THE IMPACT OF WAVELENGTH IN PLANT'S RESPONSE TO EXTREME LIGHT-INDUCED STRESS

Débora Vieira Parrine Sant'Ana

Department of Bioresource Engineering

McGill University, QC, Canada

A doctoral thesis submitted to the Faculty of Graduate Studies and Research, McGill University, in partial fulfillment of the requirements of the degree of Doctor of Philosophy.

To my mother and my sister

for being my constant inspiration.

ABSTRACT

The understanding of plant stress response is essential to develop crops that are capable of withstanding adverse growing conditions. Photosynthesis is the most important metabolic process in plants and is the one most impacted by abiotic stresses. Plants deal with extreme light conditions through the emission of energy in the form of heat, a process that helps to maintain photosynthesis efficiency, called non-photochemical quenching (NPQ). Although high-light stress response in plants is well understood, there is a lack of knowledge on how plants are affected by different wavelengths of light. Here, the hypothesis that plants undergo particular mechanisms in response to extreme high-intensity light under different wavelengths is explored at the physiological, protein, and mRNA levels. An experiment was performed to define the tomato (*Solanum lycopersicum*, Heinz H1706) leaf proteome changes under high-intensity red LED light (655 nm peak wavelength). In this study, a light-emitting diode set-up was built to create a single spot at 5,000 W m^{-2} irradiance with light gradients surrounding it. Three light stress level zones were formed: Burned (area under the spotted light), Limit (edge around the burned area), and Regular (area >1 cm from the burned section). The most impacted zone (Burned) was photo-bleached and highly dehydrated after the treatment, suggesting the death of the tissue. The proteins expressed in the leaves were extracted 10 days after the light treatment. A multiplex labeled proteomics method (iTRAQ) was carried on by 2D-LC-MS/MS. A total of 3,994 proteins were identified at 1% false discovery rate and matched additional quality filters. Hierarchical clustering analysis resulted in four types of patterns related to the protein expression, with one being directly linked to the increased LED irradiation. A total of 37, 372 and 1,003 proteins were found unique to the Regular, Limit and Burned samples, respectively. In this dataset, the proteins PsbS, PsbH, PsbR, and Psb28 presented high abundance in the Burned zone compared to other leaf zones (Limit, Regular and control). These proteins are directly involved in photoinhibition through NPQ or in the biosynthesis/assembly of PSII and their expression was further investigated. A second experiment was performed with a blue light (470 nm peak wavelength) treatment under the same LED set up, resulting in equal leaf zones. Photosynthetic parameters: NPQ, photochemical efficiency of PSII (Fv/Fm), and net photosynthesis rate (Pn) were measured under the red and blue light treatments. The measurements were taken after the light treatments and after the 10-days period of each treatment. A 3-fold NPQ value was detected on the blue light treatment compared to the red when measured after the light-induced damage. A comparative proteomics analysis between the red and the blue treatments was performed to explore the relative abundance of the key proteins, PsbS, PsbH, PsbR and Psb28. Although they presented high abundance in the Burned sample of the red treatment, their concentration was low in the corresponding blue Burned sample. To further explore the regulation control of the key proteins, the quantification of the *psbs, psbr, psb28* and *psbh* transcripts was accessed through an RT-qPCR. An 8-fold transcript abundance increase of PsbS, a key protein in one of the different NPQ response strategies, was detected in the blue dataset. The low correlation between the protein and mRNA concentrations of PsbS in the blue treatment suggested a high regulation control at the mRNA level. Altogether, the results demonstrated that blue light induced a higher response of NPQ, which was continued by a strategy containing a high regulation of PsbS at the mRNA level. The red treatment response resulted in high concentrations of the PsbS, PsbH, Psb28 and PsbR proteins.

RÉSUMÉ

L'étude de la réponse des plantes liée au stress est essentielle pour le développement de cultures résistantes à des conditions défavorables. La photosynthèse est l'un des processus métaboliques le plus fondamental des plantes et est sévèrement affectée par les stress abiotiques. Les plantes font face à des conditions de lumière extrêmes grâce à l'émission d'énergie sous forme de chaleur, un processus qui aide à maintenir l'efficacité de la photosynthèse, appelé extinction non photochimique (ENP). L'ENP est un procédé qui permet aux plantes d'émettre l'excédent de lumière sous forme de chaleur, soit une façon pour les plantes de gérer le stress lié à la lumière. Bien que la réponse au stress de lumière à haute intensité chez les plantes soit bien comprise, il existe des lacunes quant à la façon dont elles sont affectées par différentes longueurs d'onde. Ici, l'hypothèse que les plantes subissent des mécanismes différents en réponse à diverses longueurs d'onde de haute intensité est explorée aux niveaux physiologiques, protéomiques et transcriptomiques. Tout d'abord, une expérience a été réalisée pour définir les changements du protéome végétal sous diode électroluminescente (DEL) rouge à haute intensité (655 nm de longueur d'onde maximale). Dans cette étude, une analyse protéomique a été effectuée pour tester une installation DEL, construite pour créer un seul spot à 5000 W m^{-2} d'irradiance avec des gradients de lumière autour. Trois zones de niveau de stress ont été formées : la zone Brûlée (zone sous le faisceau de lumière), la zone Limite (bord autour de la zone brûlée), et la zone Régulière. La zone la plus touchée (Brûlée) était photo-blanchie et fortement déshydratée après le traitement, suggérant la mort du tissue. Le début d'une synthèse de chlorophylle a été observé après 10 jours. Les protéines exprimées dans les feuilles ont été extraites 10 jours après le traitement de lumière. Une méthode protéomique multiplex (iTRAQ) a été suivie par 2D-LC-MS / MS. Au total, 3 994

protéines ont été identifiées à un taux de fausse découverte de 1% et correspondaient à des filtres de qualité supplémentaires. L'analyse de classification hiérarchique a abouti à quatre types de modèles liés à l'expression de protéines, l'un étant directement lié à l'irradiation des DEL. Un total de 37 protéines uniques ont été trouvées à l'échantillon régulier, contre 372 pour l'échantillon de la zone Limite et 1003 pour l'échantillon de la zone Brûlée. Les protéines PsbS, PsbH, PsbR et Psb28 avaient une abondance élevée dans la zone Brûlée par rapport aux autres zones foliaires (Limite, Régulière et contrôle). Ces protéines sont directement impliquées dans la photoinhibition via NPQ ou la biosynthèse/assemblage de PSII, et leur expression a été étudiée plus avant. Une deuxième expérience a été effectuée avec un traitement à la lumière bleue (longueur d'onde maximale de 470 nm), ce qui a donné les mêmes zones de feuilles. Les paramètres de la photosynthèse, tels que l'ENP, l'efficacité photochimique du PSII (Fv/Fm) et le taux de photosynthèse (Pn), ont été mesurés sous les traitements à la lumière rouge et bleue. Les mesures ont été prises après les traitements et après une période de 10 jours après chaque traitement. Une augmentation de 3 fois de l'ENP a été détectée lors du traitement à la lumière bleue (BLT) par rapport à la RLT, mesurée après les dommages dus à la lumière. La différence entre les traitements de lumière a été étudiée au niveau des protéines. Une analyse protéomique comparative entre RLT et BLT a été réalisée pour explorer l'abondance relative des protéines clés, PsbS, PsbH, PsbR et Psb28. Bien que ces protéines aient présenté une abondance élevée dans l'échantillon Brûlé de RLT, leurs concentrations étaient faibles dans l'échantillon BLT Brûlé correspondant. Pour étudier le contrôle de la régulation des protéines clés, la quantification des transcrits *psbs*, *psbr*, *psb28* et *psbh* a été obtenue via un RT-qPCR. Les résultats ont démontré que les transcrits de la protéine PsbS, une protéine clé dans l'une des différentes stratégies de réponse aux ENP, étaient huit fois plus abondants dans les conditions BLT. Le désaccord entre les concentrations de protéines et des niveaux d'ARNm de PsbS dans le BLT suggère un contrôle de régulation au niveau transcriptionnel. En conclusion, les résultats démontrent que les traitements par BLT induisent une réponse plus élevée d'ENP, suivie d'une régulation élevée de PsbS au niveau de l'ARNm. La réponse au traitement par RLT était plutôt impliquée par de fortes concentrations de PsbS, PsbH, Psb28 et PsbR.

ACKNOWLEDGEMENTS

I thank my thesis supervisor, Dr. Mark Lefsrud, whose scientific curiosity is truly inspiring, for the encouragement, and most of all, support during this long journey. I would also like to thank Dr. Valérie Orsat, the head of the department, during my PhD, for providing immediate assistance during personal and academic obstacles.

I acknowledge the help of the staff at the BREE department, and Dr. Robert Williams and Dr. Anil Patel for their help in my first steps into the project and the university. I thank my colleagues at McGill, Edris, Bo-Sen, Marcela, Jauharah, Sophie, Peter, Guillermo, Marcos and Kiran, for their great emotional and academic support. To professors Dr. Benoit Cousineau and Dr. Gregory Marczynski, thank you for the opportunity of working, and learning, as a teaching assistant in their Molecular Microbiology laboratory course.

I would also like to thank the people who I collaborated with, and whose time and expertise had invaluable input into my work: Dr. Mårten Larsson, Dr. Todd Greco, Dr. Keith Rivera and Dr. Darryl Pappin.

To my family, my friends in Montréal and in Brazil, thank you for forgiving my physical absence in important moments of your lives, thank you for your support and patience.

Lastly, to the person who enabled me to manage this period in a very healthy manner, my best friend and partner in life, Fabio Castillo.

THESIS OFFICE STATEMENT

Candidates have the option, subject to the approval of their Department, of including, as part of their thesis, copies of the text of a paper(s) submitted for publication, or the clearly duplicated text of the published paper(s) provided that these copies are bound as an integral part of the thesis. If this option is chosen, connecting texts, providing logical bridges between the different papers are mandatory. The thesis must still conform to all other requirements of the "Guidelines Concerning Thesis Preparation" and should be in literary form that is more than a mere collection of manuscripts published or to be published. The thesis must include, as separate chapters or sections: (1) a Table of Contents, (2) a general abstract in English and French, (3) an introduction which clearly states the rationale and objectives of the study, (4) a comprehensive general review of the background literature to the subject of the thesis, when this review is appropriate, and (5) a final overall conclusion and/or summary.

Additional material (procedural and design data, as well as description of the equipment used) must be provided where appropriate and in sufficient detail (e.g., in appendices) to allow a clear and precise judgment to be made of the importance and originality of the research reported in the thesis.

In the case of manuscripts co-authored by the candidate and others, the candidate is required to make an explicit statement in the thesis as to who contributed to such work and to what extent; supervisors must attest to the accuracy of such claims at the Ph.D. Oral defense. Since the task of examiners is made more difficult in these cases, it is in the candidate's interest to make perfectly clear the responsibilities of all the authors of the co-authored papers.

STATEMENT OF CONTRIBUTING AUTHORS

In accordance with the McGill “Guidelines for a Manuscript Based Thesis,” the contributions made by the candidate and co-authors of the Ph.D. dissertation chapters are specified below by manuscript. Dr. Mark Lefsrud served as thesis advisor and was involved in critical input and guidance to experimental design, editing, and review of chapter manuscripts for publication.

Manuscript I (Chapter 2)

Sant’Ana, D.V.P., Lefsrud, L. (2018) Tomato proteomics: tomato as a model to crop proteomics. Scientia Horticulturae 239, 224–233. https://doi.org/10.1016/j.scienta.2018.05.041. Permission for using this manuscript is presented in Appendix B, section 9.2.1.

DVPS was responsible for the literature research and review, figure editing and writing of the manuscript. The critical review and editing of the manuscript were performed by ML.

Manuscript II (Chapter 4)

Parrine, D, Wu, B.-S., Muhammad, B., Rivera, K., Pappin, D., Zhao, X., Lefsrud, M. (2018) Proteome modifications on tomato under extreme high light induced-stress. Proteome Science 16(1), 20. https://doi.org/10.1186/s12953-018-0148-2.

The plant light treatments with red LED were performed by DVPS under the orientation of BSW, who together performed the light irradiation map. The leaf temperature measurements were taken under the orientation of Dr. Lucas McCartney, and its data analysis was carried out by DVPS. The author DVPS was also in charge of the sample collection, project design, and the bioinformatics analysis. The bioinformatics analysis included: i) Hierarchical clustering analysis of significant differentially abundant proteins, ii) Pattern analysis of expressions, iii) Functional analysis of proteins (GO term enrichment), iv) Network interaction analysis of differentially expressed proteins. The protein sample preparation (iTRAQ labeling) and peptide injections into the mass spectrometer, as well as the preliminary statistical analysis, were carried out by KR and DP. ML critically analyzed the project design and the manuscript.

Manuscript III and IV (Chapters 5 and 6)

Sant'Ana, D.V.P., Greco, M.T., Wu, B.-S., Orakzai, B., Zhao, X., Lefsrud, M. Plants response to extreme light-induced stress is wavelength-specific (Part I and Part II).

The experimental design, plant growth, statistical analysis, protein functional enrichment, the comparison of the blue and red LED treatments datasets, and the RT-qPCR primers design were performed by DVPS. BSW and DVPS were responsible for the plant light treatment utilizing blue LED light, as well as the light irradiation map. TG performed the data label-free expression normalization and accessed data quality. BMO performed the RT-qPCR experiment for mRNA expression validation. XZ critically reviewed the RT-qPCR experiments section of the manuscript. ML critically reviewed the project design and the manuscript.

TABLE OF CONTENTS

LIST OF TABLES

LIST OF FIGURES

GLOSSARY

2-OG:	2-oxoglutarate
ABA:	Abscisic acid
ACN:	Acetonitrile
AP-MS:	Affinity purification combined with mass spectrometry
APX:	Ascorbate peroxidase
ATP:	Adenosine triphosphate
BLAST:	Basic local alignment search tool
BLT:	Blue light treatment
BRA:	Brassinosteroid
CAT:	Catalase
CDF:	Cumulative distribution function
Chl:	Chlorophyll
CID:	Collision-induced dissociation
CMV:	Cucumber mosaic virus
CP:	Coat protein
DHAR:	Dehydroascorbate reductase
ESI:	Electrospray ionization
EST:	Expressed sequence tag
F0’:	Minimum fluorescence of light-adapted state
FA:	Formic acid
FBA:	Fructose 1,6-bisphosphate aldolase

FDR:	False discovery rate
Fm:	Maximal fluorescence
Fm’:	Maximal fluorescence of light-adapted state
GAPDH:	Glyceraldehyde 3-phosphate dehydrogenase
GM:	Genetically modified
GO:	Gene ontology
GR:	Glutathione reductase
GTP:	Guanosine triphosphate
HPLC:	High-performance liquid chromatography
HR:	Hypersensitive response
HSP:	Heat shock protein
IAA:	Iodoacetamide
ICDH:	Isocitrate dehydrogenase
IT:	Ion trap
iTAG:	International tomato annotation group
iTRAQ:	Isobaric tag for relative and absolute quantitation
KEGG:	Kyoto encyclopedia of genes and genomes
LC:	Liquid chromatography
LEA:	Late embryogenesis abundant
LED:	Light emitting diodes
LHC:	Light harvesting complex
LHCB:	Light-harvesting chlorophyll a/b binding protein family
MALDI:	Matrix assisted laser abdorption/ionization

MAPKs:	Mitogen-activated protein kinases
MDHAR:	Monodehydroascorbate reductase
MMTS:	Methyl methanethiosulfonate
MS:	Mass spectrometry
MS/MS:	Tandem mass spectrometry
MudPIT:	Multidimensional protein identification technology
NPQ:	Non-photochemical quenching
NQ:	Methionine oxidation and deamidation
OEC:	Oxygen-evolving complex
PAR:	Photosynthetically active radiation
PIC:	Protein interaction clusters (-b, burned, -l, limit)
Pn:	Net photosynthesis rate
PSI:	Photosystem I
PSII:	Photosystem II
PSM:	Peptide spectrum matches
PTIR:	Predicted tomato interactome resource
PTM:	Post-translational modifications
RH:	Relative humidity
RI:	Recombinant in-breed
RLT:	Red light treatment
ROS:	Reactive oxygen species
Rubisco:	Ribulose-1,5-bisphosphate carboxylase/oxygenase
RuBP:	Ribulose 1,5-bisphosphate

SAM:	S-adenosylmethionine
SBPase:	Sedoheptulose-1,7-bisphosphate
SCX:	Strong cation exchange
SDS:	Sodium dodecyl sulfate
SGN:	Sol genomics network
SILAC:	Stable isotope labeling by amino acids
SOD:	Peroxide dismutase
SRM:	Single reaction monitoring
TCA:	Trichloroacetic acid
TCEP:	Tris(2-carboxyethyl)phosphine
TEAB:	Triethylammonium bicarbonate buffer
TF:	Transcription factors
tMAPA:	Target mass accuracy precursor alignment
TMT:	Tandem mass tag
TMV:	Tobacco mosaic virus
TOF:	Time of flight

CHAPTER 1: Introduction and objectives

1.1 Background, problem statement, and significance

The United Nations estimates that by 2100, the global population projection will be between 9.6 billion and 12.3 billion (Gerland et al., 2014). Today, more than one in seven people still have no access to fundamental quantities of protein and energy from food (Godfray et al., 2012). By 2030, the high demand for agricultural products is estimated to increase by about 50% as the global population increases, requiring a shift toward sustainable intensification of food systems (Wheeler and Braun, 2013).

The cereal production target for the coming years will need to rise to over 400 million metric tons by 2050, with a production rate achieving 44 million metric tons per year to be able to meet the world's demands (Tester and Langridge, 2010). The production demand will be higher in developing countries. The target from the Declaration of the World Summit on Food Security (FAO, 2009) was set to a 70% increase in food by 2050. Such challenging unprecedented production increase will require substantial modifications in methods for agronomic processes and crop improvement.

The demand for agricultural feedstocks for biofuel production is estimated to increase, resulting in a higher demand for, mainly, maize and sugar cane, reducing the availability of these crops as food (FAO, 2009). This demand allows for an opportunity to increase the production of other food sources to restore the levels of nutrients in diets. In the geographic distribution of hunger defined by the Food and Agriculture Organization (FAO), the highly-affected countries are situated in sub-Saharan Africa or South Asia, making their access to food a crucial factor. The importance of incentivizing and investing in agriculture in these countries is essential to guarantee the future population's access to food.

The greenhouse effect caused by high CO_2 concentration results in increased global temperatures. The global mean temperature has risen by 0.8 ºC since the 50's, with this trend, the ability to cultivate crops in currently unstable places will be vital (Wheeler and Braun, 2013). The growth of nutrient-rich crops in adverse conditions and the exploitation of methods to increase biomass yield of crops would aid in having higher production rates.

High CO_2 levels have been utilized in field simulations, as the Free Air CO_2 Enrichment (FACE) method to estimate the modifications of crops growth (Jones et al., 2014). In these experiments, entire fields of plants are CO_2 enriched by emitters. The high CO_2 atmospheric concentrations increased the photosynthesis and water use in most plants (Wheeler and Braun, 2013).

However, the temperature rise, ozone, and pollutant traces have a negative impact on plant growth, by reducing the net photosynthesis response to below maximum values. Another negative impact of global warming consequence in plants is the "natural" selection of heat-resistant varieties, which will cause the decrease of the overall biodiversity.

The investigation of stress-resistant crops is in present demand since its development is typically associated with long-term development strategy. Increased yield is a significant goal, but the efficient use of water and nutrients is also essential. New genetic methodologies and more in-depth knowledge of crop physiology will allow a more concise approach to select desired plant traits (Godfray et al., 2012). Crops resistant to drought, high-temperature, pathogens, salinity and presenting increased photosynthetic efficiency are the target crop traits for maize, soybean, cereal, potato, fruits (tomato), and others (Godfray et al., 2012).

The main limiting factors for applying new technologies in plant breeding are the regulatory complexity and high costs in certain countries (Tester and Langridge, 2010). Still, some countries have banned cultivation or/and importation of genetically modified crops. The issue concerning food security and the environmental modifications in food production has created a new urgency in accelerating the rates of genetic gain in breeding programs. Advanced technological developments are crucial, and a significant challenge will be to make sure that the technological developments achieved are successfully effective (Tester and Langridge, 2010). Therefore, the understanding of the mechanisms of crop stress tolerance is essential to developing new crops that can withstand adverse environmental conditions. This thesis addresses this challenge as a form of data resource for future genetic engineering studies on abiotic stress response pathways in plants. The finding of a high regulation control in different light wavelengths on photosynthetic proteins (PsbH, Psb28, PsbR and PsbS) and the presence of abscisic acid in a response to extremely high light intensity are observed. The regulation of these photosynthetic proteins can be explored as targets in genetic engineering studies to generate plants with higher light stress resistance traits. The levels of nonphotochemical quenching and organization of the PSII complex can possibly be controlled by the genetic expression of PsbS, Psb28, PsbR, and PsbH, and other proteins, which can result in the regulation of light stress response and photochemistry efficiency. Finally, the study of this intricate regulation could result in crops with higher photosynthetic yield, possibly increasing the amount of biomass, and generate crops that are able to grow in adverse environments as deserts, or tropical conditions.

To further explore the crop improvement topic, a review of the latest studies on proteomics analysis of tomato plants under stress is presented in Chapter 2. This review details the current research status and the limitations of the field, focusing on the use of proteomics to achieve strategies for crop improvement. To introduce the specificities of plants response to light damage, especially photoinhibition, Chapter 3 details a literature review on this subject.

The research project presented in this thesis is the characterization of plant response to extreme light-induced stress conditions. Proteomics is applied in this project as a method for in-depth characterization of these mechanisms and the identification of the key players in response to this condition. The improvement and fast-pace of genomics and protein sequencing have pushed forward the field of proteomics, and it has become the one significant method to study gene functions (Park, 2004). Two independent proteomics methodologies were used: label-free and labeled. The label-free approach was achieved by the in-house analysis in an ion trap MS coupled to a MudPIT peptide separation technique. The labeled proteomics was performed using a high-resolution mass spectrometry along with an isobaric labeling methodology (iTRAQ).

These proteomics methodologies were implemented in the study of red and blue LED lights with an extreme level of irradiance. Two wavelengths were tested, 470 nm and 655 nm, corresponding to blue and red spectra. The choice of the wavelengths was due to the availability of plant pigments (as carotenes- and porphyrins- based) presenting either both or one of these colors as the peak absorption wavelength. The LED light treatment developed by our research group was used to generate different levels of light intensity on the plant leaves. The project consisted of exploring the differences amongst the light gradient, and between the two wavelengths (red and blue).

Although there are studies on plant response to high-light stress, the literature has not yet explored the use of extreme irradiance. Several studies have contributed to the knowledge on photoinhibition and acclimation; however, there is still the need for better clarification from the field. There is, for example, lack of consensus in what is considered a high-light stress condition. Most studies report levels from 100-400 μmol photons m^{-2} s^{-1} (Bečková et al., 2017; Miller et al., 2017) and few studies reported the use of up to 1,000 μmol m^{-2} s^{-1} (Moore et al., 2014; Suzuki et al., 2015; Vogel et al., 2014). However, yet, no study has explored the plant response at an intensity of 20,000-25,000 μmol m^{-2} s^{-1}.

There are still unanswered questions regarding the many mechanisms activated during plants response to light stress. High-light exposure generates an increase in the proton availability, caused by the electron transport chain, increasing the ATP synthesis and activating the dissipative mechanisms (Croce, 2015). Well-known ROS, antioxidants synthesis, and photoinhibition (with the degradation of the D1 protein) participate in the plant response to stress. Less characterized is the non-photochemical quenching mechanism (NPQ). NPQ is activated by the protonation of two glutamate residues of the thylakoid lumen and dissipates energy as heat (Li et al., 2004). However, the participation of the PsbS protein in NPQ has been recently questioned, due to the $^1O_2$ role in energy dissipation (Szymańska et al., 2017). As it will be discussed in the following chapters, the findings from this thesis guide towards more definite answers to the involvement of proteins in light stress response.

1.2 Hypotheses and objectives

Plants evolved to present a plethora of protection mechanisms to environment stimuli due to being sessile organisms (Külheim et al., 2002). These mechanisms are well studied due to their importance in crop improvement. The understanding of their mode of action can help to engineer plants with high levels of tolerance to environmental stress. In the context of high-light stress, response to photo-oxidation, photoinhibition, and energy excess are known strategies. Less explored is how extreme light irradiance impacts these mechanisms. Would a wavelength shift be enough to cause a difference in the activation of these mechanisms? In this section, the hypotheses and objectives of this thesis are presented.

The central hypothesis of this thesis is that plants response to extreme light stress is dependent on the wavelength. This statement is based on the fact that plants express a wide range of proteins containing variable light-absorbing peaks. These proteins have roles in various metabolic functions and are typically linked to a plant's response to light, as, phototropin, chlorophyll, and phytochrome.

The impact of the different wavelengths in plant metabolism is well characterized under normal light conditions (Casal and Yanovsky, 2005). Mechanisms of plant response to light stress are wavelength-specific activated, as, for example, the UV and blue light-dependent destruction of the manganese cluster of the oxygen-evolving complex (Szymańska et al., 2017). However, when the effect of high-light in plants is studied, the effect is rarely discussed at wavelength-level. Therefore, in this study, it is hypothesized that proteomics can detect changes at the protein level on plant response to light treatments applying different wavelengths at an extremely high intensity.

The global objective of this thesis was to clarify if plants exhibit a wavelength-dependent response to extreme light-induced stress. The specific objectives, organized by chapter, are presented below.

Chapter 2 and 3 – Literature Review

- Review and critique of the relevant literature on proteomics in the context of abiotic and biotic stress studies with tomato plants.
- Assess the latest methodologies applied to the proteome characterization of crops.
- Report on the current challenges of crop proteomics.

Chapter 4 - Quantitative proteomics analysis of light-induced stress in plants

- Characterize for the first time the plant proteome landscape under extreme light-induced stress conditions using red LED lights.
- Determine the key proteins with differential abundance compared to standard conditions (control) by a clustering analysis strategy.

- Generate a protein interaction network to help in the identification of functional clusters.
- Identify the differential activation of mechanisms in plant response.

Chapters 5 and 6- Plants response to extreme light-induced stress is wavelength-specific and supplemental findings

- Compare the photosynthetic parameters and temperature of plants under extreme light-induced stress conditions (red and blue wavelengths), measured following the application of the stress, and after a 10-day period to determine lasting effects.
- Identify the proteins differentially abundant in the plant response to extreme light-induced stress under blue light.
- Establish a comparison between the plant protein abundance under two light treatments utilizing different light wavelengths (red and blue).
- Define protein/gene candidates exhibiting differential expression profiles between the samples and the light treatments previously tested.
- Validate the expression profiles of the candidate genes by comparing the mRNA expression rates through an RT-qPCR experiment.
- Determine if plants respond to extreme light-induced stress under different wavelengths in a different manner.

1.3 Thesis organization

This thesis follows, when appropriate, the McGill University's Graduate and post-graduate studies (GPS) guidelines for thesis organization in a manuscript format (www.mcgill.ca/gps/thesis-/thesis-guidelines/preparation). It contains a total of nine chapters, containing: introduction, literature review (divided into two parts), manuscript II, manuscript III and IV, supplementary findings, conclusions, references and the appendices. Connecting texts were used to clarify the context of each chapter and link the following content to the previous chapter.

Chapter 1 contains an introduction with the background, problem statement and significance, contribution to knowledge, and the hypotheses and objectives. Chapter 2 presents the first part of the literature review, a published literature review on proteomics studies on abiotic and biotic stress on tomato plants. In Chapter 3, a continuation of the literature review is presented, addressing the specific topic of light stress as photoinhibition and non-photochemical quenching. Chapters 4 and 5 contain the methodology, results, discussion and conclusion of the experiments carried out to corroborate the hypotheses presented in this thesis. The supplementary findings resulting from the experiments that were not included in the manuscripts are discussed in Chapter 6. Chapter 7 contains the final conclusions along with the final remarks of this thesis. All the references cited in this thesis are listed in Chapter 8. Finally, the appendices are presented in Chapter 9, containing details of protocols used in the mass spectrometry experiments, the permissions from the publishing editors for reproduction of the content and figures of the manuscript, and the list of proteins identified in this study.

CHAPTER 2: Literature review (manuscript I)– Part I

Connecting statement

A literature review of the various types of plant stress is presented in this chapter. The choice of writing a literature review with a broad focus on plant stress, rather than the light stress specifically, was made after a careful review of the routes of stress signaling. Plant response to stress involves many common signaling strategies, as ROS accumulation, the involvement of heat shock proteins and hormones synthesis. Therefore, to fully understand the mechanisms of the stress response, it is necessary to define a broad view of their signaling networks. From that point of view, in nature, extreme environmental conditions normally involve simultaneous stresses, for example, high-light and heat, or drought and salinity. Their combination can influence the plant response either positively or negatively. The response mechanism of biotic and abiotic stress conditions will be further discussed in this review under the proteomics view.

This review includes studies utilizing the latest proteomics techniques and topics such as iTRAQ, post-translational modifications, and protein-protein interaction studies. A more detailed review of the literature on high-light stress and of the methodology utilized in this thesis is presented in Chapter 3, as a complement of the literature discussed in this chapter.

Manuscript I: Tomato proteomics: Tomato as a model for crop proteomics

Abstract

The understanding of plant stress response is essential to develop crops that are capable of withstanding adverse conditions. The development of proteomics led to the characterization of many of the metabolic pathways involved in plant resistance and adaptation to abiotic stresses. Mass spectrometry has been a popular tool for the study of plant protein expression under special environmental conditions due to its high throughput capacity and sensitivity. Recent studies have applied proteomics methodologies, such as phosphoproteomics, to understand metabolic dynamics and regulations. Isobaric tags, such as iTRAQ, have been used to obtain more precise and less time-consuming quantitative analysis. Although these proteomic strategies have been successfully applied to studies with tomato (*Solanum lycopersicum*), a major challenge of crop proteomics is the lack of functional genetic information when compared to the model plant, *Arabidopsis thaliana*. Still, tomato has been the model crop for genetic and molecular research of the Solanaceae family due to its attributes of diploidy, easy genetic transformation, and many genetic resources. The necessity of better strategies to increase the genetics and proteomics resources of tomato is in high demand. Here, we explore the various proteomics methodologies used in studies on tomato plants, and we discuss the present challenges of crop proteomics data interpretation.

Keywords

Proteomics; Tomato; Solanaceae; Stress; Abiotic; Crops

2.1 Introduction

Proteomics allows for the study of global gene products in various tissues and physiological cell states. With the advancement of genomic sequencing and mapping of proteins, proteomics has become one of the largest areas to study functional genomics (Park, 2004), with the most publications of any omics field for a few years (Sanchez-Lucas et al., 2016). Most of the proteomics studies have focused on humans and the majority on cancer research. Although agriculture development has been a frequent topic when discussing food security (Godfray et al., 2012; Wheeler and Braun, 2013), plant research funding has not yet achieved the same level as human proteomics, making the access to new technologies limited. The importance of using proteomics to study the dynamic and complex plant proteomes relies on the identification of proteins and its modifications in stress conditions to develop crop improvement (Hu et al., 2015; Kilambi et al., 2016). In this review, we address the proteomics studies related to stress conditions on tomato plants, due to the rising importance of tomato as a model plant in crop proteomics and the importance of agricultural development for crop improvement.

2.2 The tomato genome and proteome databases

Tomato is the most intensively studied member of the *Solanaceous* family (Barone et al., 2008), mainly due to its short generation time, elementary diploid genetics, a well-known genetic transformation methodology, inbreeding tolerance, and a vast well-characterized genetic resource (Barone et al., 2008; Van der Hoeven et al., 2002). Many datasets have been gathered regarding the tomato genome: collections of wild tomato species and mutant germplasm collections; marker collections; F2 synteny and permanent recombinant inbreed (RI) mapping population; BAC libraries and an advanced physical map; TILLING populations, tomato microarrays, gene silenced tomato lines; and VIGS libraries (for transient silencing) (Barone et al., 2008).

The whole genome sequencing of tomato (*Solanum lycopersicum*) was completed in 2012 as an initiative of the Tomato Genome Consortium, formed with more than 90 research institutions (Tomato Genome Consortium, 2012). The genome of cultivar Heinz 1706 (H1706) comprises 12 chromosome pairs with a size of 950 Mb, and a total of 35,000 genes (Van der Hoeven et al., 2002). In contrast to the genome of *Arabidopsis* and sorghum, tomato presents fewer high-copy, full-length long terminal repeat retrotransposons with an older average insertion age (2.8 compared to 0.8 million years ago) and fewer high-frequency k-mers (Tomato Genome Consortium, 2012). Amongst tomato relatives, as the wild tomato (*Solanum pimpinellifolium*), only 0.6% of nucleotide divergence is seen. Compared to the genome of another member of the Solanaceae family, the tomato and the potato (*Solanum tuberosum*) genomes present only 8% nucleotide divergence and signs of recent admixture, presenting nine large and many small inversions (Tomato Genome Consortium, 2012).

Proteome databases contain the protein sequences diverged from predicted genomic gene models and unigene transcripts. The latter is determined either by applying Hidden Markov models to find coding regions, through EstScan (Iseli et al., 1999), determining the probable translation initiation by NetStart (Pedersen and Nielsen, 1997), or by the reading of the longest open reading frame (Bombarely et al., 2011). The last version update of the tomato database (v.3.2), maintained by the international tomato annotation group (iTAG), contained 30,868 annotated genes, from which 2,300 genes were user curated. Other proteomics and genomics databases are available by Phytozome (phytozome.jgi.doe.gov), Plant Genome and Systems Biology (pgsb.helmholtzmuenchen.de/plant/tomato), and the Tomato Genomic Resources Database (TGRD) (http://59.163.192.91/tomato2). As for the functional annotation of the genome, 56.6% of the genes are associated with Gene Ontology (GO) terms. The FASTA files compatible with Mascot (Hirosawa et al., 1993), basic local alignment search tool (BLAST) (Altschul et al., 1990), and Protein Pilot (Applied Biosystems) (sciex.com/products-/software/proteinpilot-software) can be obtained via file transfer protocol (FTP). Today, numerous search algorithms, such as MASCOT, SEQUEST (Eng et al., 1994), Comet (Eng et al., 2013), X!Tandem (Craig and Beavis, 2004), MS Amanda (Dorfer et al., 2014), OMSSA (Geer et al., 2004), and others are currently used. These algorithms are implemented by various software, and have the role to assign the protein identification to the spectra, and therefore, are essential in all proteomics pipelines. There are many software for proteomics dataset analysis available nowadays, some of the most popular software are: Proteome Discoverer (Thermo Fischer Scientific), MassLynx MS (Waters, Inc.), ProteinPilot (Applied Biosystems), Byonic (Protein Metrics Inc.), Scaffold (Proteome Software), MaxQuant(Cox and Mann, 2008) (free), and Searchgui (Compomics) (free). They differ in the input file format required and in the pipeline possibilities, such as using two different search engines, performing iterative searches; data visualization options (graphics, tables), and others optional parameters.

Sol Genomics Network (SGN) has created an initiative to map the tomato secretome. The *Secretom* (https://solgenomics.net/secretom) was created to aid the study of proteins of the cell wall, proteins secreted in the exterior of the plasma membrane, and that are part of the secretory pathway. Secretome proteins are important because of their role in communication, responses to stress, and plant development (Krause et al., 2013). For fleshy fruits, the secretome is especially important due to the relationship between the mechanical and chemical characteristics of the cell wall and the fruit texture (Konozy et al., 2013). The SGN has also developed SecreTary, a tool for accurate computational prediction of proteins of the secretome. Secretom datasets are available through FTP on the Secretom website.

2.3 Plant proteomics from stress conditions

The development of stress tolerant plants is an important step in the context of food security. An in-depth investigation of gene networks and regulons that are involved in plant response is essential to precisely balance energy, adaptation, and plant development (Godfray et al., 2012; Mittler and Blumwald, 2010). Plant stress response has been a topic explored in various scientific reviews (Cramer et al., 2011; Knight and Knight, 2001; Komatsu and Hossain, 2013; Mittler, 2002; Rodziewicz et al., 2014). This paper will review the emerging studies that applied proteomics methodologies to characterize and analyze, in depth, stress responses from tomato. Tomato has emerged as the model plant for the Solanaceae family, and here we argue its role as a model for crop proteomics. Table 1 resumes important publications of the last 15 years of proteomics studies on tomato.

Table 1. Featured publications of studies on tomato proteomics in the last 15 years.

Plant organ/ tissue	Stress condition/ Physiological condition	Cellular organelle	Method	Number of identified proteins/ proteins spots on gel	Tomato cultivar(s)	Reference
Root	Biotic (*Bacillus megaterium* and *Enterobacter* sp. C7	Microsome	LC-MS/MS (LTQ-Orbitrap)	1,214 proteins	Never ripe (nr) LA0162, cv Pearson	Ibort et al., 2018
Leaf	Biotic (*Phytophthora infestans*)	Total protein	2-DE, MALDI TOF-TOF	19 proteins (MS), of 41 (protein spots)	Genotypes: (BGH)-2127, cv. Santa Clara	Laurindo et al., 2018
Apoplastic fluid	Biotic (*Ralstonia solanacearum*)	Total protein	(IP)LC-MS/MS (Orbitrap)	335 protein groups	cv. Marmande, cv. Hawaii 7996	Planas-Marquès et al., 2018
Xylem sap	Nutrient deficiency (Fe and Mn)	Total protein	LC-MS/MS (LTQ XL)	643 proteins	cv. Tres Cantos	Ceballos-Laita et al., 2018
Fruit	Development stages (5), fruit skin and flesh	Total protein	LC-MS/MS (Q Exactive)	7,738 proteins	cv. Microtom	Szymanski et al., 2017
Leaf	Abiotic (drought)	Chloroplast	2D-DIGE, LC-MS/MS	2,600 spots, (31 and 54 proteins from drought and drought-recovered, respectively, were further analyzed by MS-MS)	cv Crovarese	Tamburino et al., 2017
Pericarp	Ripe red stage	Total protein	LC-MS/MS (Q Exactive)	8.588 proteins	cv. Roterno	Mata et al., 2017
Graft Union	Heat	Total protein	2-DE, MALDI-TOF	700-900, 200-600 proteins, respectively	cv. Super Sunload, cv. Super Doterang	Muneer et al., 2016
Leaf	Biotic stress (bacteria)	Total protein	TMT, LC-MS/MS	4,348 proteins[e]	*S. lycopersicum*	Balmant et al., 2015

			(hybrid quadrupole-Orbitrap)		genotype PtoR and *prf3*	
Pollen	Biotic stress (heat-pollen)	Total protein	SDS-PAGE, LC-MS/MS (Orbitrap-LTQ)	365 proteins	cv. Hazera 3017	Chaturvedi et al., 2015
Fruit	4 developmental stages	Plastid	GeLC-MS/MS, (Orbitrap-LTQ)	605 proteins[a]	cv. Micro-Tom, Black, cv. White Beauty	Suzuki et al., 2015
Floral pedicel	Ethylene-induced flower	Total protein	iTRAQ, LC-MS/MS (Q Exactive)	1,429 proteins	*L. esculentum* Mill cv. Liaoyuanduoli	Zhang et al., 2015
Roots	Abiotic stress (salt and alkali)	Total protein	iTRAQ, LC-ESI-MS/MS (Triple TOF)	1,915 proteins	*S. lycopersicum L.*	Gong et al., 2014
-	-	Extensin peroxidases	SDS-PAGE, LC-MS/MS (LTQ-FT)	3 peroxidases	?	Dong et al., 2014
Fruit	Ripening	Cell wall protein	LC-MS/MS (Q-TOF)	185 proteins	*S. lycopersicum* var. *cerasiforme, S. lycopersicum Mill* (Levovil, VilB)	Konozy et al., 2013
Leaf	Biotic stress (bacteria)	Total protein	LC-MS/MS (hybrid quadrupole-TOF and TripleTOF)	2,369 proteins	*S. lycopersicum* PtoR and *prf3* genotypes	Parker et al., 2013

Fruit	-	Total protein	2-DE, Nano-LC-MS/MS	506 spots (333 proteins)	Various (>8 genotypes)	Xu et al., 2013
Pollen	-	Total protein	iTRAQ, LC-MS, (QTrap hybrid linear ion trap triple quadrupole)	>1,200 proteins	*S. lycopersicum*, cv. M82, SC *S. pennellii* (accession LA0716), SC S. *habrochaites* (accession LA0407), and SI *S. habrochaites* (accession LA1777)	Lopez-Casado et al., 2012
Fruit	Biotic stress (fungus)	Total protein	1D-SDS-PAGE, LC-MS/MS (LTQ-linear ion trap-ESI)	588 (tomato) 79 (*Botrytis cinerea*)	cv. Ailsa Craig	Shah et al., 2012
Fruit	-	Glycoproteins	2D LC-MALDI-MS/MS	133 proteins	*S. lycopersicum* cv. Ailsa Craig	Catalá et al., 2011
Root	Abiotic stress (salt) + genotype	Total protein	SDS-PAGE, LC-MS/MS (LCQ ion trap)	1300 spots, 90 spots further analyzed by MS/MS	*S. lycopersicum* L. cv: Roma, Super Marmande, Cervil, Levovil.	Manaa et al., 2011

Leaf	Biotic stress (virus)	Total protein	1-DE SDS-PAGE, DIGE, nLC-ESI-IT-MS/MS (XCT Ultra ion trap)	2084 spots, 71 spots further analyzed by MS/MS	*S. lycopersycum* cv. Micro-Tom	Di Carli et al., 2010
Fruit	Abiotic stress (cold)	Total protein	2-DE gels, LC-MS/MS (LCQ ion trap)	85 proteins	*S. lycopersicum* L. genotypes VilB, NIL-B9	Page et al., 2010
Root	Abiotic (cadmium toxicity)	Total protein	MALDI-TOF-MS, LIFT TOF-TOF	121 spots	*Lycopersicon esculentum* Mill cv. Tres Cantos	Rodríguez-Celma et al., 2010
Stem and petiole	Synthesis of secondary chemicals	Trichome, type VI glad protein total protein	SDS-PAGE, LC-MS/MS (linear ion trap)	1,552[d] proteins	cv. M82	Schilmiller et al., 2010
Fruit	Abiotic stress (cold/chilling injury)	Total protein	SDS-PAGE, Q-TOF-MS	~300 spots	cv. Imperial	Vega-García et al., 2010
Fruit	-	Total protein from cuticle waxes	LC-ESI-MS/MS, LC-MALDI-TOF/TOF	202 proteins	*S. lycopersicum,* cv. M82	Yeats et al., 2010
Cotyledon	Biotic stress (fungus)	Total protein	LC-ESI-MS/MS QTOF	48 phosphoproteins	Cf-4/Avr4	Stulemeijer et al., 2009
Root	Abiotic stress (iron deficiency)	Total protein	MALDI-TOF	97 proteins	Genotypes T3238 and T3238*fer*	Li et al., 2008
Fruit	Ripening	Total protein	2-DE, HPLC-ESI-MS/MS	600 spots, 32 proteins	*S. lycopersicum*,	Kok et al., 2008

					var. Moneymaker	
Xylem	Biotic stress (fungus)	Total protein	2D-PAGE, MALDI-TOF-MS, LC-QTOF-MS/MS	33 proteins (21 of tomato, 7 of fungus)	?	Houterman et al., 2007
Fruit	Biotic stress (virus)	Total protein	2-DE, MALDI-TOF-MS	256 spots (healthy), 340 spots (infected)	cv. Hungarian Italian	Casado-Vela et al., 2006
Fruit	Ripening	Total protein	2-DE, MALDI-TOF-MS, µLC-ESI-IT-MS/MS	SM: 609 (green), 631 (breaker), 638 (red) gel spots. AC: 554 (green), 532 (breaker), 497 (red) spots.	cv. Ailsa Craig (AC), SM2	Rocco et al., 2006
Whole plant	Biotic stress (virus)	Total protein	2-DE, MALDI-TOF-MS	40 spots were further analyzed	Non-GM, GM[b]	Corpillo et al., 2004

[a] Total number of identified proteins is 605, distributed among different fruit stages: 414 from green tomato; 385 from yellow; 446 from orange, and 310 from red.

[b] Non-GM: result from crossing L276 x RT, parental lines of fresh market tomato. GM: result from crossing L276-30.4 x RT, L276-30 is a homozygous line obtained following genetic transformation of L276 line with T-DNA which contained the nucleoprotein gene of TSWV (TSWV-N) as well as the *nptII* gene for selection.

[c] Total number of spots or proteins not reported.

[d] Of the 1,552 proteins identified, 1,360 were found in both samples, with 67 proteins only in the type VI trichome sample and 125 specifics to the mixed-type preparation.

[e] Total number of proteins is 4,348.217 proteins were present in all triplicates, and 529 were present in at least two replicates.

Stress conditions are commonly categorized as biotic (plant-pathogen interactions), or abiotic (extreme temperatures and light intensity, drought, salinity, and toxicity). The stress responses present some interaction level on the signaling pathways. This cross-talk has been reviewed in abiotic stresses (Knight and Knight, 2001), and resulted in the generation of a "stress matrix". In the stress matrix, the positive or the negative impact of different stress interactions are presented in a matrix format (Figure 1). The knowledge of the interactions between stresses is used as a guide for crop improvement research, through a wider and applied view of how simultaneous stresses (as ozone and UV) can result in potential positive interactions.

2.3.1 Abiotic stress

Plants cope with abiotic stress by either avoiding it or acclimating to it. Avoidance is the survival of the plant during unfavorable conditions as mature seeds. Acclimation to stress concerns the modification of plant metabolism, which is caused by significant changes at the gene expression level (Kosová et al., 2011). Both mechanisms affect plant growth and yield, causing a major constraint faced by agriculture and a negative impact on global crop production (Hossain et al., 2012; Rockström and Falkenmark, 2000).

The usual approach to studying crop abiotic stress is to compare plants under different stress environments to an optimal condition (control). Another strategy is the comparison of different genotypes (tolerant vs. control). These two approaches aim to establish correlations between protein dynamics with phenotypic changes (Abreu et al., 2013). The aim of this review is to discuss recent studies on tomato plants of different abiotic stress conditions responses that utilize these strategies and to present the latest proteomics methodologies applied in the field.

2.3.1.1 Temperature

High-temperature stress was found to cause starch depletion in tomato leaves as a result of enhanced hydrolysis and reduced biosynthesis reactions (Zhang et al., 2014). At the chloroplast level, high-temperature stress results in changes to grana stacking or swelling, modifications in the thylakoids structural organization and reduction of PSII antenna (Zhang et al., 2014). All photosynthesis reactions are susceptible to heat stress (Shaheen et al., 2015). PSII and the oxygen-evolving complexes are notably affected, thylakoid membrane carbon metabolism and stroma photochemical pathways are the first reactions to be damaged (Gerganova et al., 2016).

The suppression of Rubisco activase and S-adenosyl-L-homocysteine hydrolase has been reported in heat-induced modifications in the whole proteome of tomato leaves of different heat-tolerant cultivars (Yamamoto et al., 1981). The authors identified the differential expression of the glyoxylate shunt, carbohydrate metabolism, photosynthesis and cell defense reactions. They determined the tomato regulatory molecular mechanism for temperature coping, offering to plant geneticists many opportunities to develop heat tolerant plants. Furthermore, similarly to heat stress conditions, rubisco activase has been reported to be repressed in tomato infected with the cucumber mosaic virus (Di Carli et al., 2010). However, it was found to be upregulated during drought, salinity stress, and mineral toxicity (Salekdeh and Komatsu, 2007). Another protein, S-adenosyl-L-homocysteine hydrolase has been reported to be upregulated on the resistant line of wild tomato inoculated with *C. michiganensis* ssp (Afroz et al., 2011).

A proteomics study conducted by Muneer et al. (2016) on graft unions of three tomato genotypes revealed a high activity of peroxide dismutase (SOD), ascorbate peroxidase (APX) and, catalase (CAT). Around 40 proteins were found to be differentially expressed in the three genotypes analyzed (Super Sunload, B-blocking, and Super Doterang) when subjected to the high-low temperature treatment (Muneer et al., 2016). The identification of the stress tolerant proteins by MALDI-TOF was later confirmed by immunoblot assays. The authors saw an increased synthesis of ROS on rootstock and scions under high-low temperature treatments (30/15˚C).

Chaturvedi et al. (2015) observed the expression of heat defense proteins of tomato pollen through a quantitative shotgun proteomics methodology called target Mass Accuracy Precursor Alignment (tMAPA). The tMAPA avoids ambiguous identification of tryptic peptides and can provide the quantification of proteins isoforms (Chaturvedi et al., 2015). Heat-treated tomato pollen grains from two developmental stages were studied: post-meiotic and mature. A total of 2,000 proteins were found in the different tissues, 51 unique proteins were assigned to heat-treatment-responsive roles (Chaturvedi et al., 2015), helping to further characterize temperature stress response. In a recent publication, Chaturvedi et al. (2016) reviewed studies on pollen proteomics and their importance in "developmental priming" — a reprogramming response of proteome from various stages of pollen. The review also presented a discussion on the stress proteins expression being controlled by epigenetics, or genetics, even in non-stressed conditions. The authors suggested that the control could be related to the management of the temperature variation during pollen maturation, thus establishing the importance of further research on the proteomics changes in pollen and stress-related proteins.

In another review, Kosová et al. (2015) discuss the stress responses of cereals, leguminous plants, and others, by analyzing each response phase: alarm, acclimation, and resistance. The authors compare tolerant and sensitive genotypes and the comment on the effects of combined stress factors. They argue that, in the future, plant proteomics will be oriented towards the study of cell fractionation, posttranslational modifications, and protein-protein interaction. Kosová and collaborators also point to the importance of studying protein markers and combined abiotic stresses, since they can help develop improved crops. Although their review has a great value, mostly due to the in-depth discussion of plant protein expression under different stress conditions, their discussion is limited to abiotic stresses.

2.3.1.2 Light

Conditions of high light stress have been known to cause photosystem damage, mainly on photosystem II (PSII). The excess energy that cannot be utilized for carbon fixation and oxygen generation results in photoinhibition of PSII and a decrease of photosynthetic quantum yield (Nama et al., 2015). The singlet oxygen radicals near PSII can cause permanent damage to the D1 protein, while the production of superoxide and hydroxyl radicals near the acceptor side of PSI generates oxidative harm to chloroplast lipids and proteins (Nama et al., 2015).

The photosystem recovery is performed by PSII repair cycles, which requires the monomerization and migration of the phosphorylated dimeric PSII complexes to non-appressed regions of the thylakoid, where the components of the repair cycle are enriched (Lu et al., 2011; Suorsa et al., 2014; Yamamoto et al., 1981; Zhang et al., 2001). D1, D2 and CP43 proteins are dephosphorylated, and the degradation of D1 proteins is carried out by FtsH and Deg proteases. The synthesis and thylakoid insertion of D1 is performed by the SecY translocon and ribosomes, and various auxiliary proteins are responsible for the PSII assembly. The D1, and, sometimes D2, PsbH and CP43 proteins are replaced in the PSII complex while the other members of the complex are recycled (Aro et al., 1993; Bergantino et al., 2003; Jansen et al., 1996; Järvi et al., 2015; Nelson et al., 2014; Rokka et al., 2005).

Modern tomato cultivars are frequently exposed to continuous lighting. The result of continuous lighting is an inter-vascular chlorosis, a decrease in leaf chlorophyll, reducing net photosynthesis and increasing the concentration of starch and hexoses (Demers and Gosselin, 2002). A proteomics study of tomato leaves cultivated under continuous lighting conditions showed that this condition could occur under a low light intensity (175 µmol m^{-2} s^{-1}) without harming the leaves of the plant if the normal conditions are restored after 11 days (Haque et al., 2015). The authors observed that the tomato physiological adjustments to the lighting condition could be rapidly reversed when the light exposure is brought to normal. At 300 µmol m^{-2} s^{-1} light intensity, tomato plants reach the highest energy efficiency and photosynthesis rate activity, with no increase in photosynthetic efficiency in higher light intensities (Fan et al., 2013). A current method being explored for increasing photosynthetic efficiency is the addition of blue light when cultivating greenhouse tomato under high light intensity, which combined with red in an adequate ratio, results in higher photosynthetic rate, improving biomass production (Deram et al., 2014).

The strategy of considering two simultaneous stress conditions (temperature and high-intensity light) in tomato plants was recently studied by Gerganova et al. (2016). The authors reported a smaller impact in the photochemical quenching and PSII quantum yield when both stresses occurred simultaneously, suggesting that high-light stimulation of non-photochemical quenching (NPQ) is mitigated by high temperature. Lipid peroxidation was also diminished by simultaneous heat and light stresses, while the malondialdehyde content was increased by high-light. However, when both stresses were combined, their concentration was reduced (Gerganova et al., 2016). The combination of both stress conditions also reduced the concentration of anthocyanins (involved in an alternative NPQ reaction) photoprotection and antioxidant process and lowered the lipid peroxidation. The outcome of this interaction contradicts the “Stress Matrix,” proposed by Mittler (2006) and recently updated by Suzuki et al. (2014), which classifies heat and high-light interaction as negative, based on a publication by Hewezi et al. (2008) (Figure 1). This shows the necessity of better addressing multiple stress conditions, not only in the depth of the analysis but as well as observing the effects in different plant families.

2.3.1.3 Salinity

Saline soil is generally caused by the accumulation of NaCl, while the alkaline soil is a result of $NaHCO_3$ and Na_2CO_3. Soil salinization and alkalinization generally are presented simultaneously and causes osmotic stress and ion-induced injury (Shi and Sheng, 2005; Zhang and Mu, 2009). When compared to saline stress, alkaline stress causes a high-pH environment around plants roots, generating precipitation of metal ions and phosphorus (Zhang and Mu, 2009). It impacts the absorption of inorganic anions, and alter the ionic balance and the pH homeostasis, causing physiological drought and ion toxicity (Zhang and Mu, 2009).

Manaa et al. (2011) studied tomato root proteome variations due to salt stress utilizing a 2-DE and liquid chromatography tandem mass spectrometry (LC-MS/MS) approach. The focus of the study was to evaluate the tomato genotype variation of response to salt stress. Nine sets of proteins were found to vary amongst salt treatments, independently of the genotype and most of the proteins up-regulated were related to carbon and energy metabolism. Furthermore, they found a higher difference between the tomato genotypes on the proteome variations than the salt treatment (33 protein spots differentially expressed amongst genotypes), supporting the importance of understanding the genetic variability between cultivars (Manaa et al., 2011).

Response to stress caused by salinity-alkalinity was studied by Gong et al. (2014) in tomato roots through the iTRAQ methodology. A total of 1915 proteins, 150 in response to NaCl and 199 to $NaHCO_3$, were identified and 80 unique proteins were discovered in this study (Gong et al., 2014). The most present functions were signaling pathways, ROS scavenging pathways, metabolism, and energy conversion and transport protein regulating (Gong et al., 2014). The authors generated a map with the shared and unique pathways related to salt and alkali stress in tomato roots.

2.3.1.4 Drought

Drought is one of the most common abiotic stress, primary affecting plants roots, but also responsible for a major impact on the metabolism and physiology of the plant (Ghosh and Xu, 2014). Together with salinity, they are the higher limiting factors impacting field crop productivity (Chamoli and Verma, 2014). Drought is known to affect plant respiration and photosynthesis rates and increase roots demand for energy due to intense cellular activity (Ghosh and Xu, 2014; Rizhsky et al., 2002). Although the importance of studying the impact of drought on plant physiological responses, few papers on tomato plants have been published utilizing proteomics methodologies and are further discussed.

In one of the first publications to relate the role of Cu,Zn superoxide dismutase with drought stress, Perl-Treves and Galun, (1991) noticed the increase of cytosolic Cu,Zn superoxide dismutase transcripts and associated isozyme in respond to prolonged drought stress. More recently, Rocco et al. (2006) detected Cu,Zn superoxide dismutase in two tomato ecotypes during ripening by using more advanced proteomics techniques, MALDI-TOF-MS and µLC-ESI-IT-MS/MS.

When investigating the protein expression of tomato plants chloroplast, Tamburino et al. (2017) observed that during drought conditions, chloroplasts had a higher level of proline, abscisic acid (ABA) and late embryogenesis gene transcript. Using a 2D-DIGE-MS/MS approach, the authors detected 31 differentially expressed proteins when the tomato plants were under a drought treatment (Tamburino et al., 2017). Interestingly, after the rewatering cycle, 54 proteins were found to be differentially expressed (Tamburino et al., 2017). Together with the gene expression analysis, these findings suggest specific chloroplast-to-nucleus signaling with an ABA-network related control (Tamburino et al., 2017). Photosynthesis was the process presenting the highest impact during drought stress.

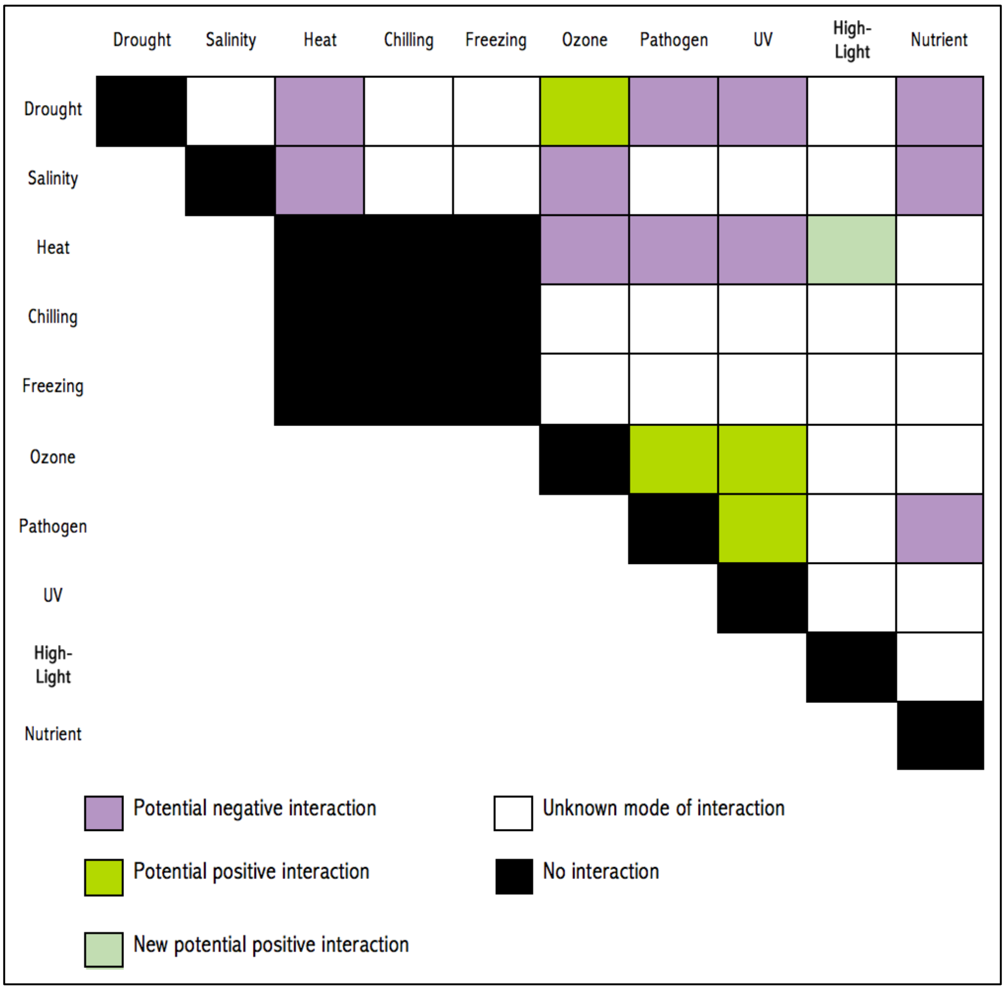

	Drought	Salinity	Heat	Chilling	Freezing	Ozone	Pathogen	UV	High-Light	Nutrient
Drought	⬛	⬜	🟪	⬜	⬜	🟩	🟪	🟪	⬜	🟪
Salinity		⬛	🟪	⬜	⬜	🟪	⬜	⬜	⬜	🟪
Heat			⬛	⬛	⬛	🟪	🟪	🟪	▨	⬜
Chilling			⬛	⬛	⬛	⬜	⬜	⬜	⬜	⬜
Freezing			⬛	⬛	⬛	⬜	⬜	⬜	⬜	⬜
Ozone						⬛	🟩	🟩	⬜	⬜
Pathogen							⬛	🟩	⬜	🟪
UV								⬛	⬜	⬜
High-Light									⬛	⬜
Nutrient										⬛

🟪 Potential negative interaction

🟩 Potential positive interaction

▨ New potential positive interaction

⬜ Unknown mode of interaction

⬛ No interaction

Figure 1. The Stress Matrix representing the agricultural important stress combinations with the new interaction between high-light and temperature. High-light and heat effects were investigated by Gerganova et al., 2016, reporting a better acclimation of tomato plants to the combined stress conditions. A smaller impact in the photochemical quenching and photosystem II quantum yield was seen when both stresses occurred simultaneously, suggesting that a high temperature might mitigate the impact of non-photochemical quenching caused by high-light (Gerganova et al., 2016). Figure modified from Mittler, 2006.

2.3.2 Biotic stress

Although the focus of this review is the abiotic stresses responses, we briefly address studies on biotic stresses to show the panorama of the latest technologies on crop proteomics.

2.3.2.1 Fungus

The sequencing of bacterial and fungal plant pathogens of model plants have enabled the study of different pathosystems as *Arabidopsis-Pseudomonas syringae* and rice-*Magnaporthe oryzae* (Vanderschuren et al., 2013). The fungus-plant interaction has been explored in rice, due to the economic importance of this crop and its sequenced genome. Proteins found in these studies were mostly related to antifungal activity, signal transduction, energy metabolism, photosynthesis, protein folding and degradation and antioxidation (Mehta et al., 2008).

Stulemeijer et al. (2009) investigated a hypersensitive-response of tomato to *Cladosporium fulvum*, a fungal leaf pathogen, utilizing label-free quantification of tomato phosphoproteins. In a comparison between resistant and susceptible plants, the authors identified novel phosphorylation sites in 48 phosphoproteins and 12 phosphopeptides subjected to changes upon hypersensitive response (HR) (Stulemeijer et al., 2009). The authors observed that photosynthesis activity suppression regulated by phosphorylation occurred in the early stages of hypersensitive response development. They identified abundance changes in phosphopeptides from four Hsp90 isoforms of control versus resistant seedlings (*Cf-4/Avr4*), suggesting a defense signaling function to the Hsp90 isoforms.

In the first study of the xylem sap proteins of tomato infected with *Fusarium oxysporum* f. sp. *lycopersici* (Fol), Houterman et al. (2007) identified 21 proteins expressed in tomato specific to the tomato-pathogen interaction, and 13 proteins present in infected plants. The authors applied a methodology of mass spectrometry analysis with a previous 2D-PAGE fractionation, and despite the limiting identification capacity of the methodology, three small protein of Fol (Six2-4) and three putative enzymes expressed during colonization of tomato were identified.

2.3.2.2 Virus

In tomato plants, one of the few studies to address virus pathogens is the investigation by Casado-Vela et al. (2006) of the tomato resistance response to the tobacco mosaic virus (TMV). The TMV infects tomato and tobacco plants, spreading to the nearby cells through the plasmodesmata, multiplicating under the control of the viral genome, resulting in cell rupture.

When comparing the protein expression of asymptomatic, but infected, tomato fruits and uninfected controls, the results showed participation of pathogenesis-related proteins (PR) (CHI, GLU) and antioxidant enzymes (DHAR, SOD, PHGPX, TPX, GST, APX) in the protection from the tobacco mosaic virus infection. The PR proteins have already been found to be related to fungus infections, and in virus infections of *N. tabacum* leaves under TMV infection (Ebrahim et al., 2011). Casado-Vela et al. (2006) also identified a variation on the expression of peptidases, endoglucanases, chitinases and proteins involved in the ascorbate-glutathione cycle. The authors suggest the use of using 2-DE and LC-MS/MS analysis as an approach to determine plant virus infections and virus species and strains.

The cucumber mosaic virus (CMV) is a major factor in agricultural losses due to biotic stresses due to its wide range of hosts, around 1,000 dicot, and monocot plants (Palukaitis et al., 1992; Tepfer et al., 2016). Di Carli et al. (2010) investigated the interaction between the cucumber mosaic virus and resistant transgenic tomato to compare compatible plant-virus interactions amongst engineered immunoprotected and susceptible tomato plants. A total of 50 differentially expressed proteins were identified, and were down-regulated in TMV-infected tomato leaves, of these proteins, 38% were related to photosynthesis, 18% to metabolism, 14%

to defense activity (Di Carli et al., 2010). Lastly, the authors observed that the CMV infection is confined to the inoculated location, and, a systemic dispersion is obstructed by the CMV coat protein (CP)-specific scFv G4 molecules, which can be helpful to develop CMV tolerant crops.

2.3.2.3 Bacteria

The interaction between *Pseudomonas syringae* pv. *tomato* DC3000 (*Pst*) causing bacterial speck disease in tomato was investigated by Parker et al. utilizing iTRAQ quantitative methodology. The study by Parker et al. (2013) reported 2,369 proteins present in tomato leaves, amongst them, 477 proteins were responsive to *Pst* inoculation. Due to the temporal analysis, the authors reported more protein/function changes on the resistance genotype at 24 h and on the susceptible genotype at 4 h (Parker et al., 2013). This research observed an effector-triggered immunity regulation of the PAMP-triggered immunity and revealed potential resistance proteins and, enabling their further characterization.

In a more recent study, protein redox functions of *P. syringae* tomato resistant (PtoR) and susceptible (prf3) genotypes were investigated by Balmant et al. (2015) through the cysteine labeling tandem mass tags (cysTMT, m/z 126-131) proteomics methodology. This study found 90 potential redox-regulated proteins related to carbohydrate and energy metabolism, cysteine, sucrose and brassinosteroid biosynthesis, cell wall biogenesis, and others. The authors observed that KAT2 (an enzyme that catalyzes β-oxidation) is highly oxidized at late stages in Pst infections in PtoR, suggesting a role as a functional switch in the reverse interaction between salicylic and jasmonic acid. The importance of the identification of novel redox-sensitive proteins pathogen-responsive relies on the increase of knowledge of the redox regulation and signaling in plant defense (Balmant et al., 2015).

Bacterial wilt agent *Ralstonia solanacearum* infection was investigated by Planas-Marquès et al. (2018) by activity-based protein profiling (ABPP), a technique that utilizes probes that marks active sites of proteins by their activity level. The authors identified the presence of papain-like cysteines proteases and serine hydrolases in the apoplast of the tolerant tomato variety Hawaii 7996 during infection with *R. solanacearum*. They found the susceptible tomato variety Marmande to present major alterations in the network topology, suggesting that the tolerant variety can resist the bacterial infection from its basal state (Planas-Marquès et al., 2018).

2.4 Other proteomic methodologies

The research of total plant protein lysates requires the use of several separation techniques to improve the proteome coverage and the inclusion of low abundance proteins (Kilambi et al., 2016). Protein separation can be obtained by an online separation method, as multidimensional protein identification technology – MudPIT (Washburn et al., 2001), or offline methods involving 2D-PAGE, and HPLC. MudPIT has been mostly implemented in shotgun studies (Abraham et al., 2013; Huang et al., 2012; Huang and Lefsrud, 2014, 2012; Patel et al., 2015; Sivagnanam et al., 2012, 2011a), while gel and offline LC-MS are more compatible with other methodologies (iTRAQ, TMT, SILAC) (Chavez et al., 2016; Gong et al., 2014; Kilambi et al., 2016; Schilmiller et al., 2010; Shah et al., 2012; Zhao et al., 2016), and require a less complex MS setup. Another strategy to reduce sample complexity is to monitor plant lysates using subcellular proteomics, which can analyze isolated organelles. Other challenges for tomato protein profiling are the identification of post-translational modifications (PTM) and the resulting interactomes based on protein-protein interactions (Sanchez-Lucas et al., 2016). Tomato fruit protein extraction and digestion, peptide separation protocols, and MS parameters were recently reviewed by Kilambi et al. (2016) providing valuable information for experiment standardization.

2.4.1 Post-translational modifications –PTM

Proteins *in vivo* can be subjected to more than 300 different known post-translational modifications, such as phosphorylation, glycosylation, acetylation, and methylation (Chen and Harmon, 2006). These modifications are responsible for the modulation of various eukaryote proteins (Mann and Jensen, 2003) and arise by covalent processing actions that change the properties of proteins through the addition of a modifying group of amino acid(s) to a determined protein or by proteolytic cleavage (Mann and Jensen, 2003).

Although the detection of PTM is important to understand the role of some proteins, only a few PTMs are known in the plant field (Chen and Harmon, 2006). They have been extensively studied in the plant model *Arabidopsis*, however, limited research has been reported with other plant species (Nakagami et al., 2010). Even though *Arabidopsis* is commonly used as a point of comparison to other plants, little is known if divergent species conserved residues follow the same modifications (Nakagami et al., 2010).

Phosphoproteomics studies have aided in the investigation of photosynthetic proteins, as phosphorylation is implicated in the photosynthetic apparatus assembly, which can occur due to damage by high light stress (Järvi et al., 2015, 2013). The PSII core proteins phosphorylation is probably related to grana lateral shrinkage and destacking and is linked to the changes of PSII location during light stress (Järvi et al., 2015).

A study by Zhang et al. (2015) of proteins and phosphoproteins from tomato flower pedicel abscission quantified 1,429 proteins, with 73 phosphoproteins exhibiting significant concentration change in response to ethylene. Isobaric tags were utilized to obtain relative and absolute quantification. Interestingly, the functional comparison amongst protein and phosphoproteins showed that the role of the protein is related to metabolic process and catalytic activity whereas the phosphoproteins have roles for signaling and transporting (Zhang et al., 2015). The phosphorylation sites found in this research can be useful as a database resource and as knowledge basis for future investigations.

2.4.2 Protein-protein interaction

Protein-protein interactions, or interactome, has led to the understanding of protein complexes and cellular protein functions through transient or stable interactions (Chen and Harmon, 2006; Park, 2004). Currently, immunoprecipitation and affinity purification combined with mass spectrometry (AP-MS) are the two most popular methodologies to study protein-protein interactions (Sanchez-Lucas et al., 2016). The interactome can be obtained by the *in vitro* analysis yeast two-hybrid (Y2H). The Y2H methodology, an experimental approach based on the transcriptional factor GAL4, results in a high false positive rate and has the limitations of the interaction of the Y3H system to the proteins in the nucleus and the difficulty in studying proteins that are toxic to yeast (Zhang et al., 2010). In AP-MS, an affinity tag is added to a bait protein, and the complex is isolated by affinity purification and analyzed by mass spectrometry. AP-MS is limited since it is dependent on the MS sensitivity and the number of proteins purified (Leene et al., 2008). The cross-linking technology, used to determine structural protein information, is also a tool to determine and guide molecular docking and modeling in protein-protein complexes (Chavez et al., 2016). Therefore, intramolecular cross-links can be used to determine the areas near an interaction and can identify their partners (Chavez et al., 2016).

Protein-protein interactions are particularly important in the context of elucidating the molecular processes of metabolic pathways and signal transduction at the cellular and systemic levels (Yue et al., 2016). The study of protein-protein interaction, along with a transcriptional regulatory network has shown a specific behavior of the expression profile perturbation in *Arabidopsis*. Where the profile was preferentially impacted by "hub" proteins (central, highly linked and module-organized), resulting in the main under/over-expressed proteins during plant defense response and after the viral infection (Rodrigo et al., 2012). A recent effort to further develop the protein-protein interactions of tomato plants resulted in the Predicted Tomato Interactome Resource (PTIR) initiative (http://bdg.hfut.edu.cn/ptir/index.html) (Yue et al., 2016). The PTIR covers 357.946 non-redundant PPIs containing 10,626 proteins, estimated to reach 30.6% of the tomato proteome, presenting a fair distribution (Yue et al., 2016).

Software and online tools have been developed to help in the visualization of these interactions. STRING (Szklarczyk et al., 2015) is a popular (free) database of protein-protein interactions and a tool to visualize protein-protein interaction networks; it maintains data from 2,031 organisms; offering, in total, 9.6 million proteins representing 184 million interactions. STRING data is generated by genomic context predictions, high-throughput lab experiments, (conserved) co-expression, automated textmining and previous knowledge in databases. Another popular tool is Cytoscape (Shannon et al., 2003), an open source software platform which not only allows visualization of molecular interactions but it provides annotations, gene expression profiles, and other enrichment sources. Cytoscape allows for the installation of plugins (apps) that enhance the analysis options.

2.5 Current challenges for tomato proteomics and conclusions

The new methodologies of proteomics have been slowly incorporated to crop proteomics. Although the speed of implementing new technologies in the plant world is not comparable to the one of human proteomics, recent publications have been applying faster mass spectrometers, phosphoproteomics studies and labeled methodologies (iTRAQ). Still, the two main challenges are sample preparation and data analysis.

Plant sample preparation is not yet standardized. Plant cells present a rigid cell wall composed of cellulose, large vacuoles containing secondary plant products (as phenolic and polyphenolic compounds), proteinases and organic acids (Laing and Christeller, 2004) making standardization difficult. Alvarez and Naldrett, (2016) have recently published a chapter extensively addressing the many issues of plant protein extraction protocols. For example, the methods utilized in different plant species (as *Arabidopsis*, maize, tobacco, rye, *Medicago sativa*) and from numerous sources (leaves, internodes, endosperm, hypocotyls, roots) were classified regarding the type of cell wall and its rigidness (CWP1-3) in relation to the salt solution used. The authors also discuss the different strategies of dealing with the high abundance of Rubisco, as Rubisco precipitation by the interaction with phytate or polyethylenimine and immunoaffinity removal; and the use of different extraction/purification methods as phenol and TCA/acetone.

Non-model plant proteomic data analysis is a challenge since there is a poor annotation of proteins, which results in many uncharacterized proteins or unmatched spectra, limiting the data interpretation. One way to overcome this issue has been the use of databases built from the iTAG database combined with an Expressed Sequence Tag (EST) list or Unigene, derived from the Harvard DFCI index (http://www.ncbi.nlm.nih.gov/pmc-/articles/PMC4205239) or the Institute for Genomic Research (http://www.tigr.org/tdb/-e2k1/plant.repeats/index.shtml) (Balmant et al., 2015; Casado-Vela et al., 2006; Catalá et al., 2011; Di Carli et al., 2010; Page et al., 2010; Rocco et al., 2006; Stulemeijer et al., 2009). ESTs can be sequenced multiple times, making their databases redundant, and the same gene sequence can come from various clones, containing (or not) an overlapping sequence which leads to increased analysis time and identification ambiguity (Champagne and Boutry, 2013). ESTs database matching relies highly on the quality and length: in short sequences protein, coverage gets compromised (Champagne and Boutry, 2013), and all these aspects put together can affect the analysis quality. Another strategy has been the search against the protein database of the whole Viridiplantae clade (green plants) (Muneer and Jeong, 2015; Rodríguez-Celma et al., 2010; Schilmiller et al., 2010; M. Suzuki et al., 2015), which leads to not only a long analysis but increases the redundancy issue. The choice of using a reliable, non-redundant protein database comes with a high price, Swiss-Prot is manually annotated, but contrary to the most popular choice – National Center for Biotechnology Information (NCBI), it contains a much lower number of protein sequences (Champagne and Boutry, 2013). The use of a database combining the specific species and a close evolutionary relative has shown to be dependent on the distance between the species, and a better-annotated database of a close relative is not always available, as in the case of tomato.

The challenges mentioned above should not discourage researchers to use proteomics for in-depth plant studies. The more protein functional annotation is obtained and is becoming available to the public, the closer we will get to being able to interpret proteomics data from non-model plants, especially crops. Sharing databases of protein identification are also highly encouraged. The information from these databases will, ultimately, result in the popularity of proteomics and the use of this powerful tool to develop tolerant crops or to enhance the synthesis of bioproducts, increasing yield and quality.

CHAPTER 3: Literature review – Part II

Connecting statement

A continuation of the literature review is presented in this chapter. The complex stress responses have their specificities, but also have signaling pathways that cross-talk (Chinnusamy et al., 2004), and they are essential to plant adaptation to extreme conditions. This second part of the literature review is focused on the key players of stress response and on details of plant response to light stress.

First, the key protein families linked to stress response are listed, and their role in the response mechanism is discussed by reviewing the literature. These protein families are part of i) the transduction process, ii) photosynthesis and metabolism, iii) oxidative stress and iv) other families of stress-responsive proteins. Later, specific aspects of high light response such as photodamage, photoinhibition, and non-photochemical quenching are described for a better understanding of the results interpretation reported in the next chapters.

3.1 Literature review

3.1.1 Key players in plant response to stress

Abiotic stress (mainly drought, salinity, and light) impacts plants development and productivity, causing high agricultural losses. It has been estimated that abiotic stresses are responsible for over 50% yield reduction in essential crops (Rodziewicz et al., 2014). The advantage of survival under abiotic stresses and maximizing the yield under unfavorable conditions is an important trait. The development of this trait in plants can aid in improving of food security. A few key metabolic pathways are involved in the abiotic stress response of plants: signal transduction, photosynthesis and metabolism, oxidative stress, and other stress-responsive proteins (Abreu et al., 2013; Shao et al., 2007).

Abiotic stresses are likely to share a common signaling transduction process (Figure 2) (Shao et al., 2007). The calcium-sensing protein family is formed by universal secondary messengers, their concentration fluctuation in the cytoplasm are identified by several Ca^{2+} sensors (Abreu et al., 2013). These sensors are typically Ca^{2+}- binding proteins that modify their conformation in the presence or absence of Ca^{2+}. Most common sensors are calmodulins, calmodulin-like proteins, and calmodulin-binding proteins. They are essential in high-temperature stress tolerance, regulating Ca^{2} influx across the membrane (Gao et al., 2012). CalM3 is involved in the activation of heat shock proteins (HSP) by specific transcription factors, and therefore, linked to temperature tolerance (Xuan et al., 2010). Overexpression of CaMPBs and CLMs are linked to salt, drought, cold and ABA sensitivity; and, the CaMBP receptor-like kinase (GsCBRLK) was found to enhance salt-tolerance in soybean (*Glycine max*) (Abreu et al., 2013).

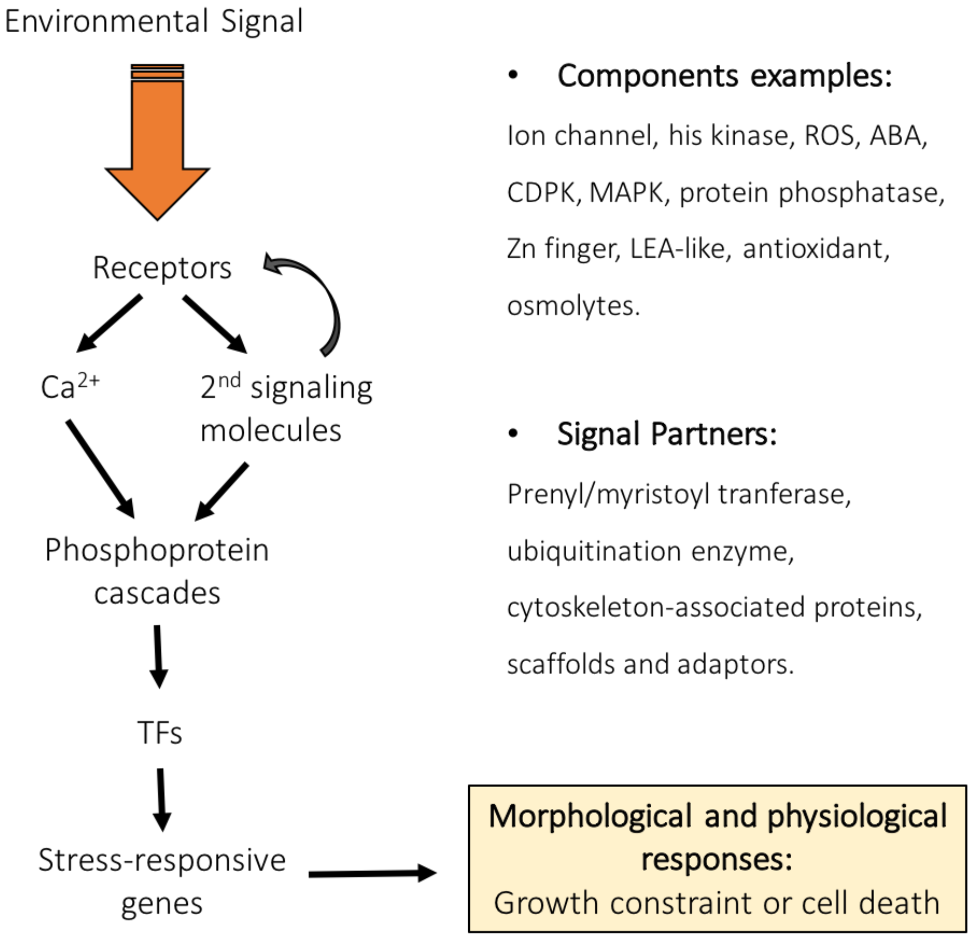

Figure 2. A general framework model for the signal transduction of abiotic stress in plants. An environmental signal is perceived by the receptors, which will enroll a cascade of signaling molecules. The process will activate transcription factors, resulting in the transcription and, later, the translation of these genes into stress-responsive proteins. Mechanisms such as photoinhibition and non-photochemical quenching will than take place, changing the plant physiology and morphology. Examples of the components of the signal transduction pathways are ion channel, kinases, ROS, hormones, as ABA, MAPK, Zinc finger, antioxidants, protein phosphatase. Signal partners may also be involved in the cascade, and some examples are ubiquitination enzyme, scaffolds, prenyl/myristoyl transferase, and cytoskeleton-associated proteins. Figure modified from Shao et al., 2007.

The 14-3-3 protein family is phosphoserine-binding proteins, modulators of many targets through protein interactions. They have been implicated in plant development, affecting central enzymes and ion channels interactions. In tomato and *Arabidopsis*, they were found to be related to nutrient deficiency reactions (Shin et al., 2011). Their differential accumulation in response to abiotic stresses as drought and salt where seen in wheat, maize, and rice. 14-3-3 proteins are involved in the abscisic acid (ABA) hormone pathway, involved in many developmental processes, including bud dormancy, they interact with regulators of ABA-responsive genes, AREB/ABF/ABI5-like transcription factors. One of the ABA-regulated responses is the stomatal closure in photorespiration water loss reduction that is indirectly related to a 14-3-3 interactor. In cotton mutants containing 14-3-3 proteins showed resistance to drought due to a higher photosynthetic efficiency caused by an increased stomatal aperture.

There is still little information about G-proteins and their relationship with abiotic stress. In rice, overexpression of Rab7B3 was salt and ABA-dependent (Pitakrattananukool et al., 2012). The kinase protein family is highly implicated in stress responses. Serine and threonine kinases, as well as mitogen-activated protein kinases (MAPKs), are implicated in a general stress signaling pathway. For example, AtMPK4 has been found in the salt-stress response and many other stress conditions (Pang et al., 2010). The receptor-like protein kinase (OsRMC) has been linked to improved salt stress tolerance in rice (*Oriza sativa*) plants (Zhang et al., 2008).

The central role of photosynthesis in plants, as the energy source pathway, is the metabolic process most affected by stress conditions as high salinity and drought, inducing stomatal closure and CO_2 slow rate assimilation. Abiotic stress conditions affect CO_2 diffusion, photosystem II efficiency, electron transport chain, ROS synthesis, RuBP content (dependent on ATP and NADPH offer), RUBISCO activity and photorespiration (Saibo et al., 2009). Light-harvesting chlorophyll a/b binding protein family (LHCB), when down-regulated, reduced responsiveness of stomatal movement caused by ABA, lowering *Arabidopsis* tolerance to drought (Xu et al., 2012). The authors showed that LHCB act in guard-cell signaling in response to ABA and may affect ABA signaling by modulating ROS homeostasis. Ferredoxin-NADP(H) reductase protein family, when overexpressed in tobacco (*Nicotiana rustica*), resulted in higher tolerance to oxidative stress, probably resulting in salt and drought tolerance (Rodriguez et al., 2006). RUBISCO activase proteins are majorly reduced under stress conditions, although some salt tolerant plants have accumulated RUBISCO as a result to high salt conditions (Pang et al., 2010). Therefore, a high concentration of this protein could be related to stress tolerance. *Arabidopsis* RCA1 granted moderate tolerance to heat stress (Kurek et al., 2007).

Carbonic anhydrase protein family has been implicated in the response of plants under drought and salt stresses (Pang et al., 2010) as they play a role in CO_2 exchange mainly in limiting conditions of CO_2, common in severe drought and high salinity. In lower carbonic anhydrase activity, plants are more susceptible to water stress, and overexpressing OsCA1 in *Arabidopsis* increased the salt tolerance at the seedling stage (Yu et al., 2007). Sedoheptulose-1,7-bisphosphatase (SBPase) are regulators of the Calvin-Benson cycle and are seen to be in lower concentrations in stress conditions (Feng et al., 2007). Transgenic rice accumulating these proteins presented higher tolerance to salt stress conditions at seedling stages, rice has also been reported as more tolerant to high temperature when presented high accumulation of SBPase (Feng et al., 2007).

For the proteins implicated in the carbohydrate metabolism, they have been found to be highly implicated in drought and salt responses. As they have not been well characterized, the information on their role in stress responses is still limited. Fructose 1,6-bisphosphate aldolase (FBA) low concentration was related to salt stress in most plants studied (Ndimba et al., 2005). FBA mutant plants of *Arabidopsis* were found to have salt and mannitol tolerance as well as an ABA sensibility at the germination stage (Lu et al., 2012). Cytosolic glyceraldehyde 3-

phosphate dehydrogenase (GAPDH), a protein involved in the glycolysis pathway was found to be accumulated under salt stresses in potato plants (Pang et al., 2010). Phosphoglycerate mutase has been highly accumulated in response to salt and drought stresses since they are critical for guard-cell function in *Arabidopsis* (Zhao and Assmann, 2011). Protein members of the tricarboxylic acid cycle are also differentially accumulated by abiotic stresses (Vanhove, 2012). NADP-dependent isocitrate dehydrogenase concentration is impacted by the response to drought or salt stress since ICDH catalyzes the reversible reaction of isocitrate to 2-oxoglutarate (2-OG) (Gallardo et al., 1995). The accumulation of NADP-dependent isocitrate has been shown to enhance salt stress in *Arabidopsis* (Liu et al., 2010).

The oxidative stress first reaction is the formation of superoxides (O_2^-) by the one-electron reduction of O_2. In plants, it occurs predominantly in the chloroplasts, and less in peroxisomes (Dietz, 2015). Mn-containing superoxide dismutases (SOD) overexpression has shown a higher survival of transgenic plants in field experiments, during winter and water-deficit (McKersie et al., 1999). Tobacco plants overexpressing a chloroplast-localized Cu, Zn-SOD showed enhanced tolerance to the high-light intensity and low-temperature conditions (Gupta et al., 1993). Cu, Zn-SOD in crops showed increases in response to drought and salinity, and low concentrations in response to high-temperature conditions (Abreu et al., 2013). Fe-SOD was increased in citrus in response to salinity. Also, barley under salt stress presented high protein accumulation in salt stress (Tanou et al., 2009).

Ascorbate peroxidase (APX) proteins are essential in the reduction of H_2O_2 to water, but its influence on the stress response of crops is tightly correlated to the pool of available glutathione S-transferase proteins (GST). A transgenic cool-season grass containing Cu, Zn-SOD, and APX genes, when tested with viologen, H_2O_2, and heavy metal exposures, presented lower H_2O_2 accumulation, lower lipid peroxidation, and higher chlorophyll content (Lee et al., 2007). Drought and heat stresses have induced APX1 expression and accumulation in *Arabidopsis*

(Koussevitzky et al., 2008). In abiotic stress responses, studies in crops have shown lower or higher accumulation of APX depending on the present protein isoform or conditions, the myriad roles of ascorbate peroxidase have been the focus of a recent publication by Pandey et al., 2017.

Catalases eliminates the H_2O_2 by producing O_2 and water. They have been shown to accumulate in wheat (*Triticum aestivum*) under drought condition (Ge et al., 2012), and in rice under salt stress (Kim et al., 2005). In wheat, a higher concentration of catalase was found in conditions of salt stress in a tolerant genotype, and lower concentration in the sensitive genotype. However, in cucumber, barley, and citrus, their concentration has shown to be lower under salt stress (Peng et al., 2009).

Glutathione-ascorbate cycle-enzymes monodehydroascorbate reductase (MDHAR), dehydroascorbate reductase (DHAR), and glutathione reductase (GR) are implicated in the maintenance of available reduced ascorbate and glutathione in cells, during the glutathione-ascorbate cycle (Abreu et al., 2013). DHAR has seen to be increased in many crops in response to abiotic stress. during, for example, dehydration followed by rehydration in drought-resistant moss and water stress of a drought tolerant tall wheatgrass (Cui et al., 2012; Gazanchian et al., 2007). Transgenic tobacco plants expressing a human DHAR in chloroplasts are more resistant to oxidative stress caused by methyl viologen of H_2O_2 treatments. Its seedlings presented better cold and salt stress, as well as high levels of glutathione reductase (Kwon et al., 2003). In wheat, GST was increased 2-fold in drought response in a genotype (Khazar-1); however, it decreased in the genotype "Arvand" and “Afghani,” demonstrating that the regulation of GST might be genotype-dependent (Hajheidari et al., 2007).

Some of the most common stress-responsive proteins are chaperones, late embryogenesis abundant proteins, and pathogenesis-related proteins (Kosová et al., 2011). Heat shock protein family are molecular chaperones, involved not only in high-temperature stress as their name suggests but also in all types of abiotic stress. HSP level oscillations in crops have been related to many abiotic stresses; they are potential targets for crop improvement since the stress conditions typically increase their expression (Jacob et al., 2017). HSP70 is the most commonly found HSP, and it was found to aid in the prevention of DNA fragmentation/degradation, as well as chlorophyll damage during heat stress conditions (Cho and Choi, 2009). A successful strategy was achieved when the ectopic expression of OsHsfA2e in *Arabidopsis* resulted in an increase of abiotic stress tolerance (Yokotani et al., 2008).

Late embryogenesis abundant proteins (LEA) accumulate in the later stages of seed maturation during the desiccation process, being responsible for the formation of bioglass, a membrane protection strategy from seeds (Banerjee and Roychoudhury, 2016). LEAs contain several families, as group 2 LEAs (dehydrins) which includes cold-regulated proteins, and Rab21, proteins induced by the ABA hormone and mechanical stress (Candat et al., 2014; Lim et al., 2015). LEAs sequestrate ions, ROS, and maintain minimum cellular-water requirements, reducing the impact of drought stress (Wang et al., 2017). Expression of Rab16A in tobacco resulted in increased salt tolerance (RoyChoudhury et al., 2007). Accumulation of ME-LeaN4 in lettuce (*Lactuca sativa*) resulted in higher growth ability under salt and drought stress conditions (Park et al., 2005). Overexpression of OsLEA3 in rice, induced by drought and salt stress, resulted in increased tolerance (Duan and Cai, 2012). Soybean hypocotyls and wheat leaves have been reported to accumulate LEAs under salt stresses. In total, 11 LEA gene products were identified in stress responses, 9 from group 3 LEAs and 2 from dehydrins (Aghaei et al., 2009; Brini et al., 2007).

Pathogenesis-related proteins (PR) are induced under pathogen infection, and its overexpression has shown to be a promising improvement to abiotic stress tolerance (Sels et al., 2008). PR-10 is involved not only in biotic stress responses but also in abiotic, such as drought, salt, low-temperature, oxidative stresses, and UV-radiation. RSOsPR10 and Osdrr genes were upregulated in rice roots under drought and salt stress conditions. PR-10 proteins were found to be highly expressed in rice seedlings and leaves under UV and high ozone stresses (Liu and Ekramoddoullah, 2006). PR proteins were found to be accumulated in response to salt-stress in various plants as grass pea (*Lathyrus sativus*), salt-tolerant barley (*Hordeum vulgare*), and wine grape (*Vitis vinifera*) variety Cabernet Sauvignon (Chattopadhyay et al., 2011; Sugimoto and Takeda, 2009; Vincent et al., 2007). The constitutive expression of PR-10 in rapeseed (*Brassica napus*) improved germination and growth rates under saline conditions (Srivastava et al., 2004). A drawback is that this group contains the known allergens *Ara h 8* and *Bet v 1* proteins, making challenging the overexpression of PR proteins (Srivastava et al., 2004).

In conclusion, the abundance of available information exploring the role of these protein families in abiotic stress responses is clear; however, most studies seem to be limited to drought, salt, and temperature stress responses (Figure 3). Little is known about their expression impact during high-light or UV-mediated stress conditions. The determination of the expression patterns of these proteins in light stress conditions is important due to the influence of photosynthesis yield to the growth and development of all plants.

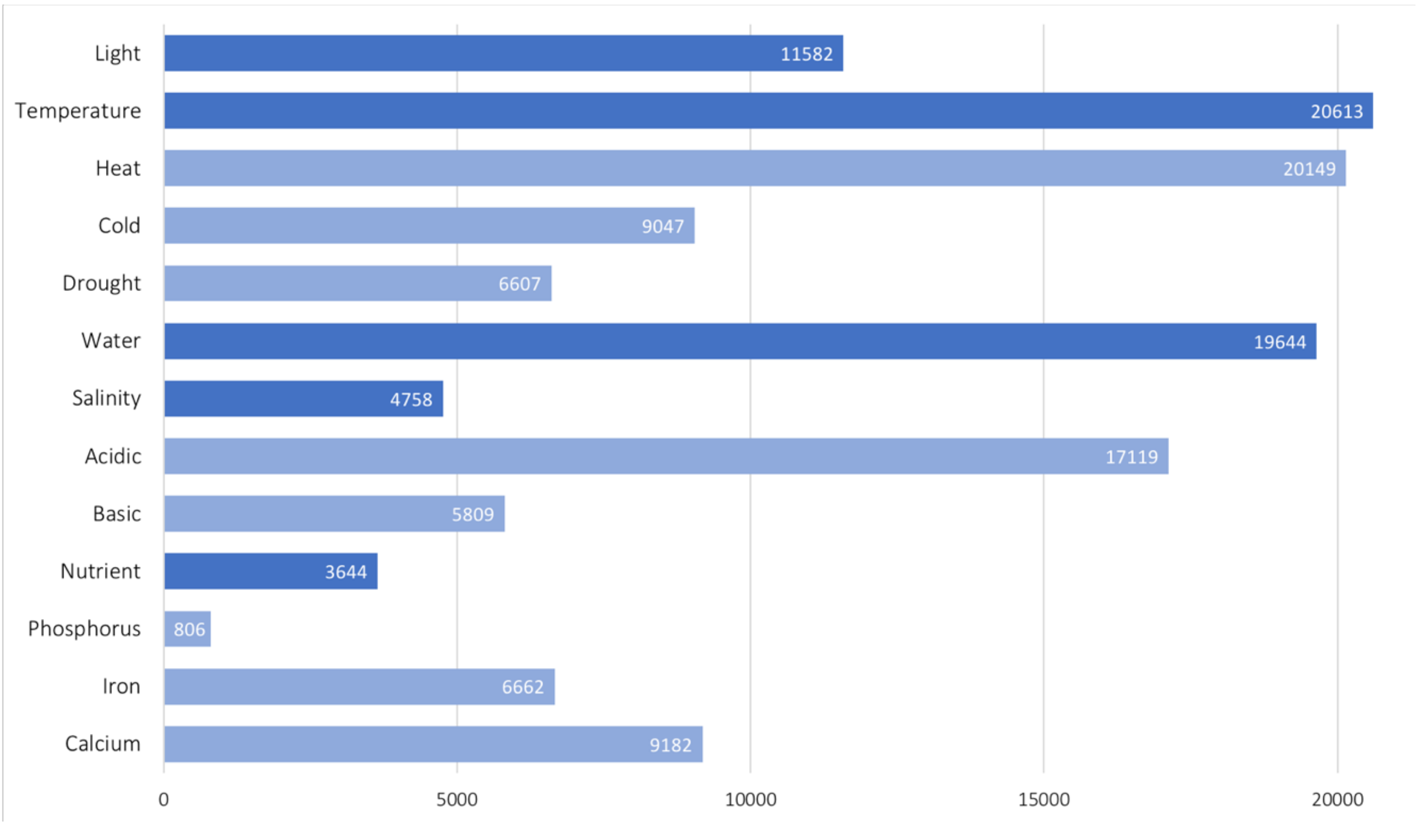

Figure 3. Number of published studies on different types of abiotic stress. Search performed on 12/10/2018. The search was performed by including the keywords “abiotic stress”, in the corresponding types, except for biotic stress, where the search was “abiotic stress”. Basic was searched as “abiotic stress basic pH”.

3.1.2 Specificities of high-light stress response

Plants respond to light changes in a multi-level dynamics that depends on the quality and intensity of the light, resulting in short or long-term responses. Short-term responses are activated in a matter of hours after the stress condition, whereas long-term responses, after days or weeks of the initial exposure, result in acclimation. Acclimation and short-term response are two distinct strategies used by the plant to deal with alterations of light and involve different cellular mechanisms (Szymańska et al., 2017). The focus of this project is set in characterizing the late response of plants to a short-term stress condition. A brief review of general light stress is reported in Chapter 2, Section 2.3.1.2, the specific effects of the high-light stress response, as photoinhibition, non-photochemical quenching, and the synthesis of antioxidants are explored.

3.1.3 Photoinhibition

An optimal light condition is needed for plants to undergo efficient photosynthesis. However, in the environment, light availability is continuously changing. Under high light conditions, plants must deal with the energy excess and its harmful consequences. One of the first consequences of high-light stress is photoinhibition (PI), which leads to damage of PSI and II. The damage causes the reduction of photosynthetic quantum yield (Nama et al., 2015), making photosynthesis less efficient. Under energy excess, singlet oxygen radicals are generated in proximity to PSII and permanently damage the D1 protein. Currently, there are a few hypotheses on how PI works. The acceptor-side PI hypothesis is based on the damage of the D1 protein, caused by its absorption of high amounts of energy from high-irradiance. The damage on PSII triggers a recycling and *de novo* synthesis of PSII complex members, as the D1 protein, which needs to be resynthesized at a high energy cost (Järvi et al., 2015). The donor-side hypothesis suggests that UV and wavelengths next to it (blue) initiates photodamage in PSII as a light-mediated release of manganese ions, resulting from the light absorption (Hakala et al., 2005; Tyystjärvi, 2008). This hypothesis, known as the donor-side PI hypothesis, agrees with the previous report that the quantum yield of PI is not dependent on light intensity, concluding that PI is carried out by an intensity-independent central mechanism (Tyystjärvi and Aro, 1996). In the next sub-sections, a detailed description of these two theories is described. The current model of the PSII protein structure (Van Eerden et al., 2017) is presented in Figure 4.

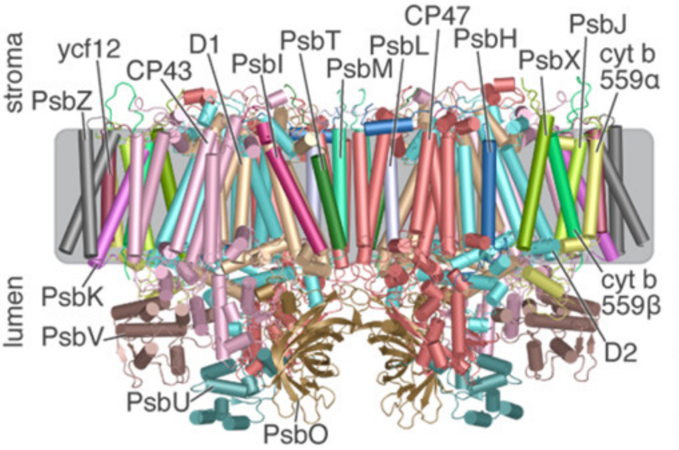

Figure 4. Model of the position of PSII subunits and cofactors. PSII dimer containing the label of 19 subunits. The thylakoid membrane is represented by a gray box, where the top is the stromal, and the bottom is the lumenal side. Figure reprinted with permission from Van Eerden, F.J., Van Den Berg, T., Frederix, P.W.J.M., De Jong, D.H., Periole, X., Marrink, S.J., 2017. Molecular dynamics of photosystem II embedded in the thylakoid membrane. Copyright (2016) Americal Chemical Society (Appendix B, section 9.2.2.1).

3.1.3.1 Donor-side photoinhibition

During PI, OEC is one of the first complexes to be inhibited, releasing one ion of Mn of the OEC per PSII complex to the lumen (Hakala et al., 2005). After the electron transfer inhibition occurs the degradation of the D1 and the simultaneous release of OEC extrinsic proteins to the lumen (Henmi et al., 2004). Although NPQ and PQ have almost no effect on photoinhibition rate, which leads to the conclusion that a significant part of PI is not generated by PSII electron transfer chain. The singlet oxygen could have originated from the light-harvesting complex II, which may have lost the link to the RC when PSII was being repaired (Rinalducci et al., 2004).

Over-saturating light causes the reorganization of the photosynthetic apparatus, due to the differential degradation of light harvesting complex I proteins (Nama et al., 2015). Two separate events take place at the beginning of PI, also known as donor-side photoinhibition: damage to the OEC, with the release of Mn ions, and P^{+}_{680} oxidizing damages to the RC. In the intense visible light, the electron transfer from P_{680} to quinone A (Q_A) is partially saturated. However, the OEC Mn-specific inactivation is not saturated. The P^{+}_{680} and $TryZ^{+}$ cationic radicals are formed when there is the impairment on the donor side (Nama et al., 2015). The interruption of the electron transfer between Q_A^- and Q_B reduces the damage generated by the remaining P^{+}_{680} since Q_A^- would recombine with free harmful P^{+}_{680} generating $P_{680}Q_A$ (Tyystjärvi, 2008). OEC33 is a metal ion-binding protein that probably retains the Mn(II) released to the lumen, acting as temporary storage of Mn(II) and a Fenton reaction mediator (Henmi et al., 2004). The action spectrum for PSII inhibition is not the same as the PSII absorption spectra, suggesting that the PSII antenna is not the main photoreceptor of photoinhibition (Santabarbara et al., 2001).

3.1.3.2 Acceptor-side photoinhibition

In the acceptor-side PI theory, PSII and LHCII are typically coupled under normal light conditions. However, under high-light conditions, they become disassociated to avoid energy transfer from LHII and PSII core. Modifications to PSII are well characterized; first, there is the inactivation of PSII activity, followed by monomerization of PSII dimer, the degradation and replacement of D1, and reassembly of PSII holocomplexes. Under typical high-light conditions, the damaged D1 proteins are dealt by proteases, and new copies are inserted in PSII by *de novo* synthesis. The vulnerability of the PSII complex has been shown to be an adaptation to avoid the damage of PSI. The PSI complex is irreparable; therefore, all the proteins must be resynthesized and re-assembled, along with the Fe-clusters, which consumes time and energy

(Järvi et al., 2015). Partial inhibition of PSII complexes seems to be a strategy for plants to avoid damage on PSI.

The FtsH and Deg proteases degrade the damaged D1, and the SecY translocon inserts the new copy of D1 in the PSII re-assembled complex, other auxiliary proteins aid in the new assembly of PSII, as Psb27, Lpa1, Cyp38/Tlp40, LQY1, and Tlp18.3 (Järvi et al., 2015). These auxiliary proteins are enriched in the thylakoid membrane non-appressed domains, where the damaged PSII will migrate to be re-assembled (Yamamoto et al., 1981). During PI, typically, only D1 is replaced, but D2, CP43, and PsbH may also be *de novo* synthesized instead of repaired (Aro et al., 1993).

The following are details on the functioning of the PSII repair cycle. In the grana, the PSII repair cycle first step is the monomerization of the PSII complex dimeric form that has been previously phosphorylated, and the dephosphorylation of D1, D2, and CP43, occurring during the migration of PSII to non-appressed stroma thylakoids, from the grana. Then, D1 protein is degraded, and the assembly of D2 takes place, forming a complex composed of Cyt b_{559}, D2, and PsbI. D1 is *de novo* synthesized by the translation of *psbA* mRNA, and the ribosome translation and insertion of D1 into the complex is enabled by the cpSecY translocation channel (Zhang et al., 2001). Cofactors bind to D1, and its interaction with D2 is established. In the next steps, a part of the low molecular mass proteins is assembled: PsbM, PsbL, PsbH, $PsbT_c$, PsbJ, and PsbR, the remaining part of these protein are linked to PSII. Last, proteins CP43, PsbK, PsbO, PsbW, and PsbZ are assembled, and PSII dimerization occurs, along with the formation of PSII-LHCII supercomplexes, which are vital for assisting electron excitation balance. The PSII repair cycle is regulated by reversible phosphorylation of its core proteins that increases membrane fluidity, allowing for PSII migration (Herbstova et al., 2012). The N-terminus threonine residues of D1, D2, CP43, and PsbH are reversibly phosphorylated, fulfilling its goal to facilitate the damaged PSII migration to stroma extrinsic membrane (Järvi et al., 2015).

The D1 protein turnover rate is known to be proportional to light intensity (Baroli and Melis, 1996), however, when light intensity is extreme, aggregation of D1 becomes permanent, signaling the suppression of D1 synthesis. Proteases cannot degrade with the accumulation of the aggregated products in PSII, and the PI becomes irreversible. The aggregated LHCII is involved in the activation of the xanthophyll cycle by a mechanism coined as energy-dependent quenching (qE) (Havaux and Niyogi, 1999).

One of the signals for the xanthophyll cycle (XC) activation is the accumulation of LHCII that is carried out by the sensing of the PsbS protein of the change in the luminal pH. PsbS is overexpressed in high-light conditions, it has a role in remodeling the energy balance control of supercomplexes PSII-LHCII, and in assuring the alignment between dissipation and excitation energy (Nama et al., 2015). In this process, the de-epoxidation of violaxanthin to zeaxanthin is catalyzed by the violaxanthin-de-epoxidase. Because violaxanthin needs to move through the thylakoid to be de-epoxidated, membrane fluidity is vital for efficient activation of XC. In extreme high-light conditions, the irreversible aggregation and crosslinking of D1, D2, CP43, alpha-subunit of b_{559}, and neighboring proteins decreases the membrane fluidity, making difficult the movement of proteins and lipids (Yamamoto, 2016). Irreversible photoinhibition can lead to permanent chloroplast damage and cell death.

Besides the energy dissipation mechanisms by NPQ and XC, quenching through state transitions is necessary to balance the energy between PSI and II. This is achieved through dissociation of the PSII surrounding antenna proteins and their binding to PSI, controlling the linear and cyclic electron flow in the chloroplast, and can take hours to days (Nama et al., 2015).

3.1.4 MS-associated methods applied in this project

For deep-characterization of a proteome, to this date, methods of MS are coupled with HPLC to allow for the identification of a higher number of peptides. HPLC can increase the identification power of MS due to its high capacity for peptide separation. Methods of HPLC include online and offline separation, according to its interface with the mass spectrometer. Offline methodologies are the most common since its set-up is less complex and virtually any HPLC equipment could be used. 2-D gels can be used for offline separation. They are a popular choice for non-complex samples than whole proteomes, due to its separation limitations. The online methods require that the HPLC separation be directly connected to columns that inject the sample into the mass spectrometer, which requires a more robust set-up. They allow for better recovery of the peptides, increasing the number of peptide identification, being a good approach for the analysis of plant proteome (Whitelegge, 2002).

MS methods are chosen accordingly to sample specificity and project objective. In this project, two different approaches were used, label-free, and labeled (iTRAQ). In the label-free approach, a MudPIT separation was applied to account for the limitation of the mass spectrometer (LTQ XL, Thermo Fischer, CA, USA) equipment limitations (MS available in our laboratory). Where in the labeled methodology, this approach was unnecessary, since a state-of-the-art mass spectrometer was utilized (Orbitrap Fusion Lumos, Thermo Fischer, CA, USA, from Dr. Darryl Pappin's laboratory at the CSHL, USA). A brief description of the MS and HPLC techniques utilized in this project are presented in this section, more details on the sample preparation, MS and HPLC parameters are presented in Appendix A.

3.1.5 Tandem mass spectrometry (MS/MS)

The identification of complex mixtures of proteins requires the digestion of proteins by proteases. This bottom-up approach is analyzed by tandem mass spectrometry (MS^2, or MS/MS), allowing for peptide sequence identification. In an MS/MS experiment, protein mixtures are digested by proteolytic enzymes, for example, trypsin. In the next step, one or two levels of peptides fragmentation are performed to allow a higher identification power. The first dimension (MS, or MS^1) is where the precursors' m/z values are generated from the ionized peptides. In the second dimension (MS/MS, or MS^2), the precursors are fragmented in the collision cell, and the MS/MS spectra are acquired. The thousands of spectra are searched against a theoretical database of peptide sequences, leading to protein identification. In any MS/MS experiment, one protein will contain thousands of MS and MS/MS spectra corresponding to the fragmented peptides (Nesvizhskii and Aebersold, 2004) (Figure 5).

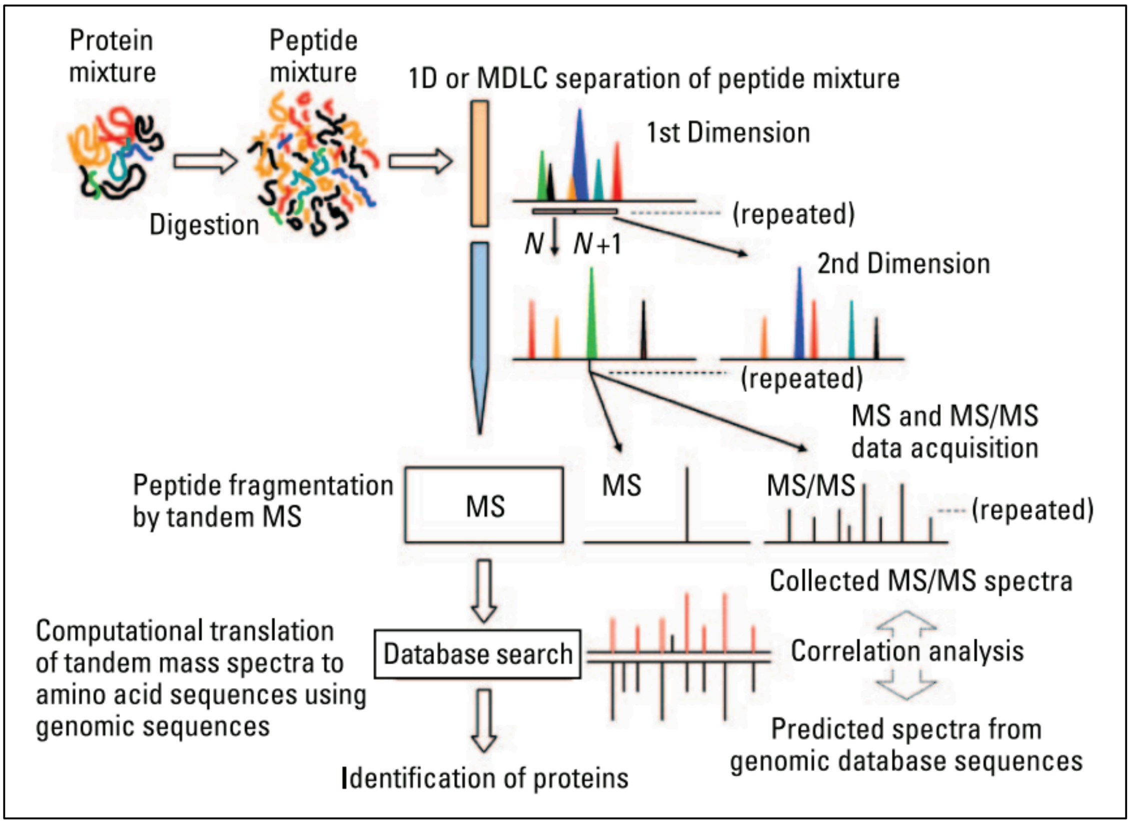

Figure 5. The workflow of a tandem mass spectrometry analysis (MS/MS). Protein mixtures are digested by proteolytic enzymes, as trypsin. In the next step, 1-dimensional or 2-dimensional isolations of peptides are performed (N represents the fraction of the sample). The first dimension (MS, or MS^1) is where the precursors' peaks are generated. In the second dimension (MS/MS, or MS^2), the precursors were further fragmented, and the MS/MS spectra are acquired. The thousands of spectra are searched against a theoretical database of peptide sequences, leading to protein identification. Reprinted with permission from Motoyama, A., Yates, J.R., 2008. Multidimensional LC separations in shotgun proteomics. Anal Chem 80, 7187–7193. doi:10.1021/ac8013669. Copyright (2008) American Chemical Society (Appendix B, section 9.2.2.2).

3.1.6 Multidimensional Protein Identification Technology (MudPIT)

In this project, shotgun proteomics applied with mass spectrometry (MS) and high efficient liquid chromatography (LC), was used through the set-up of a multidimensional protein identification technology (MudPIT) (Kislinger et al., 2005).

Shotgun proteomics is a methodology used to identify complex mixtures of proteins utilizing a theoretical fragmentation peptide sequence database. This method can identify proteins without the need of using gels or isolating the proteins. MudPIT is a protein separation methodology developed by Washburn and colleagues (2001), with the ability to identify a large number of proteins (Abraham et al., 2013; Kislinger et al., 2005). After the multidimensional separation, peptides pass through the first of a two-step isolation technique, requiring a first step of selecting an ion which will pass through a collision cell filled with gas molecules (such as helium). The ionization of the peptides is then performed by the electrospray ionization (ESI) technique, obtained by a high voltage applied to a capillary spray oriented to enter the mass spectrometer, which results in an ion beam. The ions are submitted to the second fragmentation step and sent to the mass analyzer, and the result is a pool of multiple charged ions to be identified by their different m/z ratio (Yates III, 2011).

3.1.7 isobaric Tags for Relative and Absolute Quantitation (iTRAQ)

Labeled proteomics emerged from the necessity of lowering the variance of protein quantification between samples, due to sample preparation. The first reagents to be developed used mass differences to the only label up to 2 samples for simultaneous analysis (Ross et al., 2004). Besides the low number of multiplexing possibilities, the mass difference increases the complexity of the spectra matching database. Isobaric tags were developed to account for the necessity of multiplexing samples in more complex experimental designs, and for incorporating PTM-containing peptides to the database search (Ross et al., 2004). iTRAQ is based on adding chemical labels (tags) to the peptides N-terminus and side chains of Lys that later are detected in the MS spectra. The tags are composed of a balance group, an amine peptide reactive group, and a charged reporter group (Tenga, Milagros and Lazar, 2011). There are up to eight different reporters (113, 114, 115 and 116 m/z) that can be used to analyze eight samples simultaneously. The intensity of the reporters is used to generate a relative quantitation of the peptides, allowing for an accurate comparison of protein abundance. A comparison of a label-free and an iTRAQ labeled proteomics workflow is shown in Figure 6.

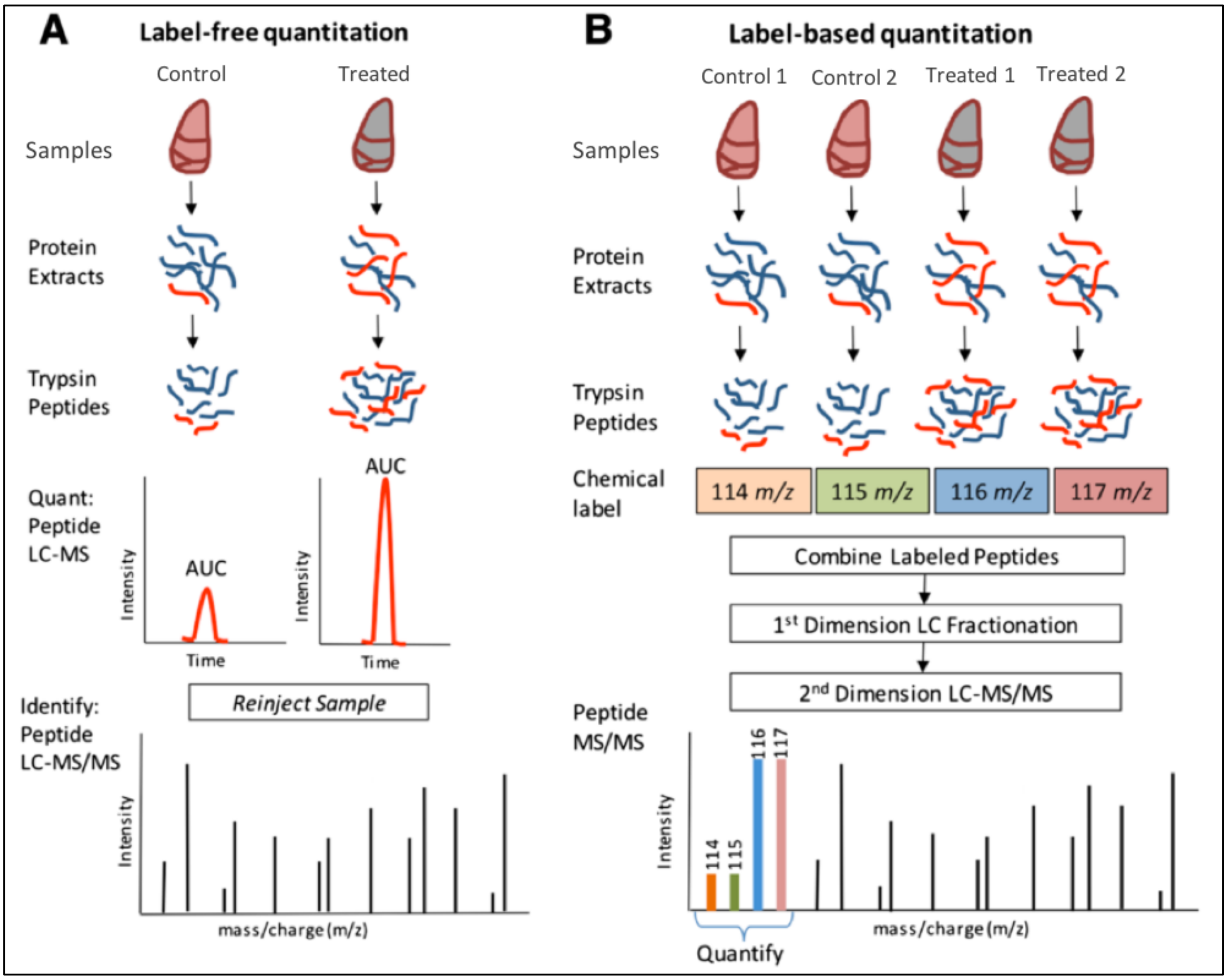

Figure 6. The workflow comparison for labeled and label-free proteomics experiments. (A) In a label-free workflow, proteins are extracted and digested with trypsin. The next step is the separation of the peptides by LC and the injection of the different conditions separately. Quantitation of the peptide (AUC) is obtained by comparing the peak area of intensity versus retention time or summed intensities. An MS/MS analysis is performed by fragmentation of the precursors and can detect target peptides. (B) In a labeled experiment (iTRAQ), after the protein digestion, peptides are labeled, in this case, a 4-plex, four labels are used (114, 115, 116, 117 m/z). The samples are combined, followed by an LC separation of the peptides, and a 1-dimension MS. Precursor ions are fragmented (MS/MS) and the reporter ions are detected. The intensity of the reporters is used to obtain relative quantitation of the peptides, while the peptide peaks are assigned to theoretical peptides by a theoretical library search. Figure

modified and reprinted (adapted) with permission from Bhargava, M., Higgins, L., Wendt, C.H., Ingbar, D.H., 2014. Application of clinical proteomics in acute respiratory distress syndrome. Clin Transl Med 3, 34. doi:10.1186/s40169-014-0034-1 . Copyright (2014) Springer (Appendix B, section 9.2.2.3).

A general workflow of an iTRAQ based experiment is detailed in Figure 6. In the project presented in this thesis, an iTRAQ strategy was applied to provide a relative quantitative analysis of the different light-induced stress areas of the tomato leaf. The proteins of the different leaf areas, generated by a LED treatment, were extracted and digested. The resulting peptide pool of each sample was labeled with a different tag (114, 115, 116 and 117 m/z) and pooled together for analysis (Figure 6). After the two-dimensional peptide separation, the results were analyzed by considering the intensity signal of the tags of each identified peptide. The comparison of the tag intensity allows for quantitative measurement of the peptide abundance. The use of iTRAQ in this project enabled the reduction of the number of injections and, more importantly, an accurate comparison of the protein abundance between samples.

3.1.8 Data analysis considerations

The two datasets (blue and red) were results of a wide-proteome search, with unlabeled peptides (blue dataset) and labeled peptides (red dataset). The data analysis workflow utilized in the analysis were similar in both datasets and used a commercial software (Proteome Discoverer, Thermo Scientific, MA, USA). Briefly, a variety of search parameters were included to reduce time and avoid false-positives, for example, the peptide's variable and fixed modifications, enzyme utilized for protein digestion, and precursor and ion mass tolerance.

These parameters were chosen after a consideration of the protein extraction and digestion methodology, the sample origin (plant), and the type of mass spectrometer utilized.

The second stage of the data analysis consisted of the statistical analysis through the use of the software Perseus (Tyanova et al., 2016). In this software, the normalized protein abundance values, NSAF (Zybailov et al., 2006) or peak intensity, were used as the input for the statistical analysis. Other filters were applied at this stage of the analysis, including filters for a minimum of 2 unique peptides, or imputation of values on missing values. The functions of hierarchical clustering, and venn diagrams, were applied to the analysis. The hierarchical clustering analysis generates protein cluster of similar expression patterns and allows for better visualization of the different patterns. Lastly, the function of GO terms enrichment was utilized to enable the identification of the function of the several proteins identified. The quality of the results was accessed by determining the Pearson correlation between the biological replicates and determining the variation between the protein abundance values in specific cases (coefficient of variation).

The tomato proteome is not fully annotated, therefore, several matches of the algorithm search (first stage analysis) are identified as uncharacterized proteins. There are other databases that contains functions of proteins that are not directly linked to the databases containing their identifications. Because of this issue, the next step is important, and it consists of searching other databases for protein functions. Protein function was estimated using a protein interaction network tools, STRING (Szklarczyk et al., 2015), or Cytoscape (Shannon et al., 2003). The proteins of each cluster present related functions that are in the input data. If the input data consisted of a list of abundant proteins, then the result will be the active functions in the cell.

The proteins must be verified to allow for confirmation of uncharacterized proteins, when the function cannot be found by the methods mentioned earlier. The amino acid sequence can be used to compare against other amino acid sequences from a database using a tool such as

BLAST (Altschul et al., 1990), from NCBI (https://blast.ncbi.nlm.nih.gov/-Blast.cgi?PROGRAM=blastp&PA-GE_TYPE=BlastSearch&LINK_LOC=blasthome). A score is provided, based on the similarity of the sequence of interest and the sequences from the database. The result is a list of characterized proteins with a similar score to the uncharacterized sequence, providing a level of certainty to the identification of the unknown function.

Together, the methodologies and the multi-level data analysis provide a robust workflow to identify and finding the function description of complex protein datasets containing thousands of proteins. The proteome quantitative analysis results in the detection of protein abundance patterns. The comparison between the abundance values of the stressed conditions and the control gives important insight into the upregulated and downregulated functions in the plant cell. For this reason, comparative proteomics is a valuable tool for observing the changes in the plant development, identifying gene function and determining the physiological responses (Voelckel et al., 2017).

CHAPTER 4: Manuscript II

Connecting statement

A study of the impact of high-intensity red lights on tomato plants is described in this chapter. An analysis at the protein level was performed aiming to understand the changes in plant survival from high-light stress. By utilizing the isobaric tags for relative and absolute quantification (iTRAQ) methodology, the proteomics study provided not only the identification of the proteins but also a semi-quantitative analysis of the protein abundance.

To reach this goal, an experiment utilizing an approach to reach high levels of light intensity was designed and performed in the leaves of tomato plants. The use of a specific LED set-up was crucial, since applying a high-intensity light on a whole plant would probably cause its death, whereas using a focused light on its leaf allowed the plant to activate the stimuli response and recovery.

In this chapter, the results of the first experiment applying extremely intense LED lights to tomato plants is reported. The goal of this study was to first define the plant response to a high level of light stress under red LEDs. The results presented here were used as a base for a comparison of the data obtained using a blue LED, presented in Chapter 5.

Manuscript II: Quantitative proteomics analysis of light-induced stress in plants.

Abstract

Light stress reduces photosynthetic yield and plant growth, negatively impacting global crop production and is a major constraint faced by agriculture. We report the main protein expression changes in a leaf tissue recovering from different levels of light stress. We introduce an in-depth analysis of plants submitted to a light treatment method developed by our research group using extremely intense light. Plant leaves were treated using light emitting diodes (LED) to create a single spot at 5,000 W m^{-2} irradiance, generating three light stress levels: Burned (area under the spotted light), Limit (edge around the burned area), and Regular (area >1 cm from the burned section). The proteins expressed in the treated tomato (*Solanum lycopersicum*, Heinz H1706) leaves were harvested 10 days after the treatment. A multiplex labeled proteomics method (iTRAQ) was analyzed by LC-MS/MS. A total of 3,994 proteins were identified at 1% false discovery rate and matched additional quality filters. Hierarchical clustering analysis resulted in four types of patterns related to the protein expression, with one being directly linked to the increased LED irradiation. A total of 37 proteins were found unique to the Regular, while the Limit had 372 proteins, and 1,003 proteins in the Burned sample. The proteome of the tissue undergoing de-etiolation resulted in the participation of salicylic acid response proteins in the recovery of this highly photodamaged tissue. The plant proteome resulted in a differential pattern of protein expression from the photosystem apparatus from which we propose the involvement of PSII 10 and 22 kDa polypeptides, and reaction centers H and Psb28 in the recovery of photosystem II in highly light-damaged leaf tissues.

4.1 Introduction

Plants cope with abiotic stress by either avoiding it or acclimating to it. Avoidance is the survival of the plant during unfavorable conditions as mature seeds, while acclimation to stress results in the modification of plant metabolism, which causes significant changes at the protein and gene-expression level (Iwai et al., 2013; Kosová et al., 2011). Both mechanisms reduce plant growth and yield, causing a major constraint to agriculture by negatively impacting global crop production (Hossain et al., 2012; Rockström and Falkenmark, 2000). Although functional photosynthetic systems are required for plant survival, most species, when exposed to full sunlight, utilize as little as 10% of the absorbed light in the photosynthetic electron transport (Demmig-Adams and Adams, 1996).

Plants use different strategies of photoprotection of the photosynthetic apparatus to control the excess exciting energy which can result in changes of the structure of the light-harvesting proteins and control the energy transference to quenching species, such as the carotenoids (Horton and Ruban, 2005). When excess energy cannot be dealt with, conditions of high light stress may cause irreversible photosystem damage (Aro et al., 2005). Photodamage is caused by the excess energy that cannot be utilized for carbon fixation and oxygen generation, resulting in photoinhibition and a decrease of photosynthetic quantum yield (Nama et al., 2015). The singlet oxygen radicals near PSII can cause permanent damage to the D1 protein, which is proportional to light intensity, while the production of superoxide and hydroxyl radicals near the acceptor side of PSI causes oxidative harm to chloroplast lipids and proteins (Nama et al., 2015). While the consequences of photodamage are clear, the signaling pathways and proteome responses that protect plants from this type of irreversible damage are less characterized.

The understanding of plants defense to abiotic stresses is essential for engineering tolerant plants, and research efforts have been placed in drought, temperature and salinity stresses (Manaa et al., 2013; Muneer and Jeong, 2015; Rizhsky et al., 2002; Zandalinas et al., 2018). Four metabolic pathways are known to act in abiotic stress response in plants: signal transduction, metabolism (especially photosynthesis), oxidative stress and stress-responsive proteins (Abreu et al., 2013; Qureshi et al., 2007; Shao et al., 2007). These pathways are found to be impacted by light stress. However, the various intrinsic pathways related to light stress requires further investigation, such as salicylic acid.

Tomatoes are part of the world's most important horticultural plants (Deram et al., 2014). They are the most intensively studied member of the Solanaceae family (Barone et al., 2008), mainly due to its short generation time, elementary diploid genetics, a well-known genetic transformation methodology, inbreeding tolerance, and a vast well-characterized genetic resource (Barone et al., 2008; Van der Hoeven et al., 2002). Few studies have been performed with tomato plants focusing on the plant response to different light offerings (A et al., 2010; Demers and Gosselin, 2002; Fellner and Sawhney, 2002; Massot et al., 2012). In tomato, the result of continuous lighting has been reported to result in inter-vascular chlorosis, a decrease in leaf chlorophyll, reduction in net photosynthesis and an increase in the concentration of starch and hexoses (Demers and Gosselin, 2002). A proteomics study of tomato leaves showed that physiological adjustments to light conditions could be rapidly reversed when the light exposure is brought to normal (Haque et al., 2015). At higher light intensities (300 μmol $m^{-2}s^{-1}$) tomato plants reach the highest energy efficiency and photosynthetic activity, and efficiency does not increase at higher light intensities (Fan et al., 2013). However, to date, no study has shown how tomato plants recover from different light levels in the same leaf tissue, and how these specialized responses can act in the plant.

To understand the recovery of irreversible photodamage caused by high light stress in plant leaves we can examine the changes in proteins expression using proteomics approaches. Proteomics allows for a global quantitative study of gene products in various tissues and cell physiological states, and is a strong tool for identifying key metabolic pathways altered upon changing external conditions as shown in the literature (Huang et al., 2012; Huang and Lefsrud, 2012; Patel et al., 2015; Sivagnanam et al., 2011a, 2011b). In this work, we used high-intensity monochromatic LED lights to create a high-light stress condition on tomato leaves, avoiding the commonly associated wavelengths interference from conventional light systems (Lefsrud et al., 2008). This approach allowed us to simultaneously generate three different zones of stress impact on the leaves at a 5,000 W m^{-2} light intensity (Burned sample), a moderately impacted zone (~3,000 W m^2) (Limit sample) and a low impact zone (<1,000 W m^2) (Regular sample). To our knowledge, this is the first characterization of this level of light stress impact and the first characterization of the different samples that were generated (Burned, and Limit). A deep characterization of proteome responses of these light stress-impacted recovered zones was performed through a multiplex iTRAQ-based quantitative proteomics approach (Ross et al., 2004). The analysis revealed four different complex responses. We report the possible exclusive involvement of the salicylic acid hormone in the Burned sample, and the probable role of PSII 10 and 22 kDa polypeptides, and reaction centers H and Psb28 in non-photochemical quenching and recovery of photosystem II.

4.2 Materials and methods

4.2.1 Plant variety

Tomato (*Solanum lycopersicum*) variety Heinz1706 was provided by HeinzSeed Stockton, CA, USA. Heinz 1706 is the variety that was recently genetically sequenced (The Tomato Genome

Consortium, 2012), the genome has a haploid chromosome number of 12, containing 900 Mb and 35,000 protein-coding genes (genes or transcript containing an open reading frame) and genome annotation is still in development.

4.2.2 Plant growth and sampling

The tomato seeds were planted and grown hydroponically in rockwool (Grodan A/S, Dk-2640, Hedehusene, Denmark) and incubated under cool-white fluorescent bulbs (4200 K, F72T8CW, Osram, USA) in a growth chamber (TC30, Conviron, MB, Canada). The environmental conditions in the chamber were controlled at 50% relative humidity (RH), 25˚C light/dark temperature, an average of 390 ppm CO_2, and a 16 h photoperiod with an irradiance level of 55 W m^{-2} (approximately 250 µmol m^{-2} s^{-1}). Fresh Hoagland (Epstein, 1972) nutrient solution was provided every other day. Hoagland composition: 6.5 mM KNO_3, 4.0 mM $Ca(NO_3)_2.4H_2O$, 2mM $NH_4H_2PO_4$, 2.0 mM $MgSO_4.7H_2O$, 4.6 µM H_3BO_3, 0.5 µM $MnCl_2.4H_20$, 0.2 µM $ZnSO_4.7H_20$, 0.1 µM $(NH_4)_6Mo_7O_{24}.4H_2O$, 0.2 µM $CuSO_4.5H_20$, 45 µM $FeCl_3$. Ten tomato plants were submitted to deep-red LED light (655 nm, LXML-PL01-0040, Philips-Lumileds, CA, USA) with an average irradiance level of 5,000 W m^{-2} (approximately ~25,000 µmol m^{-2} sec^{-1}) on a ~1.1 cm^2 spot in the center of a mature leaf for 5 min. After LED treatment, plants were continued to be grown in the growth chamber for a 10 day to recover and observe the bleached leaf area before tissue extraction. The leaves of each treatment of 10 plants were collected as one biological sample, to eliminate individual variances. The leaves were dissected, and the areas corresponding to the light treated zone (Burned), adjacent (Limit) and rest of the leave (Regular) were kept separated (Figure 7-C), the remaining parts were discarded. Plant tissues were kept under -80˚C before protein extraction (Yamamoto et al., 1981). The control plant group was kept in the growth chamber during the full experiment without the intense irradiation, and the experiment was replicated three times.

4.2.3 Light treatment

Tomato leaves were placed 2.5 cm below the LED lights, where light intensity was at 5,000 W m^{-2}, measured by a spectroradiometer (PS-300, Apogee, Logan, UT, USA). LED set up was as described by Wu et al. (2017) (not published). Briefly, the LED array was mounted to a water jacket connected to a water bath (ST-011, Guangzhou Rantion Trading Co., China) and a cluster concentrator optic (25 mm focal length, No. 263, Polymer Optics, Wokingham, Berkshire, UK) was placed in front of the array. A focal spot of 12 mm diameter was generated by the cluster concentrator optic. An isotemp (4100R20, Fisher Scientific, Hampton, NH, USA) bath circulator was used to maintain a 0 ^{o}C coolant water bath. Filtered lenses were used to attenuate the light, to measure the high irradiance level with the use of the spectroradiometer.

Leaf temperature was measured in two biological replicates as reported by Dixon & Grace (1983) with a copper constantan thermocouples (type T, 0.03 mm, Omega Engineering Canada, QC, CA). The temperature was measured during the 5 min before and after the light treatment as well as during the 5-min treatment. The thermocouples were placed on the surface of the leaf using glue extracted in chloroform from transparent adhesive tape. Data points were collected every second.

4.2.4 Tissue lysis, protein extraction, and tryptic digestion

Fresh plant tissue (20 mg) was treated with 500 µL of lysis buffer (5% SDS, 50 mM triethylammonium bicarbonate buffer (TEAB)). A volume of 5 µl of each protease inhibitor cocktail 1, phosphatase inhibitor cocktail 2, and phosphatase inhibitor cocktail 3 (Sigma-Aldrich, MO, USA) were added to the sample. The samples were then mixed at 1,250 rpm for 30 min. Tris(2-carboxyethyl)phosphine (TCEP) was added to 150 µL of the lysate to a final concentration of 5 mM. Samples were heated to 55°C for 20 min, allowed to cool to room temperature, and methyl methanethiosulfonate (MMTS) was added to a final concentration of 10 mM. Samples were incubated at room temperature for 20 min to complete blocking of free sulfhydryl groups. Methanol was added at 4x the sample volume to precipitate proteins, chloroform was added at 2x the sample volume, and deionized water was added at 3x the sample volume. The samples were then incubated at -20°C for 2 h and centrifuged at 5,000 rpm for 10 min at 4°C. Methanol was added at 3x the original sample volume, and the sample was vortexed. The sample was centrifuged at 14,000 rpm for 10 min at 4°C and air-dried.

The proteins were reconstituted with 60 µL of lysis buffer, and a BCA assay (Pierce, Thermo Fischer Scientific, MA, USA) was performed to determine protein concentration. Proteins were digested by applying 80 µg of each lysate to S-TrapTM mini spin columns (ProtiFi, NY, USA) according to the manufacturer instructions. Briefly, lysates were acidified with phosphoric acid to a final concentration of 1.2% and added to an S-Trap^{TM} containing 6x lysate volume of s-trapping buffer (90% Methanol, 100 mM TEAB). Digestion was carried out with 2 µg of sequencing grade trypsin (Promega, WI, USA) in 125 µL of 50 mM TEAB and was added to the S-TrapTM which was incubated overnight at 37°C. The peptides were eluted from the column with subsequent applications of 50 mM TEAB, 0.2% formic acid in water and 0.2% formic acid in 50% acetonitrile. After dried in a vacuum, peptides were then reconstituted in 50 µL of 0.5 M TEAB/70% isopropanol and labeled with 8-plex iTRAQ reagent for 2 h at room temperature, according to Ross et al. (2004). Labeled samples were then acidified to pH 4 with formic acid, combined, and concentrated in a vacuum until ~10 µL remained.

4.2.5 Liquid chromatography/mass spectrometry

An Orbitrap Fusion Lumos mass spectrometer (Thermo Scientific, MA, USA), equipped with a nano-ion spray source was coupled to an EASY-nLC 1200 system (Thermo Scientific, MA, USA). The LC system was configured with a self-pack PicoFrit™ 75 µm analytical column with an 8 µm emitter (New Objective, Woburn, MA) packed to 25 cm with ReproSil-Pur C18-AQ, 1.9 µM material (Dr. Maish GmbH, Ammerbuch-Entringen, DE). Mobile phase A consisted of 2% acetonitrile 0.1% formic acid and mobile phase B consisted of 90% acetonitrile 0.1% formic acid.

Peptides were then separated using the following steps: at a flow rate of 200 nL/min: 2% B to 6% B over 1 min, 6% B to 30% B over 84 min, 30% B to 60% B over 9 min, 60% B to 90% B over 1 min, held at 90% B for 5 min, 90% B to 50% B over 1 min and then flow rate was increased to 500 nL/min as 50% B was held for 9 min. Eluted peptides were directly electrosprayed into the Fusion Lumos mass spectrometer with the application of a distal 2.3 kV spray voltage and a capillary temperature of 300°C. Full-scan mass spectrum (Res=60,000 400-1600 m/z) was followed by MS/MS using the "Top N" method for selection. High-energy collisional dissociation (HCD) was used with the normalized collision energy set to 35 for fragmentation, the isolation width set to 1.2 and a duration of 10 s for the dynamic exclusion with a mass exclusion width of 10 ppm. Monoisotopic precursor selection was used for charge states 2+ and greater, and data were acquired in profile mode.

4.2.6 Database search

Peaklist files were generated by Mascot Distiller (Matrix Science, MA, USA). Protein identification and quantification were carried using Mascot 2.4 (Perkins et al., 1999) against the *Solanum lycopersicum* cv. Heinz 1706 database (UniProt, proteome reference: UP000004994). Methylthiolation of cysteine and N-terminal and lysine iTRAQ modifications were set as fixed modifications, methionine oxidation and deamidation (NQ) as a variable. Trypsin was used as a cleavage enzyme with one missed cleavage allowed. Mass tolerance was set at 30 ppm for intact peptide mass and 0.3 Da for fragment ions. Search results were rescored by Percolator to give a final 1% false discovery rate (FDR) using a randomized version of the same tomato database (score: -10log(PEP), identity threshold score for $p<0.05$: 13). Protein-level iTRAQ ratios were calculated as intensity weighted, using only peptides with expectation values <0.05. Global ratio normalization (summed) was applied across all iTRAQ channels. Protein enrichment was then calculated by dividing sample protein ratios by the corresponding control sample channel. Missing values were replaced by the single-value approach, by adding the limit of detection value, (LOD) (Webb-Robertson et al., 2015).

4.2.7 Statistical analysis

Each biological replicate consisted of samples collected from 10 treated or control plants, to account for biological variability. An empirical distribution representing total experimental variability was built, not just within each group. This was done by comparing the ratios of all replicates within each condition and forming an empirical Cumulative Distribution Function (CDF). The CDF contained the ratio of every replicate regardless of condition for all proteins identified which represented both the biological and technical variability of this dataset. The fold change cutoff for significance was determined by selecting only ratios values more than 2 standard deviations from the mean. In this study, 90% of ratios between the replicates fell between 0.61 and 1.61, with values outside this range being significant at a p-value equal to 0.05.

4.2.8 Bioinformatics

Functional annotations of the identified proteins were obtained via the UniProt Gene ontology tool (UniProt-GOA) (Huntley et al., 2015). Proteins present in samples Burned, Limit and

Regular were assigned GO-slim subcategories of the biological processes category by the PANTHER enrichment test. Bonferroni correction was applied for multiple testing. Of the total 3,994 proteins, 3,873 were mapped to a sub-category, the expression ratios were used to weight the representation of the sub-category regarding the overall expression. Protein interaction network was predicted by the STRING database (Szklarczyk et al., 2017), which obtains interactions based on genomic, experimental, co-expression or previous knowledge information context at the function or physical level. The analysis was performed with the highest confidence (0.9) interaction score. Pathway annotation was obtained by the Kyoto Encyclopedia of Genes and Genomes (KEGG) database. The KEGG Pathway Annotation tool generated visualization of the pathways involved in the high abundant proteins of the high light treated samples and control. A hierarchical clustering analysis was applied to clustering proteins based on their Euclidean distance and complete linkage to visualize the different trends of protein abundance of the dataset. The log2 transformed protein ratios (treatment/control) were clustered by the hierarchical clustering function of the Perseus software.

4.3 Results

4.3.1 High-light LED treatment

A deep-red LED (655 nm) was chosen due to the well-characterized plant physiological response to red light (Deram et al., 2014). The high-light treatment generated a highly dehydrated and damaged area on the tomato leaves (Burned sample). The light damages leaf zones were well defined after a 10-days recovery period, when a dark line was visible between Burned and Regular, representing the Limit sample (Figure 7-C). The control plants were grown for the whole period of the experiment (40 days) under normal light conditions (250 μmol m^{-2} s^{-1}), and protein abundance in each sample was relative to the control sample protein abundance. The leaf zone under extreme light intensity (Burned) appeared to be photo-bleached after 4-5 days. The color and texture change suggested the tissue's death after 10 days, while the rest of the leaf presented a healthy appearance.

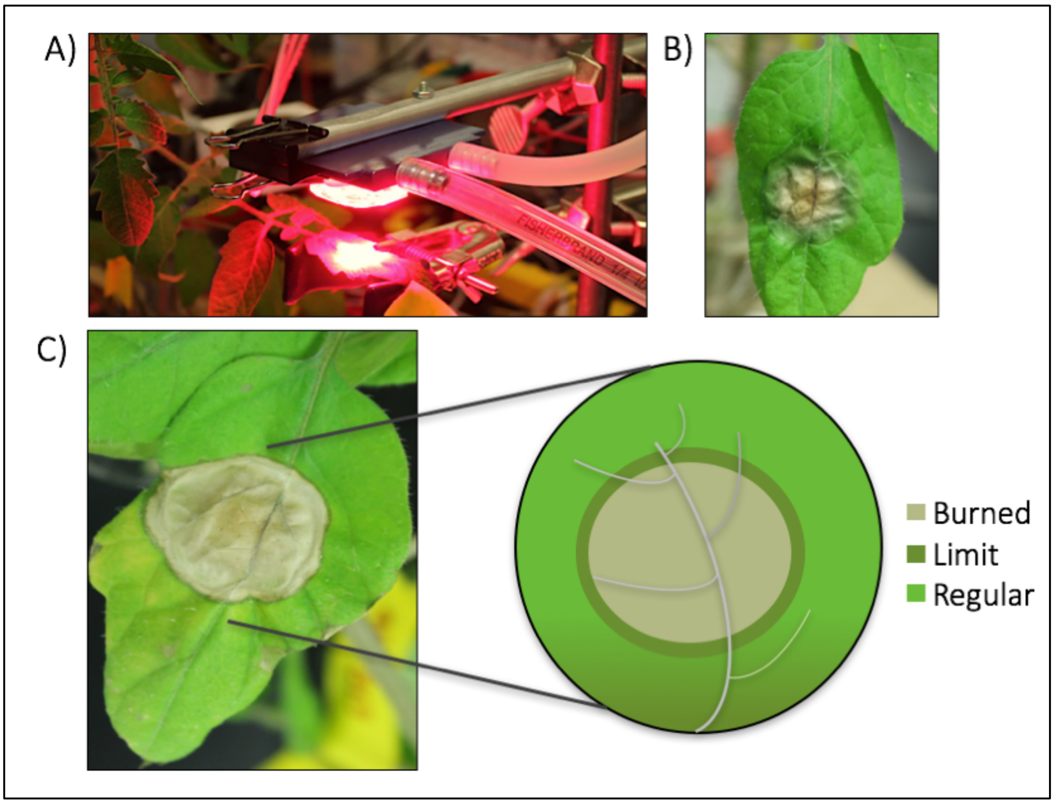

Figure 7. LED light treatment schematic. (A) Light treatment on tomato leaves using high-intensity deep-red (655 nm) LED light at 5,000 W m^{-2} (B) Tomato leaf after high-intensity light treatment (C) Photo of the leaf after the 10-days recovery from the high-light treatment and sampling zone scheme: Burned, Limit, and Regular.

Although LEDs are low-temperature lamps (varying from 60-100˚C) compared with conventional lights, a significant thermal output still exists and is dissipated from a thermal pad (Bourget, 2008). In this study, the use of a cooling strategy avoids heat dissipated from the thermal pad, reducing the interference in plant response. The cooling also helps to maintain the

LED optical characteristics (e.g., nominal wavelengths and spectral compositions) when conducting experimentation (Huang et al., 2016). Further, using a concentrator optic, we generated an extreme high irradiance level of 5,000 W m^{-2} in the Burned spot. To determine the light distribution on the leaf, a light map was generated and can be seen in Figure 8-B.

The Burned spot had a maximum light intensity of 5,000, while the Limit had ~3,000 W m^{-2}, and the Regular presented < 2,000 W m^{-2}. Because LEDs are low-temperature lights, we did not expect a high increase in leaf temperature due to the LED apparatus, but rather by a consequence of the high irradiation, resulting in heat dissipation by non-photochemical quenching. To determine the temperature change, a thermocouple was used to monitor the tomato leaf during the LED treatment. The LED treatment increased leaf temperature to a maximum of 136ºC (Figure 8-A).

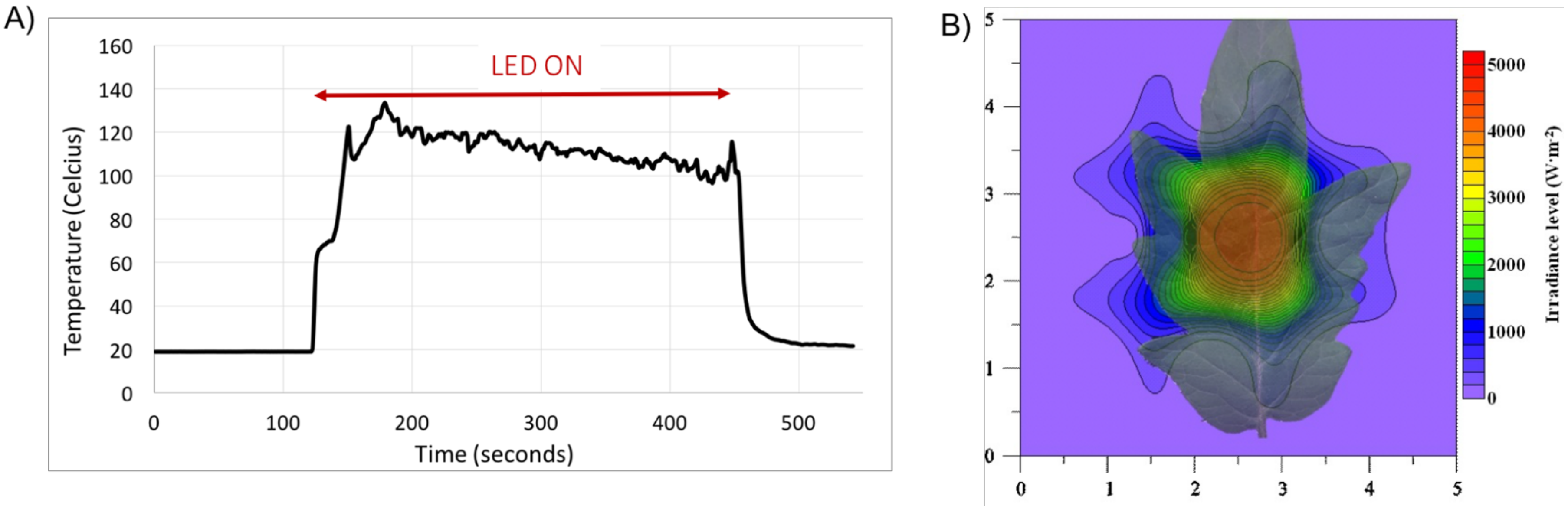

Figure 8. Light treatment temperature and light measurements. (A) Leaf temperature measurement by a thermocouple (0.03 mm, type T, Omega Engineering Canada). Data points collected every second before, during and after light treatment. The red arrow indicates the duration of the light treatment (~5 min). (B) Light mapping with a projected tomato leaf showing the irradiance distribution on the tomato leaf generated by the high-intensity light treatment with the deep-red LED. The inner circle shows the area corresponding to the Burned sample. The average of three biological replicates is reported.

4.3.2 Functional enrichment analysis

We identified 5,577 proteins in 1% FDR, which we further filtered to only proteins containing two or more unique peptides. Because identified peptides can come from more than one protein, filtering for more than 2 unique peptides increases the probability that the protein identified is indeed different from others that share a peptide. The filtered list resulted in 3,994 proteins that were further analyzed. In order to identify the protein functional groups, found in each light treated sample, the protein expression ratios (treatment/control) were calculated and used as input in a functional enrichment test. From 3,994 proteins, 120 proteins did not present functional annotation and could not be mapped; one protein presented multiple mapping information. The PANTHER enrichment test (Mi et al., 2013) (v. 12.0) was performed to obtain the proportion of each GO-slim category in relation to the protein expression of each sample treatment (Regular, Burned and Limit). The top categories are shown in Figure 9.

In the Regular sample, the trends of GO sub-categories with the unique proportion of the overall expression values were: Cellular process, RNA metabolic processes, purine nuclease metabolic process. The Limit sample unique proportion of proteins were in carbohydrate transport, fatty acid metabolic process, and fatty acid beta-oxidation.

The Burned sample had unique overrepresented categories as a cellular amino acid biosynthetic process, glycogen metabolic process, glycolysis, mRNA processing, mRNA splicing via spliceosome, protein localization, RNA splicing via transesterification reactions, steroid metabolic processes, and transcription DNA dependent. Although a high number of proteins were found to be part of the carbohydrate metabolic process, cellular amino acid metabolic process, metabolic process, monosaccharide metabolic process, generation of precursor metabolites, and energy, the expression values of these categories were sub-represented in the overall protein expression of the sample.

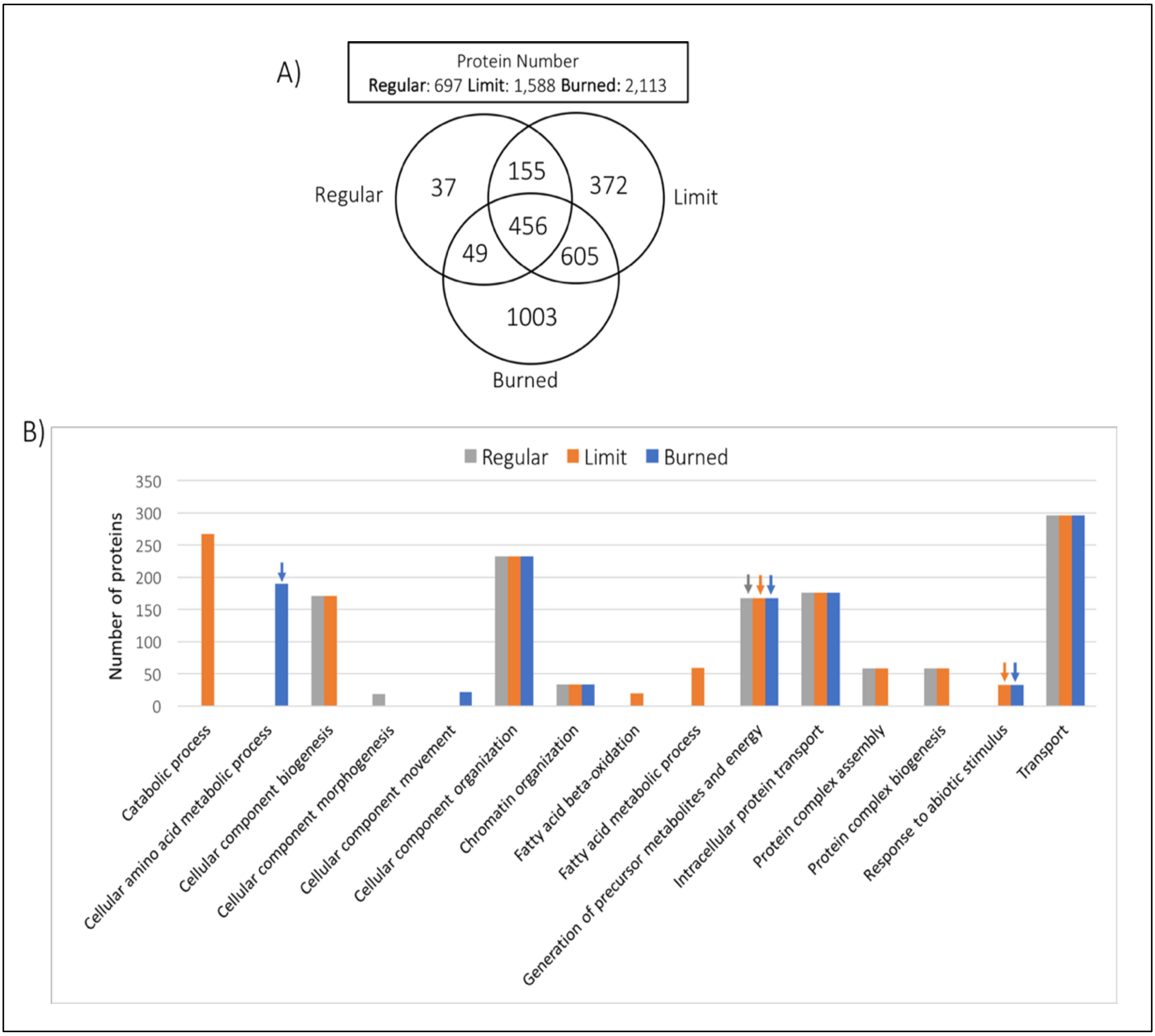

Figure 9. Quantitative functional enrichment of the detected proteins expression ratios and Venn diagram of identified proteins. (A) Venn diagram of distribution of identified proteins between samples. Statistically differentially abundant proteins ($p<0.05$) from tomato leaves recovered from high-light stress (Burned, Limit, and Regular) grouped in a Venn diagram. (B) Proteins present in samples Burned, Limit and Regular were assigned GO-slim subcategories of the biological processes category by the PANTHER enrichment test. Bonferroni correction was applied for multiple testing. Of the total 3,994 proteins, 3,873

were mapped to a sub-category, the expression ratios were used to weight the representation of the sub-category regarding the overall expression, y-axis show number of proteins. Only significant matches ($p<0.05$, Wilcoxon Rank-Sum test) top 15 categories are shown. The arrows indicate that the protein expression is shifted towards smaller values than the overall expressions. Notable trends are the high proportion of protein expression related to the cellular process in the Regular sample, when compared to Burned and Limit samples.

4.3.3 Expression patterns variations from differentially abundant proteins

We calculated an abundance ratio threshold of >0.7 and <-0.7 based on the biological replicates variability and applied it to obtain a list of statistically differentially abundant proteins ($p<0.01$). Interestingly, when analyzing the proteins detected in all samples, the Burned sample had a high total of differentially abundant proteins (2,113), while the Limit samples had 1,588 proteins (Figure 9-B). The Regular sample had the lowest number of differentially abundant proteins (697), due to the lower light intensity that the sample was submitted to, and, therefore, were similar to the proteins from the control sample. All three samples shared 456 differential proteins in common. The Burned sample presented the highest number of uniquely differential proteins (1,003). To our knowledge, this is the first time the unique set of proteins from the Burned sample are reported as involved in the recovery of a highly damaging light intensity stress (5,000 W m^{-2}) since this is the first proteomics study of the light treatment applied in this work.

A hierarchical cluster analysis was carried out to investigate the light stress recovery of tomato plants. The analysis was applied to the subset of differentially abundant proteins of samples Burned, Limit, and Regular ($p<0.01$, greater than a 0.7 log2 fold change difference) (Figure 10-A). The protein expression values used as an input for the analysis are the normalized ratios of the treatment and control (as Burned/Control, Regular/Control, Limit/Control). A total of 14 proteins clusters with different expression trends, with either a higher expression, was seen in the Burned, or Limit samples, or a linear relation to light intensity, or a similar expression in all samples, were defined. From the 14 clusters, we observed the tendency of formation of four patterns of different relative abundance (a description of the four patterns is presented in Figure 10-B). Protein lists were generated for each of the four different expression patterns, a total of 112, 102, 13, and 2,453 proteins were represented in patterns 1-4, respectively. The protein groups of each of the patterns were analyzed for their function through analysis of their associated GO term in the Biological Processes category and are resumed in Table 2. The functional groups presenting a higher number of proteins of each one of the clusters were presented.

Table 2. Functions with containing more than two proteins found in pattern 1 to 4. Patterns found in the hierarchical clustering analysis of the ratio of differentially abundant proteins found in the Burned, Regular, and Limit samples in relation to the control samples (n = 2,680 proteins).

Pattern	Pattern 1	Pattern 2	Pattern 3	Pattern 4
Number of proteins	112	102	13	2,453
Functions	Photosynthesis II reaction center, peroxidases, fruit-ripening protein.	Non-specific lipid-transfer proteins, pathogenesis-related proteins, pathogenesis-related proteins.	Carbohydrate-binding, catalytic activity, nucleic acid binding.	Anatomical structure, biosynthetic processes, cellular processes, carbohydrate metabolic processes, response/defense functions, chlorophyll a-b binding proteins, photosystem I iron-sulfur center, components of photosystem II, proteins D1, D2, CP47, CP43.

Proteins with the pattern 1 expression behavior presented high abundance in the Burned sample, and similar lower expressions in Limit and Regular samples. The trend of pattern 1 may indicate proteins with a role in long-term recovering plant tissues from extreme light damage, as they presented a very high expression value in the Burned sample. Photosystem

II reaction center protein, two peroxidases, and fruit-ripening protein were some of the proteins found in this group.

Proteins with pattern 2 showed higher expression values in the Limit sample and lower similar values for Burned and Regular. This group presented four non-specific lipid-transfer proteins, three pathogenesis-related proteins, which are proteins part of the general response/defense response to stimulus function.

The group of proteins represented by pattern 3 had high expression values in the Burned sample and decreasing values from the Limit to the Regular samples, following the intensity trend of the light treatment (high on Burned, lower on Limit, and much lower in Regular). The most frequent function was the role in binding (carbohydrate binding, catalytic activity, nucleic acid binding) and defense response. This group of proteins was characterized by mostly DNA/RNA regulators, and proteins related to defense response. Furthermore, proteins in pattern 3 can be explored by scientists interested in light-regulated genes.

The expression values of pattern 4, the largest group were either similar in all the three samples or slightly higher in the Regular sample. The proteins assign to this group were related to a large variety of roles as an anatomical structure, biosynthetic processes, cellular processes, and carbohydrate metabolic processes. 37 proteins had response/defense functions, of a total of 2,453 proteins. Interestingly, this group contained 12 chlorophyll a-b binding proteins, photosystem I iron-sulfur center, eight components of photosystem II, and proteins D1, D2, CP47, CP43. The latter are found to be involved in light stress conditions, and particularly, repair of photosystem II from photodamage. Even though the tomato plants recovered for a period of 10 days, components of the photosystem damage repair cycle could still be detected.

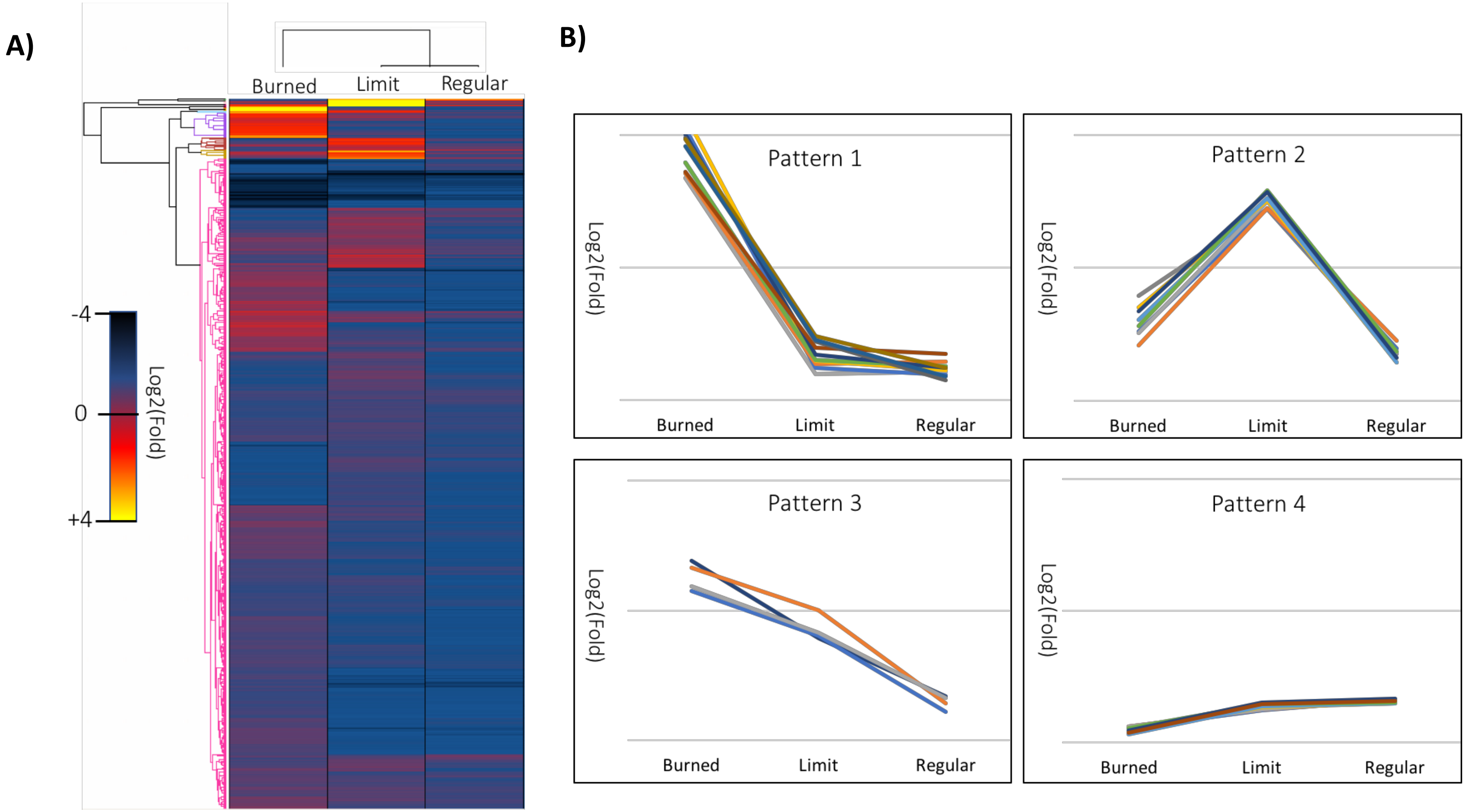

Figure 10. Hierarchical clustering analysis of all differentially abundant proteins and cluster expression patterns**.** (A) Differentially regulated proteins (n = 2,680) in Control, Burned, Limit and Regular were clustered into groups with similar log2 transformed ratio (treatment/control) patterns. The Euclidian distance was chosen to cluster proteins by abundance traits. The 8 protein clusters presenting differential abundance trend were chosen for further analysis. (B) Example of the graphical representation of the four protein abundance patterns (Pattern 1-4) found in the clusters obtained by the hierarchical clustering analysis (sample in the x-axis, fold-change on the y-axis

4.3.4 Metabolic analysis of differentially abundant proteins

We analyzed the statistically differentially abundant proteins from each sample to visualize the metabolic pathways that are involved in the recovery of the tomato leaves from the different levels of light damage recovery. The set of differentially abundant proteins detected only in the Burned sample (1,003 proteins) showed an enrichment of antennas from PSI, LHCA1, LHCA2, LHCA4 and from PSII, LHCB1, LHCB3, LHCB6, which are implicated in photoprotection mechanisms (Caffarri et al., 2005; Floris et al., 2013; Guan et al., 2016). The light treatment recovery in the Burned sample involved a general overexpression of the metabolism of proteins related to nitrogen compound metabolic process (such as fructose-bisphosphate aldolase, Glucose-6-phosphate dehydrogenase, glutamine synthetase), primary metabolism (carbohydrate, protein, and lipid processes), as ATP synthase, photosystem components, 50S ribosomal protein, and other primary metabolic functions, as methylation, developmental processes, growth, and reproductive process.

Since the differentially abundant protein of the Burned sample formed a large dataset (1,003 proteins), we used the functional analysis to filter the functions of interest. GO terms were assigned to the whole dataset, and the 194 proteins from the enriched terms immune system process and response to stimulus were further investigated. In order to better understand the role of the uncharacterized proteins and their relation to the other proteins of the dataset, the filtered proteins were analyzed with STRING (Szklarczyk et al., 2015) to obtain protein-interaction networks. The generated network was analyzed by applying high confidence (0.7) and K-means clustering. Four proteins interaction clusters (PICB) were defined in the Burned sample (Figure 11). The protein interaction analysis revealed four well-defined clusters of interactors.

PICB1 had seven uncharacterized proteins with a role in the functional terms: Positive regulation of RNA polymerase II transcriptional preinitiation complex assembly, ubiquitin-dependent ERAD pathway, DNA repair, protein K63-linked deubiquitination and response to the absence of light. PICB2 presented proteins with functions: response to heat, response to stress, regulation of gene expression, stress-activated protein kinase signaling cascade, brassinosteroid mediated signaling pathway, response to unfolded protein, and chaperone-mediated protein folding. PICB 3 functions were related to response to light stimulus, and non-photochemical quenching, where 10 of the 11 proteins where chlorophyll binding proteins. PICB 4 had functions as response to high light intensity, response to salt stress, negative regulation of plant-type hypersensitive response, and cellular response to oxidative stress.

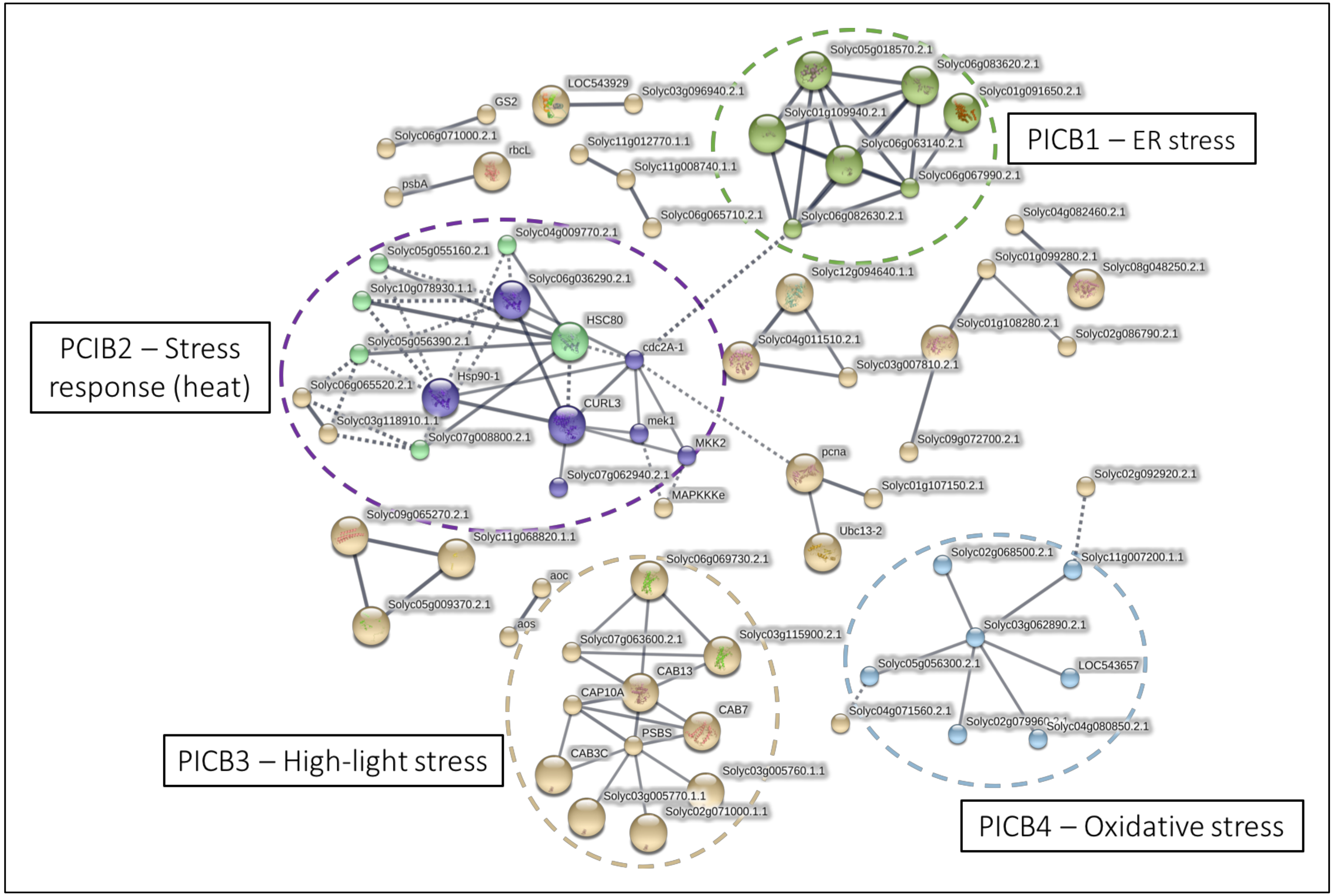

Figure 11. Protein interaction network from differentially abundant proteins found in the Burned sample. The STRING software was used to obtain a network of protein interactions at high confidence (0.7). Cluster analysis by K-means resulted in four well-defined clusters.

The same analysis was carried out with the Limit sample to compare to the response of the Burned sample. A protein interaction network was obtained from the 155 proteins from immune system process and response to stress. Three clusters (PICL) were evidenced by the protein-interaction network analysis (Figure 12). PICL 1 was composed of proteins related to chaperone, response to heat, response to cold, salt, and drought. PICL 2 proteins were related to response to light stimulus, response to hydrogen peroxide, response to endoplasmic reticulum stress, cellular response to oxidative stress, response to absence of light, response to oxygen radical. PICL 3 contained proteins with functions such as ubiquitin-dependent ERAD pathway, Proteasome-mediated ubiquitin-dependent protein catabolic process, response to salt stress, and defense response to fungus, incompatible interaction.

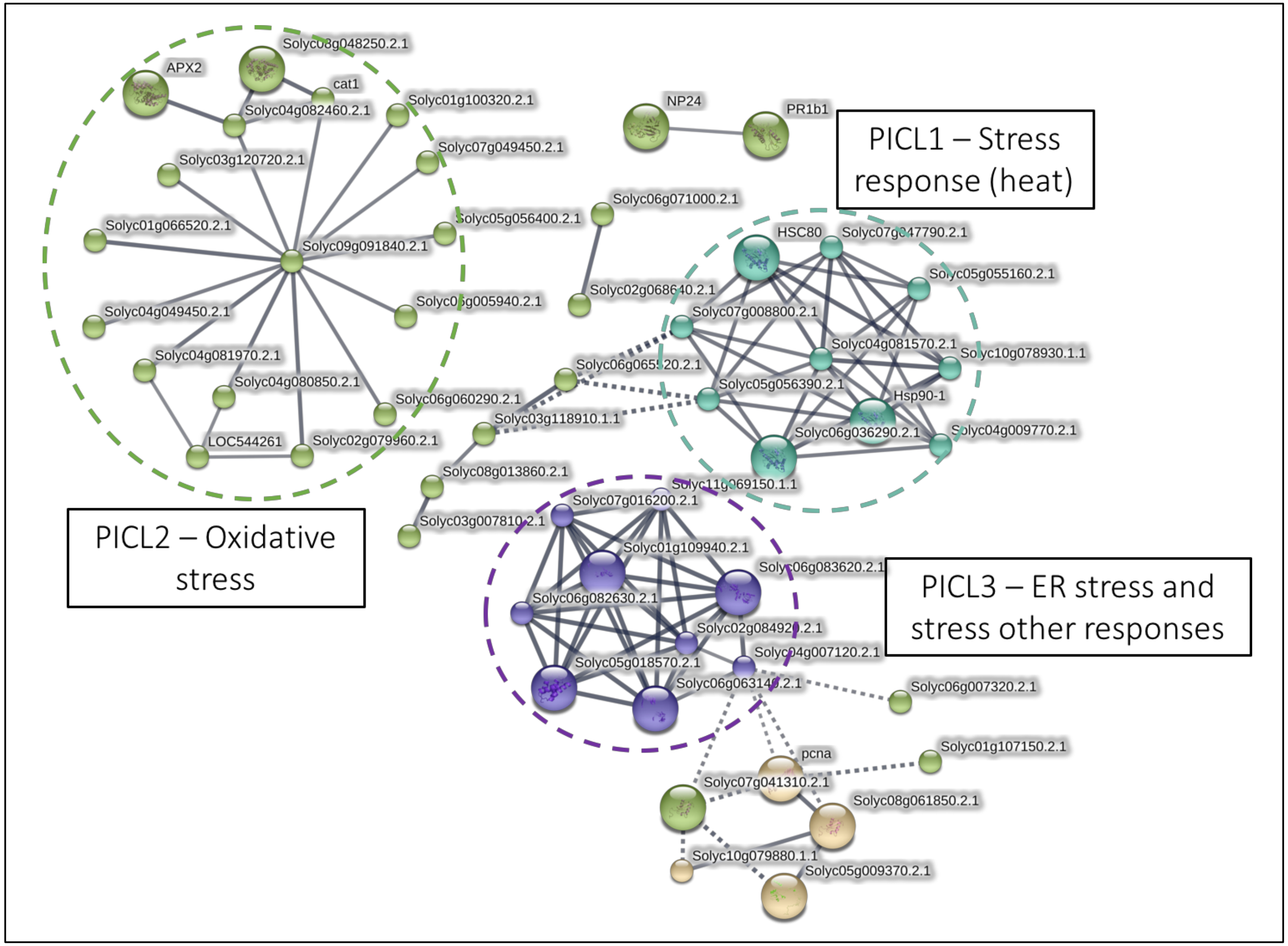

Figure 12. Protein interaction network from differentially abundant proteins found in the Limit sample. The STRING software was used to obtain a network of protein interactions at high confidence (0.7). Cluster analysis by K-means resulted in three well-defined clusters.

The set of proteins from the Regular sample were also accessed for protein interactions. A total of 85 proteins were mapped. However, only 17 proteins formed interactions, the larger cluster being formed of 5 proteins related to heat stress and chaperones, followed by three clusters of three proteins each (the list of proteins is provided in Appendix C).

4.4 Discussion

The proteomics analysis of the tomato leaves tissues submitted to the high light treatment revealed 1,003, 372, and 37 proteins specific to the samples with different light intensity (Burned, Limit, and Regular, respectively). We obtained three different levels of light stress defense in the same leaf tissue, meaning three different highly localized stress defense responses. Through a clustering analysis, we identified proteins that respond to the increase of light intensity in a direct relationship (i.e., protein concentration augments with the increasing of light intensity) and proteins that are only abundant in the higher light intensity (5,000 W m^{-2}) or the medium (~2,000 W m^{-2}).

Similar protein response in all the samples represented the largest group (pattern 4, Figure 10-B). A general enrichment of primary metabolic functions was seen. From a total of 2,455 proteins, 212 were assigned to response to stimulus function, 8 to immune system process, three to removal of superoxide radical. The response to stimulus proteins were mostly of proteins related to biotic stress (70 proteins) and chemicals (82 proteins). Since we were more interested in the uniqueness of the differentially abundant proteins in each sample and pattern 4 is composed of proteins upregulated in all samples, we decided to not explore further in this manuscript.

4.4.1 Active functions in response to medium light stress intensity

Proteins with higher expression in the Limit sample and following pattern 2 included non-specific lipid-transfer proteins, annexin proteins, R1 and PR10, and xyloglucan endotransglucosylase /hydrolases, with functions as Response to biotic and abiotic stresses, hormones, chemicals, and external stimulus. The function of the non-specific lipid-transfer proteins is still not well defined in the literature, they have been considered in the transport of monomer of cutin, deposition of lipophilic cuticular material, and plant defense (Chen et al., 2017). More recently, it has been shown to have a positive impact on drought and low-temperature stresses, where the non-specific lipid-transfer protein transcript levels were decreased in response to salicylic acid and increased during methyl jasmonate treatment (Chen et al., 2017). Attention has been focused on non-specific lipid-transfer proteins due to their role as major allergens, along with their enzymatic and heat resistance.

Annexins have been shown to be downregulated in response to low-light stress response in cotton (*Gossypium hirsutum* L.) (Hu et al., 2017). In *Arabidopsis*, phytochrome-mediated changes in annexin expression have been studied, showing a high level of *AnnAt5* transcript response to red light stimuli (Cantero et al., 2006). Still, in *Arabidopsis*, the overexpression of annexin *AnnAt1* improved drought tolerance and mitigated ROS response (Konopka-Postupolska et al., 2009). In tomato subjected to drought stress, the auxin interactor *SpUSP* increased expression of LHCB and activated other photosynthesis-related genes, maintaining regular photosynthesis levels by keeping the antenna integral while reducing ROS impact (Loukehaich et al., 2012).

R1 protein is a regulator of starch degradation in plants, and R1 deficiency has generated reduced starch phosphorylation and high starch accumulation generating phenotype with starch excess in potato and *Arabidopsis* (Yu et al., 2001). Recently, abscisic acid-induced leaf starch degradation has been reported to have an important role in osmotic stress regulation, having a synergistic role of enzymes regulated by abscisic acid through AREB/ABF-SNRK2 kinase-signaling pathway in an action to maintain carbon deviation to the roots and osmolyte accumulation (Lockhart, 2016; Thalmann et al., 2016).

Pathogenesis-related proteins (PR) are reported to be involved in different stress defenses to biotic stresses and pathogens. The overexpression of PR10 has been shown to increase salt tolerance in transgenic *Arabidopsis* containing the *SmPR10* gene from *Salix matsudana* Koidz and salt and drought tolerance in rice (Han et al., 2017; Wu et al., 2016). Xyloglucan endotransglucosylase hydrolases proteins regulate cell wall extension, construction and metabolism, are involved in the cell wall hemicellulose synthesis, and plant response to environmental stresses caused by heavy metal, salt, and drought (Xuan et al., 2016).

4.4.2 Active functions in response to strong high light stress

Besides seeing a difference in the expression behavior, we used the protein-interaction network analysis to visualize the different levels of high light stress responses represented in the Regular, Limit, and Burned samples. Presenting a higher level of complexity when compared to prokaryotic organisms, plant tissues are estimated to contain a pool of 10,000 proteins at any stage (Abraham et al., 2013). However, the sample preparation efficiency and mass spectrometry technology are limitations that highly impact the number of detectable proteins. Furthermore, plant tissues present an even greater limitation since they contain a high concentration of Rubisco, which is the most abundant protein in leaves (Ahsan et al., 2007). This makes the identification of low-abundant proteins difficult by not selecting their ions for MS^2. Methods for Rubisco removal have been developed, but they result in the removal of similar proteins by lack of antibody specificity, or coprecipitation (Alvarez and Naldrett, 2016). Also, the poor protein annotation of non-model plants is an obstacle to protein identification. The use of protein function and interaction tools are good strategies to deal with the lack of functional information since they can highlight annotated interactors and suggest protein groups of overrepresented functions. We implemented this approach to better characterize the three different levels of response to light stress obtained in this study.

Proteins with higher abundance in the Burned sample following pattern 1 abundance were nine histones, three peroxidases, three sulfotransferases, and 71 uncharacterized proteins with roles in response to stimulus, carbohydrate metabolic processes, and others. Consistent with a stress response, proteins with a role in biotic stimulus, hormone (cytokinin and abscisic acid), chemical, and other organisms were present in the sample. Redox signals have been reported to be involved in high light acclimation through the electron transport chain, variations in carbohydrate and nutrient status, and hormone levels (Dyson et al., 2015).

Interestingly, eight proteins found to be more abundant on the Burned dataset were related to plant hormone signal transduction pathways in the Burned samples (Figure 13). The eight proteins were involved in four hormonal pathways: the abscisic acid hormone (through protein SnRK2) which leads to stomatal closure and stress proteins expression activation (Thalmann et al., 2016), the ethylene hormone (through SIMKK), leading to fruit-ripening and stress responses (Guo and Ecker, 2003), the brassinosteroid hormone (through BRI1 and BSK proteins), which has a role in stem elongation, vascular differentiation and stress tolerance (Koka et al., 2000), and, lastly, the salicylic acid (PR-1), responsible for disease resistance and inducer of the systemic acquired resistance (Agarwal and Agarwal, 2014). The protein K4CX39 (uncharacterized), with role in salicylic acid response, presented a 1.75 fold change, while no protein related to the salicylic acid response was found to be differentially abundant in the Limit sample. This differential abundance could be related to the accumulation of heat shock proteins (HSPs) in heat-stressed plants, as the salicylic acid has been reported to increase Hsp70/Hsc70 in a dose and time-dependent manner (Cronjé and Bornman, 2006). The hormone cytokinin regulates cell division and maintenance of cellular redox, and most of the cytokinin-regulated genes are involved in response to light and other stimuli (Walton et al., 2015). In *Arabidopsis*, high light has been shown to induce CKX6 expression in roots, and cytokinin riboside 5'-monophosphate phosphoribohydrolase (protein K4ASD4 in tomato plants) has been shown to be highly responsive to different stimuli (Bielach et al., 2017). Brassinosteroid is a steroid hormone involved in cell elongation, vascular differentiation, senescence, and stress responses. Brassinosteroid and abscisic acid have been linked to stress responses to heat, oxidation, cold, and pathogens by inducing a rapid and transient NADPH oxidase-mediated H_2O_2 production, triggering abscisic acid biosynthesis, increasing H_2O_2 production, and prolonging stress tolerance duration (Zhou et al., 2014). In tomato plants, H_2O_2 has been found to be involved in the crosstalk between ethylene and brassinosteroids during salt stress conditions (Zhu et al., 2016).

The Burned sample presented a differentially expressed protein previously reported as related to the de-etiolation process (CURL-3) (Koka et al., 2000). The Burned sample is characterized by the etiolated leaf zone formation, the expression of the CURL-3 protein suggests that the process of de-etiolation was triggered in the Burned leaf zone after the 10-day recovery.

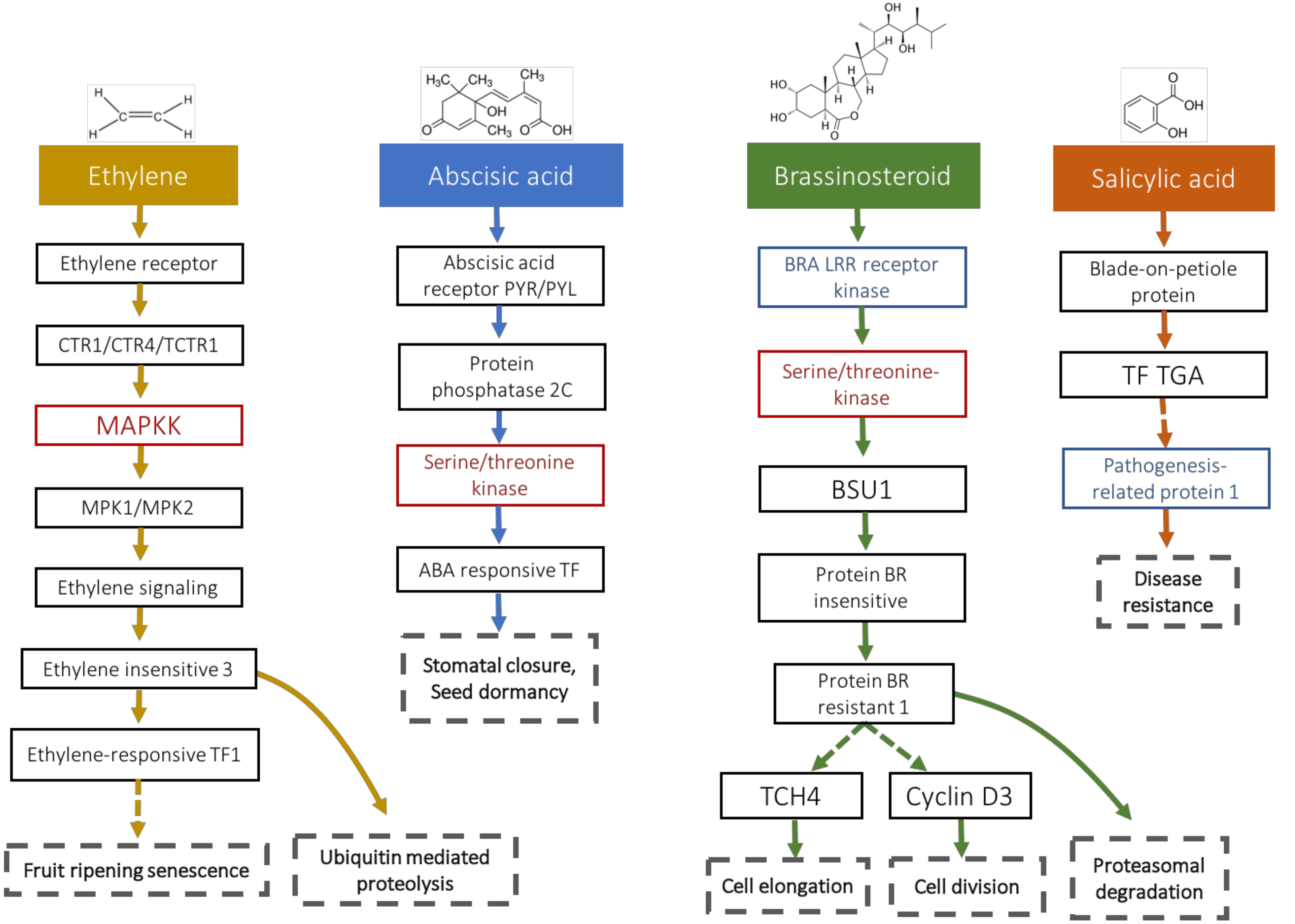

Figure 13. Simplified pathways of the hormones ethylene, abscisic acid, brassinosteroid, and salicylic acid hormones. Proteins found to be more abundant in the Limit and Burned are marked with a dashed-line, proteins only found to be more abundant in the Burned sample are marked with a dotted line. Dashed boxes are the physiological hormone response. TF: transcription factor, BRA: brassinosteroid.

The protein-interaction network analysis of the Burned sample showed a unique cluster (cluster 3) composed of proteins only related to high light stress response, those were a group of 10 chlorophyll a-b binding proteins (Q7M1K8, K4BL92, P27489, P10708, K4BE00, K4B878, K4BE01, P07369, P27524, K4CH43), and the photosystem II 22 kDa protein (P54773). This cluster is evidence of a possible recovery from photodamage by enhancing the photosynthetic antenna synthesis. The photosystem recovers using repair cycles for PSII, which requires the monomerization and migration of the phosphorylated dimeric PSII complexes to non-appressed regions of the thylakoid, where all the necessary components for the repair cycle are enriched (Suorsa et al., 2014; Yamamoto et al., 1981).

D1, D2, and CP43 proteins are dephosphorylated, and the degradation of D1 proteins is carried out by FtsH and Deg proteases. The synthesis and thylakoid insertion of D1 is performed by the SecY translocon and ribosomes, and various auxiliary proteins are responsible for the PSII assembly. The D1 and sometimes, D2, PsbH, and CP43 proteins are replaced in the PSII complex while the other members of the complex are recycled (Aro et al., 1993; Järvi et al., 2015). Furthermore, the singlet oxygen radicals near PSII can cause permanent damage to the D1 protein, which is proportional to the light intensity, while the production of superoxide and hydroxyl radicals near the acceptor side of PSI causes oxidative damage to chloroplast lipids and proteins (Nama et al., 2015).

The light harvesting chlorophyll a-b proteins (LHC) from photosystem II, a group of proteins reported in this study as part of the Burned sample differentially abundant proteins, have been found to have stabilization roles for the PSII supercomplexes structure and increase grana formation through enhancing van der Waals force amongst adjacent thylakoid membranes, and, lastly, in the excitation balance between PSII and PSI (Kim et al., 2009). It has been shown that the relative quantity of antenna proteins decrease together with the functional antenna size during high light stress, but LHCII monomers increase during plant acclimation (Bielczynski et al., 2016). In our dataset, the antenna complex proteins appeared to be downregulated in the Burned sample, along with the reaction center proteins of photosystem II CP43 and CP47, D1, D2, and PSI iron-sulfur center. However, in the same sample, PSII 10 and 22 kDa polypeptides, reaction centers H, and Psb28 proteins were found to be upregulated. While Psb28 protein has a role in PSII repair along with the CP43-lacking monomer, especially under high-temperature conditions (Sakata et al., 2013), still, the exact mechanism remains unknown. In cyanobacteria, Psb28 has been seen to bind to CP47, and to be involved in the synthesis of chlorophyll and apoproteins of chlorophyll-binding proteins CP47 and PsaA/PsaB (Dobáková et al., 2008). Therefore, the group of upregulated proteins could have similar functions with the aid of the repair and *de novo* synthesis of PSII complex proteins.

4.5 Conclusion

The importance of understanding plants defense from abiotic and biotic stresses relies on the development of strategies to grow plants in adverse conditions. We reported on proteins involved in two different levels of high light stress (~5,000 W m^{-2}, and ~3,000 W m^{-2}), with abundancies that directly respond to the light intensity increase. Also, we identified differentially abundant proteins during either only the photodamaged/de-etiolation condition or only the medium intensity light stress in a very localized leaf tissue response. The study of these proteins with a direct response to the light intensity variation is interesting because their genes can be explored as to find new light-regulated genes that can be further explored for biotechnology purposes, for the production of biomolecules of commercial value. We observed the possible exclusive involvement of the salicylic acid hormone in photodamaged tissue, and we reported on the role of PSII 10 and 22 kDa polypeptides, and reaction centers H and Psb28 in non-photochemical quenching and recovery of photosystem II. Future elucidation on the characterization of the salicylic acid role in photodamage is necessary, along with a functional genomics study of uncharacterized proteins reported in the differently light-stressed samples.

CHAPTER 5: Manuscripts III and IV

Connecting statement

The differential abundance of proteins in response to the experiments from Chapter 4 directed the experiments that are presented in the current chapter. This chapter, along with chapter 6, is expected to be published as two manuscripts (manuscripts III and IV) due to the findings and amount of data collected. The results from the red LED light treatment of high intensity, provided the starting point of the next experiment performed under the same conditions, however, using a blue LED.

The goal of this chapter was to establish the comparison between the plant responses to extreme high-light stress under different wavelengths. To accomplish this, a new proteomics experiment implementing a label-free MudPIT strategy was performed, and the abundance of key proteins was investigated. Plant stress indicators were measured and compared in both light treatments. mRNA quantification through RT-qPCR was performed to further investigate the levels of regulation control of proteins of interest (Psb28, PsbR, PsbS, and PsbH). The findings, along with the results discussion and conclusions of the comparisons achieved are presented in this chapter.

Manuscript III and IV: Plants response to extreme light-induced stress is wavelength-specific (Part I and Part II)

Abstract

Photosynthesis is the most important metabolic process in plants and is the one most affected by abiotic stresses. Plants deal with extreme light conditions through the emission of energy in the form of heat, a process that helps to maintain photosynthesis efficiency, called non-photochemical quenching (NPQ). In this study, we compared the changes in the plant proteome and photosynthetic parameters under extreme high-light conditions (5,000 W m^{-2}) with blue and red LEDs (470 and 655 nm peak wavelengths). The photosynthetic parameters analysis showed a 3-fold higher NPQ value on the blue treatment when measured after the light-induced damage when compared to the red, after a 10-day recovery period. A comparative proteomics (MudPIT 2D-LC-MS/MS) study was performed to explore the relative abundance of PSII and oxygen complex proteins that presented differential abundance between light treatments (PsbS, PsbH, PsbR, and Psb28). These four proteins are involved in photoinhibition and participate in NPQ or the biosynthesis/assembly of PSII. The mRNA differential expression of the candidates was later accessed through an RT-qPCR. An 8-fold abundance increase of PsbS was detected in the blue light treatment. This protein structure was recently unveiled, and its role as a sensor of overexcitation was suggested, although the mechanism details are still unknown. The blue light treatment had a higher response of NPQ, and most proteins of PSII and OEC complexes had no change in abundance when compared to the control. The red light treatment increased the proteins from PSII and OEC while presenting a low level of NPQ and PsbS transcripts. Altogether, our study showed that under extreme light conditions, light wavelengths impact the plant proteome differently. We suggest that the blue light appears to stimulate energy dissipation mechanisms, while red light causes a more advanced photoinhibition state.

Keywords

Abiotic Stress; Photoinhibition; Photosystem II; High Light; NPQ; LED.

5.1 Introduction

Photosynthesis is the metabolic process most impacted by abiotic stress. It is affected by photosystem II efficiency, CO_2 assimilation rate, RuBP content, RUBISCO activity, photorespiration and the electron transport chain (Saibo et al., 2009). Plants under full light absorb up to 10% of the available light, directing energy to the photosynthetic electron transport (Demmig-Adams and Adams, 1996). The excess energy must be dealt with through photoprotection mechanisms in order to protect the photosystems. One of these mechanisms is to eliminate the excess energy thought heat emission, a process known as non-photochemical quenching (NPQ). NPQ is regulated in multiple levels: through the acidification of the thylakoid lumen, caused by linear and cyclic electron flow, protein accumulation (such as PsbS) and the xanthophyll cycle (Murchie and Lawson, 2013). The protonation of PsbS and zeaxanthin formation on the xanthophyll cycle leads to PSII antenna conformational modifications, resulting in quenching of the PSII antenna excitation energy (Ruban et al., 2012). NPQ can be measured by the fluorescence emission under a high-intensity light pulse into a dark-adapted leaf and measurement of the closed PSII center maximal fluorescence (Fm) value, the maximal fluorescence of light-adapted state (Fm’), and calculating the values for the equation: *NPQ = (Fm*

– *Fm')/Fm'*. Other parameters provide insight into photosynthesis efficiency, as Fv/Fm, ETR, ΦPSII, and qP (Maxwell and Johnson, 2000)

A recent high-light-induced stress treatment utilizing a narrow red spectrum LED light under a 5,000 W m^{-2} intensity was reported (Chapter 4). The effect of the treatment was studied in depth by using a labeled proteomics strategy (iTRAQ). The authors identified key proteins involved in the long-term response to the stress condition, and the differential abundance of proteins as part of the PSII and OEC complex. These proteins present different roles on the photosynthesis reactions, from NPQ enhancement to complex assembly facilitators. Kromdijk et al. (2016) demonstrated an increase of 15% in crop productivity by utilizing transgenic tobacco containing VDE, PsbS and ZEP genes from *Arabidopsis*, due to the acceleration of NPQ relaxation duration on fluctuating light. The PsbS structure was identified, showing the pH-induced changes in the protein dimer conformation (Fan et al., 2015). PsbS has been related to NPQ, and, although the mechanism remains unknown, its role as a sensor of over-excitation has been suggested (Croce, 2015). PsbR, a 10 kDa polypeptide, has been suggested to be the PsbP and PsbQ docking protein for the oxygen-evolving complex formation (Suorsa et al., 2006). *Arabidopsis* plants lacking PsbR and PsbQ were shown a change in the PSII complex proteins organization and changes in the short-term adaptive mechanisms (Allahverdiyeva et al., 2007). Recently, a cross-linking mass spectrometry-based study elucidated the Psb28 binding to be the cytochrome b_{559} (Weisz et al., 2017). The Psb28 protein has been linked to high light stress conditions at high temperature when PSII is damaged, and increased PSII turnover is necessary (Sakata et al., 2013). The PsbH protein is part of the PSII complex core, and it has a role in its stabilization, on the acceptor side electron transportation (Pagliano et al., 2013). The cyanobacterium *Synechocystis* 6803 psbH^{-} mutant presented PSII electron transfer impairment between quinones Q_A and Q_B, and higher sensitivity to photoinhibition under high light. In *Arabidopsis*, PsbH has been shown to be important for CP47 accumulation, a component of the inner antenna complex, which directs the energy at the outer antennae to the reaction center (Bečková et al., 2017).

Light absorption capacity is wavelength dependent, mainly due to pigments absorption spectra. As pigments have their peak absorption under different wavelengths, the high-light damage could impact the pigments in a wavelength-dependent manner. To define if the differential abundance of proteins is a consequence of not only the high irradiation but also the chosen wavelength, we performed the experiment implementing two different LED wavelengths.

In this work, we used blue and red LEDs to create a high-light induced stress condition on tomato leaves, followed by our previous work using red LEDs alone. A blue light was chosen due to the plants' well-characterized plant physiological response to blue light, and the involvement of blue photoreceptors in triggering plant acclimation (Walters, 2005; Walters and Horton, 1995). Chlorophyll fluorescence parameters were measured to observe the level of damage on photosynthesis under the different wavelengths with different time spans. A proteomics approach was utilized to generate a broad characterization of the protein abundance on the leaves. The differential abundance was further investigated through a quantitative mRNA analysis. The results were compared to a recent study utilizing the same methodology but with a red LED (655 nm) (Chapter 4). We assessed the functional role of the differentially expressed proteins to determine if the plant long-term stress response was carried out in the same manner under different LED treatments.

5.2 Materials and methods

5.2.1 Plant variety

Tomato (*Solanum lycopersicum*) variety Heinz1706 was provided by HeinzSeed (Stockton, CA, USA). Heinz 1706 is the variety that was recently genetically sequenced (The Tomato Genome Consortium, 2012), the genome has a haploid chromosome number of 12, containing 900 Mb and 35,000 protein-coding genes (genes or transcript containing an open reading frame) and genome annotation is still in development.

5.2.2 Plant growth and sampling

The tomato seeds were planted and grown hydroponically in rockwool (Grodan A/S, Dk-2640, Hedehusene, Denmark). Ten plants were incubated under cool-white fluorescent bulbs (4200 K, F72T8CW, Osram, USA) in a growth chamber (TC30, Conviron, MB, Canada). The environmental conditions in the chamber were controlled at 50% relative humidity (RH), 25°C light/dark temperature, ambient CO_2 concentration, and a 16 h photoperiod with an irradiance level of 55 W m^{-2} (approximately 250 µmol m^{-2} s^{-1}). Fresh Hoagland nutrient solution was provided every other day. Hoagland composition (Epstein, 1972): 6.5 mM KNO_3, 4.0 mM $Ca(NO_3)_2.4H_2O$, 2mM $NH_4H_2PO_4$, 2.0 mM $MgSO_4.7H_2O$, 4.6 µM H_3BO_3, 0.5 µM $MnCl_2.4H_20$, 0.2 µM $ZnSO_4.7H_20$, 0.1 µM $(NH_4)_6Mo_7O_{24}.4H_2O$, 0.2 µM $CuSO_4.5H_20$, 45 µM $FeCl_3$. After the growing period of 30 days, leaves of tomato plants were placed under a royal-blue LED light (470 nm, LXML-PR01-0500, Philips-Lumileds, CA, USA) with an average irradiance level of 5,000 W m^{-2} (approximately ~25,000 µmol m^{-2} sec^{-1}) on a ~1 cm^2 spot in the center of a mature leaf for 5 min. After the LED treatment, plants were returned to the growth chamber for a 10-day period. Each group of 10 treated leaves was then collected as one biological sample, to eliminate individual variances. The leaves were dissected, and the areas corresponding to the light treated zone (Burned), adjacent (Limit) and rest of the leave (Regular) were kept separated (Figure 14-A), the remaining parts were discarded. Plant tissues were kept under -80˚C before protein extraction (Yamamoto et al., 1981). The control plant group was kept in the growth chamber during the full experiment without the treatment irradiation, and the experiment was replicated three times.

5.2.3 Light treatment and temperature measurements

Tomato leaves were set under the royal-blue LED lights, approximately 2.5 cm distance, where light intensity was stable at 5,000 W m^{-2}. The photon flux densities of the 470 and 655 nm LED light were approximately 21,000 and 25,000 µmol m^{-2} sec^{-1}, respectively. Light intensity was measured by a spectroradiometer (PS-300; Apogee, Logan, UT, USA). A filtering lens with known transmitted percentages was placed on the spectroradiometer to attenuate the high light (Wu and Lefsrud, 2018). Briefly, the LED assembly was mounted on a water jacket (ST-011, Guangzhou Rantion Trading Co., China) and attached to a cluster concentrator optic (25 mm focal length, No. 263, Polymer Optics, Wokingham, Berkshire, UK). All the rays from the diodes were collimated by the cluster concentrator optic, resulting in a small focal spot of 12 mm in diameter. An isotemp (4100R20, Fisher Scientific, Hampton, NH, USA) bath circulator was used to circulate a 0 ºC coolant in the water jacket. Leaf temperature was measured in three biological replicates with three copper constantan thermocouples (type T, 0.03 mm, Omega Engineering Canada, QC, CA) (Dixon and Grace, 1983). The temperature was recorded every five seconds for 15 min total, including 5 min before and after the light treatment as well as during the 5-min wavelength treatment. The thermocouples were placed on the surface of the leaf using glue extracted in chloroform from clear adhesive tape. The thermocouples were placed: on the center of the leaf corresponding to the Burned sample, approximately 1 cm and 2 cm from the first thermocouple (center). The temperature of the LED apparatus was also recorded for reference.

5.2.4 Fluorescence and analysis of measurements

Chlorophyll (Chl) fluorescence measurements were performed using a leaf chamber fluorometer (LI-6400-40, LI-COR Inc., Lincoln, NE, USA). Measurements were perfromed in triplicates to obtain the photochemical efficiency of PSII (Fv/Fm) of the dark-adapted leaves with a PPFD-response at 100 mmol m^{-2} s^{-1}. The measurements were performed following previously established guidelines (Murchie and Lawson, 2013). Briefly, a modulated red radiation of approximately 2 μmol $m^{−2}$ $s^{−1}$ was used to excite fluorescence by using a frequency and a pulse width of 20 kHz and 3 μs, respectively. About 8,000 μmol $m^{−2}$ $s^{−1}$ saturating radiation pulse of 0.8 s was utilized. The open PSII center (F_0) minimum Chl fluorescence and the closed PSII center maximal Chl fluorescence values were obtained after a 20 min dark-adaptation period. After, leaves were irradiated continuously, and the steady-state fluorescence (Fs) was determined. A new 8,000 μmol $m^{−2}$ $s^{−1}$ saturating pulse was emitted for obtaining the maximal fluorescence of light-adapted state (Fm’). Then, the actinic PPFD was turned off and a far-red (740 nm) light was used to measure the minimum fluorescence of light-adapted state ($F_{0'}$). The obtained values were used to calculate the following: i) Fv/Fm = (Fm − F_0)/Fm, the maximum dark-adapted PSII photochemical efficiency; ii) ΦPSII = (Fm’ − Fs)/Fm’, the effective light-adapted photochemical efficiency; iii) qP = (Fm’ − Fs)/(Fm’ – $F_{0'}$), the photochemical quenching; iv) NPQ = (Fm – Fm’)/Fm’, the non-photochemical quenching; and v) ETR = ΦPSII × 0.5 × 0.84 × PPFD, the PSII electron transport rate.

5.2.5 Net photosynthesis rate (Pn)

Net photosynthesis rate (Pn) was determined using the leaf chamber fluorometer of the portable photosynthesis system (LI-6400, LI-COR, USA) on a fully expanded tomato leaf. The light condition was set as 100 µmol m^{-2} s^{-1}, with an equal amount of 470 and 630 nm light. The environmental factors controlled during the measurement were block temperature (23 ± 1ºC), CO_2 concentration (400 ± 1 ppm) and relative humidity (RH, 50-60%). The measurements were taken every 4 s for 15 min and replicated in three different plants for each wavelength treatments and the control. Mean values of the parameters of leaf photosynthesis rated and Chl fluorescence were tested for the two wavelengths effects (red light and blue light) using Tukey's HSD test ($p<0.05$).

5.2.6 Protein extraction and digestion

A 100 mg sample was processed for protein extraction and digestion as previously described with modifications (Abraham et al., 2011). Briefly, leaves were ground by mortar and pestle in liquid nitrogen. The powder was solubilized, and proteins were extracted with buffer containing detergent (100 mMTris-HCl/4% SDS pH 8). Cells were boiled for 5 min before they were sonically disrupted on an ice bath (40% amplitude, 10s/10s on/off cycles) for a total duration of 2 min. The crude extract was processed by centrifugation at 4˚C for 10 min at 4500 x g. The sample was adjusted to 10 mM TCEP (Tris(2-carboxyethyl)phosphine) (Sigma-Aldrich Canada, Oakville, ON), instead of DTT used in the cited protocol, TCEP was used as it is a more powerful reducing agent and more resistant to oxidation. Non-protein contaminants were removed by 20 % trichloroacetic acid (TCA) precipitation and washed in ice-cold acetone followed by overnight incubation at -80 ˚C (Wu et al., 2014).

Proteins were denatured in 8M urea in Tris-HCl pH 8.0 for 30 min at room temperature, sonication pulses of 10 s and 20 s on/off during 5 min in cold water were applied to cells to solubilize proteins and avoid SDS precipitation. A fraction of the sample was diluted to 1M urea for protein concentration measurement by BCA assay (Pierce Biotechnology, Waltham, MA). The reduction was made by adjusting the sample to 20mM TCEP-HCl. Cysteines were blocked, and disulfide bridges were prevented with 20 mM iodoacetamide (IAA) at room temperature for 30 min in the dark. 1-2 mg of proteins were digested with modified sequencing grade trypsin (Promega, Madison, WI, USA), for 12 h incubation at 37 ˚C. An acidic solution (200 mM NaCl, 0.1% formic acid) was added to stop the trypsin reaction. Trypsin and undigested proteins were removed by a 30 kDa MWCO amicon ultra-centrifugal filter (Millipore Sigma). Peptides were desalted using a centrifugal column (Sep-Pak Plus C-18, Waters Limited, Mississauga, ON) before peptide quantification (Pierce Quantitative Colorimetric Peptide Assay, Thermo Fisher Scientific, San Jose, CA) and storage at -80˚C (Patel et al., 2015).

5.2.7 LC–MS/MS

A multi-dimensional protein identification technology (MudPIT) approach was performed to obtain a label-free shotgun proteomics analysis (Kislinger et al., 2005). A high-performance separation of the peptides was obtained by using a 2D-LC separation coupled online with the mass spectrometer (LTQ XL, Thermo Fisher Scientific, San Jose, CA) as previously described (Patel et al., 2015). Approximately 60 µg of peptides from three biological replicates of each condition were bomb-loaded through cell-pressure chamber into a biphasic column packed with ~5 cm of strong cation exchange (SCX) resin and ~5 cm of C18 reversed phase (RP) material (Luna 5 µm 100A and Aqua 5 µm 100A, respectively; Phenomenex, Torrance, CA). The packed column was washed through the cell-pressure chamber for 60 min with H_2O (MS-grade Optima, Thermo Fischer Scientific) with 0.1% formic acid to remove salts and impurities. Peptide spray was generated by a front column containing an integrated nanospray emitter tip (100 µm i.d., 360 µm o.d., 15 µm i.d. tip, New Objective, Woburn, MA) loaded with ~15 cm of C18 material and in-line with the back column. Liquid chromatography was carried out by an HPLC Surveyor Plus^{TM} (ThermoScientific, San Jose, CA, USA) at a ~300 nL/min flow rate at the nanospray tip. The peptides were first washed in an off-line run to remove residues that interfere with the mass spectrometry analysis, as NaCl, SDS, and urea.

A 12-step gradient (24 h analysis duration) containing salt pulses was utilized to elute the peptides from the column in a nanoESI-MS/MS approach as previously described (Abraham et al., 2011; McDonald et al., 2002; Wilmes et al., 2008). The gradients contained an increasing ammonium acetate concentration (0 – 500 mM), followed by a reverse phase gradient elution of up to 2 h duration. The data-dependent acquisition parameters inputted in Xcalibur (v.2.0.7 SP1 Thermo Fisher Scientific) where: the 5 most intense MS/MS were submitted to collision-activated dissociation (35% energy) after every full scan, 2 microscans were averaged for every full MS and MS/MS spectrum, for both full and MS/MS scans a 3 m/z isolation width was allowed. A dynamic exclusion repeat of 1 for 60 s.

5.2.8 Database searching and statistical analysis

Thermo RAW files were used to extract the MS/MS spectra which were searched against a database containing the target and reverse peptide sequences of *Solanum lycopersicum* (UNIPROT, proteome UP000004994) containing 33,952 entries, and common contaminants (cRAP v. 2012.01.01, obtained from http://www.thegpm.org/crap). MSAmanda 2.0 (Dorfer et al., 2014) algorithm was used for protein identification through the software Proteome Discoverer v.2.1.1. (Thermo Fischer Scientific, Inc). A search against the reverse sequence (decoy) tomato database. Search results were rescored by Percolator to give a final 1% false discovery rate (FDR) using a randomized version of the same tomato database (score: -10log(PEP), identity threshold score for $p<0.05$: 13). The search parameters were set to maximum 2 missed cleavages, parent ion and fragment tolerance of 2.0 Da and 0.4 Da, respectively. Methionine oxidation (+15.99 Da), carbamylation of amines (N-term) and lysine side chains were set as variable modifications, and carbamidomethylation of cysteines (+57.05 Da) was kept as a static modification. Proteins were filtered to contain ≥ 2 unique peptides, and ≥ 4 PSM in the 2 biological replicates of each sample (4 conditions x 2 biological replicates), only proteins found in 4 out of 8 samples were further analyzed. Protein identifications and abundance values were expressed as NSAF, a normalized protein abundance index that estimates absolute protein content (Zybailov et al., 2006). The results were imported into Perseus (Tyanova et al., 2016) were the NSAF values were normalized across samples to account for differences in global protein abundance. Proteins with a fold change of ≥ 2.5 and ≤ 1.5 were considered as significantly differentially abundant, considering the coefficient of variance of abundance values in the control sample. Missing values were replaced by the single-value approach, by adding the limit of detection value (LOD) (Webb-Robertson et al., 2015). Differential abundance of candidates of interest was further studied with an RT-qPCR experiment.

5.2.9 Bioinformatics

A semiquantitative comparison of the protein abundance across all samples was performed as follows. Normal distribution of data was obtained by log2-transforming the abundance values (NSAF) after their normalization (Zybailov et al., 2006). Functional annotations (GO) of the identified proteins were obtained via ClueGO (Bindea et al., 2009). The network reflects the level of relationship amongst the GO terms assigned to the proteins used as input. The nodes reflect the statistical significance of their assigned terms by their size. Kappa statistics are used to calculate the degree of connectivity (edges), and the definition of functional groups (Huang et al., 2007).

5.2.10 RT-qPCR

Total RNA from leaf samples at Day 10 was extracted with the RNeasy® Plant Mini kit (Qiagen, Germany). QuantiTect® Reverse Transcription kit (Qiagen) was used to synthesize the cDNA as presented in the manufacturer's protocol. RT-qPCR primers were designed using the online tool Primer-BLAST from the National Center for Biotechnology Information (NCBI) (Table 3). The mixed solution of RT-qPCR reaction contained Platinum® SYBR® Green qPCR SuperMix-UDG with ROX (2×, Invitrogen, USA), reverse and forward primers mix (4.28 μM) and 20-fold-diluted cDNA template. All reactions were performed on a CFX Connect Real-Time PCR system (Biorad, USA). Reaction conditions were 10 min at 95 °C, followed by 40 cycles of heating at 95 °C and annealing at 60 °C for 15 and 60 s, respectively. Melting curves were carried out in each RT-qPCR to verify single-product amplification, The relative level of gene expression was calculated with the Livak method (2- (ΔΔCt)). The genes: protein phosphatase 2A catalytic subunit (*PP2Acs*) (Løvdal and Lillo, 2009) and clathrin adaptor complex subunit (*clat*) (Dekkers et al., 2012) were used as the reference genes. Measurements were recorded from three technical and three biological replicates for each experimental condition. The significant differences in mRNA quantitation samples and their control were evaluated using ANOVA, and pair-wise comparisons were adjusted with Tukey's test ($p \leq 0.05$).

Table 3. DNA primers for RT-qPCR used in this study.

Gene	Forward primer	Reverse Primer	PCR product size (bp)	Source
psb28	CCTCGCTCTCTTCTCGGAAT	GCAAAACGCGAACGGGATAG	98	This study
psbS	GGAATTGGCTTCACTAAGCA	AGTGGCTCTGCTTCATAGAT	155	This study
psbH	TCTGGTCCAAGACGAACTGC	CAAAGGGGTAGTTCCCCACC	93	This study
psbR	CAGGAAGCCCAAGGGAAAGG	GTCACCGCCCATATGGCTAA	153	This study
TPP2Acs	CGATGTGTGATCTCCTATGGTC	AAGCTGATGGGCTCTAGAAATC	149	Løvdal and Lillo, 2009
Clat	ATGCAATCACACCAGCAC	ACTCAGCACAACAACAAAGG	61	Dekkers et al., 2012

5.3 Results and discussion

5.3.1 Plant physiological stress measurements

The blue and the red light treatments (hereafter called BLT and RLT, respectively) were compared to the level of physiological damage. Like the RLT, the BLT performed in this study generated a highly dehydrated and damaged spot of ~1 cm diameter on the tomato leaves (hereafter referred as the Burned sample), and two other zones of lower light intensity (in decreasing intensity order:

Limit and Regular). After a recovery period of 10 days, the Burned area showed symptoms of de-etiolation, the Limit area showed a slightly darker green color, and the Regular area had no change in appearance (Figure 14-A).

Plants deal with the excess energy from high-intensity lights by emitting the energy in the form of heat, a process known as non-photochemical quenching (NPQ). Therefore, high-intensity light treatments in plants will not only cause light stress but also induces heat stress. Measurements of the plant leaf temperature is essential to understand the levels of NPQ and should be included when studying light stress. The temperature of the BLT measured in the center of the leaf shifted from 20˚C to about 60˚C, in the first minutes of the experiment and reached a peak at 73˚C at the end of the light treatment (Figure 14-B). A similar trend was measured by the other two thermocouples, with a difference of approximately 10˚C. The BLT temperature rose slower, compared to the red light. It reached a peak at ~280 s of experiment, which later decreased and was maintained constant at ~82˚C. The temperatures measured during the RLT resulted in double temperature increase when compared to the BLT. The maximum reached in RLT was about 120˚C, and the difference between the measurements with the three thermocouples was of approximately 50˚C.

The difference in temperature increase is a result of wavelength specific mechanisms from plants to deal with high-light induced stress. These mechanisms are not only at the physiological level, as seen in stomata opening, but also at the protein level, by strategies of NPQ. Light induced stomatal responses to red and blue light are well characterized, and are triggered by different signals (Inoue and Kinoshita, 2017). In red light, the stomatal opening due to CO_2 concentration changes, is mostly due to a signal from the mesophyll (Mott et al., 2008). In blue light-mediated response, a more complex response is observed. The auto-phosphorylation of phototropins triggers the stomatal opening, along with the cryptochrome reduction of ABA concentration (Inoue and

Kinoshita, 2017). With lower concentrations of ABA, its stomata-closure induction does not occur, impacting the ABA signaling in guard cells (Boccalandro et al., 2012). The blue and red stomata opening responses could have different activation time requirement, resulting in different cooling observations. Different pathways leading to the activation of NPQ could be responsible for the temperature patterns observed in the treatments by requiring different trigger duration or thresholds. The hypothesis of the existence of wavelength-dependent mechanisms for high-light induced stress response will be addressed in this study.

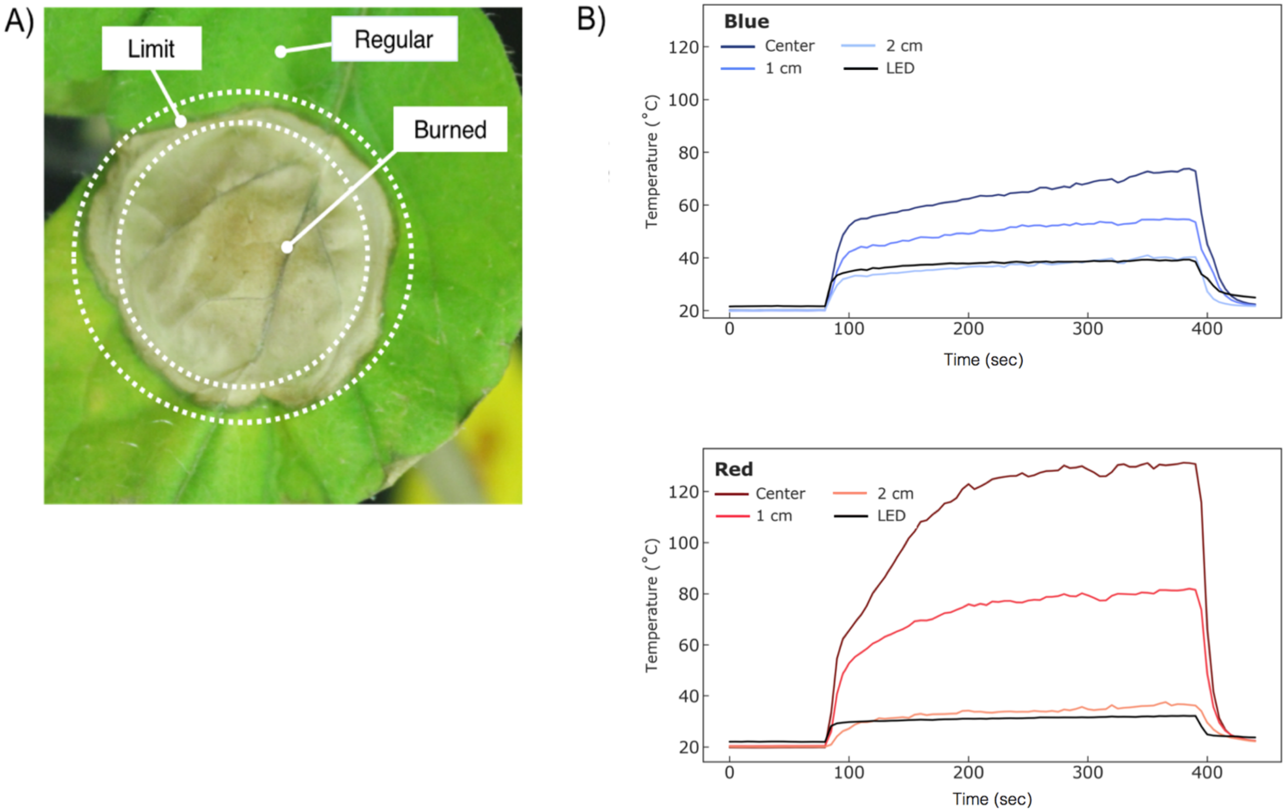

Figure 14. Sampling description and leaf temperature measurements. (A) Tomato leaf 10 days after treatment with royal blue (470 nm) LED light (~5,000 W/m^2, approximately 21,000 µmol

m^{-2} s^{-1}), the picture shows the leaf sampled areas: Burned, Limit and Regular. (B) Leaf temperature measured by 3 thermocouples positioned on the center of the leaf, and 1 cm, or 2 cm from the center, during the high-light. Treatments were performed with a blue and a red LED, separately. The temperature of the LED device was recorded. The light treatment started at 80 s and ended at 385 s (~5 min duration).

5.3.2 Impact of high-light induced heat stress in photosynthesis efficiency

We measured plant stress indicators to determine the extent of the physiological damage caused by the BLT and RLT, and if the leaf could recover its photosynthetic efficiency. A comparison of the measurements of the net photosynthesis rate (Pn), the maximum quantum efficiency of PSII photochemistry, and the non-photochemical quenching values of the BLT and RLT are shown in Figure 15.

The Pn measurement indicates the quantity of CO_2 assimilated by the plant. The control Pn value (~2.58 µmol CO_2 m^{-2} s^{-1}) agreed with values reported in the literature at 100 µmol m^{-2} s^{-1} of light (Zhang and Wang, 2011). The negative values of Pn indicate the higher levels of respiration over photosynthesis. Higher Pn values indicate a higher acclimation of photosystems for CO_2 fixation. A lower Pn would be expected from Day 0, compared to Day 10, since the measurements were taken immediately after the treatment, when components of the photosystem complexes would probably not have been yet recovered/*de novo* synthesized. The RLT had a slightly higher value for Day 0 compared to Day 10, while the blue sample had similar values in both data points. Although RLT had a small decrease on Pn from Day 0 to Day 10, both BLT and RLT indicate the non-recovery of the tissue, with the driving of energy to respiration, rather than photosynthesis.

The Fv/Fm parameter is an indicator of the maximum quantum yield of PSII. It measures the dark-adapted fluorescence emission variation in plants as a measurement of PSII damage. Two measurements are necessary: F_0 which is obtained when a low-light that cannot drive photosynthesis is utilized, and Fm, the maximum fluorescence emitted when a saturating light pulse causes the reaction centers to be closed. In stressed plants, the Fv/Fm ratio is decreased, since fewer reaction centers are open. In healthy plants, the maximum Fv/Fm value is ~0.83 (Murchie and Lawson, 2013), agreeing with the value we obtained for the control plants (0.81±0.003). The plants treated with BLT presented a slightly higher Fv/Fm (not statistically significant) on Day 10, compared to Day 0, which could indicate a slow recovery of PSII after the 10-days period. The measured Fv/Fm values from RLT did not present a change. At Day 0, different Fv/Fm values of RLT and BLT would be expected, due to the blue wavelength impact in photosystem efficiency, photosynthetic electron transport, chlorophyll content, a/b chlorophyll ratio (and chlorophyll-PSII binding proteins) (He et al., 2017).

Although we obtained similar values of Fv/Fm for RLT and BLT on Day 0 and Day 10, as expected, a light treatment wavelength impact was observed in the NPQ parameter. The NPQ results showed statistically different values for RLT and BLT on Day 0. In BLT, NPQ was 3-fold higher in the Day-0 when compared to the RLT values. Non-photochemical quenching represents the emission of heat as an energy dissipation strategy during high-light stress. A high NPQ value is interpreted as a high heat loss rate, which would be expected from stressed plants that are unable to direct light energy to the photochemical route.

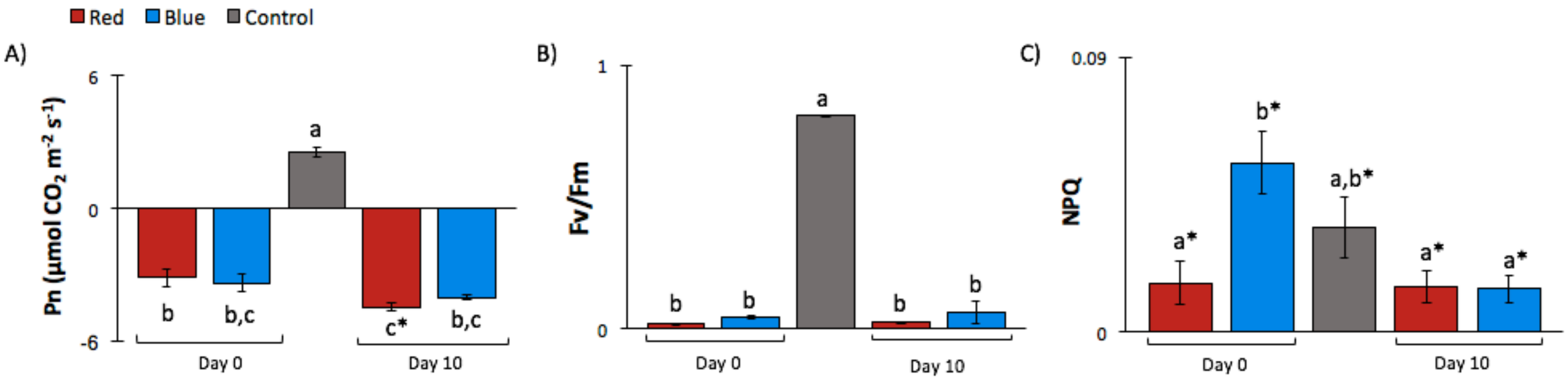

Figure 15. The photosynthetic parameters measurements. Changes in parameters from tomato plants (*Solanum lycopersicum*) stressed with deep-red (655 nm) or royal-blue (470 nm) LEDs at ~5,000 W m^{-2} intensity and control (no high-light treatment). Measurements were made using the portable photosynthesis system LI-6400 (LI-COR, USA). Data points from “Day 0” were obtained immediately after the high-light treatment, and “Day 10” data points were collected 10 days after the treatment. (A) Net photosynthesis rate (µmol CO_2 m^{-2} s^{-1}) measured at 100 µmol m^{-2} s^{-1}. (B) The maximum quantum efficiency of PSII photochemistry (F_v/F_m). (C) Induction of non-photochemical quenching (NPQ). Vertical bars indicate the ± standard error (SE) of the means (n=3). Means presenting a different letter are significantly different at $p<0.01$, or $p<0.05$ when indicated by (*), according to the Tukey's multiple comparison tests.

5.3.3 Photosystem II related proteins abundance comparisons

Proteomics analysis of the leaves after a 10-day period was performed. We chose to carry the proteomics analysis with the 10-day samples since the samples after the extreme high-light-induced stress would have yielded, in the majority, proteins degraded by the level of light and heat (as NPQ). The 10-day period allows for the observation of the functions activated after the damaged central pathways are restored. In the proteomics analysis of the RLT, we found that the Burned sample had a considerable unique pool of proteins showing high abundance when compared to the Regular and Limit samples (Chapter 4). Amongst the proteins presenting functions in photosynthesis reactions, Psb28, PsbH, PsbR, PsbS had, respectively, 2.11, 2.45, 3.1 and 2.16-fold increase in abundance when compared to the control. They were more abundant in Burned when compared to the other treatments (Limit and Regular) (Table 4). PsbH was found to have a lower abundance in the Limit sample when compared to the control. Due to their differential abundance patterns, these proteins were chosen for further investigation.

To determine if the abundance of the four proteins followed the same pattern under a different wavelength, we carried out a proteomics experiment on the plant leaves treated with the BLT. In this study, we performed a global proteomics approach for comparison with the RLT dataset. It is noteworthy that although both datasets are not comparable in quantitative terms since the abundance values are from different proteomics techniques (ion intensity for RLT and normalized spectral counting (NSAF) for BLT), the comparison of their representativeness amongst the other proteins of their datasets is still valid. While the values of protein abundance of the Burned sample on the BLT treatment were negative, these values were not significantly different from the control, since the cutoff established for BLT dataset was 2.5 and -1.5 for up and down, respectively. We validated the comparison of the proteins of interest by a quantitative mRNA experiment.

Table 4. The abundance of proteins related to the photosynthesis after red and blue high intensity LED treatments. Values are ratios of the treatment (Burned, Limit, or Regular) and Control. [a]Data from a previous experiment (Chapter 4). $^{+}$ Value statistically higher when compared to the control. $^{-}$ Value statistically lower when compared to the control. Statistical tests for the Red dataset where carried with an FDR-controlled p<0.05 and the cutoff for high or low abundant were 0.7 and -0.7 log2-transformed fold change, respectively, and 2.5 and -1.5 log2-transformed fold change for the Blue dataset.

	BLUE			RED[a]			LOCATION	FUNCTION
Protein	**Limit**	**Burned**	**Regular**	**Limit**	**Burned**	**Regular**		
Psb28	0.02	-1.27	0.14	1.01	2.12^{+}	0.97	OEC, binds to cytochrome b_{559}	PSII assembly factor
PsbS	1.45	-0.34	0.15	1.43	2.50^{+}	1.25	LHCII	NPQ relaxation process
PsbH	0.73	-0.23	0.74	0.61^{-}	3.13^{+}	1.45	PSII complex core	Electron transfer between Q_A and Q_B
PsbR	1.24	-0.12	1.52	0.89	2.16^{+}	1.11	OEC, binds to PsbQ and PsbP	OEC formation

5.3.4 Correlation of gene expression with protein abundance

We then evaluated if the protein abundance was a result of regulation at the gene transcription or mRNA translation level of Psb28, PsbH, PsbS, and PsbR. Figure 16 shows the results of the mRNA quantitative analysis by RT-qPCR of the mRNAs of interest in the various samples (Burned, Limit and Control) in the two light treatments (BLT and RLT).

The PsbH protein abundance agreed with the mRNA expression level only in the RLT Limit sample. PsbH gene is present in the chloroplast, and the regulation of chloroplast genes involved in the assembly and biosynthesis of photosystems is regulated by co-location for redox regulation (CoRR). This mechanism holds one of the current theories as to why plants retained a separate genetic system despite the energetic costs of maintaining it (Allen et al., 2011). The rbcL and psbA genes, encoding for a subunit of RUBISCO and the D1 protein, respectively, have been reported as regulated by CoRR (Allen, 2017).

The protein and mRNA quantifications of PsbR in the red Burned presented an opposite pattern, while in the other samples, the abundance was comparable (blue and red Limit) or lower (red Burned) than the control. The *psbr* gene is transcribed in the nucleus and, later, is transported to the chloroplast. The PsbR protein is localized in the proximity of the OEC docking (Pagliano et al., 2013), and is responsible for the stable assembly of PsbP, an OEC protein, to the core of PSII.

The transcription level of the *psb28* gene was stable across all treatments. Only the blue Limit sample was statistically significantly lower than the red Limit. The protein abundance measurement of Psb28 in the red Burned sample was in discordance with the mRNA trend. Psb28 is a protein with a role in the regulation of chlorophyll availability during PSI and II biosynthesis

(Dobáková et al., 2008). Recently, the Psb28 location has been determined as of a binder to cytochrome b_{559} (Weisz et al., 2017).

PsbS had no statistical difference between the control in all the treatments, except for blue Burned, where an 8-fold increase was detected. Although PsbS protein measurements in red Burned showed to be in high abundance, the mRNA level was equal to the control. The PsbS protein has been found to be a sensor of overexcitation in plants. It presents fast and transient accumulation in *Chlamydomonas reinhardtii* under high-light conditions (Tibiletti et al., 2016), although the NPQ trigger in algae is better linked to the LHCSR3 protein than to PsbS. Part of the LHC multigenic family, PsbS is the only member of the family who, probably, is not a stable pigment-binding protein (Fan et al., 2015).

Overall, the results of the mRNA analysis indicate that Psb28, PsbR, and PsbH proteins had mRNA values lower than proteins levels. Studies have suggested that protein abundances and mRNA Pearson correlation are only up to 0.40 (Maier et al., 2009), and, interestingly, the remaining variation could be explained by different levels of regulation, or by differences in the proteins and mRNA half-lives.

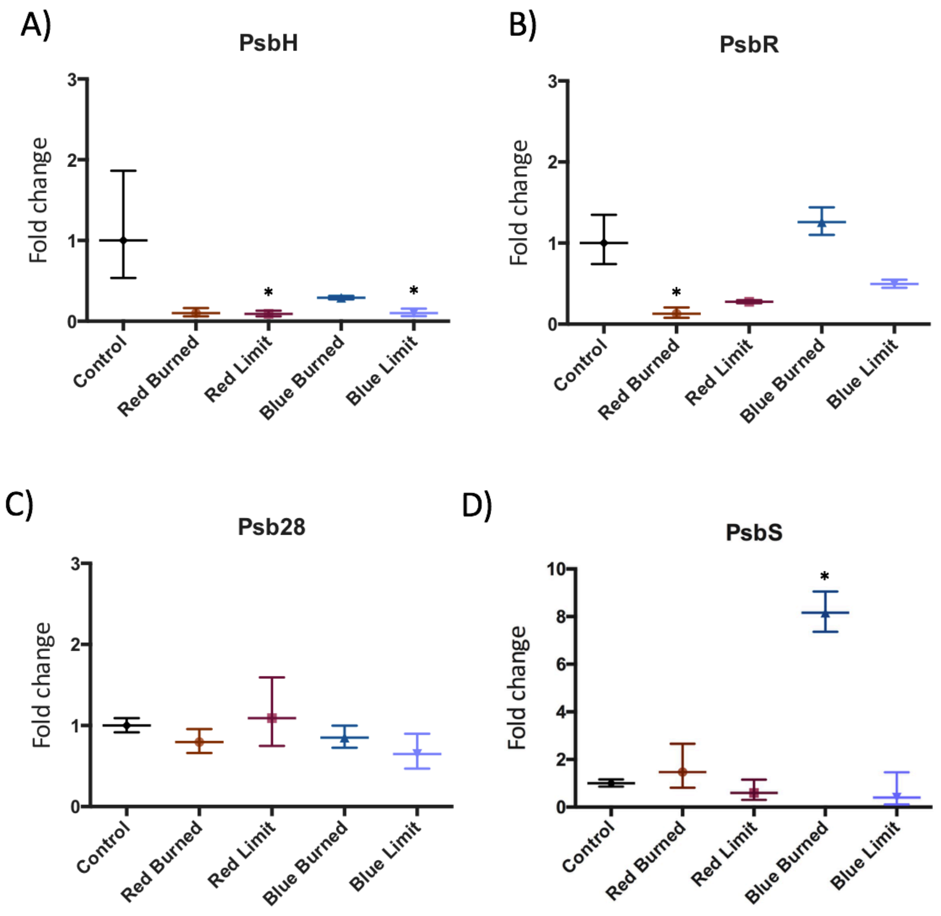

E)

	PsbH		**PsbR**		**Psb28**		**PsbS**	
	Protein	*mRNA*	*Protein*	*mRNA*	*Protein*	*mRNA*	*Protein*	*mRNA*
Red Burned	up	nc	up	down	up	nc	up	nc
Red Limit	down	down	nc	nc	nc	nc	nc	nc
Blue Burned	nc	nc	nc	nc	nc	nc	nc	up
Blue Limit	nc	down	nc	nc	nc	nc	nc	nc

Figure 16. Comparison of transcription and translation levels. A, B, C, and D) mRNA Fold changes of genes of interest (PsbH, PsbR, Psb28, and PsbS, respectively) compared to the control. The data were analyzed by ANOVA and was Tukey adjusted multiple comparison of the means with a p=0.05 significance level (* statistically different to the control). Error bars show standard

deviations with n=3 biological replicates. (E) Comparison of trends of mRNA and protein abundance in each sample treatment. nc: no change compared to the control.

5.3.5 Other proteins identified in the blue light dataset

The global proteomics analysis of BLT resulted in a total of 2,228 high confidence proteins (1% FDR), and 43 differentially abundant proteins (Table 5 and Table 6). For the group of high abundance proteins, the Limit sample was the one containing more proteins, followed by the Regular and the Burned, the last containing only one. The Burned sample presented the highest number of low abundance proteins, followed by the Limit and the Regular samples. To determine the interactions between protein functions, and to obtain the role of uncharacterized proteins, the GO functional annotation was added to the protein network.

Table 5. Proteins identified in high abundance (ratio from treatment/control > 2.5) in the blue dataset.

Sample name	Protein accession	Description	Present in BLT and RLT
Regular	Q10712	Leucine aminopeptidase 1, chloroplastic	X
	P25306	Threonine dehydratase biosynthetic, chloroplastic	X

	K4CVX0	Uncharacterized protein	X
	Q5UNS1	Arginase 2	X
	K4CVX6	Uncharacterized protein	X
Burned	K4ATA4	Uncharacterized protein	X
Limit	Q10712	Leucine aminopeptidase 1, chloroplastic	X
	K4CWC4	PR10 protein	X
	K4CVX0	Uncharacterized protein	X
	P25306	Threonine dehydratase biosynthetic, chloroplastic	X
	Q01413	Glucan endo-1,3-beta-glucosidase B	X
	K4CVQ7	Uncharacterized protein	X
	Q05539	Acidic 26 kDa endochitinase	
	K4B0B4	Uncharacterized protein	
	K4C3T2	Uncharacterized protein	X
	A0RZD0	Inducible plastid-lipid associated protein	X

	Q9LEG1	Cathepsin D Inhibitor	

Table 6. Proteins identified in low abundance (ratio from treatment/control < - 1.5) in the blue dataset.

Sample name	Protein accession	Description	Present in BLT and RLT
Regular	K4CAE2	Uncharacterized protein	
	K4ASV2	ATP-dependent Clp protease proteolytic subunit	
	K4B7W7	Uncharacterized protein	X
	K4CMI6	Uncharacterized protein	X
Burned	K4CVQ7	Uncharacterized protein	X
	K4BM57	Uncharacterized protein	X
	K4BVE2	50S ribosomal protein L31	X
	P37218	Histone H1	X
	K4AYJ8	Uncharacterized protein	X
	K4B0G3	Uncharacterized protein	X
	K4AX22	Superoxide dismutase [Cu-Zn]	X
	K4C998	Uncharacterized protein	X
	P04284	Pathogenesis-related leaf protein 6	X
	E5KBY0	Snakin-2	X
	Q2MI49	Photosystem I iron-sulfur center	X
	K4C1V2	Uncharacterized protein	
	K4CX44	Uncharacterized protein	
	Q3I5C4	Cytosolic ascorbate peroxidase 1	
	K4BJY6	Uncharacterized protein	
	P43282	S-adenosylmethionine synthase 3	

	C0KKU8	Lipoxygenase	
	P10708	Chlorophyll a-b binding protein 7, chloroplastic	
Limit	K4BVE2	50S ribosomal protein L31	
	K4BX19	Uncharacterized protein	X
	K4C1V2	Uncharacterized protein	X
	K4BLU6	Uncharacterized protein	
	K4D2D7	Uncharacterized protein	X

The proteins found more abundant in the Regular sample were mostly involved in protein and macromolecular complex subunit organization, assembly, biogenesis, metabolic process, as well as protein oligomerization and proteolysis, with protein hexamerization as the most significant function (Figure 17-A). These functions are related to the hydrolysis of proteins into amino acids or polypeptides, and formation of macromolecules and proteins (Bitrián et al., 2012), actions that are part of the cellular organization, and that are restructuring the cells, due to the stress damage. The low abundance proteins did not generate a network, but their molecular functions were related to catalytic, hydrolase and peptidase activity.

The Limit sample had the more abundant proteins distributed amongst three clusters presenting the main functions: negative regulation of cellular metabolic process, catabolic process, and cellular component organization or biogenesis (Figure 17-B). These processes prevent or reduce the rate of chemical reactions and pathways by which cells undertake chemical transformations of substances. They increase the chemical reactions resulting in compounds cleavage for energy liberation (Pianka, 1957). These functions are necessary for the recovery of damaged plant tissues and the increase in energy availability, possibly for growth. The low abundance proteins had roles in metabolic and cellular processes, regulation of biological processes and response to heat and cytokinin.

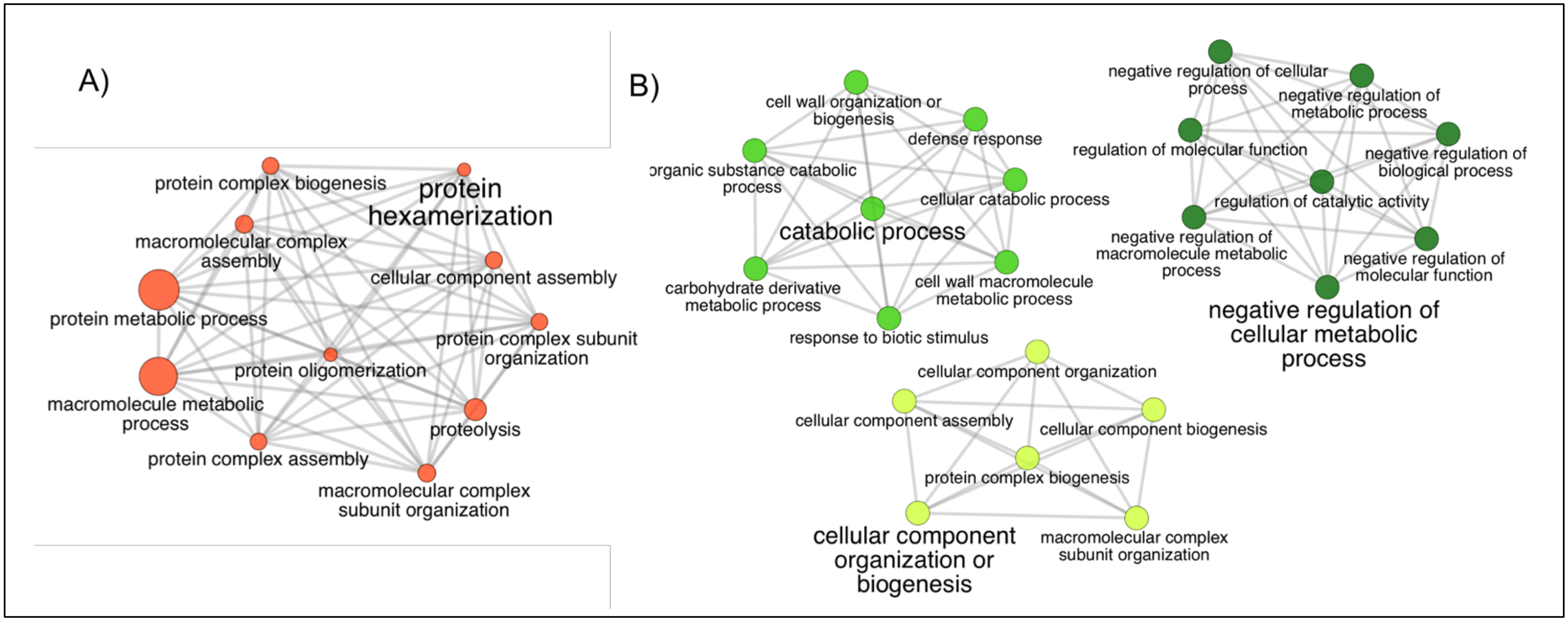

Figure 17. The network of gene ontology (GO) terms assigned to the proteins in high abundance in the Limit and Regular samples. Biological process GO terms assigned to proteins from the (A) Regular, and the (B) Limit sample. In B), each of the three clusters represents terms with a closer relationship. The leading group term (bigger font size) is the term of the higher significance of the network. The relationship between the terms is shown through the similarity of their assigned proteins. The nodes sizes represent the term's statistical significance. The edges reflect the level of connectivity amongst terms, calculated by kappa statistics.

The Burned sample presented low abundance proteins related to three major clusters: photosynthesis, coenzyme biosynthetic process, and oxidative stress response (Figure 18). Photosynthesis is an essential function for a plant and has priority in being restored by the cell for plant recovery and development. The low abundance of photosynthetic proteins is a result of a response to lowered intracellular CO_2, a condition caused by the stomatal closure (Meyer and Genty, 1998) and stress-induced senescence. During senescence, catabolism of macromolecules, such as membrane lipids, RNA, and proteins, and chlorophyll synthesis takes over photosynthesis (Gan and Amasino, 1997). Also, dehydration, abscisic acid, cytokinin, and ethylene treatments can lead to the activation of senescence-associated genes (Weaver et al., 1998). While s-adenosylmethionine (SAM) is a universal methyl donor, involved in the maintenance, and repair of proteins, DNA and RNA. SAM is a precursor to ethylene and polyamine biosynthesis, with ethylene being a known promoter of senescence, and polyamines, effective anti-senescence inducers (Pandey et al., 2000). While their antagonist roles, low abundance of SAM could indicate the activation of stress-induced senescence, with SAM redirection to ethylene production.

The protein found in significant high abundance (K4ATA4: uncharacterized protein) has the molecular function of mRNA binding, and its highest homology (59.4% score) is with the zeaxanthin epoxidase protein from the pink trumpet tree (*Handroanthus impetiginosus*). Zeaxanthin epoxidase is a protein with oxidoreductase activity, it converts zeaxanthin into antheraxanthin and lastly, to violaxanthin, and is involved in abscisic acid biosynthesis. It has an essential role in NPQ by regulation of the zeaxanthin concentration in photosynthetic energy conversion (Niyogi et al., 1998).

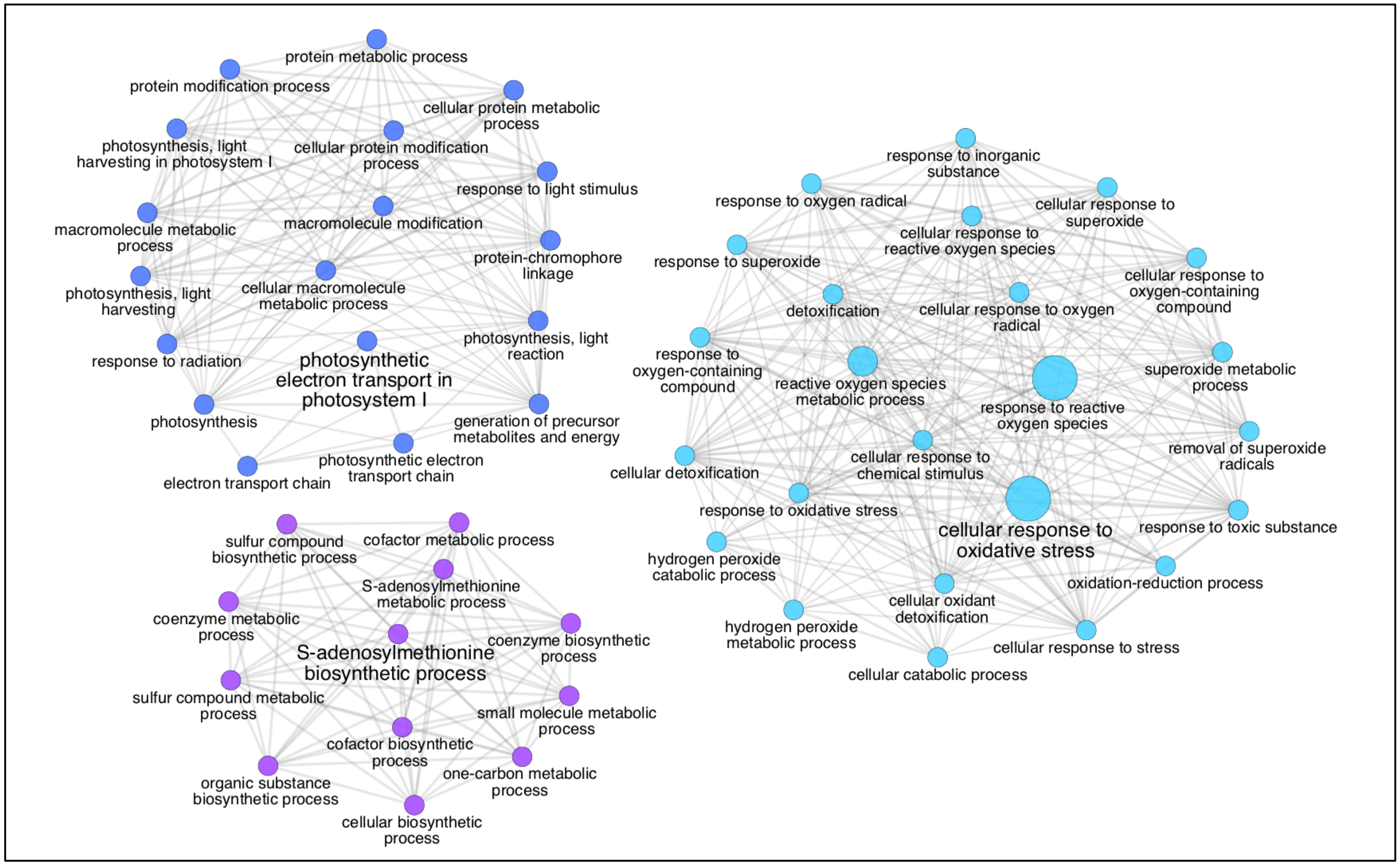

Figure 18. The network of gene ontology (GO) terms assigned to the proteins in low abundance in the Burned sample. The three clusters show different levels (< 8) of biological process GO terms for the proteins assigned and are grouped by function relationship. The relationship between the terms is shown through the similarity of their assigned proteins. The nodes sizes represent the term's

statistical significance. The leading group term (in bigger font size) is the term of the higher significance of the network. The edges reflect the level of connectivity amongst terms, calculated by kappa statistics.

From the protein functional analysis, a remarkable difference is observed between the implicated functions of the proteins from each sample (Burned, Regular, and Limit). The proteins identified in the Burned sample indicate that this tissue could be under stress-induced senescence. While the other samples presented proteins related to functions of the cellular organization and energy production, pathways that are linked to the tissue recovery and growth. This difference between active functions shows evidence of the different levels of stress response and plant development strategies.

A comparison of the protein functions found in this study (BLT) with the RLT dataset indicates differences between the responses to the treatments with red and blue LEDs. In RLT, the abundant proteins in the Burned sample were related to heat, oxidative, light, and endoplasmic reticulum stresses, while in BLT, the only abundant protein was implicated in oxidoreductase activity, thus related to oxidative stress. The low abundance proteins in the BLT indicates an undergoing senescence process on the damaged tissue. The RLT Limit sample presented similar active functions as the Burned of the same dataset, except for the particular active light-stress response. In BLT, the active functions were related to catabolic processes and cell organization. Lastly, in the Regular sample from the RLT dataset abundant proteins were identified with roles in general stress response, while in BLT, the proteins were engaged in protein hexamerization.

Put together, the results from this study suggests that the two light treatments with the same light intensity, but different wavelengths, triggered different functions in the plant. The blue light treatment had a higher response of NPQ, and most proteins of PSII and OEC complexes had no change in abundance when compared to the control, although PsbS mRNA levels had an 8-fold increase. The red light treatment caused the increase of the proteins from PSII and OEC while presenting a low level of NPQ and PsbS transcripts.

It is known that blue wavelengths cause higher photodamage when compared to other wavelengths from the visible spectrum (Arena et al., 2016; He et al., 2017). It could be hypothesized that blue light triggers photoinhibition faster and more efficiently. This could be due to the manganese cluster affinity to UV and blue wavelength range and its role of trigging photoinhibition through Mn release from the OEC (Hakala et al., 2005). With attenuation of the Mn releasing effect, the plants under red treatment would possibly be under a higher level of unbalance in PSII, having to synthesize and assemble its components, keeping their stoichiometric balance.

Indeed, it has been shown previously in *C. reinhardtii* that LHCSR3 is regulated by flavin-containing cryptochromes and/or phototropins, a photoreceptor for blue light (Petroutsos et al., 2016). LHCSR3 (light-harvesting complex stress-related protein 3) is a high-energy quenching effector (qE) (an NPQ component), and a protein from algae with similar roles to PsbS in plants. Similarly, PsbS regulation control could be linked to a blue light photoreceptor.

5.4 Conclusions

The photosynthetic parameters analysis resulted in a higher NPQ value on the blue treatment, after the light-induced damage, compared to the RLT and after the 10-days period. This result agreed with the temperature measurements, where the RLT resulted in a higher temperature compared to the BLT. The other photosynthetic parameters, however, had similar values between the BLT and

RLT treatments, between the 0-Day and 10-Days samples. The photosynthetic rate analysis showed no detectable difference in the photosynthesis efficiency between treatments and time of measurement. In accordance with the high NPQ results for BLT, the comparative quantitative analysis of the abundance of key proteins also resulted in differences between the responses to BLT and RLT. This result highlights the existence of a differential recovery of the OEC and PSII complexes under different wavelength treatments. The differential recovery of these complexes indicates the presence of, at least, two distinct mechanisms occurring in plants in response to extreme high-light stress generated by different wavelengths.

The mRNA quantification analysis suggested that regulations out of the transcriptional supervision could be involved in the control of *psbs*, *psb28*, *psbh* and *psbr* genes. Interesting, the high level of *psbs* transcripts in the BLT leads to the indication of a higher level of PsbS-dependent induction of NPQ. Particularly, the high abundance of the PsbS protein along with the low number of *psbs* transcripts suggests a high level of regulation of this gene at the transcriptional level. Our study demonstrated that in extremely high-light conditions, light wavelengths impact plants response in a different manner. Further research can be aimed at confirming, as suggested in this study, the NPQ activation cascade link to blue photoreceptors through a PsbS-dependent regulation. The characterization of the mechanisms involving *psbs* gene regulation and its role in triggering NPQ would aid in defining the different responses to high-light-induced stress.

CHAPTER 6: Supplementary findings

Connecting statement

In this chapter, the results and discussion of additional findings from Chapters 4 and 5 are shown. From Chapter 5's study, the protein-protein interaction network of the Regular sample of the RLT is presented as a result of the data analysis. Later, a discussion on the representativeness of this result considering the samples altogether is included. From the BLT, a breakdown of the results of this dataset is unfolded while the list of proteins found in this study are presented in Appendix D. The experiment workflow and assessment of data quality are described through the analysis of the Pearson correlation between biological replicates. A hierarchical clustering study of the BLT dataset containing the Limit, Burned and Regular samples was performed. The hierarchical clustering analysis had the objective of aiding the visualization of the discrepancies between the distinct samples (Limit, Burned and Regular). The presence of a differential abundance between samples defined which sampling strategy was more diverse and identified the Burned and Limit samples as objects of future investigation.

6.1 Global protein identification of tomato leaves under blue light

Presenting a higher level of complexity when compared to prokaryotic organisms, plant tissues are estimated to contain a pool of 10,000 proteins at any stage (Abraham et al., 2013). However, the sample preparation efficiency and mass spectrometry technology are limitations that highly impact the number of detectable proteins. Furthermore, plant tissues present an even greater limitation since they contain a high concentration of Rubisco, which is the most abundant protein in leaves (Ahsan et al., 2007). This makes the identification of low-abundant proteins difficult by not selecting their ions for MS^2. Methods for Rubisco removal have been developed, but they result in the removal of similar proteins by lack of antibody specificity, or coprecipitation (Alvarez and Naldrett, 2016). The poor protein annotation of non-model plants is also a great disadvantage to protein identification.

In this study, the limitations from an ion trap mass spectrometer were compensated by implementing a 12-step 2D LC gradient (in a 24 h analysis) in a MudPIT nanoESI-MS/MS methodology (McDonald et al., 2002; Wilmes et al., 2008) and a robust bioinformatics pipeline, and strict parameters (Figure 19). Peptides were searched through the MSAmanda algorithm. The MSAmanda algorithm was chosen rather than the more popular choices SEQUEST and Mascot because it has outperformed them by 4-22% when analyzing high-resolution data (Dorfer et al., 2014) and it is available in Proteome Discoverer (v. 2.0, Thermo Scientific, CA) as a free analysis node, making the use of this engine compatible and straightforward. After obtaining the identities by the algorithm matching, a global filtering parameter was applied to obtain one list of identified proteins meeting the confidence criteria (Appendix D).

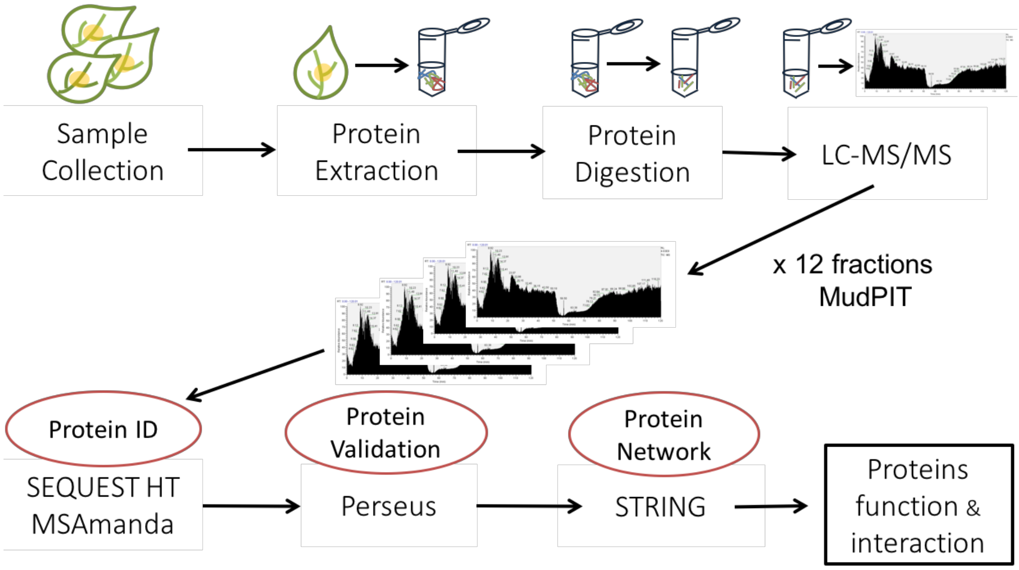

Figure 19. Schematic diagram of the proteomics workflow utilized in the BLT dataset analysis. Sample collection: leaves from 10 plants are extracted and pooled together to form samples Limit, Control and Burned. Protein extraction is performed by sonication and use of detergent in buffer (SDS). Protein digestion with modified trypsin is carried out after reduction and alkylation of disulfide bonds. LC-MS/MS analysis was done with 12 fractions of increasing salt concentration (ammonium acetate) online with a nanospray source in an ion trap mass spectrometer (LTQ XL). Protein ID (identification) was obtained by searching spectra with MSAmanda algorithm in the Proteome Discoverer software. Protein validation was done by selection of proteins meeting abundance criteria, normalization of protein abundance and statistical significance ($p<0.05$) through ANOVA, with Bonferroni's adjustment for multiple comparisons. Protein networks were generated by submitting validated protein accession numbers into STRING, clustering proteins by kmeans with high confidence (0.7 score).

6.2 Quality and reproducibility of the blue light data

We identified a total of 2,228 high confidence proteins in the tomato leaf samples treated with high-light and control. Biological replicates have a higher contribution to the sample variance when compared to technical replicates (Gan et al., 2007). For this reason, together with time and resources constriction, biological replicates were the variation measurement chosen in this experiment. Although label-free quantitation (LFQ) has been less utilized as a method to estimate protein abundance accurately, recent studies have shown that LFQ performance is comparable to extracted ion chromatogram (XIC) intensities (Bubis et al., 2017). To verify the reproducibility and quality of the data from this study, a linear regression analysis and a plot of the log2-transformed abundance values (emPAI) versus counts showing the normal distribution were obtained. As an example, the control and Limit samples analysis are shown in Figure 20, as a plot of the control replicates (C1, C2, C3) and Limit replicates (L1, L2, L3) with their corresponding R^2 values (shown in red) for the total of reliable proteins. For the Limit sample, replicate number 1 vs. 2, 1 vs. 3 and 2 vs. 3 presented the R^2 values 0.780, 0.671, 0.696, respectively. The R^2 values of the control sample replicates 1 vs. 2, 1 vs. 3 and 2 vs. 3 were 0.809, 0.696, 0.708, respectively. The R^2 average value for the biological control replicates was 0.738±0.06, and 0.716±0.06 for the Limit biological triplicates, agreeing with values reported in the literature for high-resolution MS/MS analysis (Zhou et al., 2017). The results show that the semi-quantitative analysis from the three biological replicates was reasonably linearly correlated and reproducible. The analysis of the three biological replicates of the Burned sample showed little correspondence between one of the replicates, and the replicate showing higher variance, compared to the others, was removed from the analysis.

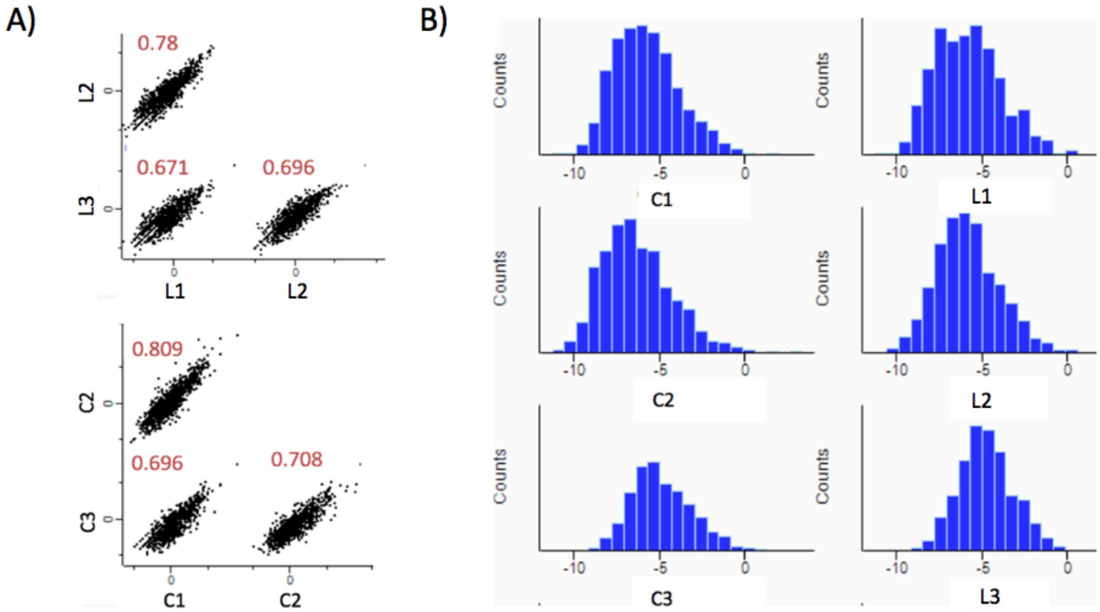

Figure 20. Example of protein abundance values distribution in control and Limit samples. (A) Linear regression analysis of the log2 abundance values (emPAI) for all proteins found in the triplicates, R^2 values in red. (B) Normal distribution obtained after log2-transformed emPAI values plotted against counts. L1-3, Limit replicates, C1-3, control replicates.

6.3 Clustering of protein abundance patterns in the blue dataset

A hierarchical clustering analysis was then performed to allow for visualization of protein abundance variation (Figure 21). Protein normalized abundance values (emPAI) from replicates were averaged. The means were transformed to a Z-score representation which was computed in the analysis.

The resulting graphical representation clearly shows the acute differences between the Burned and Limit treatments when compared to the control. In the Burned sample, several protein groups demonstrated to be in high abundance when compared to the control. Whereas the Limit sample contains a mixture of low and high protein groups similar to the control and to the Burned. The evidence of differences at the protein abundance level between the treatments and the control confirmed the interest in further analyzing these samples.

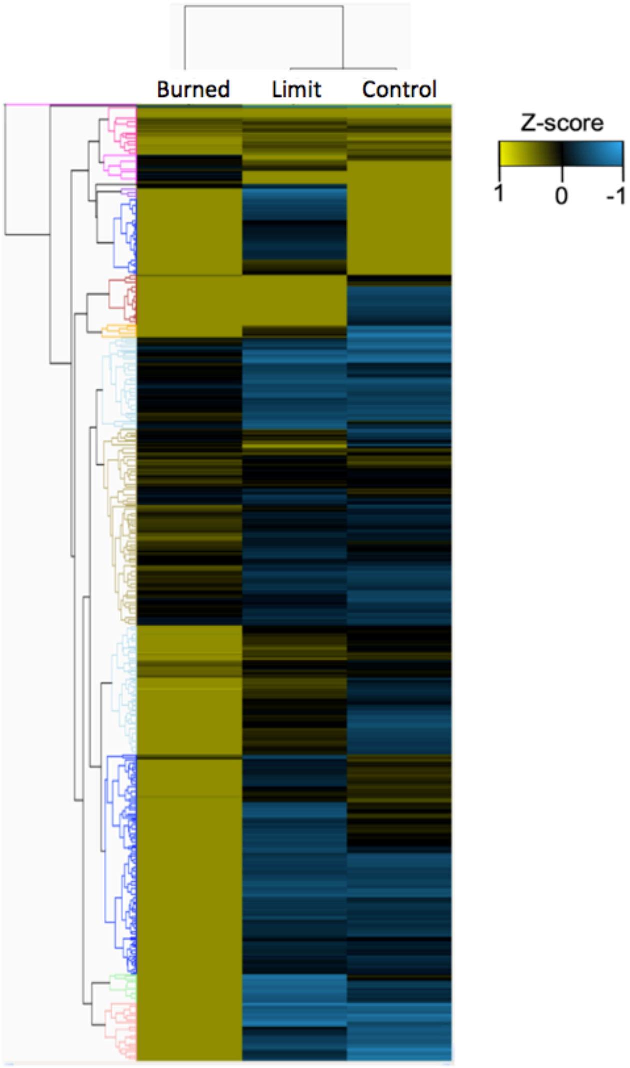

Figure 21. Hierarchical clustering analysis evidencing protein groups with similar abundance pattern. Proteins identified with a 1% FDR in control, Limit and Burned were clustered into groups with similar normalized abundance value patterns (Z-score) ranging from +1 to -1. Eucledian distance was chosen to cluster proteins by abundance traits. 12 clusters (shown in different colors) presenting differential abundance trends.

For the comparison between the datasets and the treatments, the Regular sample of the RLT dataset had shown that the differentially expressed protein were mostly general stress proteins (Figure 22), which was not the valuable candidates for further analysis. Therefore, the comparison of the RLT and BLT were performed on the Limit and Burned samples.

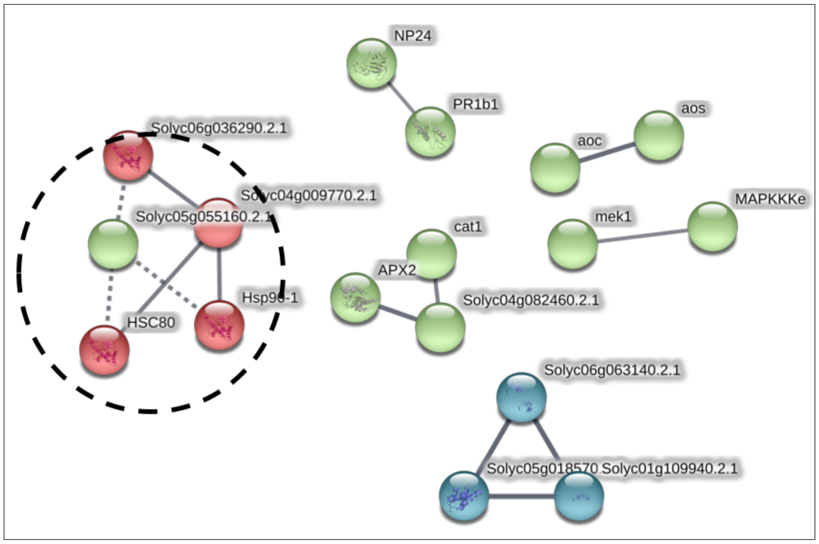

Figure 22. Protein interaction network from highly abundant proteins found in the Regular sample of the RLT. The STRING software was used to obtain a network of protein interactions with functions related to *Immune system process* and *Response to stimulus* at high confidence (0.7). Cluster analysis by K-means resulted in three distinct clusters. Proteins present in the cluster surrounded by a dashed line are part of general stress responses.

6.4 Blue dataset preliminary analysis conclusions

The analysis of the BLT dataset was performed to direct the choice of samples of interest and, most importantly, to access the data quality, which is essential in proteomics studies. Considering the results of this study, the biological replicates of Limit and Regular presented a high correlation. This is expected since the burned sample tissue was highly dehydrated, making the sample preparation more complex than the rest of the samples of the dataset. The hierarchical clustering analysis suggested that a low number of proteins were high or low abundant in the Regular sample when compared to the control. This analysis provided the basis to carry on the data analysis through the comparison of the BLT and the RLT datasets.

CHAPTER 7 - Summary

Connecting statement

A summary of the results is provided in this chapter, along with the significance of the results reported in this thesis. The methodologies developed and applied in this thesis are revisited in this chapter. As a conclusion, suggestions for future experiments are made based on the hypothesis confirmation and questions raised from the conclusions of this study.

7.1 Statement of originality, and contribution to knowledge

The results obtained in this project and presented as manuscripts in this thesis have contributed to increasing the knowledge on plants response to extreme light stress. They expand this field by adding the proteome characterization of tomato under extreme levels of light-induced stress conditions. The following are the descriptions of the original findings, their significance, and contribution to knowledge by each manuscript.

1) Tomato proteomics: Tomato as a model for crop proteomics (Chapter 2).

Contributed to the scientific community as a summary and critical analysis of the studies on tomato plants using proteomics as a tool for deep characterization of cellular changes. It discussed the latest studies, the remaining challenges, and perspectives of the field. It brought to attention the fact that crop proteomics is still behind in the level of new techniques implemented. It highlights the importance of studies focusing on combining different stress conditions, but also alerts of differences at plant species-specific response.

2) Quantitative proteomics analysis of light-induced stress in plants (Chapter 4).

This manuscript presents the first study of the proteome profile of plant response to extreme light-induced stress. In this study, an isobaric-labeled proteomics technique (iTRAQ) was implemented to define the proteome of plants under extreme light-induced stress using red LEDs. A protein-protein interaction map was generated, showing functional clusters of proteins differently abundant under the extreme condition. A hierarchical clustering study was also conducted and resulted in the finding of four protein abundance patterns between the different samples. One of the patterns showed the variable abundance of proteins with a direct relation to the increase of light intensity. Meaning that their abundance was increased according to the increase of light impacted intensity.

This first study set the grounds for a comparison between wavelengths since it presented for the first time the identification of more than 3,000 proteins expressed in the extreme condition. The analysis resulted in the detection of precursors of the salicylic acid pathway expressed only in the Burned zone, presenting a highly-specific located response. Attention was also brought to the high abundance of proteins PsbH, PsbS, PsbR, and Psb28 in the Burned sample when compared to their availability in the other zones (Limit, Regular, and control). This result was further investigated in Chapter 5 by comparison to other light treatment and comparative quantitative mRNA analysis. The observation of an initial recovery of the Burned tissue after the 10-days period was reported. The Burned zone was observed to gain a green coloration after the recovery period.

3) Plants response to extreme light-induced stress is wavelength-specific and supplemental findings (Chapters 5 and 6).

A comparison between the proteome of extreme light-induced stress in red and blue LEDs was shown. A physiological experiment was carried out to detect the differences in the levels of leaf temperature, NPQ, net photosynthetic rate, and maximum quantum efficiency of PSII photochemistry between both wavelengths and the control. A new proteomics experiment was performed, utilizing a label-free approach enhanced by a MudPIT separation technique. The data analysis was performed focusing on the proteins related to photosynthesis. The abundance of the proteins found in the previous experiment to be abundant in the Burned sample (PsbH, PsbR, PsbS, and Psb28) was further investigated. A differential abundance of these proteins was observed between the two light treatments (red and blue) and their respective control samples. Altogether, the results demonstrated that BLT induced a higher response of NPQ, carried on by a strategy containing a high regulation of PsbS at the mRNA level. The RLT treatment response resulted in high concentrations of PsbS, PsbH, Psb28 and PsbR. These results lead to the conclusion that extreme light-induced stress recovery in plants is wavelength-specific with the activation of different signaling cascades.

7.2 Thesis summary

The focus of this thesis was to deepen the knowledge of wavelength influence in high-light stress in plants. The importance of this work lies in the crucial role of photosynthesis as the primary crucial metabolic process in plants and the abiotic stress impact in its efficiency. In this thesis, a semi-quantitative proteomics analysis applying isobaric labels (iTRAQ) was carried out on plants exposed to an extreme light-induced stress condition.

The innovated LED methodology to generate the single-spot high-intensity light condition was developed by our research group. Red and blue LED lights were the chosen wavelengths to be investigated and compared, generating the RLT and BLT datasets, respectively. The high-light condition (~5,000 W m^{-2}) is achieved by using lenses as light concentrators to generate a high-intensity light. The high-intensity LED set up allowed for the generation of a leaf area of 1cm^2 treated with an extremely intense LED (~5,000 W m^{-2}), while the area surrounding where under lower intensities (see light map in Figure 8-B, section 4.3.1). This step was essential to test the hypothesis, since the burning of an entire leaf, or plant, would have caused irreparable damage.

This would lead to its death and inclusion of a 10-days period for the plant response buildup would be impossible. The three zones created as a result of the light treatment were visually distinct. The highly-impacted zone (Burned sample) was photo-bleached, while the zone around it (Limit sample) had slightly darker green color when compared to the rest of the leaf (Regular sample). The most impacted zone (Burned) was photo-bleached and highly dehydrated after the treatment, suggesting the death of the tissue. However, the beginning of a chlorophyll synthesis was observed after 10 days, suggesting a slow recovery of the tissue.

To well define the conditions created by the light treatments, photosynthetic parameters: i) non-photochemical quenching-NPQ, ii) maximum dark-adapted PSII photochemical efficiency-Fv/Fm, iii) electron transport rate-ETR, and iv) photosynthetic net rate-Pn, were obtained from data points after the light treatments and after the 10-days period. The leaf temperature was measured before and during the light treatments. The BLT presented a lower temperature increase when compared to the RLT. The results showed that the NPQ generated by the BLT was significantly higher than in the RLT at Day-0, showing the ability of plants to more efficiently activate the NPQ under blue light.

A first deep-characterization of plants after extreme light-induced stress identified central roles of proteins involved in response to a severe light condition. The three samples generated by the RLT (Burned, Limit, and Regular) were analyzed separately, proteins were extracted and digested. An isobaric-labeled methodology (iTRAQ) was applied to enable a simultaneous analysis of the samples, generating a semi-quantitative proteomics analysis. The data generated by a high-resolution mass spectrometer was searched with the iTAG protein sequence database of *Solanum lycopersicum* by the MASCOT algorithm. Quality filters to ensure high confidence matches were applied to identify a total of 3,994 proteins under 1% FDR and a minimum of 2 unique peptides.

The Regular sample contained 37 unique proteins, while the Limit and the Burned samples had 372 and 1,003, respectively. The differentially expressed proteins identified in the Burned, Limit, and Regular samples were involved in high-light, heat, endoplasmic reticulum and oxidative stress.

Protein abundance trends were investigated through a hierarchical clustering analysis performed using the Perseus software. Four patterns of protein abundance were identified, providing new lists of proteins that respond in a direct relationship to light intensity, and proteins exclusive to extreme light-induced stress. From this study, four proteins were selected for further analysis. Psb28, PsbH, PsbR, and PsbS were chosen due to their roles in photosynthesis and their differential abundance in the most severely light damaged tissue when compared to the other samples (Limit, Regular and Control). A comparative proteomics study was performed to obtain the relative abundance of key proteins of the photosystem II and the oxygen complexes (PsbS, PsbH, PsbR, Psb28). In this analysis, an in-house label-free MudPIT methodology was utilized to generate a high-level of protein separation and to allow for a high number of protein identifications.

The differential expression of the genes of interest was later studied at the mRNA level, by RT-qPCR. Two genes were chosen as internal standards for the RT-qPCR: a catalytic subunit of protein phosphatase 2A (PP2Acs), and Clathrin adaptor complex unit (Clat). Four new primers were designed and tested for the genes of interest (*psbH*, *psbR*, *psb28*, and *psbS*). The global protein abundance of the datasets was compared at the functional protein level. Overall, 7 out of 12 comparisons of mRNA and protein abundance were co-related. When protein was abundant, however, the mRNA levels were low, indicating the presence of different levels of gene regulation control.

7.3 Conclusions and future research

Photosynthesis efficiency is impacted by wavelength, since many of the proteins involved in the energy generation and the protection mechanisms have different peak absorption, as chlorophyll a and b, OEC, phytochrome, and others. Various studies have shown the effect of wavelength in plant growth and development (Brazaitytė et al., 2015; Gangadhar et al., 2012; Gómez et al., 2013; Lefsrud et al., 2008; Martineau et al., 2012); however, high-light stress response is still discussed as one universal defense mechanism with responses that do not rely on the wavelength utilized. In this thesis, the existence of a distinct impact on plant response at different wavelengths at high intensity is proven. The first steps in the characterization of these effects are taken by using proteomics, mRNA quantification and physiological measurements that provides a high level of certainty in the identification of such mechanisms.

The results obtained in the experiments, provide evidence that plants stress is mitigated when using high-intensity blue light (470 nm), compared to red light (655 nm). This statement is supported by the high level of non-photochemical quenching in the blue light treatment when compared to the red light. It is further confirmed by the high abundant proteins related to assembly and biosynthesis of PSII and OEC (PsbH, PsbR, PsbS, and Psb28) presented in the red treatment samples; indicating a possible unbalance of these essential components for efficient work of PSII and OEC, part of the main complexes of the photosynthetic apparatus. This unbalance would need to be further investigation by experiments where the stoichiometric abundance data to compare the PSII complex subunits concentrations.

It is hypothesized that blue light triggers photoinhibition faster and more efficiently than red light. This could be due to the manganese cluster affinity to UV and blue wavelength range and its role of trigging photoinhibition through Mn release from the OEC (Hakala et al., 2005). With attenuation of the Mn releasing effect, the plants under the red light treatment could possibly be under a higher level of unbalance in PSII, having to synthesize and assemble its components, keeping their stoichiometric balance.

It can be concluded that the use of the LED treatment with an in-house set-up has been shown to be a successful method to study extreme light-induced stress in plants. It provides a way of generating an impact gradient on the plant leaf, allowing it to endure an extreme irradiance level (up to 5,000 W m^{-2}) without activating plant death response. The LED set-up generated three zones of light intensity in the leaf, in which the most impacted was undergoing photo-bleaching. Although this was not the focus of this study, this light system can be an effective way to study photo-bleaching mechanisms in plants.

The identification of proteins utilizing the two proteomics methodologies (MudPIT and iTRAQ) was successful in the identification of the wavelength effects. The data comparison through the various methodologies: functional enrichment, hierarchical clustering, and protein interactions network was shown to be an effective strategy. The contrast of the mRNA and protein quantitation resulted in the suggestion of the levels of regulation mechanisms playing a role in the synthesis control of the proteins of interest (PsbR, PsbS, Psb28, and PsbH). The low levels of mRNA matched the low or unchanged levels of protein in relation to the control. This result suggests that different levels of regulation could control the expression of these genes, with up to 60% of the variability not explained by gene to mRNA correlation (Maier et al., 2009). A higher response of NPQ was seen in the BLT, possibly highlighting a high regulation of PsbS at the mRNA level. Whereas the synthesis of PsbS, PsbH, Psb28 and PsbR seems to be a consequence in the RLT response.

Finally, characterization of stress responses aids in the development of improved crops that can withstand extreme environmental conditions. Notably, the understanding of the differences caused by the wavelength in the plant response to extreme light-induced stress. Therefore, we recommend the following approaches as future research and follow up experiments:

A time course proteomics experiment. A proteomics analysis utilizing a multiplex strategy (TMT or ITRAQ, for example) to study the extreme light-induced stress in a time course strategy. The data points could be taken every day for the first 10 days and with a larger interval after this period. This would be an extensive study showing the time-frame of the stress response in the Burned and Limit leaf zones. The same methodology for plant growth and light treatment would be utilized. For each data point, a 9-plex experiment could be utilized, containing the triplicates of the control and the two treatments. This study would determine the key players in response to high-intensity stress in a time scale, evidencing the many mechanisms involved in it. The analysis of the samples after the 10-days period would allow for the characterization of the recovery of the highly-damaged tissue (Burned). Because of the number of proteomics analysis, the comparison between wavelengths would be complex and time-consuming, being more realistic to explore one of the most interesting treatment.

The identification of protein interactors. Another interesting approach would be to perform a cross-linking experiment, where an immunoprecipitation experiment would be utilized to purify for the proteins of interest (PsbH, PsbS, Psb28 or PsbR, for example). A cleavable crosslinker, as DSSO (Thermo Fischer, CA, USA), would be added to form covalent bonds between protein interactors and proteins of interest. Finally, a mass spectrometry analysis would take place, matching the resulting fragmentation patterns to protein identities from a theoretical database. This experiment would aid in the identification of these proteins mode of action, by determining the protein interactors. Finally, this approach would, for example, increase the knowledge of Psb28 role on photochemical quenching.

Comprehensive characterization of wavelengths responses. Similar experiments to the ones presented in this thesis could be performed utilizing new wavelengths, as a way to define the minimum range (in nm) that triggers a specific plant stress response. This experiment would result in the in-depth characterization of all wavelengths response to light-induced stress, or NPQ.

Extensive characterization of non-photochemical quenching. Although a widely-known process, many players and activation mechanisms of non-photochemical quenching are still unknown, as determined in this thesis. A study focusing on determining the inducers of NPQ would definitely provide a better understanding of why there are changes in the response of different wavelengths. In vitro, studies of the photosynthetic apparatus, as well as mutagenesis studies would be interesting approaches to explore these mechanisms, by carrying out knockout of genes of interest to determine functions. Although time-consuming, especially for mutagenic studies, these methodologies would generate the ultimate proof of function and involvement of the genes of interest.

Light treatment optimization. In another direction, optimization of the light treatment could greatly aid in the acquisition of samples. Due to the limited size of the Burned zone, many plants are required to obtain enough sample analysis. The design of a LED set-up that could generate greater spots of high intensity could mitigate this issue. This would have to be performed with caution, as a greater area of the Burned zone could result in high damage of the leaf, causing its release from the plant and to diminish energy consumption from the damaged tissue. Tests using various durations of light treatments could be performed since, in this thesis, a treatment of only 5 min was applied. The light treatment optimization would increase the feasibility of the above-mentioned experiments.

Verifying the direction of the electron flow. Another direction would be to further determine the mechanisms involved in the different response to wavelengths in high-light stress. It could be interesting to verify the participation of the cyclic electron flow in each different wavelength response. The cyclic electron flow has a photoprotective role in the microalga *Chlorella ohadii* by conserving water and reducing the energy of antenna biosynthesis (Ananyev et al., 2017). This mechanism could be differentially activated in the multiple stress responses by being linked to, for example, the triggering of NPQ by the OEC release of Mn to the lumen.

CHAPTER 8 – References

Abraham, P., Adams, R., Giannone, R.J., Kalluri, U., Ranjan, P., Erickson, B., Shah, M., Tuskan, G.A., Hettich, R.L., 2011. Defining the boundaries and characterizing the landscape of functional genome expression in vascular tissues of populus using shotgun proteomics. J. Proteome Res. 11, 449–460. https://doi.org/10.1021/pr200851y

Abraham, P., Giannone, R.J., Adams, R.M., Kalluri, U., Tuskan, G.A., Hettich, R.L., 2013. Putting the pieces together: High-performance LC-MS/MS provides network-, pathway-, and protein-level perspectives in *Populus*. Mol. Cell. Proteomics 12, 106–119. https://doi.org/10.1074/mcp.M112.022996

Abreu, I.A., Farinha, A.P., Negrão, S., Gonçalves, N., Fonseca, C., Rodrigues, M., Batista, R., Saibo, N.J.M., Oliveira, M.M., 2013. Coping with abiotic stress: Proteome changes for crop improvement. J. Proteomics 93, 145–168. https://doi.org/10.1016/j.jprot.2013.07.014

Afroz, A., Ali, G.M., Mir, A., Komatsu, S., 2011. Application of proteomics to investigate stress-induced proteins for improvement in crop protection. Plant Cell Rep. 30, 745–763. https://doi.org/10.1007/s00299-010-0982-x

Agarwal, P., Agarwal, P.K., 2014. Pathogenesis related-10 proteins are small, structurally similar but with diverse role in stress signaling. Mol. Biol. Rep. 41, 599–611. https://doi.org/10.1007/s11033-013-2897-4

Aghaei, K., Ehsanpour, A.A., Shah, A.H., Komatsu, S., 2009. Proteome analysis of soybean hypocotyl and root under salt stress. Amino Acids 36, 91–98. https://doi.org/10.1007/s00726-008-0036-7

Ahsan, N., Lee, D.G., Lee, S.H., Kang, K.Y., Bahk, J.D., Choi, M.S., Lee, I.J., Renaut, J., Lee, B.H., 2007. A comparative proteomic analysis of tomato leaves in response to waterlogging stress. Physiol. Plant. 131, 555–570. https://doi.org/10.1111/j.1399-3054.2007.00980.x

Allahverdiyeva, Y., Mamedov, F., Suorsa, M., Styring, S., Vass, I., Aro, E.M., 2007. Insights into the function of PsbR protein in *Arabidopsis thaliana*. Biochim. Biophys. Acta - Bioenerg. 1767, 677–685. https://doi.org/10.1016/j.bbabio.2007.01.011

Allen, J.F., 2017. The CoRR hypothesis for genes in organelles. J. Theor. Biol. 434, 50–57. https://doi.org/10.1016/j.jtbi.2017.04.008

Allen, J.F., de Paula, W.B.M., Puthiyaveetil, S., Nield, J., 2011. A structural phylogenetic map for chloroplast photosynthesis. Trends Plant Sci. 16, 645–655. https://doi.org/10.1016/j.tplants.2011.10.004

Altschul, S.F., Gish, W., Miller, W., Myers, E.W., Lipman, D.J., 1990. Basic local alignment search tool. J. Mol. Biol. 215, 403–410. https://doi.org/10.1016/S0022-2836(05)80360-2

Alvarez, S., Naldrett, M., 2016. Plant structure and specificity – challenges and sample preparation considerations for proteomics, in: Hamid, M., Martin, C. (Eds.), Modern Proteomics – Sample Preparation, Analysis and Practical Applications. Springer International Publishing AG, Cham, Switzerland, pp. 63–81. https://doi.org/10.1007/978-3-319-41448-5

Ananyev, G., Gates, C., Kaplan, A., Dismukes, G.C., 2017. Photosystem II-cyclic electron flow powers exceptional photoprotection and record growth in the microalga *Chlorella ohadii*. Biochim. Biophys. Acta - Bioenerg. 1858, 873–883. https://doi.org/10.1016/j.bbabio.2017.07.001

Arena, C., Tsonev, T., Doneva, D., De Micco, V., Michelozzi, M., Brunetti, C., Centritto, M., Fineschi, S., Velikova, V., Loreto, F., 2016. The effect of light quality on growth, photosynthesis, leaf anatomy and volatile isoprenoids of a monoterpene-emitting herbaceous species (*Solanum lycopersicum* L.) and an isoprene-emitting tree (*Platanus orientalis* L.). Environ. Exp. Bot. 130, 122–132. https://doi.org/10.1016/j.envexpbot.2016.05.014

Aro, E.M., Suorsa, M., Rokka, A., Allahverdiyeva, Y., Paakkarinen, V., Saleem, A., Battchikova, N., Rintamäki, E., 2005. Dynamics of photosystem II: A proteomic approach to thylakoid protein complexes. J. Exp. Bot. 56, 347–356. https://doi.org/10.1093/jxb/eri041

Aro, E.M., Virgin, I., Andersson, B., 1993. Photoinhibition of photosystem II. Inactivation, protein damage and turnover. Biochim. Biophys. Acta 1143, 113–134. https://doi.org/10.1016/0005-2728(93)90134-2

Balmant, K.M., Parker, J., Yoo, M., Zhu, N., Dufresne, C., Chen, S., 2015. Redox proteomics of tomato in response to *Pseudomonas syringae* infection. Hortic. Res. 2, 15043. https://doi.org/10.1038/hortres.2015.43

Banerjee, A., Roychoudhury, A., 2016. Group II late embryogenesis abundant (LEA) proteins: structural and functional aspects in plant abiotic stress. Plant Growth Regul. 79, 1–17. https://doi.org/10.1007/s10725-015-0113-3

Baroli, I., Melis, A., 1996. Photoinhibition and repair in *Dunaliella salina* acclimated to different growth irradiances. Planta 198, 640–646. https://doi.org/10.1007/BF00262653

Barone, A., Chiusano, M.L., Ercolano, M.R., Giuliano, G., Grandillo, S., Frusciante, L., 2008. Structural and Functional Genomics of Tomato. Int. J. Plant Genomics 2008, 1–12. https://doi.org/10.1155/2008/820274

Bečková, M., Gardian, Z., Yu, J., Konik, P., Nixon, P.J., Komenda, J., 2017. Association of Psb28 and Psb27 Proteins with PSII-PSI Supercomplexes upon Exposure of Synechocystis sp. PCC 6803 to High Light. Mol. Plant 10, 62–72. https://doi.org/10.1016/j.molp.2016.08.001

Bergantino, E., Brunetta, A., Touloupakis, E., Segalla, A., Szabò, I., Giacometti, G.M., 2003. Role of the PSII-H subunit in photoprotection: novel aspects of D1 turnover in *Synechocystis* 6803. J. Biol. Chem. 278, 41820–41829. https://doi.org/10.1074/jbc.M303096200

Bhargava, M., Higgins, L., Wendt, C.H., Ingbar, D.H., 2014. Application of clinical proteomics in acute respiratory distress syndrome. Clin. Transl. Med. 3, 34. https://doi.org/10.1186/s40169-014-0034-1

Bielach, A., Hrtyan, M., Tognetti, V.B., 2017. Plants under stress: Involvement of auxin and cytokinin. Int. J. Mol. Sci. 18. https://doi.org/10.3390/ijms18071427

Bielczynski, L.W., Schansker, G., Croce, R., 2016. Effect of light acclimation on the organization of photosystem II super- and sub-complexes in *Arabidopsis thaliana*. Front. Plant Sci. 7, 105. https://doi.org/10.3389/fpls.2016.00105

Bindea, G., Mlecnik, B., Hackl, H., Charoentong, P., Tosolini, M., Kirilovsky, A., Fridman, W.H., Pagès, F., Trajanoski, Z., Galon, J., 2009. ClueGO: A Cytoscape plug-in to decipher functionally grouped gene ontology and pathway annotation networks. Bioinformatics 25, 1091–1093. https://doi.org/10.1093/bioinformatics/btp101

Bitrián, M., Zarza, X., Altabella, T., Tiburcio, A.F., Alcázar, R., 2012. Polyamines under abiotic stress: Metabolic crossroads and hormonal crosstalks in plants. Metabolites 2, 516–528. https://doi.org/10.3390/metabo2030516

Boccalandro, H.E., Giordano, C. V., Ploschuk, E.L., Piccoli, P.N., Bottini, R., Casal, J.J., 2012. Phototropins But Not Cryptochromes Mediate the Blue Light-Specific Promotion of Stomatal

Conductance, While Both Enhance Photosynthesis and Transpiration under Full Sunlight. Plant Physiol. 158, 1475–1484. https://doi.org/10.1104/pp.111.187237

Bombarely, A., Menda, N., Tecle, I.Y., Buels, R.M., Strickler, S., Fischer-York, T., Pujar, A., Leto, J., Gosselin, J., Mueller, L.A., 2011. The sol genomics network (solgenomics.net): Growing tomatoes using Perl. Nucleic Acids Res. 39, 1149–1155. https://doi.org/10.1093/nar/gkq866

Bourget, C.M., 2008. An introduction to light-emitting diodes. HortScience 43, 1944–1946.

Brazaitytė, A., Sakalauskienė, S., Samuolienė, G., Jankauskienė, J., Viršilė, A., Novičkovas, A., Sirtautas, R., Miliauskienė, J., Vaštakaitė, V., Dabašinskas, L., Duchovskis, P., 2015. The effects of LED illumination spectra and intensity on carotenoid content in Brassicaceae microgreens. Food Chem. 173, 600–606. https://doi.org/10.1016/j.foodchem.2014.10.077

Brini, F., Hanin, M., Lumbreras, V., Amara, I., Khoudi, H., Hassairi, A., Pagès, M., Masmoudi, K., 2007. Overexpression of wheat dehydrin DHN-5 enhances tolerance to salt and osmotic stress in Arabidopsis thaliana. Plant Cell Rep. 26, 2017–2026. https://doi.org/10.1007/s00299-007-0412-x

Bubis, J.A., Levitsky, L.I., Ivanov, M. V., Tarasova, I.A., Gorshkov, M. V., 2017. Comparative evaluation of label-free quantification methods for shotgun proteomics. Rapid Commun. Mass Spectrom. 31, 606–612. https://doi.org/10.1002/rcm.7829

Caffarri, S., Frigerio, S., Olivieri, E., Righetti, P.G., Bassi, R., 2005. Differential accumulation of *Lhcb* gene products in thylakoid membranes of *Zea mays* plants grown under contrasting light and temperature conditions. Proteomics 5, 758–768. https://doi.org/10.1002/pmic.200402008

Candat, A., Paszkiewicz, G., Neveu, M., Gautier, R., Logan, D.C., Avelange-Macherel, M.-H., Macherel, D., 2014. The Ubiquitous Distribution of Late Embryogenesis Abundant Proteins across Cell Compartments in *Arabidopsis* Offers Tailored Protection against Abiotic Stress. Plant Cell 26, 3148–3166. https://doi.org/10.1105/tpc.114.127316

Cantero, A., Barthakur, S., Bushart, T.J., Chou, S., Morgan, R.O., Fernandez, M.P., Clark, G.B., Roux, S.J., 2006. Expression profiling of the *Arabidopsis* annexin gene family during germination, de-etiolation and abiotic stress. Plant Physiol. Biochem. 44, 13–24. https://doi.org/10.1016/j.plaphy.2006.02.002

Casado-Vela, J., Selles, S., Martinez, R.B., 2006. Proteomic analysis of tobacco mosaic virus-infected tomato (*Lycopersicon esculentum* M.) fruits and detection of viral coat protein. Proteomics 6, S196–S206. https://doi.org/10.1002/pmic.200500317

Casal, J.J., Yanovsky, M.J., 2005. Regulation of gene expression by light. Int. J. Dev. Biol. 49, 501–511. https://doi.org/10.1387/ijdb.051973jc

Catalá, C., Howe, K.J., Hucko, S., Rose, J.K.C., Thannhauser, T.W., 2011. Towards characterization of the glycoproteome of tomato (*Solanum lycopersicum*) fruit using Concanavalin A lectin affinity chromatography and LC-MALDI-MS/MS analysis. Proteomics 11, 1530–1544. https://doi.org/10.1002/pmic.201000424

Ceballos-Laita, L., Gutierrez-Carbonell, E., Takahashi, D., Abadía, A., Uemura, M., Abadía, J., López-Millán, A.F., 2018. Effects of Fe and Mn deficiencies on the protein profiles of tomato (*Solanum lycopersicum*) xylem sap as revealed by shotgun analyses. J. Proteomics 170, 117–129. https://doi.org/10.1016/j.jprot.2017.08.018

Chamoli, S., Verma, A.K., 2014. Targeting of Metabolic Pathways for Genetic Engineering to Combat Abiotic Stress Tolerance in Crop Plants, in: Gaur, R.K., Sharma, P. (Eds.), Approaches to Plant Stress and Their Management. Springer India, New Delhi, pp. 23–37. https://doi.org/10.1007/978-81-322-1620-9_2

Champagne, A., Boutry, M., 2013. Proteomics of nonmodel plant species. Proteomics 13, 663–673. https://doi.org/10.1002/pmic.201200312

Chattopadhyay, A., Subba, P., Pandey, A., Bhushan, D., Kumar, R., Datta, A., Chakraborty, S., Chakraborty, N., 2011. Analysis of the grasspea proteome and identification of stress-responsive proteins upon exposure to high salinity, low temperature, and abscisic acid treatment. Phytochemistry 72, 1293–1307. https://doi.org/10.1016/j.phytochem.2011.01.024

Chaturvedi, P., Doerfler, H., Jegadeesan, S., Ghatak, A., Pressman, E., Castillejo, M.A., Wienkoop, S., Egelhofer, V., Firon, N., Weckwerth, W., 2015. Heat-treatment-responsive proteins in different developmental stages of tomato pollen detected by targeted mass accuracy precursor alignment (tMAPA). J. Proteome Res. 14, 4463–4471. https://doi.org/10.1021/pr501240n

Chaturvedi, P., Ghatak, A., Weckwerth, W., 2016. Pollen proteomics: from stress physiology to developmental priming. Plant Reprod. 29, 119–132. https://doi.org/10.1007/s00497-016-0283-9

Chavez, J.D., Eng, J.K., Schweppe, D.K., Cilia, M., Rivera, K., Zhong, X., Wu, X., Allen, T., Khurgel, M., Kumar, A., Lampropoulos, A., Larsson, M., Maity, S., Morozov, Y., Pathmasiri, W., Perez-Neut, M., Pineyro-Ruiz, C., Polina, E., Post, S., Rider, M., Tokmina-Roszyk, D., Tyson, K., Vieira Parrine Sant'Ana, D., Bruce, J.E., 2016. A General Method for Targeted Quantitative Cross-Linking Mass Spectrometry. PLoS One 11, e0167547. https://doi.org/10.1371/journal.pone.0167547

Chen, S., Harmon, A.C., 2006. Advances in plant proteomics. Proteomics 6, 5504–5516. https://doi.org/10.1002/pmic.200600143

Chen, Y., Ma, J., Zhang, X., Yang, Y., Zhou, D., Yu, Q., Que, Y., Xu, L., Guo, J., 2017. A Novel Non-specific Lipid Transfer Protein Gene from Sugarcane (NsLTPs), Obviously Responded to Abiotic Stresses and Signaling Molecules of SA and MeJA. Sugar Tech 19, 17–25. https://doi.org/10.1007/s12355-016-0431-4

Chinnusamy, V., Schumaker, K., Zhu, J.K., 2004. Molecular genetic perspectives on cross-talk and specificity in abiotic stress signalling in plants. J. Exp. Bot. 55, 225–236. https://doi.org/10.1093/jxb/erh005

Cho, E.K., Choi, Y.J., 2009. A nuclear-localized HSP70 confers thermoprotective activity and drought-stress tolerance on plants. Biotechnol. Lett. 31, 597–606. https://doi.org/10.1007/s10529-008-9880-5

Corpillo, D., Gardini, G., Vaira, A.M., Basso, M., Aime, S., Accotto, G.P., Fasano, M., 2004. Proteomics as a tool to improve investigation of substantial equivalence in genetically modified organisms: The case of a virus-resistant tomato. Proteomics 4, 193–200. https://doi.org/10.1002/pmic.200300540

Cox, J., Mann, M., 2008. MaxQuant enables high peptide identification rates, individualized p.p.b.-range mass accuracies and proteome-wide protein quantification. Nat. Biotechnol. 26, 1367–72. https://doi.org/10.1038/nbt.1511

Craig, R., Beavis, R.C., 2004. TANDEM: Matching proteins with tandem mass spectra. Bioinformatics 20, 1466–1467. https://doi.org/10.1093/bioinformatics/bth092

Cramer, G.R., Urano, K., Delrot, S., Pezzotti, M., Shinozaki, K., 2011. Effects of abiotic stress on plants: a systems biology perspective. BMC Plant Biol. 11, 163. https://doi.org/10.1186/1471-2229-11-163

Croce, R., 2015. PsbS is the plants' pick for sun protection. Nat. Struct. Mol. Biol. 22, 650–652. https://doi.org/10.1038/nsmb.3079

Cronjé, M.J., Bornman, L., 2006. Salicylic Acid Influences Hsp70/Hsc70 Expression in *Lycopersicon esculentum*: Dose- and Time-Dependent Induction or Potentiation. Biochem. Biophys. Res. Commun. 427, 422–427. https://doi.org/10.1006/bbrc.1999.1692

Cui, S., Hu, J., Guo, S., Wang, J., Cheng, Y., Dang, X., Wu, L., He, Y., 2012. Proteome analysis of *Physcomitrella patens* exposed to progressive dehydration and rehydration. J. Exp. Bot. 63, 711–726. https://doi.org/10.1093/jxb/err296

Dekkers, B.J.W., Willems, L., Bassel, G.W., Van Bolderen-Veldkamp, R.P.M., Ligterink, W., Hilhorst, H.W.M., Bentsink, L., 2012. Identification of reference genes for RT-qPCR expression analysis in *Arabidopsis* and tomato seeds. Plant Cell Physiol. 53, 28–37. https://doi.org/10.1093/pcp/pcr113

Demers, D.A., Gosselin, A., 2002. Growing greenhouse tomato and sweet pepper under supplemental lighting: Optimal photoperiod, negative effects of long photoperiod and their causes. Acta Hortic. 580, 83–88.

Demmig-Adams, B., Adams, W.W., 1996. Xanthophyll cycle and light stress in nature: uniform response to excess direct sunlight among higher plant species. Planta 198, 460–470. https://doi.org/10.1007/BF00620064

Deram, P., Lefsrud, M.G., Orsat, V., 2014. Supplemental lighting orientation and Red-to-Blue ratio of light-emitting diodes for greenhouse tomato production. HortScience 49, 448–452.

Di Carli, M., Villani, M.E., Bianco, L., Lombardi, R., Perrotta, G., Benvenuto, E., Donini, M., 2010. Proteomic analysis of the plant-virus interaction in cucumber mosaic virus (CMV) resistant transgenic tomato. J. Proteome Res. 9, 5684–5697. https://doi.org/10.1021/pr100487x

Dietz, K.J., 2015. Efficient high light acclimation involves rapid processes at multiple mechanistic levels. J. Exp. Bot. 66, 2401–2414. https://doi.org/10.1093/jxb/eru505

Dixon, M., Grace, J., 1983. Natural convection from leaves at realistic Grashof numbers. Plant. Cell Environ. 6, 665–670. https://doi.org/10.1111/1365-3040.ep11589240

Dobáková, M., Sobotka, R., Tichy, M., Komenda, J., 2008. Psb28 protein is involved in the biogenesis of the photosystem II inner antenna CP47 (PsbB) in the *Cyanobacterium Synechocystis* sp. PCC 6803. Plant Physiol. 149, 1076–1086. https://doi.org/10.1104/pp.108.130039

Dong, W., Kieliszewski, M., Held, M.A., 2014. Identification of the pI 4.6 extensin peroxidase from *Lycopersicon esculentum* using proteomics and reverse-genomics. Phytochemistry 112, 151–159. https://doi.org/10.1016/j.phytochem.2014.09.015

Dorfer, V., Pichler, P., Stranzl, T., Stadlmann, J., Taus, T., Winkler, S., Mechtler, K., 2014. MS Amanda, a universal identification algorithm optimized for high accuracy tandem mass spectra. J. Proteome Res. 13, 3679–3684. https://doi.org/10.1021/pr500202e

Duan, J., Cai, W., 2012. OsLEA3-2, an Abiotic Stress Induced Gene of Rice Plays a Key Role in Salt and Drought Tolerance. PLoS One 7. https://doi.org/10.1371/journal.pone.0045117

Dyson, B.C., Allwood, J.W., Feil, R., Xu, Y., Miller, M., Bowsher, C.G., Goodacre, R., Lunn, J.E., Johnson, G.N., 2015. Acclimation of metabolism to light in *Arabidopsis thaliana*: The glucose 6-phosphate/phosphate translocator GPT2 directs metabolic acclimation. Plant, Cell Environ. 38, 1404–1417. https://doi.org/10.1111/pce.12495

Ebrahim, S., Usha, K., Singh, B., 2011. Pathogenesis Related (PR) Proteins in Plant Defense Mechanism Age-Related Pathogen Resistance. Curr. Res. Technol. Adv. 1043–1054.

Eng, J.K., Jahan, T.A., Hoopmann, M.R., 2013. Comet: An open-source MS/MS sequence database search tool. Proteomics 13, 22–24. https://doi.org/10.1002/pmic.201200439

Eng, J.K., Mccormack, A.L., Yates III, J.R., 1994. An approach to correlate tandem mass spectral data of peptides with amino acid sequences in a protein database. J. Am Soc Mass Spectrom 5, 976–989.

Epstein, E., 1972. Mineral Nutrition of Plants: Principles and Perspectives. J Wiley and Sons, Inc., New York.

Fan, M., Li, M., Liu, Z., Cao, P., Pan, X., Zhang, H., Zhao, X., Zhang, J., Chang, W., 2015. Crystal structures of the PsbS protein essential for photoprotection in plants. Nat. Struct. Mol. Biol. 22, 729–735. https://doi.org/10.1038/nsmb.3068

Fan, X.-X., Xu, Z.-G., Liu, X.-Y., Tang, C.-M., Wang, L.-W., Han, X., 2013. Effects of light intensity on the growth and leaf development of young tomato plants grown under a combination of red and blue light. Sci. Hortic. (Amsterdam). 153, 50–55. https://doi.org/10.1016/j.scienta.2013.01.017

Fellner, M., Sawhney, V.K., 2002. The 7B-1 mutant in tomato shows blue-light-specific resistance to osmotic stress and abscisic acid. Planta 214, 675–682. https://doi.org/10.1007/s004250100671

Feng, L., Han, Y., Liu, G., An, B., Yang, J., Yang, G., Li, Y., Zhu, Y., 2007. Overexpression of sedoheptulose-1,7-bisphosphatase enhances photosynthesis and growth under salt stress in transgenic rice plants. Funct. Plant Biol. 34, 822–834. https://doi.org/10.1071/FP07074

Floris, M., Bassi, R., Robaglia, C., Alboresi, A., Lanet, E., 2013. Post-transcriptional control of light-harvesting genes expression under light stress. Plant Mol. Biol. 82, 147–154. https://doi.org/10.1007/s11103-013-0046-z

Gallardo, F., Gálvez, S., Gadal, P., Cánovas, F.M., 1995. Changes in NADP+-linked isocitrate dehydrogenase during tomato fruit ripening: Characterization of the predominant cytosolic enzyme from green and ripe pericarp. Planta An Int. J. Plant Biol. 196, 148–154. https://doi.org/10.1007/BF00193228

Gan, C.S., Chong, P.K., Pham, T.K., Wright, P.C., 2007. Technical, experimental, and biological variations in isobaric tags for relative and absolute quantitation (iTRAQ). J. Proteome Res. 6, 821–827. https://doi.org/10.1021/pr060474i

Gan, S., Amasino, R.M., 1997. Making Sense of Senescence. Plant Physiol. 113, 313–319. https://doi.org/10.1104/pp.113.2.313

Gangadhar, B.H., Mishra, R.K., Pandian, G., Park, S.W., 2012. Comparative Study of Color , Pungency , and Biochemical Composition in Chili Pepper (*Capsicum annuum*) Under Different Light-emitting Diode Treatments 47, 1729–1735.

Gao, F., Han, X., Wu, J., Zheng, S., Shang, Z., Sun, D., Zhou, R., Li, B., 2012. A heat-activated calcium-permeable channel - Arabidopsis cyclic nucleotide-gated ion channel 6 - Is involved in heat shock responses. Plant J. 70, 1056–1069. https://doi.org/10.1111/j.1365-313X.2012.04969.x

Gazanchian, A., Hajheidari, M., Sima, N.K., Salekdeh, G.H., 2007. Proteome response of *Elymus* *elongatum* to severe water stress and recovery. J. Exp. Bot. 58, 291–300. https://doi.org/10.1093/jxb/erl226

Ge, P., Ma, C., Wang, S., Gao, L., Li, X., Guo, G., Ma, W., Yan, Y., 2012. Comparative proteomic analysis of grain development in two spring wheat varieties under drought stress. Anal. Bioanal. Chem. 402, 1297–1313. https://doi.org/10.1007/s00216-011-5532-z

Geer, L.Y., Markey, S.P., Kowalak, J.A., Wagner, L., Xu, M., Maynard, D.M., Yang, X., Shi, W., Bryant, S.H., 2004. Open mass spectrometry search algorithm. J. Proteome Res. 3, 958–964. https://doi.org/10.1021/pr0499491

Gerganova, M., Popova, A. V., Stanoeva, D., Velitchkova, M., 2016. Tomato plants acclimate better to elevated temperature and high light than to treatment with each factor separately. Plant Physiol. Biochem. 104, 234–241. https://doi.org/10.1016/j.plaphy.2016.03.030

Gerland, P., Raftery, A.E., ev ikova, H., Li, N., Gu, D., Spoorenberg, T., Alkema, L., Fosdick, B.K., Chunn, J., Lalic, N., Bay, G., Buettner, T., Heilig, G.K., Wilmoth, J., 2014. World population stabilization unlikely this century. Science 346, 234–237. https://doi.org/10.1126/science.1257469

Ghosh, D., Xu, J., 2014. Abiotic stress responses in plant roots: a proteomics perspective. Front. Plant Sci. 5, 1–13. https://doi.org/10.3389/fpls.2014.00006

Godfray, H.C.J., Beddington, J.R., Crute, I.R., Haddad, L., Lawrence, D., Muir, J.F., Pretty, J., Robinson, S., Thomas, S.M., Toulmin, C., 2012. Food security: the challenge of feeding 9 billion people. Science 327, 812. https://doi.org/10.4337/9780857939388

Gómez, C., Morrow, R.C., Bourget, M., Massa, G., Mitchell Carry, A., 2013. Comparison of Intracanopy Light-emitting Diode Towers and Overhead High-Pressure Sodium Lamps for

Supplemental Lighting of Greenhouse-grown Tomatoes. Horttechnology 23, 93–98. https://doi.org/10.1017/CBO9781107415324.004

Gong, B., Zhang, C., Li, X., Wen, D., Wang, S., Shi, Q., Wang, X., 2014. Identification of NaCl and $NaHCO_3$ stress responsive proteins in tomato roots using iTRAQ-based analysis. Biochem. Biophys. Res. Commun. 446, 417–422. https://doi.org/10.1016/j.bbrc.2014.03.005

Greco, M., Chiappetta, A., Bruno, L., Bitonti, M.B., 2012. In *Posidonia oceanica* cadmium induces changes in DNA methylation and chromatin patterning. J. Exp. Bot. 63, 695–709. https://doi.org/10.1093/jxb/err313

Guan, Z., Mou, S., Zhang, X., Xu, D., Fan, X., Wang, Y., Wang, D., Ye, N., 2016. Identification and expression analysis of four light harvesting-like (*Lhc*) genes associated with light and desiccation stress in *Ulva linza*. J. Exp. Mar. Bio. Ecol. 478, 10–15. https://doi.org/10.1016/j.jembe.2016.01.012

Guo, H., Ecker, J.R., 2003. Plant responses to ethylene gas are mediated by SCFEBF1/EBF2-dependent proteolysis of EIN3 transcription factor. Cell 115, 667–677. https://doi.org/10.1016/S0092-8674(03)00969-3

Gupta, A.S., Webb, R.P., Holaday, A.S., Allen, R.D., 1993. Overexpression of Superoxide Dismutase Protects Plants from Oxidative Stress (Induction of Ascorbate Peroxidase in Superoxide Dismutase-Overexpressing Plants). Plant Physiol. 103, 1067–1073. https://doi.org/10.1104/pp.103.4.1067

Hajheidari, M., Eivazi, A., Buchanan, B.B., Wong, J.H., Majidi, I., Salekdeh, G.H., 2007. Proteomics uncovers a role for redox in drought tolerance in wheat. J. Proteome Res. 6, 1451–1460. https://doi.org/10.1021/pr060570j

Hakala, M., Tuominen, I., Keränen, M., Tyystjärvi, T., Tyystjärvi, E., 2005. Evidence for the role of the oxygen-evolving manganese complex in photoinhibition of Photosystem II. Biochim. Biophys. Acta - Bioenerg. 1706, 68–80. https://doi.org/10.1016/j.bbabio.2004.09.001

Han, X., He, X., Qiu, W., Lu, Z., Zhang, Y., Chen, S., Liu, M., Qiao, G., Zhuo, R., 2017. Pathogenesis-related protein PR10 from *Salix matsudana* Koidz exhibits resistance to salt stress in transgenic *Arabidopsis thaliana*. Environ. Exp. Bot. 141, 74–82. https://doi.org/10.1016/j.envexpbot.2017.07.008

Haque, M.S., Kjaer, K.H., Rosenqvist, E., Ottosen, C.-O., 2015. Recovery of tomato (*Solanum lycopersicum* L.) leaves from continuous light induced injury. J. Plant Physiol. 185, 24–30. https://doi.org/10.1016/j.jplph.2015.06.011

Havaux, M., Niyogi, K.K., 1999. The violaxanthin cycle protects plants from photooxidative damage by more than one mechanism. Proc. Natl. Acad. Sci. U. S. A. 96, 8762–8767. https://doi.org/10.1073/pnas.96.15.8762

He, J., Qin, L., Chong, E.L.C., Choong, T.-W., Lee, S.K., 2017. Plant Growth and Photosynthetic Characteristics of Mesembryanthemum crystallinum Grown Aeroponically under Different Blue- and Red-LEDs. Front. Plant Sci. 8, 1–13. https://doi.org/10.3389/fpls.2017.00361

Henmi, T., Miyao, M., Yamamoto, Y., 2004. Release and Reactive-Oxygen-Mediated Damage of the Oxygen-Evolving Complex Subunits of PSII during Photoinhibition. Plant Cell Physiol. 45, 243–250. https://doi.org/10.1093/pcp/pch027

Herbstova, M., Tietz, S., Kinzel, C., Turkina, M. V., Kirchhoff, H., 2012. Architectural switch in plant photosynthetic membranes induced by light stress. Proc. Natl. Acad. Sci. 109, 20130–20135. https://doi.org/10.1073/pnas.1214265109

Hewezi, T., Léger, M., Gentzbittel, L., 2008. A comprehensive analysis of the combined effects of high light and high temperature stresses on gene expression in sunflower. Ann. Bot. 102, 127–140. https://doi.org/10.1093/aob/mcn071

Hirosawa, M., Hoshida, M., Ishikawa, M., Toya, T., 1993. MASCOT: multiple alignment system for protein sequences based on three-way dynamic programming. Comput. Appl. Biosci. 9, 161–167.

Horton, P., Ruban, A., 2005. Molecular design of the photosystem II light-harvesting antenna: Photosynthesis and photoprotection. J. Exp. Bot. 56, 365–373. https://doi.org/10.1093/jxb/eri023

Hossain, Z., Nouri, M.-Z., Komatsu, S., 2012. Plant cell organelle proteomics in response to abiotic stress. J. Proteome Res. 11, 37–48. https://doi.org/10.1021/pr200863r

Houterman, P.M., Speijer, D., Dekker, H.L., Koster, C.G., Cornelissen, B.J.C., Rep, M., 2007. The mixed xylem sap proteome of *Fusarium oxysporum*-infected. Mol. Plant 8, 215–221. https://doi.org/10.1111/J.1364-3703.2007.00384.X

Hu, J., Rampitsch, C., Bykova, N. V, 2015. Advances in plant proteomics toward improvement of crop productivity and stress resistance. Front. Plant Sci. 6, 209. https://doi.org/10.3389/fpls.2015.00209

Hu, W., Zheng, M., Wang, S., Meng, Y., Wang, Y., Chen, B., Snider, J.L., Zhou, Z., 2017. Proteomic changes in response to low-light stress during cotton fiber elongation. Acta Physiol. Plant. 39, 200. https://doi.org/10.1007/s11738-017-2499-1

Huang, D.W., Sherman, B.T., Tan, Q., Collins, J.R., Alvord, W.G., Roayaei, J., Stephens, R., Baseler, M.W., Lane, H.C., Lempicki, R.A., 2007. The DAVID Gene Functional

Classification Tool: A novel biological module-centric algorithm to functionally analyze large gene lists. Genome Biol. 8. https://doi.org/10.1186/gb-2007-8-9-r183

Huang, E.L., Lefsrud, M.G., 2014. Fermentation Monitoring of a Co-Culture Process with *Saccharomyces cerevisiae* and *Scheffersomyces stipitis* Using Shotgun Proteomics. J. Bioprocess. Biotech. 4, 1–7. https://doi.org/10.4172/2155-9821.1000144

Huang, E.L., Lefsrud, M.G., 2012. Temporal analysis of xylose fermentation by *Scheffersomyces stipitis* using shotgun proteomics. J. Ind. Microbiol. Biotechnol. 39, 1507–1514. https://doi.org/10.1007/s10295-012-1147-4

Huang, E.L., Orsat, V., Shah, M.B., Hettich, R.L., VerBerkmoes, N.C., Lefsrud, M.G., 2012. The temporal analysis of yeast exponential phase using shotgun proteomics as a fermentation monitoring technique. J. Proteomics 75, 5206–5214. https://doi.org/10.1016/j.jprot.2012.06.005

Huang, Y., Shen, S., Li, H., Gu, Y., 2016. Improved thermal design of fin heat sink for high-power LED lamp cooling. 2016 17th Int. Conf. Electron. Packag. Technol. ICEPT 2016 1069–1074. https://doi.org/10.1109/ICEPT.2016.7583311

Huntley, R.P., Sawford, T., Mutowo-Meullenet, P., Shypitsyna, A., Bonilla, C., Martin, M.J., O'Donovan, C., 2015. The GOA database: Gene Ontology annotation updates for 2015. Nucleic Acids Res. 43, D1057–D1063. https://doi.org/10.1093/nar/gku1113

Ibort, P., Imai, H., Uemura, M., Aroca, R., 2018. Proteomic analysis reveals that tomato interaction with plant growth promoting bacteria is highly determined by ethylene perception. J. Plant Physiol. 220, 43–59. https://doi.org/10.1016/j.jplph.2017.10.008

Inoue, S., Kinoshita, T., 2017. Blue Light Regulation of Stomatal Opening and the Plasma

Membrane H^+-ATPase. Plant Physiol. 174, 531–538. https://doi.org/10.1104/pp.17.00166

Iseli, C., Jongeneel, C. V, Bucher, P., 1999. ESTScan: a program for detecting, evaluating, and reconstructing potential coding regions in EST sequences. Proc. Int. Conf. Intell. Syst. Mol. Biol. 138–148.

Iwai, M., Pack, C.-G., Takenaka, Y., Sako, Y., Nakano, A., 2013. Photosystem II antenna phosphorylation-dependent protein diffusion determined by fluorescence correlation spectroscopy. Sci. Rep. 3, 2833. https://doi.org/10.1038/srep02833

Jacob, P., Hirt, H., Bendahmane, A., 2017. The heat-shock protein/chaperone network and multiple stress resistance. Plant Biotechnol. J. 15, 405–414. https://doi.org/10.1111/pbi.12659

Jansen, M. a K., Gaba, V., Greenberg, B.M., Mattoo, a K., Edelman, M., 1996. Low threshold levels of ultraviolet-B in a background of photosynthetically active radiation trigger rapid degradation of the D2 protein of photosystem II. Plant J. 9, 693–699. https://doi.org/10.1046/j.1365-313X.1996.9050693.x

Järvi, S., Gollan, P.J., Aro, E.-M., 2013. Understanding the roles of the thylakoid lumen in photosynthesis regulation. Front. Plant Sci. 4, 434. https://doi.org/10.3389/fpls.2013.00434

Järvi, S., Suorsa, M., Aro, E.M., 2015. Photosystem II repair in plant chloroplasts-Regulation, assisting proteins and shared components with photosystem II biogenesis. Biochim. Biophys. Acta 1847, 900–909. https://doi.org/10.1016/j.bbabio.2015.01.006

Jones, A.G., Scullion, J., Ostle, N., Levy, P.E., Gwynn-Jones, D., 2014. Completing the FACE of elevated CO_2 research. Environ. Int. 73, 252–258. https://doi.org/10.1016/j.envint.2014.07.021

Kilambi, H. V., Manda, K., Sanivarapu, H., Maurya, V.K., Sharma, R., Sreelakshmi, Y., 2016. Shotgun proteomics of tomato fruits: evaluation, optimization and validation of sample preparation methods and mass spectrometric parameters. Front. Plant Sci. 7, 1–14. https://doi.org/10.3389/fpls.2016.00969

Kim, D.W., Rakwal, R., Agrawal, G.K., Jung, Y.H., Shibato, J., Jwa, N.S., Iwahashi, Y., Iwahashi, H., Kim, D.H., Shim, I.S., Usui, K., 2005. A hydroponic rice seedling culture model system for investigating proteome of salt stress in rice leaf. Electrophoresis 26, 4521–4539. https://doi.org/10.1002/elps.200500334

Kim, E.H., Li, X.P., Razeghifard, R., Anderson, J.M., Niyogi, K.K., Pogson, B.J., Chow, W.S., 2009. The multiple roles of light-harvesting chlorophyll a/b-protein complexes define structure and optimize function of *Arabidopsis* chloroplasts: A study using two chlorophyll b-less mutants. Biochim. Biophys. Acta - Bioenerg. 1787, 973–984. https://doi.org/10.1016/j.bbabio.2009.04.009

Kislinger, T., Gramolini, A.O., MacLennan, D.H., Emili, A., 2005. Multidimensional protein identification technology (MudPIT): Technical overview of a profiling method optimized for the comprehensive proteomic investigation of normal and diseased heart tissue. J. Am. Soc. Mass Spectrom. 16, 1207–1220. https://doi.org/10.1016/j.jasms.2005.02.015

Knight, H., Knight, M.R., 2001. Abiotic stress signalling pathways: Specificity and cross-talk. Trends Plant Sci. 6, 262–267. https://doi.org/10.1016/S1360-1385(01)01946-X

Kok, E.J., Lehesranta, S.J., van Dijk, J.P., Helsdingen, J.R., Dijksma, W.T.P., Van Hoef, A.M. a., Koistinen, K.M., Karenlampi, S.O., Kuiper, H. a., Keijer, J., 2008. Changes in gene and protein expression during tomato ripening - consequences for the safety assessment of new crop plant varieties. Food Sci. Technol. Int. 14, 503–518. https://doi.org/10.1177/1082013208100771

Koka, C. V, Cerny, R.E., Gardner, R.G., Noguchi, T., Fujioka, S., Takatsuto, S., Yoshida, S., Clouse, S.D., 2000. A putative role for the tomato genes *DUMPY* and *CURL-3* in brassinosteroid biosynthesis and response. Plant Physiol. 122, 85–98. https://doi.org/10.1104/pp.122.1.85

Komatsu, S., Hossain, Z., 2013. Organ-specific proteome analysis for identification of abiotic stress response mechanism in crop. Front. Plant Sci. 4, 71. https://doi.org/10.3389/fpls.2013.00071

Konopka-Postupolska, D., Clark, G., Goch, G., Debski, J., Floras, K., Cantero, A., Fijolek, B., Roux, S., Hennig, J., 2009. The Role of Annexin 1 in Drought Stress in *Arabidopsis*. Plant Physiol. 150, 1394–1410. https://doi.org/10.1104/pp.109.135228

Konozy, E.H.E., Rogniaux, H., Causse, M., Faurobert, M., 2013. Proteomic analysis of tomato (*Solanum lycopersicum*) secretome. J. Plant Res. 126, 251–266. https://doi.org/10.1007/s10265-012-0516-4

Kosová, K., Vítámvás, P., Prášil, I.T., Renaut, J., 2011. Plant proteome changes under abiotic stress - Contribution of proteomics studies to understanding plant stress response. J. Proteomics 74, 1301–1322. https://doi.org/10.1016/j.jprot.2011.02.006

Kosová, K., Vítámvás, P., Urban, M.O., Klíma, M., Roy, A., Tom Prášil, I., 2015. Biological networks underlying abiotic stress tolerance in temperate crops-a proteomic perspective. Int. J. Mol. Sci. 16, 20913–20942. https://doi.org/10.3390/ijms160920913

Koussevitzky, S., Suzuki, N., Huntington, S., Armijo, L., Sha, W., Cortes, D., Shulaev, V., Mittler, R., 2008. Ascorbate peroxidase 1 plays a key role in the response of *Arabidopsis thaliana* to stress combination. J. Biol. Chem. 283, 34197–34203. https://doi.org/10.1074/jbc.M806337200

Krause, C., Richter, S., Knöll, C., Jürgens, G., 2013. Plant secretome - From cellular process to biological activity. Biochim. Biophys. Acta - Proteins Proteomics 1834, 2429–2441. https://doi.org/10.1016/j.bbapap.2013.03.024

Kromdijk, J., Głowacka, K., Leonelli, L., Gabilly, S.T., Iwai, M., Niyogi, K.K., Long, S.P., 2016. Improving photosynthesis and crop productivity by accelerating recovery from photoprotection. Science 354, 857–861. https://doi.org/10.1126/science.aai8878

Külheim, C., Agren, J., Jansson, S., 2002. Rapid regulation of light harvesting and plant fitness in the field. Science 297, 91–3. https://doi.org/10.1126/science.1072359

Kurek, I., Chang, T.K., Bertain, S.M., Madrigal, A., Liu, L., Lassner, M.W., Zhu, G., 2007. Enhanced Thermostability of *Arabidopsis* Rubisco Activase Improves Photosynthesis and Growth Rates under Moderate Heat Stress. Plant Cell 19, 3230–3241. https://doi.org/10.1105/tpc.107.054171

Kwon, S.-Y., Choi, S.-M., Ahn, Y.-O., Lee, H.-S., Lee, H.-B., Park, Y.-M., Kwak, S.-S., 2003. Enhanced stress-tolerance of transgenic tobacco plants expressing a human dehydroascorbate reductase gene. J. Plant Physiol. 160, 347–53. https://doi.org/10.1078/0176-1617-00926

Laing, W., Christeller, J., 2004. Extraction of proteins from plant tissues. Curr. Protoc. protein Sci. 4.7.1. https://doi.org/10.1002/0471140864.ps0407s38

Laurindo, B.S., Laurindo, R.D.F., Fontes, P.P., Vital, C.E., Delazari, F.T., Baracat-Pereira, M.C., da Silva, D.J.H., 2018. Comparative analysis of constitutive proteome between resistant and susceptible tomato genotypes regarding to late blight. Funct. Integr. Genomics 18, 11–21. https://doi.org/10.1007/s10142-017-0570-z

Lee, S.H., Ahsan, N., Lee, K.W., Kim, D.H., Lee, D.G., Kwak, S.S., Kwon, S.Y., Kim, T.H., Lee, B.H., 2007. Simultaneous overexpression of both CuZn superoxide dismutase and ascorbate peroxidase in transgenic tall fescue plants confers increased tolerance to a wide range of abiotic stresses. J. Plant Physiol. 164, 1626–1638. https://doi.org/10.1016/j.jplph.2007.01.003

Leene, J. Van, Witters, E., Inze, D., Aeger, G. De, 2008. Boosting tandem affinity purification of plant protein complexes. Trends Plant Sci. 13, 517–520. https://doi.org/10.1016/j.tplants.2008.08.002

Lefsrud, M.G., Kopsell, D.A., Sams, C.E., 2008. Irradiance from distinct wavelength light-emitting diodes affect secondary metabolites in kale. HortScience 43, 2243–2244.

Li, J., Wu, X.D., Hao, S.T., Wang, X.J., Ling, H.Q., 2008. Proteomic response to iron deficiency in tomato root. Proteomics 8, 2299–2311. https://doi.org/10.1002/pmic.200700942

Li, X.P., Gilmore, A.M., Caffarri, S., Bassi, R., Golan, T., Kramer, D., Niyogi, K.K., 2004. Regulation of photosynthetic light harvesting involves intrathylakoid lumen pH sensing by the PsbS protein. J. Biol. Chem. 279, 22866–22874. https://doi.org/10.1074/jbc.M402461200

Lim, C.W., Lim, S., Baek, W., Lee, S.C., 2015. The pepper late embryogenesis abundant protein CaLEA1 acts in regulating abscisic acid signaling, drought and salt stress response. Physiol. Plant. 154, 526–542. https://doi.org/10.1111/ppl.12298

Liu, J.J., Ekramoddoullah, A.K.M., 2006. The family 10 of plant pathogenesis-related proteins: Their structure, regulation, and function in response to biotic and abiotic stresses. Physiol.

Mol. Plant Pathol. 68, 3–13. https://doi.org/10.1016/j.pmpp.2006.06.004

Liu, Y., Shi, Y., Song, Y., Wang, T., Li, Y., 2010. Characterization of a stress-induced NADP-isocitrate dehydrogenase gene in maize confers salt tolerance in arabidopsis. J. Plant Biol. 53, 107–112. https://doi.org/10.1007/s12374-009-9091-1

Lockhart, J., 2016. Counting carbs: tracking fluctuations in starch-derived metabolite levels uncovers their crucial roles in osmotic stress tolerance. Plant Cell 28, 1757–1758. https://doi.org/10.1105/tpc.16.00585

Lopez-Casado, G., Covey, P.A., Bedinger, P.A., Mueller, L.A., Thannhauser, T.W., Zhang, S., Fei, Z., Giovannoni, J.J., Rose, J.K.C., 2012. Enabling proteomic studies with RNA-Seq: The proteome of tomato pollen as a test case. Proteomics 12, 761–774. https://doi.org/10.1002/pmic.201100164

Løvdal, T., Lillo, C., 2009. Reference gene selection for quantitative real-time PCR normalization in tomato subjected to nitrogen, cold, and light stress. Anal. Biochem. 387, 238–242. https://doi.org/10.1016/j.ab.2009.01.024

Lu, W., Tang, X., Huo, Y., Xu, R., Qi, S., Huang, J., Zheng, C., Wu, C. ai, 2012. Identification and characterization of fructose 1,6-bisphosphate aldolase genes in *Arabidopsis* reveal a gene family with diverse responses to abiotic stresses. Gene 503, 65–74. https://doi.org/10.1016/j.gene.2012.04.042

Lu, Y., Hall, D. a, Last, R.L., 2011. A small zinc finger thylakoid protein plays a role in maintenance of photosystem II in *Arabidopsis thaliana*. Plant Cell 23, 1861–1875. https://doi.org/10.1105/tpc.111.085456

Maier, T., Güell, M., Serrano, L., 2009. Correlation of mRNA and protein in complex biological samples. FEBS Lett. 583, 3966–3973. https://doi.org/10.1016/j.febslet.2009.10.036

Manaa, A., Ben Ahmed, H., Valot, B., Bouchet, J.P., Aschi-Smiti, S., Causse, M., Faurobert, M., 2011. Salt and genotype impact on plant physiology and root proteome variations in tomato. J. Exp. Bot. 62, 2797–2813. https://doi.org/10.1093/jxb/erq460

Manaa, A., Mimouni, H., Wasti, S., Gharbi, E., Aschi-smiti, S., Ahmed, H. Ben, 2013. Comparative proteomic analysis of tomato (*Solanum lycopersicum*) leaves under salinity stress. Plant Omics 6, 268–277.

Mann, M., Jensen, O.N., 2003. Proteomic analysis of post-translational modifications. Nat. Biotechnol. 21, 255–61. https://doi.org/10.1038/nbt0303-255

Martineau, V., Lefsrud, M., Naznin, M.T., Kopsell, D.A., 2012. Comparison of Light-emitting Diode and High-pressure Sodium Light Treatments for Hydroponics Growth of Boston Lettuce. HortScience 47, 477–482.

Massot, C., Stevens, R., Génard, M., Longuenesse, J.J., Gautier, H., 2012. Light affects ascorbate content and ascorbate-related gene expression in tomato leaves more than in fruits. Planta 235, 153–163. https://doi.org/10.1007/s00425-011-1493-x

Mata, C.I., Fabre, B., Hertog, M.L.A.T.M., Parsons, H.T., Deery, M.J., Lilley, K.S., Nicolaï, B.M., 2017. In-depth characterization of the tomato fruit pericarp proteome. Proteomics 17, 1–2. https://doi.org/10.1002/pmic.201600406

Maxwell, K., Johnson, G.N., 2000. Chlorophyll fluorescence - a practical guide. J. Exp. Bot. 51, 659–668. https://doi.org/10.1093/jexbot/51.345.659

McDonald, W.H., Ohi, R., Miyamoto, D.T., Mitchison, T.J., Yates, J.R., 2002. Comparison of three directly coupled HPLC MS/MS strategies for identification of proteins from complex mixtures: Single-dimension LC-MS/MS, 2-phase MudPIT, and 3-phase MudPIT. Int. J. Mass Spectrom. 219, 245–251. https://doi.org/10.1016/S1387-3806(02)00563-8

McKersie, B.D., Bowley, S.R., Jones, K.S., 1999. Winter Survival of Transgenic Alfalfa Overexpressing Superoxide Dismutase1. Plant Physiol. 119, 839–848. https://doi.org/10.1104/pp.119.3.839

Mehta, A., Brasileiro, A.C.M., Souza, D.S.L., Romano, E., Campos, A., Grossi-de-sa, M.F., 2008. Plant–pathogen interactions: what is proteomics telling us? FEBS J. 275, 3731–3746. https://doi.org/10.1111/j.1742-4658.2008.06528.x

Meyer, S., Genty, B., 1998. Mapping intercellular CO_2 mole fraction (Ci) in rosa rubiginosa leaves fed with abscisic acid by using chlorophyll fluorescence imaging - Significance Of ci estimated from leaf gas exchange. Plant Physiol. 116, 947–57. https://doi.org/10.1104/pp.116.3.947

Mi, H., Muruganujan, A., Casagrande, J.T., Thomas, P.D., 2013. Large-scale gene function analysis with the PANTHER classification system. Nat. Protoc. 8, 1551–1566. https://doi.org/10.1038/nprot.2013.092

Miller, M.A.E., O'Cualain, R., Selley, J., Knight, D., Karim, M.F., Hubbard, S.J., Johnson, G.N., 2017. Dynamic acclimation to high light in *Arabidopsis thaliana* involves widespread reengineering of the leaf proteome. Front. Plant Sci. 8, 1–15. https://doi.org/10.3389/fpls.2017.01239

Mittler, R., 2006. Abiotic stress, the field environment and stress combination. Trends Plant Sci. 11, 15–19. https://doi.org/10.1016/j.tplants.2005.11.002

Mittler, R., 2002. Oxidative stress, antioxidants and stress tolerance. Trends Plant Sci. 7, 405–410.

https://doi.org/10.1016/S1360-1385(02)02312-9

Mittler, R., Blumwald, E., 2010. Genetic engineering for modern agriculture: challenges and perspectives. Annu. Rev. Plant Biol. 61, 443–462. https://doi.org/10.1146/annurev-arplant-042809-112116

Moore, M., Vogel, M., Dietz, K., 2014. The acclimation response to high light is initiated within seconds as indicated by upregulation of AP2/ERF transcription factor network in *Arabidopsis thaliana*. Plant Signal. Behav. 9, 976479. https://doi.org/10.4161/15592324.2014.976479

Motoyama, A., Yates, J.R., 2008. Multidimensional LC separations in shotgun proteomics. Anal. Chem. 80, 7187–7193. https://doi.org/10.1021/ac8013669

Mott, K.A., Sibbernsen, E.D., Shope, J.C., 2008. The role of the mesophyll in stomatal responses to light and CO_2. Plant, Cell Environ. 31, 1299–1306. https://doi.org/10.1111/j.1365-3040.2008.01845.x

Muneer, S., Jeong, B.R., 2015. Proteomic analysis of salt-stress responsive proteins in roots of tomato (*Lycopersicon esculentum* L.) plants towards silicon efficiency. Plant Growth Regul. 77, 133–146. https://doi.org/10.1007/s10725-015-0045-y

Muneer, S., Ko, C.H., Wei, H., Chen, Y., Jeong, B.R., 2016. Physiological and Proteomic Investigations to Study the Response of Tomato Graft Unions under Temperature Stress. PLoS One 11, e0157439. https://doi.org/10.1371/journal.pone.0157439

Murchie, E.H., Lawson, T., 2013. Chlorophyll fluorescence analysis: A guide to good practice and understanding some new applications. J. Exp. Bot. 64, 3983–3998. https://doi.org/10.1093/jxb/ert208

Nakagami, H., Sugiyama, N., Mochida, K., Daudi, A., Yoshida, Y., Toyoda, T., Tomita, M., Ishihama, Y., Shirasu, K., 2010. Large-scale comparative phosphoproteomics identifies conserved phosphorylation sites in plants. Plant Physiol. 153, 1161–1174. https://doi.org/10.1104/pp.110.157347

Nama, S., Madireddi, S.K., Devadasu, E.R., Subramanyam, R., 2015. High light induced changes in organization, protein profile and function of photosynthetic machinery in *Chlamydomonas reinhardtii*. J. Photochem. Photobiol. B Biol. 152, 367–376. https://doi.org/10.1016/j.jphotobiol.2015.08.025

Ndimba, B.K., Chivasa, S., Simon, W.J., Slabas, A.R., 2005. Identification of *Arabidopsis* salt and osmotic stress responsive proteins using two-dimensional difference gel electrophoresis and mass spectrometry. Proteomics 5, 4185–4196. https://doi.org/10.1002/pmic.200401282

Nelson, C.J., Alexova, R., Jacoby, R.P., Millar, A.H., 2014. Proteins with high turnover rate in barley leaves estimated by proteome analysis combined with in planta isotope labeling. Plant Physiol. 166, 91–108. https://doi.org/10.1104/pp.114.243014

Nesvizhskii, A.I., Aebersold, R., 2004. Analysis, statistical validation and dissemination of large-scale proteomics datasets generated by tandem MS. Drug Discov. Today 9, 173–181. https://doi.org/10.1016/S1359-6446(03)02978-7

Niyogi, K.K., Grossman, A.R., Björkman, O., 1998. Arabidopsis mutants define a central role for the xanthophyll cycle in the regulation of photosynthetic energy conversion. Plant Cell 10, 1121–34. https://doi.org/10.1105/tpc.10.7.1121

Page, D., Gouble, B., Valot, B., Bouchet, J.P., Callot, C., Kretzschmar, A., Causse, M., Renard, C.M.C.G., Faurobert, M., 2010. Protective proteins are differentially expressed in tomato genotypes differing for their tolerance to low-temperature storage. Planta 232, 483–500.

https://doi.org/10.1007/s00425-010-1184-z

Pagliano, C., Saracco, G., Barber, J., 2013. Structural, functional and auxiliary proteins of photosystem II. Photosynth. Res. 116, 167–188. https://doi.org/10.1007/s11120-013-9803-8

Palukaitis, P., Roossinck, M.J., Dietzgen, R.G., Francki, R.I.B., 1992. Cucumber MOSAIC Virus. Adv. Virus Res. 41, 281–348. https://doi.org/http://dx.doi.org/10.1016/S0065-3527(08)60039-1

Pandey, S., Fartyal, D., Agarwal, A., Shukla, T., James, D., Kaul, T., Negi, Y.K., Arora, S., Reddy, M.K., 2017. Abiotic Stress Tolerance in Plants: Myriad Roles of Ascorbate Peroxidase. Front. Plant Sci. 8, 1–13. https://doi.org/10.3389/fpls.2017.00581

Pandey, S., Ranade, S.A., Nagar, P.K., Kumar, N., 2000. Role of polyamines and ethylene as modulators of plant senescence. J. Biosci. 25, 291–299. https://doi.org/10.1007/BF02703938

Pang, Q.Y., Chen, S.X., Dai, S.J., Chen, Y.Z., Wang, Y., Yan, X.F., 2010. Comparative proteomics of salt tolerance in *Arabidopsis thaliana* and *Thellungiella halophila*. J Proteome Res 9, 2584–2599. https://doi.org/10.1021/pr100034f

Park, B.J., Liu, Z., Kanno, A., Kameya, T., 2005. Increased tolerance to salt- and water-deficit stress in transgenic lettuce (*Lactuca sativa* L.) by constitutive expression of LEA. Plant Growth Regul. 45, 165–171. https://doi.org/10.1007/s10725-004-7924-y

Park, O.K., 2004. Proteomic studies in plants. J. Biochem. Mol. Biol. 37, 133–138.

Parker, J., Koh, J., Yoo, M.-J., Zhu, N., Feole, M., Yi, S., Chen, S., 2013. Quantitative proteomics of tomato defense against *Pseudomonas syringae* infection. Proteomics 13, 1934–46. https://doi.org/10.1002/pmic.201200402

Patel, A.K., 2015. Microalgae for wastewater treatment and biomass production : A comparative analysis of growth and nutrient removal including shotgun proteomics. McGill University.

Patel, A.K., Huang, E.L., Low-Décarie, E., Lefsrud, M.G., 2015. Comparative Shotgun Proteomic Analysis of Wastewater-Cultured Microalgae: Nitrogen Sensing and Carbon Fixation for Growth and Nutrient Removal in *Chlamydomonas reinhardtii*. J. Proteome Res. 14, 3051–3067. https://doi.org/10.1021/pr501316h

Pedersen, A.G., Nielsen, H., 1997. Neural network prediction of translation initiation sites in eukaryotes: perspectives for EST and genome analysis. Proceedings. Int. Conf. Intell. Syst. Mol. Biol. 5, 226–33.

Peng, Z., Wang, M., Li, F., Lv, H., Li, C., Xia, G., 2009. A Proteomic Study of the Response to Salinity and Drought Stress in an Introgression Strain of Bread Wheat. Mol. Cell. Proteomics 8, 2676–2686. https://doi.org/10.1074/mcp.M900052-MCP200

Perl-Treves, R., Galun, E., 1991. The tomato Cu,Zn superoxide dismutase genes are developmentally regulated and respond to light and stress. Plant Mol. Biol. 17, 745–760.

Petroutsos, D., Tokutsu, R., Maruyama, S., Flori, S., Greiner, A., Magneschi, L., Cusant, L., Kottke, T., Mittag, M., Hegemann, P., Finazzi, G., Minagawa, J., 2016. A blue-light photoreceptor mediates the feedback regulation of photosynthesis. Nature 537, 563–566. https://doi.org/10.1038/nature19358

Pianka, M., 1957. Biological activity and chemical reactivity of organophosphorus compounds. j sci food agric 8, 393–399.

Pitakrattananukool, S., Kawakatsu, T., Anuntalabhochai, S., Takaiwa, F., 2012. Overexpression of OsRab7B3, a Small GTP-Binding Protein Gene, Enhances Leaf Senescence in Transgenic Rice. Biosci. Biotechnol. Biochem. 76, 1296–1302. https://doi.org/10.1271/bbb.120050

Planas-Marquès, M., Bernardo-Faura, M., Paulus, J.K., Kaschani, F., Kaiser, M., Valls, M., van der Hoorn, R., Sanchez Coll, N., 2018. Protease activities triggered by Ralstonia solanacearum infection in susceptible and tolerant tomato lines. Mol. Cell. Proteomics mcp.RA117.000052. https://doi.org/10.1074/mcp.RA117.000052

Qureshi, M.I., Qadir, S., Zolla, L., 2007. Proteomics-based dissection of stress-responsive pathways in plants. J. Plant Physiol. 164, 1239–1260. https://doi.org/10.1016/j.jplph.2007.01.013

Rinalducci, S., Pedersen, J.Z., Zolla, L., 2004. Formation of radicals from singlet oxygen produced during photoinhibition of isolated light-harvesting proteins of photosystem II. Biochim. Biophys. Acta 1608, 63—73.

Rizhsky, L., Liang, H., Mittler, R., 2002. The combined effect of drought stress and heat shock on gene expression in tobacco. Plant Phisiology 130, 1143–1151. https://doi.org/10.1104/pp.006858

Rocco, M., D'Ambrosio, C., Arena, S., Faurobert, M., Scaloni, A., Marra, M., 2006. Proteomic analysis of tomato fruits from two ecotypes during ripening. Proteomics 6, 3781–3791. https://doi.org/10.1002/pmic.200600128

Rockström, J., Falkenmark, M., 2000. Semiarid crop production from a hydrological perspective: gap between potential and actual yields. CRC. Crit. Rev. Plant Sci. 19, 319–346. https://doi.org/10.1080/07352680091139259

Rodrigo, G., Carrera, J., Ruiz-Ferrer, V., del Toro, F.J., Llave, C., Voinnet, O., Elena, S.F., 2012. A meta-analysis reveals the commonalities and differences in *Arabidopsis thaliana* response to different viral pathogens. PLoS One 7, 1–14. https://doi.org/10.1371/journal.pone.0040526

Rodríguez-Celma, J., Rellán-Álvarez, R., Abadía, A., Abadía, J., López-Millán, A.F., 2010. Changes induced by two levels of cadmium toxicity in the 2-DE protein profile of tomato roots. J. Proteomics 73, 1694–1706. https://doi.org/10.1016/j.jprot.2010.05.001

Rodriguez, R.E., Lodeyro, A., Poli, H.O., Zurbriggen, M., Peisker, M., Palatnik, J.F., Tognetti, V.B., Tschiersch, H., Hajirezaei, M.-R., Valle, E.M., Carrillo, N., 2006. Transgenic Tobacco Plants Overexpressing Chloroplastic Ferredoxin-NADP(H) Reductase Display Normal Rates of Photosynthesis and Increased Tolerance to Oxidative Stress. Plant Physiol. 143, 639–649. https://doi.org/10.1104/pp.106.090449

Rodziewicz, P., Swarcewicz, B., Chmielewska, K., Wojakowska, A., Stobiecki, M., 2014. Influence of abiotic stresses on plant proteome and metabolome changes. Acta Physiol. Plant. 36, 1–19. https://doi.org/10.1007/s11738-013-1402-y

Rokka, A., Suorsa, M., Saleem, A., Battchikova, N., Aro, E.-M., 2005. Synthesis and assembly of thylakoid protein complexes: multiple assembly steps of photosystem II. Biochem. J. 388, 159–168. https://doi.org/10.1042/BJ20042098

Ross, P.L., Huang, Y.N., Marchese, J.N., Williamson, B., Parker, K., Hattan, S., Khainovski, N., Pillai, S., Dey, S., Daniels, S., Purkayastha, S., Juhasz, P., Martin, S., Bartlet-Jones, M., He, F., Jacobson, A., Pappin, D.J., 2004. Multiplexed Protein Quantitation in *Saccharomyces cerevisiae* Using Amine-reactive Isobaric Tagging Reagents. Mol. Cell. Proteomics 3, 1154–1169. https://doi.org/10.1074/mcp.M400129-MCP200

RoyChoudhury, A., Roy, C., Sengupta, D.N., 2007. Transgenic tobacco plants overexpressing the heterologous lea gene Rab16A from rice during high salt and water deficit display enhanced tolerance to salinity stress. Plant Cell Rep. 26, 1839–1859. https://doi.org/10.1007/s00299-

007-0371-2

Ruban, A. V., Johnson, M.P., Duffy, C.D.P., 2012. The photoprotective molecular switch in the photosystem II antenna. Biochim. Biophys. Acta - Bioenerg. 1817, 167–181. https://doi.org/10.1016/j.bbabio.2011.04.007

Saibo, N.J.M., Lourenço, T., Oliveira, M.M., 2009. Transcription factors and regulation of photosynthetic and related metabolism under environmental stresses. Ann. Bot. 103, 609–623. https://doi.org/10.1093/aob/mcn227

Sakata, S., Mizusawa, N., Kubota-Kawai, H., Sakurai, I., Wada, H., 2013. Psb28 is involved in recovery of photosystem II at high temperature in *Synechocystis* sp. PCC 6803. Biochim. Biophys. Acta - Bioenerg. 1827, 50–59. https://doi.org/10.1016/j.bbabio.2012.10.004

Salekdeh, G.H., Komatsu, S., 2007. Crop proteomics: Aim at sustainable agriculture of tomorrow. Proteomics 7, 2976–2996. https://doi.org/10.1002/pmic.200700181

Sanchez-Lucas, R., Mehta, A., Valledor, L., Cabello-Hurtado, F., Romero-Rodriguez, M.C., Simova-Stoilova, L., Demir, S., Rodriguez-de-Francisco, L.E., Maldonado-Alconada, A.M., Jorrin-Prieto, A.L., Jorrín-Novo, J. V., 2016. A year (2014-2015) of plants in *Proteomics* journal. Progress in wet and dry methodologies, moving from protein catalogs, and the view of classic plant biochemists. Proteomics 16, 866–876. https://doi.org/10.1002/pmic.201500351

Sant'Ana, D.V.P., Lefsrud, M., 2018. Tomato proteomics: Tomato as a model for crop proteomics. Sci. Hortic. (Amsterdam). 239, 224–233. https://doi.org/10.1016/j.scienta.2018.05.041

Santabarbara, S., Neverov, K. V., Garlaschi, F.M., Zucchelli, G., Jennings, R.C., 2001. Involvement of uncoupled antenna chlorophylls in photoinhibition in thylakoids. FEBS Lett.

491, 109–113. https://doi.org/10.1016/S0014-5793(01)02174-3

Schilmiller, A.L., Miner, D.P., Larson, M., McDowell, E., Gang, D.R., Wilkerson, C., Last, R.L., 2010. Studies of a biochemical factory: tomato trichome deep expressed sequence tag sequencing and proteomics. Plant Physiol. 153, 1212–1223. https://doi.org/10.1104/pp.110.157214

Sels, J., Mathys, J., De Coninck, B.M.A., Cammue, B.P.A., De Bolle, M.F.C., 2008. Plant pathogenesis-related (PR) proteins: A focus on PR peptides. Plant Physiol. Biochem. 46, 941–950. https://doi.org/10.1016/j.plaphy.2008.06.011

Shah, P., Powell, A.L.T., Orlando, R., Bergmann, C., Gutierrez-Sanchez, G., 2012a. Proteomic analysis of ripening tomato fruit infected by *Botrytis cinerea*. J. Proteome Res. 11, 2178–2192. https://doi.org/10.1021/pr200965c

Shah, P., Powell, A.L.T., Orlando, R., Bergmann, C., Gutierrez-Sanchez, G., 2012b. A Proteomic Analysis of Ripening Tomato Fruit Infected by *Botrytis cinerea*. Proteome Res. 11, 2178–2192. https://doi.org/10.1021/pr200965c

Shaheen, M.R., Ayyub, C.M., Amjad, M., Waraich, E.A., 2015. Morpho-physiological evaluation of tomato genotypes under high temperature stress conditions. J. Sci. Food Agric. 96, 2698–2704. https://doi.org/10.1002/jsfa.7388

Shannon, P., Markiel, A., Ozier, O., Baliga, N.S., Wang, J.T., Ramage, D., Amin, N., Schwikowski, B., Ideker, T., 2003. Cytoscape: A Software Environment for Integrated Models of Biomolecular Interaction Networks. Genome Res. 13, 2498–2504. https://doi.org/10.1101/gr.1239303

Shao, H., Guo, Q., Chu, L., Zhao, X., Su, Z., Hu, Y., Cheng, J., 2007. Understanding molecular mechanism of higher plant plasticity under abiotic stress. Colloids and Surfaces B-Biointerfaces 54, 37–45. https://doi.org/10.1016/j.colsurfb.2006.07.002

Shi, D., Sheng, Y., 2005. Effect of various salt-alkaline mixed stress conditions on sunflower seedlings and analysis of their stress factors. Environ. Exp. Bot. 54, 8–21. https://doi.org/10.1016/j.envexpbot.2004.05.003

Shin, R., Jez, J.M., Basra, A., Zhang, B., Schachtman, D.P., 2011. 14-3-3 Proteins fine-tune plant nutrient metabolism. FEBS Lett. 585, 143–147. https://doi.org/10.1016/j.febslet.2010.11.025

Sivagnanam, K., Raghavan, V.G.S., Shah, M., Hettich, R.L., Verberkmoes, N.C., Lefsrud, M.G., 2012. Shotgun proteomic monitoring of *Clostridium acetobutylicum* during stationary phase of butanol fermentation using xylose and comparison with the exponential phase. J. Ind. Microbiol. Biotechnol. 39, 949–955. https://doi.org/10.1007/s10295-012-1094-0

Sivagnanam, K., Raghavan, V.G.S., Shah, M., Hettich, R.L., Verberkmoes, N.C., Lefsrud, M.G., 2011a. Comparative shotgun proteomic analysis of *Clostridium acetobutylicum* from butanol fermentation using glucose and xylose. Proteome Sci. 9, 66. https://doi.org/10.1186/1477-5956-9-66

Sivagnanam, K., Raghavan, V.G.S., Shah, M., Verberkmoes, N.C., Hettich, R.L., Lefsrud, M.G., 2011b. Proteomic analysis of *Clostridium acetobutylicum* in butanol production from lignocellulosic biomass. BMC Proc. 5, P176. https://doi.org/10.1186/1753-6561-5-S7-P176

Srivastava, S., Fristensky, B., Kav, N.N. V, 2004. Constitutive Expression of a PR10 Protein Enhances the Germination of *Brassica napus* under saline conditions. Plant Cell Physiol. 45, 1320–1324.

Stulemeijer, I.J.E., Joosten, M.H.A.J., Jensen, O.N., 2009. Quantitative phosphoproteomics of tomato mounting a hypersensitive response reveals a swift suppression of photosynthetic activity and a differential role for Hsp90 Isoforms. J. Proteome Res. 8, 1168–1182. https://doi.org/10.1021/pr800619h

Sugimoto, M., Takeda, K., 2009. Proteomic analysis of specific proteins in the root of salt-tolerant barley. Biosci. Biotechnol. Biochem. 73, 2762–5. https://doi.org/10.1271/bbb.90456

Suorsa, M., Rantala, M., Danielsson, R., Järvi, S., Paakkarinen, V., Schröder, W.P., Styring, S., Mamedov, F., Aro, E.M., 2014. Dark-adapted spinach thylakoid protein heterogeneity offers insights into the photosystem II repair cycle. Biochim. Biophys. Acta - Bioenerg. 1837, 1463–1471. https://doi.org/10.1016/j.bbabio.2013.11.014

Suorsa, M., Sirpiö, S., Allahverdiyeva, Y., Paakkarinen, V., Mamedov, F., Styring, S., Aro, E.M., 2006. PsbR, a missing link in the assembly of the oxygen-evolving complex of plant photosystem II. J. Biol. Chem. 281, 145–150. https://doi.org/10.1074/jbc.M510600200

Suzuki, M., Takahashi, S., Kondo, T., Dohra, H., Ito, Y., Kiriiwa, Y., Hayashi, M., Kamiya, S., Kato, M., Fujiwara, M., Fukao, Y., Kobayashi, M., Nagata, N., Motohashi, R., 2015. Plastid proteomic analysis in tomato fruit development. PLoS One 10, 1–25. https://doi.org/10.1371/journal.pone.0137266

Suzuki, N., Devireddy, A.R., Inupakutika, M.A., Baxter, A., Miller, G., Song, L., Shulaev, E., Azad, R.K., Shulaev, V., Mittler, R., 2015. Ultra-fast alterations in mRNA levels uncover multiple players in light stress acclimation in plants. Plant J. 84, 760–772. https://doi.org/10.1111/tpj.13039

Suzuki, N., Rivero, R.M., Shulaev, V., Blumwald, E., Mittler, R., 2014. Abiotic and biotic stress combinations. New Phytol. 203, 32–43. https://doi.org/10.1111/nph.12797

Szklarczyk, D., Franceschini, A., Wyder, S., Forslund, K., Heller, D., Huerta-Cepas, J., Simonovic, M., Roth, A., Santos, A., Tsafou, K.P., Kuhn, M., Bork, P., Jensen, L.J., Von Mering, C., 2015. STRING v10: Protein-protein interaction networks, integrated over the tree of life. Nucleic Acids Res. 43, D447–D452. https://doi.org/10.1093/nar/gku1003

Szklarczyk, D., Morris, J.H., Cook, H., Kuhn, M., Wyder, S., Simonovic, M., Santos, A., Doncheva, N.T., Roth, A., Bork, P., Jensen, L.J., von Mering, C., 2017. The STRING database in 2017: quality-controlled protein–protein association networks, made broadly accessible. Nucleic Acids Res. 45, D362–D368. https://doi.org/10.1093/nar/gkw937

Szymańska, R., Ślesak, I., Orzechowska, A., Kruk, J., 2017. Physiological and biochemical responses to high light and temperature stress in plants. Environ. Exp. Bot. 139, 165–177. https://doi.org/10.1016/j.envexpbot.2017.05.002

Szymanski, J., Levin, Y., Savidor, A., Breitel, D., Chappell-Maor, L., Heinig, U., Töpfer, N., Aharoni, A., 2017. Label-free deep shotgun proteomics reveals protein dynamics during tomato fruit tissues development. Plant J. 90, 396–417. https://doi.org/10.1111/tpj.13490

Tamburino, R., Vitale, M., Ruggiero, A., Sassi, M., Sannino, L., Arena, S., Costa, A., Batelli, G., Zambrano, N., Scaloni, A., Grillo, S., Scotti, N., 2017. Chloroplast proteome response to drought stress and recovery in tomato (*Solanum lycopersicum* L.). BMC Plant Biol. 17, 40. https://doi.org/10.1186/s12870-017-0971-0

Tanou, G., Job, C., Rajjou, L., Arc, E., Belghazi, M., Diamantidis, G., Molassiotis, A., Job, D., 2009. Proteomics reveals the overlapping roles of hydrogen peroxide and nitric oxide in the acclimation of citrus plants to salinity. Plant J. 60, 795–804. https://doi.org/10.1111/j.1365-313X.2009.04000.x

Tenga, Milagros, J., Lazar, I., 2011. Impact of Peptide Modifications on iTRAQ Quantitation Accuracy. Anal Chem. 83, 701–707. https://doi.org/10.1021/ac100775s.Impact

Tepfer, M., Girardot, G., Fénéant, L., Ben Tamarzizt, H., Verdin, E., Moury, B., Jacquemond, M., 2016. A genetically novel, narrow-host-range isolate of cucumber mosaic virus (CMV) from rosemary. Arch. Virol. 161, 2013–2017. https://doi.org/10.1007/s00705-016-2874-z

Tester, M., Langridge, P., 2010. Breeding Technologies to Increase Crop Production in a Changing World. Science (80-.). 327, 818–822. https://doi.org/10.1126/science.1183700

Thalmann, M., Pazmino, D., Seung, D., Horrer, D., Nigro, A., Meier, T., Kölling, K., Pfeifhofer, H.W., Zeeman, S.C., Santelia, D., 2016. Regulation of leaf starch degradation by abscisic acid is important for osmotic stress tolerance in plants. Plant Cell 28, 1860–1878. https://doi.org/10.1105/tpc.16.00143

Tibiletti, T., Auroy, P., Peltier, G., Caffarri, S., 2016. *Chlamydomonas reinhardtii* PsbS protein is functional and accumulates rapidly and transiently under high light. Plant Physiol. pp.00572.2016. https://doi.org/10.1104/pp.16.00572

Tomato Genome Consortium, T., 2012. The tomato genome sequence provides insights into fleshy fruit evolution. Nature 485, 635–641. https://doi.org/10.1038/nature11119

Tyanova, S., Temu, T., Sinitcyn, P., Carlson, A., Hein, M.Y., Geiger, T., Mann, M., Cox, J., 2016. The Perseus computational platform for comprehensive analysis of (prote)omics data. Nat. Methods 13, 731–40. https://doi.org/10.1038/nmeth.3901

Tyystjärvi, E., 2008. Photoinhibition of Photosystem II and photodamage of the oxygen evolving manganese cluster. Coord. Chem. Rev. 252, 361–376. https://doi.org/10.1016/j.ccr.2007.08.021

Tyystjärvi, E., Aro, E.M., 1996. The rate constant of photoinhibition, measured in lincomycin-treated leaves, is directly proportional to light intensity. Proc. Natl. Acad. Sci. U. S. A. 93, 2213–2218. https://doi.org/10.1073/pnas.93.5.2213

Van der Hoeven, R., Ronning, C., Giovannoni, J., Martin, G., Tanksley, S., 2002. Deductions about the number, organization, and evolution of genes in the tomato genome based on analysis of a large expressed sequence tag collection and selective genomic sequencing. Plant Cell 14, 1441–1456. https://doi.org/10.1105/tpc.010478

Van Eerden, F.J., Van Den Berg, T., Frederix, P.W.J.M., De Jong, D.H., Periole, X., Marrink, S.J., 2017. Molecular Dynamics of Photosystem II Embedded in the Thylakoid Membrane. J. Phys. Chem. B 121, 3237–3249. https://doi.org/10.1021/acs.jpcb.6b06865

Vanderschuren, H., Lentz, E., Zainuddin, I., Gruissem, W., 2013. Proteomics of model and crop plant species: Status, current limitations and strategic advances for crop improvement. J. Proteomics 93, 5–19. https://doi.org/10.1016/j.jprot.2013.05.036

Vanhove, A.-C., 2012. Screening the banana biodiversity for drought tolerance: can an in vitro growth model and proteomics be used as a tool to discover tolerant varieties and understand homeostasis. Front. Plant Sci. 3, 1–10. https://doi.org/10.3389/fpls.2012.00176

Vega-García, M.O., López-Espinoza, G., Chávez Ontiveros, J., Caro-Corrales, J.J., Delgado Vargas, F., López-Valenzuela, J.A., 2010. Changes in protein expression associated with chilling injury in tomato fruit. J. Am. Soc. Hortic. Sci. 135, 83–89.

Velez-Ramirez, A.I., Dünner-Planella, G., Vreugdenhil, D., Millenaar, F.F., van Ieperen, W., 2017. On the induction of injury in tomato under continuous light: circadian asynchrony as the main triggering factor. Funct. Plant Biol. 44, 597. https://doi.org/10.1071/FP16285

Vincent, D., Ergül, A., Bohlman, M.C., Tattersall, E.A.R., Tillett, R.L., Wheatley, M.D., Woolsey, R., Quilici, D.R., Joets, J., Schlauch, K., Schooley, D.A., Cushman, J.C., Cramer, G.R., 2007. Proteomic analysis reveals differences between *Vitis vinifera* L. cv. Chardonnay and cv. Cabernet Sauvignon and their responses to water deficit and salinity. J. Exp. Bot. 58, 1873–1892. https://doi.org/10.1093/jxb/erm012

Voelckel, C., Gruenheit, N., Lockhart, P., 2017. Evolutionary Transcriptomics and Proteomics: Insight into Plant Adaptation. Trends Plant Sci. 22, 462–471. https://doi.org/10.1016/j.tplants.2017.03.001

Vogel, M.O., Moore, M., König, K., Pecher, P., Alsharafa, K., Lee, J., Dietz, K.-J., 2014. Fast retrograde signaling in response to high light involves metabolite export, MITOGEN-ACTIVATED PROTEIN KINASE6, and AP2/ERF transcription factors in *Arabidopsis*. Plant Cell 26, 1151–65. https://doi.org/10.1105/tpc.113.121061

Walters, R.G., 2005. Towards an understanding of photosynthetic acclimation. J. Exp. Bot. 56, 435–447. https://doi.org/10.1093/jxb/eri060

Walters, R.G., Horton, P., 1995. Acclimation of *Arabidopsis thaliana* to the light environment: regulation of chloroplast composition. Planta 197, 475–481.

Walton, A., Stes, E., De Smet, I., Goormachtig, S., Gevaert, K., 2015. Plant hormone signalling through the eye of the mass spectrometer. Proteomics 15, 1113–1126. https://doi.org/10.1002/pmic.201400403

Wang, H., Wu, Y., Yang, X., Guo, X., Cao, X., 2017. SmLEA2, a gene for late embryogenesis abundant protein isolated from *Salvia miltiorrhiza*, confers tolerance to drought and salt stress in Escherichia coli and S. miltiorrhiza. Protoplasma 254, 685–696.

https://doi.org/10.1007/s00709-016-0981-z

Washburn, M.P., Wolters, D., Yates, J.R., 2001. Large-scale analysis of the yeast proteome by multidimensional protein identification technology. Nat. Biotechnol. 19, 242–7. https://doi.org/10.1038/85686

Weaver, L.M., Gan, S., Quirino, B., Amasino, R.M., 1998. A comparison of the expression patterns of several senescence-associated genes in response to stress and hormone treatment. Plant Mol. Biol. 37, 455–469. https://doi.org/10.1023/A:1005934428906

Webb-Robertson, B.J.M., Wiberg, H.K., Matzke, M.M., Brown, J.N., Wang, J., McDermott, J.E., Smith, R.D., Rodland, K.D., Metz, T.O., Pounds, J.G., Waters, K.M., 2015. Review, evaluation, and discussion of the challenges of missing value imputation for mass spectrometry-based label-free global proteomics. J. Proteome Res. 14, 1993–2001. https://doi.org/10.1021/pr501138h

Weisz, D.A., Liu, H., Zhang, H., Thangapandian, S., Tajkhorshid, E., Gross, M.L., Pakrasi, H.B., 2017. Mass spectrometry-based cross-linking study shows that the Psb28 protein binds to cytochrome b_{559} in Photosystem II. Proc. Natl. Acad. Sci. 114, 2224–2229. https://doi.org/10.1073/pnas.1620360114

Wheeler, T., Braun, J. Von, 2013. Climate change impacts on global food security. Science 341, 508–513. https://doi.org/10.1126/science.1239402

Whitelegge, J.P., 2002. Plant proteomics: BLASTing out of a MudPIT. Proc. Natl. Acad. Sci. U. S. A. 99, 11564–11566. https://doi.org/10.1073/pnas.192449199

Wilmes, P., Andersson, A.F., Lefsrud, M.G., Wexler, M., Shah, M., Zhang, B., Hettich, R.L., Bond, P.L., VerBerkmoes, N.C., Banfield, J.F., 2008. Community proteogenomics highlights microbial strain-variant protein expression within activated sludge performing enhanced biological phosphorus removal. ISME J. 2, 853–864. https://doi.org/10.1038/ismej.2008.38

Wu, J., Kim, S.G., Kang, K.Y., Kim, J.-G., Park, S.-R., Gupta, R., Kim, Y.H., Wang, Y., Kim, S.T., 2016. Overexpression of a pathogenesis-related protein 10 enhances biotic and abiotic stress tolerance in rice. Plant Pathol. J. 32, 552. https://doi.org/10.5423/PPJ.OA.06.2016.0141

Wu, B. Sen, Lefsrud, M.G., 2018. Photobiology eye safety for horticultural LED lighting: Transmittance performance of eyewear protection using high-irradiant monochromatic LEDs. J. Occup. Environ. Hyg. 15, 133–142. https://doi.org/10.1080/15459624.2017.1395959

Wu, X., Xiong, E., Wang, W., Scali, M., Cresti, M., 2014. Universal sample preparation method integrating trichloroacetic acid / acetone precipitation with phenol extraction for crop proteomic analysis. Nat. Protoc. 9. https://doi.org/10.1038/nprot.2014.022

Xu, J., Pascual, L., Aurand, R., Bouchet, J.P., Valot, B., Zivy, M., Causse, M., Faurobert, M., 2013. An extensive proteome map of tomato (*Solanum lycopersicum*) fruit pericarp. Proteomics 13, 3059–3063. https://doi.org/10.1002/pmic.201200438

Xu, Y.H., Liu, R., Yan, L., Liu, Z.Q., Jiang, S.C., Shen, Y.Y., Wang, X.F., Zhang, D.P., 2012. Light-harvesting chlorophyll a/b-binding proteins are required for stomatal response to abscisic acid in *Arabidopsis*. J. Exp. Bot. 63, 1095–1106. https://doi.org/10.1093/jxb/err315

Xuan, Y., Zhou, S., Wang, L., Cheng, Y., Zhao, L., 2010. Nitric Oxide Functions as a Signal and Acts Upstream of AtCaM3 in Thermotolerance in *Arabidopsis* Seedlings. Plant Physiol. 153, 1895–1906. https://doi.org/10.1104/pp.110.160424

Xuan, Y., Zhou, Z.S., Li, H.B., Yang, Z.M., 2016. Identification of a group of XTHs genes responding to heavy metal mercury, salinity and drought stresses in *Medicago truncatula*. Ecotoxicol. Environ. Saf. 134, 286. https://doi.org/10.1016/j.ecoenv.2016.09.005

Yamamoto, T., Burke, J., Autz, G., Jagendorf, A.T., 1981a. Bound Ribosomes of Pea Chloroplast Thylakoid Membranes: Location and Release in Vitro by High Salt, Puromycin, and RNase. PLANT Physiol. 67, 940–949. https://doi.org/10.1104/pp.67.5.940

Yamamoto, T., Burke, J., Autz, G., Jagendorf, A.T., 1981b. Bound Ribosomes of Pea Chloroplast Thylakoid Membranes: Location and Release in Vitro by High Salt, Puromycin, and RNase. Plant Physiol. 67, 940–9. https://doi.org/10.1104/pp.67.5.940

Yamamoto, Y., 2016. Quality Control of Photosystem II: The Mechanisms for Avoidance and Tolerance of Light and Heat Stresses are Closely Linked to Membrane Fluidity of the Thylakoids. Front. Plant Sci. 7, 1–13. https://doi.org/10.3389/fpls.2016.01136

Yates III, J.R., 2011. A century of mass spectrometry: from atoms to proteomes. Nat. Methods 8, 633–637. https://doi.org/10.1038/nmeth.1659

Yeats, T.H., Howe, K.J., Matas, A.J., Buda, G.J., Thannhauser, T.W., Rose, J.K.C., 2010. Mining the surface proteome of tomato (*Solanum lycopersicum*) fruit for proteins associated with cuticle biogenesis. J. Exp. Bot. 61, 3759–3771. https://doi.org/10.1093/jxb/erq194

Yokotani, N., Ichikawa, T., Kondou, Y., Matsui, M., Hirochika, H., Iwabuchi, M., Oda, K., 2008. Expression of rice heat stress transcription factor OsHsfA2e enhances tolerance to environmental stresses in transgenic *Arabidopsis*. Planta 227, 957–967. https://doi.org/10.1007/s00425-007-0670-4

Yu, S., Zhang, X., Guan, Q., Takano, T., Liu, S., 2007. Expression of a carbonic anhydrase gene is induced by environmental stresses in Rice (*Oryza sativa L.*). Biotechnol. Lett. 29, 89–94.

https://doi.org/10.1007/s10529-006-9199-z

Yu, T.S., Kofler, H., Häusler, R.E., Hille, D., Flügge, U.I., Zeeman, S.C., Smith, A.M., Kossmann, J., Lloyd, J., Ritte, G., Steup, M., Lue, W.L., Chen, J., Weber, A., 2001. The *Arabidopsis sex1* mutant is defective in the R1 protein, a general regulator of starch degradation in plants, and not in the chloroplast hexose transporter. Plant Cell 13, 1907–1918. https://doi.org/10.1105/TPC.010091

Yue, J., Xu, W., Ban, R., Huang, S., Miao, M., Tang, X., Liu, G., Liu, Y., 2016. PTIR: Predicted Tomato Interactome Resource. Sci. Rep. 6, 25047. https://doi.org/10.1038/srep25047

Zandalinas, S.I., Mittler, R., Balfagón, D., Arbona, V., Gómez-Cadenas, A., 2018. Plant adaptations to the combination of drought and high temperatures. Physiol. Plant. 162, 2–12. https://doi.org/10.1111/ppl.12540

Zhang, J., Jiang, X.D., Li, T.L., Cao, X.J., 2014. Photosynthesis and ultrastructure of photosynthetic apparatus in tomato leaves under elevated temperature. Photosynthetica 52, 430–436. https://doi.org/10.1007/s11099-014-0051-8

Zhang, J., Wang, S., 2011. Simulation of the Canopy Photosynthesis Model of Greenhouse Tomato 16, 632–639. https://doi.org/10.1016/j.proeng.2011.08.1134

Zhang, J.T., Mu, C.S., 2009. Effects of saline and alkaline stresses on the germination, growth, photosynthesis, ionic balance and anti-oxidant system in an alkali-tolerant leguminous forage Lathyrus quinquenervius. Soil Sci. Plant Nutr. 55, 685–697. https://doi.org/10.1111/j.1747-0765.2009.00411.x

Zhang, L., Paakkarinen, V., Suorsa, M., Aro, E.M., 2001. A SecY homologue is involved in chloroplast-encoded D1 protein biogenesis. J. Biol. Chem. 276, 37809–37814.

https://doi.org/10.1074/jbc.M105522200

Zhang, L., Tian, L.-H., Zhao, J.-F., Song, Y., Zhang, C.-J., Guo, Y., 2008. Identification of an Apoplastic Protein Involved in the Initial Phase of Salt Stress Response in Rice Root by Two-Dimensional Electrophoresis. Plant Physiol. 149, 916–928. https://doi.org/10.1104/pp.108.131144

Zhang, X. lin, Qi, M. fang, Xu, T., Lu, X. jun, Li, T. lai, 2015. Proteomics profiling of ethylene-induced tomato flower pedicel abscission. J. Proteomics 121, 67–87. https://doi.org/10.1016/j.jprot.2015.03.023

Zhang, Y., Gao, P., Yuan, J.S., 2010. Plant protein-protein interaction network and interactome. Curr. Genomics 11, 40–6. https://doi.org/10.2174/138920210790218016

Zhao, F., Zhang, D., Zhao, Y., Wang, W., Yang, H., Tai, F., Li, C., Hu, X., 2016. The Difference of Physiological and Proteomic Changes in Maize Leaves Adaptation to Drought, Heat, and Combined Both Stresses. Front. Plant Sci. 7, 1471. https://doi.org/10.3389/fpls.2016.01471

Zhao, Z., Assmann, S.M., 2011. The glycolytic enzyme, phosphoglycerate mutase, has critical roles in stomatal movement, vegetative growth, and pollen production in *Arabidopsis thaliana*. J. Exp. Bot. 62, 5179–5189. https://doi.org/10.1093/jxb/err223

Zhou, D., Yang, Y., Zhang, J., Jiang, F., Craft, E., Thannhauser, T.W., Kochian, L. V., Liu, J., 2017. Quantitative iTRAQ Proteomics Revealed Possible Roles for Antioxidant Proteins in Sorghum Aluminum Tolerance. Front. Plant Sci. 7, 1–14. https://doi.org/10.3389/fpls.2016.02043

Zhou, J., Wang, J., Li, X., Xia, X.J., Zhou, Y.H., Shi, K., Chen, Z., Yu, J.Q., 2014. H2O2 mediates the crosstalk of brassinosteroid and abscisic acid in tomato responses to heat and oxidative stresses. J. Exp. Bot. 65, 4371–4383. https://doi.org/10.1093/jxb/eru217

Zhu, T., Deng, X., Zhou, X., Zhu, L., Zou, L., Li, P., Zhang, D., Lin, H., 2016. Ethylene and hydrogen peroxide are involved in brassinosteroid-induced salt tolerance in tomato. Sci. Rep. 6, 35392. https://doi.org/10.1038/srep35392

Zybailov, B., Mosley, A.L., Sardiu, M.E., Coleman, M.K., Florens, L., Washburn, M.P., 2006. Statistical analysis of membrane proteome expression changes in *Saccharomyces cerevisiae*. J. Proteome Res. 5, 2339–2347. https://doi.org/10.1021/pr060161n

CHAPTER 9 - Appendix

9.1 Appendix A: Proteomics methodology

9.1.1 MudPIT

9.1.1.1 Sample preparation

Materials

SDS Lysis buffer (SDS-LB) – 4% w/v SDS in 100 mM Tris-Cl, pH 8.0

TCEP-HCl – stock: 100mM TCEP-HCl in ammonium bicarbonate pH 7-8

150 mg am. bicarbonate + 85.98 mg TCEP for 3 mL

Use 100 µL in 500 µL of UB for 20mM

Trichloroacetic acid (TCA)

Acetone (ice cold or stored at -20 to -80˚C)

Urea Dilution Buffer (UB) – 100 mM Tris-Cl, pH 8.0

Urea (8M)

Iodoacetamide (IAA) (20mM)

Trypsin (20 ug vials)

Acidic salt solution – 4M NaCl in HPLC water, 2% formic acid

Spin filter with 30 kDa mass cutoff

Sample Lysis and Precipitation

Grind leaves well in a mortar adding liquid nitrogen until leaves become powder, keep the sample frozen at all times.

Resuspend the sample (10 – 100 mg) in 1 mL SDS-LB adjusted to 20 mM TCEP

Keeping this amount low is essential for proper BCA protein measurements.

Most if not all the TCEP will be removed during TCA ppt and cleanup.

Use 150 µL of 100 mM TCEP for 750 µL of sample.

Sonicate sample (recall 3; 20% | 2m | 10s on | 10s off) with sample tube suspended in cool water from the faucet to disperse heat.

The sample was already boiled and will be boiled again so heat is not an issue.

Boil (or 60˚C heat block) sample for 5 min.

Centrifuge sample at 21000g for 10 min to pre-clear the sample of DNA and other debris

Transfer sample, or fraction of sample, to a new Eppendorf tube.

Pre-weigh the new Eppendorf tube for the accurate weight of TCA'd pellet.

Adjust the sample to 20% TCA, vortex briefly, and spin down precipitate in tabletop microcentrifuge.

Place in -20˚ to -80˚C freezer for 1 hr to overnight.

TCA Precipitation Clean Up (~ 30 min)

Thaw TCA precipitated sample on ice and centrifuged at 21000g / 4˚C for 15 min.

Discard supernatant appropriately (hazardous waste), taking care not to disrupt the pelleted protein.

Add 1 ml of cold acetone to sample, dislodging pellet from the tube wall with a pipet tip, and vortex briefly.

Centrifuge sample at 21000g / 4˚C for 5 min.

Repeat steps 2 – 4.

Remove as much residual acetone as possible leaving the protein pellet in the tube.

Speed-vac the sample for 5 min to remove all the liquid.

If the tube was pre-weighed (see 6a in the above section), obtain the weight of the TCA'd protein pellet.

Pellet can be stored at this point.

Sample Digestion (overnight)

Add 500 µl of freshly prepared 8M urea in UB.

Adjust sample to 20 mM TCEP

Use 100 µL 100 mM TCEP for 500 µL of sample.

If pellet floats, allow it to rehydrate for 10-30 min.

Sonicate sample in an ice water bath (recall 4; 20% | 2m | 5s on | 10s off)

Keep the sample cool to room temperature to keep carbamylation to a minimum.

Repeat a second time if the pellet is still substantial.

Allow sample to denature at room temperature for 30-60 min, vortexing intermittently.

If sample concentration is unknown, remove a 20 µl aliquot for BCA assay and adjust the remaining sample to 20 mM TCEP.

Incubate sample with TCEP for 15-30 min at room temperature.

Block disulfide reformation by adjusting the sample to 20 mM IAA and incubating sample at room temperature in the dark for 15-30 min.

Transfer sample to a new Eppendorf tube for digestion and freeze the rest.

Digest 1–2 mg of sample, but try not to exceed 375 µl of crude lysate in 8M urea since by the end of the prep you'll have 4x the volume.

Digest sample with trypsin (1:20; or 1 vial of trypsin per 1 mg of the sample) that has been resuspended in 3 sample volume of UB plus 10 mM $CaCl_2$. Add resuspended trypsin directly to sample in 8M urea.

For example, if 2 mg of sample in 250 ul of 8M urea, resuspend a vial of trypsin (20 ug) in 750 ul of UB + 10 mM $CaCl_2$ and add to sample.

Digest overnight at 37ºC.

Add 20x dilution of acidic salt solution to bring sample to 200 mM NaCl, 0.1% FA

For example, add 50 ul of stock solution to 1 ml of digested sample (to remove SDS).

Briefly vortex sample and move to a 30 kDa cutoff spin filter.

Centrifuge sample for 15 – 30 min at full speed (4500 x g in swing bucket rotor) to remove undigested proteins, intact trypsin, and other debris.

Move filtrate containing peptides to a new tube.

Sample De-salting (Sep-Pak Plus C-18) for >1 mL sample

Spin in a centrifuge to remove debris.

Wash Sep-Pak column with 5 mL ACN (0.1% FA) using 10 mL syringe.

Wash Sep-Pak with 5 mL H_2O (0.1% FA).

Add 1 mL H_2O to sample to increase working volume. Use a syringe with a needle to draw up sample (avoid pellet).

Load sample onto the column

Wash with 5 mL H_2O (0.1% FA).

Elute with 2 mL ACN (0.1% FA) into 1 or 2 2mL tube.

Speedvac to ~500 μL.

Pool if 2 tubes and add 1 mL H_2O (0.1% FA) to solvent exchange.

Speedvac to ~200 μL.

Load sample onto Ultrafree-MC filter and spin to dryness in mini-centrifuge to remove large particles.

Perform a peptide quantification assay on the peptides (4x dilution to stay within measurable range).

Load <100 μg of the sample onto the back column.

Sample Loading

Load appropriate amount of sample onto a normal SCX-RP back column.

Post-load, wash sample with solvent A (95% H_2O, 5% Acetonitrile, 0.1% formic acid) for 30 minutes to desalt the column.

This step is important to recharge the SCX material.

Setup the method like always, 1^{st} step aqueous to the organic gradient, followed by 11 salt pulses. Front load the salt pulses for improved results.

i.e. 0% (1^{st} step), 5%, 7.5%, 10%, 12.5%, 15%, 17.5%, 20%, 25%, 35%, 50%, 100%

This salt pulse scheme is also relevant for traditionally prepared (guanidine) samples.

9.1.1.2 2D LC elution gradient

The methodology for the MudPIT set up with online MS was used according to the reference (Patel, 2015). Briefly, peptide separation was obtained by applying a two a 2-dimensional LC online with a linear ion trap MS. The peptides were ionized, further fragmented, and identified by an LTQ XL (Thermo Fischer Scientific, CA, USA).

In the MudPIT set-up, a biphasic column was packed with, approximately each, 5 cm of strong cation exchange resin (SCX) and C18 reversed phase (RP) (Luna 5 µm 100A and Aqua 5 µm 100A, Phenomenex, Torrance, CA). The loaded columns containing the peptides, were washed to remove impurities and contaminations, before being placed in-line with a nanospray emitter tip containing column (100 µm i.d., 360 µm o.d., 15 µm i.d. tip, New Objective, MA, USA). The latter was previously packed with C18 RP (approximately 15 cm). Finally, a flow of 12 gradients of solvents A, B, and C (salt-pulse), with a 24-hour duration is carried on in a 2D LC–nanoESI–MS/MS analysis. Compositions of solvents utilized in the LC gradient were: solvent A, 95% water, 5% ACN, 1% formic acid, solvent B, 30% water, 70% ACN, 1% formic acid, solvent D, 500 mM ammonium acetate in 95% water, 5% ACN, 1% formic acid. The 12 gradients applied in the LC analysis were as follows:

	Time (min)	Flow (nL/min)	Solvent A	Solvent B	Solvent C
Gradient #1	0	450	100	0	0
	45	450	50	50	0
	55	450	0	100	0
	60	450	100	0	0
Gradient #2	0	450	100	0	0
	5	450	100	0	0
	5.1	450	90	0	10
	7	800	90	0	10
	7.1	800	100	0	0
	10	450	100	0	0
	120	450	50	50	0
Gradient #3	0	450	100	0	0
	5	450	100	0	0
	5.1	450	85	0	15
	7	800	85	0	15
	7.1	800	100	0	0
	10	450	100	0	0
	120	450	50	50	0

	Time (min)	Flow (nL/min)	Solvent A	Solvent B	Solvent C
Gradient #4	0	450	100	0	0
	5	450	100	0	0
	5.1	450	80	0	20
	7	450	80	0	20
	7.1	450	100	0	0
	10	450	100	0	0
	120	450	50	50	0
Gradient #5	0	450	100	0	0
	5	450	100	0	0
	5.1	450	75	0	25
	7	800	75	0	25
	7.1	800	100	0	0
	10	450	100	0	0
	120	450	50	50	0
Gradient #6	0	450	100	0	0
	5	450	100	0	0
	5.1	450	70	0	30
	7	800	70	0	30
	7.1	800	100	0	0
	10	450	100	0	0

	120	450	50	50	0

	Time (min)	Flow (nL/min)	Solvent A	Solvent B	Solvent C
Gradient #7	0	450	100	0	0
	5	450	100	0	0
	5.1	450	65	0	35
	7	800	65	0	35
	7.1	800	100	0	0
	10	450	100	0	0
	120	450	50	50	0
Gradient #8	0	450	100	0	0
	5	450	100	0	0
	5.1	450	60	0	40
	7	800	60	0	40
	7.1	800	100	0	0
	10	450	100	0	0
	120	450	50	50	0
Gradient #9	0	450	100	0	0
	5	450	100	0	0
	5.1	450	55	0	45
	7	800	55	0	45

	7.1	800	100	0	0
	10	450	100	0	0
	120	450	50	50	0

	Time (min)	Flow (nL/min)	Solvent A	Solvent B	Solvent C
Gradient #10	0	450	100	0	0
	5	450	100	0	0
	5.1	450	50	0	50
	7	800	50	0	50
	7.1	800	100	0	0
	10	450	100	0	0
	120	450	50	50	0
Gradient #11	0	450	100	0	0
	5	450	100	0	0
	5.1	450	40	0	60
	7	800	40	0	60
	7.1	800	100	0	0
	10	450	100	0	0
	120	450	50	50	0

	Time (min)	Flow (nL/min)	Solvent A	Solvent B	Solvent C
Gradient #12	0	450	100	0	0
	5	450	100	0	0
	5.1	450	40	0	60
	7	800	40	0	60
	7.1	800	100	0	0
	10	450	80	20	0
	120	450	0	100	0
Column Equilibration	0	300	0	100	0
	5	300	0	100	0
	30	300	100	0	0
	35	300	100	0	0

9.1.1.3 LTQ XL parameters for data-dependent acquisition of MS/MS spectra

Calibration and tune:

The LTQ XL mass spectrometer was calibrated through the use of the positive calibration solution from Thermo Scientific (CA, USA), which contains MRFA, Caffeine, and Ultramark. The MS' tune was done using the semi-automatic program setting as target the caffeine peak (195 m/z). Instructions from the LQT XL user manual were followed to perform calibration and tune.

ESI source parameters

Sheath gas= 0, aux gas= 0, sweep gas= 0, spray voltage= 195 to 225kV, capillary temp= 275 ºC, capillary voltage= 47 kV, tube lens= 110

Ion optics

Multipole 00 offset= -45, Lens 0 voltage= -4, multipole 0 offset = -525, lens 1, voltage= -28, gate lens voltage= -22, multipole 1 offset= -155, multipole RF amplitude V p-p = 400, front lens= -575.

ACG target

full ms= 3e4, SIM= 1e4, MSn= 2e4, zoom= 3000

Instrument setup for MS/MS and data-dependent:

6 total scan events, 1 full and 5 dependent. 5 MS/MS per 1 full MS,

Global mass range: 0 to 100,000,

Global mass width: Should be 05,

Dynamic exclusion: repeat count =1, repeat duration=30s, exclusion list size=100,

exclusion duration= 60s, exclusion mass width: by mass, 15 low and high,

CID activation page for each scan event:

a) Default charge state: always 3,

b) Isolation width= 3,

c) Normalized collision energy= 35,

d) Activation Q= 025,

e) Activation time= 30 ms,

f) For the current scan event, minimum signal threshold=1000, select mass determined from the full scan, select Nth most intense ion Scan event 2 should be 1st most intense ion from scan event 1, scan 3 should be for the 2nd most intense from scan event 1.

9.1.2 iTRAQ

9.1.2.1 Sample preparation

The following protocol is provided by the manufacturer Applied Biosystems iTRAQ™ Reagents (Applied Biosystem).

1. Allow each vial of iTRAQ™ Reagent required to reach room temperature.

2. Spin to bring the solution to the bottom of the tube.

3. Add 70 µL of ethanol to each room-temperature iTRAQ™ Reagent vial.

4. Vortex each vial to mix, then spin.

5. Transfer the contents of one iTRAQ™ Reagent vial to one sample tube.

For a duplex-type experiment, transfer the contents of the iTRAQ™ Reagent 114 vial to the sample 1 protein digest tube and transfer the contents of the iTRAQ™ Reagent 117 vial to the sample 2 protein digest tube.

6. Vortex each tube to mix, then spin.

7. Incubate the tubes at room temperature for 1 hour

8. Combine the contents of each iTRAQ™ Reagent-labeled sample tube into one tube

9. Vortex to mix, then spin.

9.1.2.2 LC-MS/MS set up

An Orbitrap Fusion Lumos mass spectrometer (Thermo Scientific), equipped with a nano-ion spray source was coupled to an EASY-nLC 1200 system (Thermo Scientific). The LC system was configured with a self-pack PicoFrit™ 75-µm analytical column with an 8-µm emitter (New Objective, Woburn, MA) packed to 25cm with ReproSil-Pur C18-AQ, 1.9 µM material (Dr. Maish GmbH). Mobile phase A consisted of 2% acetonitrile; 0.1% formic acid and mobile phase B consisted of 90% acetonitrile; 0.1% formic acid. Peptides were then separated using the following steps: at a flow rate of 200 nL/min: 2% B to 6% B over 1 min, 6% B to 30% B over 84 min, 30% B to 60% B over 9 min, 60% B to 90% B over 1 min, held at 90% B for 5 min, 90% B to 50% B over 1 min and then flow rate was increased to 500 nL/min as 50% B was held for 9 min.

Eluted peptides were directly electrosprayed into the Fusion Lumos mass spectrometer with the application of a distal 2.3 kV spray voltage and a capillary temperature of 300°C. Full-scan mass spectrum (Res=60,000; 400-1600 *m/z*) were followed by MS/MS using the “Top N” method for selection. High-energy collisional dissociation (HCD) was used with the normalized collision energy set to 35 for fragmentation, the isolation width set to 1.2 and a duration of 10 seconds was set for the dynamic exclusion with a mass exclusion width of 10ppm. We used monoisotopic precursor selection for charge states 2+ and greater, and all data were acquired in profile mode.

9.2 Appendix B: Manuscript permissions (use of figures and contents)

9.2.1 Manuscript I

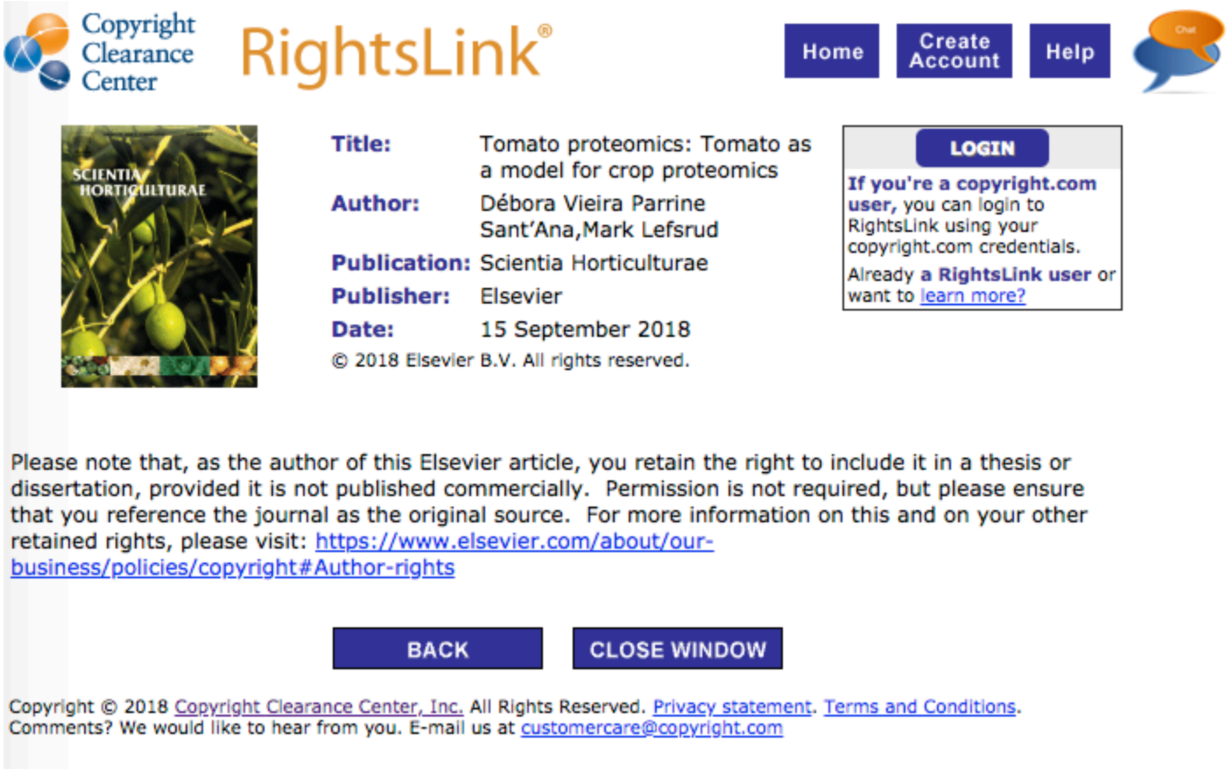

Title: Tomato proteomics: Tomato as a model for crop proteomics
Author: Débora Vieira Parrine Sant'Ana,Mark Lefsrud
Publication: Scientia Horticulturae
Publisher: Elsevier
Date: 15 September 2018
© 2018 Elsevier B.V. All rights reserved.

If you're a copyright.com user, you can login to RightsLink using your copyright.com credentials.
Already **a RightsLink user** or want to learn more?

Please note that, as the author of this Elsevier article, you retain the right to include it in a thesis or dissertation, provided it is not published commercially. Permission is not required, but please ensure that you reference the journal as the original source. For more information on this and on your other retained rights, please visit: https://www.elsevier.com/about/our-business/policies/copyright#Author-rights

Copyright © 2018 Copyright Clearance Center, Inc. All Rights Reserved. Privacy statement. Terms and Conditions.
Comments? We would like to hear from you. E-mail us at customercare@copyright.com

9.2.2 Figures

9.2.2.1 Figure 4

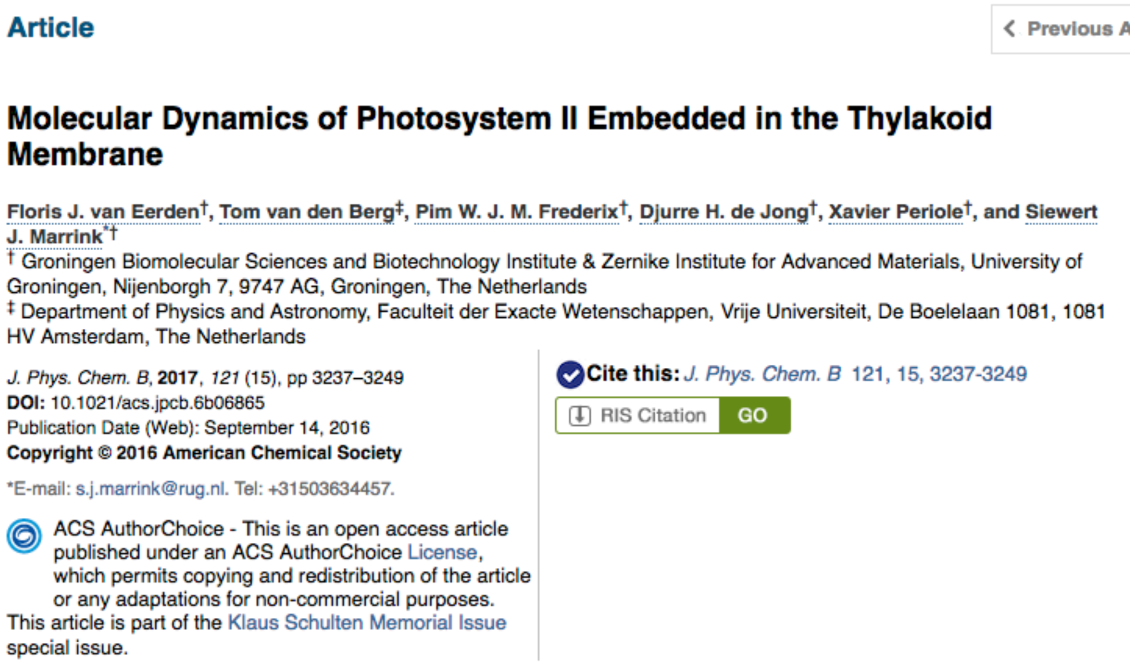

Article

Molecular Dynamics of Photosystem II Embedded in the Thylakoid Membrane

Floris J. van Eerden[†], **Tom van den Berg**[‡], **Pim W. J. M. Frederix**[†], **Djurre H. de Jong**[†], **Xavier Periole**[†], and **Siewert J. Marrink**[*†]

[†] Groningen Biomolecular Sciences and Biotechnology Institute & Zernike Institute for Advanced Materials, University of Groningen, Nijenborgh 7, 9747 AG, Groningen, The Netherlands

[‡] Department of Physics and Astronomy, Faculteit der Exacte Wetenschappen, Vrije Universiteit, De Boelelaan 1081, 1081 HV Amsterdam, The Netherlands

J. Phys. Chem. B, **2017**, *121* (15), pp 3237–3249

DOI: 10.1021/acs.jpcb.6b06865

Publication Date (Web): September 14, 2016

Copyright © 2016 American Chemical Society

*E-mail: s.j.marrink@rug.nl. Tel: +31503634457.

ACS AuthorChoice - This is an open access article published under an ACS AuthorChoice License, which permits copying and redistribution of the article or any adaptations for non-commercial purposes.

This article is part of the Klaus Schulten Memorial Issue special issue.

Cite this: *J. Phys. Chem. B* 121, 15, 3237-3249

9.2.2.2 Figure 5

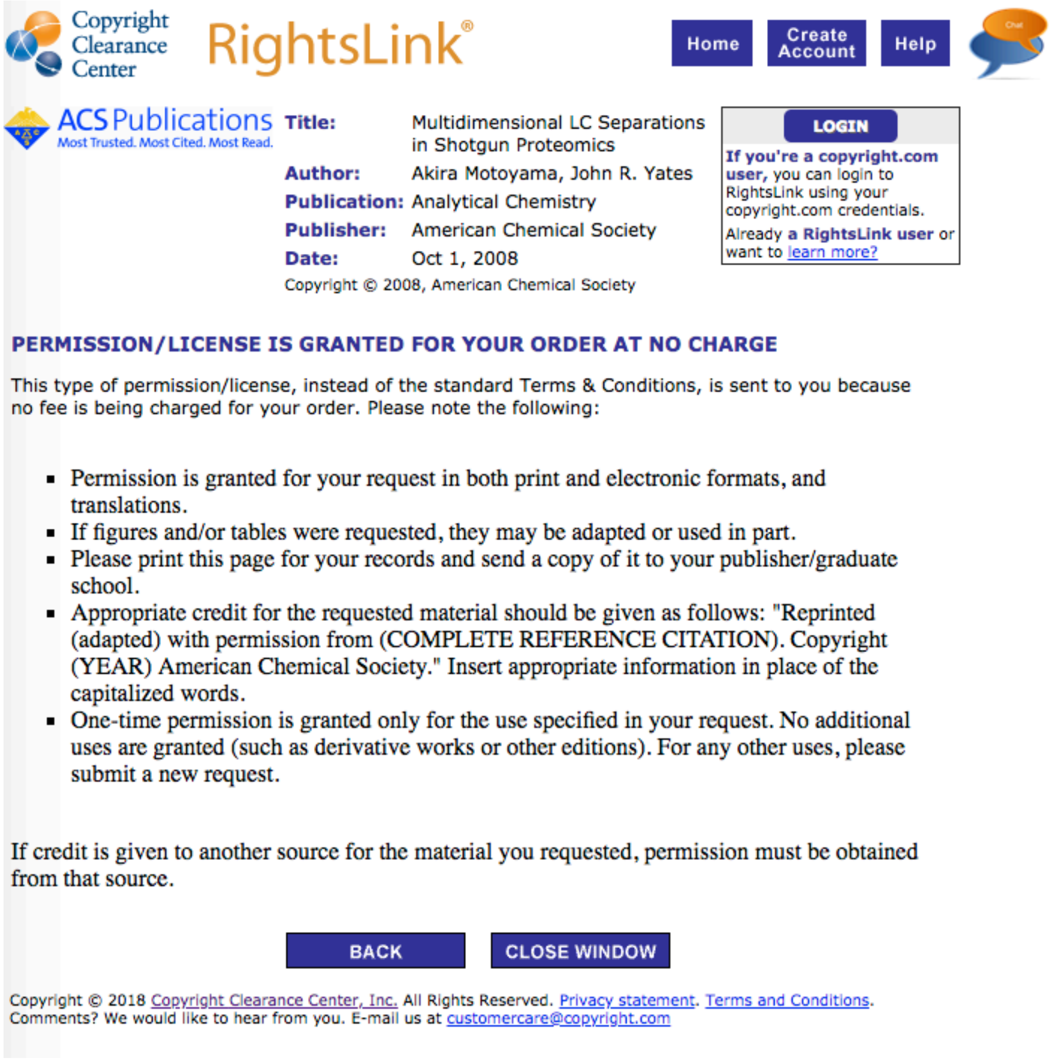

Title: Multidimensional LC Separations in Shotgun Proteomics
Author: Akira Motoyama, John R. Yates
Publication: Analytical Chemistry
Publisher: American Chemical Society
Date: Oct 1, 2008
Copyright © 2008, American Chemical Society

If you're a copyright.com user, you can login to RightsLink using your copyright.com credentials.
Already **a RightsLink user** or want to learn more?

PERMISSION/LICENSE IS GRANTED FOR YOUR ORDER AT NO CHARGE

This type of permission/license, instead of the standard Terms & Conditions, is sent to you because no fee is being charged for your order. Please note the following:

- Permission is granted for your request in both print and electronic formats, and translations.
- If figures and/or tables were requested, they may be adapted or used in part.
- Please print this page for your records and send a copy of it to your publisher/graduate school.
- Appropriate credit for the requested material should be given as follows: "Reprinted (adapted) with permission from (COMPLETE REFERENCE CITATION). Copyright (YEAR) American Chemical Society." Insert appropriate information in place of the capitalized words.
- One-time permission is granted only for the use specified in your request. No additional uses are granted (such as derivative works or other editions). For any other uses, please submit a new request.

If credit is given to another source for the material you requested, permission must be obtained from that source.

Copyright © 2018 Copyright Clearance Center, Inc. All Rights Reserved. Privacy statement. Terms and Conditions.
Comments? We would like to hear from you. E-mail us at customercare@copyright.com

9.2.2.3 Figure 6

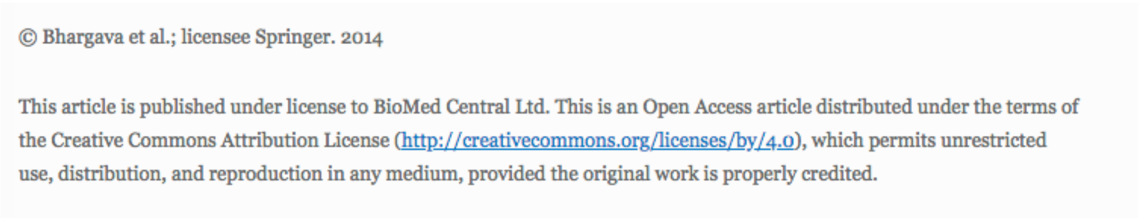

© Bhargava et al.; licensee Springer. 2014

This article is published under license to BioMed Central Ltd. This is an Open Access article distributed under the terms of the Creative Commons Attribution License (http://creativecommons.org/licenses/by/4.0), which permits unrestricted use, distribution, and reproduction in any medium, provided the original work is properly credited.

9.3 Appendix C: List of proteins identified in the red LED treatment.

Accession	Burned	Control	Regular	Limit	Description
Q4A1N1	13.572	1.067	3.166	11.66	Non-specific lipid-transfer protein
K4AYM0	12.562	1.012	1.112	1.723	Uncharacterized protein
K4BI15	12.536	1.439	2.076	4.677	Uncharacterized protein
K4DBN5	12.436	1.051	1.090	1.882	Uncharacterized protein
K4DEQ3	12.001	1.036	1.246	1.485	Uncharacterized protein
K4BNK8	11.544	1.416	2.282	5.255	Uncharacterized protein
K4D2M7	10.917	1.011	1.210	1.482	Uncharacterized protein
K4DA82	10.788	0.919	0.995	2.532	Uncharacterized protein
K4BE14	10.753	0.957	1.113	1.469	Uncharacterized protein
K4ASG5	10.246	0.810	0.965	1.200	Uncharacterized protein
K4BNH6	10.047	1.170	1.706	3.915	Uncharacterized protein
K4BKV5	10.000	1.058	1.227	1.706	Uncharacterized protein
K4BN40	9.880	0.861	0.738	2.198	Uncharacterized protein
K4C7M5	9.840	0.893	1.210	2.413	Uncharacterized protein
K4CE39	9.575	0.889	0.906	2.276	Uncharacterized protein
K4B0B5	8.946	0.970	1.282	1.510	Uncharacterized protein
K4CAY2	8.689	0.946	1.437	2.977	Uncharacterized protein
K4D062	8.620	0.960	1.741	1.960	Uncharacterized protein
K4B033	8.541	1.058	1.436	1.367	Uncharacterized protein
K4D1N6	8.523	1.049	1.633	3.719	Uncharacterized protein
K4DE42	8.364	1.364	1.073	0.968	Uncharacterized protein
K4CA81	8.108	1.558	2.628	3.477	Uncharacterized protein
K4DAU1	8.058	1.292	1.783	3.307	Uncharacterized protein
K4C1S8	7.660	1.664	2.487	3.944	Ferritin
K4CV86	7.556	1.243	1.716	4.210	Uncharacterized protein
K4C894	7.420	0.975	1.234	1.927	Uncharacterized protein
K4BKV8	7.258	0.912	1.035	1.360	Uncharacterized protein
K4C3V9	7.140	0.975	1.230	1.904	Uncharacterized protein
K4BJR2	7.028	1.053	1.272	2.024	Uncharacterized protein
K4CJT1	6.910	1.271	1.694	3.935	Uncharacterized protein
K4B1G7	6.875	0.999	1.441	1.990	Uncharacterized protein
K4C8V5	6.752	1.091	0.901	1.372	CASP-like protein
K4AR34	6.656	0.973	1.408	5.012	Uncharacterized protein
K4C9B8	6.504	1.044	1.258	2.072	Uncharacterized protein
K4BXB1	6.308	0.896	0.872	1.746	Uncharacterized protein
K4CHI8	6.290	0.947	1.102	1.607	Uncharacterized protein
K4BVR6	6.246	1.122	1.679	2.509	Uncharacterized protein
K4B115	5.946	1.168	1.631	4.144	Uncharacterized protein
K4CP59	5.934	0.926	1.532	1.402	Uncharacterized protein
Q05540	5.753	0.872	1.084	4.008	Acidic 27 kDa endochitinase
K4C9G1	5.733	1.017	1.015	2.073	Uncharacterized protein
K4CFC3	5.697	1.053	1.252	1.487	Uncharacterized protein
P27056	5.663	0.951	4.971	12.316	Non-specific lipid-transfer protein 1
K4D9W7	5.647	1.009	1.020	2.039	Uncharacterized protein
Q2MI86	5.584	0.920	0.549	0.648	Photosystem II reaction center protein J
K4BVI4	5.572	1.106	1.523	1.861	Uncharacterized protein
K4BDM8	5.520	1.081	1.213	1.605	Uncharacterized protein
K4DGL5	5.518	1.077	1.279	1.663	Uncharacterized protein
K4CLT6	5.468	0.993	1.105	1.822	Uncharacterized protein
K4D4F0	5.400	1.013	1.109	1.868	Uncharacterized protein
K4CBZ0	5.396	1.015	1.444	1.629	Uncharacterized protein
K4D1U9	5.334	0.951	5.085	12.488	Non-specific lipid-transfer protein
K4D9M4	5.333	1.212	2.204	2.980	Histone H4
K4AXF7	5.324	1.286	2.255	2.751	Histone H3

Accession	Burned	Control	Regular	Limit	Description
K4B8E7	5.316	0.860	0.978	1.196	Uncharacterized protein
K4DD05	5.259	0.804	1.067	0.953	Uncharacterized protein
K4CQZ3	5.253	0.956	1.084	1.647	Uncharacterized protein
K4CQ91	5.239	1.006	1.646	1.596	Uncharacterized protein
K4CXI7	5.239	1.088	1.818	2.381	Histone H2A
K4B2W8	5.221	1.032	1.266	1.904	Uncharacterized protein
K4D5Q4	5.187	1.155	1.297	1.815	Uncharacterized protein
K4BDU6	5.162	1.095	1.818	2.389	Histone H2A
K4AV48	5.160	0.863	1.254	1.934	Uncharacterized protein
P25469	5.156	1.113	1.892	2.460	Histone H2A.1
K4D4U3	5.146	1.021	1.249	1.667	Uncharacterized protein
K4DHD2	5.142	1.105	1.252	1.747	6,7-dimethyl-8-ribityllumazine synthase
K4DB65	5.136	1.070	1.768	2.312	Histone H2A
K4DAZ1	5.104	1.214	2.190	2.899	Histone H4
Q6T2D2	5.100	0.962	1.127	1.531	PII-like protein
K4BXE2	5.095	0.977	1.320	2.157	Uncharacterized protein
K4C5P1	5.022	1.473	1.939	2.918	Ferritin
K4AY85	4.986	1.027	1.132	1.156	Uncharacterized protein
P93205	4.945	1.136	1.171	1.498	SBT2 protein
K4CMG7	4.942	1.045	1.446	2.308	Uncharacterized protein
P93224	4.920	0.946	3.588	9.019	Non-specific lipid-transfer protein 2
K4CH96	4.904	1.002	1.223	2.056	Uncharacterized protein
K4CP19	4.898	1.100	0.978	1.928	Uncharacterized protein
K4BTH6	4.890	0.997	1.872	2.382	Peroxidase
G1DEX3	4.888	0.939	0.869	1.435	Cutin-deficient 1 protein
A0RZC9	4.887	0.901	0.876	1.253	Constitutive plastid-lipid associated protein
K4DHR7	4.885	1.002	1.228	2.068	Uncharacterized protein
Q6LB28	4.883	1.265	2.145	2.571	Histone H3
K4CX88	4.879	1.005	1.223	2.041	Uncharacterized protein
E1AZA3	4.871	1.145	2.821	15.829	Late embryogenesis abundant protein
K4BY22	4.858	1.174	1.482	1.664	Sulfotransferase
K4AT06	4.794	1.231	1.609	2.890	40S ribosomal protein S27
K4CC92	4.779	0.931	0.972	1.254	Uncharacterized protein
K4CI14	4.759	0.965	1.507	2.685	Uncharacterized protein
K4C433	4.684	0.935	1.076	1.357	Protein transport protein Sec61 subunit beta
K4CE93	4.675	1.035	1.388	1.923	Dirigent protein
K4BKV6	4.672	0.972	0.919	1.184	Uncharacterized protein
K4CFF0	4.665	1.044	1.817	1.353	Peroxidase
K4AUE2	4.646	1.023	1.525	1.673	Peroxidase
K4BR75	4.623	1.021	1.206	1.629	Uncharacterized protein
K4B3Z2	4.617	1.290	1.929	2.926	Uncharacterized protein
K4CAR4	4.616	1.110	1.813	2.310	Histone H2A
K4B0B4	4.614	0.996	1.966	3.292	Uncharacterized protein
K4CCH4	4.530	0.970	1.219	1.515	Pectinesterase
K4BY19	4.510	1.121	1.331	1.530	Sulfotransferase
K4B6S9	4.500	0.984	1.290	1.961	Uncharacterized protein
K4BDV2	4.475	1.005	0.759	0.943	Uncharacterized protein
P22240	4.451	0.992	1.616	6.064	Abscisic acid and environmental stress-inducible protein TAS14
K4BLW4	4.421	1.201	1.682	1.670	Uncharacterized protein
K4D5T9	4.392	1.113	1.414	2.675	Uncharacterized protein
K4CWC4	4.342	1.045	2.570	10.407	PR10 protein
K4CWU7	4.330	1.022	1.317	1.361	Uncharacterized protein

Accession	Burned	Control	Regular	Limit	Description
O82575	4.329	1.050	1.378	2.403	Fruit-ripening protein
K4BY17	4.286	1.117	1.353	1.573	Sulfotransferase
K4BUV9	4.276	1.032	1.405	1.880	Uncharacterized protein
K4D4H7	4.272	0.999	1.186	1.885	Uncharacterized protein
K4D287	4.271	0.999	1.125	1.783	Uncharacterized protein
K4CLW3	4.266	1.155	1.554	1.405	Uncharacterized protein
K4CVQ2	4.265	0.993	0.832	0.919	Uncharacterized protein
K4C2G9	4.250	1.131	1.345	2.310	Uncharacterized protein
Q00747	4.238	0.805	1.908	11.596	Protein LE25
K4B8D7	4.221	1.052	1.132	1.325	Uncharacterized protein
K4CR60	4.217	1.018	1.077	1.430	Nascent polypeptide-associated complex subunit beta
K4BNM3	4.202	1.109	1.254	2.375	Uncharacterized protein
Q40144	4.181	1.048	1.319	1.614	Probable xyloglucan endotransglucosylase/hydrolase 1
K4B1J8	4.163	1.472	2.154	2.155	Uncharacterized protein
K4C9X3	4.163	0.925	0.805	0.976	Uncharacterized protein
K4AWR9	4.106	1.061	1.196	2.126	Uncharacterized protein
K4BT97	4.094	1.116	1.555	2.248	Uncharacterized protein
K4CR12	4.086	1.125	0.995	1.154	Uncharacterized protein
K4B2T2	4.044	1.171	1.691	2.186	Uncharacterized protein
K4BE13	4.015	1.039	1.027	1.290	Uncharacterized protein
O80432	4.007	1.149	1.573	4.942	Mitochondrial small heat shock protein
K4CAJ4	3.977	1.071	1.725	1.484	Uncharacterized protein
K4CVW4	3.977	1.273	1.808	1.950	Uncharacterized protein
K4BXB7	3.970	1.090	2.237	5.125	Uncharacterized protein
K4CYV9	3.957	1.263	1.840	2.635	Uncharacterized protein
K4BQ64	3.953	1.130	1.177	2.124	Uncharacterized protein
K4CWC5	3.937	1.080	1.746	7.216	PR10 protein
K4B276	3.936	1.308	1.788	2.239	Uncharacterized protein
K4AXP6	3.923	1.010	1.587	12.238	Uncharacterized protein
K4CJ96	3.915	1.028	1.201	1.519	6,7-dimethyl-8-ribityllumazine synthase
Q9LKW0	3.913	1.046	0.968	1.315	Thioredoxin-like protein CITRX, chloroplastic
K4BR44	3.893	1.304	3.165	2.188	Uncharacterized protein
K4BYR5	3.852	0.750	1.278	1.343	Uncharacterized protein
K4CVC3	3.847	0.738	0.831	0.954	Uncharacterized protein
K4D9H0	3.842	0.972	1.068	1.383	Xyloglucan endotransglucosylase/hydrolase
K4B8D4	3.841	1.176	1.356	1.764	Uncharacterized protein
Q3SC87	3.804	0.974	0.751	0.934	ACI13
K4C7M6	3.802	0.983	1.431	2.454	Uncharacterized protein
K4CLV2	3.798	1.344	1.545	1.761	3-ketoacyl-CoA synthase
K4B4N0	3.789	1.400	2.646	3.318	Uncharacterized protein
K4B5D8	3.744	1.045	1.145	1.863	Uncharacterized protein
K4BTI7	3.743	0.932	1.124	2.530	Uncharacterized protein
K4D3D9	3.734	1.075	1.150	1.376	Uncharacterized protein
K4DFR5	3.715	0.999	1.022	1.200	Uncharacterized protein
K4D0U1	3.709	1.187	1.391	2.034	Uncharacterized protein
K4C5G3	3.687	1.136	0.893	0.723	Potassium transporter
K4CQV0	3.682	1.042	1.132	1.363	Uncharacterized protein
K4AT60	3.671	0.949	1.210	2.304	Uncharacterized protein
K4ASQ6	3.628	0.939	1.860	2.653	Uncharacterized protein
K4CXM8	3.614	1.200	1.835	2.240	Uncharacterized protein
K4CAT6	3.611	1.002	1.294	1.590	Uncharacterized protein

Accession	Burned	Control	Regular	Limit	Description
K4D4L7	3.607	1.070	1.083	1.128	Uncharacterized protein
K4BXG3	3.606	0.902	1.227	1.481	Uncharacterized protein
Q05539	3.601	1.106	2.092	18.027	Acidic 26 kDa endochitinase
K4BE28	3.600	0.984	1.101	1.693	Uncharacterized protein
K4BS37	3.598	0.991	0.820	1.146	Uncharacterized protein
K4CAU0	3.594	1.068	1.331	1.957	Uncharacterized protein
K4BE37	3.568	0.955	0.950	1.486	Uncharacterized protein
K4BMR7	3.563	0.881	0.954	1.043	Uncharacterized protein
K4AT91	3.559	0.825	0.824	0.937	Uncharacterized protein
K4BD63	3.538	1.018	1.466	1.719	Uncharacterized protein
K4BJT7	3.516	0.968	1.437	7.541	Uncharacterized protein
K4D304	3.514	0.823	0.818	0.926	Uncharacterized protein
P27161	3.491	0.821	0.816	0.915	Calmodulin
K4BSP6	3.489	1.281	2.418	2.152	Uncharacterized protein
K4BWV8	3.487	1.006	1.348	1.605	Uncharacterized protein
K4D8U5	3.481	1.035	1.167	1.308	Uncharacterized protein
K4C3K8	3.474	0.984	1.152	1.398	Uncharacterized protein
K4C9U5	3.447	1.239	1.902	2.214	Histone H2B
K4D553	3.446	1.239	1.902	2.214	Histone H2B
O65818	3.445	1.237	1.902	2.225	Histone H2B.2
K4D554	3.445	1.237	1.898	2.208	Histone H2B
K4C2M0	3.445	1.236	1.899	2.216	Histone H2B
O65821	3.443	1.238	1.901	2.222	Histone H2B.1
K4C9J5	3.438	1.236	1.904	2.226	Histone H2B
K4BHJ2	3.429	1.234	1.892	2.204	Histone H2B
K4DBG9	3.421	1.216	1.451	1.248	Uncharacterized protein
K4CBZ9	3.421	0.924	1.201	1.797	Uncharacterized protein
K4BCY7	3.411	0.989	0.966	1.207	Uncharacterized protein
K4DG02	3.396	1.023	1.170	1.821	Uncharacterized protein
K4D371	3.393	1.075	1.431	1.749	Uncharacterized protein
K4BTE8	3.393	0.958	1.075	1.533	Uncharacterized protein
K4AXA6	3.385	1.439	1.986	2.027	Uncharacterized protein
K4C2W3	3.372	0.922	1.210	1.789	Uncharacterized protein
Q9ZP31	3.366	1.016	1.373	1.598	Expansin
Q42871	3.360	0.946	0.990	1.525	Endoglucanase
K4B9E7	3.358	1.099	1.896	1.556	Uncharacterized protein
B2LW68	3.356	1.103	3.418	6.715	PR1 protein
P20076	3.354	0.986	1.618	7.855	Ethylene-responsive proteinase inhibitor 1
K4C6Y9	3.349	0.998	1.135	1.498	Beta-galactosidase
K4B3R6	3.344	1.113	1.601	1.460	Peptidyl-prolyl cis-trans isomerase
K4BF11	3.329	1.037	2.751	5.202	Peroxidase
K4BJ99	3.325	1.145	1.244	1.700	Uncharacterized protein
Q9SYU8	3.318	0.965	1.531	3.927	17.7 kD class I small heat shock protein
K4BFM2	3.304	1.144	1.384	1.990	Uncharacterized protein
Q9SYV0	3.297	0.975	1.546	3.959	17.6 kD class I small heat shock protein
Q53U35	3.295	1.015	1.396	4.504	Similar to pathogenesis-related protein STH-2
P37218	3.295	1.210	2.034	2.206	Histone H1
P32045	3.285	0.928	1.699	5.963	Pathogenesis-related protein P2
K4CID1	3.283	1.178	1.606	2.565	Uncharacterized protein
K4CA24	3.275	1.540	1.975	1.664	Tubulin beta chain
K4BY90	3.274	1.045	1.206	1.867	Uncharacterized protein
K4CGQ1	3.259	0.998	1.206	1.569	Uncharacterized protein
K4DBS4	3.256	1.308	2.003	2.427	Uncharacterized protein
K4B1M3	3.250	1.817	1.998	1.621	Uncharacterized protein

Accession	Burned	Control	Regular	Limit	Description
K4C8U3	3.246	1.323	2.739	5.461	Uncharacterized protein
K4C5F0	3.241	1.145	1.239	1.610	Uncharacterized protein
K4D4A7	3.239	1.532	2.024	1.704	Tubulin beta chain
K4C8U4	3.238	1.293	2.750	5.813	Uncharacterized protein
K4BU57	3.233	0.935	0.884	1.226	Uncharacterized protein
K4CME9	3.221	1.141	1.884	3.811	Uncharacterized protein
Q43528	3.220	1.006	2.311	10.988	Xyloglucan endotransglucosylase/hydrolase
K4D5T8	3.216	1.075	1.583	3.499	Uncharacterized protein
K4B422	3.213	1.204	1.606	1.553	Uncharacterized protein
K4BVZ1	3.209	0.967	0.954	1.491	Uncharacterized protein
K4BHF8	3.207	1.241	1.810	5.263	Uncharacterized protein
K4C4W6	3.205	1.532	2.126	1.860	Tubulin beta chain
K4D2Y1	3.196	1.559	2.114	1.781	Tubulin beta chain
K4CHZ9	3.192	1.064	1.348	1.517	Uncharacterized protein
B5M9E4	3.187	1.255	2.003	2.735	Beta-glucosidase 01
K4CBV4	3.184	1.047	1.335	1.925	Uncharacterized protein
K4C988	3.180	0.924	0.944	1.186	Uncharacterized protein
E0YCS8	3.179	1.086	1.321	1.944	Methylketone synthase IIa
K4CSP7	3.174	1.067	1.341	1.630	Uncharacterized protein
K4D384	3.158	1.069	1.447	5.876	Uncharacterized protein
K4CBF7	3.142	1.003	1.858	10.124	Xyloglucan endotransglucosylase/hydrolase
K4DHU1	3.132	1.002	1.525	5.554	Uncharacterized protein
K4C1R6	3.131	1.033	1.016	1.244	Uncharacterized protein
Q2MI72	3.131	0.956	1.446	0.607	Photosystem II reaction center protein H
K4BG34	3.122	1.078	1.517	2.139	Uncharacterized protein
K4C258	3.119	1.126	1.569	2.419	Uncharacterized protein
Q38MV0	3.119	1.581	2.159	1.725	Tubulin beta chain
K4BN73	3.102	1.203	1.350	1.467	Uncharacterized protein
K4BE93	3.102	1.055	2.082	4.079	Peroxidase
K4D9N7	3.096	1.050	1.657	2.774	Uncharacterized protein
K4BUT0	3.095	0.984	1.309	2.964	Uncharacterized protein
K4CVZ3	3.094	1.012	1.230	1.805	Uncharacterized protein
K4D5F6	3.091	1.147	1.667	1.547	Uncharacterized protein
K4BIL3	3.088	0.934	1.436	1.173	Uncharacterized protein
K4C6V9	3.078	1.031	1.654	2.239	Uncharacterized protein
K4B6U4	3.071	0.985	1.433	1.447	Patatin
K4C2H3	3.070	1.137	1.399	1.433	Uncharacterized protein
K4D448	3.069	1.162	0.778	0.905	Uncharacterized protein
K4DFZ3	3.065	0.833	0.800	0.959	Uncharacterized protein
K4B3L3	3.062	0.888	1.007	1.209	Beta-galactosidase
K4CEU2	3.062	1.164	1.733	2.615	Uncharacterized protein
K4C101	3.060	1.195	1.701	2.713	Uncharacterized protein
K4BNT9	3.057	0.984	0.982	1.323	Uncharacterized protein
K4B269	3.052	1.100	1.441	1.459	Uncharacterized protein
K4BBI1	3.052	0.825	0.741	1.077	Uncharacterized protein
K4D594	3.050	1.082	1.424	1.616	Uncharacterized protein
K4D0U0	3.049	1.154	1.349	1.399	Uncharacterized protein
K4BKM5	3.046	0.955	1.184	1.215	Uncharacterized protein
K4BSP7	3.046	1.224	2.962	4.294	Uncharacterized protein
K4BPD2	3.043	1.236	1.926	2.595	Uncharacterized protein
K4B922	3.042	1.082	1.418	7.624	Uncharacterized protein
K4B3Y2	3.041	1.180	1.196	1.359	Uncharacterized protein
K4BBI0	3.040	0.826	0.745	1.079	Uncharacterized protein
K4BGB7	3.035	1.411	1.863	1.774	Uncharacterized protein
K4B0B8	3.032	0.898	0.920	0.823	Uncharacterized protein

Accession	Burned	Control	Regular	Limit	Description
K4BTY3	3.030	1.143	1.373	1.715	Uncharacterized protein
K4B1J9	3.024	1.154	1.315	1.276	Uncharacterized protein
K4AZJ7	3.024	1.311	1.860	2.323	60S ribosomal protein L36
Q2MI83	3.023	0.888	0.977	0.839	Cytochrome b559 subunit alpha
K4BF25	3.023	1.314	1.869	2.339	60S ribosomal protein L36
K4D0F3	3.016	0.989	1.568	3.377	Uncharacterized protein
O82625	3.016	1.070	1.410	1.496	Expansin
B2ZPK7	3.016	0.977	1.413	3.188	BURP domain-containing protein
K4AWP9	3.011	0.994	1.042	1.282	Uncharacterized protein
K4BNF4	3.008	0.972	1.243	1.391	Uncharacterized protein
K4BEU8	3.005	1.154	1.456	1.596	Uncharacterized protein
K4BTH7	3.003	0.946	2.264	2.671	Peroxidase
K4BKB2	2.997	1.427	2.146	3.220	Uncharacterized protein
K4BJT6	2.992	0.923	1.127	2.332	Uncharacterized protein
K4DAN4	2.991	1.083	1.326	1.639	Uncharacterized protein
K4BJ98	2.990	0.996	0.822	0.752	Uncharacterized protein
K4CM15	2.988	1.216	1.700	1.546	Uncharacterized protein
K4BR30	2.986	1.515	2.322	2.200	Uncharacterized protein
K4CVB2	2.986	0.920	1.004	0.857	Pectinesterase
K4B2V0	2.978	0.949	0.920	1.171	Uncharacterized protein
K4BVZ8	2.976	1.048	1.370	1.694	Uncharacterized protein
K4CBZ1	2.976	1.025	1.023	1.215	Nascent polypeptide-associated complex subunit beta
K4BAE6	2.972	1.933	2.701	2.157	Catalase
K4AZL1	2.967	1.272	1.166	1.448	Uncharacterized protein
K4C1K9	2.966	1.004	1.242	1.561	Uncharacterized protein

Accession	Burned	Control	Regular	Limit	Description
K4B1X7	2.963	1.133	1.765	1.843	Uncharacterized protein
K4CW92	2.952	1.358	1.919	1.860	Uncharacterized protein
K4B3H9	2.946	1.148	1.319	1.490	Uncharacterized protein
K4BAE0	2.945	1.109	1.473	1.597	Uncharacterized protein
K4DCS5	2.934	0.869	1.602	2.930	Uncharacterized protein
K4C3N2	2.932	0.925	1.103	1.125	Uncharacterized protein
K4C145	2.929	1.155	1.500	2.501	Uncharacterized protein
K4B9P3	2.925	1.104	1.170	1.185	Pectinesterase
K4AXB7	2.924	0.881	0.836	1.352	Uncharacterized protein
K4C6J4	2.918	1.017	1.334	2.304	Uncharacterized protein
K4BJC2	2.913	1.399	6.119	15.045	Uncharacterized protein
K4B544	2.913	1.032	1.139	1.198	Uncharacterized protein
O48625	2.911	0.998	1.164	3.645	Lemir
K4C6M2	2.906	1.267	1.512	1.880	Uncharacterized protein
Q5NE18	2.906	1.215	4.645	11.294	Formate dehydrogenase, mitochondrial
K4C3K2	2.904	1.134	1.313	1.278	Uncharacterized protein
K4CTX7	2.904	0.954	1.142	1.438	Uncharacterized protein
K4B1X5	2.902	1.589	2.110	2.033	Serine hydroxymethyltransferase
K4BEF6	2.901	1.193	1.059	0.995	Uncharacterized protein
K4BZ85	2.901	1.408	2.008	1.798	Uncharacterized protein
K4C0P6	2.895	1.185	1.167	1.300	Uncharacterized protein
K4DH02	2.893	1.507	1.997	1.716	Tubulin beta chain
K4DCX0	2.889	1.044	1.312	2.190	Uncharacterized protein
K4B071	2.889	1.225	1.713	2.062	Cation-transporting ATPase
K4AZI7	2.884	1.006	1.146	0.984	Uncharacterized protein
K4BHT9	2.884	1.086	1.260	1.182	Uncharacterized protein

Accession	Burned	Control	Regular	Limit	Description
K4B7W7	2.877	1.273	1.626	1.919	Uncharacterized protein
K4CPG9	2.874	1.187	2.112	3.536	Reticulon-like protein
K4BRK0	2.870	1.019	1.241	1.827	Uncharacterized protein
K4CN93	2.857	0.956	1.161	1.745	Uncharacterized protein
K4D9V2	2.853	0.952	0.911	1.121	Uncharacterized protein
K4C5I8	2.852	1.063	1.671	2.143	Peroxidase
K4CPL3	2.848	0.984	1.162	1.915	Uncharacterized protein
K4CHG7	2.846	0.984	1.174	1.930	Small ubiquitin-related modifier
K4CQU7	2.846	1.262	1.570	2.354	Uncharacterized protein
K4B3X8	2.839	1.062	1.335	2.356	Uncharacterized protein
K4BMT2	2.833	1.295	1.868	2.506	Uncharacterized protein
K4BIA4	2.832	1.357	1.806	1.650	Uncharacterized protein
Q9SMD1	2.830	1.026	1.032	1.475	Small ubiquitin-related modifier
K4BXU9	2.829	0.967	1.291	1.839	Purple acid phosphatase
Q152U7	2.828	0.939	1.069	1.146	Multiprotein bridging factor 1c
K4BQC4	2.825	1.186	1.476	1.473	Nuclear pore protein
K4B351	2.824	1.027	1.404	3.389	Uncharacterized protein
K4BQX1	2.817	1.065	1.389	1.949	Uncharacterized protein
K4D482	2.817	0.978	1.169	1.424	Uncharacterized protein
K4BKZ7	2.813	1.265	1.642	1.864	Uncharacterized protein
K4D422	2.813	1.097	1.479	6.328	Uncharacterized protein
K4D4A9	2.811	1.133	1.462	1.821	Uncharacterized protein
K4BC63	2.811	0.972	1.203	1.295	MRLK5
K4BGT9	2.810	1.404	1.408	2.081	Uncharacterized protein
K4BF53	2.809	0.986	0.918	1.504	Uncharacterized protein
K4B486	2.806	1.044	1.420	1.415	Uncharacterized protein
K4C3J2	2.804	0.849	0.962	1.631	Uncharacterized protein
K4C6R9	2.803	1.092	1.222	1.307	Uncharacterized protein

Accession	Burned	Control	Regular	Limit	Description
K4B0V2	2.802	1.013	1.833	7.893	Lipoxygenase
K4DBS7	2.799	1.054	1.268	1.317	Uncharacterized protein
K4BX03	2.798	1.093	1.477	2.066	Uncharacterized protein
K4CAE7	2.797	1.052	1.408	1.310	Uncharacterized protein
K4C2J3	2.797	1.151	1.640	2.328	Uncharacterized protein
K4C382	2.796	0.939	1.049	1.090	Uncharacterized protein
K4BVG4	2.794	1.053	1.713	4.538	Uncharacterized protein
K4BDF9	2.792	1.137	1.490	1.538	Uncharacterized protein
K4BF54	2.791	1.071	1.563	4.512	Uncharacterized protein
K4C235	2.791	1.092	1.433	1.266	Uncharacterized protein
K4C5Z4	2.790	1.146	1.635	1.486	Uncharacterized protein
K4CSI7	2.789	1.101	1.191	1.553	Uncharacterized protein
K4BXA3	2.784	0.975	1.030	1.397	Uncharacterized protein
K4B1I4	2.783	1.432	2.013	2.094	Uncharacterized protein
K4CRG8	2.782	1.007	1.293	1.788	Uncharacterized protein
K4B7S0	2.780	1.020	1.145	1.519	Uncharacterized protein
K4D9Q9	2.779	0.922	1.127	1.538	Carboxypeptidase
K4D8X9	2.777	0.936	1.591	1.699	Uncharacterized protein
K4CLS9	2.777	0.922	1.028	1.306	Uncharacterized protein
K4CHA5	2.773	0.843	1.528	1.908	Uncharacterized protein
K4BKL5	2.770	1.295	1.521	1.401	Uncharacterized protein
K4B835	2.770	0.906	0.806	0.984	Uncharacterized protein
K4B0X3	2.767	1.212	1.369	1.561	Uncharacterized protein
P15003	2.765	0.785	0.951	1.653	Suberization-associated anionic peroxidase 1
K4DB22	2.764	1.103	1.163	1.418	Uncharacterized protein
K4BTX9	2.762	1.128	1.354	1.601	Uncharacterized protein
K4CH73	2.758	1.182	1.378	2.419	Uncharacterized protein
K4ASN8	2.755	1.267	1.666	2.194	Uncharacterized protein
K4CH57	2.752	0.940	1.274	1.338	Uncharacterized protein

Accession	Burned	Control	Regular	Limit	Description
Q9ZP11	2.752	1.011	1.086	1.445	Beta-galactosidase
Q672Q9	2.752	0.835	0.693	0.833	Acyl carrier protein
K4D1H1	2.749	0.976	1.895	6.613	Uncharacterized protein
K4BVR1	2.746	1.283	1.296	1.454	Uncharacterized protein
K4BA70	2.744	1.126	1.310	2.025	Uncharacterized protein
K4C7H6	2.741	1.139	1.439	1.903	RNA-binding protein 8A
K4CNY4	2.741	0.922	1.158	1.578	Uncharacterized protein
K4BTI0	2.739	0.850	0.823	1.026	Uncharacterized protein
K4C5G0	2.736	1.050	1.571	1.944	Alpha-galactosidase
K4AV57	2.733	1.065	1.460	1.667	Uncharacterized protein
K4B8K0	2.733	1.045	1.219	1.364	Uncharacterized protein
K4CEU5	2.730	1.004	1.424	1.352	Uncharacterized protein
K4BWW9	2.729	1.057	1.279	3.020	Uncharacterized protein
Q96569	2.728	0.948	1.469	2.779	L-lactate dehydrogenase
K4BKK1	2.727	0.891	1.209	1.589	Uncharacterized protein
K4C5K1	2.724	0.972	0.853	1.132	PRA1 family protein
K4CN95	2.719	1.063	1.600	2.154	Uncharacterized protein
K4BSQ9	2.719	1.371	2.102	2.894	Uncharacterized protein
K4BVQ4	2.718	1.071	1.323	1.087	Uncharacterized protein
Q9FT22	2.717	1.123	1.693	2.673	Putative glutathione S-transferase T2
K4B078	2.716	1.204	1.308	1.391	Uncharacterized protein
K4D3M6	2.716	0.899	1.523	6.345	Uncharacterized protein
K4CB09	2.709	0.856	0.700	1.228	Uncharacterized protein
K4C3U9	2.708	0.946	1.160	1.072	Pectinesterase
K4C2Y2	2.707	1.135	1.239	1.490	Uncharacterized protein
K4CQU1	2.705	1.031	1.227	1.354	Uncharacterized protein
K4B042	2.704	1.494	2.156	1.980	Uncharacterized protein
K4CRL4	2.702	1.197	1.718	1.572	Uncharacterized protein
O82777	2.699	0.912	1.581	2.122	Subtilisin-like protease

Accession	Burned	Control	Regular	Limit	Description
Q2MI94	2.691	0.938	0.776	0.921	ATP synthase epsilon chain, chloroplastic
K4BU32	2.684	0.977	1.172	1.484	Uncharacterized protein
K4DGH9	2.684	1.215	1.617	1.987	Uncharacterized protein
K4C5X0	2.680	1.217	1.451	1.645	Uncharacterized protein
Q9M726	2.680	1.101	1.196	1.132	Non-specific serine/threonine protein kinase
K4AYE4	2.679	0.956	1.117	1.847	Uncharacterized protein
K4D1H0	2.673	1.042	2.238	9.525	Uncharacterized protein
K4B456	2.669	1.074	1.469	1.988	Uncharacterized protein
K4D5E1	2.669	0.965	1.075	1.417	Beta-hexosaminidase
K4B2P6	2.667	0.974	0.858	0.763	Uncharacterized protein
K4CTS9	2.664	1.129	1.293	1.506	Uncharacterized protein
K4B4Z7	2.661	1.309	1.715	1.655	Uncharacterized protein
K4BBY2	2.660	1.205	1.910	1.793	Uncharacterized protein
K4CQ37	2.660	1.186	1.445	1.809	Uncharacterized protein
K4C2X8	2.658	1.230	1.937	1.784	Uncharacterized protein
K4ASQ2	2.657	1.132	1.661	1.677	Uncharacterized protein
K4B7P7	2.657	1.235	2.087	2.775	Uncharacterized protein
K4BY91	2.650	1.131	1.356	1.673	Uncharacterized protein
K4BW82	2.646	1.033	1.588	3.398	Uncharacterized protein
K4AYH1	2.646	0.910	1.855	2.513	Uncharacterized protein
G5EM33	2.644	0.918	1.066	1.423	Calcineurin B-like molecule
K4BLK6	2.643	1.254	1.661	1.882	Uncharacterized protein
K4BYE4	2.643	1.132	1.347	1.430	Uncharacterized protein
Q05538	2.642	1.019	2.798	10.676	Basic 30 kDa endochitinase
K4BFG3	2.642	1.473	2.247	2.063	Uncharacterized protein
K4BAX2	2.642	1.238	1.664	2.043	Uncharacterized protein

Accession	Burned	Control	Regular	Limit	Description
K4BL51	2.637	0.931	1.044	1.782	Uncharacterized protein
K4D9N5	2.635	1.095	2.425	4.633	Xyloglucan endotransglucosylase/hydrolase
K4BRX7	2.635	1.133	1.184	1.279	Uncharacterized protein
K4D8X6	2.633	0.960	1.224	3.128	Uncharacterized protein
Q2MI42	2.631	1.415	1.851	1.672	Protein TIC 214
Q9ZS44	2.630	0.885	1.757	2.433	SBT4B protein
K4BHS7	2.630	1.118	2.368	5.435	Glycosyltransferase
K4BD26	2.625	1.027	1.346	1.971	Uncharacterized protein
O22548	2.624	1.207	1.816	2.850	Inorganic phosphate transporter
K4B1A3	2.624	1.229	1.642	1.836	Importin subunit alpha
K4CHA6	2.623	1.225	1.770	2.644	Uncharacterized protein
K4B9K6	2.620	1.032	1.151	1.444	Uncharacterized protein
K4DI03	2.610	1.142	1.297	1.500	Signal recognition particle 9 kDa protein
K4CWC6	2.608	0.997	1.285	2.687	Uncharacterized protein
K4DD78	2.607	1.056	1.201	1.163	Uncharacterized protein
K4BT26	2.607	1.332	1.497	1.418	Uncharacterized protein
Q9AXQ5	2.605	1.034	1.186	1.654	Eukaryotic translation initiation factor 5A-2
K4BWN6	2.602	1.026	1.224	1.520	Uncharacterized protein
D6C447	2.601	0.900	1.184	3.692	Putative uncharacterized protein
K4DBG6	2.600	1.192	1.731	2.032	Reticulon-like protein
K4CR71	2.597	1.293	1.728	2.198	Uncharacterized protein
K4BRF6	2.597	1.025	1.965	7.230	Uncharacterized protein
K4B1I7	2.595	1.465	1.973	2.061	Uncharacterized protein
E0Z1D0	2.593	1.140	1.993	5.654	Sucrose synthase
K4B0H5	2.592	1.021	1.053	1.889	Uncharacterized protein
K4BB54	2.592	1.221	1.560	1.977	Uncharacterized protein
Q9LEG5	2.591	1.198	3.036	3.898	Allene oxide cyclase
Q42872	2.589	1.028	1.168	1.779	Endoglucanase
K4D5D4	2.588	1.014	1.156	1.179	Uncharacterized protein
K4B7H7	2.583	0.919	1.266	1.850	Uncharacterized protein
K4B1I5	2.582	1.327	1.596	1.701	Uncharacterized protein
K4DH53	2.580	1.088	1.373	1.787	Uncharacterized protein
K4CHP1	2.574	1.195	1.486	2.034	Uncharacterized protein
K4C890	2.565	1.030	0.837	0.798	Uncharacterized protein
K4CU67	2.565	1.292	1.829	2.192	Uncharacterized protein
K4C1Q9	2.565	1.051	1.611	1.827	Peroxidase
K4DH35	2.564	0.909	0.863	1.307	Uncharacterized protein
K4D345	2.563	1.125	1.315	1.539	Uncharacterized protein
K4CY94	2.562	1.064	1.584	1.498	Secretory carrier-associated membrane protein
Q0PY39	2.561	0.922	1.183	1.240	Auxin repressed/dormancy associated protein
K4DBS5	2.557	1.055	1.336	1.580	Uncharacterized protein
K4CA37	2.557	0.961	0.896	0.627	Uncharacterized protein
K4D3L8	2.556	1.024	1.659	1.929	Uncharacterized protein
K4CFP9	2.555	0.715	0.924	1.334	Uncharacterized protein
K4B9E1	2.553	1.047	1.554	2.672	Uncharacterized protein
K4B0L0	2.551	1.000	1.223	1.579	Uncharacterized protein
K4DHG3	2.548	1.235	1.283	1.508	Uncharacterized protein
K4B9C4	2.545	1.285	1.559	1.576	Uncharacterized protein
K4BX55	2.545	1.214	1.656	1.379	Uncharacterized protein
K4CRI5	2.543	0.986	1.557	3.067	Uncharacterized protein
K4BEV4	2.541	0.992	1.823	7.496	Tonoplast intrinsic protein 32

Accession	Burned	Control	Regular	Limit	Description
K4BM30	2.540	1.006	1.147	3.284	Uncharacterized protein
K4DBZ4	2.538	0.974	1.321	2.163	Uncharacterized protein
K4BCC3	2.537	1.016	1.611	4.189	Uncharacterized protein
K4CPJ0	2.534	1.019	1.107	1.197	Uncharacterized protein
K4CDF4	2.531	1.408	1.964	2.024	Coatomer subunit alpha
K4BWA5	2.530	1.342	1.909	1.977	Uncharacterized protein
K4B825	2.530	1.198	1.278	1.377	Uncharacterized protein
K4AX22	2.528	0.666	0.453	1.291	Superoxide dismutase [Cu-Zn]
Q01413	2.527	1.065	2.081	5.205	Glucan endo-1,3-beta-glucosidase B
K4CY16	2.526	0.909	1.033	1.087	Uncharacterized protein
K4CGP4	2.525	1.057	1.133	1.608	Uncharacterized protein
K4CWB2	2.525	1.029	1.179	1.468	Uncharacterized protein
K4CA55	2.523	1.106	1.710	2.878	Peptidyl-prolyl cis-trans isomerase
K4D3H7	2.520	1.042	1.201	1.359	Uncharacterized protein
K4AVG8	2.518	0.976	1.256	1.491	Uncharacterized protein
K4BWJ9	2.518	1.141	1.098	1.323	Uncharacterized protein
K4BAL4	2.515	0.944	1.292	2.676	Uncharacterized protein
K4DC67	2.514	1.188	1.695	1.880	Uncharacterized protein
E5KBY0	2.513	0.876	1.674	1.221	Snakin-2
K4BUK2	2.512	1.078	1.934	5.976	Uncharacterized protein
K4CV90	2.511	1.048	1.494	1.784	Uncharacterized protein
K4CK49	2.510	1.241	1.882	1.786	Importin subunit alpha
K4CI50	2.509	0.955	1.261	1.236	Uncharacterized protein
K4BCG1	2.508	0.958	1.110	0.918	Uncharacterized protein
K4B402	2.508	1.071	1.884	2.690	Uncharacterized protein
K4C858	2.506	1.219	1.673	1.932	Uncharacterized protein
K4C128	2.501	0.999	1.094	1.228	Small nuclear ribonucleoprotein-associated protein
K4B1U3	2.500	1.193	1.786	3.067	Uncharacterized protein
K4DA21	2.499	1.295	1.941	1.743	Uncharacterized protein
P54773	2.498	1.004	1.249	1.430	Photosystem II 22 kDa protein, chloroplastic
K4C7E9	2.498	0.922	0.971	1.164	Uncharacterized protein
K4CAB5	2.494	1.356	1.769	2.413	Uncharacterized protein
Q9SMC4	2.494	1.028	1.118	1.333	Dolichyl-diphosphooligosaccharide--protein glycosyltransferase subunit DAD1
K4D130	2.494	0.991	1.217	1.819	Uncharacterized protein
K4BTT5	2.493	0.979	1.019	1.090	Uncharacterized protein
K4DCR6	2.492	0.861	0.881	0.931	Uncharacterized protein
K4B9P2	2.491	1.109	1.192	1.231	Pectinesterase
K4D3J1	2.490	1.496	2.203	3.146	Uncharacterized protein
K4BEK3	2.489	1.314	1.413	1.943	Pyruvate kinase
K4CFU2	2.488	1.122	1.910	2.116	Uncharacterized protein
K4BID3	2.487	1.032	0.791	0.594	Uncharacterized protein
K4BP88	2.487	1.074	1.300	1.715	Uncharacterized protein
K4C1J7	2.484	1.161	1.561	2.437	Acylsugar acylhydrolase 1
K4BEJ6	2.481	1.164	1.903	2.416	Reticulon-like protein
K4D3Q3	2.481	0.987	1.101	1.255	Uncharacterized protein
K4AYQ0	2.479	1.076	1.117	1.191	Uncharacterized protein
K4BP33	2.475	0.959	1.240	1.740	Uncharacterized protein
Q152U8	2.475	0.941	1.099	1.047	Multiprotein bridging factor 1b
K4CWS9	2.473	0.984	0.872	1.129	Uncharacterized protein

Accession	Burned	Control	Regular	Limit	Description
K4CMG1	2.472	1.117	1.359	1.649	Uncharacterized protein
K4CGJ8	2.471	1.167	1.800	1.692	Uncharacterized protein
K4B1Y2	2.471	1.174	1.429	1.512	Uncharacterized protein
K4CB65	2.467	1.308	2.452	2.471	Uncharacterized protein
K4C1V2	2.466	1.090	1.169	0.831	Uncharacterized protein
K4DH50	2.465	1.153	1.153	1.235	Uncharacterized protein
Q66MH8	2.465	1.097	1.502	1.482	MAPKK
K4DC49	2.465	1.103	1.324	1.401	Uncharacterized protein
K4BBM1	2.464	1.288	1.811	1.949	Uncharacterized protein
K4BUY4	2.463	1.035	1.140	1.536	Uncharacterized protein
Q8H0Q1	2.461	1.293	1.379	1.642	Proliferating cell nuclear antigen
K4BM94	2.460	1.382	1.424	1.464	Uncharacterized protein
K4CV79	2.457	1.114	1.475	1.977	Uncharacterized protein
K4BM13	2.455	1.184	1.801	2.021	Uncharacterized protein
K4AZJ5	2.454	1.002	1.117	1.246	Small nuclear ribonucleoprotein-associated protein
Q8GUQ5	2.452	1.135	1.415	1.455	Brassinosteroid LRR receptor kinase
K4DAE7	2.451	0.992	1.192	1.457	Uncharacterized protein
K4AXN9	2.448	1.046	1.345	2.399	Uncharacterized protein
K4AV71	2.447	1.141	1.697	3.993	Uncharacterized protein
Q9FT20	2.446	0.917	1.452	3.365	Putative glutathione S-transferase T4
K4CBN8	2.446	1.221	1.944	2.071	Uncharacterized protein
F8WS84	2.446	1.049	1.150	1.118	Leucine rich repeat receptor protein kinase CLAVATA1
K4DAC8	2.444	1.475	2.147	3.045	Uncharacterized protein
K4DHZ8	2.444	1.020	1.105	1.582	Mitochondrial fission 1 protein
K4BRW8	2.444	1.218	1.427	1.308	Uncharacterized protein
K4BSR4	2.443	1.082	1.800	5.931	Annexin
K4B6B6	2.437	1.019	1.146	1.331	Uncharacterized protein
K4DHM2	2.436	1.516	1.974	1.917	Serine hydroxymethyltransferase
K4C8T5	2.435	1.005	1.607	6.048	Uncharacterized protein
K4CH02	2.433	0.872	0.957	0.994	Uncharacterized protein
B5M9E5	2.433	1.030	1.475	2.709	Beta-glucosidase 08
K4B023	2.433	1.175	1.689	1.755	Uncharacterized protein
K4BVQ6	2.432	0.929	1.286	2.735	Uncharacterized protein
K4D266	2.432	1.143	1.247	1.743	Uncharacterized protein
K4CKY7	2.430	1.071	1.763	1.513	Uncharacterized protein
K4BUX6	2.430	0.962	1.333	2.631	Uncharacterized protein
K4C2J4	2.428	0.981	0.850	1.040	Uncharacterized protein
K4C9L4	2.428	1.469	2.130	3.019	Uncharacterized protein
K4B4Z0	2.427	1.182	1.589	2.245	Uncharacterized protein
K4D479	2.427	0.874	0.937	0.892	Uncharacterized protein
K4CW83	2.426	0.948	1.424	1.248	Uncharacterized protein
K4D367	2.424	0.955	1.173	1.254	Uncharacterized protein
K4B1U6	2.424	0.932	0.706	0.738	Uncharacterized protein
K4BLP5	2.421	1.272	1.689	2.041	Uncharacterized protein
K4C1V3	2.420	1.037	1.191	1.216	Uncharacterized protein
K4B724	2.417	0.916	0.744	0.893	Uncharacterized protein
K4BLW3	2.414	0.878	0.833	1.199	Uncharacterized protein
K4BVU7	2.413	1.044	2.888	6.284	Uncharacterized protein
K4BTY1	2.410	1.055	1.241	1.293	Uncharacterized protein
A0A140TAT3	2.409	0.967	0.915	1.537	Uncharacterized protein
K4D3K7	2.407	1.093	1.663	1.415	Uncharacterized protein

Accession	Burned	Control	Regular	Limit	Description
K4CWQ3	2.404	1.225	1.924	2.798	Uncharacterized protein
K4BXN1	2.403	1.174	1.412	1.409	Uncharacterized protein
K4AZZ3	2.402	1.086	1.265	2.203	Uncharacterized protein
K4CCD4	2.401	1.241	1.555	2.230	Uncharacterized protein
K4BL05	2.400	1.028	1.418	1.843	Uncharacterized protein
Q7XAV2	2.399	0.596	0.292	0.756	Superoxide dismutase [Cu-Zn]
K4DDH5	2.397	1.140	1.443	1.522	Uncharacterized protein
K4D0Y5	2.395	0.983	1.172	2.003	Uncharacterized protein
K4D3Y2	2.394	1.354	1.806	1.958	Uncharacterized protein
K4BJB9	2.392	1.259	1.953	2.308	Uncharacterized protein
K4DBY2	2.390	1.138	1.321	1.576	Uncharacterized protein
K4CB54	2.388	1.045	0.988	1.156	Translation initiation factor IF-3
K4D5U9	2.387	0.932	1.395	3.873	Uncharacterized protein
Q2MI54	2.387	1.221	1.530	1.467	30S ribosomal protein S7, chloroplastic
K4CHM7	2.386	1.090	1.299	1.545	Uncharacterized protein
K4CJG6	2.385	0.958	1.233	1.768	Uncharacterized protein
K4CPE5	2.383	0.995	0.940	1.158	Uncharacterized protein
K4CR18	2.382	1.337	1.739	1.765	Uncharacterized protein
K4CXZ6	2.382	1.038	1.135	1.351	Uncharacterized protein
K4C2U1	2.381	1.108	1.547	2.173	Phenylalanine ammonia-lyase
K4AXH8	2.380	1.023	1.125	1.260	Uncharacterized protein
K4CFN3	2.380	0.954	1.399	3.906	Uncharacterized protein
K4BMT5	2.378	1.004	1.356	1.732	Uncharacterized protein
K4CH99	2.378	0.997	0.788	0.729	Thiamine thiazole synthase, chloroplastic
K4D7U2	2.378	1.230	1.943	2.354	Uncharacterized protein
K4B891	2.374	0.944	1.090	1.327	Uncharacterized protein
K4AX86	2.373	0.985	1.412	1.682	Tubulin-specific chaperone A
K4B8I7	2.372	1.387	2.363	3.344	Uncharacterized protein
K4AZ39	2.371	1.158	1.349	1.865	Uncharacterized protein
K4B4T2	2.371	0.956	1.078	1.704	Carboxypeptidase
K4B287	2.370	0.994	0.973	1.077	Uncharacterized protein
K4BTM6	2.368	1.094	1.234	1.354	Uncharacterized protein
K4BXT3	2.367	1.157	1.107	1.055	Uncharacterized protein
K4CCK4	2.367	1.083	1.296	1.857	Uncharacterized protein
K4D7N1	2.367	1.043	0.863	0.963	Uncharacterized protein
K4BVX3	2.365	1.806	2.749	2.393	Catalase
K4BU64	2.365	1.023	1.405	1.615	Uncharacterized protein
K4BKA0	2.363	1.187	1.161	1.258	Uncharacterized protein
K4CXC5	2.362	1.311	1.480	1.660	Uncharacterized protein
K4AZT0	2.361	1.233	1.650	2.474	Uncharacterized protein
K4CQF3	2.357	0.984	1.246	1.607	Carboxypeptidase
K4CN52	2.357	1.018	1.231	1.415	Uncharacterized protein
Q84KJ2	2.353	0.955	1.439	1.519	Copper chaperone
K4DGU7	2.352	0.880	0.935	1.475	Uncharacterized protein
K4B137	2.352	0.998	0.955	1.188	Uncharacterized protein
Q96477	2.351	1.051	1.582	2.788	LRR protein
K4AYK4	2.351	0.990	1.250	1.271	Uncharacterized protein
K4BL78	2.350	0.980	1.374	1.849	Uncharacterized protein
K4C8I5	2.349	0.983	1.003	1.062	Uncharacterized protein
Q5D8D3	2.348	1.228	1.809	3.242	Acyl-coenzyme A oxidase
K4CH98	2.347	1.112	1.556	1.633	Uncharacterized protein
K4CQR2	2.345	1.029	1.247	3.739	Uncharacterized protein
K4C349	2.344	0.953	1.080	1.434	Uncharacterized protein
K4C2E8	2.340	0.908	1.058	1.467	Beta-hexosaminidase
K4CFR4	2.340	1.049	1.182	1.333	Uncharacterized protein

Accession	Burned	Control	Regular	Limit	Description
K4DHR3	2.340	0.950	1.379	4.479	Uncharacterized protein
K4DC77	2.337	1.361	2.638	2.550	Uncharacterized protein
K4D426	2.336	1.162	1.348	1.644	Uncharacterized protein
K4AS88	2.334	1.312	1.822	1.740	Uncharacterized protein
K4CXS7	2.334	1.327	1.784	1.901	Uncharacterized protein
K4CB35	2.332	1.024	1.261	1.427	Uncharacterized protein
K4CR73	2.332	1.300	1.660	1.885	Eukaryotic translation initiation factor 3 subunit A
K4C320	2.332	1.222	2.024	2.951	Uncharacterized protein
K4B3Y6	2.332	1.120	1.315	1.498	Uncharacterized protein
K4CL64	2.331	1.381	1.924	2.598	Uncharacterized protein
O82006	2.330	0.921	1.596	2.179	Subtilisin-like protease
K4CW46	2.329	1.164	1.678	1.818	Uncharacterized protein
K4BPB8	2.329	0.972	1.210	1.634	Uncharacterized protein
K4DH72	2.327	1.381	1.932	2.610	Uncharacterized protein
K4CQH9	2.326	1.166	1.765	1.893	Phenylalanine ammonia-lyase
K4B8U9	2.326	1.230	1.438	2.334	Uncharacterized protein
K4CBV1	2.326	1.283	1.796	2.230	Calcium-transporting ATPase
P61242	2.325	1.355	1.649	1.524	Protein Ycf2
K4AZ45	2.325	1.055	1.083	1.144	Pectinesterase
K4BFL2	2.323	1.147	1.495	1.590	Vacuolar protein sorting-associated protein 35
K4CBQ8	2.321	1.101	1.326	1.569	Uncharacterized protein
K4CGW9	2.320	1.192	1.835	2.738	Uncharacterized protein
K4BFU2	2.320	1.314	1.834	2.076	Uncharacterized protein
K4BKQ1	2.317	1.174	1.290	1.789	Uncharacterized protein
K4CHH2	2.317	1.012	1.150	1.979	GrpE protein homolog

Accession	Burned	Control	Regular	Limit	Description
E1CFU1	2.316	1.096	1.456	1.333	Calcium dependent protein kinase
K4C3V7	2.315	1.078	1.267	1.300	Diacylglycerol kinase
K4BL48	2.314	1.115	1.546	1.750	Uncharacterized protein
K4BVH7	2.313	1.357	1.893	2.147	Coatomer subunit alpha
K4BF27	2.313	1.094	1.230	1.556	Uncharacterized protein
K4BI20	2.312	1.152	1.526	1.941	Uncharacterized protein
K4BS22	2.311	1.437	2.204	2.228	Uncharacterized protein
K4DAT4	2.311	0.924	0.991	1.355	Uncharacterized protein
K4AYG4	2.310	0.922	1.691	2.440	Uncharacterized protein
K4BCJ8	2.308	0.960	1.835	1.865	Patatin
K4CWU2	2.308	0.961	3.075	5.350	Uncharacterized protein
K4CIH7	2.308	1.596	2.262	1.829	Tubulin alpha chain
K4B0D8	2.307	1.064	1.800	2.584	Annexin
K4CBD9	2.305	1.246	1.607	1.578	Uncharacterized protein
K4B1D9	2.304	1.059	1.099	0.948	Uncharacterized protein
K4DG25	2.302	1.170	1.598	2.358	Uncharacterized protein
K4CHI7	2.302	1.097	1.197	1.400	Uncharacterized protein
K4BMH7	2.299	1.013	1.132	1.809	Uncharacterized protein
K4B6Z5	2.297	1.054	1.331	1.568	Uncharacterized protein
K4BH38	2.296	0.930	0.799	1.081	Superoxide dismutase [Cu-Zn]
K4CA23	2.296	0.950	0.861	0.928	Peroxidase
K4BZD5	2.294	1.158	1.433	1.889	Uncharacterized protein
K4DI17	2.294	0.888	0.818	0.919	Uncharacterized protein
C5IU71	2.294	0.806	0.538	0.594	Chloroplast sedoheptulose-1,7-bisphosphatase
K4CC09	2.294	1.076	1.151	1.416	Uncharacterized protein
K4CQR5	2.291	1.406	2.045	2.185	Uncharacterized protein
K4C5Y9	2.291	1.302	1.894	1.910	Uncharacterized protein

Accession	Burned	Control	Regular	Limit	Description
K4AYS8	2.291	1.328	1.503	1.229	Uncharacterized protein
K4CRN6	2.287	1.122	1.249	1.329	Uncharacterized protein
K4C9Z6	2.286	1.313	1.510	1.703	Uncharacterized protein
A7X331	2.285	0.956	1.747	2.136	Expansin-like protein
K4C6Y2	2.285	1.003	1.301	1.671	Uncharacterized protein
K4C603	2.285	1.353	2.231	2.623	Uncharacterized protein
K4C2V5	2.284	1.312	1.772	2.138	T-complex protein 1 subunit gamma
K4CTZ5	2.282	1.178	1.819	2.522	Uncharacterized protein
K4C386	2.277	1.134	1.320	1.516	Uncharacterized protein
K4B894	2.276	1.073	1.073	1.216	Uncharacterized protein
K4B6Q4	2.276	1.242	1.757	1.728	Calcium-transporting ATPase
K4D1B3	2.274	0.951	1.430	2.745	Dirigent protein
K4BEW7	2.271	0.913	1.002	1.667	Uncharacterized protein
K4CZZ5	2.270	1.118	1.344	1.421	Uncharacterized protein
K4BPI0	2.268	1.190	1.495	2.284	Uncharacterized protein
K4C6S7	2.267	1.030	1.505	5.093	Uncharacterized protein
K4C869	2.266	1.074	0.957	0.764	Uncharacterized protein
K4D6I5	2.262	1.297	1.340	1.152	Nitrate reductase
K4DF84	2.262	1.283	1.251	1.463	ADP,ATP carrier protein
K4D887	2.260	1.370	2.016	2.475	Uncharacterized protein
K4CI92	2.260	1.105	1.387	1.852	Uncharacterized protein
K4D681	2.260	1.228	1.661	1.786	Uncharacterized protein
K4CRC7	2.259	0.920	0.901	0.854	Uncharacterized protein
K4AZ32	2.258	1.124	1.289	1.755	Uncharacterized protein
K4BCW6	2.258	0.973	1.207	1.792	Uncharacterized protein
K4C992	2.257	1.046	1.440	2.830	Uncharacterized protein
K4ASK2	2.255	1.261	1.934	2.204	Uncharacterized protein
K4BAF6	2.255	0.978	1.097	1.291	Uncharacterized protein

Accession	Burned	Control	Regular	Limit	Description
K4AZT1	2.254	1.089	1.298	1.558	Uncharacterized protein
K4BHY2	2.254	0.983	1.124	2.110	Uncharacterized protein
K4B9R8	2.254	1.154	1.281	1.467	Uncharacterized protein
K4CPI9	2.253	1.069	1.227	1.394	Uncharacterized protein
K4CHA9	2.253	1.325	1.119	1.147	Tryptophan synthase
K4CPB3	2.252	1.117	1.286	1.613	Uncharacterized protein
K4BPJ2	2.251	1.228	1.964	2.744	Uncharacterized protein
K4CPJ7	2.250	1.154	1.531	1.591	Uncharacterized protein
K4CVT4	2.250	1.175	1.548	1.978	Uncharacterized protein
K4BD40	2.248	1.079	1.377	2.083	Uncharacterized protein
K4CTP6	2.248	0.999	1.218	1.678	Uncharacterized protein
K4AT09	2.248	0.807	0.947	1.080	Uncharacterized protein
K4CWW8	2.247	1.077	1.234	1.894	Uncharacterized protein
K4BML9	2.247	1.214	1.484	1.565	Uncharacterized protein
K4BF04	2.245	0.861	0.738	0.606	Uncharacterized protein
K4BT67	2.244	0.963	0.998	1.299	Carboxypeptidase
K4DH69	2.243	0.941	1.002	1.184	Uncharacterized protein
O04972	2.243	0.988	1.284	1.914	Endoglucanase
K4B778	2.240	1.105	1.264	1.732	Uncharacterized protein
K4BVR7	2.240	0.958	1.283	2.134	Uncharacterized protein
K4CAV7	2.240	1.220	1.599	1.707	Uncharacterized protein
K4BV79	2.239	1.073	1.142	1.686	Uncharacterized protein
K4CN33	2.239	1.089	1.299	1.451	Uncharacterized protein
O65836	2.238	0.913	0.982	1.091	p69F protein
K4BAD9	2.237	1.112	1.263	1.681	Uncharacterized protein
K4CIJ8	2.237	1.275	1.683	1.573	Uncharacterized protein
K4B7C1	2.236	1.095	1.130	0.991	Uncharacterized protein
K4AT93	2.236	1.497	2.477	3.233	Uncharacterized protein
K4AZH6	2.235	1.403	1.937	2.018	Uncharacterized protein
K4C5P5	2.233	1.029	1.752	3.961	Uncharacterized protein

Accession	Burned	Control	Regular	Limit	Description
K4ATY6	2.232	1.047	1.242	1.754	Aldehyde dehydrogenase
K4BI70	2.230	1.273	1.702	1.781	Uncharacterized protein
K4BNR3	2.230	1.203	1.583	1.542	Uncharacterized protein
K4BG21	2.229	1.316	1.551	2.218	Uncharacterized protein
K4CI43	2.228	1.079	1.174	1.445	Uncharacterized protein
K4C9U6	2.228	0.794	0.829	1.090	Uncharacterized protein
K4B7Q8	2.226	1.120	1.379	1.441	AGO2A2
K4CZF1	2.226	1.164	1.489	1.696	Peptidylprolyl isomerase
K4CJL1	2.225	1.170	1.603	1.547	Uncharacterized protein
K4BL52	2.224	1.069	1.385	1.575	Uncharacterized protein
K4D4Y1	2.224	0.873	1.214	1.700	Uncharacterized protein
K4B264	2.223	1.344	2.065	2.488	Uncharacterized protein
K4BIC8	2.221	0.904	0.989	1.384	Uncharacterized protein
K4D888	2.221	1.218	1.537	1.905	Uncharacterized protein
K4CYF5	2.220	0.866	1.259	1.348	Uncharacterized protein
K4B6X9	2.219	0.956	1.777	2.823	Uncharacterized protein
K4CHM9	2.218	1.027	1.094	1.281	Uncharacterized protein
K4BAG0	2.217	1.021	1.607	3.003	Uncharacterized protein
K4CF47	2.217	0.977	1.300	3.147	Uncharacterized protein
K4D9K1	2.214	1.080	1.388	2.179	Uncharacterized protein
K4C5A8	2.214	1.234	1.643	2.097	Uncharacterized protein
K4D3L6	2.212	1.091	1.310	2.082	Uncharacterized protein
K4BMB8	2.211	0.965	1.297	1.640	Uncharacterized protein
K4CQ16	2.210	1.446	1.403	1.946	Uncharacterized protein
K4D5N5	2.209	1.148	1.328	1.101	Uncharacterized protein
K4D8E0	2.209	0.982	1.214	1.601	Uncharacterized protein
P15004	2.208	0.949	1.152	1.674	Suberization-associated anionic peroxidase 2
K4DAM1	2.207	1.050	1.377	2.420	Uncharacterized protein
K4CQE1	2.207	0.950	1.222	2.202	Peroxidase
K4BBI6	2.204	0.986	1.050	1.194	Uncharacterized protein
K4B117	2.204	1.260	1.589	1.909	Uncharacterized protein
K4BIP4	2.204	1.151	1.581	2.194	Mago nashi protein
K4BVR9	2.204	1.044	1.680	6.140	Uncharacterized protein
K4CVX1	2.203	0.992	2.031	2.831	Uncharacterized protein
K4C4E2	2.203	1.179	1.853	3.357	Uncharacterized protein
K4CLN3	2.203	1.071	1.238	1.442	Uncharacterized protein
K4DA93	2.202	1.104	1.330	1.445	RuvB-like helicase
K4C1C0	2.201	0.949	1.339	1.244	Peroxidase
K4BGP0	2.201	1.176	1.418	1.501	Uncharacterized protein
K4D1P9	2.200	1.138	1.543	1.593	Uncharacterized protein
K4CEJ0	2.200	1.110	1.572	3.330	Uncharacterized protein
K4CV92	2.200	1.260	1.575	1.884	Uncharacterized protein
K4BVM3	2.199	1.350	2.087	1.984	Uncharacterized protein
K4DA57	2.199	1.146	1.343	1.795	Uncharacterized protein
K4BVG6	2.198	1.032	0.881	0.849	Uncharacterized protein
K4DC86	2.198	0.953	0.916	0.999	Uncharacterized protein
K4DA00	2.197	1.249	1.534	1.957	Ribosomal protein
K4C864	2.196	1.002	0.931	0.844	Uncharacterized protein
K4DGX0	2.195	1.235	1.830	1.667	Uncharacterized protein
K4B831	2.191	1.200	1.448	2.162	Uncharacterized protein
K4AXK6	2.191	1.118	1.501	2.637	Uncharacterized protein
K4D615	2.190	1.007	1.142	1.294	Uncharacterized protein
K4CXU6	2.189	0.886	0.868	1.154	Uncharacterized protein
K4D249	2.189	1.249	1.836	1.659	Uncharacterized protein
K4C036	2.188	1.267	1.558	1.368	Uncharacterized protein
K4BHZ2	2.187	1.136	0.920	1.089	Uncharacterized protein
K4BWD8	2.187	0.909	0.833	1.117	Uncharacterized protein
K4DHL5	2.186	1.202	1.277	1.503	Uncharacterized protein

Accession	Burned	Control	Regular	Limit	Description
Q9XGY1	2.186	0.981	1.354	1.989	Small zinc finger-like protein
K4BSS5	2.186	1.201	1.753	1.671	Uncharacterized protein
K4BK89	2.186	1.237	1.543	1.651	Uncharacterized protein
D7S016	2.185	1.313	1.951	1.633	Glycosyltransferase
K4DBP8	2.185	1.197	1.429	1.252	Uncharacterized protein
K4CD33	2.185	0.966	1.064	1.315	Uncharacterized protein
K4C261	2.185	1.460	1.891	1.902	Serine hydroxymethyltransferase
K4BCD1	2.183	1.118	1.281	1.406	Uncharacterized protein
K4CNZ0	2.183	0.913	1.082	1.293	Uncharacterized protein
K4CIS3	2.181	1.097	1.226	1.450	Uncharacterized protein
K4CPD8	2.181	1.171	1.509	1.817	Uncharacterized protein
K4B7Z3	2.181	1.060	1.131	3.533	Uncharacterized protein
K4C7H7	2.181	1.244	1.871	1.993	Uncharacterized protein
K4CUI0	2.181	1.124	1.852	2.074	Uncharacterized protein
K4BBM6	2.180	0.988	1.135	1.374	Peroxidase
Q5QJB4	2.180	0.767	0.870	1.110	Harpin binding protein 1
K4C131	2.180	1.016	1.373	1.918	Uncharacterized protein
K4BPF0	2.179	1.176	1.507	1.558	Uncharacterized protein
K4BBC3	2.179	1.220	1.189	1.438	Uncharacterized protein
K4BPB4	2.179	1.048	1.350	1.490	Uncharacterized protein
Q152U9	2.177	0.951	1.039	1.128	Multiprotein bridging factor 1a
K4D4B5	2.176	1.173	1.334	1.293	Protein translocase subunit SecA
Q40142	2.176	1.067	1.358	1.590	Cell wall protein
K4BVG9	2.176	1.010	1.081	1.112	Uncharacterized protein
K4BJD6	2.176	1.152	1.134	0.988	Uncharacterized protein
K4CHZ8	2.176	1.130	2.188	2.875	Uncharacterized protein
K4B459	2.175	0.935	1.544	1.656	Uncharacterized protein
K4BXZ3	2.175	1.041	1.021	1.176	Uncharacterized protein
K4CI86	2.173	1.465	1.969	1.898	Protein arginine N-methyltransferase
P17786	2.173	1.628	2.913	3.495	Elongation factor 1-alpha
K4BN48	2.173	1.012	1.241	1.391	Uncharacterized protein
K4BIU7	2.172	1.286	1.515	1.849	Uncharacterized protein
K4C7M3	2.172	1.055	1.482	1.725	Uncharacterized protein
K4BCM5	2.172	0.990	1.084	1.246	Uncharacterized protein
K4D472	2.170	1.021	1.207	1.530	Uncharacterized protein
K4D1F3	2.169	1.254	2.465	1.958	Plasmamembrane intrinsic protein 29
K4B820	2.169	1.264	1.170	1.626	Uncharacterized protein
K4CXR8	2.169	1.392	2.023	2.763	Uncharacterized protein
K4BXC1	2.169	1.034	1.250	1.878	Uncharacterized protein
K4CPW9	2.168	0.903	1.073	1.319	Purple acid phosphatase
K4CV93	2.168	1.266	1.575	1.853	Uncharacterized protein
K4CQG5	2.168	1.254	2.464	1.957	Uncharacterized protein
K4AYH0	2.165	0.913	1.476	2.025	Uncharacterized protein
K4DFH1	2.164	1.210	1.477	1.691	Uncharacterized protein
K4CQ99	2.164	1.038	1.198	1.261	Uncharacterized protein
Q40163	2.164	0.927	1.111	0.891	Photosystem II 10 kDa polypeptide, chloroplastic
K4BUC5	2.164	1.087	1.307	3.650	Uncharacterized protein
K4CDL3	2.164	1.079	1.561	2.632	Aspartate aminotransferase
K4CSE1	2.163	1.241	1.450	1.760	Uncharacterized protein
K4CPN9	2.163	1.239	1.738	2.446	Nucleoside diphosphate kinase
K4BI25	2.162	1.125	1.292	1.307	Uncharacterized protein
K4DHU5	2.162	0.890	0.964	0.993	Uncharacterized protein

Accession	Burned	Control	Regular	Limit	Description
K4BPM8	2.162	0.913	1.487	1.210	Uncharacterized protein
K4AYI7	2.162	0.990	1.250	1.566	Carboxypeptidase
K4BK27	2.162	1.219	1.787	2.263	Uncharacterized protein
K4DEI6	2.162	1.059	1.358	1.820	Uncharacterized protein
K4AZA9	2.161	1.038	1.331	1.989	Uncharacterized protein
K4BC61	2.161	1.317	1.671	1.632	Eukaryotic translation initiation factor 3 subunit M
K4CHK7	2.160	0.968	1.538	1.967	Uncharacterized protein
K4D8F6	2.159	0.995	1.713	2.482	Uncharacterized protein
K4B9Y4	2.158	1.040	1.171	1.316	Uncharacterized protein
K4B8I9	2.158	1.289	1.752	1.639	Uncharacterized protein
K4AXU7	2.157	1.031	1.185	2.027	Uncharacterized protein
K4BQZ9	2.157	1.026	1.089	1.359	Uncharacterized protein
K4CWY6	2.157	1.029	1.379	1.636	Metacaspase
G8Z254	2.155	1.241	1.243	1.099	Hop-interacting protein THI016
K4CK76	2.155	1.289	1.982	3.110	Uncharacterized protein
K4CMM0	2.155	0.994	1.252	4.041	Pectin acetylesterase
K4C2S7	2.154	0.863	1.148	1.641	V-type proton ATPase subunit G
K4AT81	2.150	1.196	2.004	2.291	Non-specific serine/threonine protein kinase
K4B5N9	2.149	1.209	1.406	1.261	Uncharacterized protein
K4BUJ6	2.149	1.165	1.391	1.404	Uncharacterized protein
K4C5S0	2.148	1.157	1.403	1.478	Uncharacterized protein
Q9FV24	2.147	1.269	1.400	1.694	Aldehyde oxidase
K4CLS8	2.147	0.888	1.160	1.499	Cytochrome b-c1 complex subunit 7
K4CUU6	2.146	1.023	1.148	1.238	Peroxidase
K4CBJ8	2.146	0.868	0.600	0.643	Uncharacterized protein
K4B428	2.146	1.255	2.427	1.932	Plasmamembrane intrinsic protein 28
K4BMU9	2.146	0.997	1.087	1.283	Uncharacterized protein
K4D1S4	2.146	0.987	1.186	1.174	Uncharacterized protein
K4CIW8	2.146	1.236	1.738	2.463	Nucleoside diphosphate kinase
K4C633	2.145	1.026	1.233	1.625	Uncharacterized protein
K4C408	2.144	0.873	0.997	1.149	Uncharacterized protein
K4D4D0	2.144	1.102	1.247	1.611	Uncharacterized protein
K4BRP6	2.144	1.141	1.249	1.393	Uncharacterized protein
K4BJE2	2.143	0.930	0.940	1.270	Uncharacterized protein
K4BTC7	2.141	1.274	1.788	1.619	Uncharacterized protein
K4C7T7	2.138	0.921	1.118	1.038	Uncharacterized protein
K4B4E9	2.138	0.957	0.905	0.840	Uncharacterized protein
O22478	2.138	1.221	1.893	1.900	Importin subunit alpha
K4C3V1	2.137	1.320	1.628	1.541	Ribosomal protein L19
K4CN82	2.135	1.013	1.576	1.766	Uncharacterized protein
K4DHC9	2.133	1.139	1.417	1.951	Uncharacterized protein
K4B1X9	2.133	1.072	1.344	1.691	Uncharacterized protein
K4B8F3	2.133	1.154	1.590	1.978	Uncharacterized protein
Q6XNM3	2.132	1.065	1.176	1.173	Non-specific serine/threonine protein kinase
K4BA58	2.132	1.019	1.289	1.267	Uncharacterized protein
K4C288	2.132	0.919	0.848	0.657	Uncharacterized protein
K4D2T3	2.131	1.065	1.301	1.365	Uncharacterized protein
K4BIW5	2.131	1.192	1.495	1.528	Uncharacterized protein
K4CIG7	2.130	0.936	1.044	1.306	Uncharacterized protein
K4BYC0	2.130	1.337	1.766	2.033	Uncharacterized protein
K4BY93	2.129	0.953	1.349	2.061	Alpha-galactosidase

Accession	Burned	Control	Regular	Limit	Description
K4BM62	2.129	1.033	1.563	1.478	Uncharacterized protein
P12670	2.129	0.903	2.390	9.335	Protein NP24
K4CXH1	2.128	1.293	1.137	1.165	Tryptophan synthase
K4BWN2	2.128	1.112	1.355	3.253	Uncharacterized protein
K4C3H8	2.128	1.152	1.605	1.523	Uncharacterized protein
K4D1X7	2.127	0.884	1.101	1.532	Uncharacterized protein
K4CAT1	2.126	1.166	1.459	1.706	Uncharacterized protein
Q2MI63	2.126	1.149	1.453	1.571	50S ribosomal protein L16, chloroplastic
K4BTE6	2.126	1.212	1.611	1.904	Uncharacterized protein
H1AC33	2.126	1.064	1.597	1.604	Beta-D-xylosidase
K4BAY4	2.125	1.122	1.333	1.730	Uncharacterized protein
K4DG27	2.125	1.060	1.347	1.228	Uncharacterized protein
Q8RXB8	2.124	1.065	1.487	4.699	N-hydroxycinnamoyl-CoA:tyramine N-hydroxycinnamoyl transferase THT1-3
K4DGY9	2.123	1.217	2.504	3.059	Sugar-porter family protein 6
K4B1Y6	2.123	0.983	1.119	2.883	Uncharacterized protein
K4BEK5	2.122	0.981	1.469	1.975	Uncharacterized protein
K4B848	2.121	1.222	1.591	1.749	Uncharacterized protein
K4D9Z8	2.121	0.960	1.596	2.045	Uncharacterized protein
K4CC52	2.120	1.119	1.554	2.570	Uncharacterized protein
K4CR56	2.119	1.230	1.262	1.406	Uncharacterized protein
K4B0X2	2.119	1.120	1.388	1.528	Uncharacterized protein
K4CU78	2.119	0.912	0.970	1.013	Photosystem II reaction center Psb28 protein
K4B8A4	2.118	1.207	1.239	1.333	Uncharacterized protein
K4CGD4	2.117	1.230	1.550	1.396	Uncharacterized protein
K4AWQ1	2.114	0.834	0.895	1.281	Uncharacterized protein
K4CXM7	2.114	0.806	0.868	0.901	Uncharacterized protein
K4C2X2	2.112	1.086	1.795	4.528	Uncharacterized protein
K4C8L5	2.112	1.052	0.995	0.966	Uncharacterized protein
K4B0A7	2.111	1.068	1.306	1.843	Uncharacterized protein
K4DBJ1	2.110	1.224	1.831	2.514	Signal peptidase I
K4CFQ7	2.108	1.004	1.188	1.808	Uncharacterized protein
K4BT25	2.107	0.979	1.235	1.997	Uncharacterized protein
K4CAP2	2.106	1.265	1.787	1.870	Structural maintenance of chromosomes protein
K4DBI5	2.105	1.170	1.500	1.400	Uncharacterized protein
K4AVY7	2.104	1.216	1.418	1.533	Uncharacterized protein
K4D2D4	2.103	1.191	1.374	2.085	Uncharacterized protein
K4AVH4	2.102	1.013	1.258	1.587	Uncharacterized protein
K4AVB7	2.102	1.299	1.908	1.997	Uncharacterized protein
K4BHQ8	2.101	1.238	1.667	2.175	Uncharacterized protein
K4DA39	2.100	0.978	0.964	0.891	Uncharacterized protein
K4BJM5	2.098	0.996	1.313	5.776	Uncharacterized protein
K4BDM3	2.098	1.138	1.410	1.320	Uncharacterized protein
K4DDB1	2.098	1.230	1.632	1.716	Uncharacterized protein
K4B3P2	2.097	1.194	1.520	1.716	Uncharacterized protein
K4CBT5	2.097	1.072	1.258	1.264	Uncharacterized protein
K4B9V8	2.096	0.946	1.179	2.340	Uncharacterized protein
Q9FT17	2.094	1.000	1.621	6.082	Lipoxygenase
K4CAB8	2.094	1.173	1.565	1.857	Uncharacterized protein
K4AT92	2.094	1.507	2.001	1.918	AGO4A
K4BMH6	2.093	1.316	1.873	2.151	Coatomer subunit beta'
K4BPV0	2.093	1.022	1.360	1.790	Uncharacterized protein
K4CNY9	2.092	0.898	1.015	1.152	Uncharacterized protein
K4B0S7	2.090	1.056	1.318	1.404	Protein YIPF
K4C4W2	2.089	0.949	1.468	1.324	Uncharacterized protein

Accession	Burned	Control	Regular	Limit	Description
K4CFM0	2.089	1.082	1.490	1.460	Uncharacterized protein
K4DBN6	2.088	1.099	1.230	1.319	Uncharacterized protein
K4AZI2	2.088	1.248	1.922	1.975	Uncharacterized protein
K4DF88	2.088	1.390	2.173	2.439	Coatomer subunit beta'
K4DHR8	2.086	1.020	1.343	1.204	Uncharacterized protein
K4CGZ3	2.086	1.121	1.458	2.628	Uncharacterized protein
K4C7M8	2.085	0.840	0.656	0.767	Uncharacterized protein
K4CUE6	2.084	1.082	1.687	2.044	Uncharacterized protein
K4C7M7	2.083	0.834	0.672	0.778	Uncharacterized protein
K4D5S0	2.083	0.990	1.136	1.912	Uncharacterized protein
K4BS74	2.083	0.932	0.964	1.084	Uncharacterized protein
O81536	2.082	1.073	2.242	7.235	Annexin
K4D358	2.082	0.857	0.999	1.199	Uncharacterized protein
K4B1K6	2.082	1.263	1.661	1.927	Uncharacterized protein
Q9XH50	2.082	1.527	1.300	1.036	1-D-deoxyxylulose 5-phosphate synthase
K4C1T2	2.081	1.488	2.436	2.123	Clathrin heavy chain
K4C3A1	2.081	1.308	1.648	3.121	Uncharacterized protein
K4C6M9	2.079	1.097	1.248	1.716	Uncharacterized protein
K4B6V2	2.079	1.034	1.188	1.406	Uncharacterized protein
K4CAL7	2.079	1.168	1.490	1.676	Uncharacterized protein
K4CIF3	2.079	1.139	1.505	1.873	Uncharacterized protein
K4CXV6	2.079	1.146	1.347	1.355	Uncharacterized protein
K4D919	2.078	1.196	1.586	1.591	Uncharacterized protein
K4B170	2.078	1.000	0.827	0.962	Uncharacterized protein
K4C3F2	2.077	1.032	1.267	1.887	Uncharacterized protein
K4C3B4	2.076	1.200	1.345	1.329	Uncharacterized protein
K4AWQ5	2.074	1.067	1.680	1.855	Dihydrolipoamide acetyltransferase component of pyruvate dehydrogenase complex
K4BTY2	2.074	1.094	1.175	1.276	Uncharacterized protein
K4BXG8	2.071	1.228	1.772	1.647	Uncharacterized protein
K4BJZ7	2.070	1.045	1.143	1.326	Uncharacterized protein
K4CMC3	2.069	1.452	1.060	0.884	Delta-aminolevulinic acid dehydratase
K4CGT2	2.068	1.016	1.526	2.653	Uncharacterized protein
K4AT98	2.066	0.974	1.285	1.849	Cysteine proteinase inhibitor
K4BWD6	2.066	1.145	1.923	1.482	Uncharacterized protein
K4BV44	2.066	1.168	1.611	2.270	Uncharacterized protein
K4B8D8	2.065	0.981	1.754	1.673	Uncharacterized protein
K4CK56	2.065	1.113	1.451	1.926	Uncharacterized protein
K4CHS4	2.064	1.092	1.469	1.810	Uncharacterized protein
K4BT18	2.063	0.994	1.351	1.344	Uncharacterized protein
K4BP39	2.060	0.957	0.936	1.188	Uncharacterized protein
K4BP29	2.056	0.971	1.179	1.461	Alpha-galactosidase
P10967	2.055	1.052	1.310	4.685	1-aminocyclopropane-1-carboxylate oxidase homolog
K4BJT0	2.055	1.109	1.236	2.824	Uncharacterized protein
K4B3K7	2.055	1.286	1.879	2.302	Uncharacterized protein
K4C7I6	2.054	1.164	1.486	2.239	Uncharacterized protein
K4CHE0	2.053	1.158	1.533	1.497	Uncharacterized protein
K4BFH8	2.052	1.150	1.420	1.684	RuvB-like helicase
K4B2Y0	2.052	1.008	1.313	1.327	Uncharacterized protein
K4CRC8	2.051	1.019	1.280	1.433	Uncharacterized protein
K4BKE4	2.051	1.279	1.590	1.632	Uncharacterized protein
K4CR83	2.051	1.187	1.427	1.733	Uncharacterized protein
K4BJT9	2.051	1.063	1.553	2.829	Uncharacterized protein
K4CQ25	2.050	1.037	1.283	2.087	Uncharacterized protein
K4B978	2.050	0.973	1.043	1.521	Clathrin light chain

Accession	Burned	Control	Regular	Limit	Description
K4B286	2.049	1.282	1.449	1.606	Uncharacterized protein
K4B046	2.049	1.166	1.402	1.772	Uncharacterized protein
K4CBD5	2.049	1.092	1.567	2.061	Uncharacterized protein
K4C7Y9	2.048	0.978	1.069	0.982	Uncharacterized protein
K4C472	2.048	1.369	2.124	2.265	Uncharacterized protein
K4CX79	2.048	1.107	1.306	1.226	Uncharacterized protein
K4DBV9	2.047	1.102	1.459	1.677	Uncharacterized protein
K4AXK4	2.046	1.244	1.983	2.752	Uncharacterized protein
K4BLU6	2.046	1.145	1.619	1.772	Uncharacterized protein
K4B785	2.046	1.018	1.193	1.656	Uncharacterized protein
K4CAK9	2.045	1.073	1.261	1.660	Uncharacterized protein
K4CC14	2.044	1.285	1.747	2.301	Uncharacterized protein
K4CB85	2.043	1.199	1.887	3.033	Uncharacterized protein
K4BYQ5	2.042	1.038	1.978	3.283	Uncharacterized protein
K4BNY4	2.041	1.119	1.477	2.200	4-hydroxy-4-methyl-2-oxoglutarate aldolase
K4BK43	2.040	1.086	1.668	1.384	Uncharacterized protein
K4BK26	2.040	1.107	1.449	1.848	Uncharacterized protein
K4C646	2.038	0.895	0.978	1.077	Uncharacterized protein
K4CX56	2.038	0.940	1.163	1.282	Uncharacterized protein
Q6QDC5	2.038	0.921	1.080	1.297	Early light inducible protein
K4BML2	2.038	0.973	0.969	0.945	Uncharacterized protein
K4BEW0	2.036	0.973	1.304	1.478	Uncharacterized protein
K4C7X4	2.036	1.184	1.467	1.579	Uncharacterized protein
K4BS97	2.035	1.314	2.077	1.925	Uncharacterized protein
K4BXK7	2.035	1.061	1.240	1.510	Uncharacterized protein
K4D9E0	2.035	0.944	1.117	1.579	Uncharacterized protein
K4BJ22	2.033	1.456	2.347	2.102	Clathrin heavy chain
K4BQC6	2.032	1.174	1.502	1.481	Calcium-transporting ATPase
K4CHS9	2.031	1.240	1.676	2.080	Uncharacterized protein
K4CPH0	2.030	1.119	1.064	1.367	Uncharacterized protein
K4C2H7	2.030	1.338	1.457	1.145	Uncharacterized protein
K4AWS0	2.029	1.177	1.504	1.649	Uncharacterized protein
K4CTW4	2.028	1.048	1.319	1.935	Uncharacterized protein
K4AZJ6	2.027	1.130	1.457	1.999	Uncharacterized protein
K4CNE9	2.027	1.088	1.602	2.585	Uncharacterized protein
K4CY53	2.025	1.123	1.223	1.405	Uncharacterized protein
K4BIG5	2.024	0.972	1.364	1.734	Uncharacterized protein
K4AYS0	2.024	1.171	1.644	2.401	Uncharacterized protein
K4D2H8	2.023	1.197	1.398	1.618	Uncharacterized protein
K4CMI0	2.022	0.964	1.501	1.200	Uncharacterized protein
K4D1T4	2.022	1.110	1.175	1.129	Uncharacterized protein
K4BAN9	2.021	1.065	1.227	1.648	Uncharacterized protein
K4CFF9	2.021	1.075	1.489	1.948	Uncharacterized protein
K4B7G4	2.020	1.084	1.223	1.447	Uncharacterized protein
K4C4Z6	2.019	1.324	1.882	2.929	Uncharacterized protein
K4C7I7	2.019	1.315	1.826	2.114	Uridine kinase
K4AST1	2.018	1.502	2.300	2.308	Coatomer subunit beta
K4C1Z0	2.018	0.959	0.746	0.789	Uncharacterized protein
K4C5P4	2.014	0.986	1.202	1.541	Uncharacterized protein
K4B6F8	2.014	1.226	1.891	2.279	Uncharacterized protein
K4DBB0	2.013	0.990	1.768	1.501	Uncharacterized protein
K4B2H4	2.011	1.274	1.832	2.147	Uncharacterized protein
K4CAD5	2.011	1.001	1.251	1.817	Uncharacterized protein
O65834	2.011	0.914	1.084	1.334	p69C protein
K4AZF6	2.010	1.095	1.220	1.910	Uncharacterized protein
K4B212	2.009	1.022	1.153	1.720	Uncharacterized protein
K4CX24	2.009	1.025	1.118	1.112	Uncharacterized protein

Accession	Burned	Control	Regular	Limit	Description
K4AYT8	2.008	0.940	0.947	1.257	Nucleoside diphosphate kinase
K4B0V5	2.008	0.959	1.202	3.302	Lipoxygenase
K4BNV4	2.008	0.999	1.423	3.066	Uncharacterized protein
K4C1M1	2.007	1.031	1.310	1.458	Uncharacterized protein
K4CIG6	2.007	0.966	1.067	1.055	Uncharacterized protein
K4BYS9	2.007	1.069	1.327	1.475	Uncharacterized protein
K4D815	2.006	1.242	1.910	2.019	Protein phosphatase methylesterase 1
K4C7I1	2.006	1.305	1.780	2.057	Uncharacterized protein
Q6QLU0	2.006	1.066	1.767	4.308	Protein phosphatase 2C
K4CA69	2.005	1.278	1.694	1.873	Uncharacterized protein
K4D421	2.005	1.179	1.271	1.176	Uncharacterized protein
K4D3B5	2.005	1.234	1.558	1.689	Uncharacterized protein
K4BQ07	2.005	0.796	0.871	1.025	Peptidylprolyl isomerase
K4C935	2.004	0.997	1.093	1.130	Uncharacterized protein
K4BU29	2.003	1.046	1.156	1.205	40S ribosomal protein S21
K4DAG1	2.002	1.067	1.424	1.627	Uncharacterized protein
K4C6Y4	2.002	1.202	1.485	1.642	Serine/threonine-protein phosphatase 2A 55 kDa regulatory subunit B
K4CUU2	2.002	1.143	1.028	0.985	Uncharacterized protein
K4B012	2.002	1.076	1.269	1.345	Uncharacterized protein
K4CWV0	2.002	0.906	2.411	1.428	Uncharacterized protein
K4AY49	2.001	0.983	1.063	0.905	Uncharacterized protein
Q9XEX8	2.000	0.926	1.278	1.256	Remorin 1
K4D794	2.000	1.101	1.192	1.326	Uncharacterized protein
K4BD54	2.000	1.034	2.156	3.942	Peroxidase
K4BPE9	2.000	1.077	1.064	1.136	Uncharacterized protein
K4C875	2.000	1.198	1.563	1.918	Uncharacterized protein
K4AZY6	1.999	1.212	1.666	2.078	Uncharacterized protein
K4BQ70	1.999	1.233	1.679	2.120	Uncharacterized protein
K4ASA5	1.999	1.094	1.339	1.511	Uncharacterized protein
K4BWH9	1.998	1.062	1.304	1.444	Uncharacterized protein
K4B1C7	1.998	1.013	1.456	1.367	Uncharacterized protein
K4DDZ0	1.998	0.958	1.366	1.303	Uncharacterized protein
K4C253	1.998	0.938	1.132	1.494	Uncharacterized protein
K4CPQ4	1.997	1.157	1.216	1.588	Uncharacterized protein
K4C7B1	1.996	1.025	1.053	1.225	Uncharacterized protein
K4CP11	1.995	1.032	1.101	1.178	Uncharacterized protein
K4DHW5	1.994	1.180	1.664	3.722	Uncharacterized protein
K4CPD0	1.993	1.029	1.193	1.440	Uncharacterized protein
K4C7T6	1.993	0.973	1.069	1.073	Uncharacterized protein
K4D5P0	1.993	1.120	1.346	1.307	Uncharacterized protein
K4B0Q7	1.992	1.216	1.476	1.638	Uncharacterized protein
K4BDH9	1.991	1.184	2.059	3.300	Glucose-6-phosphate 1-dehydrogenase
K4BQX5	1.989	1.079	1.350	1.705	Uncharacterized protein
K4C192	1.989	1.197	1.569	1.924	Uncharacterized protein
K4BTV1	1.989	1.193	1.331	1.254	Uncharacterized protein
K4C1Z2	1.988	1.171	1.480	1.153	Uncharacterized protein
K4D2V6	1.988	1.119	1.278	1.731	Uncharacterized protein
K4D2C0	1.987	1.090	1.268	1.594	Uncharacterized protein
K4DG37	1.987	1.313	1.290	1.526	Glycosyltransferase
K4BIC0	1.987	1.168	1.216	1.404	Uncharacterized protein
K4CK63	1.986	1.496	1.433	1.256	Uncharacterized protein
K4CEF1	1.986	1.200	1.773	2.331	Uncharacterized protein
K4BP45	1.985	1.106	1.306	1.490	Uncharacterized protein
K4CEN4	1.985	1.381	1.519	1.546	Uncharacterized protein
K4CVM4	1.984	1.205	1.716	1.797	Uncharacterized protein

Accession	Burned	Control	Regular	Limit	Description
K4CUC7	1.984	1.069	1.254	2.030	Uncharacterized protein
K4C1V6	1.983	1.126	1.705	1.930	Phosphoinositide phospholipase C
K4BEF5	1.983	1.382	1.787	1.608	Uncharacterized protein
K4B7E1	1.983	1.071	1.244	1.076	Uncharacterized protein
K4DFB7	1.982	1.093	1.206	1.329	Uncharacterized protein
K4C5S4	1.982	1.449	2.311	2.061	Clathrin heavy chain
K4CHD8	1.982	1.092	1.256	1.334	Uncharacterized protein
K4BBN7	1.982	1.267	1.897	2.028	Uncharacterized protein
K4CFT1	1.981	1.006	1.060	1.273	Uncharacterized protein
K4CYB7	1.981	0.981	1.431	2.877	Uncharacterized protein
K4CR41	1.981	1.039	0.985	0.820	Uncharacterized protein
K4B3R1	1.980	1.093	1.199	1.482	Uncharacterized protein
K4D7R0	1.980	1.197	1.709	1.193	Uncharacterized protein
K4AYW0	1.980	1.019	1.109	1.070	Uncharacterized protein
K4CHS1	1.979	1.123	1.444	1.236	Uncharacterized protein
K4B3Q4	1.978	1.206	1.598	2.048	Uncharacterized protein
K4CF07	1.977	1.046	1.039	1.363	Uncharacterized protein
P54928	1.977	0.972	0.730	1.156	Inositol monophosphatase 3
K4DBV7	1.976	1.011	1.065	1.369	Uncharacterized protein
K4C9I3	1.976	1.322	1.926	1.785	Uncharacterized protein
K4BAZ6	1.975	0.963	1.039	1.242	Uncharacterized protein
K4BUE1	1.974	1.221	1.695	1.891	Uncharacterized protein
K4D5B1	1.973	1.159	1.464	1.808	Uncharacterized protein
K4BBL8	1.973	0.978	1.574	2.663	Uncharacterized protein
K4B101	1.972	1.133	1.206	1.504	Uncharacterized protein
K4CGX7	1.972	1.043	1.188	1.357	Uncharacterized protein
K4D9A2	1.972	1.176	1.778	1.574	Uncharacterized protein
K4D417	1.971	1.141	1.053	1.116	Uncharacterized protein

Accession	Burned	Control	Regular	Limit	Description
K4CA25	1.970	1.157	1.499	1.750	Uncharacterized protein
K4DHC7	1.969	1.132	1.204	1.502	Uncharacterized protein
K4BVY4	1.969	1.053	1.394	1.459	RING-type E3 ubiquitin transferase
Q2MI43	1.968	1.061	1.373	1.668	30S ribosomal protein S15, chloroplastic
K4D529	1.967	0.857	0.954	0.879	Uncharacterized protein
K4CP14	1.967	1.278	1.659	1.993	Uncharacterized protein
K4AU60	1.967	1.191	1.591	1.905	RING-type E3 ubiquitin transferase
K4BXD4	1.967	1.339	1.814	1.823	Uncharacterized protein
K4C3P2	1.967	1.089	1.987	3.294	Uncharacterized protein
K4DAG8	1.965	0.994	1.253	1.592	Uncharacterized protein
K4CIK9	1.965	1.026	1.113	1.269	Uncharacterized protein
K4B123	1.965	1.106	1.256	1.776	Uncharacterized protein
K4BF00	1.964	1.358	2.554	2.758	Uncharacterized protein
K4CQL3	1.964	1.220	1.384	1.272	Uncharacterized protein
K4C3D5	1.964	0.962	1.723	2.405	Uncharacterized protein
K4B3W7	1.963	0.977	1.221	1.965	Uncharacterized protein
Q10712	1.962	1.061	2.717	10.782	Leucine aminopeptidase 1, chloroplastic
K4B5N6	1.962	1.089	1.689	2.344	Uncharacterized protein
K4DFU2	1.962	1.112	1.754	2.539	Uncharacterized protein
K4AXZ9	1.962	1.199	1.515	1.525	Uncharacterized protein
K4CN65	1.961	1.276	1.400	1.080	Uncharacterized protein
K4CWH0	1.961	1.035	1.106	1.147	Histone deacetylase
K4CP63	1.960	0.994	2.816	9.053	Uncharacterized protein
K4BT15	1.960	1.091	0.995	0.931	Uncharacterized protein
K4B2M5	1.960	1.078	1.074	1.069	Uncharacterized protein
K4D305	1.960	0.968	1.108	1.685	Uncharacterized protein
K4BEC1	1.959	0.984	1.511	2.252	Uncharacterized protein

Accession	Burned	Control	Regular	Limit	Description
K4D7A1	1.958	1.088	1.399	1.837	Transmembrane 9 superfamily member
K4CXQ6	1.958	1.062	1.136	1.527	UBC13-2
K4B110	1.958	1.219	1.679	2.049	Uncharacterized protein
Q9LKW3	1.957	0.869	0.762	0.722	Dehydration-induced protein ERD15
K4BDG0	1.956	1.234	1.705	1.921	Uncharacterized protein
E0Z1D1	1.956	1.057	1.310	2.440	Sucrose synthase
K4D398	1.956	1.315	1.649	1.983	4-hydroxy-tetrahydrodipicolinate synthase
K4DCW6	1.955	0.959	1.105	1.149	Uncharacterized protein
K4CV78	1.955	1.006	1.131	1.449	Uncharacterized protein
K4CPQ3	1.955	0.998	1.142	0.946	Uncharacterized protein
K4BVZ4	1.953	1.174	1.569	2.099	Dolichyl-diphosphooligosaccharide--protein glycosyltransferase subunit 1
K4B364	1.953	0.892	1.235	2.151	Carboxypeptidase
K4CXC4	1.952	1.176	1.465	1.284	Uncharacterized protein
K4B3P3	1.951	1.044	1.264	1.509	Uncharacterized protein
K4AXM9	1.951	1.141	1.358	1.686	Uncharacterized protein
P25306	1.951	0.925	2.546	11.911	Threonine dehydratase biosynthetic, chloroplastic
K4B7W2	1.950	0.974	1.499	2.057	Uncharacterized protein
K4BWY7	1.950	1.092	1.485	1.790	Uncharacterized protein
K4D4X8	1.950	1.122	1.464	1.544	Uncharacterized protein
K4D1M3	1.949	1.233	1.746	2.012	Uncharacterized protein
K4B8V5	1.949	1.297	1.303	1.231	Uncharacterized protein
K4B3W5	1.949	1.396	1.532	1.478	Uncharacterized protein
K4CP20	1.948	1.138	1.137	1.151	Uncharacterized protein
K4B9L7	1.947	0.991	1.441	1.640	Thioredoxin
K4CG69	1.947	1.107	1.288	1.388	Uncharacterized protein
K4BU15	1.946	1.078	1.319	1.208	Uncharacterized protein
K4CDY9	1.946	1.318	1.742	1.534	Uncharacterized protein
K4D2N4	1.946	1.233	1.853	2.805	Glycosyltransferase
K4AYN8	1.944	1.107	1.242	1.481	UMP-CMP kinase
Q8RY07	1.943	1.200	1.441	1.568	Serine/threonine protein kinase pk23
K4BLH0	1.943	0.935	1.127	1.588	Uncharacterized protein
K4DDK9	1.942	1.092	1.131	1.257	Uncharacterized protein
K4CZZ2	1.942	1.046	1.429	1.631	Uncharacterized protein
O65004	1.941	1.273	1.809	1.589	Farnesyl pyrophosphate synthase
K4CN78	1.941	1.200	1.556	1.725	Pyruvate kinase
K4CMJ7	1.941	1.205	1.431	1.841	Eukaryotic translation initiation factor 3 subunit G
K4C2V4	1.940	0.957	0.674	0.674	Uncharacterized protein
K4D2Z4	1.940	1.032	1.075	1.223	Uncharacterized protein
K4AZZ5	1.940	1.351	1.946	1.853	Uncharacterized protein
Q9XEX9	1.938	0.929	1.412	1.543	Remorin 2
K4CWI4	1.938	1.022	0.919	1.112	Uncharacterized protein
K4CBT8	1.938	1.136	1.356	1.791	Uncharacterized protein
K4C2T7	1.938	1.083	1.425	1.983	Dolichyl-diphosphooligosaccharide--protein glycosyltransferase subunit 1
K4AXG8	1.938	1.012	0.886	0.902	Uncharacterized protein
K4BU70	1.938	1.329	1.586	1.389	Uncharacterized protein

Accession	Burned	Control	Regular	Limit	Description
K4CNX5	1.937	1.105	1.254	1.379	Uncharacterized protein
K4CP66	1.935	1.051	1.501	2.633	Uncharacterized protein
K4BAC4	1.935	0.971	1.131	1.361	Uncharacterized protein
K4CIV5	1.934	1.109	1.762	2.512	Uncharacterized protein
K4DFZ2	1.933	1.139	1.352	1.301	Uncharacterized protein
K4BZB1	1.933	1.286	1.842	2.096	Uncharacterized protein
K4ATN9	1.933	1.067	1.171	1.170	Uncharacterized protein
K4CGP6	1.932	1.341	1.798	1.916	Uncharacterized protein
K4BQD6	1.932	1.145	1.611	2.193	S-formylglutathione hydrolase
K4D2Y4	1.931	1.255	1.809	1.957	Uncharacterized protein
K4CB89	1.931	1.001	1.141	1.442	Uncharacterized protein
K4CB52	1.930	1.153	1.226	1.371	Uncharacterized protein
A0A0C5CEC8	1.929	1.412	1.834	1.686	Acetyl-coenzyme A carboxylase carboxyl transferase subunit beta, chloroplastic
K4BLA1	1.929	1.116	1.241	1.929	Uncharacterized protein
K4BCR3	1.928	1.154	1.269	1.203	Uncharacterized protein
K4D808	1.927	0.978	1.026	1.271	Uncharacterized protein
K4AYJ2	1.927	1.239	1.775	1.897	Uncharacterized protein
K4AS92	1.927	1.160	1.468	1.627	Uncharacterized protein
K4BVZ5	1.927	1.077	1.265	1.483	Uncharacterized protein
K4AXI7	1.927	1.046	1.499	1.783	Uncharacterized protein
K4B989	1.926	0.921	0.887	2.995	Uncharacterized protein
K4B1G1	1.926	1.032	1.546	1.918	Uncharacterized protein
K4CYX6	1.926	1.105	1.331	1.438	Uncharacterized protein
K4CB29	1.926	1.134	1.378	1.451	1-acyl-sn-glycerol-3-phosphate acyltransferase
K4CHP6	1.926	1.018	1.349	2.037	Uncharacterized protein
K4D2N0	1.925	1.003	1.282	2.207	Uncharacterized protein
K4BMJ6	1.925	1.030	1.597	1.396	Uncharacterized protein
K4BM02	1.925	1.040	1.067	1.056	Uncharacterized protein
K4CLH6	1.925	1.010	1.332	1.564	Uncharacterized protein
K4BTX3	1.924	1.190	1.280	1.024	Glycosyltransferase
K4C2F7	1.923	0.955	1.087	1.403	Uncharacterized protein
K4B202	1.923	1.222	1.206	1.144	Uncharacterized protein
K4CU14	1.922	1.153	1.748	3.708	Uncharacterized protein
K4B3D9	1.922	1.147	1.207	1.354	Uncharacterized protein
K4C9E3	1.921	1.126	1.532	1.828	Uncharacterized protein
K4B0Q2	1.920	1.079	1.124	1.211	Uncharacterized protein
K4CP92	1.919	1.058	1.434	4.037	Glutathione peroxidase
K4BUA0	1.919	1.130	1.362	1.500	Uncharacterized protein
K4BS23	1.919	1.266	1.340	1.179	Uncharacterized protein
K4DB34	1.917	1.123	1.066	1.408	Uncharacterized protein
K4D5F9	1.917	0.847	0.767	0.928	Uncharacterized protein
K4C7V3	1.917	1.481	2.186	2.030	Uncharacterized protein
K4D645	1.916	1.142	1.597	1.433	Uncharacterized protein
K4D2U2	1.916	1.218	1.647	1.442	Uncharacterized protein
K4BS21	1.916	1.293	1.640	1.946	Uncharacterized protein
K4CAY1	1.915	0.959	1.147	1.575	Uncharacterized protein
K4DAL9	1.915	1.230	1.557	1.597	Uncharacterized protein
K4AZE7	1.915	1.273	1.505	1.527	Uncharacterized protein
K4C069	1.913	1.013	1.164	1.381	Uncharacterized protein
K4DA97	1.913	1.042	1.492	1.776	Uncharacterized protein
K4CPS9	1.911	1.173	1.343	1.400	Glutamine-dependent NAD(+) synthetase
K4ASM9	1.910	1.059	1.107	1.426	Uncharacterized protein
K4B3F4	1.910	1.131	1.695	2.097	Dolichyl-diphosphooligosaccharid

Accession	Burned	Control	Regular	Limit	Description
					e--protein glycosyltransferase 48 kDa subunit
K4BF45	1.910	1.080	0.939	1.537	Uncharacterized protein
K4CMA9	1.910	0.987	1.336	1.765	Uncharacterized protein
K4C8M3	1.909	1.032	1.107	1.084	Uncharacterized protein
K4D451	1.909	1.112	1.480	1.894	Phenylalanine ammonia-lyase
K4CY40	1.908	1.099	1.488	1.903	Uncharacterized protein
K4CVG0	1.908	1.013	1.205	1.360	Uncharacterized protein
K4CQQ1	1.907	0.961	1.144	1.282	Peptidylprolyl isomerase
K4DHP7	1.907	1.003	1.172	1.368	Uncharacterized protein
K4C891	1.907	1.412	1.962	1.831	Uncharacterized protein
K4CV71	1.907	1.026	0.868	0.907	Uncharacterized protein
K4CWI5	1.907	1.029	1.195	1.448	Uncharacterized protein
K4CF12	1.906	1.329	1.491	1.247	Uncharacterized protein
K4BZZ2	1.906	0.992	1.232	1.611	Uncharacterized protein
K4CES2	1.905	1.058	1.247	1.666	Uncharacterized protein
K4CAU9	1.904	1.073	1.378	1.943	Uncharacterized protein
K4C0A1	1.904	1.013	1.163	3.486	4-hydroxyphenylpyruvate dioxygenase
K4C2I6	1.902	1.245	1.604	1.901	Uncharacterized protein
K4B1G3	1.902	1.013	1.260	3.173	Pectin acetylesterase
K4BNL3	1.902	1.330	2.231	2.529	Uncharacterized protein
K4CFU3	1.902	1.162	1.657	1.914	Uncharacterized protein
K4BNV2	1.901	0.878	0.997	1.055	Uncharacterized protein
K4CV87	1.900	1.184	1.354	1.423	Uncharacterized protein
K4CWK9	1.900	1.255	1.348	1.212	Uncharacterized protein
K4AY44	1.899	1.251	1.626	1.537	Uncharacterized protein
K4BAX9	1.899	1.120	1.569	1.601	Aldehyde dehydrogenase
K4DDP2	1.899	1.506	2.256	2.050	DNA gyrase subunit B
K4CGF7	1.898	0.895	0.773	0.673	Uncharacterized protein
K4BM40	1.898	1.181	1.540	1.912	T-complex protein 1 subunit delta
K4BM57	1.897	1.120	1.662	1.692	Uncharacterized protein
K4CQ15	1.897	1.168	1.078	1.247	Uncharacterized protein
K4CKK5	1.897	1.025	1.113	1.351	Uncharacterized protein
Q1T7C2	1.896	1.179	1.273	1.595	Cytochrome P450 710A11
K4DH59	1.896	1.646	1.409	1.451	Uncharacterized protein
K4ASA8	1.895	0.889	1.364	4.595	Uncharacterized protein
B1VK36	1.895	1.103	1.176	5.475	Carbonic anhydrase
K4BMY5	1.895	1.060	1.402	1.986	Uncharacterized protein
K4BUW7	1.894	1.174	1.815	3.399	Annexin
K4BVU1	1.893	0.947	1.373	1.444	Uncharacterized protein
K4BI78	1.893	1.037	1.367	1.529	Uncharacterized protein
K4ASX2	1.892	0.841	0.675	0.886	Uncharacterized protein
K4BWL7	1.890	1.252	1.837	1.885	Uncharacterized protein
K4BN85	1.890	1.084	1.313	1.378	Uncharacterized protein
K4C8L9	1.890	1.001	1.087	1.519	Uncharacterized protein
K4C8P4	1.890	1.226	1.746	2.287	Uncharacterized protein
K4CX95	1.889	1.071	1.462	1.506	Uncharacterized protein
K4B1X0	1.888	1.137	1.239	1.413	Uncharacterized protein
K4DHN2	1.888	1.157	1.556	1.368	Glycosyltransferase
K4C619	1.887	1.163	1.370	1.590	Uncharacterized protein
K4D389	1.886	0.826	0.657	0.865	Uncharacterized protein
K4B283	1.886	0.950	1.070	1.300	Uncharacterized protein
K4CMH3	1.886	1.208	1.530	1.394	Uncharacterized protein
K4BWA7	1.886	1.196	1.485	1.404	Uncharacterized protein
Q2MI78	1.886	1.143	1.064	0.980	30S ribosomal protein S18, chloroplastic
K4ASG7	1.886	0.930	1.031	1.237	Uncharacterized protein

Accession	Burned	Control	Regular	Limit	Description
P93220	1.886	1.051	1.609	2.306	Ethylene-responsive late embryogenesis-like protein
K4CWM3	1.886	1.114	1.489	1.498	Uncharacterized protein
K4BFU1	1.885	1.016	0.840	0.859	Uncharacterized protein
K4CFE7	1.885	1.025	0.833	1.580	Isocitrate lyase
K4BY28	1.884	1.064	1.402	1.524	Uncharacterized protein
K4B7M2	1.884	1.125	1.957	1.778	Uncharacterized protein
K4BPH6	1.884	1.093	1.308	1.545	Uncharacterized protein
K4B1W9	1.884	1.165	1.656	2.344	Uncharacterized protein
K4BDU3	1.883	1.130	0.857	0.770	Uncharacterized protein
K4CKK0	1.883	1.128	1.388	1.508	Uncharacterized protein
K4B838	1.883	1.221	1.555	1.629	Uncharacterized protein
K4D1R2	1.883	1.224	1.458	1.810	Uncharacterized protein
K4B381	1.883	1.414	2.243	2.064	N-acetylglutamate-5-P reductase
K4BF26	1.883	1.072	1.243	1.515	Uncharacterized protein
K4BVN3	1.882	0.939	0.995	1.250	Uncharacterized protein
K4CZD5	1.881	1.030	1.184	1.701	Coatomer subunit delta
K4BXF2	1.880	1.222	1.110	1.086	Methionine aminopeptidase
K4BY27	1.879	1.039	1.109	1.327	Uncharacterized protein
K4B3H0	1.879	0.956	1.147	1.746	Uncharacterized protein
K4BNU8	1.878	1.040	1.140	1.176	Uncharacterized protein
K4B230	1.877	0.859	0.839	0.986	Uncharacterized protein
K4BWN3	1.877	1.486	1.779	1.505	Alpha-amylase
K4DBX2	1.876	0.917	1.117	2.391	Beta-galactosidase
K4AXT4	1.876	1.032	1.271	1.400	Uncharacterized protein
K4BA01	1.874	1.051	1.348	1.506	Uncharacterized protein
K4C1Q1	1.874	1.095	1.413	1.476	Uncharacterized protein
K4BIS6	1.873	0.971	1.490	2.113	Glutamate dehydrogenase
K4BT73	1.871	1.081	1.170	1.397	Uncharacterized protein
K4AZ16	1.871	1.199	1.605	2.159	Uncharacterized protein
K4D9U4	1.871	1.188	1.296	1.399	Uncharacterized protein
K4DF51	1.869	1.090	1.790	2.158	Glycosyltransferase
K4ASJ6	1.869	0.909	2.899	3.047	Peroxidase
K4D9Q3	1.868	0.919	1.244	1.383	Uncharacterized protein
K4CPT1	1.868	1.232	1.336	1.606	Uncharacterized protein
K4B6G9	1.867	0.905	0.933	0.997	Signal recognition particle subunit SRP68
K4DBC9	1.867	1.068	1.687	2.271	Uncharacterized protein
K4CF87	1.866	0.917	1.104	2.087	Uncharacterized protein
K4BP62	1.866	0.947	1.032	1.326	Uncharacterized protein
K4B7K5	1.866	1.104	1.314	1.500	Uncharacterized protein
K4BEU0	1.866	1.200	1.503	1.633	Uncharacterized protein
K4CMY1	1.866	1.076	1.400	1.909	Uncharacterized protein
K4D4V2	1.865	0.965	1.602	2.957	Ferredoxin
K4BWJ3	1.865	0.932	1.031	1.014	Uncharacterized protein
K4B041	1.865	1.045	1.236	1.453	Uncharacterized protein
Q41350	1.864	1.118	1.184	2.040	Osmotin-like protein
K4C7K0	1.863	1.141	1.350	1.427	Uncharacterized protein
K4BVL0	1.863	1.109	1.265	1.589	Uncharacterized protein
G8Z288	1.862	1.117	1.599	1.860	Hop-interacting protein THI141
K4CC35	1.862	1.024	1.262	1.746	Uncharacterized protein
K4D9C3	1.862	1.059	1.093	1.335	Mitochondrial fission 1 protein
K4CVQ4	1.861	1.113	1.564	2.030	Uncharacterized protein
K4CXI0	1.861	1.041	1.239	1.447	Uncharacterized protein
K4CA71	1.861	1.014	1.327	1.900	Uncharacterized protein

Accession	Burned	Control	Regular	Limit	Description
K4AW53	1.859	1.258	1.545	1.473	Uncharacterized protein
K4B8A9	1.859	0.985	1.071	1.425	Uncharacterized protein
K4B0S9	1.858	1.143	1.540	1.936	Mitochondrial Rho GTPase
K4D9I3	1.858	1.135	1.177	1.652	Uncharacterized protein
K4CXP2	1.857	0.898	0.959	0.911	Uncharacterized protein
K4CB87	1.857	1.056	1.522	2.029	Uncharacterized protein
K4CWD3	1.856	1.118	1.191	1.779	Malate dehydrogenase
K4BK19	1.856	1.187	1.521	1.590	Uncharacterized protein
K4CVY0	1.856	1.017	1.597	2.587	Uncharacterized protein
K4BGK0	1.856	1.375	2.053	2.240	Uncharacterized protein
K4D832	1.854	0.954	0.860	0.876	Uncharacterized protein
K4CN87	1.854	1.039	1.113	1.209	Phosphoacetylglucosamine mutase
K4D5Q9	1.853	0.964	1.160	1.103	Uncharacterized protein
K4BJS3	1.853	1.200	1.756	2.252	Uncharacterized protein
K4C291	1.853	1.047	1.372	1.614	Cysteine proteinase inhibitor
K4BMH2	1.852	0.979	0.863	0.820	Uncharacterized protein
K4C7X8	1.852	1.062	1.230	1.539	Uncharacterized protein
K4D0T6	1.851	1.164	1.487	1.618	Adenylyl cyclase-associated protein
K4D486	1.851	1.217	1.643	2.092	Uncharacterized protein
K4CR47	1.849	1.015	1.247	1.418	Peptidyl-prolyl cis-trans isomerase
K4BX90	1.849	1.059	1.227	1.593	Uncharacterized protein
K4D3A7	1.848	1.071	1.229	1.515	Uncharacterized protein
K4BMX2	1.847	1.091	1.166	1.281	Uncharacterized protein
K4AZP0	1.847	0.927	1.440	1.280	Uncharacterized protein
K4CMP8	1.845	1.411	1.950	1.811	Uncharacterized protein
K4B3G7	1.844	1.278	1.665	1.719	Coatomer subunit gamma

Accession	Burned	Control	Regular	Limit	Description
K4BV11	1.844	0.976	1.146	1.545	Uncharacterized protein
Q5NE21	1.844	1.144	1.436	1.701	Carbonic anhydrase
K4B2Z4	1.844	0.942	1.169	1.470	Glycosyltransferase
K4B9T8	1.844	1.100	1.511	1.470	Uncharacterized protein
Q2MIA8	1.843	1.419	1.680	1.274	DNA-directed RNA polymerase subunit beta
K4BF07	1.843	1.163	1.611	1.995	Uncharacterized protein
K4BLG1	1.843	1.195	2.233	1.622	Uncharacterized protein
K4AVE6	1.840	1.179	1.289	1.687	Pyruvate kinase
K4CN26	1.840	1.300	1.944	1.890	Uncharacterized protein
K4BEC3	1.840	1.158	1.707	2.116	Uncharacterized protein
O48616	1.840	1.180	1.704	1.830	MAP kinase kinase
K4CPP9	1.839	1.278	1.374	1.314	Uncharacterized protein
K4B6K2	1.838	0.957	1.144	1.579	Uncharacterized protein
K4DBB6	1.838	1.080	1.283	1.662	Uncharacterized protein
K4C240	1.838	1.148	1.705	1.948	Uncharacterized protein
K4CU16	1.838	1.148	1.730	1.507	Uncharacterized protein
K4CN16	1.838	0.927	1.107	1.812	Uncharacterized protein
K4DFF9	1.837	1.276	1.857	2.605	Uncharacterized protein
K4CF10	1.836	1.055	1.269	1.793	Uncharacterized protein
K4AYR0	1.836	1.058	1.164	1.379	Uncharacterized protein
K4CJI7	1.836	1.201	1.451	1.850	Uncharacterized protein
K4B960	1.836	1.146	1.655	2.331	Uncharacterized protein
K4C2C7	1.835	1.324	2.249	2.494	Uncharacterized protein
K4BCV1	1.835	1.077	0.930	0.856	Uncharacterized protein
K4CXD7	1.835	1.078	1.361	1.547	Uncharacterized protein
K4DC90	1.835	1.069	2.726	11.481	Uncharacterized protein
K4C7X3	1.834	1.084	1.648	3.540	Uncharacterized protein
K4C958	1.834	1.184	1.421	1.453	Uncharacterized protein

Accession	Burned	Control	Regular	Limit	Description
K4CM58	1.834	1.279	1.552	1.862	Eukaryotic translation initiation factor 3 subunit L
K4CUL0	1.834	1.151	1.073	1.194	Uncharacterized protein
K4DDI0	1.834	0.947	1.141	0.851	Uncharacterized protein
K4CQ64	1.833	1.159	1.120	1.332	Uncharacterized protein
K4C926	1.832	1.043	1.323	1.693	Uncharacterized protein
K4B087	1.831	0.975	1.176	1.421	Uncharacterized protein
K4B2Y3	1.831	0.992	1.367	2.091	Uncharacterized protein
K4CB84	1.830	1.192	1.401	2.429	Uncharacterized protein
K4DF81	1.829	1.087	1.504	2.261	Uncharacterized protein
K4CLG8	1.829	1.028	1.233	1.401	Uncharacterized protein
P38546	1.828	1.406	2.465	3.718	GTP-binding nuclear protein Ran1
K4CWN7	1.828	0.848	0.700	0.663	Uncharacterized protein
K4CBG0	1.828	1.049	1.490	2.734	Uncharacterized protein
K4C239	1.827	1.147	1.707	1.947	Uncharacterized protein
K4B298	1.826	1.107	1.560	1.867	Uncharacterized protein
K4BYN8	1.825	1.051	1.357	1.669	Uncharacterized protein
K4C6W7	1.824	0.922	1.111	1.811	Uncharacterized protein
K4AYP6	1.824	1.064	1.468	1.822	Uncharacterized protein
E7EC27	1.824	1.240	2.524	1.948	Aquaporin
K4D0B9	1.823	1.126	1.257	1.442	Uncharacterized protein
K4B280	1.822	1.038	1.206	1.809	Uncharacterized protein
K4C2B5	1.821	1.130	1.442	2.847	Uncharacterized protein
K4BJV3	1.820	1.308	1.474	1.425	Uncharacterized protein
K4CI11	1.819	0.925	1.114	1.801	Uncharacterized protein
K4CRJ2	1.819	1.166	2.253	3.576	Uncharacterized protein
K4D619	1.819	1.368	1.776	1.923	Uncharacterized protein
Q9STA8	1.818	1.141	1.666	4.318	Hexose transporter
K4D1F8	1.817	1.413	1.380	1.393	Methyltransferase
Q38JD4	1.817	0.908	1.093	1.508	Temperature-induced lipocalin
K4BC78	1.817	1.117	1.371	1.206	Uncharacterized protein
K4C2L9	1.817	1.237	1.248	1.164	Uncharacterized protein
K4B1G9	1.817	1.399	1.868	1.887	Uncharacterized protein
K4D293	1.816	0.857	1.142	1.461	Uncharacterized protein
K4BB81	1.815	1.189	0.928	0.944	Uncharacterized protein
K4CN84	1.814	1.079	1.209	1.271	Uncharacterized protein
K4CH93	1.814	0.906	0.800	1.042	Uncharacterized protein
K4D4Y8	1.813	1.213	1.145	1.095	Uncharacterized protein
K4B3E9	1.812	1.041	1.184	1.376	Uncharacterized protein
K4C3B7	1.811	0.851	1.181	1.735	Uncharacterized protein
K4DC52	1.810	1.441	1.911	1.329	Uncharacterized protein
K4AW81	1.810	1.227	1.587	1.868	Uncharacterized protein
K4BTI3	1.809	1.371	1.173	1.129	Uncharacterized protein
K4AZT2	1.809	0.888	1.455	1.345	Uncharacterized protein
K4BV98	1.808	1.045	1.127	1.115	Uncharacterized protein
K4C7X1	1.806	0.932	1.033	1.873	Uncharacterized protein
Q40159	1.806	0.986	1.879	2.824	Late embryogenesis (Lea)-like protein
K4CBX5	1.806	0.911	1.142	1.419	Purple acid phosphatase
K4AZ93	1.805	0.807	1.011	1.213	Uncharacterized protein
K4BK60	1.804	1.253	1.319	1.197	Uncharacterized protein
K4C2M1	1.804	1.066	1.054	1.644	Uncharacterized protein
K4CKQ1	1.804	1.002	0.973	1.192	Uncharacterized protein
K4ATR9	1.803	1.002	1.207	1.699	Uncharacterized protein
K4BWU3	1.803	1.174	1.291	1.354	Uncharacterized protein
K4B1V5	1.803	1.084	1.308	1.829	40S ribosomal protein S12
K4D2K2	1.802	1.013	1.429	1.598	Uncharacterized protein

Accession	Burned	Control	Regular	Limit	Description
K4BIZ4	1.802	0.933	0.887	1.166	Alpha-amylase
K4AUB9	1.802	1.054	1.111	1.083	Uncharacterized protein
K4BJE4	1.801	1.049	1.531	2.715	Cysteine proteinase inhibitor
K4BKW0	1.801	1.001	1.165	1.331	Uncharacterized protein
K4C2J8	1.801	1.198	1.406	2.377	Uncharacterized protein
K4CJW3	1.800	1.023	1.350	4.049	Lipoxygenase
K4AT25	1.800	0.992	1.131	1.358	Uncharacterized protein
K4BFF1	1.799	1.058	1.278	1.587	Uncharacterized protein
K4D9C1	1.799	1.062	1.184	1.366	Uncharacterized protein
K4B9T4	1.799	0.950	1.165	2.000	Lactoylglutathione lyase
K4ATR8	1.798	1.107	1.718	3.099	Uncharacterized protein
K4AY68	1.797	1.344	1.775	1.689	Clustered mitochondria protein homolog
K4BME2	1.797	1.009	1.224	1.424	Uncharacterized protein
K4DAX8	1.796	1.056	1.439	0.847	Uncharacterized protein
K4B8A8	1.796	1.014	1.250	1.090	Uncharacterized protein
K4BJU1	1.796	1.471	4.200	8.442	Uncharacterized protein
K4BKR9	1.796	0.978	1.024	1.179	Uncharacterized protein
K4ASM0	1.796	1.105	1.383	0.933	Lipoxygenase
K4C760	1.794	1.148	1.375	1.407	Uncharacterized protein
K4CNU3	1.794	0.949	1.434	4.394	Amine oxidase
K4BLT8	1.793	1.155	1.876	2.448	Uncharacterized protein
K4D7R1	1.793	1.170	1.592	2.335	Uncharacterized protein
K4DBM4	1.792	0.991	1.051	1.378	Uncharacterized protein
K4C6Z0	1.792	1.111	1.817	2.424	Transmembrane 9 superfamily member
K4DFQ7	1.792	0.960	1.008	1.080	Uncharacterized protein
K4ASC0	1.792	1.259	1.454	1.269	Lysine--tRNA ligase
K4BD88	1.792	1.158	1.267	1.233	Uncharacterized protein
K4DFK7	1.791	1.216	1.613	1.893	Uncharacterized protein
K4C9K5	1.791	0.863	0.823	1.000	Uncharacterized protein
K4ATE8	1.790	1.222	1.483	1.786	Ribosomal protein
K4D3Q4	1.790	0.935	1.087	1.154	Uncharacterized protein
K4CAM0	1.789	0.924	0.818	0.992	Uncharacterized protein
K4DAA0	1.789	1.035	1.182	1.676	Uncharacterized protein
K4BMI4	1.789	1.439	1.997	1.890	Uncharacterized protein
Q2MIB4	1.789	0.987	0.774	0.866	ATP synthase subunit b, chloroplastic
K4CHE1	1.789	1.023	1.539	1.983	Uncharacterized protein
K4B0U7	1.788	1.076	1.403	2.361	Uncharacterized protein
K4BX96	1.788	1.255	1.694	1.969	Uncharacterized protein
K4AW91	1.787	1.237	1.494	2.693	Uncharacterized protein
K4CFS1	1.787	1.105	1.784	3.793	Uncharacterized protein
K4C467	1.786	0.967	1.074	1.823	Uncharacterized protein
K4BB90	1.786	1.205	1.484	1.737	Uncharacterized protein
K4BN88	1.786	0.990	1.214	1.821	alpha-1,2-Mannosidase
K4D4S7	1.785	1.195	1.406	2.380	Uncharacterized protein
K4CMI1	1.784	0.983	1.600	1.296	Uncharacterized protein
K4CRC1	1.783	1.174	1.509	1.912	Uncharacterized protein
K4DC84	1.783	1.171	1.438	1.453	Uncharacterized protein
K4CZC1	1.782	1.091	1.349	1.711	Uncharacterized protein
K4CPC9	1.782	1.268	1.750	1.812	Beta-adaptin-like protein
K4ASK1	1.782	1.230	1.782	1.855	Uncharacterized protein
K4DAC6	1.782	1.657	2.917	3.304	Elongation factor 1-alpha
K4C500	1.781	1.085	1.633	2.634	Uncharacterized protein
K4BT72	1.781	0.907	1.090	1.322	Uncharacterized protein
K4D3V4	1.781	1.095	1.723	4.967	Uncharacterized protein
K4CEE9	1.781	1.314	2.127	1.964	Uncharacterized protein
K4C708	1.781	0.976	1.255	1.055	Uncharacterized protein
K4DAV6	1.781	1.149	1.163	1.140	Uncharacterized protein

Accession	Burned	Control	Regular	Limit	Description
K4B0J0	1.781	1.108	1.473	1.724	Uncharacterized protein
K4CSX7	1.780	1.171	1.355	1.755	Uncharacterized protein
K4DEL2	1.780	0.942	0.898	1.092	Uncharacterized protein
K4B088	1.780	0.995	1.073	1.520	Uncharacterized protein
K4B319	1.780	1.110	1.911	2.048	Uncharacterized protein
K4D2H0	1.780	1.182	1.523	1.490	Uncharacterized protein
K4CMI6	1.780	0.985	1.889	1.943	Uncharacterized protein
K4AXB1	1.779	1.177	1.571	1.641	Serine/threonine-protein phosphatase
K4D5D7	1.779	1.004	1.321	1.916	Uncharacterized protein
K4D1R6	1.778	1.054	1.300	1.435	Uncharacterized protein
B2Z9Y5	1.778	1.048	1.421	1.748	Gamma-glutamylhydrolase 2
K4B341	1.778	1.062	1.425	1.652	Uncharacterized protein
K4CA47	1.778	0.950	1.075	1.290	Uncharacterized protein
K4B769	1.777	1.011	1.106	1.572	Uncharacterized protein
K4CM55	1.777	1.158	1.485	2.141	Uncharacterized protein
K4CKX0	1.777	0.957	1.024	1.134	Uncharacterized protein
K4C3Y3	1.775	1.122	1.327	1.734	Uncharacterized protein
K4BUN4	1.775	1.020	1.118	1.545	Uncharacterized protein
K4DH10	1.775	1.005	1.596	3.129	Uncharacterized protein
K4CZJ5	1.774	0.977	1.079	1.432	Uncharacterized protein
K4B2X5	1.774	1.145	1.388	1.353	Uncharacterized protein
P36181	1.773	1.377	1.944	2.714	Heat shock cognate protein 80
K4B171	1.773	1.062	1.371	1.789	Uncharacterized protein
K4D4T0	1.772	1.115	1.410	1.994	Uncharacterized protein
K4D1V6	1.772	1.008	2.696	6.331	Uncharacterized protein
K4B2A7	1.772	0.992	1.354	3.628	Uncharacterized protein
K4BF94	1.772	1.195	1.290	1.281	Uncharacterized protein

Accession	Burned	Control	Regular	Limit	Description
P05116	1.771	1.073	2.046	3.655	1-aminocyclopropane-1-carboxylate oxidase 1
K4BJ21	1.770	0.990	0.824	0.685	Uncharacterized protein
K4CXG8	1.770	0.875	0.728	0.658	Uncharacterized protein
K4C745	1.768	1.336	2.024	2.073	Uncharacterized protein
K4BMT0	1.767	1.071	1.066	1.297	Uncharacterized protein
E2FYC4	1.767	1.013	1.524	1.644	LysM receptor-like kinase
K4AXV8	1.766	1.219	1.643	2.546	Uncharacterized protein
K4CFM8	1.766	1.004	1.110	1.183	Uncharacterized protein
K4BV83	1.766	1.090	1.055	0.719	Uncharacterized protein
K4BKT5	1.765	0.953	0.978	1.449	Uncharacterized protein
K4C2T5	1.764	1.283	1.864	1.981	Uncharacterized protein
K4C6I9	1.763	1.045	1.706	2.063	Uncharacterized protein
K4CNL0	1.763	1.125	1.651	2.570	Uncharacterized protein
K4BJV9	1.763	0.917	0.876	1.060	Nucleoside diphosphate kinase
K4D202	1.762	1.056	1.566	4.364	Uncharacterized protein
K4CWJ2	1.761	1.153	1.749	1.998	Uncharacterized protein
K4BP30	1.761	1.232	1.826	2.597	Pyruvate kinase
K4CQY0	1.761	1.031	1.363	1.433	Uncharacterized protein
K4BML3	1.760	0.868	1.106	1.225	Uncharacterized protein
K4B8R4	1.760	1.124	1.509	1.523	Uncharacterized protein
K4D613	1.760	1.118	1.518	1.607	Mitochondrial pyruvate carrier
K4BVA3	1.757	1.132	1.262	1.753	Uncharacterized protein
K4DDL2	1.757	0.904	1.086	1.585	Uncharacterized protein
K4CQ62	1.757	1.076	1.119	1.912	Uncharacterized protein
K4C8R8	1.757	0.918	0.884	1.067	Nucleoside diphosphate kinase
K4BDT2	1.756	1.047	1.451	1.634	Protoporphyrinogen oxidase

Accession	Burned	Control	Regular	Limit	Description
K4C4P0	1.756	1.076	1.356	1.498	Autophagy-related protein 3
D1MAF2	1.755	1.186	1.565	1.721	Exportin-1
K4C726	1.755	0.913	0.968	1.036	Uncharacterized protein
K4CAM3	1.755	0.978	1.227	1.053	Uncharacterized protein
K4B7E6	1.754	1.191	1.548	1.423	Uncharacterized protein
K4BWV6	1.754	1.219	1.474	1.825	Uncharacterized protein
K4BE26	1.754	1.088	1.267	1.271	Uncharacterized protein
K4D938	1.754	1.170	1.398	1.671	Signal recognition particle subunit SRP72
K4BDB7	1.754	0.973	1.041	1.207	Uncharacterized protein
Q6J1L7	1.754	1.204	1.406	1.549	GDP-mannose pyrophosphorylase
K4CU43	1.754	0.975	1.212	1.056	Uncharacterized protein
K4CJR2	1.754	1.071	1.827	2.122	Uncharacterized protein
K4CGH0	1.753	0.936	1.231	1.930	Uncharacterized protein
K4BAA5	1.753	1.040	1.235	1.222	Uncharacterized protein
K4C245	1.753	1.281	1.774	1.831	Uncharacterized protein
K4D9T1	1.752	1.092	1.788	2.129	Uncharacterized protein
K4B3R8	1.752	1.021	0.727	0.965	Uncharacterized protein
K4CZX0	1.752	1.226	1.489	1.439	Uncharacterized protein
K4BQC3	1.752	1.082	1.152	1.479	Uncharacterized protein
K4C8F8	1.751	1.373	1.954	2.747	Uncharacterized protein
K4DD79	1.751	0.940	1.286	1.391	Uncharacterized protein
K4BLV2	1.751	1.271	1.584	2.318	Uncharacterized protein
K4CTF8	1.750	0.995	1.250	1.619	Peptidylprolyl isomerase
K4CX39	1.750	0.861	1.028	0.759	Uncharacterized protein
K4BVQ3	1.750	1.003	1.265	2.012	Uncharacterized protein
K4BLZ4	1.748	1.610	1.632	1.252	Uncharacterized protein
K4CEW0	1.748	1.341	1.585	1.690	Glucose-6-phosphate 1-dehydrogenase
K4BME6	1.748	1.286	1.146	1.385	ADP,ATP carrier protein
K4CJ92	1.747	0.913	1.060	1.269	Uncharacterized protein
Q6UJX4	1.747	1.388	1.958	2.741	Molecular chaperone Hsp90-1
K4CEC3	1.747	0.891	0.948	1.041	Uncharacterized protein
K4ASJ5	1.746	0.920	2.383	3.156	Peroxidase
K4CRS5	1.746	0.997	1.553	1.813	Uncharacterized protein
K4BVK2	1.745	1.077	1.246	1.996	Uncharacterized protein
K4CA08	1.744	0.846	0.926	1.002	Uncharacterized protein
K4D4I1	1.743	1.193	1.555	1.931	Uncharacterized protein
K4DA61	1.741	1.077	1.619	2.676	Uncharacterized protein
K4CR42	1.741	1.078	1.277	1.613	Uncharacterized protein
K4B2T0	1.741	0.991	1.053	1.478	Uncharacterized protein
Q5K2N1	1.741	1.182	1.382	1.289	Steroid 5-alpha-reductase DET2
K4BPX0	1.740	1.065	1.248	1.796	Uncharacterized protein
K4CGD5	1.740	1.085	0.952	0.811	Uncharacterized protein
K4BVY3	1.740	0.909	0.952	1.149	Uncharacterized protein
K4BIB5	1.740	1.068	1.266	1.770	Uncharacterized protein
K4BVU3	1.739	0.901	1.103	1.273	Uncharacterized protein
E5L4Q6	1.739	1.149	1.299	1.419	ABA aldehyde oxidase
K4CN90	1.738	1.065	1.332	1.522	UMP-CMP kinase
K4D621	1.736	1.140	1.448	1.717	Uncharacterized protein
K4AXC1	1.736	1.066	1.269	1.228	Uncharacterized protein
K4CUC1	1.736	0.966	1.344	3.256	Uncharacterized protein
K4BLV3	1.735	1.272	1.600	2.309	Uncharacterized protein
K4BDZ9	1.735	1.028	1.088	1.160	Uncharacterized protein
K4AX07	1.735	1.197	1.459	1.644	Uncharacterized protein
K4BDL4	1.734	1.137	1.517	2.033	Uncharacterized protein
K4CRV3	1.734	1.240	1.872	1.874	Uncharacterized protein

Accession	Burned	Control	Regular	Limit	Description
K4D4Q2	1.734	0.963	1.001	0.970	Uncharacterized protein
K4DHY6	1.734	0.794	0.976	0.689	Uncharacterized protein
K4C5K3	1.734	1.243	1.321	1.517	Uncharacterized protein
K4AYE2	1.733	0.838	0.772	0.736	Uncharacterized protein
K4CNU9	1.733	1.002	1.056	1.099	Uncharacterized protein
K4BCT9	1.732	1.222	1.402	1.746	Uncharacterized protein
K4BJB2	1.732	1.092	1.390	1.530	NADH dehydrogenase [ubiquinone] 1 alpha subcomplex subunit 12
K4D515	1.731	1.350	1.437	1.410	Uncharacterized protein
K4BQ58	1.731	0.965	1.171	1.595	Uncharacterized protein
K4B576	1.730	1.113	1.306	1.586	Coatomer subunit epsilon
K4CND7	1.730	1.181	1.731	2.012	Uncharacterized protein
K4B344	1.730	1.193	1.646	1.943	Uncharacterized protein
K4D3L7	1.729	1.261	1.436	1.505	Uncharacterized protein
K4C757	1.729	1.013	1.196	1.892	alpha-1,2-Mannosidase
K4BJW8	1.729	1.305	1.467	1.235	Uncharacterized protein
K4CD10	1.728	0.893	1.174	1.041	Uncharacterized protein
K4CSM2	1.728	1.237	1.379	1.368	Uncharacterized protein
K4BLU9	1.728	1.197	1.963	2.001	Uncharacterized protein
K4ATT0	1.727	1.066	1.130	1.368	Uncharacterized protein
K4BT90	1.727	1.206	1.547	1.612	Terpene cyclase/mutase family member
K4BLX8	1.727	1.108	1.125	1.497	Uncharacterized protein
K4D4B9	1.726	1.002	1.336	1.440	Uncharacterized protein
K4BJP3	1.725	1.308	1.856	1.587	Uncharacterized protein
K4CVI0	1.725	0.813	0.884	0.855	Uncharacterized protein
K4CCJ2	1.725	1.316	1.991	2.649	Plasma membrane ATPase
K4BMU5	1.723	0.903	1.485	1.668	PRA1 family protein
K4BV52	1.722	1.032	1.685	1.601	Allene oxide synthase 1, chloroplastic
K4DAV5	1.722	1.005	1.336	1.133	Uncharacterized protein
K4BRW6	1.722	0.978	0.983	0.981	Uncharacterized protein
K4D348	1.722	1.185	1.595	1.774	Uncharacterized protein
K4C952	1.721	1.412	1.794	1.975	Lysine--tRNA ligase
K4CPE0	1.721	1.096	1.589	1.901	Uncharacterized protein
K4CC07	1.720	1.219	1.535	1.600	Uncharacterized protein
K4C8Q1	1.720	1.356	1.899	1.828	Uncharacterized protein
K4D5G7	1.720	1.168	1.181	1.229	Uncharacterized protein
K4B3A4	1.719	1.077	1.100	1.118	Uncharacterized protein
Q2MIA9	1.719	1.432	1.602	1.471	DNA-directed RNA polymerase subunit beta'
K4BJY9	1.719	1.226	1.695	1.524	Uncharacterized protein
K4C9N4	1.719	1.014	1.131	1.611	Uncharacterized protein
K4AZ18	1.719	0.972	1.180	1.363	Uncharacterized protein
K4B1M7	1.718	1.503	2.391	2.443	Uncharacterized protein
K4AWA0	1.718	1.096	1.621	2.830	Uncharacterized protein
K4C8V0	1.718	1.313	1.688	1.481	AGO1A
K4C0W6	1.717	1.176	1.716	2.436	Uncharacterized protein
K4CAS6	1.716	1.036	1.190	1.253	Uncharacterized protein
K4CUX6	1.716	1.268	1.821	2.136	Elongation factor Tu
K4CPP0	1.715	1.087	1.279	2.846	Uncharacterized protein
K4CB99	1.715	0.891	1.581	1.807	Uncharacterized protein
K4AZG7	1.715	0.894	1.381	3.667	Uncharacterized protein
K4D5E7	1.714	1.322	1.621	1.999	Methylenetetrahydrofolate reductase
K4CGY4	1.714	1.012	1.261	1.542	Uncharacterized protein
K4AZ10	1.714	1.215	1.429	1.823	Elongation factor G, mitochondrial
K4CX51	1.713	0.914	0.835	0.775	Uncharacterized protein

Accession	Burned	Control	Regular	Limit	Description
K4CWH3	1.713	1.143	1.717	3.650	Uncharacterized protein
P26300	1.713	1.029	1.110	1.787	Enolase
K4AV84	1.713	1.181	1.499	1.539	Serine/threonine-protein phosphatase
K4BGM2	1.712	1.550	1.416	1.029	Uncharacterized protein
K4BX61	1.711	1.085	1.229	1.476	Uncharacterized protein
K4BI74	1.711	1.183	1.234	1.472	Uncharacterized protein
K4B612	1.711	1.098	1.238	1.240	Uncharacterized protein
K4BKU8	1.711	1.230	1.534	1.672	Uncharacterized protein
K4D5C3	1.711	1.292	1.015	0.987	Uncharacterized protein
K4AZ59	1.710	1.265	1.593	1.977	3-phosphoshikimate 1-carboxyvinyltransferase
K4BCN5	1.709	1.262	1.613	1.877	Uncharacterized protein
K4CB23	1.709	1.490	1.106	0.832	Uncharacterized protein
K4BVK0	1.709	1.087	1.124	1.223	Uncharacterized protein
K4BE74	1.708	0.985	0.942	1.187	Clathrin light chain
K4BJ06	1.708	1.357	1.918	2.252	Uncharacterized protein
K4BDP2	1.708	1.238	2.234	2.746	Phosphorus transporter
K4BJW4	1.707	1.168	1.926	3.418	Glyceraldehyde-3-phosphate dehydrogenase
K4DH83	1.707	0.975	0.795	0.671	Uncharacterized protein
O04897	1.707	0.947	1.461	2.780	Fructokinase
K4CWK8	1.706	0.952	1.306	1.439	Uncharacterized protein
K4CSI5	1.706	0.973	1.189	1.480	Uncharacterized protein
K4CUF4	1.706	0.778	0.674	0.724	Uncharacterized protein
K4AZG6	1.705	0.894	1.423	3.833	Uncharacterized protein
K4C627	1.705	1.061	1.181	1.257	Isopropylmalate synthase
K4AXC0	1.704	1.092	1.479	1.584	Citrate synthase
K4CXV5	1.702	1.095	1.299	1.797	Uncharacterized protein
K4BBF4	1.701	0.941	0.815	0.674	Uncharacterized protein
K4BVK8	1.701	1.035	0.990	1.753	Cytokinin riboside 5'-monophosphate phosphoribohydrolase
K4B2A4	1.700	1.215	1.440	1.572	Uncharacterized protein
K4CLJ5	1.700	1.200	1.381	1.480	Uncharacterized protein
P21568	1.700	1.226	2.207	3.736	Peptidyl-prolyl cis-trans isomerase
K4DBW0	1.699	1.173	1.512	1.907	Uncharacterized protein
K4BVC3	1.699	1.019	1.176	1.603	Uncharacterized protein
K4D5D0	1.699	1.214	1.519	1.507	Uncharacterized protein
K4BBJ0	1.699	0.999	1.262	1.501	Uncharacterized protein
K4BTY6	1.697	1.226	1.270	1.992	Phospho-2-dehydro-3-deoxyheptonate aldolase
P38415	1.697	1.084	1.379	3.508	Linoleate 9S-lipoxygenase A
K4C973	1.697	1.487	1.850	1.582	Uncharacterized protein
K4DCV3	1.697	0.933	1.030	1.611	Malate dehydrogenase
K4AZ08	1.696	0.964	1.096	1.160	Uncharacterized protein
K4BA13	1.694	1.073	1.411	1.936	Uncharacterized protein
K4BU61	1.694	0.994	1.154	1.297	Uncharacterized protein
A8DUB0	1.694	1.120	1.617	2.271	Glutathione S-transferase-like protein
K4BCZ0	1.693	1.049	1.092	1.204	Xyloglucan endotransglucosylase/hydrolase
K4DB11	1.693	1.079	1.595	2.106	Uncharacterized protein
K4B692	1.693	1.071	1.504	1.641	Uncharacterized protein
K4CEV0	1.693	0.865	1.210	1.135	Uncharacterized protein
K4BM50	1.692	1.081	1.204	1.378	Uncharacterized protein
K4CM99	1.691	1.132	1.502	3.324	Uncharacterized protein
K4CNR1	1.691	1.094	1.115	1.262	Uncharacterized protein
K4BNP4	1.691	1.001	1.251	1.538	Uncharacterized protein

Accession	Burned	Control	Regular	Limit	Description
K4CB27	1.689	1.073	1.194	1.259	Uncharacterized protein
K4BVV8	1.689	0.924	0.899	0.973	Uncharacterized protein
K4BCY8	1.689	1.128	1.347	1.433	Uncharacterized protein
K4CZ51	1.688	1.029	1.237	1.475	Uncharacterized protein
Q6IV07	1.688	1.074	1.562	2.742	UDP-glucose:protein transglucosylase-like protein SlUPTG1
K4B2Z8	1.687	1.167	1.799	2.943	Glycosyltransferase
K4BMV8	1.687	1.147	1.577	1.868	Protein ROOT HAIR DEFECTIVE 3 homolog
K4B445	1.686	1.506	1.354	1.080	Methyltransferase
K4B1P8	1.686	0.924	1.238	1.826	Uncharacterized protein
K4BAK2	1.685	1.120	1.552	1.537	Phospholipase D
Q5UNS2	1.684	1.082	2.278	3.367	Arginase 1
K4AWR0	1.683	1.130	1.265	1.077	Uncharacterized protein
K4DAZ4	1.683	1.263	1.604	1.993	Uncharacterized protein
K4DAV2	1.683	0.878	1.062	1.360	ATP synthase subunit d, mitochondrial
K4D343	1.682	0.979	1.190	2.327	Uncharacterized protein
K4BXK3	1.682	1.147	1.293	1.356	Uncharacterized protein
K4DHU7	1.682	1.249	1.710	1.807	Uncharacterized protein
K4CY98	1.681	1.123	1.254	1.476	Uncharacterized protein
K4CFW6	1.679	1.756	1.569	0.851	Uncharacterized protein
K4CNT2	1.679	0.907	0.573	0.603	Uncharacterized protein
K4CQ21	1.679	1.093	1.665	2.024	Uncharacterized protein
K4BB66	1.679	1.103	1.529	1.544	Uncharacterized protein
K4B3Y8	1.678	1.137	2.247	1.978	Uncharacterized protein
K4CII8	1.678	1.245	1.021	1.186	Uncharacterized protein
K4CBY0	1.678	1.147	1.295	1.695	Uncharacterized protein
K4B1D4	1.678	1.267	1.862	2.032	Uncharacterized protein
K4D0H2	1.677	0.984	1.164	3.961	Uncharacterized protein
K4D2A4	1.677	1.137	1.315	1.620	Uncharacterized protein
P43282	1.677	1.396	1.468	1.328	S-adenosylmethionine synthase 3
K4B893	1.677	1.043	1.241	1.375	Uncharacterized protein
K4CC89	1.676	1.145	1.500	2.021	Uncharacterized protein
K4C8H3	1.676	0.969	1.916	5.237	Uncharacterized protein
K4CB74	1.676	1.341	1.042	0.834	Uncharacterized protein
K4D5N9	1.675	1.241	1.572	1.254	Uncharacterized protein
K4DHY7	1.675	0.964	1.143	1.567	Uncharacterized protein
K4C8R4	1.675	1.172	1.798	2.938	Glyceraldehyde-3-phosphate dehydrogenase
Q9LWA3	1.674	0.887	1.317	1.713	Subtilisin-like protease
K4BPJ1	1.674	1.074	1.594	2.145	Uncharacterized protein
K4D633	1.674	1.044	1.024	0.907	Uncharacterized protein
K4CHJ1	1.674	0.791	1.045	1.253	Uncharacterized protein
K4BBS8	1.674	1.109	1.583	1.992	Uncharacterized protein
K4BKZ4	1.673	1.171	1.636	1.513	Uncharacterized protein
K4BEE2	1.671	0.929	1.236	1.885	Uncharacterized protein
K4DC48	1.671	0.815	0.858	0.855	Uncharacterized protein
K4B7I2	1.671	0.893	1.107	1.341	Uncharacterized protein
K4CLE4	1.669	0.978	1.265	1.607	Uncharacterized protein
K4BDZ2	1.669	1.045	1.166	1.457	Uncharacterized protein
K4B166	1.669	0.998	1.461	3.284	Uncharacterized protein
K4BDC1	1.669	0.972	1.052	3.137	Uncharacterized protein
K4B7R9	1.669	0.978	1.181	1.805	Uncharacterized protein
K4CQ83	1.669	1.160	1.516	1.409	Uncharacterized protein
K4BN86	1.669	1.537	1.299	1.552	Uncharacterized protein
K4BKF6	1.669	0.851	1.168	1.764	Aldose 1-epimerase
P05119	1.669	1.203	5.413	10.369	Wound-induced proteinase inhibitor 2

Accession	Burned	Control	Regular	Limit	Description
K4C7K8	1.669	0.981	1.309	1.821	Uncharacterized protein
K4BED0	1.669	1.003	1.139	1.301	Uncharacterized protein
K4B6A4	1.669	1.219	1.601	1.462	Uncharacterized protein
K4DCS4	1.668	1.259	1.396	1.261	Uncharacterized protein
K4CNB0	1.668	1.229	1.835	2.187	Uncharacterized protein
K4B3E8	1.667	1.226	1.695	1.807	Uncharacterized protein
K4CAV3	1.667	1.139	1.256	1.145	Uncharacterized protein
K4B1S0	1.667	1.218	1.371	1.291	Uncharacterized protein
K4C0H2	1.666	1.043	1.569	1.655	Uncharacterized protein
K4DG54	1.665	1.288	1.501	1.375	Uncharacterized protein
K4DI04	1.665	1.199	1.908	1.716	Uncharacterized protein
K4CXZ7	1.664	1.224	1.902	1.481	Uncharacterized protein
Q8RW36	1.664	1.007	1.147	1.230	Calcium-dependent protein kinase
K4C465	1.664	1.148	1.267	2.073	Uncharacterized protein
K4B6W4	1.664	1.379	1.820	1.737	Uncharacterized protein
K4C3W7	1.664	1.060	1.652	2.815	Uncharacterized protein
K4CAB6	1.663	1.071	1.221	1.336	Uncharacterized protein
K4BBG4	1.662	0.982	1.152	1.091	Uncharacterized protein
K4C379	1.662	1.025	1.319	2.180	Uncharacterized protein
K4DB26	1.662	0.990	1.518	2.976	Uncharacterized protein
K4B861	1.662	1.059	1.101	1.067	Uncharacterized protein
K4BF28	1.661	1.110	1.451	1.713	Uncharacterized protein
K4BE91	1.661	1.130	1.489	1.801	Uncharacterized protein
K4B862	1.661	1.007	1.134	1.285	Uncharacterized protein
K4D5S8	1.661	1.087	1.311	2.008	Uncharacterized protein
K4BJY6	1.660	1.234	1.526	1.889	Uncharacterized protein
K4BKV2	1.660	0.985	1.025	1.226	Uncharacterized protein
K4BYC5	1.659	0.919	1.083	1.281	Uncharacterized protein
K4ASJ4	1.659	1.445	2.457	2.378	Uncharacterized protein

Accession	Burned	Control	Regular	Limit	Description
K4BJB3	1.658	1.046	1.428	1.482	Vacuolar glucose transporter 2
K4DCU0	1.658	1.065	1.465	1.660	Uncharacterized protein
K4CW14	1.657	0.966	1.375	2.124	Uncharacterized protein
K4DHP1	1.657	1.395	1.843	2.020	Eukaryotic translation initiation factor 3 subunit H
K4CT86	1.656	0.994	1.024	1.198	Uncharacterized protein
K4BF05	1.655	1.117	1.124	1.285	Alcohol acyl transferase
K4CHI2	1.655	0.930	1.086	1.246	Uncharacterized protein
K4DEF2	1.655	1.016	1.100	1.335	Uncharacterized protein
G5EM34	1.655	0.891	1.006	1.129	Calcineurin B-like molecule
K4C2P8	1.653	1.274	1.208	1.269	Methylenetetrahydrofolate reductase
K4B414	1.652	1.049	1.422	1.439	Uncharacterized protein
K4C9Q1	1.652	0.995	1.391	1.315	Uncharacterized protein
K4C7N1	1.652	0.897	0.782	0.997	Uncharacterized protein
K4B9G5	1.652	1.132	1.496	1.799	Uncharacterized protein
K4B315	1.652	0.912	1.009	1.134	Uncharacterized protein
K4C2W4	1.652	1.024	1.300	3.795	Protein disulfide-isomerase
K4BXY3	1.652	1.165	1.375	1.351	Uncharacterized protein
K4AYJ8	1.651	1.316	1.763	2.004	Uncharacterized protein
K4C6B2	1.651	1.017	0.966	0.966	Uncharacterized protein
K4CDN1	1.651	0.877	0.980	1.187	Uncharacterized protein
K4ASD4	1.650	0.911	1.128	0.980	Cytokinin riboside 5'-monophosphate phosphoribohydrolase
G3K2M5	1.650	1.041	1.092	1.366	Methionine sulfoxide reductase A5
K4CM05	1.649	0.941	1.001	1.002	Uncharacterized protein

Accession	Burned	Control	Regular	Limit	Description
K4CR32	1.648	0.965	1.046	1.218	Uncharacterized protein
K4DA24	1.647	1.041	1.184	1.815	Uncharacterized protein
K4D3Y9	1.647	1.045	0.969	1.407	Uncharacterized protein
K4BID7	1.647	1.066	1.167	1.287	Uncharacterized protein
Q40140	1.647	0.969	1.208	2.232	Aspartic protease
K4CHU3	1.647	1.106	1.213	1.289	Uncharacterized protein
K4AT14	1.646	1.011	0.987	1.234	Uncharacterized protein
K4D2X7	1.646	1.044	1.464	3.251	Uncharacterized protein
K4C753	1.646	1.044	1.402	1.696	Uncharacterized protein
K4AZA5	1.646	1.139	1.442	1.504	Uncharacterized protein
K4BGK4	1.646	1.126	0.825	0.780	Uncharacterized protein
K4CAS1	1.645	1.169	1.278	1.303	Uncharacterized protein
K4BJF4	1.645	1.242	1.627	1.106	Uncharacterized protein
K4DHI9	1.645	1.099	1.466	2.289	Uncharacterized protein
K4BPI5	1.645	1.029	1.107	1.088	Uncharacterized protein
K4C034	1.644	1.210	1.580	2.368	Uncharacterized protein
K4AT78	1.644	1.339	1.877	2.983	Uncharacterized protein
K4CIT0	1.644	0.991	0.907	0.884	Uncharacterized protein
K4BI42	1.643	1.341	1.706	1.971	Uncharacterized protein
K4BBM2	1.643	0.841	0.791	0.976	Uncharacterized protein
K4B437	1.642	1.051	1.122	1.110	Uncharacterized protein
K4CBJ2	1.642	1.122	1.294	1.537	Uncharacterized protein
K4B3V9	1.642	1.424	1.123	0.854	Uncharacterized protein
K4D4P7	1.642	1.137	1.440	1.341	Uncharacterized protein
K4DGP6	1.641	1.147	1.281	1.991	Uncharacterized protein
K4CMZ9	1.640	1.137	1.198	1.571	Uncharacterized protein
K4D9S9	1.640	1.038	1.230	1.783	Uncharacterized protein
K4BMS6	1.639	1.040	1.586	2.040	Uncharacterized protein
K4C772	1.639	1.012	1.126	1.257	Uncharacterized protein
K4CZB3	1.639	1.295	1.252	1.345	Uncharacterized protein
K4C6C7	1.639	1.057	1.196	1.354	Uncharacterized protein
K4CR64	1.638	1.073	1.588	2.153	Uncharacterized protein
K4B406	1.638	1.057	1.659	2.463	Uncharacterized protein
K4CX43	1.638	0.910	1.638	1.834	Uncharacterized protein
K4CVP8	1.637	1.082	1.620	2.023	Uncharacterized protein
K4D6Q4	1.636	1.026	1.255	1.321	Beta-galactosidase
K4BV51	1.636	1.061	1.374	1.614	Uncharacterized protein
K4CH51	1.635	1.130	1.496	1.807	Uncharacterized protein
K4B846	1.635	1.188	1.509	1.578	60S ribosomal protein L18a
K4BN07	1.635	1.157	1.449	1.828	Uncharacterized protein
K4BQF1	1.635	1.064	1.213	1.111	Uncharacterized protein
K4AY22	1.634	0.986	1.006	1.078	Uncharacterized protein
Q9FT21	1.633	0.986	1.233	2.125	Putative glutathione S-transferase T3
K4DA99	1.632	1.249	2.639	1.867	Uncharacterized protein
K4AW47	1.631	1.161	1.628	1.801	Uncharacterized protein
K4CP41	1.631	0.965	1.088	1.724	Uncharacterized protein
K4BT02	1.630	0.919	0.985	1.214	Uncharacterized protein
K4BMK3	1.630	1.042	1.176	1.406	Uncharacterized protein
K4B0C2	1.630	0.906	0.969	1.413	Uncharacterized protein
K4CY57	1.630	1.162	1.237	1.379	Uncharacterized protein
K4AZG0	1.630	1.047	1.045	1.030	Uncharacterized protein
K4BGI7	1.630	1.266	1.386	1.197	Uncharacterized protein
K4CZD4	1.629	1.113	1.581	2.143	Coatomer subunit delta
K4B6B3	1.629	1.028	1.211	1.426	Uncharacterized protein
K4BVC5	1.629	1.263	2.359	2.343	Uncharacterized protein
K4C2P5	1.629	0.978	1.107	1.465	Uncharacterized protein
K4CV09	1.629	1.039	1.222	1.311	Serine/threonine-protein phosphatase

Accession	Burned	Control	Regular	Limit	Description
K4CNA3	1.629	1.148	1.352	1.515	Lon protease homolog 2, peroxisomal
K4CR79	1.629	1.029	1.226	1.413	Uncharacterized protein
K4CIN9	1.628	0.987	1.065	1.212	Uncharacterized protein
K4CI96	1.627	1.053	1.070	1.139	Uncharacterized protein
K4C6U7	1.626	1.083	1.590	1.900	Uncharacterized protein
K4DEF3	1.626	1.149	1.391	1.535	Uncharacterized protein
K4C734	1.626	1.158	1.446	1.807	Uncharacterized protein
K4D467	1.625	1.074	1.596	2.134	Uncharacterized protein
K4C8C0	1.624	0.947	1.226	1.531	Uncharacterized protein
K4C8Q9	1.624	1.241	1.505	1.809	Uncharacterized protein
K4D588	1.623	1.057	1.231	2.353	Carboxypeptidase
K4CUI2	1.623	1.061	1.265	3.165	Uncharacterized protein
K4B120	1.623	1.157	1.384	1.559	Serine/threonine-protein phosphatase
K4B0W5	1.623	1.036	1.251	1.421	Uncharacterized protein
K4CM57	1.622	1.072	1.242	1.822	Aspartate aminotransferase
K4BA73	1.622	1.014	1.126	1.335	Uncharacterized protein
K4CHP7	1.622	1.084	1.314	1.512	Uncharacterized protein
K4CW84	1.621	0.986	1.217	1.243	Uncharacterized protein
K4BBG0	1.621	0.901	1.046	1.067	Uncharacterized protein
K4BG35	1.621	0.994	1.121	1.183	Uncharacterized protein
K4CNL2	1.620	1.118	1.315	1.036	Uncharacterized protein
K4C4V7	1.620	0.954	1.280	2.769	Uncharacterized protein
K4CWK1	1.620	1.226	1.684	1.760	Uncharacterized protein
K4DHA3	1.619	1.361	1.775	1.832	40S ribosomal protein S6
K4B3Q2	1.618	0.963	1.347	1.554	Uncharacterized protein
K4D368	1.618	0.981	1.191	1.214	Uncharacterized protein
K4BE81	1.617	0.972	1.158	1.441	Uncharacterized protein
K4B1H9	1.617	1.019	1.213	1.229	Uncharacterized protein
K4BSG5	1.616	1.204	1.473	1.411	Uncharacterized protein
K4BDF1	1.616	1.103	1.288	1.277	Uncharacterized protein
K4C9A2	1.616	0.982	1.221	1.304	Uncharacterized protein
K4B182	1.616	0.990	1.300	1.520	Uncharacterized protein
K4D184	1.616	1.164	2.208	3.522	Peptidyl-prolyl cis-trans isomerase
K4B5Z2	1.616	0.972	1.179	1.401	Uncharacterized protein
K4BKS7	1.615	0.934	0.895	0.994	Uncharacterized protein
K4CGT3	1.614	1.149	1.839	3.033	Uncharacterized protein
Q2MI60	1.614	1.115	1.233	1.230	30S ribosomal protein S19, chloroplastic
K4CHX2	1.613	1.071	0.715	0.812	Uncharacterized protein
K4C310	1.613	0.943	1.384	2.019	Uncharacterized protein
K4ATD8	1.613	1.045	1.224	1.755	Uncharacterized protein
K4CX23	1.612	0.949	1.265	1.337	Uncharacterized protein
K4D935	1.612	0.977	1.143	1.538	Uncharacterized protein
K4DAN7	1.612	1.104	1.338	1.549	Uncharacterized protein
K4CXN7	1.612	0.932	1.634	3.191	Uncharacterized protein
K4CH72	1.611	1.260	1.497	1.512	Uncharacterized protein
Q2MI81	1.611	0.951	0.785	0.714	Cytochrome b6-f complex subunit 5
K4BU76	1.610	1.167	1.488	1.857	NADPH--cytochrome P450 reductase
K4CNY6	1.610	0.913	1.122	1.332	Uncharacterized protein
K4CSI6	1.609	1.030	1.262	1.754	Uncharacterized protein
K4CG84	1.609	1.178	1.679	2.237	Uncharacterized protein
K4DBI1	1.609	1.033	1.226	1.184	Uncharacterized protein
K4BK69	1.609	1.307	1.826	1.744	Elongation factor Tu
K4C975	1.609	1.001	1.349	2.036	Uncharacterized protein
K4BMP7	1.608	1.097	1.415	1.735	Uncharacterized protein

Accession	Burned	Control	Regular	Limit	Description
K4CG60	1.608	1.106	1.526	1.672	Aspartate aminotransferase
Q93X45	1.607	1.130	1.547	1.837	Xaa-Pro aminopeptidase 2
K4CBR2	1.607	1.003	1.157	2.036	Uncharacterized protein
K4B1F9	1.607	0.790	0.935	0.625	Uncharacterized protein
K4BWH1	1.606	0.969	0.998	0.933	Uncharacterized protein
K4DBR8	1.606	0.894	0.740	0.937	Uncharacterized protein
K4BIX1	1.606	1.042	1.399	1.695	Uncharacterized protein
K4DA30	1.605	0.930	0.839	1.139	Uncharacterized protein
K4BNS3	1.603	1.033	1.156	1.299	Uncharacterized protein
K4DBV2	1.603	0.995	1.090	1.207	Uncharacterized protein
K4BDC5	1.603	1.465	2.286	2.080	Uncharacterized protein
K4BZ35	1.602	1.092	1.308	1.361	Uncharacterized protein
K4DAF8	1.601	1.028	1.268	1.504	Uncharacterized protein
K4D4F5	1.601	0.867	1.156	1.067	Uncharacterized protein
K4BL25	1.600	1.062	1.099	2.215	Uncharacterized protein
K4BIS2	1.600	0.844	0.782	0.846	Signal recognition particle subunit SRP68
K4C2R0	1.599	1.021	0.859	0.871	Uncharacterized protein
K4CIV1	1.599	0.986	1.144	1.268	Uncharacterized protein
K4CZH2	1.599	1.218	1.686	2.136	Chloride channel protein
K4BM35	1.599	1.516	2.245	2.376	Uncharacterized protein
K4ATT7	1.599	0.989	1.061	1.527	Uncharacterized protein
K4C289	1.599	0.951	0.996	1.350	ER membrane protein complex subunit 3
K4ATD5	1.598	1.076	1.236	1.213	Uncharacterized protein
K4AWF0	1.597	1.161	1.514	1.634	Importin subunit alpha
K4CBP9	1.597	1.193	1.585	1.702	Uncharacterized protein
K4BTS8	1.597	1.020	1.233	1.631	Uncharacterized protein
K4D6A1	1.596	0.949	1.414	1.882	Uncharacterized protein
K4C362	1.596	1.170	1.384	1.569	Serine/threonine-protein phosphatase
K4BC34	1.595	1.000	1.345	2.346	Uncharacterized protein
K4BLN0	1.595	0.950	1.039	1.297	Uncharacterized protein
K4DB71	1.595	1.266	1.529	1.517	Uncharacterized protein
K4B2P9	1.593	0.980	1.601	2.617	Uncharacterized protein
K4BMV6	1.592	1.149	1.397	1.783	Transmembrane 9 superfamily member
K4C946	1.592	1.160	1.503	1.622	Golgi apparatus membrane protein TVP23
K4BXG6	1.592	1.008	1.200	1.278	Uncharacterized protein
K4CJX3	1.591	1.093	1.417	1.877	Uncharacterized protein
K4C998	1.591	1.299	1.963	2.290	Uncharacterized protein
K4BF68	1.590	0.950	1.282	2.790	Uncharacterized protein
K4BBT4	1.589	1.172	1.614	2.315	Aldose 1-epimerase
K4C654	1.589	0.973	1.340	2.655	Uncharacterized protein
K4CE53	1.587	1.156	1.351	1.601	Uncharacterized protein
K4CY27	1.587	1.032	1.553	1.417	Uncharacterized protein
K4D2T4	1.586	1.132	1.516	1.436	Uncharacterized protein
K4DHW4	1.586	1.000	1.467	3.240	Uncharacterized protein
K4BJC4	1.586	0.971	1.108	1.396	Uncharacterized protein
K4CPS0	1.586	1.099	1.427	1.586	Uncharacterized protein
K4BP82	1.585	1.307	1.999	1.731	Uncharacterized protein
K4CXK7	1.585	1.112	1.443	1.724	Uncharacterized protein
K4AXU5	1.585	0.838	0.727	0.786	Uncharacterized protein
K4CZ49	1.584	1.135	1.722	1.693	Uncharacterized protein
E3UVW7	1.584	0.990	1.257	2.171	Beta-galactosidase
K4C870	1.584	1.062	1.358	1.283	Uncharacterized protein
K4D3F8	1.584	1.265	1.844	2.974	Pyruvate kinase
K4DHD8	1.584	0.932	1.157	1.297	Uncharacterized protein
K4C679	1.584	0.976	0.814	0.848	Uncharacterized protein

Accession	Burned	Control	Regular	Limit	Description
K4B0D3	1.583	0.777	0.727	0.903	Uncharacterized protein
K4BF36	1.583	1.096	1.240	1.606	Uncharacterized protein
K4D4R4	1.582	1.019	1.195	1.370	Uncharacterized protein
K4BDD0	1.582	0.987	1.015	1.472	Uncharacterized protein
K4BYG6	1.582	1.184	1.810	2.785	Glyceraldehyde-3-phosphate dehydrogenase
K4D9G1	1.582	1.044	1.452	2.064	Uncharacterized protein
K4D6E8	1.582	1.018	1.052	1.332	Eukaryotic translation initiation factor 3 subunit F
K4BN62	1.582	1.012	1.709	2.340	Pectinesterase
K4CW78	1.582	0.990	0.984	1.330	Uncharacterized protein
K4DH49	1.581	1.292	2.023	1.871	Pyrophosphate--fructose 6-phosphate 1-phosphotransferase subunit alpha
K4D1P2	1.581	1.109	1.679	1.892	Uncharacterized protein
K4BMF8	1.581	1.066	0.819	0.994	Uncharacterized protein
K4D7D0	1.581	0.891	1.287	1.620	Uncharacterized protein
K4CX83	1.580	1.169	1.835	2.774	Glyceraldehyde-3-phosphate dehydrogenase
K4BEU5	1.580	1.101	1.239	1.358	Uncharacterized protein
K4DFA0	1.579	1.152	1.396	1.705	Uncharacterized protein
K4C5A1	1.578	1.009	0.784	0.973	Uncharacterized protein
K4CQR9	1.577	1.267	1.791	2.735	Pyruvate kinase
K4BT00	1.577	1.059	1.169	1.325	Uncharacterized protein
K4CGB7	1.576	1.105	1.475	3.575	Citrate synthase
K4B541	1.575	1.027	1.446	1.616	3-hydroxyisobutyrate dehydrogenase
K4B937	1.575	1.194	1.454	1.853	Eukaryotic translation initiation factor 3 subunit D
K4CM61	1.574	1.177	1.645	1.293	Uncharacterized protein
K4BMV7	1.573	1.180	1.563	1.831	Uncharacterized protein
K4CWD6	1.572	1.111	1.316	1.739	Uncharacterized protein
K4BPV5	1.572	0.972	1.075	0.919	Glutamine synthetase
K4D2L3	1.571	1.066	1.250	1.274	Uncharacterized protein
K4C874	1.571	1.364	1.808	1.771	Uncharacterized protein
K4D585	1.571	1.050	1.105	1.411	Uncharacterized protein
K4AYD7	1.569	1.034	1.315	1.773	Uncharacterized protein
K4CBK7	1.568	1.061	1.234	1.430	Uncharacterized protein
K4DCI6	1.567	1.123	1.645	4.108	Citrate synthase
K4BDV8	1.567	1.251	1.670	1.486	Uncharacterized protein
K4CCS9	1.566	1.079	1.455	2.242	Uncharacterized protein
K4CPJ8	1.565	1.086	1.306	1.200	Uncharacterized protein
K4D1T3	1.565	0.887	0.863	0.864	Uncharacterized protein
K4BRZ1	1.564	1.288	1.724	1.967	Uncharacterized protein
K4CUA7	1.563	1.153	1.349	1.271	Uncharacterized protein
K4D3T8	1.563	0.906	0.992	1.075	Uncharacterized protein
K4CEJ1	1.561	0.996	1.045	1.082	Uncharacterized protein
K4CWS1	1.561	1.145	1.377	1.560	Uncharacterized protein
K4DBU5	1.561	1.414	2.001	1.785	Uncharacterized protein
K4CYL4	1.560	1.055	1.346	1.468	Cysteine synthase
K4D3P8	1.559	0.986	1.043	1.237	Uncharacterized protein
K4CQP7	1.559	1.035	1.313	1.536	Uncharacterized protein
K4BZG0	1.559	1.123	1.321	1.180	Uncharacterized protein
K4C4N5	1.558	0.892	0.739	0.964	Uncharacterized protein
K4DA25	1.558	1.090	0.808	0.797	Uncharacterized protein
K4BMM4	1.557	1.069	1.464	1.815	Uncharacterized protein

Accession	Burned	Control	Regular	Limit	Description
P30264	1.557	1.455	3.915	4.140	Catalase isozyme 1
Q672Q2	1.556	0.951	0.981	1.019	Chloroplast-specific ribosomal protein
K4BY24	1.555	1.204	1.634	1.820	Uncharacterized protein
K4B7M5	1.555	0.904	1.054	1.123	Uncharacterized protein
K4BLV4	1.554	0.989	1.355	1.638	Uncharacterized protein
K4BW77	1.554	1.232	1.415	1.948	Uncharacterized protein
K4B9D0	1.553	1.013	1.277	1.605	Eukaryotic translation initiation factor 3 subunit J
K4ASZ8	1.553	1.119	1.655	1.925	Uncharacterized protein
K4DHB2	1.553	1.030	1.171	1.285	Uncharacterized protein
K4DF99	1.552	1.145	1.372	1.663	Uncharacterized protein
K4AVE9	1.551	1.000	1.188	1.441	Uncharacterized protein
K4DD89	1.551	1.111	1.480	2.084	Guanosine nucleotide diphosphate dissociation inhibitor
K4DB46	1.550	0.952	1.310	1.915	Uncharacterized protein
K4D6M7	1.550	0.988	1.032	1.506	Chorismate mutase
K4CH34	1.550	1.064	1.110	1.081	Uncharacterized protein
K4CAS8	1.550	1.155	1.728	2.364	40S ribosomal protein S24
K4D9R6	1.550	1.033	1.531	1.908	Uncharacterized protein
K4B753	1.549	1.256	1.563	1.814	Uncharacterized protein
K4BMM1	1.549	0.991	1.149	1.661	Uncharacterized protein
K4AYP1	1.548	1.307	1.816	1.823	Uncharacterized protein
K4BRR1	1.548	0.868	1.254	1.624	V-type proton ATPase subunit G
K4CJ46	1.548	1.104	1.109	1.105	Isopropylmalate synthase
K4C6U8	1.547	1.068	1.233	1.142	Uncharacterized protein
Q9FV54	1.547	0.927	0.910	0.879	Peptide deformylase 1B, chloroplastic
K4DCV6	1.547	1.083	1.395	1.519	Uncharacterized protein
K4DCC6	1.546	1.172	1.260	1.772	Transmembrane 9 superfamily member
K4B102	1.546	0.901	1.242	1.829	Uncharacterized protein
K4CPR6	1.545	1.262	1.676	1.939	Uncharacterized protein
K4CWC9	1.545	0.854	0.716	0.807	Beta-amylase
K4CAM8	1.545	1.036	1.133	1.529	Uncharacterized protein
K4BMX1	1.544	1.145	1.461	1.557	Uncharacterized protein
K4B7J6	1.543	0.989	1.250	1.717	Uncharacterized protein
K4CXV2	1.543	0.974	0.847	0.870	Uncharacterized protein
K4C4N4	1.543	1.060	1.223	1.631	Uncharacterized protein
K4BL13	1.542	1.134	1.613	1.899	Uncharacterized protein
K4DAA5	1.542	1.054	1.076	1.182	Uncharacterized protein
K4B9P8	1.542	1.058	1.295	1.526	Vacuolar protein sorting-associated protein 28 homolog
K4D3T7	1.541	0.943	1.133	1.180	Uncharacterized protein
K4AZ76	1.541	0.905	0.973	1.040	Uncharacterized protein
K4D245	1.539	1.024	1.285	1.708	Proteasome subunit alpha type
K4BSC0	1.539	1.085	1.447	1.330	Uncharacterized protein
K4CF67	1.539	1.056	1.236	1.137	Uncharacterized protein
K4BD52	1.539	1.246	1.673	1.154	Uncharacterized protein
K4BK30	1.539	0.943	1.071	1.096	Uncharacterized protein
K4ATR3	1.538	1.054	1.265	2.185	Uncharacterized protein
K4C876	1.538	1.012	1.056	1.172	Uncharacterized protein
K4BQ13	1.537	1.007	1.164	1.714	Uncharacterized protein
K4BSR7	1.537	1.427	1.541	1.509	Uncharacterized protein
K4BRZ6	1.537	1.210	1.625	1.979	Uncharacterized protein
K4DI33	1.536	1.013	1.239	1.709	Uncharacterized protein

Accession	Burned	Control	Regular	Limit	Description
K4AT27	1.536	1.016	1.249	1.389	Dihydroorotate dehydrogenase (quinone), mitochondrial
K4D4X3	1.535	0.919	1.000	1.356	Uncharacterized protein
K4BYW1	1.535	1.284	1.503	1.854	Glucose-6-phosphate 1-dehydrogenase
K4CJ39	1.535	1.145	1.202	1.146	Eukaryotic translation initiation factor 2A
K4CHF9	1.534	0.960	1.339	2.017	Uncharacterized protein
K4CHP2	1.533	0.902	1.557	1.218	Uncharacterized protein
K4BUX5	1.533	0.908	0.831	0.879	Uncharacterized protein
K4BEL9	1.532	1.199	1.311	1.550	Uncharacterized protein
K4DBQ4	1.532	1.197	1.618	2.413	Uncharacterized protein
K4C6Q2	1.532	1.023	0.986	1.008	Uncharacterized protein
K4AZX9	1.531	1.425	1.122	0.887	Uncharacterized protein
K4CAM4	1.530	0.954	1.100	1.490	Uncharacterized protein
K4BY55	1.530	1.179	1.433	1.555	Uncharacterized protein
K4DHE3	1.530	1.192	1.609	1.919	Uncharacterized protein
K4D3Z7	1.529	0.964	1.222	1.561	Uncharacterized protein
Q6DUX2	1.529	0.995	1.372	1.723	Regulator of gene silencing
K4CF48	1.528	1.010	1.204	1.884	Uncharacterized protein
K4CGU0	1.528	1.002	1.101	1.359	Fen-interacting protein 3
K4AYM5	1.527	0.951	0.909	1.055	Uncharacterized protein
K4CWB9	1.527	1.030	1.296	1.436	Uncharacterized protein
K4BC10	1.527	1.083	1.256	1.403	Uncharacterized protein
K4CBC8	1.527	0.967	2.358	5.511	Uncharacterized protein
K4BP93	1.527	1.020	0.952	1.038	Uncharacterized protein
K4AT35	1.526	1.207	1.485	2.728	Uncharacterized protein
K4BH28	1.526	1.008	1.221	1.545	Uncharacterized protein
K4CBD6	1.526	0.977	1.336	2.420	Xylose isomerase
K4D9A5	1.525	0.966	1.485	1.872	Uncharacterized protein
K4BHY1	1.525	0.988	1.270	2.120	Uncharacterized protein
K4CPB7	1.525	0.966	0.970	1.319	Uncharacterized protein
K4AY21	1.525	1.101	1.241	1.430	Uncharacterized protein
K4AT29	1.524	1.241	1.537	1.568	Uncharacterized protein
K4AS91	1.523	1.159	1.340	1.127	Uncharacterized protein
K4CG47	1.522	0.935	1.169	1.999	Proteasome subunit alpha type
K4DCQ6	1.522	1.670	1.293	0.806	Uncharacterized protein
K4CNI4	1.521	1.004	1.253	1.422	Uncharacterized protein
K4CJB4	1.521	1.124	1.496	2.110	Guanosine nucleotide diphosphate dissociation inhibitor
K4D809	1.521	1.127	1.231	1.454	Uncharacterized protein
K4C1K8	1.520	0.935	0.943	1.132	Uncharacterized protein
K4B2G9	1.520	0.952	1.263	2.958	Uncharacterized protein
K4C376	1.519	0.988	1.244	3.333	Protein disulfide-isomerase
K4BNE1	1.519	0.941	0.983	1.247	Uncharacterized protein
K4C8E9	1.519	1.116	1.229	1.478	Uncharacterized protein
K4BJ82	1.519	1.054	1.295	1.438	Uncharacterized protein
K4C5F9	1.519	1.268	1.726	2.090	Uncharacterized protein
K4CQH4	1.518	0.981	0.566	0.484	Uncharacterized protein
K4B2C6	1.518	1.269	1.089	1.016	Uncharacterized protein
K4C1Z4	1.518	1.263	1.807	2.084	Uncharacterized protein
K4CWT1	1.518	1.062	1.101	0.805	Uncharacterized protein
K4B2H7	1.518	0.889	0.916	1.145	Uncharacterized protein
K4CRH1	1.518	1.016	1.355	1.552	Uncharacterized protein
K4CZD6	1.517	0.933	0.987	1.080	Pectin acetylesterase
K4BDL0	1.517	0.975	1.304	1.430	Uncharacterized protein
Q5UNS1	1.516	1.096	2.718	3.974	Arginase 2

Accession	Burned	Control	Regular	Limit	Description
K4DHX8	1.515	0.863	0.916	0.754	Uncharacterized protein
K4C286	1.515	1.338	1.677	1.860	Uncharacterized protein
K4DFC8	1.515	1.281	1.432	1.498	Uncharacterized protein
K4DHQ5	1.515	1.140	1.553	1.590	Uncharacterized protein
K4BW06	1.515	1.096	1.395	1.654	Uncharacterized protein
K4CBW8	1.514	0.921	0.898	1.052	Uncharacterized protein
Q9M7N6	1.514	0.844	0.735	0.822	MFP1 attachment factor 1
K4BPH3	1.512	0.952	0.890	0.937	Uncharacterized protein
K4B1J4	1.512	1.048	1.587	3.010	Uncharacterized protein
K4D1R1	1.511	1.103	1.326	1.799	Uncharacterized protein
K4CND0	1.511	1.330	1.757	1.869	Uncharacterized protein
K4AZ11	1.511	1.001	1.124	1.365	Uncharacterized protein
K4CJ85	1.510	1.207	1.532	1.843	Uncharacterized protein
K4CF32	1.510	1.379	2.113	1.314	Uncharacterized protein
K4D4Z3	1.509	1.001	1.270	1.396	Uncharacterized protein
K4CWZ8	1.509	1.335	1.700	1.860	Eukaryotic translation initiation factor 3 subunit H
K4CXX8	1.509	0.926	1.169	1.852	Proteasome subunit alpha type
K4DF02	1.509	1.223	1.767	1.965	Uncharacterized protein
K4BK81	1.509	1.037	1.306	1.479	Uncharacterized protein
K4D5Z6	1.508	1.078	1.204	1.603	Transmembrane 9 superfamily member
K4CXV1	1.508	1.035	1.195	1.054	Uncharacterized protein
K4CEU8	1.507	0.987	1.100	1.241	Uncharacterized protein
K4CBF4	1.507	1.010	1.228	1.032	Uncharacterized protein
K4BPX5	1.507	1.328	1.672	1.899	Uncharacterized protein
K4D246	1.507	1.314	1.137	0.848	Uncharacterized protein
K4C785	1.507	1.313	1.319	1.313	Uncharacterized protein
K4C219	1.507	0.987	1.122	1.368	Prefoldin subunit 3
K4B6E8	1.507	1.071	1.377	1.543	Uncharacterized protein
K4CGL3	1.506	1.056	1.461	1.528	Uncharacterized protein
K4CTL7	1.506	0.997	1.111	1.475	Uncharacterized protein
K4D860	1.506	1.010	1.201	1.924	Uncharacterized protein
K4CX99	1.506	1.009	1.162	1.545	Uncharacterized protein
K4AZH5	1.506	1.242	1.409	1.138	Uncharacterized protein
K4D2F4	1.506	1.145	1.383	1.386	Uncharacterized protein
K4D4H5	1.506	1.138	1.487	1.505	N-acetylglutamate kinase
K4C7V8	1.505	1.105	1.161	1.221	Uncharacterized protein
K4DAV8	1.504	1.237	1.705	1.526	Uncharacterized protein
Q41340	1.504	1.070	1.470	2.106	Small GTP-binding protein
K4C7Z8	1.504	1.370	1.110	0.958	Uncharacterized protein
K4DD26	1.504	1.004	0.916	1.000	Uncharacterized protein
K4D3J0	1.504	0.881	0.989	1.208	Uncharacterized protein
K4BRH8	1.504	1.145	1.550	1.776	Ubiquitin thioesterase
K4D413	1.504	1.093	1.404	1.651	Uncharacterized protein
K4D3R4	1.504	1.139	1.527	1.646	Uncharacterized protein
K4AW95	1.503	1.201	1.667	1.886	Uncharacterized protein
K4CHL0	1.503	1.048	1.033	1.189	Uncharacterized protein
K4D2J1	1.502	1.077	1.183	1.546	Inosine-5'-monophosphate dehydrogenase
K4CEJ5	1.502	1.350	1.761	2.151	60S ribosomal protein L27
E0XN34	1.502	0.899	1.133	1.271	Alpha-mannosidase
K4DAQ8	1.501	1.368	1.438	1.482	Homoserine dehydrogenase
K4CC33	1.501	1.180	1.567	1.768	Uncharacterized protein

Accession	Burned	Control	Regular	Limit	Description
K4BRS2	1.500	0.953	1.081	1.715	Protein disulfide-isomerase
K4D5L7	1.500	1.128	1.247	1.016	Uncharacterized protein
K4C949	1.499	1.271	1.549	1.968	60S ribosomal protein L27
K4DC81	1.499	1.040	1.415	1.197	Glycosyltransferase
K4AZ19	1.499	1.124	1.324	1.218	Uncharacterized protein
K4DBF5	1.499	0.940	1.036	1.211	Uncharacterized protein
K4C2U7	1.498	1.085	1.629	1.848	Uncharacterized protein
K4BTV7	1.498	1.081	1.577	1.667	Uncharacterized protein
K4B8T5	1.498	1.003	1.267	1.725	Uncharacterized protein
K4CB31	1.497	1.317	1.605	2.292	Transmembrane 9 superfamily member
K4C8M7	1.497	1.273	1.042	1.204	Uncharacterized protein
K4D6R2	1.496	1.344	1.771	1.609	Uncharacterized protein
K4BVB8	1.496	0.940	1.139	1.199	Uncharacterized protein
K4BQ47	1.495	1.370	1.579	1.292	Translation factor GUF1 homolog, chloroplastic
K4B0D2	1.495	1.122	1.532	2.374	Uncharacterized protein
K4DA74	1.495	1.011	1.429	2.431	Uncharacterized protein
K4CP17	1.494	1.542	2.454	1.890	Uncharacterized protein
K4D616	1.494	1.327	1.690	1.960	Uncharacterized protein
K4BP32	1.494	1.013	1.114	1.272	Uncharacterized protein
K4CBN7	1.494	0.844	1.002	1.733	Purple acid phosphatase
K4CWI3	1.493	1.045	1.457	2.047	Ubiquinone biosynthesis monooxygenase COQ6, mitochondrial
K4BM53	1.493	1.394	1.837	1.750	Uncharacterized protein
K4D6D0	1.493	0.973	1.275	1.952	Uncharacterized protein
K4AT08	1.493	0.811	1.205	1.424	Uncharacterized protein
K4BNA1	1.493	0.982	0.941	0.949	Uncharacterized protein
K4B7E5	1.492	1.062	1.329	2.081	Uncharacterized protein
K4D7K7	1.492	0.998	1.109	1.520	Uncharacterized protein
K4C8G1	1.492	0.968	1.060	1.315	Uncharacterized protein
A9Q2P8	1.492	1.190	0.816	0.613	Phytoene synthase 2
K4BHX0	1.491	0.982	1.431	2.433	Uncharacterized protein
K4CU71	1.491	1.055	1.009	0.913	Uncharacterized protein
K4BAQ4	1.491	1.034	1.271	1.534	Uncharacterized protein
K4BXY1	1.491	0.989	1.273	1.554	Uncharacterized protein
K4AYA3	1.491	0.933	1.193	1.634	Uncharacterized protein
K4AX99	1.490	1.260	1.653	1.948	Uncharacterized protein
K4D4L9	1.490	1.405	1.258	1.166	Uncharacterized protein
K4BWB5	1.489	1.221	1.329	1.186	Uncharacterized protein
K4CI93	1.488	1.401	1.847	1.925	40S ribosomal protein S6
K4BIA1	1.487	1.015	1.222	1.410	Uncharacterized protein
K4CNG6	1.486	1.071	1.507	2.239	Uncharacterized protein
K4D533	1.486	0.921	1.113	1.413	Dihydrolipoamide acetyltransferase component of pyruvate dehydrogenase complex
K4B3K6	1.486	1.068	1.049	1.240	Uncharacterized protein
K4CEK4	1.485	1.570	2.631	1.505	Uncharacterized protein
K4C9K6	1.485	0.840	0.613	0.775	Uncharacterized protein
K4DBZ7	1.485	1.019	1.171	1.447	Uncharacterized protein
K4BNE0	1.485	1.063	1.432	2.210	Uncharacterized protein
Q1M319	1.485	1.145	1.524	1.786	Putative beta-glycosidase
K4BSV7	1.484	0.870	1.037	1.389	Uncharacterized protein
K4C7G1	1.484	1.008	1.279	1.504	Uncharacterized protein
K4DHX7	1.484	1.094	1.233	1.433	Uncharacterized protein
K4CA29	1.484	1.005	0.923	1.164	Uncharacterized protein
K4C7G6	1.483	0.865	1.163	1.780	Uncharacterized protein

Accession	Burned	Control	Regular	Limit	Description
K4C9I5	1.483	1.061	1.266	1.628	Uncharacterized protein
K4BXV0	1.481	1.159	1.284	1.290	Argininosuccinate synthase
K4BXJ8	1.481	0.933	0.992	1.066	Uncharacterized protein
K4BPF1	1.481	0.973	1.107	2.133	Uncharacterized protein
K4B464	1.480	1.226	1.664	1.347	Uncharacterized protein
K4CVA7	1.479	1.158	1.488	1.620	Uncharacterized protein
K4CWR9	1.478	1.009	1.681	2.530	Uncharacterized protein
K4CA95	1.478	1.045	1.215	1.512	Uncharacterized protein
K4C961	1.475	1.015	1.417	1.603	Uncharacterized protein
K4D5F8	1.475	0.968	1.202	1.347	Uncharacterized protein
K4B3I4	1.475	1.033	1.553	1.806	Response to dessication 2
K4BBN2	1.474	0.892	0.919	1.196	Uncharacterized protein
K4C762	1.472	1.076	1.707	2.160	Uncharacterized protein
K4CM80	1.472	1.061	1.374	1.718	Uncharacterized protein
K4DFV6	1.471	1.079	1.836	3.181	Uncharacterized protein
K4BA43	1.471	1.089	1.245	1.149	Uncharacterized protein
K4B030	1.470	0.884	1.222	2.465	Uncharacterized protein
K4C950	1.469	1.201	1.600	1.863	Uncharacterized protein
K4BJ07	1.469	0.977	1.008	1.447	Uncharacterized protein
K4BKZ5	1.469	0.952	1.050	1.193	Uncharacterized protein
K4C4N6	1.468	0.963	1.127	1.326	Uncharacterized protein
K4BZC4	1.468	0.926	1.028	1.320	Uncharacterized protein
K4CDQ9	1.468	1.243	1.721	1.589	Uncharacterized protein
K4CIY9	1.467	1.079	1.400	1.392	Uncharacterized protein
K4CLQ6	1.467	1.113	1.560	1.959	Phospholipase D
K4CGL2	1.467	1.041	1.552	2.774	Uncharacterized protein
K4D0E5	1.466	1.321	1.861	1.936	D-3-phosphoglycerate dehydrogenase
K4C2D6	1.466	1.179	1.446	2.194	60S acidic ribosomal protein P0
K4B371	1.466	0.942	1.291	2.115	Uncharacterized protein
K4BSH6	1.466	1.275	1.104	0.958	Uncharacterized protein
K4BLU5	1.465	0.988	1.078	1.316	Uncharacterized protein
K4BT42	1.465	1.071	1.478	2.261	Uncharacterized protein
K4CMY8	1.465	1.164	1.589	1.151	Secretory carrier-associated membrane protein
K4D126	1.465	0.968	0.986	1.133	Uncharacterized protein
K4CQN4	1.465	1.082	1.513	2.343	Uncharacterized protein
K4CA36	1.464	0.991	1.299	2.104	Uncharacterized protein
K4BTQ4	1.463	0.946	0.949	1.112	Uncharacterized protein
K4D9S3	1.462	1.105	1.202	1.125	Uncharacterized protein
K4CHC5	1.462	0.937	1.061	1.639	Uncharacterized protein
K4BV28	1.462	0.975	1.315	1.892	Uncharacterized protein
K4BP55	1.460	1.069	1.041	1.126	Uncharacterized protein
K4D955	1.460	0.930	0.929	1.040	Uncharacterized protein
K4BK90	1.459	1.066	1.366	1.595	Uncharacterized protein
K4CHV3	1.459	1.004	1.276	1.608	Uncharacterized protein
Q38JE1	1.459	0.900	1.194	1.791	Temperature-induced lipocalin
K4BGT4	1.458	1.017	1.148	1.133	Uncharacterized protein
K4BA68	1.457	1.060	1.267	1.248	Uncharacterized protein
K4B3G5	1.457	1.072	1.517	1.891	Uncharacterized protein
Q40143	1.457	0.852	1.640	3.503	Cysteine proteinase 3
K4CPF3	1.457	1.069	1.039	1.033	2-C-methyl-D-erythritol 2,4-cyclodiphosphate synthase
K4BUC6	1.457	1.042	1.313	1.602	Ubiquitin-fold modifier-conjugating enzyme 1
K4CPR0	1.457	1.502	2.383	3.139	Uncharacterized protein
K4B7I5	1.456	1.131	1.418	1.235	Uncharacterized protein

Accession	Burned	Control	Regular	Limit	Description
K4BP05	1.456	0.910	0.956	0.931	Uncharacterized protein
K4BPB0	1.455	0.879	0.780	1.002	Uncharacterized protein
K4AZG9	1.455	1.173	1.415	1.587	Uncharacterized protein
A0RZD0	1.454	0.876	1.966	4.913	Inducible plastid-lipid associated protein
K4CRN4	1.453	1.226	1.281	1.195	Uncharacterized protein
K4C755	1.453	0.949	1.011	1.116	Uncharacterized protein
K4CJ02	1.453	0.975	1.322	0.925	Uncharacterized protein
K4BZW9	1.453	1.021	1.231	1.686	Uncharacterized protein
K4CMS0	1.452	1.029	1.162	1.355	Uncharacterized protein
Q2MI58	1.452	1.053	1.302	1.504	50S ribosomal protein L23, chloroplastic
K4ATA6	1.451	1.143	1.354	1.913	Uncharacterized protein
K4B418	1.451	1.092	1.492	1.453	Uncharacterized protein
K4D0H9	1.451	1.008	1.016	1.217	Uncharacterized protein
K4C779	1.451	1.255	1.673	2.039	Uncharacterized protein
K4AXA9	1.450	0.948	1.053	1.190	Uncharacterized protein
Q9LKW2	1.450	1.087	1.426	1.823	Putative uncharacterized protein
K4B476	1.450	1.029	1.192	1.360	Uncharacterized protein
K4C9N2	1.449	0.988	0.937	0.958	Uncharacterized protein
K4D2D7	1.449	1.279	1.986	2.304	Uncharacterized protein
K4D297	1.448	0.963	1.372	2.128	Glutamate dehydrogenase
K4C2Q2	1.448	1.207	1.356	1.715	Uncharacterized protein
K4CGD8	1.447	1.144	1.326	1.741	Transmembrane 9 superfamily member
K4BW18	1.447	1.004	1.057	1.001	Chlorophyll a-b binding protein, chloroplastic
Q9LEG1	1.446	1.363	7.002	7.725	Cathepsin D Inhibitor
Q9AXQ6	1.446	0.994	1.238	1.562	Eukaryotic translation initiation factor 5A-1
K4DGM6	1.446	0.925	1.215	1.454	Uncharacterized protein
K4BAF0	1.445	0.885	0.905	0.939	Uncharacterized protein
K4BKI1	1.445	1.031	1.093	1.088	Uncharacterized protein
K4DFH0	1.445	0.953	1.170	1.299	Uncharacterized protein
K4B2B1	1.444	1.048	2.736	1.998	Uncharacterized protein
K4BKN0	1.444	0.992	1.088	1.094	NAD(P)H-hydrate epimerase
C6KI36	1.443	1.268	1.507	1.009	Starch synthase III
K4B1A8	1.442	0.952	0.947	1.326	Uncharacterized protein
K4CXM0	1.441	1.727	1.339	0.814	Uncharacterized protein
K4AT23	1.441	0.857	0.800	0.898	Uncharacterized protein
A2SXR3	1.440	1.003	1.367	1.905	Uricase
K4CWZ4	1.440	1.125	1.324	1.415	Uncharacterized protein
K4CSN4	1.439	1.377	1.525	1.107	Uncharacterized protein
K4BJZ4	1.439	0.981	1.591	2.463	Uncharacterized protein
K4BLP9	1.438	1.095	1.253	1.383	Uncharacterized protein
K4CNH2	1.438	1.072	1.347	1.597	Uncharacterized protein
K4C252	1.436	1.031	1.089	1.332	Uncharacterized protein
K4DEU5	1.436	1.386	1.812	1.692	Uncharacterized protein
K4BRN5	1.436	1.053	1.255	1.623	Uncharacterized protein
K4BZ70	1.436	1.060	1.207	1.578	Uncharacterized protein
K4D2T9	1.435	0.851	0.760	0.966	Uncharacterized protein
K4BN81	1.435	1.394	1.783	1.768	D-3-phosphoglycerate dehydrogenase
K4BVZ3	1.434	1.008	1.121	1.107	Peptidylprolyl isomerase
Q2MIB0	1.434	1.269	1.352	1.119	DNA-directed RNA polymerase subunit beta''
K4B427	1.434	1.023	1.177	1.583	S-phase kinase-associated protein 1
K4D347	1.433	1.079	1.341	1.044	Uncharacterized protein
K4BI68	1.431	1.052	1.190	2.081	Uncharacterized protein

Accession	Burned	Control	Regular	Limit	Description
K4CFR0	1.429	1.213	1.560	1.784	Uncharacterized protein
K4AX61	1.429	0.944	1.037	1.262	Uncharacterized protein
K4BKN1	1.428	1.277	1.638	1.622	Uncharacterized protein
K4CI48	1.428	1.123	1.182	0.987	Uncharacterized protein
P17340	1.428	0.742	0.684	0.578	Plastocyanin, chloroplastic
K4ATA1	1.428	1.027	1.107	1.300	Uncharacterized protein
K4CL50	1.428	1.163	1.584	1.928	Aminopeptidase
K4AYW1	1.427	1.127	1.110	0.926	Uncharacterized protein
K4CUW3	1.427	1.223	1.607	1.894	Uncharacterized protein
K4CXP8	1.425	1.100	1.405	1.628	Uncharacterized protein
K4B504	1.424	1.184	1.536	1.970	Uncharacterized protein
Q2MI65	1.424	1.288	1.443	1.204	30S ribosomal protein S8, chloroplastic
K4BM58	1.424	1.081	1.303	1.386	Uncharacterized protein
K4B7S8	1.423	0.929	1.109	1.139	Uncharacterized protein
K4BI97	1.422	1.041	1.198	1.408	Uncharacterized protein
K4B5D7	1.422	1.033	1.173	0.971	Uncharacterized protein
K4C8V8	1.421	1.084	1.372	1.877	Uncharacterized protein
P04284	1.421	1.063	4.075	8.210	Pathogenesis-related leaf protein 6
K4C047	1.421	1.062	1.286	1.348	Uncharacterized protein
K4BKH7	1.420	1.002	1.267	1.344	Uncharacterized protein
K4C263	1.420	1.188	1.644	1.778	Uncharacterized protein
K4D258	1.420	0.961	0.996	1.157	Uncharacterized protein
Q941P9	1.419	1.043	1.102	1.955	Non-symbiotic hemoglobin 2
K4D300	1.419	1.021	1.272	1.682	Proteasome subunit alpha type
K4BW27	1.418	1.045	1.044	1.211	Uncharacterized protein
K4CJT5	1.418	0.935	1.088	1.213	Uncharacterized protein
K4CIH0	1.418	1.280	1.434	2.011	Transmembrane 9 superfamily member
Q94K24	1.418	1.013	1.229	1.251	Ran binding protein-1
K4BRA1	1.418	1.079	1.147	1.298	Uncharacterized protein
K4BF16	1.417	1.074	1.544	1.697	Uncharacterized protein
K4BR52	1.417	1.244	1.606	1.891	Uncharacterized protein
K4CGZ7	1.417	0.735	0.504	0.368	Glutamyl-tRNA(Gln) amidotransferase subunit C, chloroplastic/mitochondrial
K4BTJ3	1.416	1.060	1.503	1.791	Uncharacterized protein
K4BBU9	1.416	1.365	1.890	2.425	Uncharacterized protein
K4CHJ6	1.416	1.421	2.190	2.517	40S ribosomal protein S8
K4C9B4	1.416	1.149	1.384	1.320	Serine/threonine-protein phosphatase
K4B803	1.416	1.031	1.115	1.136	Uncharacterized protein
K4CX59	1.416	1.254	1.661	1.755	Uncharacterized protein
K4D331	1.416	1.114	1.396	1.824	NADH-cytochrome b5 reductase
K4C807	1.416	1.192	1.440	1.566	Uncharacterized protein
K4CV95	1.415	1.280	1.122	1.028	Uncharacterized protein
Q8H6B5	1.415	1.040	1.391	2.316	Putative dehydrogenase
K4B7S7	1.414	0.928	1.106	1.137	Uncharacterized protein
K4BF34	1.414	1.166	1.284	1.488	Uncharacterized protein
K4CNT6	1.413	1.214	1.156	0.982	Uncharacterized protein
K4B9M8	1.413	0.933	1.093	1.208	Uncharacterized protein
K4B9R3	1.412	1.249	1.649	1.746	Uncharacterized protein
Q8SA58	1.412	1.035	1.652	2.239	Putative uncoupling protein
K4CI75	1.411	1.126	1.287	1.327	Uncharacterized protein
K4CMM8	1.411	1.214	2.381	2.414	Uncharacterized protein

Accession	Burned	Control	Regular	Limit	Description
K4CL75	1.411	1.386	1.816	2.105	Uncharacterized protein
K4BM85	1.411	1.258	1.661	2.408	Uncharacterized protein
K4BC75	1.411	0.976	0.990	1.175	Uncharacterized protein
K4BY66	1.411	0.835	0.956	0.907	Protein DETOXIFICATION
K4C882	1.410	1.253	1.657	2.393	Uncharacterized protein
K4D5H3	1.410	0.936	1.278	1.182	Peroxidase
K4B407	1.410	0.982	1.237	1.777	Proteasome subunit alpha type
K4C108	1.410	1.023	1.024	1.386	Phosphomannomutase
K4CQE3	1.409	1.203	1.404	1.562	Uncharacterized protein
K4BVV3	1.409	1.040	1.270	1.245	Uncharacterized protein
K4ATC4	1.409	1.137	1.368	1.291	Serine/threonine-protein phosphatase
K4CEB8	1.409	1.068	1.102	1.419	Eukaryotic translation initiation factor 3 subunit K
K4DHQ6	1.409	1.095	1.424	1.456	Uncharacterized protein
G8Z246	1.408	0.826	0.744	0.816	Hop-interacting protein THI002
K4D3W3	1.407	0.962	1.112	1.086	Uncharacterized protein
K4C1P5	1.407	0.870	1.191	1.481	Uncharacterized protein
K4BWK4	1.407	0.935	1.091	1.046	Uncharacterized protein
K4CIE2	1.405	0.829	0.938	1.068	Peptidylprolyl isomerase
K4CYE5	1.405	1.146	1.310	1.400	Uncharacterized protein
K4DHT1	1.405	0.988	1.027	1.093	Dihydrolipoyl dehydrogenase
K4B7B8	1.405	0.977	1.175	2.515	Uncharacterized protein
K4C8I0	1.405	0.957	1.091	1.501	Uncharacterized protein
K4D3I3	1.404	1.354	1.438	1.269	S-adenosylmethionine synthase
K4CW45	1.404	1.108	1.225	1.316	Uncharacterized protein
K4BA08	1.404	0.993	1.053	1.455	Uncharacterized protein

Accession	Burned	Control	Regular	Limit	Description
K4BP76	1.403	1.234	1.202	1.013	Uncharacterized protein
K4CVX4	1.403	1.005	2.438	3.122	Uncharacterized protein
K4B4Z2	1.403	1.121	1.498	1.607	Uncharacterized protein
K4B7E7	1.402	1.195	1.617	1.683	Uncharacterized protein
Q9AXQ3	1.401	0.992	1.207	1.509	Eukaryotic translation initiation factor 5A-4
D2CV80	1.401	1.221	0.835	0.693	Cytochrome P450-type monooxygenase 97A29
Q04108	1.401	1.062	4.051	8.199	Pathogenesis-related leaf protein 4
A9LRT7	1.400	1.028	1.347	1.898	Isopentenyl diphosphate isomerase
K4BG16	1.399	1.072	1.561	1.576	Uncharacterized protein
K4DAX1	1.398	0.961	1.003	1.147	Uncharacterized protein
K4DBZ1	1.398	1.149	1.376	1.149	Uncharacterized protein
K4ASY4	1.398	1.148	1.431	1.562	Uncharacterized protein
K4CZP2	1.397	1.142	1.885	2.005	Uncharacterized protein
K4DFE6	1.397	1.152	0.857	1.220	Malic enzyme
K4B1M0	1.397	1.172	1.668	1.776	Methionine S-methyltransferase
K4B6Q3	1.396	1.343	1.822	2.321	Uncharacterized protein
K4BKB8	1.395	0.993	1.241	1.679	Uncharacterized protein
K4BWI5	1.395	1.214	1.692	1.679	Serine/threonine-protein phosphatase
K4DEQ8	1.395	1.177	1.306	1.631	Uncharacterized protein
K4CA11	1.394	0.972	0.913	1.085	Uncharacterized protein
K4BMW6	1.394	0.999	1.079	1.005	Uncharacterized protein
K4D5U3	1.394	1.095	1.540	2.191	Glutamine synthetase
K4CUY3	1.394	0.822	0.818	0.702	Uncharacterized protein
K4D399	1.394	1.145	1.427	1.556	Uncharacterized protein
K4C227	1.393	1.009	1.240	1.753	Uncharacterized protein

Accession	Burned	Control	Regular	Limit	Description
K4B6F2	1.392	0.936	1.064	1.036	Uncharacterized protein
K4DAP9	1.392	1.064	1.149	1.155	Serine/threonine-protein phosphatase
K4BQ51	1.392	1.531	1.229	1.004	Mg-protoporphyrin IX chelatase
K4BTL0	1.392	0.991	1.321	1.561	Uncharacterized protein
K4CN56	1.391	0.961	1.158	1.088	Uncharacterized protein
K4CNW6	1.390	0.976	0.908	1.226	Uncharacterized protein
K4CIZ7	1.390	1.034	1.273	1.186	Uncharacterized protein
K4CVC2	1.390	1.054	1.385	1.555	Uncharacterized protein
K4BDW9	1.390	1.007	1.431	1.541	Uncharacterized protein
K4CIH6	1.389	1.226	1.527	1.268	Uncharacterized protein
K4B6T0	1.389	0.901	0.862	0.985	Uncharacterized protein
K4CPS8	1.389	1.069	1.163	2.021	Uncharacterized protein
K4CAC2	1.389	1.452	1.957	1.924	Uncharacterized protein
K4C6T9	1.389	0.988	1.021	1.075	Uncharacterized protein
K4BX09	1.388	1.322	1.823	1.376	Uncharacterized protein
K4DCW2	1.388	0.892	0.989	1.205	Uncharacterized protein
K4BMW3	1.388	0.995	1.271	1.584	Uncharacterized protein
K4BIE9	1.387	0.908	1.149	1.037	Uncharacterized protein
K4DGU3	1.387	1.103	1.181	1.206	Polyadenylate-binding protein
K4CAH3	1.387	1.436	2.245	2.547	40S ribosomal protein S8
K4BI65	1.387	0.791	0.775	0.889	Uncharacterized protein
K4B433	1.387	1.253	1.616	1.622	Uncharacterized protein
K4BJ57	1.386	1.304	2.071	2.534	Uncharacterized protein
K4BCQ9	1.386	1.083	1.513	2.461	Uncharacterized protein
K4CSC5	1.386	0.994	1.092	1.151	Uncharacterized protein
K4CU99	1.386	0.882	1.010	1.114	Uncharacterized protein
K4CB98	1.385	0.853	1.061	0.891	Cytochrome c oxidase subunit
K4BP98	1.385	0.849	0.888	1.008	Uncharacterized protein
K4D925	1.384	1.295	2.432	2.768	Uncharacterized protein
K4CRV2	1.383	1.135	1.286	1.576	Uncharacterized protein
K4B031	1.383	0.885	1.105	1.579	Uncharacterized protein
K4C2B1	1.383	1.116	1.326	1.444	Uncharacterized protein
K4C5J9	1.383	1.040	1.104	1.396	Uncharacterized protein
K4DD22	1.382	0.916	1.015	1.009	Uncharacterized protein
K4CMZ2	1.382	1.116	1.239	1.043	Uncharacterized protein
K4CET1	1.381	1.056	1.235	1.939	Uncharacterized protein
K4AZU6	1.381	1.180	1.357	1.409	Uncharacterized protein
K4CWS6	1.381	1.043	1.432	2.074	Glycosyltransferase
K4DGE8	1.380	1.424	1.974	1.359	Uncharacterized protein
K4C2U0	1.380	1.048	1.355	1.823	Proteasome subunit beta type
K4C273	1.379	1.076	1.438	2.033	Uncharacterized protein
K4D5I0	1.378	0.944	1.173	1.665	Uncharacterized protein
K4DGM3	1.378	0.963	0.970	1.162	Uncharacterized protein
K4D9P9	1.377	1.107	1.174	1.348	Uncharacterized protein
K4CQL9	1.377	1.028	1.038	1.127	Uncharacterized protein
K4AZL9	1.376	1.061	1.565	1.558	Cysteine synthase
K4CXD9	1.376	1.421	2.192	2.491	40S ribosomal protein S8
K4AY40	1.375	1.034	1.153	0.967	Uncharacterized protein
K4CGM9	1.375	0.980	1.114	1.245	Uncharacterized protein
K4AXA7	1.374	1.030	1.167	1.304	Uncharacterized protein
K4CLJ1	1.374	1.163	1.176	0.805	Uncharacterized protein
K4D4V8	1.374	1.038	1.490	1.705	Uncharacterized protein
K4D6C1	1.374	1.126	1.251	1.282	Uncharacterized protein
K4BPH8	1.373	1.084	1.670	2.538	Uncharacterized protein
K4BCV6	1.373	1.242	1.400	1.472	Uncharacterized protein
K4AX85	1.372	1.015	1.022	1.079	Uncharacterized protein

Accession	Burned	Control	Regular	Limit	Description
K4CR11	1.372	1.121	1.249	1.174	Uncharacterized protein
K4C2E1	1.372	1.174	2.642	4.661	Uncharacterized protein
K4B9Y9	1.372	1.071	1.454	1.425	Uncharacterized protein
K4CMS1	1.371	1.100	1.460	1.472	Ubiquinol oxidase
K4BNF1	1.369	0.949	1.360	1.265	Purple acid phosphatase
Q7Y240	1.369	1.036	1.599	1.926	Thioredoxin peroxidase 1
K4BQ85	1.369	1.137	1.707	2.318	Uncharacterized protein
Q84K11-2	1.368	1.154	1.300	1.506	Isoform 2 of Serine/threonine-protein phosphatase 5
P27058	1.368	0.972	1.145	0.974	Systemin
K4C3U7	1.368	1.118	1.413	1.660	Uncharacterized protein
K4DH66	1.367	1.217	1.487	1.223	Serine hydroxymethyltransferase
K4CWX5	1.367	1.252	1.469	1.403	Uncharacterized protein
Q41328	1.367	1.095	1.469	1.468	Pto-interacting protein 1
K4BJC8	1.367	0.834	0.893	1.251	Uncharacterized protein
K4C1X2	1.367	1.082	1.190	1.301	Folylpolyglutamate synthase
K4AYV8	1.365	1.065	1.388	1.939	Uncharacterized protein
Q9ZS45	1.365	1.048	1.123	1.774	Spermidine synthase
Q9FZ05	1.364	0.871	1.325	1.099	Xyloglucan endotransglucosylase/hydrolase
K4B1S4	1.364	1.063	1.336	1.674	Coatomer subunit delta
K4BCT2	1.364	0.976	1.074	1.501	Uncharacterized protein
K4BQ77	1.363	1.294	1.042	0.775	Uncharacterized protein
K4CSD5	1.363	1.069	1.207	1.240	Ubiquitin carboxyl-terminal hydrolase
K4CXY8	1.362	1.149	1.448	1.706	Acyl-coenzyme A oxidase
K4BU44	1.362	1.007	1.086	1.578	Uncharacterized protein
K4C744	1.362	1.110	1.534	1.614	Uncharacterized protein
K4DAN1	1.362	0.916	1.090	0.808	Uncharacterized protein
K4CGE8	1.361	1.037	1.369	1.726	Uncharacterized protein
K4B489	1.361	1.011	1.429	1.817	Uncharacterized protein
K4C2D7	1.361	1.170	1.248	1.766	Uncharacterized protein
K4BPC0	1.360	1.092	1.370	1.665	Diphosphomevalonate decarboxylase
K4C7N4	1.360	1.229	1.508	2.145	Uncharacterized protein
K4AYM7	1.360	1.305	1.608	1.907	Eukaryotic translation initiation factor 3 subunit B
K4C1K6	1.360	0.973	1.146	0.974	Uncharacterized protein
Q41339	1.360	1.078	1.430	1.990	Small GTP-binding protein
K4CFW4	1.360	0.928	0.934	1.140	Uncharacterized protein
K4D530	1.359	1.267	1.673	2.250	Pyruvate kinase
K4B7P5	1.358	0.978	0.992	0.977	Peptidylprolyl isomerase
K4CN74	1.358	1.413	1.295	1.005	Uncharacterized protein
K4BG89	1.356	1.078	1.219	1.317	Uncharacterized protein
K4B277	1.356	0.866	1.260	1.166	Peroxidase
K4C3T2	1.355	0.876	1.410	3.118	Uncharacterized protein
K4B0G4	1.355	1.125	1.410	0.941	Uncharacterized protein
K4CRR7	1.355	0.969	1.061	0.792	Uncharacterized protein
K4BA95	1.355	1.036	1.171	1.799	Thioredoxin reductase
K4BRT9	1.355	0.998	1.049	1.368	Uncharacterized protein
K4CV19	1.355	1.229	1.438	1.161	Uncharacterized protein
K4C5W1	1.354	1.065	1.267	1.536	Uncharacterized protein
K4BLI1	1.354	1.110	1.411	1.293	Uncharacterized protein
K4CMT7	1.353	1.090	1.251	1.768	60S ribosomal protein L13
K4D025	1.352	1.012	1.123	1.354	Uncharacterized protein

Accession	Burned	Control	Regular	Limit	Description
K4BMV1	1.351	0.811	0.760	0.875	Uncharacterized protein
K4C868	1.351	1.201	1.216	1.033	Uncharacterized protein
K4BMZ4	1.350	1.001	1.184	1.529	Uncharacterized protein
K4CQU8	1.350	1.214	1.236	0.844	Uncharacterized protein
K4CWR4	1.349	1.294	1.621	2.087	Adenosylhomocysteinase
K4B8T1	1.349	0.946	1.153	1.383	Uncharacterized protein
K4CF29	1.349	1.134	1.254	1.397	Uncharacterized protein
K4B5E3	1.349	0.984	1.066	1.362	Uncharacterized protein
K4DHC5	1.348	1.028	1.225	2.241	Uncharacterized protein
K4AZE2	1.348	1.034	1.305	1.375	Uncharacterized protein
K4D5K6	1.348	1.116	1.619	2.037	ATP-dependent 6-phosphofructokinase
K4BNB5	1.348	1.018	1.154	1.183	Uncharacterized protein
K4AT05	1.347	0.884	1.084	1.654	Uncharacterized protein
K4C7V4	1.347	1.048	1.222	1.139	Uncharacterized protein
K4BXJ9	1.346	1.136	1.494	2.141	Uncharacterized protein
K4BLQ1	1.346	1.091	1.422	1.757	Uncharacterized protein
K4CRI4	1.345	1.141	1.587	2.261	Uncharacterized protein
K4BLA0	1.345	1.412	0.853	0.680	Uncharacterized protein
K4DB58	1.345	0.939	1.265	2.280	Uncharacterized protein
K4BFE4	1.344	1.222	1.597	1.726	Uncharacterized protein
K4B267	1.344	0.920	1.040	0.957	Uncharacterized protein
K4B0G3	1.344	1.257	1.650	1.957	Uncharacterized protein
K4C2F8	1.344	1.094	1.707	2.599	Uncharacterized protein
K4CEY6	1.343	1.050	1.381	1.969	Uncharacterized protein
K4B0D9	1.343	1.076	2.265	3.292	Uncharacterized protein
Q9SPD5	1.343	1.235	1.656	1.632	Plasma membrane ATPase
K4BJK1	1.342	1.270	2.245	2.710	Uncharacterized protein
K4B302	1.342	0.894	0.941	1.206	Uncharacterized protein

Accession	Burned	Control	Regular	Limit	Description
K4CY71	1.341	1.114	1.327	1.262	Uncharacterized protein
K4C3D8	1.341	1.411	2.153	2.435	40S ribosomal protein S8
K4BBE3	1.341	1.030	1.092	0.861	Uncharacterized protein
K4BDK9	1.340	1.110	1.304	1.511	Uncharacterized protein
K4D1U0	1.340	1.023	1.141	2.102	Uncharacterized protein
K4B7P2	1.339	0.917	1.207	2.454	Uncharacterized protein
Q2MI99	1.339	1.004	0.845	0.819	Photosystem I assembly protein Ycf3
K4DAF9	1.339	1.012	1.314	1.232	Uncharacterized protein
K4DH61	1.339	1.139	1.499	1.951	ATP-dependent 6-phosphofructokinase
K4CLC9	1.338	1.236	1.484	1.175	Serine hydroxymethyltransferase
B1Q3F2	1.338	1.164	1.792	1.884	Glutamate decarboxylase
K4DEI9	1.338	1.093	1.223	1.241	Uncharacterized protein
K4B0E1	1.338	1.039	1.527	2.136	Annexin
K4C203	1.337	1.089	1.471	1.454	Uncharacterized protein
K4BVE2	1.337	1.007	1.018	0.921	50S ribosomal protein L31
K4AXJ9	1.336	1.027	1.397	2.135	Uncharacterized protein
K4C2K1	1.336	0.880	1.222	1.001	Uncharacterized protein
K4B2P1	1.336	1.125	1.127	1.076	Uncharacterized protein
K4CBE9	1.335	1.005	1.073	1.033	Uncharacterized protein
K4BBN6	1.335	1.005	1.036	1.250	Alpha-mannosidase
K4C9P9	1.335	1.260	1.572	1.256	Uncharacterized protein
K4DDC7	1.334	0.944	1.017	1.664	Uncharacterized protein
K4CNT4	1.334	1.013	1.298	1.801	Uncharacterized protein
K4BN29	1.334	0.984	1.494	3.136	Uncharacterized protein
K4BDB0	1.333	0.894	0.867	0.991	Uncharacterized protein
K4B8W9	1.332	0.912	1.356	1.030	Uncharacterized protein

Accession	Burned	Control	Regular	Limit	Description
K4CNF1	1.332	1.220	2.083	2.430	Isocitrate dehydrogenase [NAD] subunit, mitochondrial
K4BD23	1.332	0.936	1.204	1.504	Uncharacterized protein
K4BD39	1.332	1.307	1.731	2.080	Uncharacterized protein
K4B860	1.331	1.195	1.466	1.461	Uncharacterized protein
K4AXX4	1.331	1.007	0.931	0.859	Uncharacterized protein
K4CZS1	1.329	1.062	1.385	1.785	Uncharacterized protein
K4B2T3	1.329	1.081	1.350	1.658	Uncharacterized protein
K4D3A3	1.328	0.973	1.147	1.289	Uncharacterized protein
K4D5D8	1.328	1.071	0.832	0.873	Uncharacterized protein
K4BVN6	1.327	1.089	1.305	1.797	Uncharacterized protein
P52884	1.327	1.031	1.401	2.132	GTP-binding protein SAR2
K4D810	1.327	1.293	1.472	1.549	Uncharacterized protein
K4CLM9	1.327	0.846	0.728	0.768	Uncharacterized protein
Q42884	1.326	1.204	1.372	1.335	Chorismate synthase 1, chloroplastic
K4CRG0	1.326	1.127	1.310	1.395	Uncharacterized protein
K4AZJ1	1.326	1.109	1.315	1.312	Uncharacterized protein
K4BL38	1.326	1.175	1.314	1.646	Uncharacterized protein
K4BJL6	1.325	0.958	0.869	1.241	Uncharacterized protein
K4CPG6	1.325	1.148	0.974	0.970	Uncharacterized protein
K4CPR3	1.324	1.542	2.403	2.737	Uncharacterized protein
K4D340	1.324	1.063	1.468	1.623	Uncharacterized protein
K4C2V1	1.324	0.925	0.991	1.078	Uncharacterized protein
K4BFI7	1.323	0.869	0.900	0.840	Uncharacterized protein
K4BDE0	1.323	1.023	1.160	1.262	Uncharacterized protein
K4D4P8	1.322	1.015	1.034	1.280	Uncharacterized protein
K4BFH1	1.322	1.049	1.161	1.664	Thioredoxin reductase
K4BVD6	1.322	0.993	1.253	1.465	Uncharacterized protein

Accession	Burned	Control	Regular	Limit	Description
K4CN15	1.322	0.825	0.779	0.960	Uncharacterized protein
K4B9J8	1.321	1.099	1.167	1.060	Uncharacterized protein
K4BEP5	1.321	1.178	1.803	1.553	Uncharacterized protein
K4BPT1	1.321	1.095	1.579	1.974	ATP-dependent 6-phosphofructokinase
K4C849	1.321	0.795	1.011	1.177	Uncharacterized protein
K4CVS3	1.319	1.238	1.287	1.344	Pyruvate kinase
K4C5M1	1.319	1.067	1.279	1.793	Uncharacterized protein
K4D6Y2	1.319	1.075	0.850	0.774	Uncharacterized protein
K4CS37	1.318	1.064	1.196	2.227	Uncharacterized protein
K4BMF0	1.318	1.096	1.238	1.561	Uncharacterized protein
K4BVA5	1.318	0.941	1.233	1.544	Uncharacterized protein
K4C8T6	1.318	1.233	1.659	1.676	Serine/threonine-protein phosphatase
G8Z271	1.317	1.348	1.607	1.083	Hop-interacting protein THI044
K4BPJ4	1.317	1.170	1.251	1.732	Uncharacterized protein
Q9SDZ6	1.316	1.167	1.790	2.467	Phospholipase D alpha (Fragment)
K4AZC8	1.316	1.040	1.156	1.667	ATPase ASNA1 homolog
K4CYU9	1.315	1.401	1.958	2.278	Uncharacterized protein
K4AXY5	1.315	1.122	1.235	1.984	Uncharacterized protein
K4BYA2	1.314	0.980	1.238	1.465	Uncharacterized protein
K4AZQ1	1.313	1.093	1.176	1.370	Uncharacterized protein
K4BJY3	1.313	0.868	1.058	1.438	Uncharacterized protein
K4CWE4	1.313	1.005	1.229	1.725	Uncharacterized protein
K4CC51	1.311	1.005	1.137	1.415	Uncharacterized protein
K4D6T1	1.309	1.221	1.240	1.245	Uncharacterized protein
K4CMT6	1.309	0.841	0.925	0.902	Uncharacterized protein
K4CAI5	1.309	0.974	1.080	1.420	Uncharacterized protein
K4CXB5	1.308	0.873	0.795	0.841	Uncharacterized protein

Accession	Burned	Control	Regular	Limit	Description
K4B7U1	1.307	1.127	1.284	1.594	Coatomer subunit epsilon
K4BZT8	1.307	0.921	1.140	1.394	Uncharacterized protein
K4BUT9	1.307	0.840	1.522	2.856	Uncharacterized protein
K4CMQ6	1.307	0.981	1.096	1.645	Uncharacterized protein
K4B169	1.305	1.029	1.418	2.178	Uncharacterized protein
K4D2B6	1.305	0.977	1.323	1.462	Uncharacterized protein
K4B3K2	1.304	1.016	1.210	1.674	Uncharacterized protein
K4BVF6	1.303	1.217	1.237	1.100	Uncharacterized protein
K4CTF7	1.303	1.013	1.173	2.007	Peptidylprolyl isomerase
K4CJY1	1.303	1.166	1.359	1.065	Uncharacterized protein
K4CT32	1.302	1.083	1.146	1.308	Uncharacterized protein
K4BVH5	1.301	0.946	1.161	3.192	Uncharacterized protein
K4DA40	1.300	1.107	1.267	1.608	Uncharacterized protein
K4CNF2	1.300	1.216	2.061	2.404	Isocitrate dehydrogenase [NAD] subunit, mitochondrial
K4C8R3	1.300	1.071	1.067	1.284	Uncharacterized protein
K4AXR6	1.300	0.950	1.232	2.063	Uncharacterized protein
K4CE78	1.300	0.960	1.137	1.434	Uncharacterized protein
K4C7I8	1.300	1.315	1.644	1.884	60S ribosomal protein L18a
K4DH88	1.300	1.082	1.237	1.737	60S ribosomal protein L13
K4BXG7	1.299	1.095	1.117	0.903	Uncharacterized protein
K4BDQ9	1.299	1.259	1.637	1.347	Acetyl-coenzyme A synthetase
K4AZ98	1.299	1.227	1.399	1.385	Uncharacterized protein
K4CCD7	1.299	1.061	1.432	2.031	Proteasome subunit beta type
K4B7E0	1.298	1.128	1.524	2.293	Chloride channel protein
K4B2Y6	1.297	0.949	1.166	2.029	Uncharacterized protein
K4DFH8	1.297	1.043	1.285	1.580	Uncharacterized protein
K4BT93	1.297	0.997	1.029	1.068	Uncharacterized protein
K4CU73	1.297	0.923	1.120	1.336	Uncharacterized protein
Q9SWW0	1.296	0.960	1.162	1.330	Elongation factor Ts, mitochondrial
K4BB89	1.296	1.039	1.439	1.398	Uncharacterized protein
K4B3F3	1.295	0.936	1.181	1.169	Uncharacterized protein
K4BIM9	1.294	1.192	1.594	1.941	ATP-dependent 6-phosphofructokinase
K4B7W0	1.294	1.081	1.151	1.184	Uncharacterized protein
K4C793	1.294	1.384	2.045	2.122	Ribosomal protein L15
K4BTC4	1.294	1.138	1.449	1.370	Uncharacterized protein
B2MWN0	1.294	1.074	1.187	1.416	D-cysteine desulfhydrase
K4D557	1.293	1.057	1.221	1.096	Uncharacterized protein
K4CVQ7	1.292	0.908	2.697	7.192	Uncharacterized protein
K4BC04	1.292	1.093	1.554	1.627	Uncharacterized protein
K4BKH5	1.292	0.916	1.491	1.370	Uncharacterized protein
K4D0V1	1.291	1.342	1.664	3.927	Uncharacterized protein
K4B779	1.291	0.898	1.383	1.470	Uncharacterized protein
K4CGN9	1.291	0.994	1.191	1.195	Uncharacterized protein
K4D2M9	1.291	1.425	1.837	1.745	Eukaryotic translation initiation factor 3 subunit E
K4B0G1	1.291	1.119	1.349	1.493	Uncharacterized protein
K4BSK2	1.291	0.931	1.205	1.387	Uncharacterized protein
K4BNY7	1.291	1.161	1.556	1.406	Glycosyltransferase
K4C502	1.291	1.028	1.250	1.367	Uncharacterized protein
K4C8H8	1.290	0.908	1.470	1.333	Uncharacterized protein
K4D6L1	1.290	1.113	1.292	1.666	Eukaryotic translation initiation factor 3 subunit I

Accession	Burned	Control	Regular	Limit	Description
K4CWL0	1.290	0.995	1.597	3.324	Uncharacterized protein
K4AXB5	1.290	1.037	1.663	2.342	Uncharacterized protein
K4BU77	1.290	1.202	1.293	1.085	Uncharacterized protein
K4DFB8	1.290	1.111	1.144	1.250	Uncharacterized protein
K4BIU4	1.289	0.927	1.160	1.451	Uncharacterized protein
K4DHS9	1.289	1.113	1.601	1.775	Uncharacterized protein
K4DHN3	1.288	1.228	1.270	1.072	Glycosyltransferase
K4B139	1.287	1.168	1.509	1.822	Uncharacterized protein
K4C841	1.286	0.975	0.966	0.938	Uncharacterized protein
K4BV87	1.286	1.098	1.253	1.096	Glycosyltransferase
K4CP57	1.286	1.080	1.353	2.393	Uncharacterized protein
K4DCZ2	1.286	0.823	1.063	1.243	Uncharacterized protein
K4B5Z5	1.286	1.101	1.103	1.299	Uncharacterized protein
K4BBV6	1.285	1.155	1.375	1.096	Starch synthase, chloroplastic/amyloplastic
K4CRN9	1.285	0.972	1.019	1.368	Uncharacterized protein
K4BG20	1.285	1.296	1.698	2.019	Uncharacterized protein
K4C3B5	1.285	1.161	1.486	2.015	Uncharacterized protein
K4BF35	1.285	1.269	1.539	1.777	Uncharacterized protein
K4CXU9	1.284	1.028	1.333	1.615	Uncharacterized protein
K4B159	1.284	0.964	1.086	1.315	Uncharacterized protein
K4CBV3	1.283	1.237	1.288	1.556	Uncharacterized protein
P22180	1.283	1.227	1.674	1.685	Plasma membrane ATPase 1
K4BWZ2	1.283	1.105	1.239	1.422	Uncharacterized protein
K4BJY1	1.282	1.030	1.294	1.612	Uncharacterized protein
K4B3M9	1.282	0.937	0.782	0.834	Uncharacterized protein
K4BZT0	1.281	0.916	1.373	1.075	Uncharacterized protein
K4BR45	1.281	1.060	1.088	1.641	Uncharacterized protein
K4BYA3	1.281	1.054	1.322	1.802	Proteasome subunit beta type
K4BDU9	1.280	1.205	1.110	1.225	Uncharacterized protein
K4CNY3	1.280	1.005	0.871	1.081	Uncharacterized protein
K4CVA6	1.279	1.230	1.506	1.923	Uncharacterized protein
K4D5G8	1.278	1.386	1.025	1.024	Phospho-2-dehydro-3-deoxyheptonate aldolase
K4B9Y6	1.277	1.118	1.388	1.329	Pyrophosphate--fructose 6-phosphate 1-phosphotransferase subunit beta
K4AT97	1.277	1.101	1.093	1.150	Uncharacterized protein
K4BET8	1.276	0.877	0.854	0.923	Uncharacterized protein
K4B2G7	1.276	1.057	1.400	1.141	Uncharacterized protein
K4CSQ2	1.276	1.290	1.614	1.435	Alpha-1,4 glucan phosphorylase
K4CE22	1.275	0.912	1.034	1.267	Uncharacterized protein
K4BEI8	1.275	1.029	1.257	1.360	Uncharacterized protein
K4B895	1.274	0.912	1.027	1.018	Uncharacterized protein
K4BK44	1.274	0.959	1.056	1.151	Protein-L-isoaspartate O-methyltransferase
O04678	1.274	0.908	1.108	1.225	Subtilisin-like protease
K4C6L0	1.274	1.004	1.330	2.652	Protein disulfide-isomerase
K4BUZ1	1.273	1.067	1.174	1.556	Uncharacterized protein
K4CEL3	1.273	0.919	0.957	1.441	Uncharacterized protein
K4BM64	1.273	0.946	0.928	0.778	Peptidylprolyl isomerase
K4CN80	1.273	1.108	1.103	1.054	Uncharacterized protein
K4D691	1.272	0.764	0.916	0.966	Uncharacterized protein
K4BNB4	1.272	1.023	1.308	1.423	Pyruvate dehydrogenase E1 component subunit alpha

Accession	Burned	Control	Regular	Limit	Description
K4BXH2	1.272	0.964	1.044	1.433	Uncharacterized protein
E5LBC4	1.272	1.069	1.194	1.363	Prephenate aminotransferase
K4B513	1.272	1.077	1.115	1.554	Uncharacterized protein
K4DA96	1.272	0.969	1.095	1.382	Protein disulfide-isomerase
K4B813	1.272	1.224	1.608	1.810	Uncharacterized protein
K4BMJ4	1.271	1.094	1.095	1.417	Uncharacterized protein
Q8VWR0	1.271	0.868	1.564	2.224	Profilin
K4BY65	1.270	1.155	1.240	1.254	Amine oxidase
K4CR69	1.270	0.990	1.110	1.295	Arginine biosynthesis bifunctional protein ArgJ, chloroplastic
K4D4K3	1.270	0.965	1.010	1.218	Uncharacterized protein
K4CSY9	1.270	1.146	1.670	1.229	Uncharacterized protein
K4BXT5	1.269	1.190	1.394	1.292	Uncharacterized protein
K4BL65	1.268	1.307	1.637	1.405	Uncharacterized protein
K4BKW6	1.268	0.977	0.906	1.007	Uncharacterized protein
K4BWQ2	1.268	0.752	0.659	1.017	Ribulose-phosphate 3-epimerase
A8WBX7	1.267	1.161	1.597	1.976	Diphosphomevalonate decarboxylase
K4CP24	1.267	0.946	1.235	1.358	Uncharacterized protein
K4D318	1.267	1.028	1.454	1.444	Uncharacterized protein
K4BQX4	1.266	1.141	1.067	0.930	Uncharacterized protein
K4AZH0	1.265	0.995	0.944	0.819	Uncharacterized protein
Q66YT8	1.265	1.277	1.667	1.161	DWARF1/DIMINUTO
Q8GT30	1.264	0.987	0.958	0.950	Dihydrolipoyl dehydrogenase
K4DAV9	1.263	1.151	1.239	1.389	Arogenate dehydratase
K4BBJ6	1.263	1.195	0.901	0.591	Uncharacterized protein
K4BRG8	1.263	1.122	1.297	1.527	Uncharacterized protein
K4BL04	1.263	1.034	1.232	1.053	Uncharacterized protein
K4DFV5	1.262	0.912	1.275	1.562	Glutathione peroxidase
K4BF57	1.262	1.038	1.307	1.337	Uncharacterized protein
K4D3B7	1.262	0.973	1.313	1.593	Uncharacterized protein
K4CNY2	1.261	0.915	0.989	1.166	Uncharacterized protein
K4BG30	1.261	0.978	2.442	4.451	Peroxidase
K4B4U8	1.261	1.409	1.764	1.402	Uncharacterized protein
H9BYP6	1.260	1.123	1.103	0.901	Sucrose-phosphate synthase B
K4DBI3	1.259	1.309	2.033	2.101	Uncharacterized protein
K4CFX4	1.258	0.816	0.975	0.997	Uncharacterized protein
K4BSB7	1.258	0.968	0.951	1.148	Uncharacterized protein
K4D452	1.258	1.071	1.236	1.668	Uncharacterized protein
K4B2C4	1.257	1.164	1.547	1.345	Uncharacterized protein
K4CJP1	1.257	1.155	1.505	1.466	Methylthioribose-1-phosphate isomerase
K4BP07	1.257	0.990	1.178	1.072	UBX domain-containing protein
K4CEK6	1.256	1.336	1.738	1.372	Uncharacterized protein
Q84MI6	1.255	1.063	1.192	1.283	Mitogen-activated protein kinase
K4BFA5	1.255	1.065	1.376	1.244	Uncharacterized protein
K4BNT6	1.255	1.124	1.319	1.734	Uncharacterized protein
K4C3D3	1.255	1.389	1.767	1.733	Uncharacterized protein
K4ATF7	1.253	1.181	1.570	1.713	Uncharacterized protein
Q7XZS6	1.253	0.924	1.225	1.640	Glutathione peroxidase
K4CES8	1.252	1.062	0.968	1.020	Uncharacterized protein
K4BSD7	1.252	1.276	1.119	0.870	Uncharacterized protein
K4CWD1	1.252	1.072	1.321	1.130	Uncharacterized protein
K4CJ21	1.251	1.016	1.394	1.612	Malic enzyme
K4C390	1.251	1.138	0.974	0.841	Uncharacterized protein

Accession	Burned	Control	Regular	Limit	Description
K4CNR6	1.251	0.990	0.899	0.771	Uncharacterized protein
K4BP02	1.251	1.401	2.095	2.170	Ribosomal protein L15
A4ZYQ6	1.251	1.077	1.531	0.921	1-aminocyclopropane-1-carboxylate oxidase
K4C464	1.249	1.091	1.113	2.019	Uncharacterized protein
K4ATB4	1.248	1.089	0.866	1.243	Uncharacterized protein
K4BGC0	1.248	1.200	1.625	1.958	Uncharacterized protein
K4D1U4	1.247	1.150	1.303	1.445	Uncharacterized protein
K4CES3	1.247	1.105	1.355	1.642	ATP-dependent 6-phosphofructokinase
K4B066	1.247	0.962	1.083	1.052	Uncharacterized protein
K4CA68	1.247	1.168	1.364	1.662	Uncharacterized protein
K4BQ23	1.246	1.084	1.486	2.087	ATP-dependent 6-phosphofructokinase
K4BNA9	1.246	0.962	1.044	1.301	Uncharacterized protein
K4BVZ7	1.246	1.000	1.038	1.358	Uncharacterized protein
K4ATA4	1.245	0.815	0.699	0.818	Uncharacterized protein
K4CWP2	1.245	0.991	1.314	1.529	Beta-galactosidase
K4DBT9	1.244	1.098	1.146	1.409	Phosphotransferase
K4B0P2	1.244	1.005	1.010	1.150	Uncharacterized protein
K4B0S5	1.244	1.110	1.158	1.318	Uncharacterized protein
K4CQI3	1.243	1.120	1.411	1.722	Uncharacterized protein
K4CRF6	1.243	1.053	0.856	0.792	Uncharacterized protein
K4BZB6	1.243	1.075	1.109	1.049	Uncharacterized protein
K4BQW1	1.242	1.028	1.226	1.122	Uncharacterized protein
K4CGX0	1.242	0.901	0.856	0.937	Uncharacterized protein
K4BCG0	1.242	1.110	1.122	1.112	Uncharacterized protein
K4CU01	1.241	1.100	1.366	1.299	Uncharacterized protein
K4BDV0	1.241	1.285	1.086	1.151	Uncharacterized protein
C6K8M2	1.240	1.125	1.500	1.859	Plastid isopentenyl diphosphate isomerase
K4CXC8	1.239	0.840	1.015	1.305	Uncharacterized protein
K4CBC4	1.239	1.049	1.004	0.882	Adenylosuccinate lyase
K4BVW7	1.239	1.164	1.524	1.449	Uncharacterized protein
K4CXZ1	1.239	0.926	1.197	1.848	Uncharacterized protein
Q42886	1.238	1.139	1.247	1.169	ATP-dependent Clp protease proteolytic subunit
K4BI85	1.238	1.219	1.350	0.972	Starch synthase, chloroplastic/amyloplastic
K4BDD3	1.238	1.088	1.299	1.694	Uncharacterized protein
K4CNS0	1.238	0.797	0.800	0.861	Uncharacterized protein
K4CEY5	1.238	1.257	1.399	1.673	Uncharacterized protein
K4CW98	1.238	1.157	1.561	1.717	Uncharacterized protein
K4C607	1.238	0.894	1.238	1.574	Uncharacterized protein
K4B725	1.237	1.010	1.226	1.434	Uncharacterized protein
K4BV04	1.237	1.008	1.168	1.587	Uncharacterized protein
K4BFE2	1.237	1.291	1.023	0.850	Uncharacterized protein
K4CN88	1.235	0.933	1.034	1.103	Uncharacterized protein
K4BGP1	1.235	0.904	1.018	0.952	Uncharacterized protein
K4CHG0	1.235	1.103	1.331	1.281	Uncharacterized protein
K4CH48	1.235	1.074	1.345	1.435	Ubiquitinyl hydrolase 1
A0FKE6	1.234	1.197	0.983	0.964	Threonine dehydratase
K4CUE3	1.234	1.043	1.126	1.135	Uncharacterized protein
K4BP97	1.233	1.109	1.360	2.003	Proteasome subunit beta type
Q4W5U7	1.233	1.016	1.152	1.737	Calnexin-like protein
K4B3M5	1.232	1.079	1.719	2.041	V-type proton ATPase subunit a
K4CV97	1.231	0.959	1.107	1.397	Uncharacterized protein
K4CQK3	1.231	1.060	1.316	1.417	Uncharacterized protein

Accession	Burned	Control	Regular	Limit	Description
A5JV19	1.230	1.321	1.739	1.082	Zeaxanthin epoxidase, chloroplastic
K4C4Y0	1.230	1.016	1.016	2.003	Uncharacterized protein
K4C7X6	1.229	1.037	1.092	1.129	Uncharacterized protein
K4B0U6	1.229	1.019	1.426	1.266	Uncharacterized protein
K4BI32	1.229	1.017	1.208	1.046	Uncharacterized protein
K4DHF0	1.228	1.085	1.061	1.105	Uncharacterized protein
K4C8C6	1.228	0.982	0.974	1.106	Uncharacterized protein
K4D9U6	1.228	1.014	1.004	1.071	Arogenate dehydratase
K4D5K9	1.227	0.806	0.530	0.404	Uncharacterized protein
K4BNL8	1.226	1.127	1.376	1.299	Uncharacterized protein
K4DFI3	1.226	1.008	1.436	1.930	Uncharacterized protein
K4BJG4	1.226	1.026	1.026	1.237	Uncharacterized protein
K4D2Z0	1.225	0.965	1.045	1.129	Uncharacterized protein
K4AVT4	1.225	1.030	1.191	1.079	Uncharacterized protein
K4D698	1.224	0.883	0.870	0.908	Glutaredoxin-like protein
K4ATU6	1.224	1.106	1.146	1.040	Uncharacterized protein
K4CP88	1.224	1.135	1.427	1.489	Uncharacterized protein
Q2MIB8	1.223	1.115	1.217	1.137	30S ribosomal protein S16, chloroplastic
K4BUC0	1.223	1.056	1.365	1.034	Uncharacterized protein
K4CPM4	1.222	0.989	1.186	1.306	Uncharacterized protein
K4D2Q1	1.222	1.192	1.825	2.752	Uncharacterized protein
K4CKX4	1.222	1.209	1.465	1.945	Uncharacterized protein
K4B1W8	1.222	1.243	1.461	1.867	Transmembrane 9 superfamily member
K4BDE9	1.222	0.993	1.112	1.276	Uncharacterized protein
K4BNQ2	1.221	1.049	1.246	1.437	Uncharacterized protein
K4CGV3	1.221	1.208	2.975	3.491	Uncharacterized protein
K4C589	1.221	0.902	1.242	1.504	Superoxide dismutase
K4BIY5	1.220	0.960	1.110	1.712	Uncharacterized protein
K4BM18	1.220	1.176	1.308	1.473	Uncharacterized protein
K4BTT8	1.219	0.999	1.253	1.321	Uncharacterized protein
K4C1S9	1.218	1.104	1.185	1.157	Uncharacterized protein
K4B740	1.218	1.218	1.474	1.801	UDP-glucose 6-dehydrogenase
K4B727	1.218	1.068	1.278	0.938	Uncharacterized protein
K4BVL2	1.217	0.988	1.058	0.954	Uncharacterized protein
K4CJX8	1.217	0.941	1.148	1.805	Uncharacterized protein
K4BWK0	1.216	1.051	1.263	1.151	Uncharacterized protein
O49877	1.216	0.861	1.375	2.297	CYP1
B2CPI9	1.215	1.290	1.092	0.773	Lycopene epsilon cyclase
K4DEP4	1.215	1.117	1.167	1.135	Uncharacterized protein
K4CPX6	1.214	1.574	1.423	0.889	Starch synthase, chloroplastic/amyloplastic
K4DCA5	1.213	1.063	1.131	1.173	Uncharacterized protein
K4CWS4	1.212	0.974	1.124	1.468	Glycosyltransferase
K4DHW1	1.211	1.154	1.723	1.774	Uncharacterized protein
K4CV43	1.211	1.017	1.181	1.684	Uncharacterized protein
K4D637	1.210	0.717	0.690	0.453	Uncharacterized protein
K4CVX5	1.210	1.056	2.772	5.043	Uncharacterized protein
K4D465	1.209	1.091	1.190	1.892	Uncharacterized protein
K4B7K7	1.209	1.198	1.513	1.498	Probable tRNA N6-adenosine threonylcarbamoyltransferase
K4CAH4	1.209	1.027	1.170	2.055	Peptidylprolyl isomerase
K4C455	1.209	1.183	1.443	1.969	Uncharacterized protein
K4BXV7	1.208	0.978	1.002	1.062	Uncharacterized protein
K4DBL8	1.207	1.012	1.100	1.016	Uncharacterized protein
K4CIC2	1.207	1.042	1.090	1.381	Glycosyltransferase

Accession	Burned	Control	Regular	Limit	Description
K4CPU7	1.207	1.082	0.835	0.832	Uncharacterized protein
K4D450	1.206	1.020	1.082	1.033	Uncharacterized protein
K4B089	1.206	0.928	0.924	1.098	Uncharacterized protein
K4CV83	1.205	1.161	1.799	1.883	Uncharacterized protein
K4CCD2	1.205	1.015	1.246	2.089	Uncharacterized protein
B2Z9Y3	1.205	0.983	1.193	1.534	Gamma-glutamylhydrolase 1
K4DCX9	1.205	0.967	1.205	1.317	Uncharacterized protein
K4BK61	1.204	1.289	1.794	1.805	D-3-phosphoglycerate dehydrogenase
K4C7S0	1.204	1.063	1.255	1.587	Phosphotransferase
Q2MI76	1.204	1.009	1.135	1.269	ATP-dependent Clp protease proteolytic subunit
K4CRC9	1.203	0.927	0.955	1.079	Uncharacterized protein
K4D671	1.202	1.621	1.513	0.965	Uncharacterized protein
K4B0I4	1.202	0.884	0.916	1.084	Uncharacterized protein
K4AXY6	1.202	0.974	1.025	1.184	Uncharacterized protein
K4AYQ1	1.200	0.947	0.825	0.956	Uncharacterized protein
K4BX11	1.199	1.110	0.917	1.119	Uncharacterized protein
K4BT19	1.199	1.278	1.548	1.774	Uncharacterized protein
K4CXD5	1.199	1.066	1.107	1.085	Uncharacterized protein
K4CM64	1.196	1.063	1.093	1.262	Uncharacterized protein
K4BJQ9	1.195	1.343	1.284	0.863	Uncharacterized protein
K4BFN4	1.194	0.908	1.210	1.714	Uncharacterized protein
K4DB56	1.194	0.775	0.903	0.976	Uncharacterized protein
K4BWE4	1.194	1.138	1.144	1.016	Uncharacterized protein
K4B0M5	1.193	1.028	1.189	1.129	Uncharacterized protein
K4C7H8	1.192	0.908	1.029	1.073	Uncharacterized protein
G8Z278	1.191	1.003	1.123	1.440	Hop-interacting protein THI111
K4D4S1	1.191	0.929	0.915	0.971	Uncharacterized protein
K4C8W7	1.191	0.854	0.817	0.965	Uncharacterized protein
K4CZP0	1.189	0.934	0.867	1.157	Uncharacterized protein
K4B0I7	1.189	1.035	1.249	1.932	Uncharacterized protein
K4AYF1	1.189	0.978	1.107	1.226	Uncharacterized protein
K4CNR8	1.188	0.838	0.956	0.983	Uncharacterized protein
K4B832	1.187	0.987	1.287	1.840	Proteasome subunit alpha type
K4BGV0	1.187	0.960	1.054	1.374	Uncharacterized protein
K4CQ60	1.186	1.178	1.236	1.106	Uncharacterized protein
K4BLY5	1.186	1.194	1.048	1.047	Uncharacterized protein
K4DDF7	1.186	1.081	0.976	1.042	Uncharacterized protein
K4BNC2	1.185	1.122	1.502	2.107	6-phosphogluconate dehydrogenase, decarboxylating
K4B546	1.185	1.111	1.271	1.514	Obg-like ATPase 1
K4BT41	1.184	1.011	1.040	1.685	Uncharacterized protein
K4CM82	1.184	1.047	1.394	1.669	Uncharacterized protein
K4D052	1.184	1.016	1.189	0.967	Uncharacterized protein
K4CN04	1.182	1.117	0.876	0.825	Uncharacterized protein
K4BB06	1.182	1.052	1.330	1.663	Proteasome subunit beta type
K4DC47	1.182	0.873	0.905	0.796	Uncharacterized protein
K4BTP3	1.181	0.917	0.874	0.927	Uncharacterized protein
K4DG14	1.180	0.832	0.629	0.805	Uncharacterized protein
K4CXG4	1.180	1.014	1.146	1.033	Uncharacterized protein
K4CJC4	1.179	0.968	0.889	0.855	Uncharacterized protein
K4D2B1	1.179	1.005	1.375	1.604	Uncharacterized protein
K4B7F0	1.179	0.942	0.900	0.975	Uncharacterized protein
K4B0U8	1.178	1.190	1.224	1.116	Uncharacterized protein

Accession	Burned	Control	Regular	Limit	Description
K4CJH4	1.178	0.986	1.286	1.838	Proteasome subunit alpha type
K4CRB3	1.178	1.176	1.172	0.883	Uncharacterized protein
K4CVK9	1.178	1.009	1.258	1.791	Uncharacterized protein
K4BY72	1.178	1.085	1.090	0.885	Phosphate transporter
K4CLL3	1.178	1.055	1.068	1.241	Malic enzyme
K4BV02	1.177	0.910	1.190	1.427	Uncharacterized protein
K4BYL6	1.176	0.835	1.014	1.419	Uncharacterized protein
K4B469	1.176	0.784	1.164	1.096	Uncharacterized protein
K4CA57	1.174	1.076	0.687	0.729	Uncharacterized protein
B1Q3F8	1.174	1.003	1.186	1.546	Succinic semialdehyde dehydrogenase
K4DCH7	1.172	1.058	1.251	1.317	Uncharacterized protein
K4BL40	1.172	1.270	1.586	1.913	UDP-glucose 6-dehydrogenase
K4CJE1	1.172	1.182	1.479	1.468	Uncharacterized protein
K4BLF9	1.172	0.934	1.209	1.264	Uncharacterized protein
K4DBC4	1.169	1.074	1.470	2.340	Aconitate hydratase
Q944F3	1.169	0.951	1.046	1.072	Arabinosidase ARA-1
K4CVX0	1.169	1.142	3.856	11.193	Uncharacterized protein
K4BA10	1.169	1.023	1.098	1.541	Uncharacterized protein
K4D9W3	1.169	1.072	1.330	1.191	Uncharacterized protein
K4D338	1.168	1.097	0.854	1.193	Uncharacterized protein
K4DA09	1.167	0.877	1.428	1.677	Uncharacterized protein
K4C8S6	1.167	0.949	0.924	0.999	Uncharacterized protein
K4CQ52	1.166	1.127	1.331	1.353	Uncharacterized protein
K4CE04	1.166	1.221	1.438	1.873	Uncharacterized protein
K4BB18	1.166	0.949	1.093	1.191	Uncharacterized protein
K4DF00	1.165	1.187	1.040	1.024	Uncharacterized protein
K4BTZ3	1.165	0.787	0.869	0.697	Uncharacterized protein

Accession	Burned	Control	Regular	Limit	Description
K4CVI9	1.164	0.918	1.024	1.469	Uncharacterized protein
K4D0C8	1.163	0.984	0.979	1.107	ATP-dependent Clp protease proteolytic subunit
K4CV84	1.163	1.152	1.783	1.866	Uncharacterized protein
K4CBT6	1.162	0.850	0.903	0.869	Uncharacterized protein
K4AXN2	1.162	0.947	0.936	1.019	Uncharacterized protein
Q93X44	1.161	1.430	1.806	1.103	Protein tyrosine phosphatase
K4D9Q1	1.161	1.107	1.531	1.826	Uncharacterized protein
Q84MI5	1.160	1.014	1.088	1.205	Mitogen-activated protein kinase
K4BLR5	1.160	1.025	1.220	2.414	Uncharacterized protein
K4AXQ9	1.160	0.992	1.106	1.204	Uncharacterized protein
K4DA71	1.159	1.034	1.247	1.630	Proteasome subunit beta
K4BNL9	1.159	0.892	1.085	1.637	Uncharacterized protein
K4CHH3	1.159	0.947	0.953	1.039	Uncharacterized protein
K4BEF0	1.158	0.956	0.997	1.196	Uncharacterized protein
Q09IV6	1.158	1.052	0.914	0.785	Solanesyl diphosphate synthase
K4D892	1.158	0.910	0.869	0.555	Uncharacterized protein
K4BA90	1.158	1.106	1.056	1.184	Uncharacterized protein
K4B2X1	1.158	1.085	1.281	1.446	Uncharacterized protein
K4BJU9	1.157	0.948	0.922	0.995	Uncharacterized protein
O65917	1.157	1.261	1.334	1.457	Dehydroquinate dehydratase/shikimate:NADP oxidoreductase
K4BFA4	1.156	1.241	1.595	1.217	Uncharacterized protein
K4CD97	1.156	0.982	1.020	1.098	Uncharacterized protein
K4D7X4	1.155	1.115	1.643	1.543	Uncharacterized protein
K4BLX5	1.154	1.210	1.196	1.178	Uncharacterized protein

Accession	Burned	Control	Regular	Limit	Description
K4BC62	1.154	0.906	1.259	1.348	Uncharacterized protein
K4DCK2	1.153	1.131	1.378	2.051	Uncharacterized protein
K4BJE6	1.153	1.203	1.391	1.624	Alanine--tRNA ligase
K4BF72	1.152	0.894	0.857	0.861	Uncharacterized protein
K4CVW7	1.152	0.979	1.119	1.639	Uncharacterized protein
K4B9W9	1.152	1.181	1.378	1.160	Uncharacterized protein
K4D5A8	1.152	0.975	1.081	0.898	Uncharacterized protein
K4C0M5	1.152	0.832	0.879	1.125	Uncharacterized protein
K4CMU2	1.150	0.947	0.905	1.136	ATP-dependent Clp protease proteolytic subunit
K4BYF1	1.150	1.066	1.187	1.061	Uncharacterized protein
D2KQI9	1.150	1.091	1.620	1.650	Succinate dehydrogenase [ubiquinone] iron-sulfur subunit, mitochondrial
K4BAN0	1.149	0.910	0.890	1.062	Uncharacterized protein
I6ZAC9	1.149	1.149	1.083	2.064	Lutescent 2
Q93YH0	1.149	0.980	0.960	0.947	ATP-dependent Clp protease proteolytic subunit
K4B124	1.148	1.389	2.072	2.415	Uncharacterized protein
K4B318	1.148	0.969	1.154	0.921	Uncharacterized protein
K4B3K9	1.147	1.021	1.120	1.137	Uncharacterized protein
K4C6K6	1.146	1.030	1.379	1.966	Aldehyde dehydrogenase
K4D6T3	1.146	0.911	0.899	0.917	Peroxidase
K4CNE8	1.146	0.956	1.010	1.325	ATP-dependent Clp protease proteolytic subunit
K4CAD0	1.145	0.922	0.940	1.208	Uncharacterized protein
K4D5H1	1.145	1.072	1.319	1.496	Uncharacterized protein
Q9M5A8	1.145	1.048	0.719	1.157	Chaperonin 21
K4BSI6	1.145	1.032	1.188	1.220	Uncharacterized protein
K4B1R4	1.145	1.045	1.362	1.669	Uncharacterized protein
K4CWK0	1.143	1.273	1.442	1.684	Uncharacterized protein
Q4PS96	1.143	1.012	1.212	1.430	Phosphotransferase
K4BP08	1.142	0.901	0.860	0.858	Uncharacterized protein
K4CIA5	1.140	1.144	0.996	0.828	Uncharacterized protein
K4BHX1	1.140	1.034	1.059	1.263	Uncharacterized protein
K4C2A3	1.140	1.015	1.195	1.226	Uncharacterized protein
K4AT31	1.139	1.125	1.194	1.430	Uncharacterized protein
K4CI13	1.138	0.910	1.103	1.430	Uncharacterized protein
K4BB37	1.138	1.155	1.623	1.538	Uncharacterized protein
Q52QQ4	1.138	1.248	1.768	1.921	Ascorbate peroxidase
K4AZG3	1.137	1.018	1.257	1.263	Uncharacterized protein
K4DCU5	1.137	0.794	0.956	1.307	Uncharacterized protein
Q8RXB7	1.136	1.073	1.177	1.480	N-hydroxycinnamoyl-CoA:tyramine N-hydroxycinnamoyl transferase THT7-1
K4D3G5	1.136	1.243	1.290	0.964	Uncharacterized protein
Q8GZR6	1.136	1.508	1.432	0.916	GcpE
K4CV42	1.135	1.306	1.289	1.006	Uncharacterized protein
K4CI69	1.133	0.928	1.349	1.518	Pectin acetylesterase
Q672Q8	1.133	1.278	0.979	0.738	Adenylyl-sulfate reductase
K4BMY2	1.132	0.980	1.094	1.552	Glycylpeptide N-tetradecanoyltransferase
K4CNU5	1.132	1.038	1.467	1.643	Uncharacterized protein
K4C6Q9	1.132	1.085	1.044	1.022	Uncharacterized protein
K4CK77	1.131	1.016	1.053	1.144	Uncharacterized protein
K4B111	1.131	1.063	1.177	1.725	Uncharacterized protein
K4DF79	1.130	1.022	1.308	1.308	Uncharacterized protein

Accession	Burned	Control	Regular	Limit	Description
K4D738	1.130	1.034	1.105	1.153	Uncharacterized protein
K4C2D8	1.130	1.158	1.247	0.948	Uncharacterized protein
K4C618	1.130	0.977	0.934	0.907	Uncharacterized protein
K4BQC2	1.129	1.189	0.943	0.857	Uncharacterized protein
K4AZG1	1.128	1.011	1.392	1.599	Malic enzyme
Q2MIA1	1.128	1.077	1.284	1.008	Photosystem I P700 chlorophyll a apoprotein A2
K4BDQ0	1.127	1.197	1.986	1.719	Uncharacterized protein
K4CKD9	1.127	1.091	1.135	1.362	Uncharacterized protein
K4B9R5	1.127	1.293	1.018	0.857	Uncharacterized protein
K4CPV7	1.127	0.952	1.033	1.630	Uncharacterized protein
K4DBP9	1.126	0.921	0.820	0.824	Uncharacterized protein
K4CKP3	1.126	1.210	1.454	1.854	Uncharacterized protein
K4D9D7	1.125	1.077	1.323	1.476	Uncharacterized protein
K4DDB9	1.125	1.232	1.772	1.597	Potassium transporter
K4D109	1.124	1.303	2.524	3.635	Uncharacterized protein
K4BW49	1.124	1.230	1.227	1.283	Uncharacterized protein
K4D4M0	1.124	0.947	1.156	1.278	Peptidyl-prolyl cis-trans isomerase
Q9FEW9	1.124	1.046	1.283	1.572	12-oxophytodienoate reductase 3
K4DCG6	1.124	1.034	1.298	1.622	Uncharacterized protein
K4DC02	1.123	0.980	1.177	1.803	Proteasome subunit alpha type
K4BC16	1.121	1.055	0.951	1.413	Uncharacterized protein
K4BVG7	1.121	0.881	1.140	1.279	Uncharacterized protein
K4B9D4	1.121	0.868	1.028	1.268	Uncharacterized protein
K4BLU0	1.119	0.965	0.941	1.225	Uncharacterized protein
K4B0S1	1.119	1.095	1.216	1.283	Mevalonate kinase
Q93YG7	1.118	0.986	1.362	1.435	Profilin-2
K4CAN7	1.118	1.085	1.191	1.612	Uncharacterized protein
K4BLB3	1.117	1.200	1.415	1.397	Uncharacterized protein
K4AY97	1.116	0.858	0.936	1.029	Uncharacterized protein
K4BH04	1.115	0.984	1.129	1.182	Uncharacterized protein
K4AWX8	1.115	1.197	1.297	0.815	Uncharacterized protein
K4BS18	1.115	0.900	1.056	1.287	Uncharacterized protein
K4C399	1.114	1.088	1.331	1.131	Uncharacterized protein
K4C2U9	1.114	1.249	1.646	1.751	Uncharacterized protein
K4DAM7	1.113	1.159	1.378	1.422	Uncharacterized protein
K4B303	1.113	1.099	1.259	1.473	Polyadenylate-binding protein
K4B3R5	1.113	1.266	1.310	0.873	Amidophosphoribosyltransferase
K4BB41	1.113	0.925	0.852	0.970	Uncharacterized protein
K4D4X0	1.112	1.086	1.191	1.046	Uncharacterized protein
K4CET8	1.112	1.179	1.226	1.267	Uncharacterized protein
K4CFL8	1.112	0.865	0.893	1.171	Uncharacterized protein
K4CFR7	1.112	1.088	1.440	2.189	Uncharacterized protein
K4B857	1.112	0.903	1.099	1.253	Uncharacterized protein
K4AYG5	1.111	1.117	1.189	1.110	Uncharacterized protein
K4B9W8	1.111	1.155	1.346	1.155	Uncharacterized protein
K4BDB3	1.111	1.126	1.273	1.517	Uncharacterized protein
K4CLE1	1.111	0.906	1.410	1.412	Uncharacterized protein
K4BA40	1.110	0.948	1.105	1.413	Proteasome subunit alpha type
K4D6M8	1.110	1.020	0.839	1.108	Dihydrolipoamide acetyltransferase component of pyruvate dehydrogenase complex
K4BA92	1.109	0.994	1.232	1.282	Uncharacterized protein
K4BWQ1	1.108	1.452	2.014	2.002	Uncharacterized protein

Accession	Burned	Control	Regular	Limit	Description
K4CK47	1.108	1.059	1.243	1.475	Aspartate aminotransferase
K4B3Q8	1.106	1.047	1.142	1.508	Uncharacterized protein
K4CTF6	1.105	1.413	2.057	2.193	40S ribosomal protein S8
E1U7P9	1.105	1.077	1.072	1.081	Glutathione synthetase
K4ASF7	1.105	1.042	1.247	1.249	Uncharacterized protein
K4C3B9	1.105	1.250	1.567	1.885	40S ribosomal protein S4
K4D899	1.105	1.136	1.494	1.966	Proline iminopeptidase
P43280	1.104	1.280	1.498	1.235	S-adenosylmethionine synthase 1
K4CGU4	1.104	1.059	1.278	1.645	Uncharacterized protein
K4DCU3	1.104	1.025	1.322	1.663	Uncharacterized protein
K4DB01	1.104	0.686	0.551	0.647	Uncharacterized protein
K4DF56	1.104	1.252	1.449	1.537	40S ribosomal protein S12
K4DBN8	1.103	1.305	1.137	0.642	Uncharacterized protein
K4CXX9	1.103	1.083	0.922	0.671	Uncharacterized protein
K4CY51	1.103	1.551	1.148	0.715	Mg-protoporphyrin IX chelatase
K4DH58	1.102	1.089	1.267	1.089	Uncharacterized protein
B1Q3F0	1.100	1.174	1.874	2.242	Glutamate decarboxylase
K4C3K6	1.100	1.085	1.187	1.613	Uncharacterized protein
K4ATQ2	1.100	1.447	1.998	1.993	Uncharacterized protein
K4CUR8	1.100	1.098	1.236	1.706	Uncharacterized protein
K4CUW6	1.099	0.921	0.856	0.952	Uncharacterized protein
K4BCF4	1.099	0.799	0.827	0.844	Uncharacterized protein
K4B814	1.099	1.261	1.598	1.898	40S ribosomal protein S4
K4DHK7	1.098	1.269	1.454	1.687	Uncharacterized protein
K4D7V9	1.098	1.197	1.298	1.325	Uncharacterized protein
K4B7K2	1.097	1.014	1.271	1.353	Uncharacterized protein
K4B461	1.096	1.260	1.105	0.764	Probable alanine--tRNA ligase, chloroplastic
K4BED4	1.095	0.951	1.114	1.336	Uncharacterized protein
K4CBC3	1.095	1.136	1.247	1.277	Uncharacterized protein
K4CID9	1.093	0.985	1.444	2.868	Uncharacterized protein
K4B490	1.093	1.236	1.063	0.889	Uncharacterized protein
Q84T86	1.092	0.954	1.005	1.225	Biotin carboxylase carrier protein
K4C740	1.092	1.055	1.463	2.323	Uncharacterized protein
K4CVI4	1.091	1.300	1.252	1.577	Cysteine synthase
K4BNH1	1.091	0.856	0.700	1.113	Uncharacterized protein
K4BAJ6	1.091	0.944	0.952	0.758	Uncharacterized protein
K4BLH7	1.091	1.126	1.294	1.319	Uncharacterized protein
D3TI69	1.089	0.938	1.080	1.118	Beta-hexosaminidase
Q2MI87	1.088	0.937	0.826	1.110	Cytochrome f
K4BXC7	1.087	1.042	0.964	1.233	Dihydrolipoamide acetyltransferase component of pyruvate dehydrogenase complex
K4C247	1.087	1.270	1.455	1.686	Uncharacterized protein
K4C712	1.087	0.928	0.998	1.313	Glycylpeptide N-tetradecanoyltransferase
K4CMH4	1.087	1.094	1.068	1.214	Uncharacterized protein
K4CJ99	1.087	0.930	1.257	2.068	Uncharacterized protein
K4B438	1.086	0.903	1.210	1.733	Uncharacterized protein
K4B818	1.086	1.262	1.605	1.907	40S ribosomal protein S4
K4B7A1	1.086	1.118	1.250	1.693	Uncharacterized protein
K4C715	1.085	1.320	1.442	1.169	Uncharacterized protein
K4B2L3	1.085	1.040	1.111	1.047	Uncharacterized protein
K4BTM7	1.084	1.222	1.307	0.933	Uncharacterized protein
K4B2J4	1.084	0.958	1.127	1.854	Uncharacterized protein

Accession	Burned	Control	Regular	Limit	Description
P23322	1.084	0.801	0.838	0.848	Oxygen-evolving enhancer protein 1, chloroplastic
K4CMX6	1.084	0.965	0.968	0.974	Uncharacterized protein
K4B7D7	1.081	1.069	1.010	0.960	Uncharacterized protein
K4BWD5	1.081	1.249	1.746	2.190	Uncharacterized protein
K4C363	1.081	1.032	1.340	1.671	Uncharacterized protein
K4CWG8	1.080	0.878	0.701	0.760	Inosine triphosphate pyrophosphatase
K4BM14	1.079	0.988	1.234	1.446	Aldose 1-epimerase
K4D1F7	1.079	0.901	1.202	1.719	Uncharacterized protein
K4CAF8	1.078	0.803	1.091	1.232	Carboxypeptidase
K4BEV1	1.078	0.904	1.128	0.971	Alpha-galactosidase
K4BWH8	1.078	1.031	1.302	1.388	Pyruvate dehydrogenase E1 component subunit alpha
K4D7F1	1.078	1.176	1.417	1.875	Uncharacterized protein
K4BDN7	1.077	1.026	0.885	0.786	Uncharacterized protein
K4DC28	1.077	1.214	0.961	0.992	Pyruvate dehydrogenase E1 component subunit alpha
K4CN08	1.076	0.977	1.053	1.175	Uncharacterized protein
K4DG42	1.075	0.772	0.894	0.714	Uncharacterized protein
K4BBG9	1.075	0.976	1.095	1.598	Isocitrate dehydrogenase [NADP]
K4BMI0	1.075	0.890	1.088	0.785	Uncharacterized protein
K4C635	1.074	1.154	0.895	0.949	Acyl-[acyl-carrier-protein] desaturase
K4CQS3	1.074	1.197	0.926	0.814	Uncharacterized protein
K4DA65	1.074	0.882	0.734	0.859	Uncharacterized protein
Q9XGI9	1.073	0.909	0.940	1.354	N-carbamoylputrescine amidase
Q8H0Q2	1.073	1.008	1.129	1.362	Phosphotransferase
K4BY37	1.073	1.139	0.949	0.712	Uncharacterized protein
K4C6R8	1.072	1.110	1.261	0.879	Uncharacterized protein
K4DG11	1.071	0.899	0.930	1.210	Uncharacterized protein
K4BAL8	1.071	0.865	0.898	1.107	Uncharacterized protein
B1Q3F1	1.070	1.079	1.531	1.865	Glutamate decarboxylase
K4BSK7	1.070	1.003	1.199	1.079	Peptidylprolyl isomerase
K4B7P1	1.069	0.823	0.939	1.617	Uncharacterized protein
K4D5A3	1.069	0.952	1.192	1.440	Uncharacterized protein
K4C948	1.068	1.080	0.886	0.641	Uncharacterized protein
K4D5J1	1.067	1.490	1.256	1.136	Uncharacterized protein
K4B2I9	1.067	0.952	1.118	1.834	Uncharacterized protein
K4B440	1.067	1.145	1.374	1.299	Uncharacterized protein
K4BGW4	1.066	0.967	1.014	0.812	Uncharacterized protein
K4C2N1	1.066	0.885	0.758	0.716	Uncharacterized protein
K4DG16	1.065	0.872	0.838	1.003	Uncharacterized protein
K4CAD9	1.065	0.861	0.685	0.724	Uncharacterized protein
K4CCQ8	1.065	1.195	1.769	1.476	NADPH--cytochrome P450 reductase
K4D9I4	1.065	0.990	0.788	0.833	Uncharacterized protein
K4CAF9	1.064	0.750	0.920	1.024	Carboxypeptidase
K4CG62	1.064	1.212	1.643	2.045	Uncharacterized protein
K4BKE0	1.062	1.025	0.993	0.850	Uncharacterized protein
K4B5N0	1.061	1.506	1.121	0.725	Uncharacterized protein
K4BXN9	1.061	1.387	1.325	1.234	Uncharacterized protein
K4CUB2	1.060	0.927	1.222	1.467	Glutathione peroxidase
K4CZH3	1.060	1.190	1.437	1.769	Transmembrane 9 superfamily member
K4CFD4	1.060	1.067	1.416	2.097	Aconitate hydratase
K4CFP5	1.059	1.034	1.308	1.612	Uncharacterized protein

Accession	Burned	Control	Regular	Limit	Description
K4CAN2	1.059	1.187	1.221	0.936	Uncharacterized protein
K4BXJ1	1.058	1.007	1.040	0.925	Uncharacterized protein
K4AWC1	1.058	1.269	1.371	1.072	Uncharacterized protein
K4CQW8	1.057	0.975	1.309	1.826	Uncharacterized protein
K4ASL1	1.055	0.992	1.198	1.349	Uncharacterized protein
K4BHZ4	1.055	1.213	1.266	1.595	Uncharacterized protein
K4CVP1	1.055	1.040	1.284	1.731	1,2-dihydroxy-3-keto-5-methylthiopentene dioxygenase
K4C7G8	1.054	0.934	0.952	1.098	Uncharacterized protein
K4DBP0	1.054	0.865	0.786	1.216	Uncharacterized protein
Q2MI70	1.053	1.032	1.132	1.202	Cytochrome b6-f complex subunit 4
K4BNH5	1.053	1.016	1.120	1.473	Uncharacterized protein
K4CW69	1.052	0.835	0.953	1.229	Cyanate hydratase
K4C9W3	1.052	1.042	1.254	2.100	Uncharacterized protein
K4B369	1.052	0.869	1.077	1.804	Uncharacterized protein
K4CG68	1.052	0.998	1.265	1.538	Uncharacterized protein
Q3I5C4	1.051	1.234	1.668	1.795	Cytosolic ascorbate peroxidase 1
K4BHG4	1.050	1.201	1.502	1.193	Alpha-1,4 glucan phosphorylase
K4B0H9	1.050	1.152	1.352	1.794	Cysteine synthase
K4DC06	1.050	0.913	0.891	1.345	Uncharacterized protein
K4BA66	1.049	1.012	1.109	1.468	Uncharacterized protein
K4C3J6	1.049	1.076	0.996	0.840	Uncharacterized protein
K4C2H1	1.048	0.999	1.117	1.381	Uncharacterized protein
H1ZXA9	1.048	1.033	1.209	2.078	Heat shock protein 70 isoform 3
K4BSE0	1.048	1.064	1.300	1.310	Uncharacterized protein
A0A0H2UIA1	1.048	1.037	0.941	0.799	1,2-dihydroxy-3-keto-5-methylthiopentene dioxygenase
K4CEH6	1.048	1.077	1.071	0.861	Glycosyltransferase
K4BXX0	1.048	0.897	1.117	1.279	Uncharacterized protein
K4B2H0	1.047	1.134	1.283	1.241	Uncharacterized protein
K4DH44	1.047	0.835	0.862	0.988	Uncharacterized protein
K4CNW2	1.047	0.982	0.899	0.977	ATP-dependent Clp protease proteolytic subunit
K4C1Q7	1.046	1.007	1.174	1.209	Uncharacterized protein
K4DCH3	1.046	1.016	1.098	0.932	Uncharacterized protein
K4D9L5	1.046	1.051	1.167	1.815	Uncharacterized protein
K4BX93	1.045	1.222	1.389	1.510	Uncharacterized protein
K4CBK0	1.045	1.153	1.444	1.504	Uncharacterized protein
K4BPL5	1.045	0.863	0.679	0.727	Peptidylprolyl isomerase
K4BVS6	1.043	1.115	1.015	2.089	Uncharacterized protein
K4B0H3	1.043	1.245	1.185	0.806	Uncharacterized protein
K4CGU8	1.043	0.886	0.974	1.502	Malate dehydrogenase
K4B6V8	1.043	0.938	1.043	2.517	Uncharacterized protein
Q9STA6	1.041	0.922	0.948	1.019	RAD23 protein
K4ASW3	1.039	1.143	1.384	1.324	Uncharacterized protein
K4D9N3	1.039	0.828	0.863	1.065	Carboxypeptidase
K4D4C1	1.038	0.869	0.962	0.768	Uncharacterized protein
K4BPA9	1.038	0.905	0.888	0.974	Uncharacterized protein
K4B0W1	1.036	0.967	0.959	1.210	Uncharacterized protein
K4DF31	1.035	0.948	1.091	1.794	Uncharacterized protein
K4BU13	1.034	0.960	0.936	0.904	Uncharacterized protein
K4D6M3	1.033	0.922	0.857	1.001	Uncharacterized protein
K4DFS5	1.033	1.283	1.509	1.109	Uncharacterized protein
K4C2B3	1.032	1.132	1.302	1.270	Uncharacterized protein

Accession	Burned	Control	Regular	Limit	Description
K4CSA9	1.031	1.161	1.272	1.425	Uncharacterized protein
K4CVT9	1.029	1.173	1.538	1.147	Uncharacterized protein
K4D650	1.029	1.034	1.274	1.486	Uncharacterized protein
K4BAJ5	1.028	0.900	1.227	1.226	Vitamin K epoxide reductase
K4C1L6	1.028	1.175	1.019	0.920	Uncharacterized protein
K4BX20	1.027	0.907	0.975	1.175	ATP synthase subunit beta
K4C7W9	1.027	0.987	1.258	1.388	Uncharacterized protein
K4C9H1	1.026	1.007	0.973	1.035	Arogenate dehydratase
K4CHH4	1.026	1.201	0.873	0.690	Uncharacterized protein
K4CJD3	1.025	1.247	1.486	1.091	Uncharacterized protein
K4ASY9	1.025	1.069	1.522	1.856	Succinate--CoA ligase [ADP-forming] subunit alpha, mitochondrial
Q8GZD8	1.025	0.978	1.562	4.167	Neutral leucine aminopeptidase preprotein
K4BVD8	1.024	0.962	1.091	1.499	Proteasome subunit alpha type
Q2MI98	1.024	1.344	1.634	1.253	30S ribosomal protein S4, chloroplastic
K4CPX9	1.024	0.943	0.928	0.996	Uncharacterized protein
K4BBT1	1.023	1.007	1.259	1.487	UBC41
K4DF39	1.022	0.897	0.941	0.906	Uncharacterized protein
K4C9A8	1.021	0.907	1.219	1.345	Uncharacterized protein
K4BLS9	1.021	0.907	0.898	1.019	Uncharacterized protein
K4BI34	1.021	1.035	1.239	1.363	Uncharacterized protein
K4C5F4	1.019	0.914	1.115	1.416	Superoxide dismutase
K4BEH7	1.019	1.648	1.014	0.919	Uncharacterized protein
K4BNR2	1.019	0.903	0.974	1.170	ATP synthase subunit beta
K4BGL3	1.019	0.962	1.070	1.233	Uncharacterized protein
K4CFM5	1.019	1.196	1.321	1.308	Ketol-acid reductoisomerase
K4B6K0	1.019	0.903	0.924	1.020	Uncharacterized protein
K4BK33	1.018	1.100	1.902	1.652	Uncharacterized protein
K4CWC2	1.018	1.048	0.748	0.624	Uncharacterized protein
K4DAS6	1.017	0.975	1.144	1.605	Uncharacterized protein
K4BJJ6	1.017	1.004	1.461	1.754	V-type proton ATPase subunit C
K4BUC1	1.017	0.917	0.831	1.048	Uncharacterized protein
K4AXL3	1.016	1.006	1.012	0.954	Uncharacterized protein
K4B103	1.015	0.970	0.958	1.140	ATP-dependent Clp protease proteolytic subunit
K4D9L9	1.015	1.035	1.222	2.109	Uncharacterized protein
K4DI41	1.014	0.965	0.910	0.874	Uncharacterized protein
K4CBI2	1.014	0.907	1.052	0.994	Peptidyl-prolyl cis-trans isomerase
K4CR90	1.013	1.050	1.169	1.852	Uncharacterized protein
K4B8G4	1.013	0.955	0.809	0.812	Histidinol dehydrogenase, chloroplastic
K4CHU1	1.012	1.042	1.532	1.077	Uncharacterized protein
K4B6R3	1.012	1.053	1.584	1.235	Uncharacterized protein
K4BMN4	1.012	1.214	0.886	1.107	Uncharacterized protein
K4BC25	1.012	0.981	1.269	1.557	Uncharacterized protein
K4DA85	1.011	1.011	0.826	0.967	Uncharacterized protein
K4CUJ9	1.011	1.211	1.594	1.377	Uncharacterized protein
K4CMW6	1.010	1.040	1.054	0.930	Uncharacterized protein
K4BTI1	1.010	1.061	1.046	1.056	Uncharacterized protein
K4BJD0	1.010	1.038	1.163	1.133	Uncharacterized protein
K4CRJ9	1.010	1.024	0.917	0.946	Uncharacterized protein

Accession	Burned	Control	Regular	Limit	Description
Q43503	1.010	1.100	1.034	1.110	Lycopene beta cyclase, chloroplastic
K4CLR1	1.008	0.853	0.778	0.907	Lactoylglutathione lyase
K4CSX9	1.008	0.983	0.860	0.916	Uncharacterized protein
K4ASU4	1.008	0.855	0.624	0.701	Uncharacterized protein
K4BT58	1.007	0.923	1.111	1.006	Uncharacterized protein
K4CS35	1.007	0.916	1.161	1.259	Uncharacterized protein
K4BKU9	1.006	1.265	1.132	0.798	Uncharacterized protein
K4D7D1	1.006	0.964	1.384	1.181	Uncharacterized protein
K4CV38	1.006	0.904	0.772	0.636	Uncharacterized protein
K4BAK9	1.005	0.897	0.963	0.979	Uncharacterized protein
K4CNV2	1.005	1.013	1.114	1.138	Uncharacterized protein
K4B7S3	1.005	1.072	0.959	0.798	Uncharacterized protein
K4AXN3	1.004	0.950	1.064	0.805	Uncharacterized protein
K4B9S5	1.004	0.942	0.779	0.926	Uncharacterized protein
K4CMN8	1.003	1.093	1.324	1.169	Uncharacterized protein
K4BDI6	1.003	0.915	1.104	1.438	Uncharacterized protein
Q672Q6	1.001	0.801	0.813	0.783	Photosystem II oxygen-evolving complex protein 3
K4CVM9	1.000	1.230	1.594	1.574	40S ribosomal protein S3a
K4DDW3	1.000	0.902	0.750	0.748	Uncharacterized protein
Q42896	1.000	0.917	1.056	1.589	Fructokinase-2
K4BT48	1.000	0.740	0.589	0.942	Uncharacterized protein
K4C3Z3	1.000	0.678	0.557	0.381	Uncharacterized protein
K4B010	0.999	1.061	1.329	1.511	Uncharacterized protein
K4BRP1	0.999	0.849	0.740	0.766	Uncharacterized protein
K4C2V9	0.998	0.871	0.902	1.154	Uncharacterized protein
K4B4D7	0.997	1.088	1.579	1.954	Succinate--CoA ligase [ADP-forming] subunit alpha, mitochondrial
K4D402	0.997	1.042	1.171	1.034	Uncharacterized protein
K4DDD8	0.997	1.034	0.962	0.869	Uncharacterized protein
K4BWS5	0.996	1.062	1.240	1.107	Uncharacterized protein
K4BPJ0	0.994	1.119	1.752	2.088	Uncharacterized protein
K4D2I8	0.993	0.983	1.280	1.442	Uncharacterized protein
K4B1N6	0.993	1.143	1.297	1.024	Uncharacterized protein
K4CSD7	0.992	0.950	1.288	1.379	Uncharacterized protein
K4D9J3	0.992	1.130	1.425	1.124	Uncharacterized protein
K4CEK7	0.992	1.158	1.717	1.203	Glycosyltransferase
Q7YK44	0.992	0.872	1.205	1.312	Superoxide dismutase
K4CTJ3	0.992	0.948	1.469	1.980	Uncharacterized protein
K4C3B8	0.991	0.960	0.984	1.047	Uncharacterized protein
K4B768	0.990	0.926	0.970	1.119	Uncharacterized protein
K4CN10	0.990	0.912	1.171	1.568	Uncharacterized protein
K4D0N8	0.989	0.982	1.179	1.442	Uncharacterized protein
K4BMY9	0.987	1.256	1.264	1.022	Uncharacterized protein
K4CHD1	0.986	1.217	1.431	1.415	Uncharacterized protein
G8Z286	0.985	1.120	1.317	1.078	Hop-interacting protein THI135
K4CMM7	0.985	1.098	1.234	1.667	Uncharacterized protein
K4BIU3	0.985	0.889	1.156	1.259	Uncharacterized protein
K4ASC2	0.985	0.971	1.157	1.858	Isocitrate dehydrogenase [NADP]
K4BW33	0.984	1.190	1.244	1.150	Uncharacterized protein
K4B9B8	0.983	1.038	1.370	2.757	Uncharacterized protein
K4B2K8	0.983	1.080	1.128	0.722	Uncharacterized protein
K4AU58	0.983	1.311	2.495	2.807	Uncharacterized protein
K4DFU6	0.982	0.903	0.729	0.895	Uncharacterized protein

Accession	Burned	Control	Regular	Limit	Description
K4BBN1	0.982	1.002	1.168	1.176	Uncharacterized protein
K4C3F7	0.981	1.071	0.908	0.768	Uncharacterized protein
K4CBF0	0.981	0.947	1.259	1.591	Acetyltransferase component of pyruvate dehydrogenase complex
K4BJK7	0.980	1.237	1.533	1.660	40S ribosomal protein S3a
K4CBN0	0.980	1.057	1.139	1.063	Uncharacterized protein
K4CHY6	0.979	1.027	0.994	1.367	Uncharacterized protein
K4D3M1	0.978	1.164	1.251	1.524	Uncharacterized protein
K4D2U9	0.977	1.054	1.340	1.565	Uncharacterized protein
K4C392	0.977	1.067	1.189	1.055	Uncharacterized protein
K4D5Y9	0.976	1.027	1.087	1.192	Uncharacterized protein
Q3C2L6	0.976	1.167	1.194	0.991	Sorbitol related enzyme
K4B0I9	0.976	0.969	1.311	1.590	Uncharacterized protein
K4CDC2	0.976	1.166	1.600	1.802	Uncharacterized protein
K4C8W9	0.976	1.235	1.531	1.659	40S ribosomal protein S3a
P93213	0.976	1.002	1.122	1.426	14-3-3 protein 8
K4BD29	0.976	1.063	1.561	1.551	Uncharacterized protein
K4B1V0	0.975	1.338	1.400	1.305	Uncharacterized protein
K4ASW1	0.975	1.154	1.124	1.006	Uncharacterized protein
K4D212	0.975	0.958	1.065	1.101	Uncharacterized protein
K4C030	0.972	1.089	0.912	0.749	Uncharacterized protein
K4D2D3	0.972	0.819	0.894	0.992	Uncharacterized protein
K4CQU6	0.972	1.063	1.321	1.355	Uncharacterized protein
K4CA74	0.971	1.095	1.145	0.963	Uncharacterized protein
K4D473	0.971	1.045	1.170	1.853	Uncharacterized protein
K4C4E5	0.969	0.988	1.213	1.021	Uncharacterized protein
K4ASZ0	0.969	0.907	0.910	0.974	Uncharacterized protein
K4B3W9	0.969	0.950	1.033	1.516	Uncharacterized protein
K4BW98	0.969	0.915	1.106	0.947	Uncharacterized protein
Q2MI62	0.968	1.444	1.803	1.332	30S ribosomal protein S3, chloroplastic
K4BSM2	0.968	1.201	0.929	0.699	Uncharacterized protein
K4CKM0	0.967	0.855	0.902	0.969	Uncharacterized protein
K4B858	0.967	0.904	1.162	1.250	Uncharacterized protein
K4C2X3	0.967	0.978	1.085	1.271	Uncharacterized protein
K4B9G0	0.967	1.011	0.724	0.386	Uncharacterized protein
Q56R04	0.965	1.061	1.032	1.104	Putative betaine aldehyde dehyrogenase
K4BKB7	0.964	1.001	1.372	1.304	Uncharacterized protein
K4BYZ6	0.964	1.185	1.371	1.103	Uncharacterized protein
K4AVZ4	0.964	1.071	0.979	0.837	Uncharacterized protein
K4CVP9	0.960	1.024	1.482	1.845	Uncharacterized protein
K4CWE3	0.959	0.949	1.189	1.294	Uncharacterized protein
K4BC01	0.959	1.042	1.167	1.889	Chorismate mutase
K4CGI1	0.959	0.881	1.161	1.800	Uncharacterized protein
K4CGN6	0.957	1.069	1.251	1.320	Chalcone-flavonone isomerase family protein
K4DD04	0.956	1.056	0.886	0.708	Uncharacterized protein
K4B0G7	0.956	0.956	1.143	1.510	Uncharacterized protein
K4CVP2	0.954	0.913	1.083	0.906	Anthocyanin O-methyltransferase
K4AXJ2	0.953	0.598	0.335	0.209	Uncharacterized protein
K4CW67	0.953	0.939	1.061	1.100	Uncharacterized protein
G8XSL1	0.953	1.043	1.078	1.138	GSH1
K4B7G7	0.953	0.812	0.732	0.876	Uncharacterized protein
K4B1Z2	0.953	0.965	0.939	0.699	Uncharacterized protein
K4BG52	0.951	1.156	0.882	0.690	Acetolactate synthase

Accession	Burned	Control	Regular	Limit	Description
K4BCS6	0.951	1.093	1.132	1.004	ATP-dependent Clp protease proteolytic subunit
K4BP87	0.951	1.028	1.203	1.424	ATP-dependent Clp protease proteolytic subunit
K4BDQ1	0.950	1.111	1.559	1.452	Uncharacterized protein
K4CBV6	0.950	1.104	1.246	1.606	Uncharacterized protein
K4DFR1	0.949	0.942	1.296	1.712	Uncharacterized protein
K4CUL6	0.949	0.886	0.766	1.025	Uncharacterized protein
K4BZA6	0.948	0.932	1.258	1.848	NADH-cytochrome b5 reductase
K4B0T9	0.948	0.826	0.788	1.117	Uncharacterized protein
K4BU02	0.948	0.831	0.938	1.100	Uncharacterized protein
K4B274	0.948	0.836	0.742	0.637	Uncharacterized protein
Q2MI71	0.947	0.993	0.867	0.982	Cytochrome b6
K4CAN4	0.947	0.928	1.205	1.599	Succinate--CoA ligase [ADP-forming] subunit beta, mitochondrial
K4ASR4	0.947	1.089	1.117	1.011	Uncharacterized protein
K4CBK1	0.945	1.209	1.534	1.719	Uncharacterized protein
K4B1S7	0.940	1.336	1.613	1.957	Uncharacterized protein
K4CBS3	0.939	1.149	1.369	1.415	Uncharacterized protein
K4B553	0.938	0.981	1.118	1.415	Ferredoxin--NADP reductase
A6N6K8	0.938	1.063	1.493	1.641	Phenylacetaldehyde reductase
K4CWA1	0.936	0.929	0.864	0.866	Uncharacterized protein
K4D435	0.935	1.153	1.265	1.549	Uncharacterized protein
K4D1Q1	0.934	1.018	1.203	1.697	Uncharacterized protein
P43281	0.934	1.280	1.386	1.181	S-adenosylmethionine synthase 2
K4CEH3	0.934	1.058	1.132	1.156	Uncharacterized protein
K4CGY7	0.933	0.964	1.104	1.592	Probable bifunctional methylthioribulose-1-phosphate dehydratase/enolase-phosphatase E1
K4BBN0	0.933	0.935	0.859	0.790	Ferredoxin-thioredoxin reductase, catalytic chain
K4D171	0.933	1.213	1.504	1.134	Uncharacterized protein
A0A0J9YZP8	0.932	0.968	1.090	1.383	Uncharacterized protein
K4BBJ8	0.932	0.830	0.841	0.969	Uncharacterized protein
K4C7F6	0.931	0.951	1.018	0.908	Uncharacterized protein
K4BBZ1	0.931	1.149	0.942	0.783	Uncharacterized protein
K4CBC9	0.931	1.029	1.330	0.881	Diacylglycerol kinase
Q6R8F6	0.929	1.146	0.853	0.848	Cystathionine gamma synthase
K4BP91	0.928	1.169	1.137	0.945	Uncharacterized protein
K4BU47	0.927	1.008	0.968	0.924	Glucose-6-phosphate isomerase
K4C2F3	0.927	0.932	1.216	1.932	Uncharacterized protein
K4DD75	0.926	1.039	1.167	1.156	Uncharacterized protein
Q672Q7	0.926	0.836	0.787	0.620	Putative uncharacterized protein
Q42891	0.926	0.821	0.932	1.103	Lactoylglutathione lyase
K4B8B4	0.926	0.939	0.875	0.624	Uncharacterized protein
K4B413	0.925	1.047	0.767	1.083	Uncharacterized protein
K4BLW8	0.925	1.199	1.294	1.211	Uncharacterized protein
K4C764	0.924	0.941	1.282	1.691	Uncharacterized protein
K4ASV9	0.923	1.310	1.580	1.196	Ribosomal protein
K4BG66	0.923	1.003	1.178	1.228	Uncharacterized protein

Accession	Burned	Control	Regular	Limit	Description
K4C5B9	0.921	1.016	0.682	0.668	Uroporphyrinogen decarboxylase
K4DH95	0.921	1.103	1.233	1.622	Uncharacterized protein
K4DFU3	0.921	1.103	1.299	1.531	6-phosphogluconate dehydrogenase, decarboxylating
K4B4C5	0.920	1.088	1.302	1.241	Uncharacterized protein
K4B075	0.920	1.048	0.952	0.933	Uncharacterized protein
K4D4A4	0.918	1.063	0.920	0.802	Uncharacterized protein
K4CXU8	0.917	0.907	1.219	1.211	Chlorophyll a-b binding protein, chloroplastic
Q9LLB0	0.917	0.927	1.209	1.179	Allene oxide synthase 2, chloroplastic
K4CEK8	0.917	1.131	1.527	1.469	Glycosyltransferase
Q2MI93	0.916	0.851	0.618	0.690	ATP synthase subunit beta, chloroplastic
Q2MI97	0.916	0.999	1.006	0.947	NAD(P)H-quinone oxidoreductase subunit J, chloroplastic
K4C2V0	0.913	1.300	1.258	1.007	Uncharacterized protein
Q2MI89	0.910	1.279	1.138	0.912	Photosystem I assembly protein Ycf4
K4AXU0	0.910	1.130	1.598	1.407	Uncharacterized protein
K4CEJ7	0.909	1.297	2.196	1.200	Uncharacterized protein
K4CMN4	0.909	1.148	1.072	1.042	Uncharacterized protein
K4CM08	0.909	0.892	0.996	1.039	Uncharacterized protein
K4ATQ7	0.908	0.855	0.814	0.770	Uncharacterized protein
K4BIG6	0.908	0.887	0.973	1.312	Uncharacterized protein
K4B188	0.905	0.834	0.723	0.754	Uncharacterized protein
K4BFZ6	0.904	1.030	1.283	1.394	Uncharacterized protein
K4DHH6	0.903	0.847	0.937	1.030	Uncharacterized protein
K4D5D2	0.903	1.187	1.595	1.212	Beta-glucosidase
P93212	0.902	0.980	1.094	1.337	14-3-3 protein 7
Q2MIB1	0.900	1.346	1.697	1.214	30S ribosomal protein S2, chloroplastic
K4DH15	0.900	0.871	0.896	0.990	Uncharacterized protein
K4B173	0.900	1.071	1.161	1.077	Uncharacterized protein
P93211	0.899	0.982	1.111	1.452	14-3-3 protein 6
P93214	0.898	0.981	1.120	1.356	14-3-3 protein 9
K4BY69	0.898	0.974	0.861	0.869	Uncharacterized protein
K4CQA9	0.897	0.897	0.949	0.982	Uncharacterized protein
K4CWP0	0.895	0.841	0.657	0.429	Uncharacterized protein
K4BLI9	0.895	0.993	0.972	0.843	Uncharacterized protein
K4CL08	0.894	0.910	0.903	1.187	Uncharacterized protein
K4CU54	0.894	0.972	1.203	1.047	Uncharacterized protein
K4BV58	0.892	0.868	0.779	0.858	Uncharacterized protein
K4C9R9	0.891	1.084	1.285	1.688	Uncharacterized protein
K4DCP3	0.891	0.863	0.902	0.969	Uncharacterized protein
K4C3V2	0.891	0.933	0.872	1.073	Uncharacterized protein
P12372	0.890	0.999	1.224	1.111	Photosystem I reaction center subunit II, chloroplastic
K4BPR4	0.890	0.982	1.115	1.477	Uncharacterized protein
K4BK46	0.889	1.008	1.017	1.047	Uncharacterized protein
K4CR23	0.888	1.067	0.929	0.788	Uncharacterized protein
K4CQE5	0.887	0.979	0.908	0.816	Uncharacterized protein
K4D9M0	0.886	1.059	0.918	0.778	Uncharacterized protein
K4B7U4	0.885	0.912	0.835	0.832	Uncharacterized protein
K4BQ37	0.885	0.879	0.922	1.126	Carboxypeptidase
Q6SKP4	0.885	1.316	1.604	1.949	Ribosomal protein L3
K4BCZ3	0.884	0.956	1.126	0.992	Uncharacterized protein
K4BLT6	0.883	1.026	0.967	0.733	Uncharacterized protein

Accession	Burned	Control	Regular	Limit	Description
K4DBV1	0.883	0.893	1.100	1.352	Uncharacterized protein
K4DHE9	0.883	0.996	1.388	1.296	Uncharacterized protein
K4D3B1	0.882	0.868	0.910	1.030	Uncharacterized protein
C0KZ34	0.881	0.901	0.874	0.788	Violaxanthin de-epoxidase
K4BZB9	0.881	0.901	0.790	0.980	Ferrochelatase
K4B8Z3	0.880	1.171	1.417	0.990	Alpha-1,4 glucan phosphorylase
K4BTY9	0.880	0.977	1.093	1.414	Uncharacterized protein
K4BFT9	0.879	1.123	1.093	0.794	Uncharacterized protein
K4CQB5	0.877	1.140	1.297	1.549	Uncharacterized protein
K4BWV3	0.876	0.882	0.740	0.858	Uncharacterized protein
K4BJA3	0.874	1.006	1.049	0.928	Uncharacterized protein
K4CGE7	0.873	1.068	1.034	1.052	Glucose-1-phosphate adenylyltransferase
K4DDQ3	0.871	1.035	1.207	1.434	Uncharacterized protein
K4C5R3	0.871	0.872	0.805	1.085	Uncharacterized protein
K4B614	0.870	1.152	1.380	1.511	Uncharacterized protein
K4BCZ5	0.870	1.071	0.925	0.763	Branched-chain-amino-acid aminotransferase
Q1PCD2	0.869	1.002	1.059	1.253	Glucose-6-phosphate isomerase
K4B125	0.869	1.143	1.290	1.194	Uncharacterized protein
K4B9E9	0.868	0.980	0.985	0.979	Uncharacterized protein
K4AV63	0.867	1.243	0.981	1.275	Uncharacterized protein
K4CYD3	0.865	0.931	0.915	0.863	Uncharacterized protein
Q49B52	0.865	0.867	1.079	1.090	Monodehydroascorbate reductase
K4BSG9	0.865	0.941	1.000	0.916	4-alpha-glucanotransferase
K4DAD5	0.864	1.093	0.721	1.041	Uncharacterized protein
K4C9L7	0.864	1.108	0.758	1.060	Uncharacterized protein
K4BCS7	0.863	1.030	1.218	1.111	Uncharacterized protein
K4DFB4	0.862	1.138	1.282	1.316	Uncharacterized protein
K4BFU0	0.862	0.978	1.101	1.414	Uncharacterized protein
Q0ZPA3	0.862	0.904	1.053	2.415	Plastid lipid associated protein CHRC
K4DF90	0.861	0.939	0.900	0.883	Uncharacterized protein
K4B7N3	0.861	0.906	0.776	0.875	Uncharacterized protein
P0CD46	0.861	1.123	1.122	1.015	NAD(P)H-quinone oxidoreductase subunit 2 A, chloroplastic
P93208	0.860	0.978	1.090	1.385	14-3-3 protein 2
K4BA62	0.860	0.949	0.827	0.846	Uncharacterized protein
K4CID0	0.860	0.851	0.887	1.000	Uncharacterized protein
K4BDK7	0.859	0.981	0.869	0.806	Uncharacterized protein
K4C7Z7	0.858	1.268	1.528	0.866	Uncharacterized protein
K4CD46	0.858	0.947	1.036	0.836	Chlorophyll a-b binding protein, chloroplastic
K4BNK4	0.858	1.014	1.064	1.367	Uncharacterized protein
K4CB67	0.858	0.910	0.979	1.192	Carboxypeptidase
K4BEU4	0.858	0.999	1.350	1.643	Uncharacterized protein
K4D5V2	0.857	0.990	1.210	1.143	Uncharacterized protein
K4C7C4	0.855	0.934	1.508	1.022	Uncharacterized protein
Q9SE20	0.855	1.330	1.314	0.866	Zeta-carotene desaturase, chloroplastic/chromoplastic
K4B2B2	0.855	1.106	1.517	1.274	Phospho-2-dehydro-3-deoxyheptonate aldolase
K4BIJ5	0.854	1.160	1.208	1.031	Uncharacterized protein
K4C7W7	0.854	0.907	1.100	1.424	Uncharacterized protein
K4DAK3	0.853	1.127	0.912	0.768	Uncharacterized protein
K4CVX8	0.850	0.955	2.139	3.058	Uncharacterized protein

Accession	Burned	Control	Regular	Limit	Description
K4AXX7	0.849	1.200	1.134	0.885	Protein translocase subunit SecA
K4AYB0	0.849	0.918	0.627	0.550	Uncharacterized protein
P28554	0.849	1.032	0.917	0.752	Phytoene dehydrogenase, chloroplastic/chromoplastic
K4DFV4	0.848	1.006	1.204	1.307	Glutathione peroxidase
K4BH71	0.847	1.051	1.128	0.921	Uncharacterized protein
K4BXX3	0.844	1.443	1.250	0.844	Alpha-1,4 glucan phosphorylase
K4CGM3	0.841	0.860	0.663	0.891	Uncharacterized protein
K4CHW8	0.841	1.088	1.148	1.331	Obg-like ATPase 1
K4AZV6	0.841	0.925	0.987	0.943	Uncharacterized protein
K4CLB7	0.840	1.031	1.103	0.935	Uncharacterized protein
K4CLI9	0.839	1.176	1.286	1.033	Uncharacterized protein
K4DHC8	0.838	1.216	1.645	1.174	Uncharacterized protein
K4CPN6	0.838	0.993	0.957	0.781	Uncharacterized protein
K4C2T9	0.837	0.938	0.983	0.902	1-(5-phosphoribosyl)-5-[(5-phosphoribosylamino)methylideneamino] imidazole-4-carboxamide isomerase, chloroplastic
K4CXN5	0.836	0.856	0.878	1.202	Uncharacterized protein
K4D2W1	0.835	1.135	1.220	1.372	Uncharacterized protein
Q9FUZ0	0.834	1.119	1.308	1.098	Peptide deformylase 1A, chloroplastic
K4DDD7	0.833	1.052	0.883	0.786	Uncharacterized protein
K4D311	0.833	0.812	0.688	0.768	GrpE protein homolog
K4BDU7	0.833	1.136	1.484	1.222	Uncharacterized protein
K4B1M1	0.830	0.983	0.834	0.829	Uncharacterized protein

Accession	Burned	Control	Regular	Limit	Description
K4BBC4	0.828	1.109	1.619	1.373	Plastidic glucose transporter 1
K4DCL4	0.828	0.899	1.212	1.179	Chlorophyll a-b binding protein, chloroplastic
K4CHY3	0.825	0.994	1.136	1.445	Phosphoglycerate kinase
K4BXY4	0.825	0.956	0.748	0.729	Uncharacterized protein
K4D2Z7	0.824	0.918	0.818	0.691	Uncharacterized protein
K4C804	0.824	1.021	1.020	0.862	Uncharacterized protein
K4CGI2	0.824	0.936	1.196	1.436	Uncharacterized protein
P93207	0.822	0.973	1.078	1.300	14-3-3 protein 10
K4BEB0	0.822	1.036	0.997	0.911	Uncharacterized protein
K4AXM4	0.822	0.974	0.858	0.896	Glucose-1-phosphate adenylyltransferase
K4D3V6	0.821	0.957	1.135	1.572	Uncharacterized protein
K4BAF3	0.821	1.034	1.105	0.936	Phosphoserine aminotransferase
K4DDF6	0.821	1.062	1.021	1.285	Uncharacterized protein
K4B172	0.821	0.952	0.988	1.384	Uncharacterized protein
Q32516	0.820	1.160	1.455	1.145	NAD(P)H-quinone oxidoreductase subunit 5, chloroplastic
K4BP27	0.817	0.801	0.742	0.641	Uncharacterized protein
K4ASR0	0.816	0.847	0.735	0.698	Uncharacterized protein
K4BEI9	0.815	1.015	1.149	1.121	SGT1-1
K4BUZ0	0.815	0.947	1.001	1.086	Uncharacterized protein
K4BPP3	0.815	0.946	0.949	0.867	Uncharacterized protein
K4BRC3	0.813	0.826	0.578	0.688	Uncharacterized protein
K4D5Z8	0.812	0.999	1.147	1.766	Isocitrate dehydrogenase [NADP]
K4CXW3	0.812	1.050	0.927	0.888	Glutamyl-tRNA(Gln) amidotransferase subunit A,

Accession	Burned	Control	Regular	Limit	Description
					chloroplastic/mitochondrial
K4BDS4	0.811	0.904	0.868	0.681	Uncharacterized protein
K4BHI9	0.810	0.933	0.981	1.087	Uncharacterized protein
K4BMD5	0.808	0.940	1.044	0.903	Uncharacterized protein
K4BJF3	0.808	0.696	0.594	0.577	Uncharacterized protein
Q6E4P5	0.806	1.018	0.979	0.996	Carotenoid cleavage dioxygenase 1A
Q9LEG3	0.802	1.192	1.609	1.088	Putative alcohol dehydrogenase
K4BB47	0.802	1.022	1.353	1.622	Succinate dehydrogenase [ubiquinone] flavoprotein subunit, mitochondrial
K4CUK9	0.802	0.974	1.185	1.253	Uncharacterized protein
C0LIR4	0.802	0.958	1.104	1.053	Sulfurtransferase
K4BTH5	0.801	1.117	1.296	1.223	Vacuolar-type H+-translocating inorganic pyrophosphatase
K4CP05	0.798	0.914	1.158	0.963	Uncharacterized protein
K4BHN8	0.798	0.958	0.730	0.690	Uncharacterized protein
K4CEG5	0.798	0.841	0.896	0.873	Glycosyltransferase
K4BTL1	0.798	0.868	0.904	1.287	Uncharacterized protein
G3K2M4	0.797	1.054	1.145	0.915	Methionine sulfoxide reductase A4
K4CN44	0.796	0.994	0.929	0.804	Uncharacterized protein
K4CXR1	0.796	1.096	0.943	0.812	Uroporphyrinogen decarboxylase
K4B3J8	0.795	1.351	1.327	0.807	Uncharacterized protein
K4CVX6	0.795	0.955	2.130	3.046	Uncharacterized protein
K4BKR7	0.794	0.962	1.371	1.242	Uncharacterized protein
K4D8C1	0.794	0.979	1.179	1.301	Uncharacterized protein
K4CNG0	0.794	0.976	1.003	0.967	Uncharacterized protein
K4D054	0.792	0.817	0.699	0.834	Uncharacterized protein
K4BRF4	0.789	1.285	1.214	0.730	Uncharacterized protein
K4D9S4	0.789	1.082	1.329	1.220	Glycosyltransferase
K4D5K8	0.786	0.961	1.047	1.233	Uncharacterized protein
K4C234	0.786	0.941	0.918	0.897	Uncharacterized protein
K4BKU7	0.785	1.021	1.123	0.943	Uncharacterized protein
K4BH21	0.784	0.960	0.950	0.892	Uncharacterized protein
K4BJI5	0.782	0.958	1.222	1.337	Uncharacterized protein
K4DC08	0.781	1.160	1.180	1.273	Chlorophyll a-b binding protein, chloroplastic
K4CWB0	0.781	1.017	0.842	0.811	Glutamyl-tRNA(Gln) amidotransferase subunit B, chloroplastic/mitochondrial
K4BF12	0.781	0.982	0.960	0.742	Uncharacterized protein
K4BEC6	0.781	0.876	0.843	0.783	Uncharacterized protein
Q6E4P4	0.779	1.010	0.921	0.824	Carotenoid cleavage dioxygenase 1B
K4BN59	0.779	1.038	1.410	2.093	Uncharacterized protein
K4CEA5	0.778	1.071	1.467	1.424	Uncharacterized protein
K4CQB7	0.777	1.184	1.572	1.892	Uncharacterized protein
K4BEW6	0.776	1.063	1.021	0.878	Uncharacterized protein
K4BL84	0.776	0.899	1.009	0.850	Uncharacterized protein
K4D4L5	0.776	0.869	0.778	0.764	Uncharacterized protein
K4DFK8	0.775	1.016	1.043	0.901	Uncharacterized protein
K4D7W0	0.775	0.937	1.278	1.439	Cytochrome b-c1 complex subunit Rieske, mitochondrial
C6K2L0	0.774	1.005	0.843	0.788	GDP-mannose 3',5'-epimerase
K4BPG2	0.773	1.063	1.343	1.009	Uncharacterized protein

Accession	Burned	Control	Regular	Limit	Description
K4CQA5	0.773	0.821	1.141	1.068	Uncharacterized protein
K4CFG8	0.772	0.899	0.746	0.653	Beta-amylase
K4B3H5	0.769	1.036	1.408	1.252	Uncharacterized protein
D3J5I7	0.762	0.917	0.813	0.919	Plastid-dividing ring protein
K4CXQ8	0.761	1.105	1.138	1.428	Uncharacterized protein
K4C1B2	0.760	1.007	1.222	1.096	Uncharacterized protein
K4DHP4	0.760	1.138	1.279	1.118	Uncharacterized protein
K4BDZ7	0.760	1.185	1.000	0.857	Uncharacterized protein
C0LIR5	0.760	0.976	1.101	1.057	Thiosulfate:cyanide sulfurtransferase-like protein (Fragment)
K4B6W2	0.759	0.915	0.967	1.921	Uncharacterized protein
K4D834	0.757	1.029	1.019	0.942	Uncharacterized protein
C6K2K9	0.754	1.024	0.837	0.756	GDP-mannose 3',5'-epimerase
K4CU44	0.752	1.001	1.110	1.144	Uncharacterized protein
K4CPC2	0.752	1.105	1.077	1.103	Uncharacterized protein
K4CLQ8	0.751	0.957	1.051	1.058	Uncharacterized protein
Q96483	0.750	1.060	1.205	1.215	Actin-51 (Fragment)
K4CN57	0.749	0.847	1.854	4.558	Uncharacterized protein
K4BKN2	0.748	1.046	1.091	1.139	Uncharacterized protein
C0LIR3	0.746	1.089	0.859	0.816	UDP-sulfoquinovose synthase
K4BT78	0.746	1.061	1.143	1.201	Uncharacterized protein
K4BKJ8	0.746	1.011	1.027	0.935	Uncharacterized protein
K4D2U0	0.743	1.056	1.167	1.128	Uncharacterized protein
K4CN58	0.742	0.863	1.843	4.517	Uncharacterized protein
K4D9S5	0.740	1.114	1.383	1.320	Glycosyltransferase
K4B0H8	0.738	0.800	0.606	0.556	Uncharacterized protein

Accession	Burned	Control	Regular	Limit	Description
Q2MI64	0.738	0.879	0.801	0.775	50S ribosomal protein L14, chloroplastic
K4BGW5	0.734	0.980	1.061	0.822	Uncharacterized protein
K4B196	0.732	0.872	0.807	0.761	Uncharacterized protein
Q5NE17	0.732	0.918	0.960	1.082	Malate dehydrogenase
K4CG46	0.731	1.092	1.040	1.407	Uncharacterized protein
K4CVG3	0.730	0.944	1.196	1.703	Lipoxygenase
K4D3D6	0.730	0.983	0.869	0.839	Uncharacterized protein
Q9FVN0	0.730	1.068	1.409	0.739	Ammonium transporter 1 member 3
K4CIG0	0.728	0.797	0.968	1.046	Glutathione peroxidase
K4BML6	0.727	1.138	1.231	1.177	Uncharacterized protein
K4CEP4	0.727	0.883	0.969	0.968	Uncharacterized protein
K4C144	0.727	1.032	1.292	1.497	Malic enzyme
B1N662	0.726	1.083	1.221	1.025	Mitochondrial carrier protein
K4CQX2	0.726	0.954	0.847	0.803	Uncharacterized protein
P29795	0.725	0.883	0.969	0.968	Oxygen-evolving enhancer protein 2, chloroplastic
K4CB78	0.724	0.924	0.895	0.949	Uncharacterized protein
K4B6N4	0.724	1.062	0.816	0.979	Malate dehydrogenase
K4DGZ2	0.724	1.035	1.197	1.037	Uncharacterized protein
H6WYS2	0.721	1.089	1.188	1.275	Sulfite reductase
K4CPR5	0.721	0.935	0.780	0.901	Uncharacterized protein
K4D4E7	0.719	0.937	0.981	0.943	Uncharacterized protein
D0VNY3	0.719	1.084	0.844	0.705	ISPH protein
K4CN59	0.719	0.873	1.885	4.595	Uncharacterized protein
K4ASC8	0.718	1.056	1.268	1.204	Uncharacterized protein
K4DCC5	0.718	1.036	1.108	0.774	Uncharacterized protein
K4CEP2	0.718	0.943	0.849	1.115	Uncharacterized protein

Accession	Burned	Control	Regular	Limit	Description
K4B375	0.716	0.902	0.890	1.376	Uncharacterized protein
K4C6K7	0.716	0.911	1.052	1.237	Uncharacterized protein
K4BN60	0.716	0.980	1.105	1.303	Uncharacterized protein
K4CN09	0.715	1.065	0.726	0.561	Glycerol-3-phosphate acyltransferase, chloroplastic
K4AZB8	0.715	0.930	0.899	0.802	Uncharacterized protein
K4BKT6	0.715	1.084	0.741	0.540	Uncharacterized protein
K4B2L1	0.711	0.820	0.756	0.876	Uncharacterized protein
K4B8P9	0.708	0.937	0.938	0.870	Uncharacterized protein
K4B6P1	0.708	0.970	1.050	0.798	Uncharacterized protein
K4BJA2	0.707	0.849	0.892	0.639	Uncharacterized protein
K4DE74	0.707	0.938	0.839	0.684	Uncharacterized protein
K4B9J6	0.707	0.847	1.170	1.344	Uncharacterized protein
K4C8T4	0.707	1.064	1.086	1.260	40S ribosomal protein SA
K4C2H5	0.706	1.052	1.317	0.977	Uncharacterized protein
K4C3E8	0.706	1.137	1.173	1.524	Uncharacterized protein
K4DCW0	0.705	1.105	1.156	1.383	Uncharacterized protein
K4B924	0.705	1.013	0.952	0.844	Uncharacterized protein
K4D140	0.705	0.950	0.954	0.964	Uncharacterized protein
K4DCH1	0.704	1.146	1.122	0.875	Uncharacterized protein
K4BW05	0.704	1.052	1.108	1.224	Uncharacterized protein
K4CW40	0.702	1.036	1.311	1.755	Malate dehydrogenase
K4BK45	0.701	0.798	0.689	0.673	Uncharacterized protein
K4BU01	0.701	0.969	0.911	0.805	Uncharacterized protein
K4BTB8	0.698	1.051	1.162	1.125	Uncharacterized protein
K4C2C6	0.697	1.059	1.171	1.135	Uncharacterized protein
K4CSH4	0.696	1.138	1.159	1.452	Uncharacterized protein
P14278	0.696	0.872	1.055	1.021	Chlorophyll a-b binding protein 4, chloroplastic

Accession	Burned	Control	Regular	Limit	Description
K4CP37	0.694	1.066	0.908	0.777	Uncharacterized protein
K4D0R4	0.694	1.013	1.138	0.833	Uncharacterized protein
K4D2S2	0.694	0.995	0.975	0.882	Adenylosuccinate synthetase, chloroplastic
K4DH24	0.693	0.993	1.397	1.467	Uncharacterized protein
K4CLD5	0.691	0.972	1.181	1.102	Uncharacterized protein
K4CH79	0.691	0.798	0.689	0.709	Uncharacterized protein
K4CQW5	0.689	1.156	1.662	1.577	Uncharacterized protein
K4C353	0.689	0.945	1.063	1.011	Uncharacterized protein
K4CF70	0.686	0.898	0.929	0.927	Fatty acid hydroperoxide lyase, chloroplastic
K4C8X8	0.684	0.930	1.114	1.173	Uncharacterized protein
K4AXM7	0.683	0.848	0.953	1.172	Uncharacterized protein
K4BPK3	0.683	1.065	1.185	1.146	Uncharacterized protein
K4B467	0.682	1.170	1.291	0.945	Uncharacterized protein
Q94FW7	0.679	0.964	0.772	0.871	Heme oxygenase 1
K4CAE9	0.677	0.999	1.338	1.195	Uncharacterized protein
K4DBF1	0.677	0.869	1.039	1.000	Chlorophyll a-b binding protein, chloroplastic
K4B8J0	0.676	0.917	0.898	0.890	Uncharacterized protein
K4AXF5	0.675	1.065	0.775	0.619	Protoporphyrinogen oxidase
K4BBP7	0.673	1.023	0.700	0.563	Uncharacterized protein
K4BSV6	0.673	0.967	0.879	0.839	Uncharacterized protein
K4CRS9	0.670	0.896	0.926	0.926	Chlorophyll a-b binding protein, chloroplastic
K4BX77	0.670	0.934	0.826	0.809	3-isopropylmalate dehydrogenase
K4DCX4	0.669	0.928	0.809	0.895	Uncharacterized protein
K4ASB8	0.668	0.864	0.781	0.665	Uncharacterized protein
K4C768	0.666	0.865	0.971	0.906	Chlorophyll a-b binding protein, chloroplastic

Accession	Burned	Control	Regular	Limit	Description
K4AX51	0.666	0.887	0.894	0.875	Uncharacterized protein
K4D5T1	0.665	0.865	0.806	0.810	Uncharacterized protein
Q2MIB5	0.664	0.875	0.622	0.571	ATP synthase subunit alpha, chloroplastic
K4CY65	0.662	0.963	1.342	1.695	Uncharacterized protein
K4AXJ0	0.660	1.004	1.045	1.206	Uncharacterized protein
K4DFV3	0.660	1.186	1.923	1.411	Plasmamembrane intrinsic protein 13
K4CSF0	0.660	0.844	0.753	0.676	Uncharacterized protein
Q5NE20	0.659	1.128	1.289	1.422	Carbonic anhydrase
P05118	0.659	0.735	1.338	1.095	Wound-induced proteinase inhibitor 1
K4ATJ2	0.659	1.043	1.057	1.021	Uncharacterized protein
K4D3F2	0.658	0.954	0.968	1.064	Uncharacterized protein
K4BEV0	0.657	1.040	1.025	1.203	40S ribosomal protein SA
K4CVU1	0.657	0.903	0.867	0.716	Uncharacterized protein
K4BY59	0.655	1.467	1.440	1.029	Uncharacterized protein
K4CV65	0.654	1.032	1.049	0.909	Uncharacterized protein
P27525	0.652	0.842	0.874	0.933	Chlorophyll a-b binding protein CP24 10B, chloroplastic
K4D6Q9	0.651	0.870	1.019	1.093	Uncharacterized protein
K4CRB9	0.649	0.869	0.828	0.979	Uncharacterized protein
K4D8S6	0.647	0.872	1.274	1.015	Uncharacterized protein
K4BBH8	0.646	1.079	1.079	1.174	Uncharacterized protein
K4DHR2	0.646	0.938	0.826	0.779	Uncharacterized protein
K4CRK7	0.646	0.872	0.648	0.670	Uncharacterized protein
K4DF66	0.644	0.939	0.860	0.869	Uncharacterized protein
K4CCQ6	0.642	1.055	0.999	1.070	Glucose-1-phosphate adenylyltransferase
K4BT84	0.641	0.967	0.933	0.817	Uncharacterized protein

Accession	Burned	Control	Regular	Limit	Description
K4CHY4	0.640	1.036	1.074	0.870	Phosphoglycerate kinase
K4ASJ9	0.639	0.987	1.091	0.945	Uncharacterized protein
K4CGT6	0.637	1.094	1.078	1.339	Uncharacterized protein
K4CFC8	0.637	1.083	1.180	1.024	Uncharacterized protein
K4CWW3	0.635	1.084	0.996	0.692	Uncharacterized protein
K4DI37	0.633	0.914	0.820	0.871	Uncharacterized protein
K4B0Q1	0.631	0.861	1.011	0.965	Uncharacterized protein
Q2MIA0	0.631	1.105	1.350	1.066	Photosystem I P700 chlorophyll a apoprotein A1
K4CGH5	0.629	0.907	1.145	1.430	Uncharacterized protein
K4B4L4	0.628	0.917	1.052	1.105	Uncharacterized protein
K4DDP7	0.628	1.029	1.055	0.619	Uncharacterized protein
K4BVE0	0.628	1.036	1.221	1.088	Ornithine carbamoyltransferase
K4C823	0.627	1.059	1.162	0.923	Uncharacterized protein
K4B4C4	0.627	1.241	1.040	0.644	Uncharacterized protein
K4DBA1	0.627	0.849	0.726	0.686	Cytochrome b6-f complex iron-sulfur subunit
K4DC13	0.624	0.898	0.847	1.076	Uncharacterized protein
K4D4F1	0.617	0.990	1.404	1.849	Uncharacterized protein
K4CXJ6	0.614	0.803	1.059	1.185	Uncharacterized protein
K4CYL8	0.614	0.823	0.712	0.694	Uncharacterized protein
K4D9X3	0.614	0.976	0.784	0.585	Uncharacterized protein
K4B207	0.613	0.909	0.956	0.999	Uncharacterized protein
K4CYY2	0.611	0.938	1.099	0.861	Uncharacterized protein
K4B830	0.610	1.042	1.205	0.816	Uncharacterized protein
K4BP59	0.609	1.298	1.630	1.257	Glyceraldehyde-3-phosphate dehydrogenase
K4CNE7	0.608	1.019	0.650	0.529	Uncharacterized protein

Accession	Burned	Control	Regular	Limit	Description
K4CAE2	0.605	1.138	1.157	1.495	Uncharacterized protein
K4AX11	0.603	0.987	0.991	0.939	Uncharacterized protein
K4AT88	0.600	0.966	1.062	0.724	Uncharacterized protein
K4CB91	0.597	0.906	0.879	0.922	Uncharacterized protein
K4CEL4	0.596	0.861	0.650	0.792	Uncharacterized protein
K4B4U4	0.594	1.301	1.616	1.255	Glyceraldehyde-3-phosphate dehydrogenase
K4D5C2	0.593	0.838	0.643	0.660	Uncharacterized protein
K4CE57	0.591	0.709	0.362	0.384	Uncharacterized protein
P10708	0.591	0.965	1.213	1.043	Chlorophyll a-b binding protein 7, chloroplastic
K4CGQ2	0.588	0.893	0.760	0.781	Uncharacterized protein
K4C9G9	0.588	0.912	1.000	0.827	Uncharacterized protein
Q84LQ3	0.586	0.893	0.971	1.029	Putative FtsH protease
K4BVV2	0.586	0.873	0.806	0.820	Uncharacterized protein
K4BE00	0.584	0.912	1.070	0.930	Chlorophyll a-b binding protein, chloroplastic
K4BE01	0.582	0.912	1.070	0.930	Chlorophyll a-b binding protein, chloroplastic
K4BEJ8	0.581	0.903	0.817	0.768	Uncharacterized protein
P27489	0.580	0.948	0.942	1.011	Chlorophyll a-b binding protein 13, chloroplastic
Q9XG54	0.580	0.962	0.887	0.759	12-oxophytodienoate reductase 1
K4B1K8	0.578	0.913	0.957	1.017	Uncharacterized protein
K4CH43	0.577	0.947	0.940	1.010	Chlorophyll a-b binding protein, chloroplastic
K4CNS6	0.576	1.163	0.958	0.672	Elongation factor G, chloroplastic
Q08451	0.576	1.205	2.220	1.621	Probable aquaporin PIP-type pTOM75
K4C601	0.573	0.991	1.131	1.015	Uncharacterized protein
K4BCU7	0.572	0.927	0.942	1.047	Uncharacterized protein
K4BX19	0.572	0.972	0.879	0.688	Uncharacterized protein
K4BTC6	0.572	0.991	0.716	0.669	Uncharacterized protein
K4D1Q0	0.567	0.988	0.770	0.559	Uncharacterized protein
Q8RU74	0.567	0.948	0.850	0.741	3-dehydroquinate synthase, chloroplastic
K4BSZ1	0.566	0.878	0.789	0.647	Uncharacterized protein
K4D6V7	0.566	0.846	0.674	0.849	Uncharacterized protein
K4CX44	0.565	1.077	0.848	0.865	Uncharacterized protein
P07369	0.564	0.914	1.075	0.947	Chlorophyll a-b binding protein 3C, chloroplastic
K4CCP7	0.564	0.952	0.645	0.456	Elongation factor Ts, mitochondrial
K4BI72	0.561	1.149	1.308	0.666	Uncharacterized protein
K4D3E4	0.561	0.899	0.817	0.871	Fructose-bisphosphate aldolase
Q2MI96	0.560	0.987	1.083	0.774	NAD(P)H-quinone oxidoreductase subunit K, chloroplastic
K4BUB7	0.559	0.991	0.847	0.792	Serine hydroxymethyltransferase
Q9FYW9	0.558	0.979	0.844	0.662	Adenylosuccinate synthetase, chloroplastic
K4DFY4	0.556	0.984	0.718	0.679	Uncharacterized protein
K4BUF0	0.554	0.997	1.086	0.681	Uncharacterized protein
K4CPY0	0.551	0.889	0.776	0.640	Uncharacterized protein
K4CJ67	0.550	0.988	0.822	0.748	Cysteine synthase
K4D601	0.550	1.005	0.973	1.138	Uncharacterized protein
K4D2P9	0.547	1.084	1.288	0.899	Thioredoxin reductase
C0KKU8	0.545	1.111	1.604	0.916	Lipoxygenase

Accession	Burned	Control	Regular	Limit	Description
P08706	0.542	1.127	0.932	0.499	Ribulose bisphosphate carboxylase small chain 1, chloroplastic
P07179	0.540	1.126	0.930	0.499	Ribulose bisphosphate carboxylase small chain 2A, chloroplastic
K4B7T1	0.538	1.167	1.515	0.845	Uncharacterized protein
K4CAF2	0.538	0.917	0.823	0.668	Uncharacterized protein
K4C947	0.531	0.948	0.770	0.716	Uncharacterized protein
K4CG24	0.531	0.924	0.853	0.866	Uncharacterized protein
K4BHN0	0.529	1.075	1.503	1.444	Vacuolar glucose transporter 1
K4CY74	0.528	1.160	1.622	1.212	Uncharacterized protein
K4BL92	0.517	0.912	1.201	1.022	Chlorophyll a-b binding protein, chloroplastic
K4B876	0.514	0.910	1.067	1.032	Chlorophyll a-b binding protein, chloroplastic
K4AYG3	0.513	0.904	0.745	0.746	Ribosomal protein
K4BVZ0	0.511	1.232	1.442	1.065	Glyceraldehyde-3-phosphate dehydrogenase
Q7M1K8	0.507	0.920	1.209	1.030	Chlorophyll a-b binding protein, chloroplastic
K4BCV4	0.507	1.014	0.912	0.906	Serine hydroxymethyltransferase
K4CQV5	0.505	0.879	0.783	0.845	Fructose-bisphosphate aldolase
K4C647	0.503	0.891	0.798	0.810	Uncharacterized protein
K4B878	0.503	0.910	1.068	1.032	Chlorophyll a-b binding protein, chloroplastic
K4B6A3	0.501	0.925	0.742	0.787	Ferredoxin--NADP reductase
K4BDH8	0.500	0.483	0.206	0.258	Uncharacterized protein
K4BF14	0.500	0.865	0.878	0.717	Uncharacterized protein
K4DH36	0.498	1.212	1.427	1.054	Glyceraldehyde-3-phosphate dehydrogenase
Q2MI44	0.496	0.950	0.927	0.768	NAD(P)H-quinone oxidoreductase subunit H, chloroplastic
Q40131	0.496	1.133	1.638	0.887	Putative uncharacterized protein
K4BPK4	0.495	0.893	0.795	0.809	Uncharacterized protein
K4BAP9	0.493	0.918	0.750	0.795	Ferredoxin--NADP reductase
K4CMY9	0.492	0.867	0.644	0.614	Phosphoribulokinase
K4CB11	0.490	1.023	0.973	1.025	Uncharacterized protein
K4BZF3	0.487	1.043	1.263	0.984	Uncharacterized protein
K4CL87	0.483	0.877	0.953	0.986	Uncharacterized protein
G8Z261	0.481	0.924	0.717	0.532	Hop-interacting protein THI032
K4C945	0.476	1.086	1.131	0.850	Uncharacterized protein
K4ATJ4	0.474	0.854	0.788	0.706	Peptidyl-prolyl cis-trans isomerase
K4C377	0.467	0.827	0.736	0.778	Uncharacterized protein
K4C9D8	0.460	1.147	1.650	1.518	Uncharacterized protein
Q2MI46	0.460	0.903	0.839	0.706	NAD(P)H-quinone oxidoreductase subunit I, chloroplastic
K4DG90	0.460	1.383	1.715	1.016	Uncharacterized protein
K4BW79	0.459	0.900	0.787	0.852	2-methylene-furan-3-one reductase
Q2MIA5	0.458	1.013	1.184	0.898	Photosystem II D2 protein
K4BMJ2	0.457	0.996	0.845	0.591	Uncharacterized protein

Accession	Burned	Control	Regular	Limit	Description
K4C035	0.454	1.001	0.980	0.747	Uncharacterized protein
K4C423	0.450	1.035	1.554	1.107	Uncharacterized protein
P27524	0.449	0.814	0.927	0.945	Chlorophyll a-b binding protein CP24 10A, chloroplastic
K4B1S1	0.448	0.844	0.653	0.746	Uncharacterized protein
Q15I66	0.443	0.935	0.834	0.766	Glucose-1-phosphate adenylyltransferase
K4BLS5	0.439	0.936	0.897	0.742	Uncharacterized protein
K4C331	0.438	0.874	0.795	0.839	Uncharacterized protein
K4B9B4	0.421	1.115	1.491	1.351	Uncharacterized protein
K4CUE5	0.421	0.989	0.875	0.636	Uncharacterized protein
Q2MI49	0.413	0.922	1.060	0.735	Photosystem I iron-sulfur center
K4CHR6	0.412	0.826	0.645	0.560	Fructose-bisphosphate aldolase
K4B9V1	0.408	1.083	1.212	1.051	Aminomethyltransferase
K4D0P3	0.406	0.942	0.751	0.620	Uncharacterized protein
K4AXS2	0.404	1.234	1.413	0.766	Glutamine synthetase
K4BB24	0.403	0.904	0.823	0.760	Uncharacterized protein
K4B3X5	0.398	0.767	0.615	0.555	Uncharacterized protein
K4BK24	0.395	0.923	0.733	0.506	Uncharacterized protein
K4D180	0.391	0.750	0.555	0.476	Uncharacterized protein
A0A0J9YZP9	0.382	0.865	1.018	0.828	Chlorophyll a-b binding protein, chloroplastic
Q2MI77	0.380	0.941	0.776	0.755	50S ribosomal protein L20, chloroplastic
K4BBK4	0.378	0.970	1.559	1.464	Uncharacterized protein
K4B378	0.376	0.948	0.732	0.532	Uncharacterized protein
K4CIJ1	0.373	0.773	0.737	0.674	Glycine cleavage system H protein
K4D5G2	0.364	0.987	0.974	0.877	Uncharacterized protein
Q4W5U8	0.364	0.865	0.756	0.749	FtsH protease
Q43517	0.363	0.673	0.461	0.317	Ferredoxin-1, chloroplastic
K4CIK5	0.355	1.073	0.688	0.591	Uncharacterized protein
K4C6T7	0.350	0.775	0.746	0.668	Glycine cleavage system H protein
K4C1C9	0.350	1.029	0.945	0.690	Uncharacterized protein
K4DBI4	0.349	0.922	0.889	0.606	Uncharacterized protein
P27065	0.348	1.205	1.018	0.328	Ribulose bisphosphate carboxylase large chain
Q2MIA4	0.347	0.912	0.920	0.731	Photosystem II CP43 reaction center protein
K4D489	0.343	1.004	0.768	0.410	Uncharacterized protein
Q2MI75	0.335	0.960	1.075	0.841	Photosystem II CP47 reaction center protein
K4CRD4	0.331	1.007	0.763	0.404	Uncharacterized protein
K4CVU5	0.327	0.879	0.829	0.737	Uncharacterized protein
Q40129	0.311	0.882	1.491	1.352	Putative uncharacterized protein
K4CYV4	0.309	1.038	0.943	0.678	Uncharacterized protein
K4BHA1	0.305	0.864	0.684	0.525	Uncharacterized protein
K4AZA6	0.300	1.248	1.427	0.878	Uncharacterized protein
K4CGI6	0.297	0.973	0.790	0.571	Uncharacterized protein
K4B425	0.285	0.941	0.674	0.588	Uncharacterized protein
K4CKH7	0.285	0.977	0.811	0.581	Uncharacterized protein
K4CXT9	0.281	0.957	0.757	0.576	Uncharacterized protein
Q2MIC0	0.270	0.973	1.065	0.687	Photosystem II protein D1
K4BAW0	0.261	0.906	0.738	0.458	Fructose-bisphosphate aldolase
K4B6C3	0.259	0.931	0.680	0.443	Fructose-bisphosphate aldolase

Accession	Burned	Control	Regular	Limit	Description
K4CLA3	0.255	0.956	0.829	0.602	Glycine cleavage system P protein
K4B3P9	0.251	0.940	0.703	0.455	Fructose-bisphosphate aldolase
K4BX34	0.242	0.902	0.750	0.488	Fructose-bisphosphate aldolase
K4D1V7	0.221	0.657	0.484	0.275	Ferredoxin

9.4 Appendix D: List of proteins identified on the blue LED treatment.

Accession	Burned	Control	Regular	Limit	Description
A0A0C5CEC8	-0.27	-0.01	-0.46	0.12	Acetyl-coenzyme A carboxylase carboxyl transferase subunit beta, chloroplastic
A0A0J9YZP8	0.06	-0.04	0.10	0.08	Uncharacterized protein
A0A0J9YZP9	-1.75	0.00	-0.42	-1.16	Chlorophyll a-b binding protein, chloroplastic
A0RZC9	0.07	-0.11	-0.01	0.00	Constitutive plastid-lipid associated protein
A0RZD0	0.02	0.00	2.45	2.53	Inducible plastid-lipid associated protein
A4ZYQ6	-1.19	-0.54	-0.34	-0.64	1-aminocyclopropane-1-carboxylate oxidase
A5JV19	-1.80	-0.11	-0.45	-0.28	Zeaxanthin epoxidase, chloroplastic
A6N6K8	-0.36	-0.08	-0.27	0.96	Phenylacetaldehyde reductase
A7X331	0.25	-0.28	-0.07	0.26	Expansin-like protein
B1N662	0.00	0.00	0.79	0.38	Mitochondrial carrier protein
B1Q3F1	-2.12	-0.02	0.09	-1.03	Glutamate decarboxylase
B2CPI9	-0.55	-0.04	-1.05	-0.88	Lycopene epsilon cyclase
B5M9E4	0.02	-0.13	-1.22	0.67	Beta-glucosidase 01
C0KKU8	-2.96	-0.27	0.37	-1.18	Lipoxygenase
C0KZ34	0.76	0.00	-0.23	-1.05	Violaxanthin de-epoxidase
C0LIR3	-0.34	-0.04	0.98	-0.82	UDP-sulfoquinovose synthase
C0LIR4	-0.34	0.00	-0.46	-0.86	Sulfurtransferase
C5IU71	0.89	-0.05	0.03	0.29	Chloroplast sedoheptulose-1,7-bisphosphatase
C6K2K9	-0.54	-0.14	0.03	-0.42	GDP-mannose 3',5'-epimerase
C6K2L0	-1.02	-0.13	-0.07	-0.59	GDP-mannose 3',5'-epimerase
C6KI36	-0.76	-0.04	-1.04	-0.22	Starch synthase III
D0VNY3	-1.76	-0.07	-0.59	-1.00	ISPH protein
D1MAF2	1.55	0.00	-0.30	-0.31	Exportin-1
D2KQI9	-0.34	-0.03	0.24	-1.38	Succinate dehydrogenase [ubiquinone] iron-sulfur subunit, mitochondrial
D3J5I7	1.45	-0.04	0.19	0.12	Plastid-dividing ring protein
D7S016	0.17	-0.49	0.03	0.57	Glycosyltransferase
E0XN34	0.16	0.00	-1.12	-0.21	Alpha-mannosidase
E0Z1D0	-0.63	-0.25	0.15	0.58	Sucrose synthase
E1U7P9	-0.73	-0.02	0.57	-0.76	Glutathione synthetase
E3UVW7	-0.96	-0.15	-0.25	-0.34	Beta-galactosidase
E5KBY0	-2.99	-1.19	-1.01	-0.81	Snakin-2
E5LBC4	0.80	-0.01	0.65	1.10	Prephenate aminotransferase
G1DEX3	0.84	-0.38	0.08	-0.03	Cutin-deficient 1 protein

Accession	Burned	Control	Regular	Limit	Description
G3K2M4	-0.81	-0.02	-0.16	0.21	Methionine sulfoxide reductase A4
G8XSL1	-0.06	-0.04	-0.33	0.91	GSH1
G8Z254	-0.07	-0.01	-0.08	-1.68	Hop-interacting protein THI016
G8Z261	-1.64	-0.06	-0.48	-2.31	Hop-interacting protein THI032
G8Z271	0.70	-0.19	0.64	0.44	Hop-interacting protein THI044
G8Z278	-0.69	-0.13	-0.21	-0.87	Hop-interacting protein THI111
H1AC33	-0.76	-0.01	-0.17	-0.50	Beta-D-xylosidase
H1ZXA9	-0.48	-0.05	-0.74	0.26	Heat shock protein 70 isoform 3
H6WYS2	-1.19	-0.13	-0.67	-1.12	Sulfite reductase
K4AS92	-0.80	-0.23	0.11	0.16	Uncharacterized protein
K4ASB8	-0.43	-0.02	0.08	-0.99	Uncharacterized protein
K4ASC0	0.59	0.00	-0.30	0.29	Lysine--tRNA ligase
K4ASC2	-1.38	-0.15	0.18	-0.30	Isocitrate dehydrogenase [NADP]
K4ASC8	0.25	-0.01	0.13	0.65	Uncharacterized protein
K4ASG2	-0.07	-0.06	0.27	0.42	Uncharacterized protein
K4ASJ4	-1.52	-0.01	0.82	-0.43	Uncharacterized protein
K4ASJ5	0.67	-0.31	0.86	1.78	Peroxidase
K4ASJ6	0.29	-0.01	0.80	1.93	Peroxidase
K4ASJ9	-0.29	-0.29	-0.06	-0.84	Uncharacterized protein
K4ASL1	0.19	-0.11	0.69	0.11	Uncharacterized protein
K4ASM0	-0.03	0.00	0.20	-0.78	Lipoxygenase
K4ASQ6	0.44	-0.08	0.63	1.42	Uncharacterized protein
K4ASR0	1.39	-0.03	-0.94	-0.34	Uncharacterized protein
K4ASR4	-0.97	-0.45	-0.75	-0.13	Uncharacterized protein
K4AST1	-1.24	0.00	-0.39	-0.72	Coatomer subunit beta
K4ASV2	-1.24	-0.43	-2.52	-1.54	ATP-dependent Clp protease proteolytic subunit
K4ASV3	-0.17	0.00	-0.55	-0.27	Photosystem II CP47 reaction center protein
K4ASV9	0.98	0.00	0.56	-0.05	Ribosomal protein
K4ASW1	-0.31	-0.20	-0.71	-1.08	Uncharacterized protein
K4ASW3	0.29	-0.10	-0.56	-0.59	Uncharacterized protein
K4ASX2	-0.77	-0.13	-0.47	-0.52	Uncharacterized protein
K4AT06	1.40	-0.25	-1.14	1.28	40S ribosomal protein S27
K4AT23	-1.47	-0.36	-0.58	-0.76	Uncharacterized protein
K4AT31	-0.73	-0.06	-0.54	-0.45	Uncharacterized protein
K4AT35	-1.42	-0.28	-1.00	-1.24	Uncharacterized protein
K4AT88	0.20	-0.05	-0.53	-0.03	Uncharacterized protein
K4AT91	1.60	0.00	-0.64	1.54	Uncharacterized protein
K4AT92	-1.58	-0.44	0.19	-0.37	AGO4A
K4ATA1	1.12	-0.04	0.25	0.22	Uncharacterized protein
K4ATA4	2.64	-0.05	-0.37	0.35	Uncharacterized protein
K4ATB4	-0.35	0.00	-0.33	0.26	Uncharacterized protein
K4ATD8	0.52	-0.02	-0.04	0.04	Uncharacterized protein
K4ATJ4	-1.58	-0.17	-2.43	-1.40	Peptidyl-prolyl cis-trans isomerase
K4ATQ2	0.82	-0.23	-0.09	0.82	Uncharacterized protein
K4ATR8	0.46	-0.04	0.25	-0.72	Uncharacterized protein
K4ATR9	-0.99	-0.07	-0.37	0.18	Uncharacterized protein
K4AUB9	-0.09	-0.01	0.78	0.01	Uncharacterized protein
K4AV63	-0.74	-0.24	-0.39	-0.13	Uncharacterized protein
K4AV84	0.36	-0.19	-0.33	0.21	Serine/threonine-protein phosphatase
K4AVB7	0.39	-0.09	-0.58	0.06	Uncharacterized protein
K4AVE9	1.87	0.00	0.87	1.43	Uncharacterized protein
K4AVY7	0.07	-0.28	-1.72	-0.24	Uncharacterized protein

Accession	Burned	Control	Regular	Limit	Description
K4AVZ4	-0.65	-0.05	-0.56	0.32	Uncharacterized protein
K4AW95	-0.44	-0.01	0.88	-0.23	Uncharacterized protein
K4AWA0	0.45	-0.04	-1.25	0.36	Uncharacterized protein
K4AWC1	-0.05	-0.04	-0.58	-1.27	Uncharacterized protein
K4AWF0	0.69	0.00	0.44	0.56	Importin subunit alpha
K4AWT4	-0.54	-0.04	0.54	0.07	40S ribosomal protein S21
K4AWX8	-0.82	-0.07	-0.36	-1.04	Uncharacterized protein
K4AX22	-2.84	-0.07	-0.41	0.52	Superoxide dismutase [Cu-Zn]
K4AX51	-0.38	-0.04	-0.05	0.10	Uncharacterized protein
K4AX99	-1.73	-0.02	-1.76	0.10	Uncharacterized protein
K4AXB5	-1.29	-0.31	0.36	-0.99	Uncharacterized protein
K4AXC0	0.64	0.00	0.70	0.58	Citrate synthase
K4AXF5	-0.63	-0.19	-0.44	-0.06	Uncharacterized protein
K4AXJ0	-1.11	-0.27	0.52	0.06	Uncharacterized protein
K4AXJ2	-0.80	-0.03	-0.58	-1.50	Uncharacterized protein
K4AXL3	0.31	0.00	0.31	0.36	Uncharacterized protein
K4AXM4	-0.23	-0.03	-0.27	-0.96	Glucose-1-phosphate adenylyltransferase
K4AXM7	-0.54	-0.07	1.49	0.03	Uncharacterized protein
K4AXN3	-0.09	-0.01	0.26	0.05	Uncharacterized protein
K4AXS2	-1.88	-0.04	-0.55	-1.01	Glutamine synthetase
K4AXU0	-0.01	-0.36	0.92	-0.17	Uncharacterized protein
K4AXU5	-0.31	-0.01	-0.51	-1.01	Uncharacterized protein
K4AXX7	-1.75	-0.01	-0.40	-1.60	Protein translocase subunit SecA
K4AY97	-0.29	-0.05	-0.41	-0.02	Uncharacterized protein
K4AYA3	-0.17	-0.04	-0.73	0.66	Uncharacterized protein
K4AYE2	-1.37	-0.18	-0.96	-0.99	Uncharacterized protein
K4AYE4	-0.24	-0.02	-1.25	-1.21	Uncharacterized protein
K4AYG3	-1.33	-0.25	-0.60	-1.11	Ribosomal protein
K4AYG5	0.37	-0.07	-0.70	0.14	Uncharacterized protein

Accession	Burned	Control	Regular	Limit	Description
K4AYH0	0.44	-0.02	1.64	0.80	Uncharacterized protein
K4AYJ2	-1.68	-0.02	-0.13	-0.26	Uncharacterized protein
K4AYJ8	-2.72	-0.21	-1.26	-1.56	Uncharacterized protein
K4AYM7	-1.50	-0.01	-1.80	-1.04	Eukaryotic translation initiation factor 3 subunit B
K4AYP1	0.31	0.00	-1.20	-0.35	Uncharacterized protein
K4AYP6	1.19	-0.01	0.17	1.58	Uncharacterized protein
K4AYQ1	0.85	-0.32	-0.09	0.19	Uncharacterized protein
K4AYT8	1.11	0.00	-0.29	1.26	Nucleoside diphosphate kinase
K4AYW1	-0.22	0.00	-0.09	0.13	Uncharacterized protein
K4AZ16	-0.43	-0.10	-0.42	-0.30	Uncharacterized protein
K4AZ93	-1.10	-0.25	-1.09	-1.10	Uncharacterized protein
K4AZ98	0.66	-0.06	0.25	-0.12	Uncharacterized protein
K4AZG1	-0.85	-0.01	-0.04	0.80	Malic enzyme
K4AZH0	-0.49	0.00	0.04	0.14	Uncharacterized protein
K4AZH5	0.11	-0.10	-0.52	0.97	Uncharacterized protein
K4AZL9	-0.17	-0.21	0.11	0.42	Cysteine synthase
K4AZT2	0.57	-0.07	-0.15	-0.49	Uncharacterized protein
K4AZV6	-0.03	-0.27	-0.61	0.15	Uncharacterized protein
K4AZZ3	-0.08	0.00	0.28	-0.90	Uncharacterized protein
K4B012	-1.06	-0.01	1.08	-1.17	Uncharacterized protein
K4B033	0.98	-0.02	-0.24	0.46	Uncharacterized protein
K4B046	0.09	-0.93	1.32	-0.41	Uncharacterized protein
K4B075	0.19	-0.05	-0.36	0.27	Uncharacterized protein
K4B0B4	1.19	0.00	1.58	2.80	Uncharacterized protein
K4B0D3	-0.85	-0.39	0.17	-0.92	Uncharacterized protein
K4B0D9	0.18	-0.01	1.09	1.22	Uncharacterized protein
K4B0G3	-2.72	-0.70	-1.01	-1.49	Uncharacterized protein
K4B0G4	-0.33	-0.33	-0.30	-0.54	Uncharacterized protein
K4B0I7	-0.12	-0.70	-1.01	0.45	Uncharacterized protein

Accession	Burned	Control	Regular	Limit	Description
K4B0Q1	0.39	0.00	0.09	0.46	Uncharacterized protein
K4B0S5	0.03	0.00	0.07	0.36	Uncharacterized protein
K4B0U8	1.12	-0.19	1.00	0.79	Uncharacterized protein
K4B0W1	-0.08	-0.08	-0.43	0.44	Uncharacterized protein
K4B101	0.98	0.00	0.54	0.80	Uncharacterized protein
K4B103	-0.03	-0.15	-0.57	-1.29	ATP-dependent Clp protease proteolytic subunit
K4B110	-1.11	-0.41	-0.57	-0.02	Uncharacterized protein
K4B111	0.50	-0.16	0.26	0.91	Uncharacterized protein
K4B117	0.40	0.00	0.59	-1.02	Uncharacterized protein
K4B124	-0.89	-0.20	-0.59	1.13	Uncharacterized protein
K4B137	1.01	-0.14	0.22	0.94	Uncharacterized protein
K4B166	-1.13	-0.09	0.19	0.51	Uncharacterized protein
K4B169	-0.99	-0.11	-0.19	-1.08	Uncharacterized protein
K4B170	-1.04	-0.15	-1.82	-0.97	Uncharacterized protein
K4B172	-0.88	-0.21	-1.19	0.83	Uncharacterized protein
K4B196	-0.34	-0.05	0.45	-0.36	Uncharacterized protein
K4B1B8	0.52	-0.10	0.49	0.55	Uncharacterized protein
K4B1F9	0.92	0.00	0.50	0.43	Uncharacterized protein
K4B1G3	0.00	0.00	-0.18	-1.65	Pectin acetylesterase
K4B1G9	0.28	-0.01	0.57	-0.63	Uncharacterized protein
K4B1H9	-0.76	-1.13	-0.69	-0.41	Uncharacterized protein
K4B1J4	-1.29	-0.16	0.09	-0.61	Uncharacterized protein
K4B1K6	1.74	-0.08	1.53	0.62	Uncharacterized protein
K4B1K8	-0.32	-0.03	0.22	-0.54	Uncharacterized protein
K4B1M7	0.62	-0.10	0.63	-1.07	Uncharacterized protein
K4B1N6	1.38	-0.29	0.54	1.00	Uncharacterized protein
K4B1R4	-0.37	-0.36	0.41	-0.05	Uncharacterized protein
K4B1S1	-0.22	-0.02	-0.39	-0.42	Uncharacterized protein
K4B1S4	0.75	-0.12	1.13	-0.09	Uncharacterized protein
K4B1S7	-1.13	-0.11	-0.57	-1.39	Uncharacterized protein
K4B1U6	-0.73	-0.12	-1.35	-1.66	Uncharacterized protein
K4B1V0	-0.65	-0.59	-0.02	-1.13	Uncharacterized protein
K4B1X9	-0.01	-0.48	-1.79	-1.67	Uncharacterized protein
K4B1Z2	0.07	-0.22	0.01	0.72	Uncharacterized protein
K4B202	0.58	-0.07	0.15	-0.18	Uncharacterized protein
K4B212	-0.40	-0.51	0.19	-1.27	Uncharacterized protein
K4B264	-0.31	-0.69	0.82	0.71	Uncharacterized protein
K4B267	-1.09	-0.14	0.48	-0.52	Uncharacterized protein
K4B274	0.84	-0.70	-1.39	0.30	Uncharacterized protein
K4B276	0.80	-0.37	1.23	-0.12	Uncharacterized protein
K4B277	-0.30	0.00	0.68	0.98	Peroxidase
K4B2A4	-1.87	-0.02	-0.68	-1.45	Uncharacterized protein
K4B2C4	-0.30	-0.07	-0.94	-1.33	Uncharacterized protein
K4B2H0	0.88	-0.01	0.89	1.07	Uncharacterized protein
K4B2H7	1.23	0.00	0.02	0.54	Uncharacterized protein
K4B2I9	-0.48	-0.02	0.37	0.50	Uncharacterized protein
K4B2J4	-1.25	-0.05	0.26	0.13	Uncharacterized protein
K4B2L1	-0.84	-0.04	-0.25	-0.78	Uncharacterized protein
K4B2L3	-0.30	-0.06	-0.44	0.13	Uncharacterized protein
K4B2Y0	0.11	0.00	0.64	1.08	Uncharacterized protein
K4B2Y6	-0.10	0.00	-0.48	0.35	Uncharacterized protein
K4B303	-0.76	-0.15	-0.14	0.09	Polyadenylate-binding protein
K4B364	-0.10	0.00	-1.13	-0.78	Carboxypeptidase
K4B375	-2.04	-0.01	-0.74	-0.33	Uncharacterized protein
K4B378	-0.50	0.00	-0.18	-0.97	Uncharacterized protein
K4B381	0.37	-0.04	0.71	0.30	N-acetylglutamate-5-P reductase
K4B3F4	-0.64	-0.36	0.59	-0.25	Dolichyl-diphosphooligosaccharide--protein

Accession	Burned	Control	Regular	Limit	Description
					glycosyltransferase 48 kDa subunit
K4B3G5	-1.79	-0.19	-0.40	-1.16	Uncharacterized protein
K4B3G7	-0.50	-0.17	-0.45	0.90	Coatomer subunit gamma
K4B3H9	0.54	-0.14	0.32	0.52	Uncharacterized protein
K4B3J8	-1.26	-0.01	-0.18	-0.14	Uncharacterized protein
K4B3K7	-1.01	-0.31	-1.47	-0.89	Uncharacterized protein
K4B3L3	0.16	-0.02	0.14	1.34	Beta-galactosidase
K4B3M5	-0.83	-0.09	0.05	-0.07	V-type proton ATPase subunit a
K4B3M9	0.29	0.00	0.09	-0.03	Uncharacterized protein
K4B3P9	-0.09	-0.01	0.07	0.16	Fructose-bisphosphate aldolase
K4B3X5	-0.57	-0.07	-1.03	-1.09	Uncharacterized protein
K4B3Y2	0.75	-0.06	-0.65	0.78	Uncharacterized protein
K4B3Y8	-0.43	-0.01	0.79	-1.01	Uncharacterized protein
K4B402	-0.02	-0.04	1.19	1.37	Uncharacterized protein
K4B406	-1.06	-0.02	-0.06	0.16	Uncharacterized protein
K4B413	-0.92	-0.16	-1.00	-0.65	Uncharacterized protein
K4B414	0.05	0.00	0.78	-0.67	Uncharacterized protein
K4B425	-1.60	-0.01	-0.80	-1.25	Uncharacterized protein
K4B428	-0.59	-0.01	0.19	0.37	Plasmamembrane intrinsic protein 28
K4B433	-0.72	-0.02	0.37	0.54	Uncharacterized protein
K4B438	0.13	-0.10	0.76	0.70	Uncharacterized protein
K4B461	-1.10	-0.01	-0.52	-0.67	Probable alanine--tRNA ligase, chloroplastic
K4B467	0.43	-0.04	-0.14	0.44	Uncharacterized protein
K4B489	-0.14	-0.02	0.75	0.39	Aminoacylase
K4B4L4	0.07	-0.22	0.19	0.30	Uncharacterized protein
K4B4N0	-1.54	-0.01	-0.27	-1.87	Uncharacterized protein
K4B4U1	1.22	0.00	1.52	-0.39	Uncharacterized protein
K4B4U4	-0.68	-0.02	-0.29	-0.01	Glyceraldehyde-3-phosphate dehydrogenase
K4B4U8	-0.60	-0.01	0.06	-1.39	Uncharacterized protein
K4B4Z2	1.94	0.00	1.27	0.69	Uncharacterized protein
K4B553	0.66	-0.04	-0.25	0.28	Ferredoxin--NADP reductase
K4B5Z5	-1.02	-0.04	-0.38	-0.82	Uncharacterized protein
K4B6A3	-0.80	-0.09	-0.28	-0.36	Ferredoxin--NADP reductase
K4B6C3	-0.24	-0.02	-0.14	-0.46	Fructose-bisphosphate aldolase
K4B6E8	0.10	-0.11	0.17	-0.39	Uncharacterized protein
K4B6K0	-1.63	-0.04	-0.97	-0.11	Uncharacterized protein
K4B6N4	-0.46	0.00	-0.02	1.09	Malate dehydrogenase
K4B6P1	-0.51	-0.26	0.22	-1.82	Uncharacterized protein
K4B6Q3	-0.02	0.00	-0.28	-0.22	Uncharacterized protein
K4B6Q4	-0.57	-0.19	-0.42	0.02	Calcium-transporting ATPase
K4B6S9	-0.43	-0.11	0.04	0.12	Uncharacterized protein
K4B6V8	-0.63	-0.01	0.17	2.02	Uncharacterized protein
K4B6W4	0.13	-0.04	-0.39	0.24	Uncharacterized protein
K4B727	1.55	-0.04	-0.46	1.55	Uncharacterized protein
K4B740	-0.76	-0.10	-0.28	-0.34	UDP-glucose 6-dehydrogenase
K4B768	-0.44	-0.01	-0.48	0.07	Uncharacterized protein
K4B778	-1.43	-0.04	-0.99	-0.03	Uncharacterized protein
K4B779	0.95	-0.01	0.56	2.23	Uncharacterized protein
K4B7E1	-0.66	-0.25	0.02	-1.65	Uncharacterized protein
K4B7N3	-0.94	-0.03	-0.64	-1.72	Uncharacterized protein
K4B7S8	1.91	-0.01	-0.62	0.73	Uncharacterized protein
K4B7T1	-2.38	-0.02	0.95	-1.58	Uncharacterized protein
K4B7U1	0.62	-0.25	1.22	-0.17	Uncharacterized protein
K4B7W7	0.16	-0.04	-2.85	0.06	Uncharacterized protein

Accession	Burned	Control	Regular	Limit	Description
K4B814	-0.26	-0.07	-0.61	0.56	40S ribosomal protein S4
K4B831	-0.68	-0.19	0.28	-0.01	Uncharacterized protein
K4B832	-0.19	-0.12	0.36	0.93	Proteasome subunit alpha type
K4B857	0.57	-0.02	0.37	0.45	Uncharacterized protein
K4B858	1.18	-0.02	1.41	1.13	Uncharacterized protein
K4B878	-0.17	-0.06	-0.46	-0.22	Chlorophyll a-b binding protein, chloroplastic
K4B8D4	-0.36	0.00	0.65	-1.54	Uncharacterized protein
K4B8D7	-0.45	-0.20	-0.53	-1.29	Uncharacterized protein
K4B8D8	-0.12	-0.03	1.52	1.24	Uncharacterized protein
K4B8E7	1.63	0.00	0.35	1.00	Uncharacterized protein
K4B8G4	0.47	-0.14	0.65	0.61	Histidinol dehydrogenase, chloroplastic
K4B8I9	0.98	-0.05	1.16	0.96	Uncharacterized protein
K4B8J0	-0.50	-0.05	-0.98	-0.52	Uncharacterized protein
K4B8P9	-0.64	-0.04	0.08	-0.17	Uncharacterized protein
K4B924	-0.46	0.00	-0.63	-0.52	Uncharacterized protein
K4B937	-0.78	0.00	-0.72	0.23	Eukaryotic translation initiation factor 3 subunit D
K4B978	0.68	-0.01	1.11	-0.18	Clathrin light chain
K4B9B8	0.23	-0.08	1.56	1.44	Uncharacterized protein
K4B9D4	-0.72	0.00	-0.37	0.04	Uncharacterized protein
K4B9J6	1.79	-0.13	1.27	1.19	Uncharacterized protein
K4B9P2	-0.49	-0.45	-0.04	-1.22	Pectinesterase
K4B9R3	-0.09	-0.02	-0.07	-0.78	Uncharacterized protein
K4B9S5	0.91	-0.01	-0.11	0.92	Uncharacterized protein
K4B9T4	0.96	0.00	0.40	1.72	Lactoylglutathione lyase
K4B9V1	-1.87	-0.05	-0.80	-0.80	Aminomethyltransferase
K4B9W8	-0.17	-0.05	0.41	-0.78	Uncharacterized protein
K4B9Y6	-2.05	-0.10	0.09	0.56	Pyrophosphate--fructose 6-phosphate 1-phosphotransferase subunit beta
K4BA10	1.19	0.00	0.34	0.69	Uncharacterized protein
K4BA40	-1.40	-0.49	-0.23	-0.61	Proteasome subunit alpha type
K4BA68	0.00	-0.04	0.27	0.35	Uncharacterized protein
K4BA70	0.37	-0.17	0.68	-1.07	Uncharacterized protein
K4BA73	-0.28	-0.03	-0.86	-1.11	Uncharacterized protein
K4BA90	-0.21	-0.05	-0.76	0.38	Uncharacterized protein
K4BAE6	-1.85	-0.01	-0.92	-0.59	Catalase
K4BAF0	-1.26	-0.07	-0.30	0.79	Uncharacterized protein
K4BAF3	-1.84	-0.41	-1.13	-1.46	Phosphoserine aminotransferase
K4BAK2	0.46	-0.09	-2.08	-1.96	Phospholipase D
K4BAK9	0.24	0.00	1.17	0.49	Uncharacterized protein
K4BAL8	-1.10	-0.33	-0.87	-0.61	Uncharacterized protein
K4BAN9	-0.57	-0.01	0.46	0.68	Uncharacterized protein
K4BAP9	-1.03	-0.06	-0.42	-0.21	Ferredoxin--NADP reductase
K4BAW0	-0.31	-0.02	0.05	-0.05	Fructose-bisphosphate aldolase
K4BB06	0.01	-0.10	1.57	1.39	Proteasome subunit beta type
K4BB24	0.20	-0.12	0.94	0.74	Uncharacterized protein
K4BB47	0.20	-0.02	1.05	0.54	Succinate dehydrogenase [ubiquinone] flavoprotein subunit, mitochondrial
K4BB90	0.70	-0.05	-1.14	0.51	Uncharacterized protein
K4BBC4	-0.67	-0.05	-0.42	0.36	Plastidic glucose transporter 1
K4BBF4	-0.56	-0.02	0.41	-0.52	Uncharacterized protein
K4BBG9	-1.71	-0.09	0.07	0.10	Isocitrate dehydrogenase [NADP]
K4BBI0	0.44	-1.38	-0.73	-0.72	Uncharacterized protein

Accession	Burned	Control	Regular	Limit	Description
K4BBI1	0.86	-1.44	-1.70	-0.07	Uncharacterized protein
K4BBJ0	-0.51	-0.10	-0.14	-0.64	Uncharacterized protein
K4BBJ8	0.45	-0.03	-0.35	0.19	Uncharacterized protein
K4BBM2	-0.70	-0.11	-0.31	-0.69	Uncharacterized protein
K4BBN1	-0.33	-0.05	0.92	-0.15	Uncharacterized protein
K4BBY2	-1.17	-0.01	0.42	-0.92	Uncharacterized protein
K4BC16	-0.40	0.00	-1.17	0.08	Uncharacterized protein
K4BC25	-1.16	-0.04	0.87	0.23	Uncharacterized protein
K4BCF4	0.60	-0.04	0.62	-0.03	Uncharacterized protein
K4BCQ9	-0.82	-0.24	-0.34	-0.42	Uncharacterized protein
K4BCS6	-1.00	-0.11	-0.37	-1.41	ATP-dependent Clp protease proteolytic subunit
K4BCU7	-0.51	-0.11	0.50	-0.11	Uncharacterized protein
K4BCV4	-0.70	-0.01	0.15	-0.20	Serine hydroxymethyltransferase
K4BCV6	-1.80	0.00	0.22	-0.33	Uncharacterized protein
K4BCZ0	-1.90	-0.04	-0.88	-1.87	Xyloglucan endotransglucosylase/hydrolase
K4BCZ5	0.33	0.00	0.20	-0.57	Branched-chain-amino-acid aminotransferase
K4BD40	-0.23	-0.08	0.74	0.73	Uncharacterized protein
K4BD54	-0.62	0.00	0.37	0.82	Peroxidase
K4BD63	1.29	-0.02	1.26	1.25	Uncharacterized protein
K4BDB3	-1.20	-0.07	0.22	-0.32	Uncharacterized protein
K4BDD0	-0.25	0.00	-0.54	0.22	Uncharacterized protein
K4BDE9	0.48	-0.09	-0.63	-0.17	Uncharacterized protein
K4BDF9	-0.12	0.00	-0.09	-0.60	Uncharacterized protein
K4BDK7	-1.58	-0.41	-0.99	-1.91	Uncharacterized protein
K4BDP2	0.21	0.00	0.57	0.53	Phosphorus transporter
K4BDQ9	-0.77	-0.02	-1.11	-1.21	Acetyl-coenzyme A synthetase
K4BDU7	-0.56	-0.02	-0.33	1.21	Uncharacterized protein
K4BDV0	-1.38	-0.05	-0.35	-1.25	Uncharacterized protein
K4BDZ7	-0.68	-0.01	-1.50	-0.34	Uncharacterized protein
K4BE13	0.59	-0.01	0.16	-0.21	Uncharacterized protein
K4BE37	0.06	-0.35	-0.55	-0.18	Uncharacterized protein
K4BEB0	-0.48	0.00	-0.46	-0.65	Uncharacterized protein
K4BEI9	-0.09	0.00	-0.24	-0.78	SGT1-1
K4BET8	1.60	-0.06	0.98	-0.11	Uncharacterized protein
K4BEV0	-0.15	-0.18	-0.15	-0.08	40S ribosomal protein SA
K4BEW6	-0.83	-0.29	-1.28	-0.95	Uncharacterized protein
K4BF05	-0.54	-0.07	-1.28	-0.70	Alcohol acyl transferase
K4BF11	-0.59	0.00	0.61	1.47	Peroxidase
K4BF14	-0.50	0.00	0.06	-0.29	Uncharacterized protein
K4BF25	-0.91	-0.23	0.44	-0.80	60S ribosomal protein L36
K4BF34	1.60	-0.02	0.34	2.13	Uncharacterized protein
K4BFA4	-0.02	-0.04	-0.42	-0.53	Uncharacterized protein
K4BFE4	0.24	-0.02	0.26	-0.32	Uncharacterized protein
K4BFH1	-0.07	0.00	-0.59	-0.09	Thioredoxin reductase
K4BFI7	-0.07	0.00	-0.22	0.77	Uncharacterized protein
K4BFT9	-1.29	-0.01	-1.15	-1.44	Uncharacterized protein
K4BG20	-0.51	0.00	-0.48	-0.29	Uncharacterized protein
K4BG21	-1.19	0.00	0.11	0.43	Uncharacterized protein
K4BG34	0.78	-0.04	1.08	0.61	Uncharacterized protein
K4BGK0	-0.60	-0.01	-0.01	-0.38	Uncharacterized protein
K4BGT9	-2.29	-0.01	-1.38	-0.27	Uncharacterized protein
K4BGW4	0.18	-0.61	-0.11	-0.15	Uncharacterized protein
K4BGW5	0.31	-0.28	0.16	-1.03	Uncharacterized protein
K4BH21	-1.61	-0.08	-0.47	-1.08	Uncharacterized protein
K4BH28	1.82	-0.05	0.38	1.05	Uncharacterized protein
K4BHA1	-0.14	0.00	0.25	0.04	Uncharacterized protein

Accession	Burned	Control	Regular	Limit	Description
K4BHG4	-1.84	-0.36	0.28	-1.05	Alpha-1,4 glucan phosphorylase
K4BHI9	-1.52	-0.02	-0.89	-0.32	Uncharacterized protein
K4BHJ2	-2.36	-0.09	-0.97	-0.11	Histone H2B
K4BHQ8	-0.02	-0.07	0.52	0.89	Uncharacterized protein
K4BHX1	-0.37	-0.12	-0.10	0.52	Uncharacterized protein
K4BHY1	0.33	-0.05	-0.09	0.67	Uncharacterized protein
K4BHZ2	0.00	-0.51	-1.79	-0.69	Uncharacterized protein
K4BI32	0.08	-0.10	0.76	-0.53	Uncharacterized protein
K4BI65	0.73	-0.10	0.44	0.44	Uncharacterized protein
K4BI68	-0.79	-0.06	-1.04	-0.10	Uncharacterized protein
K4BIC0	0.44	0.00	-0.60	-1.93	Uncharacterized protein
K4BIC8	0.80	-0.40	-0.27	0.00	Uncharacterized protein
K4BIG6	0.07	0.00	-0.23	-0.77	Uncharacterized protein
K4BIU3	1.25	-0.01	1.25	-0.72	Uncharacterized protein
K4BJ22	-0.44	0.00	0.26	0.22	Clathrin heavy chain
K4BJA3	0.35	-0.03	-1.19	-0.73	Uncharacterized protein
K4BJC8	0.32	-0.05	0.13	0.91	Uncharacterized protein
K4BJE6	-1.28	-0.03	-0.12	-0.46	Alanine--tRNA ligase
K4BJF4	-1.54	0.00	0.89	-0.25	Uncharacterized protein
K4BJG4	-0.38	-0.18	-0.45	-0.91	Uncharacterized protein
K4BJI5	-0.12	0.00	0.87	0.36	Uncharacterized protein
K4BJJ6	-0.18	-0.35	0.53	0.47	Uncharacterized protein
K4BJT6	0.41	-0.08	0.96	0.31	Uncharacterized protein
K4BJU1	0.52	-0.06	1.53	2.07	Uncharacterized protein
K4BJW4	-1.14	0.00	-0.62	-0.27	Glyceraldehyde-3-phosphate dehydrogenase
K4BJY3	0.84	-0.11	0.62	1.34	Uncharacterized protein
K4BJY6	-2.78	-0.29	-0.91	-1.71	Uncharacterized protein
K4BJZ7	-0.48	0.00	-0.43	-0.57	Uncharacterized protein
K4BK24	0.48	-0.04	-0.41	-0.10	Uncharacterized protein
K4BK27	0.05	-0.38	-0.49	-1.53	Uncharacterized protein
K4BK30	-1.43	-0.12	0.02	-0.49	Uncharacterized protein
K4BK43	-0.52	-0.11	0.67	-0.62	Uncharacterized protein
K4BK45	1.20	0.00	-0.89	-0.31	Uncharacterized protein
K4BK46	-0.58	-0.10	-0.31	0.51	Uncharacterized protein
K4BK61	-0.70	-0.01	1.06	-0.03	D-3-phosphoglycerate dehydrogenase
K4BK69	0.49	0.00	0.19	0.35	Elongation factor Tu
K4BK89	0.11	-0.22	-0.71	-0.04	Uncharacterized protein
K4BK90	0.99	-0.38	-1.15	0.24	Uncharacterized protein
K4BKE4	0.50	-0.04	1.01	0.98	Uncharacterized protein
K4BKF6	0.79	-0.19	0.26	2.31	Aldose 1-epimerase
K4BKH5	-0.14	-0.16	1.21	1.47	Uncharacterized protein
K4BKH7	1.48	-0.24	-0.45	1.37	Uncharacterized protein
K4BKN1	-1.63	-0.26	0.37	-1.01	Uncharacterized protein
K4BKN2	-0.07	-0.03	0.55	-0.69	Uncharacterized protein
K4BKR7	-1.32	0.00	0.13	-0.32	Uncharacterized protein
K4BKT6	0.15	-0.38	-1.56	-0.33	Uncharacterized protein
K4BKU7	-0.39	-0.04	-0.09	0.06	Uncharacterized protein
K4BKV8	1.70	-0.19	0.50	1.35	Uncharacterized protein
K4BKZ5	0.69	-0.02	0.33	0.09	Uncharacterized protein
K4BL04	2.01	-0.19	0.15	1.43	Uncharacterized protein
K4BL13	-0.98	-0.19	-0.74	-0.39	Uncharacterized protein
K4BL38	-0.27	-0.42	0.07	0.12	Uncharacterized protein
K4BL65	-0.42	-0.05	-1.27	-1.31	Uncharacterized protein
K4BL84	0.57	-0.15	0.40	0.37	Uncharacterized protein
K4BL92	0.67	-0.27	0.24	-0.07	Chlorophyll a-b binding protein, chloroplastic
K4BLA0	-0.76	-0.02	-0.68	-0.49	Uncharacterized protein
K4BLA1	0.27	-0.02	0.57	0.66	Uncharacterized protein
K4BLI1	-0.21	-0.11	0.11	-0.54	Uncharacterized protein

Accession	Burned	Control	Regular	Limit	Description
K4BLI9	0.96	-0.10	1.75	0.44	Uncharacterized protein
K4BLP5	-0.72	-0.21	-0.92	-0.05	Uncharacterized protein
K4BLR5	-0.75	-0.19	-1.22	0.17	Uncharacterized protein
K4BLS5	-0.21	-0.07	-0.27	0.54	Uncharacterized protein
K4BLT6	0.51	0.00	-0.27	-0.92	Uncharacterized protein
K4BLU0	0.17	0.00	0.17	0.07	Uncharacterized protein
K4BLU5	0.09	-0.01	-0.26	-1.04	Uncharacterized protein
K4BLU6	-0.32	-0.03	-2.06	-2.89	Uncharacterized protein
K4BLV3	-0.81	-0.06	0.47	0.40	Uncharacterized protein
K4BLW8	-1.13	0.00	-0.75	-1.13	Uncharacterized protein
K4BLX5	-1.12	0.00	-1.11	-0.22	Uncharacterized protein
K4BLY5	0.00	0.00	-0.25	-0.38	Uncharacterized protein
K4BM13	0.51	-0.14	0.17	-0.64	Uncharacterized protein
K4BM40	-0.96	-0.58	1.00	-0.62	T-complex protein 1 subunit delta
K4BM53	0.75	0.00	-0.65	0.18	Uncharacterized protein
K4BM57	-2.61	-0.03	0.10	-1.77	Uncharacterized protein
K4BM62	0.07	-0.22	0.08	-0.15	Uncharacterized protein
K4BM85	-0.10	-0.38	-1.42	-0.18	Uncharacterized protein
K4BMB8	0.70	-0.35	0.52	0.62	Uncharacterized protein
K4BMD5	0.01	-0.01	-0.01	-0.95	Uncharacterized protein
K4BMH6	0.80	-0.10	0.24	-0.91	Uncharacterized protein
K4BMI4	-0.02	0.00	1.00	-1.18	Uncharacterized protein
K4BMJ2	-0.93	-0.02	0.01	-1.17	Uncharacterized protein
K4BMJ4	-0.52	0.00	-0.94	1.12	Uncharacterized protein
K4BML3	-1.09	-0.21	-0.36	-1.62	Uncharacterized protein
K4BML6	-0.58	0.00	-0.61	-0.50	Uncharacterized protein
K4BMM4	-0.67	-0.19	-0.19	0.42	Uncharacterized protein
K4BMN4	-0.51	-0.15	-1.23	-0.19	Uncharacterized protein
K4BMR7	-0.33	-0.03	-0.60	-0.49	Uncharacterized protein
K4BMT2	-2.49	-0.81	-0.14	-1.12	Uncharacterized protein
K4BMX1	-0.59	-0.07	0.16	0.58	Uncharacterized protein
K4BMY2	-0.47	-0.88	-0.28	0.05	Glycylpeptide N-tetradecanoyltransferase
K4BMY9	-0.48	-0.04	0.57	0.13	Uncharacterized protein
K4BN29	-0.77	-0.04	1.25	0.60	Uncharacterized protein
K4BN40	1.97	-0.06	0.70	1.36	Uncharacterized protein
K4BN60	-0.83	0.00	-0.30	-0.64	Uncharacterized protein
K4BN62	-0.73	-0.45	0.48	-0.16	Pectinesterase
K4BN81	0.74	-0.01	1.52	0.51	D-3-phosphoglycerate dehydrogenase
K4BNC2	-0.80	-0.05	-0.42	-0.68	6-phosphogluconate dehydrogenase, decarboxylating
K4BNE0	0.37	-0.01	0.11	1.23	Uncharacterized protein
K4BNF7	-1.09	-0.43	-0.41	-1.18	Eukaryotic translation initiation factor 5A
K4BNH6	-0.41	-0.42	-1.23	-1.33	Uncharacterized protein
K4BNL9	-0.77	-0.07	-0.42	-0.80	Uncharacterized protein
K4BNR2	-0.08	-0.01	-0.15	0.18	ATP synthase subunit beta
K4BNT6	-0.66	-0.04	0.48	-1.07	Uncharacterized protein
K4BNV4	-0.76	-0.08	0.67	0.25	Uncharacterized protein
K4BNY4	0.54	-0.03	0.15	0.53	4-hydroxy-4-methyl-2-oxoglutarate aldolase
K4BP02	-0.79	-0.14	-0.97	-0.62	Ribosomal protein L15
K4BP08	-0.45	-0.17	0.62	-1.43	Uncharacterized protein
K4BP30	-1.36	0.00	0.34	-0.14	Pyruvate kinase
K4BP59	-0.70	-0.01	-0.24	-0.17	Glyceraldehyde-3-phosphate dehydrogenase
K4BP76	-0.70	-0.04	-1.12	-0.85	Uncharacterized protein
K4BP98	1.51	-0.01	-0.63	0.70	Uncharacterized protein
K4BPB0	-0.45	-1.00	-1.45	-0.51	Uncharacterized protein
K4BPJ0	1.84	-0.05	0.94	1.64	Uncharacterized protein
K4BPJ4	-0.66	-0.16	-0.07	-0.06	Uncharacterized protein

Accession	Burned	Control	Regular	Limit	Description
K4BPK3	-0.97	-0.04	0.06	-0.77	Uncharacterized protein
K4BPK4	-0.28	-0.08	-0.03	-0.40	Uncharacterized protein
K4BPP3	0.02	-0.27	-0.78	-0.14	Uncharacterized protein
K4BPR4	0.05	-0.01	-0.08	0.11	Uncharacterized protein
K4BPV5	-1.09	0.00	-0.12	-1.25	Glutamine synthetase
K4BPX5	0.01	-0.01	0.08	-0.50	Uncharacterized protein
K4BQ07	-0.14	-0.06	0.89	-0.26	Peptidylprolyl isomerase
K4BQ47	-1.35	-0.01	-0.38	-0.99	Translation factor GUF1 homolog, chloroplastic
K4BQ51	-0.68	-0.15	-1.37	-0.37	Mg-protoporphyrin IX chelatase
K4BQ58	-0.28	-0.01	0.41	0.98	Uncharacterized protein
K4BQ77	-1.85	-0.11	-0.87	-0.96	Uncharacterized protein
K4BQ85	-1.16	0.00	0.14	-0.67	Uncharacterized protein
K4BQC6	-0.55	-0.22	-0.75	-1.16	Calcium-transporting ATPase
K4BQD6	-1.60	-0.01	-0.64	-0.44	S-formylglutathione hydrolase
K4BQW1	0.09	-0.02	0.29	0.64	Uncharacterized protein
K4BR52	-1.66	-0.03	-1.85	0.37	Uncharacterized protein
K4BRC3	1.47	-0.06	0.11	0.60	Uncharacterized protein
K4BRG8	-0.96	0.00	-0.05	-0.27	Uncharacterized protein
K4BRR1	0.52	-0.13	1.08	2.04	Uncharacterized protein
K4BRS2	-0.07	0.00	-0.14	0.09	Protein disulfide-isomerase
K4BRX7	0.90	-0.33	0.64	-1.20	Uncharacterized protein
K4BS18	-0.19	-0.09	-0.13	0.03	Uncharacterized protein
K4BS22	0.51	-0.14	-0.09	-1.83	Uncharacterized protein
K4BS37	1.31	-0.32	1.04	0.54	Uncharacterized protein
K4BSB7	-0.11	0.00	-0.33	-0.81	Uncharacterized protein
K4BSK7	0.83	-0.02	0.13	1.52	Peptidylprolyl isomerase
K4BSM2	-0.03	-0.56	-1.77	-1.35	Uncharacterized protein
K4BSP6	-0.79	-0.01	0.15	0.26	Uncharacterized protein
K4BSR4	0.70	-0.19	1.69	2.16	Annexin
K4BSV6	0.71	-0.26	0.84	0.80	Uncharacterized protein
K4BSZ1	0.39	0.00	-1.00	0.48	Uncharacterized protein
K4BT19	-0.95	-0.05	-1.51	-0.12	Uncharacterized protein
K4BT58	-0.72	-0.03	-0.52	-1.23	Uncharacterized protein
K4BT84	0.77	-0.36	-0.14	0.19	Uncharacterized protein
K4BTC6	-0.68	0.00	-0.93	0.25	Uncharacterized protein
K4BTH6	0.61	-0.08	1.06	1.33	Peroxidase
K4BTH7	0.44	-0.10	0.00	1.28	Peroxidase
K4BTI0	0.61	0.00	-0.25	-0.42	Uncharacterized protein
K4BTI1	0.72	-0.03	0.24	0.07	Uncharacterized protein
K4BTI3	-0.06	-0.01	-0.42	-0.85	Uncharacterized protein
K4BTL1	-1.76	-0.24	0.86	-0.91	Uncharacterized protein
K4BTX9	0.65	0.00	1.64	2.00	Uncharacterized protein
K4BTY6	0.03	-0.10	-0.04	0.28	Phospho-2-dehydro-3-deoxyheptonate aldolase
K4BTY9	0.03	-0.08	0.18	0.12	Uncharacterized protein
K4BTZ3	-0.55	-0.20	-0.58	-0.67	Uncharacterized protein
K4BU02	-0.47	-0.20	-0.01	-0.35	Uncharacterized protein
K4BU13	-1.08	-0.34	-1.62	-0.63	Uncharacterized protein
K4BU47	-0.19	-0.11	-0.23	-0.22	Glucose-6-phosphate isomerase
K4BUB7	-0.80	-0.02	0.10	-0.81	Serine hydroxymethyltransferase
K4BUC5	0.35	-0.32	0.02	0.34	Uncharacterized protein
K4BUN4	0.25	-0.28	-0.41	-0.76	Uncharacterized protein
K4BV02	-0.71	-0.12	-0.63	1.15	Uncharacterized protein
K4BV04	-2.21	-0.21	-0.77	-0.89	Uncharacterized protein
K4BV16	-0.20	-0.31	-0.13	0.92	Uncharacterized protein
K4BV58	0.44	0.00	-1.13	0.40	Uncharacterized protein
K4BV98	-0.59	-0.40	-0.61	-0.55	Uncharacterized protein

Accession	Burned	Control	Regular	Limit	Description
K4BVB8	0.49	-0.12	0.80	0.23	Uncharacterized protein
K4BVD6	-0.95	-0.07	0.35	0.05	Uncharacterized protein
K4BVD8	-0.77	0.00	0.03	0.40	Proteasome subunit alpha type
K4BVE2	-2.64	-0.01	-1.33	-2.67	50S ribosomal protein L31
K4BVG4	-1.10	-0.01	-1.04	-1.33	Uncharacterized protein
K4BVG6	0.38	-0.02	-1.74	-1.70	Uncharacterized protein
K4BVH5	-0.43	-0.04	-0.26	-0.43	Uncharacterized protein
K4BVH7	-0.20	-0.08	0.88	0.36	Coatomer subunit alpha
K4BVL2	-0.20	-0.09	-0.09	-0.69	Uncharacterized protein
K4BVN6	-1.08	-0.03	0.44	-1.04	Uncharacterized protein
K4BVR7	0.71	-0.10	0.37	1.30	Uncharacterized protein
K4BVS6	-1.60	-0.01	-0.88	-1.26	Uncharacterized protein
K4BVU1	1.09	-0.05	0.95	1.54	Uncharacterized protein
K4BVU7	-1.26	-0.02	-0.08	0.54	Uncharacterized protein
K4BVV2	-0.35	-0.01	0.01	-0.74	Uncharacterized protein
K4BVZ0	-0.71	0.00	-0.10	-0.19	Glyceraldehyde-3-phosphate dehydrogenase
K4BVZ3	0.75	-0.01	0.91	-0.20	Peptidylprolyl isomerase
K4BW05	-1.28	-0.11	-0.70	0.89	Uncharacterized protein
K4BW27	0.96	-0.08	0.68	-0.67	Uncharacterized protein
K4BW33	-2.03	-0.10	0.30	-1.01	Uncharacterized protein
K4BW79	0.28	-0.05	0.34	-0.09	2-methylene-furan-3-one reductase
K4BWB5	-0.59	-0.19	-0.15	0.01	Uncharacterized protein
K4BWE4	-0.12	0.00	0.15	-0.44	Uncharacterized protein
K4BWH8	-2.05	-0.02	-0.33	-0.92	Pyruvate dehydrogenase E1 component subunit alpha
K4BWH9	1.01	-0.49	2.03	1.20	Uncharacterized protein
K4BWZ2	-0.87	-0.01	-1.11	-0.28	Uncharacterized protein
K4BX09	0.10	0.00	0.60	-0.48	Uncharacterized protein
K4BX19	-1.15	-0.11	-1.98	-2.68	Uncharacterized protein
K4BX20	-0.02	-0.01	-0.05	0.20	ATP synthase subunit beta
K4BX34	-0.97	0.00	0.01	-1.16	Fructose-bisphosphate aldolase
K4BX77	-0.61	-0.13	-0.90	0.34	3-isopropylmalate dehydrogenase
K4BX96	0.36	0.00	-0.64	-0.13	Uncharacterized protein
K4BXB1	-0.26	-0.37	0.03	-0.72	Uncharacterized protein
K4BXC1	-0.50	-0.12	0.06	-0.87	Uncharacterized protein
K4BXC7	-0.95	-0.08	0.03	-1.27	Dihydrolipoamide acetyltransferase component of pyruvate dehydrogenase complex
K4BXD4	-0.64	-0.16	0.12	-0.08	Uncharacterized protein
K4BXJ1	0.25	-0.20	0.61	0.17	Uncharacterized protein
K4BXJ9	-0.35	-0.02	0.87	0.80	Uncharacterized protein
K4BXN9	-1.35	0.00	-0.65	-1.01	Uncharacterized protein
K4BXX0	-1.68	-0.03	0.34	0.08	Uncharacterized protein
K4BXX3	-1.82	-0.23	0.02	-0.43	Alpha-1,4 glucan phosphorylase
K4BXY4	0.41	-0.02	-0.62	-0.59	Uncharacterized protein
K4BY24	0.67	-0.02	0.51	1.08	Uncharacterized protein
K4BY28	-0.14	-0.01	-0.28	0.18	Uncharacterized protein
K4BY59	-0.64	-0.01	-0.33	-0.71	Uncharacterized protein
K4BYA6	0.82	-0.03	0.80	-0.02	Uncharacterized protein
K4BYA8	0.39	-0.07	-0.56	0.06	Uncharacterized protein
K4BYC0	-0.21	-0.14	1.06	-1.43	Uncharacterized protein
K4BYF1	1.19	-0.15	-0.15	0.62	Uncharacterized protein
K4BYG6	-0.72	0.00	-0.58	-0.25	Glyceraldehyde-3-phosphate dehydrogenase
K4BYL6	-0.04	-0.05	0.05	0.94	Uncharacterized protein
K4BZB1	-1.29	-0.10	-1.31	-0.24	Uncharacterized protein
K4BZB6	-0.83	-0.25	-1.08	-0.22	Uncharacterized protein

Accession	Burned	Control	Regular	Limit	Description
K4BZT0	-1.68	0.00	-1.01	-0.81	Uncharacterized protein
K4BZT8	0.77	-0.49	0.53	0.23	Uncharacterized protein
K4C030	-1.15	-0.04	0.04	-1.56	Uncharacterized protein
K4C034	-0.39	-0.06	-0.09	0.09	Uncharacterized protein
K4C036	-0.59	-0.01	0.46	-1.46	Uncharacterized protein
K4C0W6	-1.65	-0.09	0.60	-0.04	Uncharacterized protein
K4C144	-0.76	0.00	0.52	-0.66	Malic enzyme
K4C1C9	-0.38	-0.02	0.49	-0.33	Uncharacterized protein
K4C1D2	-0.48	-0.14	0.43	-0.19	Uncharacterized protein
K4C1L6	0.13	-0.44	-1.59	-1.32	Uncharacterized protein
K4C1Q9	0.67	-0.31	0.35	2.46	Peroxidase
K4C1T2	-1.76	0.00	0.57	-0.01	Clathrin heavy chain
K4C1V2	-2.52	-1.11	-0.67	-2.84	Uncharacterized protein
K4C1V6	-0.66	-0.12	-0.58	-0.28	Phosphoinositide phospholipase C
K4C1Z0	0.32	-0.01	-0.08	-0.52	Uncharacterized protein
K4C227	-0.61	-0.25	-0.29	0.80	Uncharacterized protein
K4C245	0.54	-0.06	1.06	0.10	Uncharacterized protein
K4C247	-1.13	-1.04	0.21	-1.06	Uncharacterized protein
K4C261	-0.70	-0.01	-0.32	0.12	Serine hydroxymethyltransferase
K4C273	1.36	-0.16	0.45	1.43	Uncharacterized protein
K4C2B3	0.27	-0.18	0.24	-0.40	Uncharacterized protein
K4C2D6	0.02	-0.36	-0.56	0.19	60S acidic ribosomal protein P0
K4C2D8	0.26	-0.03	-0.89	-0.22	Uncharacterized protein
K4C2E1	-1.00	0.00	1.09	-0.50	Uncharacterized protein
K4C2F3	-0.23	-0.64	1.12	0.52	Uncharacterized protein
K4C2H1	-1.03	-0.02	-0.75	-1.12	Uncharacterized protein
K4C2J3	-0.52	0.00	-0.23	-1.60	Uncharacterized protein
K4C2U0	-0.73	-0.08	-1.15	0.61	Proteasome subunit beta type
K4C2U9	-1.30	-0.01	-0.14	0.21	Uncharacterized protein
K4C2V0	-0.65	-0.04	-1.21	-0.51	Uncharacterized protein
K4C2V1	0.29	-0.12	0.59	1.14	Uncharacterized protein
K4C2V4	-0.09	-0.62	-2.06	0.09	Uncharacterized protein
K4C2V5	-0.95	0.00	-1.07	-0.25	T-complex protein 1 subunit gamma
K4C2Y2	1.53	-0.49	0.24	0.49	Uncharacterized protein
K4C310	-1.29	0.00	-0.27	0.18	Uncharacterized protein
K4C353	0.20	-0.01	-0.12	0.28	Uncharacterized protein
K4C376	-2.02	-0.06	0.41	0.57	Protein disulfide-isomerase
K4C390	-0.57	-0.08	-1.44	-0.55	Uncharacterized protein
K4C392	0.60	-0.39	0.41	-1.13	Uncharacterized protein
K4C399	-0.37	-0.61	0.59	-0.08	Uncharacterized protein
K4C3A3	-1.08	-0.19	0.33	0.73	Uncharacterized protein
K4C3B5	0.89	-0.92	-0.73	-0.56	Uncharacterized protein
K4C3B9	-0.24	-0.02	-0.73	0.58	40S ribosomal protein S4
K4C3D3	-0.95	-0.01	-0.75	-1.38	Uncharacterized protein
K4C3D8	-0.51	-0.01	-0.62	-0.46	40S ribosomal protein S8
K4C3E8	-1.44	-0.34	-1.97	-2.07	Uncharacterized protein
K4C3F7	0.38	0.00	0.04	0.97	Uncharacterized protein
K4C3H8	-0.55	-0.25	1.17	-0.09	Uncharacterized protein
K4C3J6	0.09	-0.05	-1.01	-0.33	Uncharacterized protein
K4C3T2	0.10	0.00	1.56	2.72	Uncharacterized protein
K4C3U9	-0.58	-0.01	-0.95	0.21	Pectinesterase
K4C3Y3	0.02	-0.49	0.11	-2.41	Uncharacterized protein
K4C3Z3	-1.31	-0.07	-0.41	-0.39	Uncharacterized protein
K4C424	-1.68	-0.29	-0.48	-1.15	Uncharacterized protein
K4C455	-0.49	0.00	-0.01	0.20	Uncharacterized protein
K4C4E2	-0.19	-0.36	0.09	0.34	Uncharacterized protein
K4C4Z6	-1.57	-0.05	-0.31	-0.57	Uncharacterized protein

Accession	Burned	Control	Regular	Limit	Description
K4C5A1	-0.35	0.00	-1.37	-1.43	Uncharacterized protein
K4C5B9	-0.59	0.00	-0.72	-1.42	Uroporphyrinogen decarboxylase
K4C5F4	-0.44	-0.01	-0.52	0.16	Superoxide dismutase
K4C5P1	1.03	0.00	0.66	0.16	Ferritin
K4C5R3	-0.29	-0.03	-0.09	-0.34	Uncharacterized protein
K4C5Y9	-1.25	0.00	-0.55	-0.28	Uncharacterized protein
K4C5Z4	-0.83	-0.09	0.09	-0.74	Uncharacterized protein
K4C601	-0.94	-0.02	-0.46	-0.67	Uncharacterized protein
K4C627	1.09	-0.02	1.28	-0.83	Isopropylmalate synthase
K4C635	-0.65	-0.10	-0.19	-0.42	Acyl-[acyl-carrier-protein] desaturase
K4C647	-0.29	0.00	-0.13	-1.10	Uncharacterized protein
K4C6K6	-0.25	-0.07	0.40	-0.66	Aldehyde dehydrogenase
K4C6K7	-0.56	-0.02	0.31	-0.86	Uncharacterized protein
K4C6L0	-0.84	-0.16	-0.03	-0.32	Protein disulfide-isomerase
K4C6Q9	-1.54	-0.54	-0.71	-1.72	Uncharacterized protein
K4C6T7	-1.30	-0.38	0.61	-1.11	Uncharacterized protein
K4C715	-0.44	-0.05	0.63	0.15	Uncharacterized protein
K4C726	0.41	0.00	0.14	0.08	Uncharacterized protein
K4C745	-1.10	-0.08	-0.13	0.68	Uncharacterized protein
K4C768	0.45	-0.07	0.69	0.32	Chlorophyll a-b binding protein, chloroplastic
K4C779	-2.33	-0.14	-1.02	-0.80	Uncharacterized protein
K4C785	0.32	0.00	-0.09	-1.26	Uncharacterized protein
K4C7C4	-0.08	0.00	0.01	-0.04	Uncharacterized protein
K4C7F6	-0.69	-0.05	0.23	-0.52	Uncharacterized protein
K4C7G8	0.76	-0.02	-1.20	0.08	Uncharacterized protein
K4C7H8	-0.01	-0.04	0.29	-2.21	Uncharacterized protein
K4C7I1	0.26	-0.03	-0.06	-0.12	Uncharacterized protein
K4C7I8	-1.22	-0.28	-0.18	-0.06	60S ribosomal protein L18a
K4C7K0	0.35	-0.03	0.39	-0.09	Uncharacterized protein
K4C7M5	-0.25	-0.21	0.18	-0.92	Uncharacterized protein
K4C7M8	1.97	-0.34	0.65	1.17	Uncharacterized protein
K4C7Y9	-0.30	0.00	0.04	-1.08	Uncharacterized protein
K4C7Z7	0.65	-0.29	-1.16	-0.23	Uncharacterized protein
K4C7Z8	0.92	0.00	-1.23	-0.33	Uncharacterized protein
K4C807	0.42	-0.06	0.36	0.26	Uncharacterized protein
K4C823	-1.69	-0.14	-0.94	0.23	Uncharacterized protein
K4C841	-0.92	0.00	-1.92	-0.36	Uncharacterized protein
K4C874	-0.30	0.00	-0.61	0.15	Uncharacterized protein
K4C875	-0.34	-0.16	0.95	-0.55	Uncharacterized protein
K4C890	1.01	-0.11	0.51	-0.03	Uncharacterized protein
K4C8H3	-0.10	0.00	1.08	1.10	Uncharacterized protein
K4C8P4	-1.01	-0.39	-0.61	0.85	Uncharacterized protein
K4C8Q1	0.45	0.00	-0.13	0.54	Uncharacterized protein
K4C8Q9	-2.47	-0.39	-1.07	-2.08	Uncharacterized protein
K4C8R3	0.23	-0.20	-0.86	0.18	Uncharacterized protein
K4C8R4	-0.93	0.00	-0.61	-0.20	Glyceraldehyde-3-phosphate dehydrogenase
K4C8R8	-1.27	-0.06	0.14	0.02	Nucleoside diphosphate kinase
K4C8X4	1.45	-0.01	0.30	0.45	Uncharacterized protein
K4C8X8	-0.18	-0.04	0.42	0.18	Uncharacterized protein
K4C945	-0.75	-0.02	-0.33	-0.90	Uncharacterized protein
K4C947	-0.83	0.00	-1.25	-1.04	Uncharacterized protein
K4C952	-1.08	-0.04	-1.05	-1.05	Lysine--tRNA ligase
K4C956	-0.17	-0.07	0.16	0.26	Uncharacterized protein
K4C973	-0.55	-0.33	0.25	0.34	Uncharacterized protein
K4C998	-2.86	-0.22	-1.44	-1.25	Uncharacterized protein
K4C9B8	-0.19	-0.01	-0.96	-0.13	Uncharacterized protein

Accession	Burned	Control	Regular	Limit	Description
K4C9G9	-0.63	0.00	1.25	0.11	Uncharacterized protein
K4C9K5	1.10	-0.01	0.65	0.69	Uncharacterized protein
K4C9L4	-1.06	-0.03	-0.17	0.19	Uncharacterized protein
K4C9L7	-0.45	-0.16	-0.46	-0.14	Uncharacterized protein
K4C9N4	1.80	-0.25	0.20	1.52	Uncharacterized protein
K4C9P9	-2.23	-0.01	-0.43	-1.01	Uncharacterized protein
K4C9Z6	-0.74	0.00	-0.71	-0.08	Uncharacterized protein
K4CA08	0.74	-0.52	-0.03	0.32	Uncharacterized protein
K4CA24	-0.94	-0.03	0.33	-0.38	Tubulin beta chain
K4CA37	-0.77	-0.12	-2.04	-0.40	Uncharacterized protein
K4CA55	-1.06	-0.02	-0.63	-0.12	Peptidyl-prolyl cis-trans isomerase
K4CA57	0.04	-0.02	-0.11	-0.19	Uncharacterized protein
K4CA68	-1.70	-0.04	0.18	-0.20	Uncharacterized protein
K4CA74	-0.09	-0.01	-0.52	-0.64	Uncharacterized protein
K4CAE2	-1.83	-0.40	-2.50	-1.65	Uncharacterized protein
K4CAE9	0.23	0.00	0.17	-0.13	Uncharacterized protein
K4CAF9	-1.47	-0.06	-0.46	-0.29	Carboxypeptidase
K4CAH3	-1.25	-0.03	-1.37	-0.92	40S ribosomal protein S8
K4CAH4	0.48	-0.14	0.52	-0.06	Peptidylprolyl isomerase
K4CAL7	-1.15	-0.34	-0.50	0.17	Uncharacterized protein
K4CAM0	0.10	-0.14	-0.07	0.23	Uncharacterized protein
K4CAM3	0.48	0.00	0.13	-0.97	Uncharacterized protein
K4CAM8	1.22	-0.02	1.11	0.33	Uncharacterized protein
K4CAN4	-1.16	-0.13	1.12	0.30	Succinate-CoA ligase subunit beta
K4CAR4	-2.22	-0.58	-2.43	-2.58	Histone H2A
K4CAS8	-1.33	-0.12	-0.76	-0.06	40S ribosomal protein S24
K4CAU9	-0.49	-0.01	-0.52	-0.64	Uncharacterized protein
K4CB11	-0.75	-0.02	0.70	-0.97	Uncharacterized protein
K4CB52	-0.50	-0.02	-0.54	-1.65	Uncharacterized protein
K4CB54	-0.64	0.00	0.02	-1.55	Translation initiation factor IF-3
K4CB65	-0.47	-0.08	0.09	-0.40	Uncharacterized protein
K4CB74	-1.76	-0.12	-2.10	-0.34	Uncharacterized protein
K4CBD6	-0.73	-0.03	0.82	0.77	Xylose isomerase
K4CBF0	-1.06	-0.02	0.64	-0.95	Acetyltransferase component of pyruvate dehydrogenase complex
K4CBN0	-1.57	-0.02	0.07	-1.63	Uncharacterized protein
K4CBN7	-0.04	0.00	-0.63	-0.72	Purple acid phosphatase
K4CBT5	0.82	-0.08	1.76	-0.47	Uncharacterized protein
K4CBV6	-0.60	-0.01	-0.43	0.09	Uncharacterized protein
K4CBX2	0.25	-0.34	0.61	-0.03	Tyrosine--tRNA ligase
K4CBY0	-0.40	-0.09	-1.49	-1.96	Uncharacterized protein
K4CC33	-1.01	-0.16	0.06	-0.46	Uncharacterized protein
K4CC35	0.23	0.00	0.53	-0.33	Uncharacterized protein
K4CCD2	-0.89	-0.20	-0.42	0.34	Uncharacterized protein
K4CCD7	-0.74	-0.55	0.08	-0.28	Proteasome subunit beta type
K4CCJ2	-2.09	-0.01	-0.21	-1.07	Plasma membrane ATPase
K4CCP7	-1.20	-0.05	-0.46	-1.12	Elongation factor Ts, mitochondrial
K4CDF4	0.54	0.00	0.20	-0.47	Coatomer subunit alpha
K4CDY9	0.90	-0.02	0.92	0.95	Uncharacterized protein
K4CE22	0.72	-0.28	-0.06	0.91	Uncharacterized protein
K4CE39	1.30	-0.02	0.41	0.57	Uncharacterized protein
K4CE78	0.55	0.00	-0.27	0.36	Uncharacterized protein
K4CEA5	-1.12	-0.09	-0.99	-0.71	Uncharacterized protein
K4CEJ0	-0.11	-0.01	0.24	-0.18	Uncharacterized protein
K4CEJ1	-1.83	-0.01	0.21	-0.18	Uncharacterized protein
K4CEJ7	-1.09	-0.01	0.67	0.51	Uncharacterized protein
K4CEK7	-0.79	-0.01	1.27	-1.11	Glycosyltransferase

Accession	Burned	Control	Regular	Limit	Description
K4CEL3	0.64	-0.27	-0.23	-0.70	Uncharacterized protein
K4CEL4	-1.31	-0.28	-0.29	-1.31	Uncharacterized protein
K4CEN4	0.27	-0.03	-1.52	0.21	Uncharacterized protein
K4CEP2	-2.06	-0.06	-0.72	-0.16	Uncharacterized protein
K4CEW0	0.21	-0.02	-1.74	-0.75	Glucose-6-phosphate 1-dehydrogenase
K4CEY5	-0.99	0.00	0.25	-0.57	Uncharacterized protein
K4CF48	0.17	-0.01	0.39	0.16	Uncharacterized protein
K4CF70	-0.92	-0.08	0.19	0.10	Fatty acid hydroperoxide lyase, chloroplastic
K4CF87	-1.67	-0.10	-0.71	-0.16	Uncharacterized protein
K4CFC8	-0.36	-0.18	-0.45	0.12	Uncharacterized protein
K4CFD4	-0.70	0.00	0.70	0.55	Aconitate hydratase
K4CFE7	-0.22	-0.07	-1.81	0.48	Isocitrate lyase
K4CFM5	-1.73	-0.18	-1.02	-0.91	Ketol-acid reductoisomerase
K4CFR0	-1.60	-0.02	-0.97	-2.01	Uncharacterized protein
K4CFU2	0.73	-0.36	-0.07	-0.22	Uncharacterized protein
K4CFW6	-1.91	-0.12	-1.22	-0.73	Uncharacterized protein
K4CFX4	0.66	-0.08	-0.22	0.48	Uncharacterized protein
K4CG24	0.41	0.00	-0.72	-0.86	Uncharacterized protein
K4CG46	-0.91	-0.04	-0.32	-0.32	Uncharacterized protein
K4CG62	0.51	0.00	0.01	0.67	Uncharacterized protein
K4CG68	-1.27	-0.19	-1.47	-0.22	Uncharacterized protein
K4CG69	0.98	-0.05	0.31	0.42	Uncharacterized protein
K4CGD5	-0.97	-0.07	-0.40	-1.08	Uncharacterized protein
K4CGE7	-1.59	-0.16	-0.44	-0.17	Glucose-1-phosphate adenylyltransferase
K4CGE8	-0.50	-0.05	-1.02	-1.10	Uncharacterized protein
K4CGH5	-0.83	0.00	-0.86	1.12	Uncharacterized protein
K4CGI6	-0.23	-0.05	-0.34	-0.08	Uncharacterized protein
K4CGL2	-0.41	-0.05	-0.57	-0.23	Uncharacterized protein
K4CGM3	-0.40	-0.30	-0.62	0.38	Uncharacterized protein
K4CGP6	-0.26	-0.04	0.00	0.20	Uncharacterized protein
K4CGU0	0.33	0.00	-0.46	-1.03	Fen-interacting protein 3
K4CGU4	0.81	0.00	0.50	1.71	Uncharacterized protein
K4CGU8	-0.50	-0.02	0.07	0.17	Malate dehydrogenase
K4CGX0	0.24	-0.04	-0.64	0.76	Uncharacterized protein
K4CH02	0.03	-0.20	0.13	-1.10	Uncharacterized protein
K4CH43	-0.83	-0.01	-1.55	-1.65	Chlorophyll a-b binding protein, chloroplastic
K4CH72	-2.06	-0.44	-0.15	-0.40	Uncharacterized protein
K4CH79	-1.58	-0.28	-0.71	0.71	Uncharacterized protein
K4CH96	-0.36	-0.03	0.12	1.43	Uncharacterized protein
K4CH99	-1.60	-0.20	-0.88	-1.59	Thiamine thiazole synthase, chloroplastic
K4CHD1	-0.69	-0.06	-0.94	0.03	Uncharacterized protein
K4CHF9	-0.08	-0.05	0.34	0.53	Uncharacterized protein
K4CHH3	0.97	-0.23	1.62	0.87	Uncharacterized protein
K4CHH4	-0.31	-0.43	-0.39	-0.42	Uncharacterized protein
K4CHI2	0.54	0.00	0.18	0.63	Uncharacterized protein
K4CHJ1	-0.10	0.00	0.33	-0.40	Uncharacterized protein
K4CHJ6	-0.57	-0.04	-0.66	0.13	40S ribosomal protein S8
K4CHK7	-0.12	-0.54	-1.89	-1.21	Uncharacterized protein
K4CHR6	-0.20	-0.07	0.02	-0.29	Fructose-bisphosphate aldolase
K4CHU1	-2.48	-0.01	-0.87	-2.38	Uncharacterized protein
K4CHW8	0.03	-0.19	-0.65	0.07	Obg-like ATPase 1
K4CHX2	0.01	-0.01	-0.53	-0.49	Uncharacterized protein
K4CHY3	-0.74	-0.01	-0.31	-0.70	Phosphoglycerate kinase
K4CHY4	-0.66	0.00	-0.47	-1.04	Phosphoglycerate kinase
K4CI69	-1.09	-0.01	0.63	-0.31	Pectin acetylesterase
K4CI93	-1.66	-0.04	-0.08	-1.55	40S ribosomal protein S6
K4CIE2	-1.33	-0.06	-0.04	-0.38	Peptidylprolyl isomerase

Accession	Burned	Control	Regular	Limit	Description
K4CIG0	-0.64	-0.01	0.07	0.32	Glutathione peroxidase
K4CIG6	1.40	-0.19	0.48	0.21	Uncharacterized protein
K4CIH6	-1.41	-0.56	-1.07	-1.53	Uncharacterized protein
K4CIJ1	-2.33	-0.32	0.80	-1.15	Uncharacterized protein
K4CIK9	-1.96	-0.03	-1.46	-2.03	Uncharacterized protein
K4CIV5	-1.26	0.00	0.36	-1.04	Uncharacterized protein
K4CJ02	-0.68	0.00	-0.18	-0.32	Uncharacterized protein
K4CJ46	0.14	-0.01	0.59	-0.70	Isopropylmalate synthase
K4CJ67	-0.14	-0.01	-0.07	-0.18	Cysteine synthase
K4CJ85	-1.55	-0.07	-2.02	-1.55	Uncharacterized protein
K4CJ99	1.77	-0.01	0.40	2.12	Uncharacterized protein
K4CJC4	0.35	0.00	0.03	-0.73	Uncharacterized protein
K4CJD3	-2.36	0.00	-0.68	-1.61	Uncharacterized protein
K4CJH4	-0.71	-0.18	-0.04	0.42	Proteasome subunit alpha type
K4CJP1	0.38	-0.21	0.61	-0.91	Methylthioribose-1-phosphate isomerase
K4CJT1	0.55	-0.12	0.81	-0.15	Uncharacterized protein
K4CK47	-0.64	-0.06	-0.02	0.41	Aspartate aminotransferase
K4CK49	0.83	-0.18	-0.31	-0.12	Importin subunit alpha
K4CK63	-0.54	-0.20	-1.78	-0.86	Uncharacterized protein
K4CK76	-0.26	-0.07	0.30	-0.17	Uncharacterized protein
K4CKH7	0.27	-0.08	-0.16	0.26	Uncharacterized protein
K4CKX4	-0.98	-0.10	-0.59	-0.67	Uncharacterized protein
K4CL08	-1.08	-0.44	0.24	-0.03	Uncharacterized protein
K4CL50	0.59	0.00	1.34	1.43	Uncharacterized protein
K4CL64	-0.41	0.00	-0.39	0.31	Uncharacterized protein
K4CL75	-2.01	-0.04	-0.62	-1.27	Uncharacterized protein
K4CLA3	-1.21	-0.03	0.20	-0.62	Uncharacterized protein
K4CLC9	-1.71	-0.41	-0.48	0.20	Serine hydroxymethyltransferase
K4CLD5	-0.44	-0.16	1.71	0.67	Uncharacterized protein
K4CLJ1	-1.05	-0.30	0.48	-0.82	Uncharacterized protein
K4CLJ5	0.52	-0.01	-0.46	0.53	Uncharacterized protein
K4CLQ6	0.04	-0.02	-0.37	-0.57	Phospholipase D
K4CLR1	-0.07	-0.03	0.71	0.87	Lactoylglutathione lyase
K4CLS8	1.08	-0.68	-0.73	-0.08	Cytochrome b-c1 complex subunit 7
K4CLS9	1.25	-0.10	0.53	0.86	Uncharacterized protein
K4CLT6	0.90	-0.48	1.50	0.57	Uncharacterized protein
K4CM08	-1.44	-0.19	0.05	-1.96	Uncharacterized protein
K4CM55	0.16	-0.01	-0.14	-1.39	Uncharacterized protein
K4CMC3	-0.12	-0.02	-1.72	-1.06	Delta-aminolevulinic acid dehydratase
K4CME9	-0.82	-0.12	-0.40	-1.04	Uncharacterized protein
K4CMI0	-0.41	0.00	0.57	0.09	Uncharacterized protein
K4CMI1	-0.45	0.00	0.82	0.40	Uncharacterized protein
K4CMI6	0.00	0.00	-3.31	-1.02	Uncharacterized protein
K4CMJ7	-0.22	-0.01	-0.01	-0.39	Eukaryotic translation initiation factor 3 subunit G
K4CMM7	-0.20	0.00	0.12	0.76	Uncharacterized protein
K4CMQ6	-0.17	-0.13	0.99	0.70	Uncharacterized protein
K4CMU2	0.02	-0.14	0.61	-0.05	ATP-dependent Clp protease proteolytic subunit
K4CMY9	0.50	-0.02	0.29	-0.42	Phosphoribulokinase
K4CN08	0.15	0.00	0.86	0.30	Uncharacterized protein
K4CN09	-1.45	-0.06	-1.11	-1.00	Glycerol-3-phosphate acyltransferase, chloroplastic
K4CN10	-0.91	-0.43	0.48	-1.32	Uncharacterized protein
K4CN44	1.31	0.00	1.13	1.82	Uncharacterized protein
K4CN57	0.10	-0.04	1.34	1.86	Uncharacterized protein

Accession	Burned	Control	Regular	Limit	Description
K4CNE7	-0.59	-0.02	-0.25	-0.34	Uncharacterized protein
K4CNE8	-0.45	-0.05	0.05	-0.27	ATP-dependent Clp protease proteolytic subunit
K4CNF1	-0.50	-0.02	0.79	0.07	Isocitrate dehydrogenase [NAD] subunit, mitochondrial
K4CNG0	0.50	-0.27	-0.69	0.43	Uncharacterized protein
K4CNR6	-2.15	-0.01	-0.69	-0.86	Uncharacterized protein
K4CNR8	-0.13	0.00	0.36	0.24	Uncharacterized protein
K4CNS0	0.17	-0.07	-0.53	-0.26	Uncharacterized protein
K4CNS6	-0.56	0.00	-0.48	-0.69	Elongation factor G, chloroplastic
K4CNT2	0.36	-0.58	-1.07	-0.34	Uncharacterized protein
K4CNT4	0.30	-0.07	0.43	0.60	Uncharacterized protein
K4CNW2	0.66	-0.02	-0.24	-0.02	ATP-dependent Clp protease proteolytic subunit
K4CNW6	0.97	-0.20	-0.32	-0.39	Uncharacterized protein
K4CNY4	0.03	-0.04	1.82	0.33	Uncharacterized protein
K4CP05	-0.99	-0.01	-0.66	-1.19	Uncharacterized protein
K4CP14	0.42	-0.02	-0.15	0.67	Uncharacterized protein
K4CP17	-1.89	-0.07	-0.33	-0.87	Uncharacterized protein
K4CP37	-0.37	-0.02	0.10	-0.38	Uncharacterized protein
K4CPC2	-1.83	0.00	-0.44	-0.43	Uncharacterized protein
K4CPC9	0.03	-0.05	1.00	1.21	Beta-adaptin-like protein
K4CPJ7	-0.87	-0.46	-1.33	-2.00	Uncharacterized protein
K4CPN6	1.59	-0.11	-0.50	-1.33	Uncharacterized protein
K4CPN9	-1.09	-0.02	-1.22	-2.29	Nucleoside diphosphate kinase
K4CPQ3	0.14	-0.04	-0.69	-1.29	Uncharacterized protein
K4CPS2	0.27	-0.13	-0.76	0.74	Mitochondrial pyruvate carrier
K4CPS8	-0.54	-0.09	-0.95	-0.31	Uncharacterized protein
K4CPX6	-0.43	-0.26	0.68	-0.58	Starch synthase, chloroplastic/amyloplastic
K4CPX9	-1.53	-0.61	-2.02	-1.11	Uncharacterized protein
K4CPY0	-1.35	-0.04	-0.15	-1.39	Uncharacterized protein
K4CQ52	-0.46	-0.31	-0.30	-0.52	Uncharacterized protein
K4CQ62	-0.59	0.00	-0.11	-0.22	Uncharacterized protein
K4CQ64	-0.79	0.00	-0.12	-1.04	Uncharacterized protein
K4CQA9	-0.52	-0.06	0.05	-0.14	Uncharacterized protein
K4CQB5	-0.50	-0.04	0.55	-0.41	Uncharacterized protein
K4CQE3	-0.33	-0.16	-1.53	0.08	Uncharacterized protein
K4CQE5	0.57	-0.73	-1.01	0.59	Uncharacterized protein
K4CQH4	-0.12	-0.16	-0.99	-1.28	Uncharacterized protein
K4CQH9	0.39	-0.08	-0.48	-1.55	Phenylalanine ammonia-lyase
K4CQQ1	1.65	0.00	0.30	0.65	Peptidylprolyl isomerase
K4CQT3	-0.66	-0.04	-0.20	-0.98	Uncharacterized protein
K4CQU8	-0.80	0.00	0.09	-1.37	Uncharacterized protein
K4CQV5	-0.46	-0.04	-0.20	-0.48	Fructose-bisphosphate aldolase
K4CQW8	-1.28	-0.10	-0.42	0.28	Uncharacterized protein
K4CQX2	1.12	-0.09	0.89	-0.32	Uncharacterized protein
K4CR23	-0.48	-0.03	-1.82	-0.90	Uncharacterized protein
K4CR69	-2.02	-0.88	-0.65	-0.64	Arginine biosynthesis bifunctional protein ArgJ, chloroplastic
K4CR73	-0.48	-0.05	-0.74	-0.04	Eukaryotic translation initiation factor 3 subunit A
K4CR90	-0.49	-0.02	-0.51	0.15	Uncharacterized protein
K4CRB9	-0.86	-0.01	-0.29	-1.23	Uncharacterized protein
K4CRD4	-0.40	-0.02	-0.18	-0.44	Uncharacterized protein
K4CRE0	-0.30	-0.18	-0.24	-1.66	Uncharacterized protein

Accession	Burned	Control	Regular	Limit	Description
K4CRF6	-0.82	-0.09	-0.41	-1.06	Uncharacterized protein
K4CRK7	-0.16	0.00	-0.41	-0.93	Uncharacterized protein
K4CRN4	0.27	-0.26	-0.27	-0.49	Uncharacterized protein
K4CRS9	-0.37	-0.30	-0.58	-0.36	Chlorophyll a-b binding protein, chloroplastic
K4CRV2	-0.73	-0.29	-1.06	-0.63	Uncharacterized protein
K4CSA9	-0.56	0.00	-0.84	-1.76	Uncharacterized protein
K4CSD7	0.68	0.00	-0.14	1.36	Uncharacterized protein
K4CSE1	-0.52	0.00	-0.07	-0.98	Uncharacterized protein
K4CSF0	0.10	-0.06	-0.89	-1.00	Uncharacterized protein
K4CSH4	-1.02	-0.04	-1.72	-1.34	Uncharacterized protein
K4CSN4	-0.90	-0.02	-0.38	-0.36	Uncharacterized protein
K4CSQ2	-1.59	-0.08	-0.59	-0.01	Alpha-1,4 glucan phosphorylase
K4CTF6	-0.66	0.00	-0.42	-0.38	40S ribosomal protein S8
K4CTF7	0.18	-0.04	-0.39	0.10	Peptidylprolyl isomerase
K4CTF8	-0.65	-0.05	-0.88	0.88	Peptidylprolyl isomerase
K4CTJ3	-0.08	-0.16	0.72	1.21	Uncharacterized protein
K4CU14	1.49	-0.19	2.24	1.41	Uncharacterized protein
K4CU16	-0.17	-0.43	1.82	-0.05	Uncharacterized protein
K4CU43	0.12	-0.04	-0.23	-0.69	Uncharacterized protein
K4CU67	-0.63	-0.15	-1.37	-0.07	Uncharacterized protein
K4CU73	-0.93	-0.04	0.62	-0.38	Uncharacterized protein
K4CU78	0.66	-0.03	0.23	-0.05	Photosystem II reaction center Psb28 protein
K4CUE5	-0.43	-0.01	-0.15	-0.08	Uncharacterized protein
K4CUF4	0.52	-0.14	0.23	0.11	Uncharacterized protein
K4CUL6	-0.91	-0.02	-0.01	-0.36	Uncharacterized protein
K4CUR8	0.13	-0.05	-0.73	-0.11	Uncharacterized protein
K4CUW3	-1.54	-0.89	-1.23	-1.29	Uncharacterized protein
K4CUW6	-0.42	0.00	0.61	0.91	Uncharacterized protein
K4CUX6	-1.62	-0.02	0.32	0.38	Elongation factor Tu
K4CV19	-0.50	-0.02	0.05	-0.86	Uncharacterized protein
K4CV65	-0.93	-0.01	-0.12	-0.74	Uncharacterized protein
K4CV71	-0.49	-0.14	0.15	-0.72	Uncharacterized protein
K4CV78	1.04	-0.02	-0.32	1.35	Uncharacterized protein
K4CVC0	-1.60	-0.17	-0.69	-0.42	Ribosomal protein L19
K4CVC2	-0.84	-0.33	0.48	-1.09	Uncharacterized protein
K4CVI4	-0.17	-0.01	0.13	0.13	Cysteine synthase
K4CVK9	-0.06	-0.24	1.74	-0.26	Uncharacterized protein
K4CVM9	-1.35	0.00	-1.95	-1.58	40S ribosomal protein S3a
K4CVP8	-0.62	0.00	0.27	0.35	Uncharacterized protein
K4CVP9	-1.85	0.00	0.10	-0.13	Uncharacterized protein
K4CVQ4	-0.73	-0.01	0.32	-0.41	Uncharacterized protein
K4CVQ7	-2.57	-1.02	1.94	3.05	Uncharacterized protein
K4CVS3	-1.58	-0.01	-0.92	-0.64	Pyruvate kinase
K4CVU1	-0.83	-0.01	-0.56	-0.70	Uncharacterized protein
K4CVU5	-1.26	-0.20	-1.18	-1.59	Uncharacterized protein
K4CVW4	-1.25	-0.30	-0.29	-2.50	Uncharacterized protein
K4CVW7	1.06	0.00	1.07	0.37	Uncharacterized protein
K4CVX0	-0.86	-0.16	3.75	4.02	Uncharacterized protein
K4CVX6	0.56	-0.06	2.85	2.22	Uncharacterized protein
K4CW40	-0.71	-0.09	-0.56	-0.02	Malate dehydrogenase
K4CW45	0.26	-0.03	-1.00	-0.84	Uncharacterized protein
K4CW69	-0.16	-0.04	0.35	1.08	Cyanate hydratase
K4CW78	0.31	-0.01	-0.13	0.53	Uncharacterized protein
K4CW84	-0.17	-0.07	-0.53	0.04	Uncharacterized protein
K4CW92	0.34	-0.53	-0.02	0.53	Uncharacterized protein
K4CWB0	-0.74	-0.03	0.14	-0.22	Glutamyl-tRNA(Gln) amidotransferase subunit B, chloroplastic/mitochondrial

Accession	Burned	Control	Regular	Limit	Description
K4CWC2	1.10	-0.28	-0.07	0.26	Uncharacterized protein
K4CWC4	0.20	-0.03	1.90	4.10	PR10 protein
K4CWD3	-0.58	-0.01	0.36	0.69	Malate dehydrogenase
K4CWE3	-1.47	-0.51	-0.22	-0.16	Uncharacterized protein
K4CWE4	-0.78	-0.23	-0.02	0.54	Uncharacterized protein
K4CWH3	0.35	-0.02	1.68	0.13	Uncharacterized protein
K4CWK1	0.35	-0.01	0.01	-0.27	Uncharacterized protein
K4CWK9	1.16	-0.36	0.38	0.21	Uncharacterized protein
K4CWL0	-0.68	-0.19	0.01	1.14	Uncharacterized protein
K4CWM3	-0.22	-0.25	0.65	-0.46	Uncharacterized protein
K4CWU2	-1.05	-0.57	-0.20	-1.14	Uncharacterized protein
K4CWW3	-0.78	0.00	0.06	-0.31	Uncharacterized protein
K4CWX5	0.55	-0.01	0.21	-1.04	Uncharacterized protein
K4CX43	0.53	-0.03	0.04	0.92	Uncharacterized protein
K4CX44	-2.57	-0.24	-0.66	-1.19	Uncharacterized protein
K4CX88	-0.34	-0.04	0.15	1.45	Uncharacterized protein
K4CXC8	-0.33	-0.10	-1.12	-0.88	Uncharacterized protein
K4CXD5	-0.98	-0.35	-0.25	-1.38	Uncharacterized protein
K4CXD9	-0.68	-0.07	-0.53	-0.11	40S ribosomal protein S8
K4CXG4	-0.06	-0.04	0.35	0.69	Uncharacterized protein
K4CXG8	1.35	-0.17	-0.93	-0.88	Uncharacterized protein
K4CXH1	-0.81	-0.04	-0.11	-0.63	Tryptophan synthase
K4CXJ6	0.53	-0.04	-0.39	0.51	Uncharacterized protein
K4CXM0	-1.45	-0.42	-1.08	-1.86	Uncharacterized protein
K4CXM7	0.13	-0.03	-0.17	0.15	Uncharacterized protein
K4CXQ6	0.92	-0.30	-0.87	-0.48	Ubc13-type ubiquitin-conjugating enzyme 2
K4CXR1	-0.82	-0.02	0.06	-0.48	Uroporphyrinogen decarboxylase
K4CXS7	0.03	-0.10	0.14	0.61	Uncharacterized protein
K4CXT9	0.16	-0.02	-1.03	-0.10	Uncharacterized protein
K4CXV5	0.10	-0.10	0.00	-0.99	Uncharacterized protein
K4CXW3	-0.51	0.00	-0.30	0.90	Glutamyl-tRNA(Gln) amidotransferase subunit A, chloroplastic/mitochondrial
K4CXX8	0.68	-0.23	0.90	0.19	Proteasome subunit alpha type
K4CXY8	0.86	-0.61	0.59	0.19	Acyl-coenzyme A oxidase
K4CXZ1	-1.58	-0.21	0.21	0.37	Uncharacterized protein
K4CY51	-0.88	-0.05	-1.62	-1.46	Mg-protoporphyrin IX chelatase
K4CY74	-0.71	-0.51	0.97	0.32	Uncharacterized protein
K4CYD3	-0.36	0.00	-0.65	-0.76	Uncharacterized protein
K4CYF5	0.83	-0.05	-0.45	0.99	Uncharacterized protein
K4CYL4	-1.31	-0.93	-1.04	0.91	Cysteine synthase
K4CYV4	-0.94	-0.03	0.08	-0.74	Uncharacterized protein
K4CYY2	-0.75	-0.02	-0.48	0.17	Uncharacterized protein
K4CZF1	-0.16	-0.02	0.35	-0.16	Peptidylprolyl isomerase
K4CZS1	-0.30	-0.01	-0.75	0.08	Uncharacterized protein
K4D025	0.76	0.00	1.86	0.94	Uncharacterized protein
K4D054	-0.90	-0.01	-2.21	-1.97	Uncharacterized protein
K4D0C8	-0.51	-0.01	0.22	0.34	ATP-dependent Clp protease proteolytic subunit
K4D0R4	-1.08	-0.16	-0.19	-0.55	Uncharacterized protein
K4D0T6	-1.06	0.00	0.72	-0.36	Adenylyl cyclase-associated protein
K4D0U0	0.60	-0.68	-0.67	0.15	Uncharacterized protein
K4D0U1	-0.41	-0.12	-0.52	-0.14	Uncharacterized protein
K4D0Y5	0.12	-0.49	0.59	1.56	Uncharacterized protein
K4D180	-0.51	-0.08	-1.17	-1.13	Uncharacterized protein
K4D1H0	-0.60	-0.02	0.78	2.03	Uncharacterized protein

Accession	Burned	Control	Regular	Limit	Description
K4D1N6	0.82	-0.49	0.67	1.76	Uncharacterized protein
K4D1P2	-0.21	0.00	-0.41	-1.00	Uncharacterized protein
K4D1Q0	-2.12	-0.11	-1.00	-1.74	Uncharacterized protein
K4D1U4	1.07	-0.07	0.07	0.34	Uncharacterized protein
K4D1V7	-1.10	-0.13	-0.21	-1.11	Uncharacterized protein
K4D246	0.19	-0.31	-0.57	-1.37	Uncharacterized protein
K4D258	0.67	-0.01	0.28	-0.76	Uncharacterized protein
K4D2A4	-1.11	-0.64	-1.02	-0.99	Uncharacterized protein
K4D2B6	0.43	-0.01	0.93	0.84	Uncharacterized protein
K4D2D7	-2.40	-0.01	-2.04	-3.69	Uncharacterized protein
K4D2I8	0.15	0.00	0.59	0.97	Uncharacterized protein
K4D2J1	-0.61	-0.07	0.20	-0.24	Inosine-5'-monophosphate dehydrogenase
K4D2L3	-0.16	-0.02	0.78	0.71	Uncharacterized protein
K4D2M7	0.34	-0.03	0.40	0.10	Uncharacterized protein
K4D2P9	-0.92	-0.03	0.15	-1.12	Thioredoxin reductase
K4D2T9	0.67	-0.01	0.27	-0.50	Uncharacterized protein
K4D2W1	-1.55	-0.01	0.43	0.26	Uncharacterized protein
K4D2Y1	-0.94	-0.05	0.24	-0.25	Tubulin beta chain
K4D2Y4	-0.36	-0.10	0.58	0.01	Uncharacterized protein
K4D2Z0	0.46	-0.01	-0.23	-0.95	Uncharacterized protein
K4D2Z4	0.61	-0.02	0.46	-0.21	Uncharacterized protein
K4D300	0.15	-0.16	0.21	0.35	Proteasome subunit alpha type
K4D304	2.12	-0.04	-0.83	1.44	Uncharacterized protein
K4D311	0.56	-0.72	-0.72	0.22	GrpE protein homolog
K4D331	0.46	-0.11	1.15	-0.05	NADH-cytochrome b5 reductase
K4D338	-2.24	-0.01	-0.72	-0.93	Uncharacterized protein
K4D340	-0.71	0.00	-0.49	-0.08	Uncharacterized protein
K4D378	0.44	-0.05	0.36	0.22	Coatomer subunit beta
K4D389	0.33	-0.13	-0.69	-1.68	Uncharacterized protein
K4D3B5	-0.16	-0.02	0.20	-1.53	Uncharacterized protein
K4D3D6	1.00	-0.14	0.76	-0.15	Uncharacterized protein
K4D3E4	-0.49	-0.04	-0.19	-0.44	Fructose-bisphosphate aldolase
K4D3F2	-0.26	-0.03	-0.48	0.19	Uncharacterized protein
K4D3F8	0.54	-0.34	0.58	-0.44	Pyruvate kinase
K4D3G5	-0.98	0.00	-0.09	-1.46	Uncharacterized protein
K4D3I3	-1.52	-0.14	-1.11	0.15	S-adenosylmethionine synthase
K4D3J0	0.33	-0.28	-1.20	-0.45	Uncharacterized protein
K4D3J1	-1.13	-0.08	-0.28	0.10	Uncharacterized protein
K4D3K7	0.76	0.00	0.20	0.74	Uncharacterized protein
K4D3L8	-1.00	-0.05	1.77	0.85	Uncharacterized protein
K4D3M1	-0.31	0.00	0.27	-0.19	Uncharacterized protein
K4D3R4	0.32	-0.02	-0.29	-0.33	Uncharacterized protein
K4D3V6	1.68	-0.10	1.79	0.09	Uncharacterized protein
K4D3Y2	-0.38	-0.55	-1.03	-1.31	Uncharacterized protein
K4D3Y9	0.12	0.00	-0.32	0.01	Uncharacterized protein
K4D402	-0.50	0.00	0.18	-1.12	Uncharacterized protein
K4D426	-0.33	-0.02	-0.08	-0.36	Uncharacterized protein
K4D435	-0.58	-0.02	0.03	-0.32	Uncharacterized protein
K4D448	0.29	-0.13	-0.96	-0.58	Uncharacterized protein
K4D452	-0.43	-0.01	0.11	1.19	Uncharacterized protein
K4D467	-0.89	0.00	0.17	1.05	Uncharacterized protein
K4D489	-0.18	-0.02	0.04	-0.41	Uncharacterized protein
K4D4A4	-0.82	-0.09	-0.17	-0.29	Uncharacterized protein
K4D4E6	-0.74	-0.03	0.01	-0.44	Uncharacterized protein
K4D4L9	-2.17	-0.05	-0.51	-1.74	Uncharacterized protein
K4D4P7	-0.09	-0.01	0.49	-0.77	Uncharacterized protein
K4D4T0	-1.56	-0.02	-1.30	-0.87	Uncharacterized protein
K4D4V8	0.62	-0.05	0.97	-0.49	Uncharacterized protein

Accession	Burned	Control	Regular	Limit	Description
K4D4Y1	1.76	-0.25	0.07	1.14	Uncharacterized protein
K4D530	-0.67	-0.23	0.60	-0.16	Pyruvate kinase
K4D533	0.02	0.00	-0.43	-0.68	Dihydrolipoamide acetyltransferase component of pyruvate dehydrogenase complex
K4D5C2	-0.59	-0.06	-1.02	0.07	Uncharacterized protein
K4D5E1	-0.09	-0.08	0.39	-0.54	Beta-hexosaminidase
K4D5E7	-2.27	-0.01	-0.86	-1.22	Methylenetetrahydrofolate reductase
K4D5F9	1.33	-0.14	-0.08	0.70	Uncharacterized protein
K4D5G2	-0.54	-0.23	-0.71	-0.31	Uncharacterized protein
K4D5G8	0.10	-0.30	0.03	-0.58	Phospho-2-dehydro-3-deoxyheptonate aldolase
K4D5I0	-0.02	-0.01	0.43	0.77	Uncharacterized protein
K4D5I1	0.02	-0.01	0.03	0.39	Uncharacterized protein
K4D5K8	0.35	-0.02	-0.11	0.04	Uncharacterized protein
K4D5K9	-0.20	-0.14	-0.43	-0.45	Uncharacterized protein
K4D5L7	-1.09	-0.16	0.15	-0.57	Uncharacterized protein
K4D5T1	-0.89	-0.18	-0.93	0.72	Uncharacterized protein
K4D5U3	-0.72	-0.05	0.01	-0.44	Glutamine synthetase
K4D5V2	-1.47	-0.03	0.25	0.13	Uncharacterized protein
K4D601	-0.77	-0.04	0.11	0.30	Uncharacterized protein
K4D616	-0.13	-0.04	0.29	-0.86	Uncharacterized protein
K4D619	-1.04	-0.13	-0.77	-1.38	Uncharacterized protein
K4D6D0	0.92	-0.01	0.46	2.07	Uncharacterized protein
K4D6E8	0.21	-0.11	-0.95	-0.20	Eukaryotic translation initiation factor 3 subunit F
K4D6I5	0.51	-0.01	-0.12	-0.13	Nitrate reductase
K4D6M3	0.08	-0.01	-0.92	-0.40	Uncharacterized protein
K4D6M8	-1.78	-0.69	-0.77	-2.49	Dihydrolipoamide acetyltransferase component of pyruvate dehydrogenase complex
K4D6Q9	-0.30	-0.13	0.58	-0.54	Uncharacterized protein
K4D6Y2	-0.11	-0.20	0.11	-0.56	Uncharacterized protein
K4D7D1	0.25	-0.03	-0.97	-1.64	Uncharacterized protein
K4D7F1	-0.87	0.00	-0.42	-0.05	Uncharacterized protein
K4D7R1	-0.80	-0.04	-0.41	-0.65	Uncharacterized protein
K4D7U2	0.07	-0.01	-0.31	-0.19	Uncharacterized protein
K4D7V9	-1.03	0.00	-0.49	-1.21	Uncharacterized protein
K4D7X4	-0.44	-0.01	0.73	0.23	Uncharacterized protein
K4D810	-1.26	-0.03	0.79	-0.75	Uncharacterized protein
K4D834	0.09	-0.01	-0.52	-0.43	Uncharacterized protein
K4D8C1	0.21	-0.01	-0.17	1.94	Uncharacterized protein
K4D8F6	-0.77	0.00	0.90	-1.02	Uncharacterized protein
K4D8S6	-1.06	-0.09	0.76	-0.51	Uncharacterized protein
K4D8X9	-1.44	-0.06	0.06	-0.98	Uncharacterized protein
K4D930	-0.33	0.00	0.23	1.24	Uncharacterized protein
K4D9A2	0.25	-0.13	0.16	-0.43	Uncharacterized protein
K4D9L5	-0.68	-0.01	-0.68	-0.14	Uncharacterized protein
K4D9P9	0.61	-0.01	-1.01	0.34	Uncharacterized protein
K4D9Q1	-0.37	-0.24	-0.69	-0.17	Uncharacterized protein
K4D9S4	-0.23	-0.25	0.48	-0.35	Glycosyltransferase
K4D9W7	-0.78	-0.47	-1.25	0.18	Uncharacterized protein
K4D9X3	-1.02	0.00	-0.96	-0.54	Uncharacterized protein
K4DA24	-1.35	-0.05	0.33	0.05	Uncharacterized protein
K4DA30	0.66	-0.05	0.32	0.43	Uncharacterized protein
K4DA40	-0.02	-0.05	0.15	0.27	Uncharacterized protein
K4DA57	-0.52	-0.01	0.56	-1.25	Uncharacterized protein
K4DA65	1.72	-0.08	1.37	1.40	Uncharacterized protein
K4DA71	0.06	-0.03	-1.70	0.28	Proteasome subunit beta type

Accession	Burned	Control	Regular	Limit	Description
K4DA96	0.10	0.00	-0.66	-1.53	Protein disulfide-isomerase
K4DA99	-1.75	0.00	-0.58	-1.60	Uncharacterized protein
K4DAD5	-0.05	-0.07	-0.40	-0.24	Uncharacterized protein
K4DAL9	-1.14	-0.08	-1.22	-0.89	Uncharacterized protein
K4DAM1	-1.37	-0.06	0.08	0.50	Uncharacterized protein
K4DAS6	-0.58	-0.11	-0.13	0.42	Uncharacterized protein
K4DAV2	0.43	-0.10	0.38	-0.35	Uncharacterized protein
K4DAX6	0.31	-0.02	1.07	0.51	Uncharacterized protein
K4DAX8	0.22	-0.01	0.65	-0.22	Uncharacterized protein
K4DAZ4	0.86	-0.39	-0.12	0.17	Uncharacterized protein
K4DB46	-0.96	-0.08	0.22	-0.89	Uncharacterized protein
K4DB56	0.70	-0.39	-0.17	-0.34	Uncharacterized protein
K4DB71	-2.24	-0.51	-0.33	-0.58	Uncharacterized protein
K4DBA1	-1.30	0.00	-0.29	-0.99	Cytochrome b6-f complex iron-sulfur subunit
K4DBB0	-0.06	0.00	-0.09	0.43	Uncharacterized protein
K4DBC4	-0.78	0.00	0.63	0.57	Aconitate hydratase
K4DBF1	0.42	-0.05	-0.08	-0.45	Chlorophyll a-b binding protein, chloroplastic
K4DBI3	0.17	-0.01	-0.58	0.19	Uncharacterized protein
K4DBI4	-0.09	-0.01	0.55	0.35	Uncharacterized protein
K4DBL8	-0.58	-0.08	-0.58	-0.73	Uncharacterized protein
K4DBN8	-0.73	-0.02	-0.64	-0.83	Uncharacterized protein
K4DBP9	-0.89	-0.01	-2.07	-0.45	Uncharacterized protein
K4DBR8	-0.46	-0.01	-1.09	0.46	Uncharacterized protein
K4DBU5	-0.27	-0.02	-0.13	-0.45	Uncharacterized protein
K4DBV1	-1.07	-0.19	-0.17	-0.56	Uncharacterized protein
K4DC02	-1.16	0.00	0.02	0.57	Proteasome subunit alpha type
K4DC13	-0.72	-0.10	0.07	-0.23	Uncharacterized protein
K4DC48	-0.03	-0.34	-1.55	-0.03	Uncharacterized protein
K4DC81	0.73	-0.42	0.93	0.48	Glycosyltransferase
K4DC84	-0.72	-0.04	-0.40	-1.27	Uncharacterized protein
K4DC86	2.13	-0.13	0.74	0.91	Uncharacterized protein
K4DCC5	-1.79	-0.07	-0.20	-0.56	Uncharacterized protein
K4DCH1	-1.02	-0.03	0.32	-0.97	Uncharacterized protein
K4DCI6	0.47	-0.10	0.84	0.39	Citrate synthase
K4DCL4	-2.26	-0.13	-2.12	-1.73	Chlorophyll a-b binding protein, chloroplastic
K4DCP3	-0.65	-0.05	-1.04	-1.11	Uncharacterized protein
K4DCQ6	-0.86	-0.21	-1.60	-2.48	Uncharacterized protein
K4DCR6	0.11	-0.09	0.06	-1.22	Uncharacterized protein
K4DCS5	0.15	-0.03	-0.71	-1.03	Uncharacterized protein
K4DCU3	-1.56	-0.07	-1.26	-0.41	Uncharacterized protein
K4DCV3	-0.82	-0.11	0.98	0.98	Malate dehydrogenase
K4DCW0	-1.23	-0.04	-0.40	-0.47	Uncharacterized protein
K4DD79	-0.52	-0.02	-0.16	0.87	Uncharacterized protein
K4DD89	-0.44	-0.15	-0.39	-0.59	Guanosine nucleotide diphosphate dissociation inhibitor
K4DDP7	-0.81	-0.36	-0.99	-1.55	Uncharacterized protein
K4DDW3	0.24	-0.02	-0.22	0.58	Uncharacterized protein
K4DEQ3	1.12	-0.36	0.26	0.55	Uncharacterized protein
K4DEQ8	-0.67	-0.50	0.02	-0.65	Uncharacterized protein
K4DF81	-1.14	0.00	-0.99	-0.57	Uncharacterized protein
K4DF88	0.87	-0.14	0.03	-1.14	Uncharacterized protein
K4DF90	-0.41	-0.14	1.38	0.88	Uncharacterized protein
K4DF99	-1.59	-0.56	-0.55	-1.52	Uncharacterized protein
K4DFA0	-1.28	-0.10	-0.19	-1.60	Uncharacterized protein
K4DFF9	-0.32	-0.01	1.12	-0.64	Uncharacterized protein
K4DFH1	0.44	0.00	0.20	1.41	Uncharacterized protein
K4DFK8	-0.40	0.00	-0.43	-0.23	Uncharacterized protein

Accession	Burned	Control	Regular	Limit	Description
K4DFR1	-0.67	-0.01	0.23	0.43	Uncharacterized protein
K4DFU3	-1.04	0.00	-0.22	-0.41	6-phosphogluconate dehydrogenase, decarboxylating
K4DFV3	-0.75	-0.09	0.19	-1.11	Plasmamembrane intrinsic protein 13
K4DFV4	-0.26	-0.05	0.27	0.70	Glutathione peroxidase
K4DFY4	-0.75	0.00	-0.94	0.26	Uncharacterized protein
K4DG11	0.05	0.00	0.17	-0.60	Uncharacterized protein
K4DG14	1.02	-0.04	0.41	0.33	Uncharacterized protein
K4DG25	1.70	-0.19	0.46	0.53	Uncharacterized protein
K4DG27	0.69	-0.53	0.37	0.71	Uncharacterized protein
K4DGU3	0.22	-0.15	0.04	0.71	Polyadenylate-binding protein
K4DGU7	0.75	0.00	1.43	1.25	Uncharacterized protein
K4DGZ2	-0.93	-0.34	-1.11	-0.45	Uncharacterized protein
K4DH15	-0.02	0.00	-0.27	-0.10	Uncharacterized protein
K4DH34	-2.08	-0.07	-0.16	-0.13	Catalase
K4DH36	-0.72	0.00	-0.16	-0.35	Glyceraldehyde-3-phosphate dehydrogenase
K4DH44	0.11	-0.13	-0.91	1.18	Uncharacterized protein
K4DH49	0.27	0.00	-0.19	-0.21	Pyrophosphate--fructose 6-phosphate 1-phosphotransferase subunit alpha
K4DH66	-1.19	-0.32	0.69	0.59	Serine hydroxymethyltransferase
K4DH69	0.91	-0.01	1.29	0.73	Uncharacterized protein
K4DH72	-0.42	-0.01	-0.25	0.44	Uncharacterized protein
K4DH85	0.36	0.00	0.79	-0.24	Ubiquitin-fold modifier 1
K4DH95	-0.36	-0.03	-0.22	0.39	Uncharacterized protein
K4DHA3	-1.62	-0.06	-0.02	-1.73	40S ribosomal protein S6
K4DHC8	-0.64	-0.01	-0.25	-0.92	Uncharacterized protein
K4DHE9	-0.45	-0.04	0.32	-0.18	Uncharacterized protein
K4DHH6	0.79	-0.26	0.85	-0.15	Uncharacterized protein
K4DHI9	0.66	-0.17	0.29	0.60	Uncharacterized protein
K4DHL5	-0.13	-0.01	0.20	-0.33	Uncharacterized protein
K4DHQ5	-0.63	-0.02	0.53	0.08	Uncharacterized protein
K4DHT1	-0.62	0.00	0.42	-0.20	Dihydrolipoyl dehydrogenase
K4DHU1	0.00	0.00	0.10	2.08	Uncharacterized protein
K4DHU7	-0.90	0.00	0.63	0.03	Uncharacterized protein
K4DHW8	-0.27	-0.04	-0.15	-0.19	Uncharacterized protein
K4DI33	1.60	-0.05	0.23	0.69	Uncharacterized protein
K4DI37	0.10	-0.03	-0.11	-0.04	Uncharacterized protein
O04678	0.11	-0.05	1.46	0.16	Subtilisin-like protease
O24030	-0.39	-0.36	0.41	0.37	Proteasome subunit alpha type-7
O49877	-1.36	-0.57	0.78	0.34	CYP1
O65821	-0.61	-0.01	-0.81	0.51	Histone H2B.1
O65834	1.11	-0.02	1.09	1.01	p69C protein
O65836	-1.34	-0.09	-0.12	-0.26	p69F protein
O65917	-0.96	-0.02	-1.32	-0.52	Dehydroquinate dehydratase/shikimate:NADP oxidoreductase
O81536	0.70	-0.19	1.08	0.87	Annexin
O82777	0.20	-0.05	1.07	0.30	Subtilisin-like protease
P04284	-2.86	-1.31	0.31	1.42	Pathogenesis-related leaf protein 6
P05349	0.52	-0.09	-0.21	0.37	Ribulose bisphosphate carboxylase small chain 3B, chloroplastic
P07369	-0.04	-0.03	-1.23	-0.77	Chlorophyll a-b binding protein 3C, chloroplastic
P08706	0.72	0.00	0.11	0.32	Ribulose bisphosphate carboxylase small chain 1, chloroplastic

Accession	Burned	Control	Regular	Limit	Description
P10708	-3.34	-0.16	-1.43	-1.06	Chlorophyll a-b binding protein 7, chloroplastic
P12372	0.41	0.00	0.54	-0.39	Photosystem I reaction center subunit II, chloroplastic
P12670	0.14	0.00	0.62	0.97	Protein NP24
P14831	-2.16	-0.13	-0.93	-2.35	Superoxide dismutase [Cu-Zn], chloroplastic
P17340	0.98	-0.01	0.33	0.97	Plastocyanin, chloroplastic
P17786	-1.77	-0.25	-0.54	-0.80	Elongation factor 1-alpha
P21568	-0.47	-0.15	-0.42	0.62	Peptidyl-prolyl cis-trans isomerase
P22180	-1.27	-0.01	0.15	-0.61	Plasma membrane ATPase 1
P23322	0.61	-0.09	0.40	-0.29	Oxygen-evolving enhancer protein 1, chloroplastic
P25306	-1.39	-0.79	3.78	3.55	Threonine dehydratase biosynthetic, chloroplastic
P26300	-0.21	0.00	-0.47	-0.01	Enolase
P27065	-0.99	0.00	-0.16	-0.67	Ribulose bisphosphate carboxylase large chain
P27161	0.36	-0.02	-0.01	1.23	Calmodulin
P27489	-0.79	-0.02	-1.81	-1.44	Chlorophyll a-b binding protein 13, chloroplastic
P27524	-0.64	0.00	-0.86	-0.60	Chlorophyll a-b binding protein CP24 10A, chloroplastic
P27525	-0.60	0.00	-0.81	-0.59	Chlorophyll a-b binding protein CP24 10B, chloroplastic
P36181	-1.55	-0.01	0.06	-0.80	Heat shock cognate protein 80
P37218	-2.67	-0.23	0.78	-1.95	Histone H1
P38546	-0.29	-0.11	-0.77	-0.62	GTP-binding nuclear protein Ran1
P43280	-1.32	-0.63	0.38	-1.34	S-adenosylmethionine synthase 1
P43282	-2.94	-0.14	-0.27	-0.28	S-adenosylmethionine synthase 3
P54773	-0.59	-0.28	-1.00	-0.97	Photosystem II 22 kDa protein, chloroplastic
P54928	1.00	-0.10	-0.13	0.17	Inositol monophosphatase 3
P93205	-0.70	-0.07	0.56	0.10	SBT2 protein
P93207	-0.07	-0.08	-0.01	-0.49	14-3-3 protein 10
P93208	0.25	-0.06	-0.05	0.21	14-3-3 protein 2
P93212	-0.70	-0.26	-0.32	-0.90	14-3-3 protein 7
P93214	0.06	-0.05	-0.22	-0.14	14-3-3 protein 9
P93541	-0.27	-0.22	-0.23	-0.53	Glutamate dehydrogenase
Q01413	0.57	-0.10	0.92	3.46	Glucan endo-1,3-beta-glucosidase B
Q05538	-0.16	0.00	0.63	1.99	Basic 30 kDa endochitinase
Q05539	0.04	0.00	0.40	2.96	Acidic 26 kDa endochitinase
Q08451	-0.74	-0.12	0.18	-1.27	Probable aquaporin PIP-type pTOM75
Q0ZPA3	1.17	-0.01	0.71	0.43	Plastid lipid associated protein CHRC
Q10712	-0.03	-0.36	4.14	4.18	Leucine aminopeptidase 1, chloroplastic
Q1PCD2	-0.46	0.00	1.15	1.06	Glucose-6-phosphate isomerase
Q202I0	-0.17	-0.17	-0.17	-0.34	Zeta-carotene desaturase
Q2MI42	0.95	-0.01	0.91	0.44	Protein TIC 214
Q2MI43	1.27	-0.36	-0.97	-0.51	30S ribosomal protein S15, chloroplastic
Q2MI44	-1.13	-0.01	-0.78	-1.67	NAD(P)H-quinone oxidoreductase subunit H, chloroplastic
Q2MI46	-1.01	-0.02	0.64	0.16	NAD(P)H-quinone oxidoreductase subunit I, chloroplastic

Accession	Burned	Control	Regular	Limit	Description
Q2MI49	-3.35	-0.03	-1.46	-1.47	Photosystem I iron-sulfur center
Q2MI54	0.42	-0.46	-0.40	-0.38	30S ribosomal protein S7, chloroplastic
Q2MI63	0.62	-0.03	-0.80	-0.27	50S ribosomal protein L16, chloroplastic
Q2MI64	-0.57	-0.02	0.87	-0.98	50S ribosomal protein L14, chloroplastic
Q2MI71	-0.11	-0.10	-0.28	0.05	Cytochrome b6
Q2MI72	-0.97	-0.01	-1.81	-1.76	Photosystem II reaction center protein H
Q2MI78	-0.24	-0.14	0.24	0.25	30S ribosomal protein S18, chloroplastic
Q2MI87	0.14	0.00	0.26	-0.50	Cytochrome f
Q2MI93	0.21	0.00	-0.03	0.05	ATP synthase subunit beta, chloroplastic
Q2MI96	-0.84	-0.09	-0.18	0.12	NAD(P)H-quinone oxidoreductase subunit K, chloroplastic
Q2MI98	1.00	-0.65	0.89	0.41	30S ribosomal protein S4, chloroplastic
Q2MIA0	-1.19	-0.21	-0.01	-1.19	Photosystem I P700 chlorophyll a apoprotein A1
Q2MIA1	-0.83	-0.22	-0.30	-0.37	Photosystem I P700 chlorophyll a apoprotein A2
Q2MIA4	0.02	-0.01	0.44	-0.53	Photosystem II CP43 reaction center protein
Q2MIA5	-0.75	-0.26	-0.66	-0.67	Photosystem II D2 protein
Q2MIB4	0.85	-0.02	-0.03	0.12	ATP synthase subunit b, chloroplastic
Q2MIB5	1.29	-0.03	0.17	0.39	ATP synthase subunit alpha, chloroplastic
Q2MIC0	-0.58	-0.02	0.23	-0.32	Photosystem II protein D1
Q38JD4	-1.09	-0.11	-1.37	-1.41	Temperature-induced lipocalin

Accession	Burned	Control	Regular	Limit	Description
Q38MV0	-0.80	0.00	0.17	-0.47	Tubulin beta chain
Q3C2L6	-0.35	-0.01	0.19	0.81	Sorbitol related enzyme
Q3I5C4	-2.69	-0.06	0.31	-0.86	Cytosolic ascorbate peroxidase 1
Q40129	0.28	-0.02	1.12	1.16	Uncharacterized protein
Q40131	-0.77	-0.04	1.07	-0.17	Uncharacterized protein
Q40140	-0.17	-0.07	-0.01	0.86	Aspartic protease
Q40143	-0.18	-0.71	0.21	-0.60	Cysteine proteinase 3
Q40144	0.02	-0.04	-0.62	0.10	Probable xyloglucan endotransglucosylase/hydrolase 1
Q40163	-1.10	-0.02	0.18	-1.15	Photosystem II 10 kDa polypeptide, chloroplastic
Q41339	0.35	-0.05	0.12	0.57	Small GTP-binding protein
Q41350	-0.83	-0.05	-0.74	0.39	Osmotin-like protein
Q42884	-0.05	-0.01	0.37	0.49	Chorismate synthase 1, chloroplastic
Q42891	-1.16	-0.38	-0.37	0.22	Lactoylglutathione lyase
Q42896	-1.31	0.00	-0.43	0.34	Fructokinase-2
Q43517	-2.46	0.00	-0.51	-1.35	Ferredoxin-1, chloroplastic
Q49B52	0.47	-0.01	0.91	-0.10	Monodehydroascorbate reductase
Q4A1N1	-0.54	-0.06	-0.54	1.20	Non-specific lipid-transfer protein
Q4W5U7	0.90	-0.02	0.14	1.01	Calnexin-like protein
Q4W5U8	-0.76	-0.18	-1.13	-1.81	FtsH protease
Q52QQ4	-2.12	0.00	-0.50	-0.95	Ascorbate peroxidase
Q56R04	0.22	-0.02	0.66	0.03	Putative betaine aldehyde dehyrogenase
Q5NE17	-0.38	-0.01	0.24	0.52	Malate dehydrogenase
Q5NE18	0.00	0.00	1.29	1.33	Formate dehydrogenase, mitochondrial
Q5NE20	-0.41	-0.01	-0.06	-0.72	Carbonic anhydrase
Q5NE21	-0.08	0.00	-0.57	-0.17	Carbonic anhydrase

Accession	Burned	Control	Regular	Limit	Description
Q5QJB4	-0.11	-0.12	-0.04	-0.07	Harpin binding protein 1
Q5UNS1	0.89	-0.08	3.57	2.19	Arginase 2
Q66YT8	-1.40	-0.26	-0.23	-0.54	DWARF1/DIMINUTO
Q672Q2	-0.02	-0.01	-0.21	0.43	Chloroplast-specific ribosomal protein
Q672Q6	0.73	-0.30	0.33	0.74	Photosystem II oxygen-evolving complex protein 3
Q672Q7	-0.24	-0.11	0.31	-0.98	Uncharacterized protein
Q672Q9	0.19	-0.04	-0.05	-1.21	Acyl carrier protein
Q6E4P4	-0.91	-0.01	-0.12	-0.17	Carotenoid cleavage dioxygenase 1B
Q6J1L7	-1.30	-0.09	-1.24	-0.83	GDP-mannose pyrophosphorylase
Q6R8F6	-0.63	-0.10	-0.22	-1.08	Cystathionine gamma synthase
Q6SKP4	-1.18	-0.17	-0.13	-1.21	Ribosomal protein L3
Q6T2D2	1.20	-0.02	-0.24	0.27	PII-like protein
Q6UJX4	-1.54	0.00	0.02	-0.96	Molecular chaperone Hsp90-1
Q7M1K8	-1.18	-0.06	0.23	-1.24	Chlorophyll a-b binding protein, chloroplastic
Q7XZS6	0.49	-0.01	0.46	0.93	Glutathione peroxidase
Q7Y240	-0.14	-0.02	-0.72	0.38	Thioredoxin peroxidase 1
Q7YK44	-0.30	-0.17	-0.04	-0.31	Superoxide dismutase
Q84T86	0.51	-0.01	-0.09	-1.27	Biotin carboxylase carrier protein
Q8GT30	0.10	0.00	0.24	-0.17	Dihydrolipoyl dehydrogenase
Q8GZD8	-1.10	-0.05	1.13	1.07	Neutral leucine aminopeptidase preprotein
Q8GZR6	-1.13	0.00	-0.17	-0.66	GcpE
Q8H0Q2	-0.05	0.00	1.66	0.53	Phosphotransferase
Q8RU74	-0.66	-0.08	0.41	0.13	3-dehydroquinate synthase, chloroplastic
Q93X45	1.02	-0.08	2.08	1.06	Xaa-Pro aminopeptidase 2
Q93YG7	1.15	0.00	-0.64	0.19	Profilin-2
Q93YH0	0.59	-0.03	-0.47	-0.23	ATP-dependent Clp protease proteolytic subunit
Q944F3	0.89	-0.40	0.17	0.07	Arabinosidase ARA-1
Q94K24	0.76	-0.05	1.11	0.62	Ran binding protein-1
Q9FT17	0.16	-0.28	-1.59	0.45	Lipoxygenase
Q9FV24	-0.78	-0.01	-0.73	-0.90	Aldehyde oxidase
Q9FYW9	-0.80	-0.06	-0.78	-0.25	Adenylosuccinate synthetase, chloroplastic
Q9FZ05	-1.24	-0.07	0.37	-1.07	Xyloglucan endotransglucosylase/hydrolase
Q9LEG1	0.56	-0.14	2.14	2.51	Cathepsin D Inhibitor
Q9LEG3	-0.28	0.00	0.15	1.19	Putative alcohol dehydrogenase
Q9LLB0	-0.73	-0.25	0.15	-0.01	Allene oxide synthase 2, chloroplastic
Q9M5A8	1.25	-0.08	-0.68	0.37	Chaperonin 21
Q9M7N6	1.18	-0.04	-0.37	0.19	MFP1 attachment factor 1
Q9SDZ6	-1.07	-0.10	-0.59	-0.97	Phospholipase D alpha (Fragment)
Q9SPD5	-1.31	-0.02	0.05	-0.79	Plasma membrane ATPase
Q9STA6	-0.24	0.00	-0.56	-0.23	RAD23 protein
Q9XEX8	0.27	-0.01	-0.12	-1.25	Remorin 1
Q9ZP31	-0.22	-0.18	-0.51	-0.98	Expansin